Novel and potentially non-invasive techniques to predict preterm birth

Dr Brenda Fernanda Narice

(MBBS, MSc)

A thesis submitted in partial fulfilment of the requirements for the degree of Doctor of Philosophy

The University of Sheffield

Faculty of Medicine, Dentistry and Health

Department of Oncology and Metabolism

Academic Unit of Reproductive and Developmental Medicine

Registration number: 160268520

November 2019

Abstract

The diagnosis of spontaneous preterm birth (sPTB) remains a major obstetric challenge. Prediction is currently confined to evaluating historical risk factors, clinically assessing uterine activity and cervical changes, and measuring cervical length (CL) and fetal fibronectin (fFN). These approaches have not managed to inform treatment to improve neonatal outcome or to reduce sPTB incidence. Hence, there remains a need to develop new minimally-invasive and cost-effective techniques which can better risk stratify and predict sPTB. I tested whether a series of innovative spectroscopic and light-based technologies could hold predictive value for sPTB.

I first employed Raman spectroscopy to assess mid-cervical cervicovaginal fluid (CVF) in pregnant women as a predictive tool for sPTB, and identified spectral changes in protein conformation, aminoacids, lactic acid, urea and acetate between birth outcomes.

I then used Polarisation-sensitive optical coherence tomography (PS-OCT) on the *in vitro* cervix to assess collagen orientation which is thought to change preceding sPTB. PS-OCT distinguished the preferential orientation of different cervical regions, which was consistent with histology and previous X-ray diffraction findings. PS-OCT may prove useful to assess *in vivo* cervical remodelling pending the development of a probe.

The cervical microstructure was further assessed with Magnetic induction spectroscopy (MIS). *In vitro* cervical transresistance significantly differed between the epithelial and stromal surfaces. When tested on pregnant women in a pilot preliminary study (the ECCLIPPx II study), MIS was shown to perform better than fFN and CL both in asymptomatic high-risk (AHR) and symptomatic (SYMP) women.

Finally, metabolite concentrations in CVF were assessed with enzyme-based spectrophotometry within the ECCLIPPx II study. Combining CVF lactate, urea and acetate significantly improved the clinical performance of fFN and CL within the AHR and the SYMP cohorts.

Overall, these new techniques hold promise for predicting sPTB, and support the need for larger fully-powered studies.

Dedication

This PhD thesis is lovingly dedicated to my wonderful parents and brother, Alicia B Motto, Rodolfo A Narice and Leonel E Narice; and my amazing long-life partner and mentor, Mauro A Rinaldi. Thank you for making life so worthwhile.

"*Discovery consists of seeing what everybody has seen and thinking what nobody has thought.*"

Albert Szent-Györgyi

Acknowledgement

I want to thank my supervisor, Professor Dilly Anumba, for opening the door to the wonderful world of clinical research, and giving me the opportunity to develop myself as a researcher within a great team of scientists and clinicians. Thank you for believing in me and for supporting me every step of the way.

I dedicate this thesis to my wonderful parents, Alicia B Motto and Rodolfo A Narice, and the best brother in the world, Leonel E Narice, for their unconditional love and support, for their endless hours of listening and guiding me without ever asking for anything in return. My love for you knows no limits, and I could not be more grateful for having you in my life.

I also want to dedicate this thesis to Mauro A Rinaldi, my scientific mentor and the love of my life. His own passion for science and dedicated career as a researcher instilled in me the desire to do science. I owe him my deep respect for scientists, and the daily curiosity with which I embrace life. These last two decades with you have been nothing but exceptional, and I know the best is yet to come.

I also want to express my gratitude to Dr Jill Tozer for sharing her contagious love for electrical engineering, always welcoming me into the medical engineering lab (aka “the cave”) with a smile and plenty of wonderful ideas, and for lending me a sympathetic ear when I needed it the most.

I extend my gratitude to the ECCLIPPx and PRIME teams for their fantastic companionship and for giving me a sense of belonging; a big thanks to Jamie for always coming to my rescue when the system misbehaved, the Emeritus professors, Brian Brown and Tony Baker for bringing new perspectives into the projects with their wealth of knowledge, and Evy and Anna for being great project managers and fantastic colleagues.

I thank my awesome office, lab mates and friends, Shumona, Megan, Kerry, Neha, Hiba, Gertrude, Siobhan, Sara, Sallwa, Emmanuel and Khondoker for their enthusiasm and energy, and for their 24/7 company these last three years. A special thanks to Kerry and Megan for taking the time to support me through the long and winding thesis-writing process.

I want to thank my Raman Spectroscopy collaborators, Marcela, Daniela and Professor Ihteshan Rehman for their infinite patience to train me so that I could independently perform my own studies and for believing in my project. My gratitude also extends to my PS-OCT collaborators, Wei Li and Professor Stephen Matcher, who gave me the opportunity to explore my research questions in a very supportive and friendly environment.

I thank my wonderful parents-in-law, Agustina and Augusto, and my sister-in-law, Rop, for welcoming me into their family with open arms and for always believing in me; and my extended family in Mendoza, Gaby, Cris, Gonza, Fran, and Aldu for their love and support.

I wish to extend my gratitude to my Kroto Research Institute friends, Mehri and Marcela, who have always been by my side since I moved to Sheffield; my wonderful friends from medical school back in Argentina, Agustina, Claudia, Nela, Caro, Paula, Ana and Ange, who have kept me in their lives despite the distance; and my dear speculum team, Rose, Monica and Pri, for making O&G training so much more fun.

I thank Rik for his unconditional support and love, and my long-term friends from life and the translation course, Agus, la Tana, Celes, Cyn and Vir.

I also want to thank Sheffield NHS teaching Hospitals O&G registrars, consultants and midwives for their invaluable contribution and support during my PhD. A special thanks to Mr Mostafa Metwally for his friendly advice and constant support, and registrars Jo Almeida and Vanou for their amazing sense of humour and endless energy. Immense appreciation goes to the fantastic Fetomaternal team, Dr Emma Ferriman, Mr Roobin Jokhi and Dr Vicky Stern, and midwives Jo, Caz, Kate, Jill, Rio and Emma, as well as the wonderful G1 team, for helping me during these last three years both as a colleague and as a patient. I will be forever grateful.

I also want to thank my mentor, Lisa Parker, for always listening to me without judgement; my student Kate Rahnejat whom I have had the pleasure to mentor and who has filled me with great satisfaction; the research midwifery team for their patience and good disposition; the lab managers and team secretary, the wonderful Sarah duet and Gill Burkinshaw, for dealing with my many admin requests; and the domestic assistants, Michael and Kelly, for their company during the many out-of-hours I spent in the lab and in the office.

Finally, I want to express my profound appreciation to the members of the Jessop Wing PPI team, and all the mums and dads who have taken part in our studies. Without their support, this PhD would not have been possible or meaningful. Thank you for believing in our research and for helping us in our attempt to make the world a better place.

This research has been generously supported by the National Institute of Health Research (II-LB-0216-20001), and the Jessop Wing Small Grant Scheme.

Awards, publications and presentations related to the work presented in this thesis

Grants

- "Exploring novel techniques for the prediction of spontaneous preterm birth in multiple pregnancies." British Maternal and Fetal Medicine Society (BMFMS) and Twins And Multiple Births Association (TAMBA). Principal Investigator. March 2019 (£19,614.10).
- "Intercellular matrix protein expression in non-gravid human cervix: characterisation using non-invasive optical coherence tomography." Jessop Wing Small Research Grant at Sheffield NHS Teaching Hospitals. Principal Investigator. February 2018 (£4,999.50).
- "A story across gestations: new technology to improve the prediction of preterm birth." Festival of the Mind grant at the University of Sheffield. Co-applicant. February 2018 (£5,000.00).

Travel Fellowships

- Sir Ernest Finch Travel Fellowship to attend the Preterm Birth Dialogues Conference in South Africa. January 2019 (£1,000.00).
- Department of Oncology and Metabolism Learned Society Fund to attend the BMFMS annual conference in Brighton. April 2018. (£250.00).

Prizes

- Raman spectroscopic analysis of cervicovaginal fluid may help us predict preterm birth. Oral presentation at the Preterm Birth Dialogues Conference. University of Cape Town. January 2019. 1st prize.
- Magnetic induction spectroscopy: a new technology to predict preterm birth. 3M thesis presentation at AURDM 7th Annual Symposium. University of Sheffield. November 2017. 1st prize.

Publications

- Li Wei*, Narice BF*, Anumba D and Matcher S. Polarization-sensitive optical coherence tomography with a conical beam scan for the investigation of birefringence and collagen alignment in the human cervix. Biomedical Optics Express. August 2019. Vol. 10 (8). ***Equal contribution**. https://doi.org/10.1364/BOE.10.004190.
- Narice BF, Martinez M, Lazaro Pacheco D, Amabebe E, Rehman I and Anumba D. Spectroscopic techniques as potential screening tools for preterm birth: a review and an exploratory study. Applied Spectroscopic Reviews. June 2018. https://doi.org/10.1080/05704928.2018.1473873.

Poster/oral presentations

- Narice BF, Li Wei, Matcher S and Anumba D. Polarisation-sensitive optical coherence tomography as a potential tool for assessing the orientation of collagen fibres in the human cervix. *Reproductive Sciences*. March 2019. Vol.26 (1): 63. Proceedings of the 66th annual scientific meeting of the Society for Reproductive Investigation (Poster).

- Narice BF, Martinez M, Amabebe E, Rehman I and Anumba D. Raman spectroscopic analysis of cervicovaginal fluid as a predictive tool for spontaneous preterm birth. *BJOG: An International Journal of Obstetrics and Gynaecology*. April 2012. 125 (S2), 108-109. Proceedings of the 20th annual conference of the BMFMS (Poster).
- Narice BF, Martinez M, Lazaro Pacheco D, Amabebe E, Rehman I and Anumba D. Analysing cervicovaginal fluid using Raman Spectroscopy as a predictive tool for preterm birth. *Reproductive Sciences*. March 2018. Vol 25 (1): 123(A). Proceedings of the 65th annual scientific meeting of the Society for Reproductive Investigation (Poster).
- Narice BF. Devices helping to prevent preterm birth: the ECCLIPPx II study. Royal College of Obstetrics and Gynaecology Visiting Gynaecological Society of Great Britain and Ireland. Sheffield, UK. September 2017 (Oral).

Authorship contribution

Raman spectroscopy (RS, chapter 2): I devised the study with support from my supervisor Professor Dilly Anumba, screened and recruited most participants, processed the CVF samples, conducted the experiments, interpreted the data and prepared the manuscript for publication based on preliminary results. Professor Ihtesham Rehman, Chair in Bioengineering, and his team provided critical feedback for processing the samples and aided in interpreting the spectral results. Dr Vicky Stern contributed to patients' recruitment.

Polarisation-sensitive optical coherence tomography (PS-OCT, chapter 3): I conceived the study, secured funding (Jessop Wing Small Grant), approached and recruited all participants, assisted in hysterectomies to excise the samples, performed the histology of the cervical specimens with support from Maggie Glover, histology technician at the University of Sheffield, and independently analysed the relationship between clinical variables and PS-OCT data. In collaboration with Wei Li, PhD candidate at the Department of Materials Science and Engineering, we equally contributed to sample scanning, PS-OCT raw data analysis and manuscript preparation for publication. Professor in Bioptical Engineering, Stephen Matcher, built the PS-OCT prototype and supervised the experiments and data analysis.

Magnetic induction spectroscopy (MIS, chapter 4): I secured Ethics for the study, helped the Clinical Engineering team at Sheffield NHS Teaching Hospital develop a working device by providing clinical input about cervical anatomy and physiology, screened and recruited all participants, conducted the study visits and analysed the MIS data. I also coordinated the PPI Preterm Birth group meetings and participation in outreach events including the Mobile Festival (2017) and the Festival of the Mind (2018) to raise awareness about the study. Professor Dilly Anumba conceived and supervised the study, Professor in Medical Statistics Stephen Walters provided expert input regarding sample size, and engineers Dr Jamie Healey and Dr Jill Tozer with support from Professor Emeritus Brian Brown and Tony Baker developed a clinical working MIS device.

Enzyme-based spectrophotometry (chapter 5): I screened and recruited all patients, processed CVF samples and analysed clinical and metabolomics data under the co-supervision of Dr Emmanuel Amabebe and bioinformatician Dr Neha Kulkarni.

Table of contents

Table of figures

Table of tables

List of abbreviations and acronyms

+LR	Positive likelihood ratio
-LR	Negative likelihood ratio
17-α OHPC	17-α hydroxyprogesterone caproate
^{1}H-NMR	Proton nuclear magnetic resonance spectroscopy
8-OHdG	8-hydroxydeoxyguanosine
A	Amide
a.u.	Arbitrary unit
AA	Aminoacids
AC	Alternating current
ADP	Adenosine diphosphate
ADP-GK	ADP-glucokinase
AHR	Asymptomatic high risk
AK	Acetate kinase
ATP	Adenosine triphosphate
AuROC	Area under the receiver operating characteristic curve
BASHH	British Association for Sexual Health and HIV
BMFMS	British Maternal and Fetal Medicine Society
BMI	Body mass index
BV	Bacterial vaginosis
C_{1-3}	Cervical measurement (1^{st}, 2^{nd} and 3^{rd})
CC	Creative Commons
CFLUP	Cervical length + fFN + lactate + urea + pyruvate
CI	Confidence interval
CIN	Cervical intraepithelial neoplasia
CL	Cervical length
CRF	Case report form
CS	Caesarean section
CVF	Cervicovaginal fluid
DC	Direct current
D-GPT	D-glutamate-pyruvate transaminase suspension
D-LDH	D-lactate dehydrogenase
DU	D-lactate + urea
e.m.f.	Electromotive force

ECCLIPPx	**E**le**C**tri**C**a**L** **I**mpedance **P**rediction of **P**reterm birth by spectroscopy of the cervi**X**
ECM	Extracellular matrix
EIS	Electrical impedance spectroscopy
ELISA	Enzyme-linked immunosorbent assay
EM	Electron microscopy
EMR	Electromagnetic radiation
EMS	Electromagnetic spectrum
FD-NRS	Frequency domain near-infrared spectroscopy
fFN	Fetal fibronectin
FP	Fingerprint
FPGA	Field-programmable gate array
GBS	Group B streptococci
GCSF	Granulocyte colony stimulating factors
GDPR	General Data Protection Regulation
GIDH	Glutamate dehydrogenase
GnRH	Gonadotrophin-releasing hormone
GR	General region
GS-MS	Gas chromatography-mass spectrometry
H&E	Haematoxylin & Eosin
HPA	Human Protection Agency
HRA	Human Research Authority
HTA	Human Tissue Authority
HVS	High-vaginal swab
HWN	High wavenumber
i4i	Invention for Innovation
IBP-4	Insulin-like growth factor-binding protein-4
ICC	Intra-class correlation coefficient
ICNIRP	International Commission on Non-Ionizing Radiation Protection
IGFBP-1	Insulin-like growth factor-binding protein-1
IL-10	Interleukin 10
IL-1β	Interleukin 1 beta
IL-6	Interleukin 6
IL-8	Interleukin 8
IMS	Industrial methylated spirit

IQR	Interquartile range
IUGR	Intrauterine growth restriction
JW	Jessop Wing
LC-MS	Liquid chromatography-mass spectrometry
LDA	Linear discriminant analysis
LIF	Light-induced fluorescence
L-LDH	L-lactate dehydrogenase
LLETZ	Large loop excision of the transformation zone
LMIC	Low-middle income country
LMP	Last menstrual period
LP	Linear polariser
LPS	Lipopolysaccharides
LR	Likelihood ratio
LUA	Lactate + urea + acetate
MHRA	Medicine and Healthcare products Regulatory Agency
MIAC	Microbial invasion of the amniotic cavity
MIP-1β	Macrophage inflammatory protein 1β
MIS	Magnetic induction spectroscopy
MMP	Matrix metalloproteinases
MRDTI	Magnetic resonance diffusion tensor imaging
MRI	Magnetic resonance imaging
mRNA	Messenger ribonucleic acid
MS	Mass spectrometry
NAD^+	Nicotinamide adenine dinucleotide
$NADP^+$	Nicotinamide adenine dinucleotide phosphate
NEC	Necrotising enterocolitis
NHS	National Health Service
NICE	The National Institute for Health and Care Excellence
NIHR	The National Institute for Health Research
NPV	Negative predictive value
OCT	Optical coherence tomography
PA	Photoacoustic spectroscopy
PAMG-1	Placental α-microglobulin
PANIR	Photoacoustic near-infrared
PAPR	Proteomic Assessment of Preterm Risk

PBS	Phosphate buffered saline
PC	Principal component
PCA	Principal component analysis
PG	Prostaglandin
PGN	Peptidoglycan
PIL	Patient information leaflet
PMF	Polarisation-maintaining fibre
POP	Pelvic organ prolapse
PPI	Patient and participant involvement
PPROM	Prelabour premature rupture of membranes
PPV	Positive predictive value
PRISMA	Preferred Reporting Items for Systematic Reviews and Meta- analysis
PS-OCT	Polarisation-sensitive optical coherence tomography
PTA	Phosphotransacetylase
PTB	Preterm birth
PTL	Preterm labour
PVP	Polyvinylpyrrolidone
qfFN	Quantitative fetal fibronectin
QUiPP	Quantitative Innovation in Predicting Preterm birth
QWP	Quarter wave plate
R	Reflectivity
RCOG	Royal College of Obstetricians and Gynaecologists
RCT	Randomised controlled trial
REC	Research Ethics Committee
ROS	Reactive oxygen species
RPM	Revolutions per minute
RR	Risk ratio
rRNA	Ribosomal ribonucleic acid
RS	Raman spectroscopy
SAE	Serious adverse event
SAR	Specific absorption rate
SCFA	Short-chain fatty acid
SD	Standard deviation
SGA	Small for gestational age
SHBG	Sex hormone-binding globulin

SHG	Second Harmonic Generation
SNV	Standard normal variate
SOP	Standard operating procedure
SP	Salivary progesterone
spp	Species
sPTB	Spontaneous preterm birth
SRI	Society for Reproductive Investigation
SS-OCT	Source-swept optical coherence tomography
SYMP	Symptomatic
TAH	Total abdominal hysterectomy
TLH	Total laparoscopic hysterectomy
TNF-α	Tumour necrosis factor α
TVU	Transvaginal ultrasound
USA	United States of America
UTI	Urinary tract infection
UV	Ultraviolet light
VB	Vaginal birth
VDBP	Vitamin D-binding protein
VH	Vaginal hysterectomy
WHO	World Health Organization
Z	Impedance

Chapter 1

Introduction to preterm birth

1.1. Preterm birth

1.1.1. **Definition and epidemiology**

Preterm birth (PTB) is normally defined on the basis of gestational age as any birth occurring before 37 completed weeks of gestation or alternatively lasting fewer than 259 days since the first day of the woman's last menstrual period (Blencowe et al., 2013). The PTB rate is calculated as the number of live births with a gestational age<37 weeks per 100 live births in a specific geographic area and period of time. PTB may be classified into extremely preterm (<28 weeks), very preterm (28 to<32 weeks) and moderate preterm (32 to<37). Within the moderate preterm category, those born between 34 to<37 may also be referred to as late preterm (WHO, 2012).

However, there is debate in the field regarding defining PTB based just on gestation at the time of delivery. For a start, the definition lacks an explicit boundary between what is considered a spontaneous miscarriage and a livebirth (Quinn et al., 2016). What may be regarded in some countries as a non-viable pregnancy due to extreme prematurity may be considered as a live birth in others thanks to advanced neonatal facilities. These perceptions dramatically affect the way live birth, deaths and PTB are recorded in each country, and this lack of consistency in the data does not only make comparisons across countries less reliable but it also challenges any public health effort to accurately quantify the global burden of disease (Krause et al., 2006).

Another difficulty associated with the use of gestational age at delivery to define PTB is the inability to guarantee all pregnancies are accurately and consistently dated around the world. Reliability is significantly affected by the dating method employed: whereas high and middle-income countries favour the use of prenatal ultrasound, low-middle income countries with limited access to scans tend to rely on less precise methods to estimate gestational age such as menstrual history or clinical examination (Macaulay et al., 2019).

Finally, it is worth highlighting that prematurity, as a concept and not as a standardised and arbitrary variable, is better understood as a continuum rather than a discrete entity. Prematurity refers to the degree of biological immaturity experienced by a newborn to cope with the demands of extra-uterine life (Morton and Brodsky, 2016). Survival is greatly affected by factors that go beyond gestational age at delivery such as the maternal burden of disease, the pathophysiological process triggering PTB and the neonatal birthweight among others (Draper et al., 1999). Small for gestational age babies, for example, carry a higher risk of peri- and postnatal mortality and morbidity than their appropriately-sized counterparts (Delobel-Ayoub et al., 2006, Lee et al., 2017).

Assessment of the global burden of PTB has been rather challenging given the scarce and inconsistent data available from some regions around the world. However, this has not stopped collective efforts to estimate the worldwide incidence and prevalence of PTB (WHO, 2012). Every year, more than 15 million children are thought to be born prematurely around the world, with prevalence rates that range from 5% to 18% (WHO, 2012, Georgiou et al., 2015, Liu et al., 2016). Low and middle-income countries such as India, Pakistan and Sierra Leone are disproportionally more affected by the burden of PTB than the rest of the world with higher incidence and mortality rates. Nonetheless, the developed world is far from being immune to prematurity. In the UK, around 8% of babies are born prematurely every year whereas in the USA approximately 12% of live births occur before term (Blencowe et al., 2013, Stern and Anumba, 2016).

Despite advances in perinatal health which have significantly improved the survival of premature babies, the rate of PTB has seen no decline in most countries in recent years. In some, the incidence has actually risen (Chawanpaiboon et al., 2019). Obesity, a greater use of assisted conception technology, and an increased rate of medically induced PTB are thought to be contributing to this paradoxical trend (Sung et al., 2018, Cavoretto et al., 2018).

1.1.2. **Consequences of preterm birth**

PTB, which accounts for over 1 million neonatal deaths a year, is the leading cause of neonatal mortality and morbidity worldwide and the second most common cause of death in children under five after pneumonia (WHO, 2012, Blencowe et al., 2013).

While neonatal survival for those born extremely early, especially for those born around the age of viability, has significantly increased in the last decades thanks to advances in perinatal care such as the introduction of antenatal steroids in 1995 (Chandiramani et al., 2007) and technological improvements in special care units, premature babies who survive are still at very high risk of severe short and long-term morbidity (Liu et al., 2016). The EPICURE studies, which have been following preterm babies throughout their early life to assess the short and long-term developmental implications of being born early, have shown that the earlier the gestation at birth the poorer the developmental outcomes. However, even late premature babies are not exempt of complications (Marlow, 2015). Preterm babies are more likely to experience short-term complications such as intraventricular haemorrhage, necrotising enterocolitis and respiratory distress syndrome than their term counterparts. In the long term, they are also at an increased risk of neurodevelopmental disorders such as cerebral palsy, learning difficulties with attention deficit, slow processing of information, hearing loss and visual impairment. Prematurity is also linked to a higher incidence of

respiratory infections, episodes of asthma and chronic lung disease as well as of adult-onset chronic disorders such as obesity, hypertension and diabetes (Chandiramani et al., 2007, Rubens et al., 2014, Marlow, 2015, Georgiou et al., 2015).

Apart from the huge clinical implications associated with PTB, there are also major costs to the economy to be considered (Honest et al., 2009). In the UK, the additional average costs for provision of care in spontaneous preterm labour have been estimated to be £15,688 for births below 34 weeks, and £12,104 for births before 37 weeks (Honest et al., 2009). Data from the USA shows that the fiscal cost for PTB in America is equally high sitting at over $26 million (Dimes, 2017). On top of the added financial costs derived from longer times of hospitalisation and readmissions in the first years of life in a healthcare system which is already under strain, there is also the emotional and psychological burden on families to be considered, as well as lost productivity costs when parents have to give up their jobs to become the main carers for their babies (Honest et al., 2009, Georgiou et al., 2015).

The colossal implications of PTB support the need for further research to better predict and prevent prematurity which may result in improved physical and neurological outcomes and better quality of life for preterm babies as well as micro- and macro-socioeconomic savings (Behrman and Butler, 2007).

1.2. Aetiologies and pathogeneses of preterm birth

Premature deliveries can be further classified into either iatrogenic or spontaneous preterm birth (sPTB). Iatrogenic or induced PTB, which accounts for approximately 20-30% of all premature births, is the result of medical interventions aiming to expedite delivery due to worsening maternal or fetal conditions such as preeclampsia or severe intrauterine growth restriction (IUGR). sPTB, on the other hand, occurs as a result of a complex myriad of factors which are still largely unknown even when there is every intention to prolong the pregnancy, and it is responsible for up to 70-80% of all preterm deliveries (Menon et al., 2011, Feltovich et al., 2012, Georgiou et al., 2015, Stern and Anumba, 2016). PTB can be further subdivided into preterm labour (PTL) and prelabour premature rupture of membranes (PPROM) even though some authors have suggested that PPROM may actually be a different disorder altogether as it does not always lead to PTB (Caughey et al., 2008).

The complex and heterogeneous aetiologies implicated in the pathogenesis of PTB have challenged the dogma of it being a single entity and proposes instead that PTB should be regarded as a syndrome (Romero et al., 2006b). According to the current paradigm (Menon et al., 2011,

Feltovich et al., 2012, Stern and Anumba, 2016), PTB represents the culmination of multiple pathophysiological pathways which can be triggered by a wide range of conditions such as:

1.2.1. **Abnormal uterine overdistension**

During pregnancy, myocytes undergo hypertrophy and hyperplasia to accommodate the growing fetus. Intraamniotic pressure, however, remains relatively constant throughout pregnancy mainly due to progesterone and nitric oxide (Sladek et al., 1999, Romero et al., 2006b). However, excessive uterine distension may increase intraamniotic pressure and facilitate contractions by inducing expression of gap junctions, prostaglandin release, and proteins associated with contractibility such as oxytocin receptors, G proteins and calcium channels (Chow and Lye, 1994, Ou et al., 1997, Ou et al., 1998)

Multiple pregnancies are at particularly higher risk of sPTB with 50% of twin pregnancies delivering before 37 weeks of gestation and 10% prior to 32 weeks (Murray *et al.*, 2018). Similarly, polyhydramnios, macrosomia and Müllerian duct abnormalities such as unicornuate uterus may impair the capacity of the uterus to increase in size without significantly altering intrauterine pressure, thus inducing sPTB (Heinonen, 1997, Adams Waldorf et al., 2015).

Recent studies conducted in non-human primate models showed that stretching amniocytes with increasing pressure can trigger a significant rise in tumour necrosis factor alpha (TNF-α), interleukin 6 (IL-6), interleukin 8 (IL-8) and interleukin 1 beta (IL-1β). These observations have led some authors to hypothesise that early inflammation after a mechanical stress rather than the stretching itself may be responsible for preterm labour (Adams Waldorf et al., 2015). *In vitro* distension of the amnion has also been shown to cause an upregulation of a series of transcripts such as a huntingtin-interacting protein 2 and an interferon-stimulated gene encoding a 54-kDa protein, all of which have been linked to PPROM (Nemeth et al., 2000). However, ethical considerations have limited *in vivo* work on humans, and except for a few early studies which reported an increase in intraamniotic cytokines in women undergoing stretch-induced abortions, evidence on how overdistention leads to sPTB in pregnant women is still lacking (Manabe et al., 1984, Romero et al., 2006b).

1.2.2. **Infection and inflammation**

At least 25%-40% of all sPTB are associated with infections, especially those which happen at earlier gestational age (Minkoff, 1983, Romero et al., 1988, Goldenberg et al., 2002, Witkin et al., 2013b). In rodent models, the causality between infection and PTB has been firmly established after

the administration of systemic, vaginal and/or intrauterine microbial products such as lipopolysaccharides (LPS) and peptidoglycans (PGN) was shown to cause premature labour (Elovitz et al., 2003, Gomez-Lopez et al., 2018). In humans, even when the association may not be as compelling as it is in animal models, there is enough evidence to support the link between intrauterine infection and PTB. It has even been suggested that premature delivery in the context of infection may constitute an adaptive response to guarantee the mother's survival and preserve reproductive function by emptying the infected uterine cavity (Williams and Drake, 2019).

The amniotic cavity is thought to be sterile until labour starts (Wassenaar and Panigrahi, 2014, Lim et al., 2018). Previous studies found that while less than 1% of term non-labouring women grew bacteria in their amniotic fluid cultures, this rate increased to 75% once labour began (Romero et al., 2006b). In early gestations, however, isolation of any bacteria from the amniotic fluid is considered pathological until proven otherwise. A positive amniotic fluid culture, often referred to as microbial invasion of the amniotic cavity (MIAC), may be as high as 22% in women who present in preterm labour with intact membranes and go on to deliver prematurely (Goncalves et al., 2002, Romero et al., 2006b). Amniotic fluid cultures may also be positive in 32.4% of pregnant women with PPROM. However, it is important to note that these rates are likely to be underestimations of the true incidence of MIAC as conventional culture techniques are unable to detect all PTB-related bacteria (Relman, 1999).

The commonest microorganisms involved in intrauterine infections are *Mycoplasma hominis* and *Ureaplasma urealyticum*, and to a lesser extent, *Escherichia coli*, *Streptococcus agalactiae*, Fusobacterium, Bacteroides and *Gardnerella vaginalis* (Goncalves et al., 2002). Interestingly, *Neisseria gonorrhoeae* and *Chlamydia trachomatis* which are so common in non-pregnant women are almost never isolated in intraamniotic infection (Goldenberg et al., 2002). However, colonisation of the chorioamnionitic membranes is not enough to cause infection and preterm labour: an intra-amniotic inflammatory response is also needed.

Most intrauterine infections are caused by an ascending genital tract infection which may result from changes in the vaginal microflora (Mirmonsef et al., 2011). Less commonly, systemic infections through the placenta, retrograde infections from the abdominal cavity and inoculation of pathogens during invasive procedures such as amniocentesis or chorionic villus sampling may also play a contributing role (Agrawal and Hirsch, 2012). Pathogens that evade or overcome the complex innate immune system may reach the choriodecidual space and cause chorioamnionitis by releasing LPS, PGN, short-chain fatty acids (SCFAs) and lipoproteins. The resulting inflammation of the fetal membranes contributes to a feedforward pro-inflammatory signalling pathway by further synthesising TNF-α, IL-1, IL-2, IL-6 and granulocyte colony stimulating factors (GCSF) which will

ultimately facilitate cervical remodelling and uterine contractions by activation of matrix metalloproteinases (MMP) such as MMP-8 and 9, and prostaglandins (PG) such as PGF2-α and PGE2 respectively (Saito et al., 1993, Arntzen et al., 1998, Goldenberg et al., 2002, Peltier, 2003). The breakdown of the extracellular matrix of the cervix (ECM) by MMPs leads not only to cervical ripening and shortening but also to a disruption of the mechanical integrity of the fetal membranes which may result in PPROM. This cervical remodelling added to increased PG-activated myometrial contractibility culminates in a premature and pathological activation of the parturition mechanism (Guzeloglu-Kayisli et al., 2015).

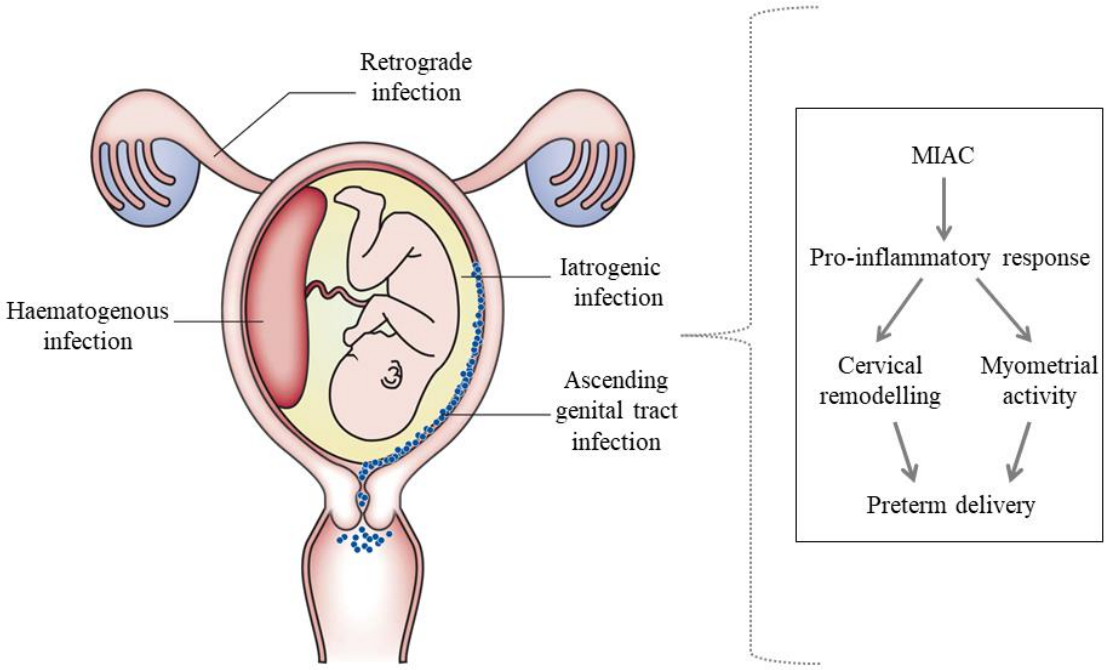

Figure 1.1. Main routes for intraamniotic infection are displayed with a proposed pathogenic pathway for infection-induced PTB. *MIAC: microbial infection of the amniotic cavity*. Adapted with permission from Goldenberg et al. (2008).

1.2.3. **Decidual haemorrhage**

A large body of observational data supports the link between uteroplacental ischaemia and PTB although the exact mechanism has not been fully elucidated (Romero et al., 2006b).

Unprovoked bleeding in the first and second trimester as well as the presence of subchorionic haematomas detected early in the second trimester are considered independent risk factors for adverse obstetric outcomes such as PTB, IUGR, miscarriage and stillbirth (Ball et al., 1996, Signore et al., 1998). Similarly, the risk of both a spontaneous or medically-indicated PTB increases if

pregnant women develop pregnancy-induced hypertension and pre-eclampsia, or if their umbilical and uterine artery Dopplers are found to be persistently abnormal (Brar et al., 1988, Sibai, 2006).

Histologically, a higher incidence of fetal and maternal vascular lesions has been noted in women who deliver prematurely when compared to term controls. In women with PPROM and/or PTB, uterine spiral arteries are more likely to be poorly remodelled with evidence of atherosis and thrombosis which suggests defective placentation (Kim et al., 2002, Romero et al., 2011). Similarly, and despite the scarce data on fetal vascular lesions in PTB, villous fibrosis and abnormal fetal angiogenesis which are much more commonly seen in the placenta of preterm babies also support the hypothesis of abnormal placental development (Romero et al., 2006b, Kelly et al., 2009).

1.2.4. **Cervical and uterine disorders**

Significant changes in the structure of the cervix and the uterus, which may be congenital or acquired following surgery or trauma, can also lead to sPTB (Stern and Anumba, 2016).

Cervical insufficiency, described as the incapacity of the cervix to retain a pregnancy in the absence of increasing contractions, has been traditionally associated with cone biopsies employed for surgical treatment of cervical intraepithelial neoplasia (CIN), and with repeated dilation and curettage for termination of pregnancy (Romero et al., 2006a, Vink and Feltovich, 2016). The development of new and less invasive surgical techniques to manage cervical lesions such as the loop excision of the transition zone (LLETZ) has seen a reduction in the number of cone biopsies. However, more effective screening programmes for CIN in industrialised countries have led to a higher number of women being subjected to LLETZ every year (Sasieni et al., 2016). The implications of LLETZ for PTB are still poorly understood. Evidence has been conflicting with some initial meta-analyses reporting a statistically significant higher risk of PTB in women who had undergone LLETZ (Kyrgiou et al., 2006, Bruinsma and Quinn, 2011). However, subsequent studies have failed to replicate these results or reach a consensus on how to better provide obstetric care to these women when they become pregnant (Conner et al., 2014). Since cervical insufficiency manifests as cervical ripening, its clinical presentation may overlap with other pathological processes making its diagnosis quite challenging. For example, evidence of intrauterine infection was found in at least 50% of women who presented with a diagnosis of acute cervical insufficiency (Romero et al., 2006b).

Uterine Müllerian anomalies such as unicornuate, bicornuate, septate and didelphys uteri as well as those caused by diethylbestrol have also been associated with PTB and other adverse fetomaternal outcomes such as miscarriage, PPROM, breech presentation, caesarean section (CS),

abnormal placentation and IUGR (Hua et al., 2011, Hoover et al., 2011, Ibeto et al., 2012). The mechanism through which congenital uterine anomalies trigger sPTB is still not completely understood, but some authors have hypothesised it could be due to underlying cervical insufficiency, abnormal placentation and/ or a decrease in muscle mass which limits the capacity of the uterus to increase in size as pregnancy progresses (Caserta et al., 2014). Clear guidance on how to best manage these patients obstetrically to reduce the risk of sPTB is currently lacking which supports the need for more and larger studies (Khander et al., 2018).

1.2.5. **Others**

Progesterone deficiency, maternal and fetal stress, and a breakdown in the maternal-fetal immunological tolerance have also been proposed as potential mechanisms of action behind sPTB (Romero et al., 2006b, Stern and Anumba, 2016).

However, regardless of what triggers sPTB, all these pathophysiological mechanisms seem to converge in a common pathway known as cervical remodelling. This process is characterised by a series of gradual and microscopic changes within the extracellular matrix (ECM) which macroscopically translate into cervical shortening, softening and dilation to allow the passage of the fetus (Feltovich et al., 2012). A better understanding of the mechanisms that lead to cervical remodelling and PTB would therefore facilitate the development of strategies that could contribute to earlier identification, more timely prevention and better stratification of PTB management (NICE, 2015a).

1.3. Strengths and limitations of the current predictive tests for preterm birth

1.3.1. **Who do we screen for preterm birth?**

In the UK, there are two main approaches to assessing PTB risk during pregnancy depending on the history and presenting symptoms –screening women without symptoms of preterm labour but who are at high risk of PTB, and screening women who regardless of their previous obstetric history present with symptoms of preterm labour but no signs of advanced cervical dilation.

- ❖ Asymptomatic high-risk women in Antenatal Clinic (AHR):

These are women who are considered to be at higher risk of sPTB on the basis of their previous obstetric history and/or due to an incidentally shortened cervix at their 20 week scan (NICE, 2015a).

Many modifiable and non-modifiable factors have been associated with PTB including socioeconomic status, smoking and extremes of maternal age (Morgen et al., 2008, Cavazos-Rehg et al., 2015). However, the history of a previous sPTB or late second-trimester miscarriage remains the strongest risk factor of PTB which can carry a 2.5-fold increase in the risk of a recurrent premature delivery compared to those who previously experienced a term pregnancy (Mercer et al., 1999, ACOG, 2001). If the cervix is incidentally found to be shortened in these women, their risk of a subsequent sPTB significantly increases.

In the UK, high-risk women are offered more intensive antenatal surveillance than their lower risk counterparts. Follow-up may include serial cervical length scans between 16 and 24 weeks and prophylactic interventions such as cerclage or progesterone (NICE, 2015a).

However, the assessment of obstetric risk factors is not enough to accurately predict sPTB since most women deemed at high risk will still deliver after 33 weeks, and over 60% of pregnancies which deliver prematurely will not have had any risk factors of significance identified antenatally (Honest et al., 2009, Georgiou et al., 2015).

❖ Symptomatic women on Labour Ward/ Maternal Assessment Unit (SYMP):

These are women who present with symptoms suggestive of PTB such as lower abdominal pain between 24^{+0} weeks and 36^{+6} weeks but with intact membranes and a cervical dilatation less than 4 cm (NICE, 2015a). In order to determine whether they are in true labour, these women are normally offered a clinical assessment and a speculum and/or vaginal digital examination. However, diagnosis of preterm labour based purely on symptoms and examination of the cervix has been shown to be imprecise as it is subjected to significant inter-observer variability (Copper et al., 1990, Lee et al., 2009).

1.3.2. **How do we screen for preterm birth?**

As PTB cannot be accurately screened based solely on the previous obstetric history and clinical examination of the cervix, a series of ancillary tests may be offered in an attempt to improve the diagnostic accuracy of sPTB and guide further management (ACOG, 2001, NICE, 2015a):

- Cervical ultrasonography:

Transvaginal ultrasound (TVU) has become the gold standard technique for measuring progressive cervical shortening which appears to precede preterm labour (Taipale and Hiilesmaa, 1998, Hibbard et al., 2000, Di Tommaso and Berghella, 2013). TVU has many advantages compared to digital examination: it is acceptable for patients, reproducible (intra-class correlation 0.90) and relatively easy to perform (Lee et al., 2009, Souka and Pilalis, 2019). It provides not only

information about cervical length (CL) but also about other cervical parameters such as "funnelling" which is the dilation of the internal portion of the cervical canal, and intraamniotic "sludge" (Mancuso et al., 2010). Cervical index (funnel length + 1/closed CL) or cervical score (CL minus cervical dilatation) have been proposed as predictive markers of PTB (Hartmann et al., 1999, Berghella et al., 2007). However, CL is still the standard marker for screening PTB because when there is funnelling the cervix is almost always short (Figure 1.2; Di Tommaso and Berghella, 2013).

A short cervix behaves as an independent predictive factor for adverse perinatal outcomes such as PTB, and thus measuring CL has now become common practice in the work-up of women at high risk of PTB (Watson et al., 1999, ACOG, 2001, Crane and Hutchens, 2011, NICE, 2015a). A comprehensive systematic review by Honest et al. (2003) showed that in high-risk women, a CL<2.5 cm (10^{th} centile) in the mid-trimester has a positive likelihood ratio (+LR) of 6.29 (95% CI: 3.29-12.02) for PTB, increasing the 4.1% pre-test probability to a 15.8% post-test probability. A subsequent meta-analysis by Crane and Hutchens (2008) which included six studies with over 663 women at high risk of sPTB further confirmed these results and suggested that the earlier the gestation at which a short cervix is identified the higher the likelihood of sPTB. Using the same cut-off of 2.5 cm to define a short cervix, they reported a +LR of 11.30 (95% CI: 3.59-35.57) for TVU before 20 weeks' gestation and a much lower +LR of 2.86 (95% CI: 2.12-3.87) if the scan was performed later between 20 and 24 weeks (Table 1.1; Crane and Hutchens, 2008, Suff et al., 2019). Based on this evidence, the UK Preterm Clinical Network currently recommends that women who fall into this category should be offered ultrasound cervical length screening from at least 16 weeks of gestation (Story et al., 2019).

Despite its extensive use for screening high-risk populations, there is still insufficient data to recommend CL as a routine test for low-risk women (Berghella et al., 2009). A shortened cervix may be a natural biological variation in some women and not necessarily be associated with PTB (Georgiou et al., 2015). However, some studies have suggested that a short cervix or cervical funnelling in low-risk women may still increase the risk of PTB (Iams et al., 1996, Lee et al., 2009), and NICE (2015a) has issued a recommendation, not free from controversy, to offer these patients prophylactic progesterone (Khandelwal, 2012).

TVU CL has also been proposed for the assessment of women with symptoms of sPTB but who are not yet in established labour (NICE, 2015a). A comprehensive meta-analysis by Sotiriadis et al. (2010) showed that CL could significantly improve the detection of sPTB within one week of presenting with symptoms (Table 1.1). However, these results should be interpreted with caution as the authors concluded that some of the primary studies included in the review were likely to be methodologically flawed (Sotiriadis et al., 2010).

Despite its use in the clinical setting, TVU does not come without its limitations and challenges. For a start, CL measurements are largely dependent on gestational age. Because the cervix is expected to shorten as pregnancy progresses, the gestation at which the measurements are taken significantly impacts on its interpretation (Suff et al., 2019). There is not currently enough evidence about the predictive value of CL outside the mid-trimester (Crane and Hutchens, 2011). Additionally, sonographic CL measurements are highly operator-dependent and require trained users, with previous studies suggesting that more than 25% of the images may not meet quality requirements (Iams et al., 2013).

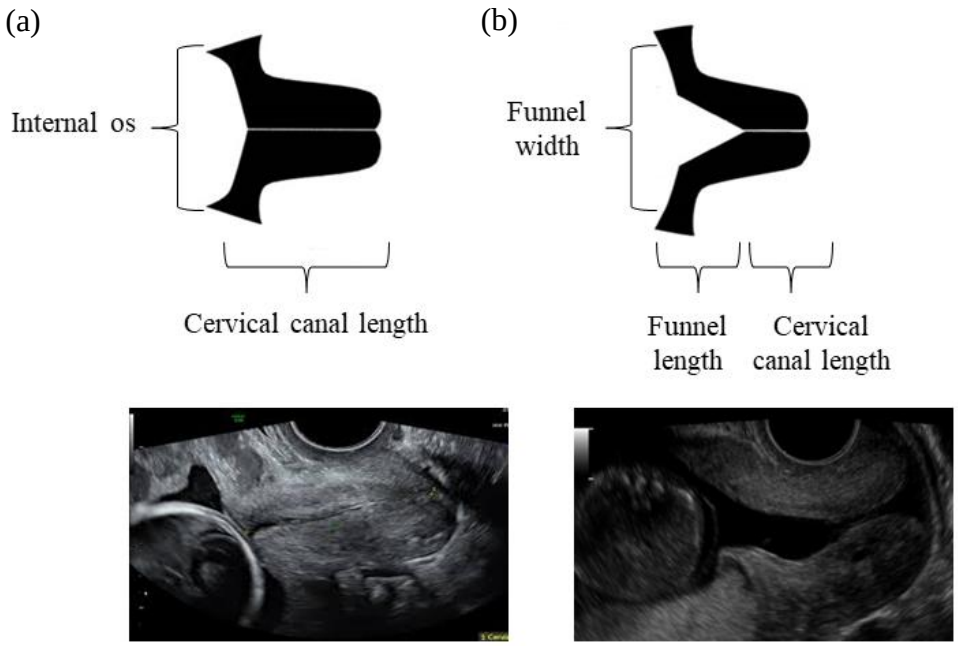

Figure 1.2. Visualisation of the human cervix. Schematic (top) and sonographic images (bottom) of **(a)** a normal and **(b)** a shortened and funnelled cervix in longitudinal view. Pictures from Sheffield NHS Teaching Hospital Preterm Birth Clinic.

Table 1.1. Clinical performance of TVU CL in AHR and SYMP women for the prediction of sPTB

	Outcome	CL cut-off	Gestational age at scan	Positive likelihood ratio (95% CI)	Number of studies in meta-analysis (n=women)
AHR (Crane and Hutchens, 2008)	Birth<35 weeks	2.5 cm	<20 weeks	11.30 (3.59-35.57)	Six (n=663)
			20-24 weeks	2.86 (2.12-3.87)	
			>24 weeks	4.01 (2.53-6.34)	
SYMP (Sotiriadis et al., 2010)	Birth within 1 week of presentation	1.5 cm	<37 weeks	5.71 (3.77-8.65)	Six (n=1781)
	Birth<34 weeks		≤34 weeks	4.31 (2.73-6.82)	Four (n=429)

AHR: asymptomatic high-risk women, CI: confidence interval, CL: cervical length, PTB: preterm birth, SYMP: symptomatic women

- Infection screening:

There is strong evidence to suggest that bacterial vaginosis (BV) is an independent risk factor for PTB (Hillier et al., 1995b, Nejad and Shafaie, 2008). BV, originally known as non-specific vaginitis, is defined as a dysbiosis of the normal vaginal microflora, and it is clinically characterised by the Amsel criteria namely offensive white discharge, positive amine test, vaginal pH>4.5 and the presence of microscopic clue cells (Wilson, 2004, Cauci et al., 2005). BV is considered one of the most common vaginal infections affecting childbearing-age women worldwide, with a prevalence that ranges from 5 to 70% (Tolosa et al., 2006). It is a polymicrobial infection, in which the normal ratio of anaerobic and facultative anaerobic bacteria to H_2O_2-producing lactobacilli increases from 2:1-5:1 to 100:1-1000:1 (Pararas et al., 2006, Guaschino et al., 2006).

However, it is not clear whether antibiotic treatment of BV is capable of preventing sPTB. A Cochrane review in 2013 analysed 21 trials involving 7847 women and concluded that the use of antibiotics during pregnancy was capable of eradicating BV and reducing the risk of late miscarriage (RR 0.2, 95% CI: 0.05-0.76) but it did not lead to a decrease in the rate of PTB (Brocklehurst et al., 2013). Nonetheless, in most maternity units in the UK, women who present with threatened sPTB are routinely assessed for BV, candidiasis, trichomoniasis, amongst others (NICE, 2015a). The UK National Screening Committee, however, does not currently recommend universal screening and treatment of BV in pregnant women for prevention of PTB given the conflicting and insufficient data available (UK, 2017).

Treatment for asymptomatic bacteriuria has also been associated with reduced sPTB, and even though current evidence is scarce to fully support this observation, antibiotic treatment does seem to be associated with a reduction in the incidence of low fetal birthweight (Smaill and Vazquez, 2015).

- Fetal fibronectin:

Fetal Fibronectin (fFN) is a complex adhesive glycoprotein which is usually found between the decidua basalis and the intervillous space (Kiefer and Vintzileos, 2008). Even though its role has not been fully elucidated, it is thought to promote cellular adhesion at the maternal-fetal interface (Farag et al., 2015). In the cervicovaginal fluid (CVF), fFN is normally detectable in the first 18 weeks of pregnancy until the decidua fuses with the fetal membranes. After fusion occurs, fFN concentration drops to low levels and it may even become undetectable until 34 weeks of gestation. High concentration of fFN in the CVF between 18-34 weeks could therefore indicate impending PTB as it may result from mechanical or inflammation-induced perturbation to the choriodecidual space which may precede preterm labour (Kiefer and Vintzileos, 2008, Farag et al., 2015, Stern and Anumba, 2016).

CVF samples for assessment of fFN are obtained from the posterior fornix of the vagina using a Dacron swab during speculum examination. The CVF specimen is subsequently extracted into a buffer solution, 200 μL of which is then pipetted onto a cassette which contains a lateral flow, solid-phase immune-chromatographic assay. The CVF sample flows across a nitrocellulose membrane via capillary action and reacts with murine monoclonal anti-fetal fFN antibodies which are conjugated to blue microspheres. These fibronectin-conjugate complexes are then captured by polyclonal anti-human fibronectin antibodies forming the test line whereas the free conjugates get bound to goat polyclonal anti-mouse IgG antibody and become the control line (Rapid fFN® Cassette Kit, Hologic®). The difference in intensities between the test and control lines, which may be visually assessed on a dipstick test or automatically interpreted by a bedside reader, is used to determine the presence and/ or the quantity of fFN in the sample respectively (Kiefer and Vintzileos, 2008, Abbott et al., 2013). Any positive results obtained in the context of vaginal bleeding, recent sexual intercourse and the use of vaginal lubricants during the speculum examination should be interpreted with caution as they have been shown to interfere with the assay and cause false positive results (Bruijn et al., 2017).

Until recently, fFN has been exclusively used as a qualitative test which can give a positive or negative result based on a cut-off concentration of 50 ng/mL (Suff et al., 2019). The main advantage of this test is its high negative predictive value for sPTB which was reported to be as

high as 96% for asymptomatic women tested between 24-26 weeks, and 99% in women with symptoms of preterm labour (Goldenberg et al., 1996, Hezelgrave and Shennan, 2016). Symptomatic women who test negative for fFN are unlikely to deliver within 7-14 days. As a result, healthcare professionals may decide against admission to hospital or administration of prophylactic intervention on the basis of a negative fFN test. On the other hand, a positive test may not be as clinically useful. Given the low positive predictive value of qualitative fFN (<30%), most symptomatic women who test positive will still not deliver within two weeks but may end up being unnecessarily admitted to hospital or treated with prophylactic measures.

The advent of a quantitative version of the technique has significantly improved the clinical performance of the test without affecting the high negative predictive value previously reported with the traditional fFN test (Table 1.2). Higher thresholds (200 and 500 ng/mL) may increase the probability that women with a positive fFN test deliver prematurely, but at the expense of reducing sensitivity (Radford et al., 2012, Foster and Shennan, 2014). While an optimal cut-off for fFN continues to be explored, there is growing evidence to support its use in the prediction of sPTB in symptomatic women especially between 30-34 weeks when CL may not be available (NICE, 2015a). However, the same cannot be said about asymptomatic both low and high-risk women in whom a lower incidence and thus pre-test probability does not seem to significantly improve with fFN testing (Radford et al., 2012, Abbott et al., 2013, Hezelgrave and Shennan, 2016, Faron et al., 2018).

Table 1.2. Performance of quantitative fFN in AHR and SYMP women. Data extracted from the meta-analysis by Faron et al. (2018)

	Outcome	**Positive likelihood ratio (95% CI)**	**Negative likelihood ratio (95%)**	**Number of studies in meta-analysis (n=women)**
AHR	Birth<34 weeks	4.3 (2.7-6.8)	0.5 (0.4-0.7)	Eleven (n=2409)
SYMP	Birth within 1 week of presentation	3.8 (3.3-4.5)	0.4 (0.3-0.5)	Fifty-four (n=11255)
	Birth<37 weeks	3.6 (3.2-4.2)	0.6 (0.5-0.6)	Sixty-eight (n=9139)

AHR: asymptomatic high-risk women, CI: confidence interval, fFN: fetal fibronectin, PTB: preterm birth, SYMP: symptomatic women

- Insulin-like growth factor-binding protein-1 (Actim Partus®) and placental α-microglobulin-1 (PartoSure®):

Phosphorylated insulin-like growth factor binding protein-1 (IGFBP-1) and placental α-microglobulin-1 (PAMG-1) are alternative biomarker tests which may aid in the prediction of sPTB (Balic et al., 2008, Khambay et al., 2012). Similarly to fibronectin, IGFBP-1 is presumably released into the choriodecidual space following disruption of the feto-maternal interface (Kosinska-Kaczynska et al., 2015). PAMG-1, on the other hand, is a 34-kDa protein found in the amniotic fluid with a concentration several thousand times higher than that in the CVF; an increased trace of PAMG-1 in CVF may indicate PPROM and a higher risk of preterm labour (Cekmez et al., 2017).

Two bedside kits known as Actim Partus® (Medix Biochemica, Finland) and PartoSure® (Quagen, Germany) have been developed to qualitatively assess the presence of IGFBP-1 and PAMG-1 in cervicovaginal secretions. Like fFN Rapid (Hologic, Inc.), these tests rely on monoclonal antibodies for detection of the protein of interest.

A recent diagnostic accuracy review and health economic analysis conducted by NICE to assess the clinical effectiveness of PAMG-1, IGFBP-1 and fFN (with thresholds of 50 ng/mL) for prediction of sPTB in symptomatic women with intact membranes failed to demonstrate the superiority of one technique over the others (Varley-Campbell et al., 2019). Larger and more standardized trials are required before clinical recommendations can be drawn.

In conclusion, the majority of sPTB occurs in women who have no risk factors identified during pregnancy. Therefore, a clinical algorithm for prediction sPTB which is solely based on previous risk factors is bound to fail at identifying women who are at real risk of going into preterm labour. As a result, some women may receive unnecessary interventions such as cerclage or progesterone, whereas others who may have actually benefited from these procedures may be diagnosed with preterm labour too late when birth is imminent and there is insufficient time for prophylactic measures. Early and accurate identification of women who will deliver prematurely is therefore paramount to better stratify management, avoid unnecessary interventions and target scarce resources to those who need them the most in clear alignment with the bioethical principles of beneficence, non-maleficence and social justice (Beauchamp and Childress, 2001). Currently, none of the methods available in the clinical setting has met this demand, thus supporting the need for more research (Ross et al., 2013, NICE, 2015a).

1.4. Prevention of preterm birth

1.4.1. **Primary prevention of preterm birth**

The aim of primary preventative strategies is to reduce the risk of PTB in the general population by addressing potential risk factors from before conception or early in pregnancy. Even though not all contributory factors of PTB have been identified, observational data suggests that there is a complex interplay of risk factors behind a premature delivery, some of which may be amenable to potential therapeutic interventions (Rubens et al., 2014).

In the USA, African-American women have been found to be at least 40-60% at greater risk of sPTB than their Hispanic and non-Hispanic Caucasian counterparts even after adjusting for socioeconomic status (Culhane and Goldenberg, 2011, Mohamed et al., 2014). The correlation between ethnicity and PTB is still poorly understood, but it is thought to involve social marginalisation and unequal access to healthcare as much as genetic and biological health determinants (Menon et al., 2009, Dominguez, 2011). Other non-modifiable risk factors associated with PTB include obstetric history of previous PTB or late miscarriage, conceiving with assisted reproductive technology, lower adult height in women, and extremes of maternal age at conception (Oliver-Williams et al., 2015, Derraik et al., 2016, Fuchs et al., 2018).

On the contrary, short intervals between pregnancies, periodontal disease, BV, low and high maternal BMI, inadequate weight gain during pregnancy, low-socioeconomic status as well as substance abuse and smoking have been increasingly recognised as modifiable risk factors for PTB (Dekker et al., 2012, Dahlin et al., 2016, Lengyel et al., 2017). For many decades, efforts have been made to target these factors by focused public health initiatives. Unfortunately, the lack of adequate risk stratification has meant that most of the current primary preventive interventions have remained largely inefficient to reduce the risk of PTB as evidenced by a recent meta-analysis which assessed 86 Cochrane's reviews of interventions (Behrman and Butler, 2007, Rubens et al., 2014, Medley et al., 2018). Only three primary strategies were found to be potentially beneficial to prevent PTB including access to continuous midwifery-led antenatal care, screening for lower genital tract infection before 37 weeks of gestation and zinc supplementation (Sangkomkamhang et al., 2015, Ota et al., 2015, Sandall et al., 2016, Alfirevic et al., 2017, Medley et al., 2018, Matei et al., 2019).

1.4.2. **Secondary prevention of preterm birth**

Secondary prevention focuses on reducing the risk of recurrent PTB which constitutes the strongest risk factor for a woman to deliver prematurely. A history of a previous PTB carries a 2.5-

fold increased risk of recurrence (Mercer et al., 1999), and therefore, interventions are targeted at either women who have experienced PTB or late miscarriage (asymptomatic high-risk women, AHR) or women presenting with incidental short cervix or symptoms of threatened PTB (symptomatic women, SYMP; Flood and Malone, 2012).

In most high-income countries, women at increased risk of PTB are offered extra surveillance (section 1.3.1) as well as prophylactic measurements (NICE, 2015a). Widely accepted strategies include progesterone supplementation and cerclage, with more recent evidence suggesting that cervical pessaries may also play a prophylactic role (Jarde et al., 2019).

In the UK, progesterone is commonly used in its natural form either per vagina (PV) or per rectum (PR), whereas the USA tends to favour intramuscular administration of a synthetic progesterone: 17-α hydroxyprogesterone caproate (17-OHPC; NICE, 2015a, SMFM, 2017). The role of progesterone has not been fully elucidated yet, but proposed mechanisms of action include suppression of the calcium-calmodulin-myosin light chain kinase system as well as local and systemic inflammatory regulation by reducing T-helper differentiation and blocking natural killer cells degranulation (Dodd and Crowther, 2010, Shah et al., 2019).

Progesterone has been found to significantly reduce the risk of PTB before 34 weeks in AHR women (RR 0.31, 95% CI: 0.14-0.69) and improve short-term neonatal complications such as the need for assisted ventilation, necrotising enterocolitis (NEC) and admission to intensive care according to the latest Cochrane's review which assessed 36 randomised controlled trials (RCTs) with over 8523 women (Dodd et al., 2013). The study, however, failed to demonstrate any long-term neonatal benefits of administering antenatal progesterone. For women found to have an incidental short cervix on ultrasound, progesterone was also reported to decrease the rate of PTB (RR 0.64, 95% CI: 0.45-0.90). No statistically significant difference was seen in multiple pregnancies, and data on symptomatic women was too limited to reach a firm conclusion on the clinical utility of progesterone (Dodd et al., 2013).

Even though progesterone is already used prophylactically in the clinical setting, there is still little information available about its optimal dose, mode of administration and best gestational age to start and stop the medication (Choi, 2017).

An alternative to progesterone has been cerclage, the placement of a suture around the cervix to prevent dilation and delivery (Alfirevic et al., 2017). It was first performed in 1902 but the procedure was not described until 1955. This first technique, known as Shirodkar, involved mobilising the bladder before inserting a transvaginal purse-string suture. Soon after in 1957, a modified technique which did not require bladder mobilisation, the McDonald's suture, was introduced (Goulding and Lim, 2014). In 1967, Benson and Durfee reported the first

transabdominal placement of a cervical cerclage(Gibb and Saridogan, 2016). Since then, these techniques have been extensively employed in the prevention of PTB despite the conflicting evidence about its true effectiveness (Romero et al., 2006a). Evidence-based practice has been limited by trial heterogeneity with a clear lack of standardisation in the population studied (singleton vs multiple pregnancy, high-risk vs low-risk) and in the outcomes assessed as well as in the indication for cerclage and techniques used (Rafael et al., 2014, Alfirevic et al., 2017).

History-indicated cerclages may be advised in women who have experienced previous late miscarriage or early PTB, and may be prophylactically inserted between 12-16 weeks of gestation. USS-indicated cerclage, on the other hand, might be suggested if cervical shortening is incidentally detected in a TVU in asymptomatic women regardless of any historical risk factors. Finally, rescue cerclage may be indicated if the cervix is dilating with intact membranes in the absence of uterine activity or evidence of infection (Cook et al., 2017). There is currently not enough primary research to accurately assess how effective cerclage is for each of these indications. However, when they are all combined, cerclage seems to significantly reduce the risk of PTB (RR 0.77, 95% CI: 0.66-0.89) according to a recent Cochrane's review which included nine RCTs with data from over 2415 women (Alfirevic et al., 2017).

More recently, cervical pessaries have been proposed as an alternative to prevent PTB. But the evidence to support this is quite limited arising from one single RCT which included 385 women with a short cervix between 11-22 weeks of gestation. The study reported a significant reduction in the risk of PTB compared with expectant management (RR 0.36, 95% CI: 0.27-0.49). More studies are still needed before any clinical recommendation can be made (Abdel-Aleem et al., 2013).

1.4.3. **Tertiary prevention of preterm birth**

Once the pathophysiological mechanism initiating preterm labour has begun, obstetric interventions may be applied in an attempt to reduce neonatal mortality and morbidity (Iams et al., 2008). These tertiary measures include the administration of steroids, magnesium sulphate and antibiotics as well as tocolytic agents to enable fetal lungs development and *in utero* transfer to a larger specialist unit (NICE, 2015a).

The use of antenatal steroids between 24^{+0} and 33^{+6} weeks has significantly reduced the risk of perinatal death (RR 0.72, 95% CI: 0.58-0.89), respiratory distress syndrome (RR 0.66, 95% CI: 0.56-0.77), intraventricular haemorrhage (RR 0.55, 95% CI: 0.40-0.76) and NEC (RR 0.50, 95% CI: 0.32-0.78) in preterm infants (NICE, 2015a, Roberts et al., 2017). However, it has not showed significant differences in long-term outcomes.

Corticosteroids are thought to accelerate the development of pneumocytes in the lung, which are responsible for the synthesis of surfactant, a key protein for lung compliance. They have also been implicated in the upregulation of alveolar epithelium sodium channels which are essential for fluid clearance from the fetal lung, and in the maturation of the lung microvasculature by promoting thickening of the basement membrane (Vinagre and Marba, 2010, Martin and Fanaroff, 2013). Regimes of administration may slightly vary from one country to another; WHO recommends one single course of two doses of 12 mg betamethasone 24 hours apart or alternatively four doses of 6 mg dexamethasone administered 12 hours apart (Romejko-Wolniewicz et al., 2014, NICE, 2015a).

The antenatal administration of magnesium sulphate for deliveries<34 weeks of gestation has been validated as a neuroprotective intervention which reduces the risk of cerebral palsy in the preterm infant (RR 0.68, 95% CI: 0.54-0.87) according to a Cochrane's review which involved five RCTs with data from 6145 infants (Doyle et al., 2009, NICE, 2015a, Chollat et al., 2018). It is estimated that at least 63 preterm foetuses would have to be treated<34 weeks to avoid one case of cerebral palsy (Usman et al., 2017). Magnesium is a ubiquitous ion in the human body which is involved in over 300 enzymatic reactions and physiological processes including storage, metabolism and energy utilisation (Chollat et al., 2018). It is likely that magnesium sulphate contributes to reducing cerebral palsy by blocking the entry of calcium into the cells after crossing the placenta, thus preventing ischaemic cell death. Further research is still needed to fully elucidate how magnesium sulphate works (Mildvan, 1987, Usman et al., 2017, Chollat et al., 2018).

In the early 2000s, a series of large multicentre trials, known as ORACLE I and II, assessed the use of prophylactic antibiotics in the routine management of women who had experienced PPROM and in women who presented with symptoms of preterm labour with intact membranes and no signs of infection (Kenyon et al., 2002, King and Flenady, 2002). Given the large populations sampled, these studies greatly influenced the subsequent Cochrane's reviews on which current clinical recommendations are based.

The administration of erythromycin to pregnant women who had PPROM (n=4826) was associated with a longer interval to delivery: relative ratio of 0.71 (95% CI: 0.58-0.87) for babies born within 48 hours and of 0.67 (95% CI: 0.52-0.85) for babies born within seven days. It was also linked with a reduction in chorioamnionitis (RR 0.66, 95% CI: 0.46-0.96), oxygen requirements and abnormal cerebral ultrasounds at birth but with no changes in neonatal death or long-term outcomes at a seven-year follow-up (Kenyon et al., 2002).

On the contrary, a Cochrane's review on the use of antibiotics in women in spontaneous labour with intact membranes involving 14 studies and 7837 women showed no changes in PTB and a significant increase in neonatal death if exposed to macrolides alone +/- beta lactam versus no

treatment (RR 1.52, 95% CI: 1.05-2.19), or if exposed to beta lactam alone +/- macrolides versus no treatment (RR 1.51, 95% CI: 1.06-2.15). The only clear benefit of administering antibiotics was a significant reduction in maternal infection (any antibiotics versus placebo, RR 0.74, 95% CI: 0.63-0.86; Flenady et al., 2013). In view of the higher risk of neonatal death, administration of antibiotics to women in preterm labour and intact membranes is not currently recommended unless there is strong evidence of infection (Flenady et al., 2013). Despite its robust methodology, the design of this Cochrane review has faced criticism as it only includes three randomised controlled trials which were carried out, totally or partially, in low and middle-income countries, and its results are significantly influenced by one single study, the ORACLE II, which has mainly UK recruits (Norman et al., 1994, Kenyon et al., 2001, Rajaei et al., 2006). The review acknowledges this limitation and concludes there might be a subgroup of women who may benefit from antibiotics in some regions, and highlights the need for further research to develop more accurate sensitive markers of subclinical infection which can help identify potential beneficiaries (Flenady et al., 2013).

Tocolytic agents are drugs designed to slow down or stop contractions with the ultimate goal of improving perinatal outcomes (Tsatsaris et al., 2004). They include a wide range of pharmacological agents namely oxytocin antagonists (Atosiban®), calcium channel blockers (nifedipine and nicardipine for example), prostaglandin inhibitors (e.g. indomethacin) and β-agonists (such as ritodrine and terbutaline; Haas et al., 2012). Even though postponing delivery by tocolysis has not shown to directly improve neonatal outcomes, it does have indirect benefits on the preterm infant as a short-term delay between 24^{+0} and 33^{+6} weeks allows corticosteroids to work and patients to be transferred to larger and better equipped neonatal facilities prior to birth (Haas et al., 2009, NICE, 2015a). *In utero* transfer to a unit with appropriate neonatal care has been reported to improve neonatal mortality and morbidity as well as reduce costs compared to *ex utero* transfers (Shlossman et al., 1997, Gale et al., 2012, Watson et al., 2019).

Overall, the landscape of PTB prevention at all levels has dramatically changed in the last few decades with the advent of new technology and the introduction of several of the aforementioned strategies. Whereas many of these interventions have positively impacted on neonatal outcomes, others still need to be further explored before any firm conclusion can be drawn. Successful prevention of PTB requires a better and more tailored targeting of therapies which may only be possible with a deeper understanding of why and how PTB occurs. Given the complexity of PTB, answers are only likely to arise from a multidisciplinary and cohesive research agenda (Flood and Malone, 2012, Rubens et al., 2014, Keelan and Newnham, 2017).

1.5. Potential biomarkers for preterm birth

There are currently no reliable clinical tools for objective evaluation and quantification of PTB risk, and this inability to accurately predict PTB partly explains why its global incidence is still rising (Lee et al., 2019). Given the substantial burden that prematurity poses on patients, families and communities, and the strain it adds on healthcare and socioeconomic resources (Petrou et al., 2019), a large number of new technologies continues to be developed and tested in the quest for superior and more cost-effective screening tools (Feltovich et al., 2012). These new technologies can be classified depending on the nature of the marker they are trying to identify which can be biochemical, bioelectrical or biomechanical.

1.5.1. **Biochemical markers**

Biological fluids such as saliva, blood (serum/plasma), urine and CVF have attracted wider interest than histological assessment of cervical, endometrial, placental or vaginal tissue in the search for a rapid bedside biomarker test for PTB given their relatively easy availability and acceptability by patients (Georgiou et al., 2015). By comparing the profiles of normal and pathogenic biological samples, novel marker candidates can be identified and extracted from small samples of tissue or body fluid for further study (Rice et al., 2006). These markers may hold predictive value for the early diagnosis of a disease as a stand-alone test or when combined together in larger panels of biomarkers (Shankar et al., 2004, Liu et al., 2014).

The detailed study of these key changes between control and case biological samples has been made possible thanks to the development of high-throughput "-omics" technologies which allow the assessment of a complex biological system at different levels with unparalleled efficiency and resolution (Zierer et al., 2015). The suffix "-omics" which is thought to stem from the Greek "-oma" refers to the wholeness of a biological system, and conceptualises the need to regard each molecule not in isolation but as an integral part of a cell, tissue or organism (Horgan and Kenny, 2011). By combining approaches that primarily aim to assess genes (genomics), mRNA (transcriptomics), proteins (proteomics) and metabolites (metabolomics), the "-omics" technology provides a holistic view of the system biology and generates novel hypotheses to inform future research (Horgan and Kenny, 2011, Zierer et al., 2015).

- Biomarkers in saliva

Salivary progesterone (SP) has been shown to be significantly lower in AHR women who deliver<34 weeks (Lachelin et al., 2009, Priya et al., 2013). The cut-off value of 2575 pg/mL for SP

measured with ELISA between 20-28 weeks was reported to predict delivery<34 weeks in AHR women with a sensitivity of 83% (95% CI: 58.6-96.4%), a specificity of 86% (95% CI: 75.9-93.1%) and a positive and a negative predictive value of 60% (95% CI: 38.6-78.8%) and 95% (95% CI: 87.1-99.0%). The resulting area under the receiver operating characteristic curve (AuROC) for SP was higher (0.89) than the AuROC for TVU CL (0.77; Priya et al., 2013). More recent studies have reported that when SP is combined with fFN values (cut-off 50 ng/L), the fFN AuROC for predicting PTB can be increased from 0.61 to 0.67 (Carter et al., 2014). The potential clinical application of SP for the prediction of PTB in AHR women and for guiding supplemental progesterone therapy as a preventive measure for PTB still remains unclear but it may be further clarified once the results from the prospective POPPY and PROMISES studies become available (Lachelin et al., 2009, Carter et al., 2013, Sharma et al., 2018).

- Biomarkers in blood (plasma/serum)

The large volume and remoteness from gestational tissues have posed some challenges for the analysis of highly diluted molecules in the blood (Georgiou et al., 2015). However, various studies have managed to assess biochemical markers for PTB in the serum and plasma using new proteomics techniques such as multiplex sandwich immunoassay which allows the simultaneous analysis of a large array of proteins in small volume samples (Goldenberg et al., 2001, Tsiartas et al., 2012). IL-10 and CCL5/RANTES are two of the proteins which were reported to significantly vary in maternal serum between control and PTB cases. In SYMP women, cut-off values of 48 pg/mL for IL-10 and 49.293 pg/mL for CCL5/RANTES were predictive of delivery within 7 days of presentation with an AuROC of 0.69 ($p<0.001$) and 0.61 ($p<0.001$) respectively, both values below the AuROC of TVU CL (0.77). When these two markers were combined together with CL, the resulting AuROC was high sitting at 0.88, with a sensitivity of 74% and a specificity of 76% for PTB (Tsiartas et al., 2012).

More recently, the Proteomic Assessment of Preterm Risk (PAPR), a large prospective multicentre study in the USA which assessed the serum proteome of over 5500 pregnant women using multiple reaction monitoring mass spectrometry reported that women who delivered prematurely had higher levels of insulin-like growth factor binding protein-4 (IBP-4) and lower levels of sex hormone-binding globulin (SHBG) than their term counterparts, and that the resulting ratio between the two was capable of discriminating PTB with an AuROC of 0.75 (95% CI: 0.56-0.91) and a sensitivity and a specificity of 75% and 74% respectively (Saade et al., 2016b, Bradford et al., 2017). The findings of the PAPR study are thought to be associated with the

inflammation/infection pathway behind PTB since higher expression of pro-inflammatory TNF-α and IL-1β signalling are known to result in an upregulated expression of insulin-like growth factors and a suppression of SHBG transcription in the liver. The clinical value of this proteomic classifier has continued to be validated in smaller studies, but as most patients in the PAPR study did not have their cervical length measured by TVU CL, it is still not possible to determine the true added value of IBP-4/SHBG for predicting PTB when compared to routine care (Saade et al., 2016a).

The quest for plasma biomarkers has not been limited to proteomics. Recent studies by Elovitz et al. (2014) and Cook et al. (2019) have shown that differential expression of maternal plasma microRNA in the first trimester of pregnancy may enable better prediction of cervical shortening and preterm birth, and response evaluation to outcome-modifying interventions such as progesterone and cerclage. Similarly, Nguyen et al. (2019) have reported that quantification of placental exosomes may hold predictive value for inflammation-induced PTB as the linearly increase of placental extracellular vesicles seen across pregnancy significantly plummets in LPS murine models prior to birth.

Maternal serum has also been subjected to metabolomics studies which aim to identify characteristic metabolic profiles associated with poor pregnancy outcomes such as PTB, small for gestational age (SGA) and IUGR to help in the early diagnosis and treatment of these conditions (Heazell et al., 2012). Some of these hypothesis-generating studies have shown that the serum metabolic profile of women with poor pregnancy outcomes has substantial differences in glycerolipids, fatty acids and vitamin D metabolites when compared to those with uncomplicated pregnancies using liquid chromatography-mass spectrometry (LC-MS). However, more targeted metabolomics studies are needed to further characterise and determine the relative abundance of these markers before they can be clinically validated (Romero et al., 2010, Heazell et al., 2012).

- Biomarkers in urine

Urine has always been considered an attractive source of potential biomarkers of human disease thanks to its relatively easy and non-invasive collection process which allows repeated sampling for early diagnosis, long-term monitoring and response assessment to treatment (Maitre et al., 2014). Its low cellular and protein concentration but high presence of metabolites makes it an ideal biofluid for metabolic assessment with little need for sample pre-processing. Despite all these advantages, there is scarce data about urinary metabolic profiles which may be associated with PTB. A recent case-control in which women who delivered preterm were matched to healthy controls (n=438) showed that the urine profile of those who delivered early had significantly higher concentration of lysine and lower amount of formate in the first trimester (between weeks 11-13) when measured

with proton nuclear magnetic resonance spectroscopy (^{1}H-NMR; Maitre et al., 2014). The study did not manage to fully explain why these metabolites differed so significantly between cases and controls but opened up a series of new hypotheses that may help elucidate the pathogenesis of PTB and improve its diagnosis.

Similarly, Ferguson et al. (2015) reported that the urine samples of women who delivered prematurely had higher oxidative stress biomarkers such as 8-isoprostate than their term counterparts at weeks 10, 18, 26 and 35. The authors hypothesised that these higher values seen in PTB could reflect the abnormal activation of inflammatory cascades which may lead to increased production of reactive oxygen species (ROS), collagen damage and an abnormal process of arteriolar spiralisation in early placentation.

- Biomarkers in cervicovaginal fluid (CVF)

CVF, a potential source of predictive markers of PTB, consists of secretions from cervical mucus glands, exfoliated cells, bacterial products, and plasma transudate through the vaginal mucosa and the choriodecidual space during pregnancy (Zegels et al., 2010). As previously postulated, the majority of infections that trigger PTB and compromise neonatal outcomes are thought to be associated with pathogens ascending from the vagina through the cervix into the uterus and surrounding fetal membranes (Pararas et al., 2006).

However, not every microorganism in the lower genital tract is capable of causing an ascending infection. The vagina, far from being a sterile reservoir, hosts millions of microorganisms known as the vaginal microbiota with which it maintains a symbiotic relationship (Ma et al., 2012). These *Lactobacillus*-dominated microbial communities find in the vaginal environment the necessary nutrients to maintain their growth and keep up with the daily microbial loss exacerbated by epithelial desquamation and the shedding of vaginal secretions. In return, these microorganisms prevent further colonisation of the vagina by non-indigenous and potentially pathogenic bacterial and fungal species, urinary tract infections and sexually-transmitted diseases by producing lactic acid and acidifying the milieu to an average pH of 3.0-4.5 (Ma et al., 2012, Romero et al., 2014b, Aldunate et al., 2015). *Lactobacillus* spp rely on the homofermentative pathway to produce lactic acid from the glycolytic breakdown of carbohydrates (Figure 1.3). Pyruvate, end-point of glycolysis, may be converted into the two isomers of the unprotonated anion of lactic acid namely D-lactate or L-lactate (Tachedjian et al., 2017). The high levels of lactid acid contributes to the low pH seen in the CVF of healthy women (Amabebe and Anumba, 2018).

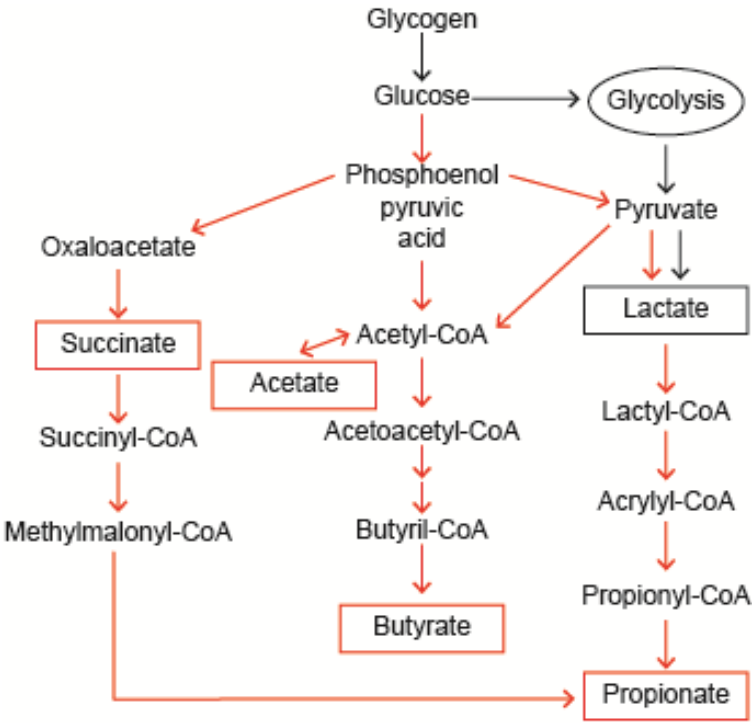

Figure 1.3. Schematic of the main fermentative reactions involved in the production of short-chain fatty acids by the vaginal microbiota (squared in orange). The homofermentative pathway is represented with black arrows whereas the anaerobic fermentation appears in orange arrows. Adapted from Richards et al. (2016)

Any perturbation to the vaginal ecosystem which may sometimes be caused by local or systemic antibiotic therapy or hygiene habits such as vaginal douching can alter the vaginal pH and upset this association between the polymicrobial microflora and the human host and cause infections such as BV. BV is characterised by a shift from a healthy *Lactobacillus*-abundant micro-environment to an abnormal and potentially pathogenic state with overgrowth of mixed anaerobes e.g. *Gardnerella*, *Bacteroides*, *Prevotella*, etc. (Petricevic et al., 2014, Amabebe et al., 2016b). It is thought that BV-associated bacteria are responsible for accentuating a dysbiotic vaginal environment by synthesising SCFAs such as acetate, propionate, butyrate and succinate (Figure 1.3). These in turn increase the pH in the vagina and downregulate the innate vaginal mucosal immunity by inhibiting monocyte chemotaxis (Al-Mushrif et al., 2000, Yeoman et al., 2013, Aldunate et al., 2015, Amabebe et al., 2016b).

The development of powerful genome sequencing techniques has allowed a better understanding of the complex diversity of microorganisms in the human vaginal microflora (Allen-Vercoe, 2013). For example, 16S rRNA gene sequence-based techniques have been employed to classify the microbiota of women at high risk of PTB, with some studies suggesting that lower concentration of certain *Lactobacillus* species in the second trimester may predispose to PTB

(Romero et al., 2014a, Rodriguez-Martinez et al., 2017). These approaches have facilitated access to a huge amount of genomic data in a relatively short period of time, compared to the lengthy and fastidious process of culturing anaerobes *in vitro*.

However, it has not been possible so far to accurately elucidate which microorganisms trigger inflammation/infection-induced PTB (Graves and Haystead, 2002). While techniques such as next-generation sequencing provide invaluable information about the abundance and genetic diversity of microorganisms in the vaginal ecosystem, they do not explain the metabolic readouts and interactions of vaginal microbes with the mucosa in health and disease. Hence, the need to combine genomics with complementary approaches that can provide information about how these microbial species behave and interact with one another (Horgan and Kenny, 2011, Allen-Vercoe, 2013). With that aim in mind, Stafford et al. (2017) carried out a pilot study to investigate the relationship between the vaginal microbiota and the metabolic profile of CVF in women who delivered prematurely compared to controls using 16S rRNA and ^{1}H-NMR, and showed that women who delivered prematurely had significantly higher amounts of *Lactobacillus jensenii* and lower number of *Lactobacillus crispatus* in their CVF samples at 20-22 weeks which in turn was associated with a higher pH (4.2 vs 3.8, $p<0.05$) and lower concentration of lactate ($p<0.01$). Similarly, Kindinger et al. (2017) found that a *Lactobacillus iners*-dominated microbiome at 16 weeks was associated with a short cervix<25 mm ($p<0.05$) and PTB before 34 weeks with a PPV of 69% ($p<0.01$). On the contrary and consistent with Stafford et al. (2017) results, *Lactobacillus crispatus* was linked to term birth with a PPV of 98%.

Some of the alternative and complementary approaches to genomics include the study of the proteome in the CVF of pregnant women. The development of more efficient proteomic technology from 2D gel electrophoresis techniques to the more advanced MS work has led to the creation of the first CVF proteome map in pregnant women by facilitating the rapid and simultaneous identification of multiple proteins (Dasari et al., 2007, Di Quinzio et al., 2007). Since then, over 150 proteins have been detected and their functions characterised, but only fibronectin and IGFBP-1 have been shown to be predictive enough of PTB to be introduced in the clinical setting (Musilova et al., 2011, Heng et al., 2015a).

Most CVF proteins have been found to be engaged in inflammatory processes (such as IL-1β), oxidative stress, mucosal defence (lactoferrin) and matrix remodelling (metalloproteinases and cysteine proteases; ACOG, 2001, Heng et al., 2015a). The dual biomarker model of albumin/vitamin D-binding protein (VDBP), for example, has been recently proposed by Liong et al. (2015) to predict PTB with a sensitivity of 66.7%, a specificity of 100%, a PPV of 100% and a NVP of 96.7% in symptomatic women between 22-35 weeks, compared to the qualitative fFN test

which yielded a sensitivity of 66.7%, specificity of 87.9%, and PPV and NPV of 36.4% and 96.2% respectively. Overall, the discovery of CVF proteins has helped improve our understanding of the mechanisms underlying labour, and it still holds promise as a potential source of predictive biomarkers for PTB (Georgiou et al., 2015). However, the clinical application of many of the proteins isolated has been limited by a lack of reproducibility and the absence of a rapid bedside test which can detect polymorphisms or isoforms of target proteins with the accuracy and precision achieved by laboratory assays (Heng et al., 2015a), a flaw that metabolomics may address.

Compared to genomics and proteomics, metabolomics has the advantage of not having to deal directly with polymorphisms as the core metabolic reactions are largely conserved across the different biological species (Veenstra, 2012, Amabebe et al., 2016a). Furthermore, metabolic changes are the closest indication of the response of the body to an external or internal stressor, a disease process or a drug therapy (Auray-Blais et al., 2011), and therefore, provide unique information about the functional phenotype. No comprehensive analysis of CVF can therefore be achieved without performing metabolomics studies.

Auray-Blais et al. (2011) used mass spectrometry to compare the vaginal metabolome of women who delivered PTB with those who gave birth at term, and concluded that the metabolomics analysis of CVF could be used to identify putative biomarkers of PTB. Further studies showed that symptomatic women who delivered before 37 weeks had significantly higher concentration of acetate (Amabebe et al., 2016a). This ^{1}H-NMR-based model was further validated by targeted enzyme-based spectrophotometric absorption of NADH using an acetic acid assay kit. Spectrophotometry is a relatively easy-to-perform analytical technique which is capable of quantifying the concentration of analytes in a sample based on their ability to transmit or absorb light at a certain wavelength (Trumbo et al., 2013). CVF acetate was predictive of delivery within two weeks of testing with an AuROC of 0.77 (95% CI: 0.58–0.96), and when CVF acetate was combined with fFN and TVU CL, the prediction of PTB increased to an AuROC of 0.86 with a sensitivity of 83% and a specificity of 89% (Table 1.3; Amabebe et al., 2016a). Similarly, when acetate was used in conjunction with glutamate, the ratio acetate-glutamate enhanced the prognostic value of acetate and yielded an AuROC of 0.86 (95% CI: 0.76-0.95%), (Amabebe et al., 2017). The combination of glutamate, acetate, lactate, fFN and CL in low-risk symptomatic women also increased the AuROC for prediction of PTB to 0.94 (95% CI: 0.88-0.98; Amabebe and Anumba, 2017).

Table 1.3. Combined test performance of CVF metabolites, fFN and CL in symptomatic and low-risk women (Amabebe et al., 2016a, Amabebe and Anumba, 2017).

	Outcome	**Sensitivity (95% CI)**	**Specificity (95% CI)**	**PPV (95% CI)**	**NPV (95 CI)**
Acetate + fFN + CL in symptomatic women	Delivery within two weeks of presentation	83% (74.18-89.77)	89% (81.17-94.38)	88% (81.10- 92.99)	84% (77.15-89.03)
Acetate + Glutamate + D-Lactate + fFN + CL in low-risk women	Delivery <37 weeks	100% (54.07-100)	72.31% (63.78-79.79)	14.3% (11.21-18.03)	100%

CI: confidence interval, CL: cervical length, fFN: fetal fibronectin

Ghartey et al. (2015) also found differences in monoacylglycerols, markers of the extracellular matrix and protein hydrolysis when comparing the biochemical profiles of CVF between women who delivered prematurely and those who delivered at term with gas chromatography-mass spectrometry (GC-MS). Particularly in the PTB group, the authors found a significant increase in the expression of mannitol and methylphosphate, a reduction in medium fatty acids such as azelate and sebacate, and a change in collagen degradation-related metabolites such as hydroxyproline, proline and glycine.

These encouraging findings further support the need for more proteomics and metabolomics studies which can provide a quick and affordable high-throughput screening of CVF for potential biomarkers of PTB followed by supervised confirmatory experiments (Cherney et al., 2007). As ^{1}H-NMR cannot be employed in clinical assays and spectrophotometry requires modestly expensive analysers and reagent kits, new cost-effective ways of assessing CVF are needed. Raman Spectroscopy (RS) may potentially fill in this role (Chapter 2).

1.5.2. **Cervical biomechanical and bioelectrical markers**

The cervix plays an essential part in maintaining a pregnancy to term (Myers et al., 2015). Throughout gestation, the cervix has to remain closed so that the foetus can develop *in utero*. However, for birth to occur, it has to shorten, soften and dilate. This crucial remodelling process is required for uterine contractions to lead to delivery (Danforth, 1983, Feltovich et al., 2012). Because PTB also requires premature cervical remodelling, improved understanding of this process is essential for the development of more accurate screening tools for PTB (Facchinetti et al., 2005).

Macroscopically, the cervix is a firm tubular structure which is situated at the lower pole of the uterine body. In non-pregnant women, a normal cervix usually has an average length of 30-40 mm, and anteroposterior and transverse diameters which range from 20 to 25 and from 25 to 30 mm respectively (Andrade et al., 2017). But these values are not categorical as the cervical size greatly varies depending on parity, age and menopausal status (Nott et al., 2016). Along the cervix, there is the cervical canal which is connected to the uterine cavity through the internal os at the top and to the vagina through the external os at the bottom (Chue-Sang et al., 2017). The upper cervix is lined by a single columnar layer of cells, whereas the lower cervix, known as ectocervix, is comprised of a 200-500 μm thick stratified squamous epithelium (Walker et al., 2002, Walker et al., 2003, Reich and Fritsch, 2014). Microscopically, approximately 90% of all the cervical tissue is comprised of an ECM which is abundant in collagen, proteoglycans and mucopolysaccharides but poor in smooth muscle fibres and elastin, the majority of which is found in the vessel walls within the cervix (Oxlund et al., 2010a). The remaining 10% is usually attributed to different types of cells including fibroblasts, smooth muscle cells, and vascular and immune cells (Nott et al., 2016).

The strength of the cervical tissue mainly relies on the collagen cross-linking within the ECM (Zork et al., 2015), although the covalent bonds between proteoglycans and glycosaminoglycan chains such as dermatan, chondroitin sulphate and hyaluronic acid also play their part (Facchinetti et al., 2005). As these molecules are hydrophilic, they bind large amounts of water which results in an increased volume-to-weight ratio in the ECM.

The main alterations in the ECM during cervical remodelling are thought to occur in the orientation and cross-linking of collagen, the amount of water content, and proteoglycans and hyaluronic acid binding (Feltovich et al., 2012). However, the process of cervical remodelling has not yet been fully characterised in humans, and most of the evidence available stems from studies on rodents. Research in mice suggests that cervical remodelling comprises four different stages: the first phase known as progressive softening begins quite early on around mid-conception, and it is characterised by a decrease in cross-linked collagen fibres. It is quickly followed by an accelerated softening phase during which collagen solubility continues to increase. After both softening stages conclude, the cervix undergoes a ripening process which culminates in full dilatation of the cervix and delivery of the foetus. This ripening phase is characterised by a higher production of hyaluronic acid which in turn will lead to a marked increase in tissue hydration. Collagen fibres have also been noted to have larger diameters during this phase. Finally, after parturition, the cervix is quickly repaired to protect the uterine cavity and upper genital tract from microbial agents. The immune system plays a leading role in this recovery phase which is microscopically characterised by increased presence of neutrophils and less soluble collagen fibres (Read et al., 2007).

Until recently, assessment of the cervical remodelling in women was limited to TVU CL and digital examination. However, as these methods lack precision and consistency, new more objective and accurate techniques have been proposed to assess changes in the microstructure of the cervix. Broadly speaking, this emerging technology which aims to assess cervical remodelling *in vivo* can be classified into three categories depending on the targeted area of interest: structure of the collagen, tissue elasticity and tissue hydration (Feltovich et al., 2012).

- Morphology of cervical collagen

Collagen fibres, which represent 60-80% of the dry weight of the cervix, have been proposed as potential functional biomarkers of the cervix. Collagen has been implicated not only in the physiological process of cervical remodelling but also in the pathological loss of biomechanical integrity seen in PTB (Ekman et al., 1986, House et al., 2009, Myers et al., 2015). As in most extracellular matrices in the human body, type I and III collagen fibres are the most abundant in the cervix. These collagen types do not only serve a mechanical function as they provide tensile strength to the cervix, but also a physiological role by acting as scaffolding for cell migration and attachment (Bode, 2002).

Collagen I and III are two types of fibrillary collagen that share a similar synthesis pathway. They are initially synthesised as large precursors with pro-peptides at both the N- and C-ends, which are ultimately cleaved off by proteinases before the fibres can interact with one another through cross-linking, forming supramolecular aggregates (Prockop and Kivirikko, 1995).

Each collagen fibre consists of three identical polypeptide chains, known as chains α, with a repeating Gly-X-Y sequence (a glycine in every third position followed by hydroxylated proline and lysine in the X- and Y-position) coiled into a left-handed helix. This molecular sequence is crucial for further intermolecular interaction (Bode, 2002, Shoulders and Raines, 2009). Three of these left-handed helices will twist around one another and wind together to form a right-handed super helix, stabilised by hydrogen bonds and water bridges, which will resemble a rope-like rod (Prockop and Kivirikko, 1995, House et al., 2009). This complex and relatively rigid triple helix conformation enables collagen to polymerise by placing the side chains of the aminoacids in the X- and Y-position on the surface, resist compression and extension (Prockop and Kivirikko, 1995, Bode, 2002) and display unique anisotropic (directionality-dependent) properties (Yao et al., 2016, Chue-Sang et al., 2017).

Studies addressing the role of collagen in cervical remodelling have mainly assessed four areas of interest: collagen concentration, solubility, morphology and functionality (Myers et al., 2009).

For many years, it was assumed that the process of parturition was associated with an actual decrease in the amount of cervical collagen as a result of an exacerbated breakdown of collagen fibres by ECM-activated metalloproteases and collagenases. Evidence to support this hypothesis, however, has been conflicting as results have been shown to greatly vary depending on the method employed to quantify collagen. When collagen concentration is normalised per dry weight, no significant difference is seen between non-pregnant and labouring pregnant women (Kleissl et al., 1978, Leppert and Yu, 1991). However, when wet weight is used instead, collagen concentration is noted to decrease significantly in labour as cervical ECM hydration dramatically increases (Uldbjerg et al., 1983). More recently, research has shown that the concentration of cervical collagen and the mechanical quality of the collagen does not significantly differ in women who have experienced cervical insufficiency in pregnancy from healthy controls when it is adjusted by age and parity. These observations further suggest that collagen concentration may not be enough to explain cervical remodelling in humans (Oxlund et al., 2010b).

Even though the absolute amount of cervical collagen may not significantly change throughout pregnancy, there is an increased body of work to suggest collagen solubility and morphology do increase. Danforth and Buckingham (1964) reported that the extractability of cervical collagen reached a maximum point during labour and in the postpartum period. This early observation was further validated by Maillot and Zimmermann (1976) who noted that 11% of cervical collagen was water-soluble at term compared to only 3% in early pregnancy and 6% in the postpartum period. It was proposed that either a reduction in the degree of collagen cross-linking or alternatively a re-arrangement of collagen fibres in the cervix could account for this increase in collagen solubility before delivery (Kucharz, 1992, Nallasamy et al., 2017a).

In mice, cervical collagen fibres have been found to significantly re-model during pregnancy from mature cross-linked collagen to more immature with fewer cross-linked fibres (Ekman-Ordeberg and Dubicke, 2012). The decrease in the collagen maturity ratio seen (total mature to total immature collagen crosslinks) during the softening phase of labour has been positively correlated with a reduction in cervical strength and stiffness by Yoshida et al. (2014). These observations further support the association between the degree of maturity and type of collagen, and the mechanical properties of the cervix (Mahendroo, 2012).

The preferential orientation the cervical collagen exhibits in non-pregnant women is thought to be lost during pregnancy (Aspden, 1988, Kirby et al., 1988). As birth approaches collagen fibres in the cervix have been reported to become more soluble, thicker, and disorganised leaving larger gaps amongst them (Read et al., 2007, Akins et al., 2010, Timmons et al., 2010). The disorganisation of collagen fibres affects its mechanical function and impacts on the ability of the cervix to maintain

the pregnancy until term (House et al., 2009). Unfortunately, most techniques which are capable of properly assessing the morphology of collagen are either invasive or can only be performed *in vitro* (Feltovich et al., 2012, Vargis et al., 2012). For premature labour to be predicted and prevented more appropriately there remains a need to develop non-invasive imaging techniques which are capable of assessing the *in vivo* remodelling from early stages.

A series of candidate technological approaches for studying cervical remodelling non-invasively have been tested including Second harmonic generation (SHG), Mueller matrix polarimetry and Optical coherence tomography (OCT).

SHG is a label-free nonlinear high-resolution imaging modality (0.5 µm) which is particularly powerful to assess non-centrosymmetric structures (structures which lack a centre of symmetry) such as fibrillar collagen. Previous research in mice has shown that SHG is capable of detecting *ex vivo* changes in the size and porosity of cervical collagen during pregnancy without destroying the sample (Akins et al., 2010). A recent study assessing human cervical biopsies also showed that SHG is able to detect and quantify differences in the alignment of cervical collagen between pre- and postmenopausal women without the need for any sample preparation (Narice et al., 2016). These results suggest that SHG may prove useful to predict PTB in the clinical setting pending the development and testing of an *in vivo* endoscopic probe (Figure 1.4; Feltovich et al., 2012).

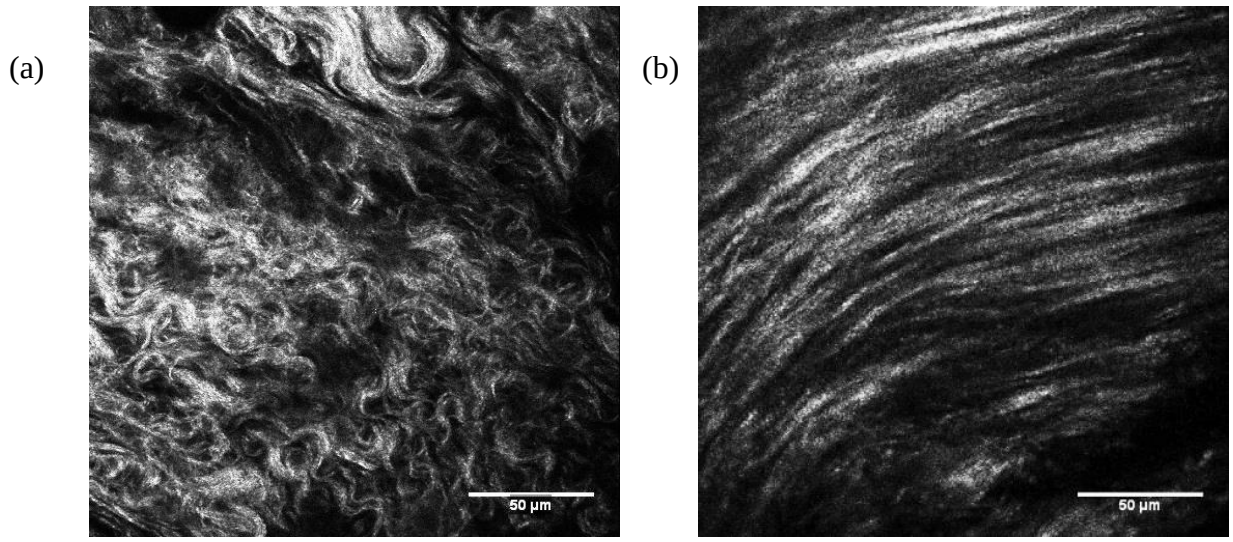

Figure 1.4. SHG images of cervical collagen. SHG allows non-destructive assessment and comparison of cervical collagen alignment between **(a)** pre- and **(b)** postmenopausal women. From Narice et al. (2016), CC BY License 4.0

Mueller matrix polarimetry and OCT are two non-invasive imaging techniques which rely on the optical properties of the tissue to explore its ultrastructure (Gan et al., 2014, Sharma and Sujatha, 2018). After successfully pioneering in ophthalmology and dermatology, Mueller matrix

polarimetry and OCT have been employed to experimentally characterise the complex topology of the human cervix and its potential role in the diagnosis of gynaecological cancer and obstetrics disorders (Yao et al., 2016, Kirillin et al., 2017). However, their translation to the clinical setting has been impaired by a reduced field of view which requires complex stitching algorithm to develop 3D imaging, low specificity for distinguishing between different tissues and limited depth-resolved changes in birefringence (Matcher, 2011, Kirillin et al., 2017). Functional extensions of OCT such as Polarisation-sensitive optical coherence tomography (PS-OCT) may be able to address these issues by enhancing tissue-specific contrast through its ability to polarise light (Chapter 3).

- Cervical tissue elasticity

Cervical remodelling in pregnancy entails gradual softening and opening of the cervix prior to labour and delivery (Cabrol, 1991). Therefore, mechanical devices that can objectively assess these variations in tissue stiffness would allow earlier identification of patients who are at higher risk of PTB.

Strain elastography, a technique which measures tissue displacement under manual compression, is a method to study the mechanical properties of the cervix during pregnancy that is attracting increasing interest (Swiatkowska-Freund and Preis, 2017). As the elastogram can be superimposed on B-mode ultrasound imaging, results are obtained in real time and non-invasively and they can be easily interpreted with colour codes. These features make elastography an attractive technique for the clinical setting (Khalil et al., 2013). However, the lack of reproducibility has limited clinical application because the pressure exerted on the probe tends to vary from one operator to another (Molina et al., 2012). Despite this source of variation, pilot clinical trials have been quite encouraging so far (Swiatkowska-Freund and Preis, 2017). Wozniak et al. (2014) showed that the evaluation of the internal cervical os in the second trimester using elastography was capable of predicting PTB in asymptomatic low-risk patients with a sensitivity of 85.7% and a specificity of 97.6%. Swiatkowska-Freund et al. (2014) also found that in women who presented with symptoms suggestive of PTB, elastography of the internal os significantly correlated with the Bishop Score ($p<0.002$). This evidence suggests elastography may be useful for prediction of PTB, but further research to standardise the force applied by the operator and improve reproducibility is still needed before its true clinical utility can be determined.

- Cervical tissue hydration

Cervical tissue proteoglycan and water concentration seem to increase as pregnancy progresses, a finding which correlates with the gradual disorganisation of the matrix seen throughout pregnancy and which culminates with the softening and full dilatation of the cervix prior to birth (Aspden, 1988, Feltovich et al., 2012). A reliable technique to measure hydration would then allow a more accurate identification of when delivery may happen.

Over 20 years ago, Oláh (1994) proposed to assess the changes in cervical hydration during pregnancy using Magnetic resonance imaging (MRI). In his study, T2 weighted scans were taken serially from a 34-week pregnant woman. Image density between the cervical connective tissue and the lower buttock adipose tissue was then used to estimate the hydration index which was shown to markedly increase closer to term. Although the study was based on serial observations from only one patient, it provided proof-of-concept data about the potential value of MRI for predicting the onset of labour. However, the limited availability and high costs associated with MRI make it less than an ideal candidate for PTB screening, and the need to develop non-invasive technology which could assess cervical hydration remains (Avis et al., 1996).

Bioimpedance techniques, though not strictly measuring hydration, assess how the electrical current, which is largely dependent on hydration and on the cellular architecture of the epithelium and the complex histology of the underlying stroma, flows within the tissue. Even the slightest variations in cervical anatomy are expected to alter the inherent electrical features of the tissue (Barai et al., 2012). This presumed physical relationship between cellular size, density and extracellular rearrangement, and electrical properties underlies the rationale for employing bioimpedance techniques in the prediction of sPTB (Anumba et al., 2011).

A recent trial was conducted at Sheffield NHS Teaching Hospital Trust to assess the role of Electrical impedance spectroscopy (EIS) as a predictive tool for PTB. By applying electrodes on the cervix of pregnant women, the cervical electrical properties throughout pregnancy were measured, and it was found that women who delivered prematurely had significantly lower tissue impedance than those who delivered at term (Stern et al., 2016, Anumba et al., 2018). The study also highlighted some intrinsic disadvantages with the EIS technique such as the variation in cervical resistivity seen with the varying contact pressure used for data collection (Jokhi et al., 2009a, Jokhi et al., 2009b). A need to overcome this limitation led to our hypothesis that Magnetic induction spectroscopy (MIS), a technique which also measures conductivity and impedance but unlike EIS does not need electrodes to do so, may be capable of assessing electrical changes associated with cervical remodelling thus improving prediction of PTB (Chapter 4).

1.6. Hypothesis and aims

1.6.1. **Hypothesis**

Pilot studies using ^{1}H-NMR and MS have shown that women who are destined to deliver earlier present different concentration of metabolites and proteins in their CVF when compared to those who deliver at term. I hypothesised that a technique capable of performing a multiple-dimensional analysis of these CVF biomarkers such as Raman spectroscopy, a non-destructive imaging technique which provides a characteristic molecular signature based on the set of chemical bonds present in the sample, would be capable of identifying markers of sPTB and improving the performance of current screening techniques in both pregnant women deemed at high risk of PTB as well as in women presenting with symptoms of threatened preterm labour. I further hypothesised that some of these specific CVF metabolomics changes could be quantified with enzyme-based spectrophotometry, a technique which may have point-of-care diagnostic potential for vaginal dysbiosis.

At a biomechanical level, I proposed the use of PS-OCT to non-destructively characterise the ultrastructure and orientation of the collagen in the human non-gravid cervix. I expected PS-OCT to fully and consistently recreate the preferential orientation of cervical collagen fibres previously described with X-ray diffraction, and its findings to significantly correlate with conventional histology to support the future creation of an endoscopic probe for *in vivo* assessment of cervical remodelling.

Finally, I hypothesised that MIS would be capable of measuring the electrical properties of the gravid human cervix *in vivo* by magnetically inducing small currents on the cervix without the need for electrodes. By removing contact coupling, MIS would overcome EIS limitations associated with varying probe pressure and the presence of cervical surface mucus.

1.6.2. **Aims**

The aim of this PhD project was to explore new applications of innovative and potentially non-invasive technologies which could improve the prediction of PTB and provide a better understanding of human cervical remodelling. I aimed to assess whether:

(1) RS molecular signature of CVF samples from high-risk pregnancies and women presenting with symptoms of preterm labour bears any predictive value for sPTB,

(2) PS-OCT is capable of measuring, reliably and non-destructively, the arrangement of collagen fibres in the *in vitro* human cervix which may justify the development of an endoscopic probe for *in vivo* use,

(3) MIS can measure, accurately and reproducibly, cervical electrical transresistance in pregnant women as a potential predictive tool for sPTB and,

(4) Metabolomics analysis of CVF performed by enzyme-based spectrophotometry can improve the prediction of sPTB as a stand-alone test or combined with fFN and cervical length.

Chapter 2

Assessing cervicovaginal fluid with vibrational Raman spectroscopy as a predictive tool for spontaneous preterm birth

2.1. Introduction and background

The cervicovaginal fluid (CVF) constitutes a potential source of biomarkers to assist in the prediction of sPTB. Secreted by the lower genital tract, it contains bacterial products, cholesterol, lipids, mucin, carbohydrates, proteins, aminoacids, nucleic acids and inorganic ions (Zegels et al., 2010, Heng et al., 2015a). Currently, there are no cost-effective techniques to assess the molecular composition of CVF in the clinical setting. I therefore proposed the use of Raman spectroscopy (RS), a non-destructive technique which relies on the scattering of electromagnetic radiation (EMR), to provide a characteristic molecular signature of the CVF in pregnant women in their second and early third trimester of gestation and assess its predictive value for sPTB.

2.1.1. **Electromagnetic radiation and vibrational spectroscopy**

Spectroscopic techniques study the interaction between EMR and matter to learn about the content of a sample. As a result, they are dependent upon both the characteristics of the radiation as well as the chemical composition of the sample. An understanding of the principles of EMR enables a better appreciation of RS and its biochemical application.

The broad range of wavelengths across which EMR spans is known as the electromagnetic spectrum (EMS), and it can be used to classify the different spectroscopic techniques. The EMS is normally subdivided into seven regions: radio waves, microwaves, infrared light, visible light, ultraviolet light (UV), X-rays, and gamma rays. Every EMS region has a natural way of interacting with atoms and molecules. Therefore, when matter is exposed to radiation, the molecules are excited in different ways depending on the wavelength of the incident light. If the photons that strike on the sample fall within the range of ultraviolet light, for example, the atom's electrons get excited to a higher level of energy. However, this higher energy level is rather unstable, and the excited electrons tend to naturally transition back to the rest level, that is, the original low-energy level at which they were before. In doing so, the electrons release energy in the form of photons. These photons generate an emission spectrum which is unique to that atom because the energy needed to move an electron from one energy level to another is fixed for each particular atom and differs from one element to another. The UV spectroscopy, in particular, relies on the specificity of the emission spectrum generated when UV light interacts with a sample to identify its atomic content (Zumdahl and Zumdahl, 2013).

On the other hand, if the wavelength of the EMR falls within the infrared or microwave ranges, which are lower in energy than UV light, the radiation cannot excite electrons to higher levels of energy but it may still affect the sample molecules in other ways. Microwaves may cause the

chemical bonds between atoms to rotate, whereas infrared radiation may not only cause the chemical bonds within the molecules to rotate but also to vibrate. Similar to what happens with atomic transitions, the energy needed to produce rotational or vibrational changes is also fixed for each particular chemical bond. Therefore, chemical groups within a sample may be identified based on the type of vibrations EMR produces, which may be stretching or bending in nature (Figure 2.1; Coates, 2006):

- Stretching vibrations (ν) are characterised by keeping the bond angles between atoms constant while bond length varies. Stretching vibrations are symmetric if the bond movements of functional groups happen in the same direction and at the same time, or asymmetric (as), if the changes in bond lengths oppose each other.
- In bending vibrations, atom bond length remains constant whereas angles change. Depending on the nature of the vibration, bending vibrations can be further classified into scissoring (δ), rocking (ρ), twisting (τ) and wagging (ω; Figure 2.1).

Vibrational spectroscopy, such as Infrared Spectroscopy and RS, relies on vibrational spectra to identify the chemical structure of a sample (dos Santos et al., 2017). RS, in particular, uses EMR from the visible and near infrared spectrum to characterise the content of a sample (740-380 nm; Talari et al., 2015).

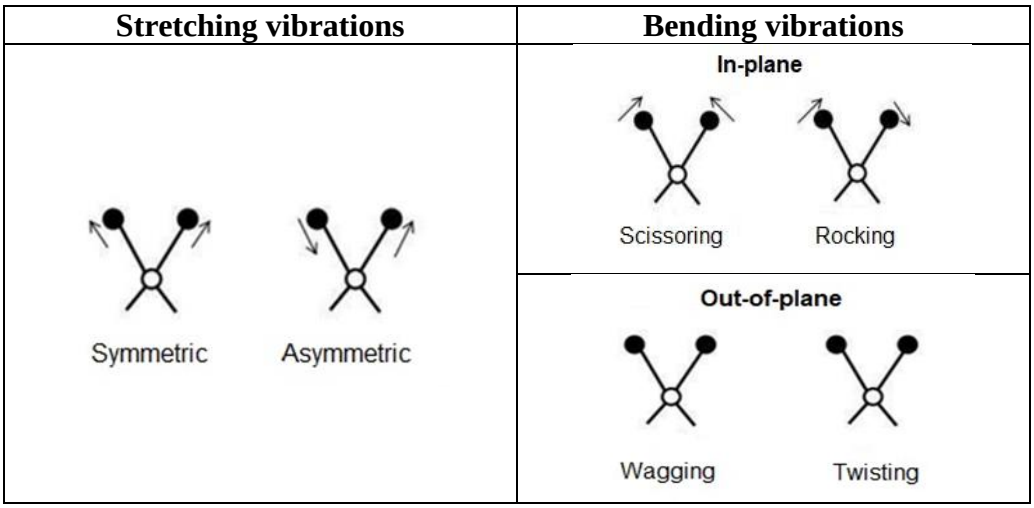

Figure 2.1. Chemical bonds between atoms interact with electromagnetic radiation in the microwave region by either stretching symmetrically (two atoms stretching in the same direction relative to an atom they both are bound to) or asymmetrically (opposite directions), or bending in plane or out of plane. Adapted from Olawumi (2015)

2.1.2. **Interaction between EMR and matter in Raman spectroscopy**

When light interacts with matter, it may be transmitted through the medium, absorbed and transformed into a different type of energy (most commonly heat), reflected back after interacting

with the surface or the interior of the medium, or scattered, that is, deviated from a straight pathway and deflected into multiple directions (Figure 2.2; Jacques, 2013). RS analyses one specific type of scattered radiation to characterise the chemical composition of a sample.

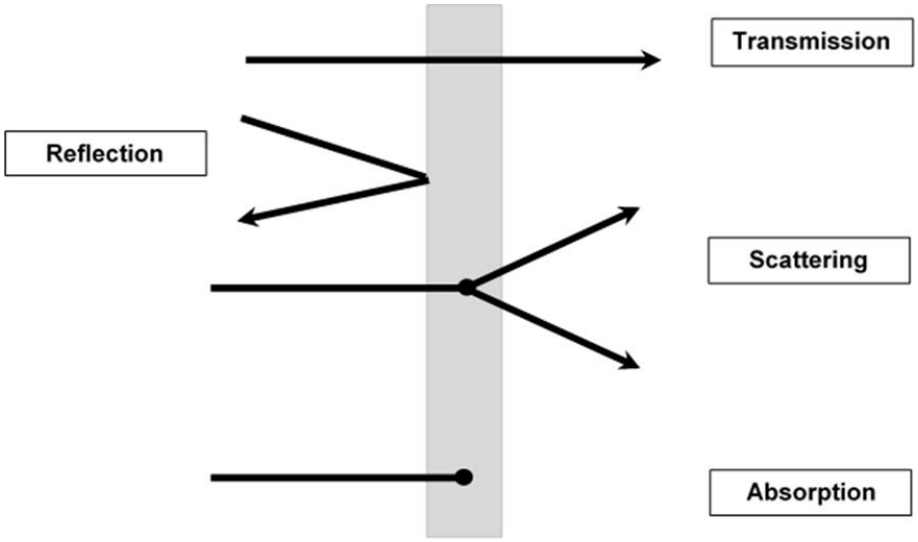

Figure 2.2. Electromagnetic waves (black lines) undergo transmission, reflection, scattering or absorption when they interact with matter (grey rectangle)

Before light is scattered, incident photons which are shining at a particular frequency (v_0) interact with the molecules of a sample by deforming their electron cloud to a degree determined by the attribute known as polarizability. As a result, energy from the photons is momentarily absorbed by the molecules which are promoted to a short-lived "virtual state" (v_m) from their ground vibrational state (Bumbrah and Sharma, 2016, Larkin, 2018). The molecules then relax back to a lower vibrational state by releasing the extra energy as photons which may be scattered with lower, higher or the same frequency as the incident light (Figure 2.3). If the frequency is conserved, scattering is classified as elastic whereas any increase or decrease in frequency is known as inelastic scattering.

1. *Elastic scattering*: also known as Rayleigh scattering, occurs when the scattered light has the same frequency as the incident radiation. After absorbing the photon, the excited molecule returns to its rest level after emitting radiation with the same frequency as the excitation source ($v_0 = v_0$).

2. *Inelastic scattering*: if the emitting radiation has lower frequency than the incident light, the scattering is known as Stokes scattering. This type of inelastic scattering occurs when part of the incident radiation is absorbed by a molecule that is at a rest vibrational state before being illuminated(v_m). The transfer of energy enables the molecule to reach a higher vibrational state at the expense of reducing the frequency of the scattered light ($v_0 - v_m$). If, on the contrary, the scattered radiation has a higher frequency than the incident light, the scattering is referred to as anti-

Stokes scattering. For this to happen, the photon of the incident light interacts with a molecule which is already in an excited vibrational level before it is illuminated; the excessive energy is released from the molecule to the scattered light (v_m) resulting in a higher frequency than that of the incident light ($v_0 + v_m$).

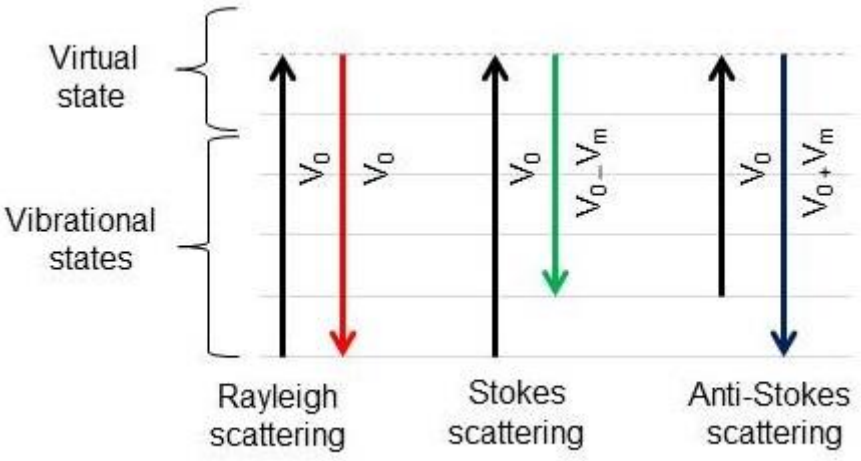

Figure 2.3. Graphic representation of Rayleigh, Stokes and Anti-Stokes scattering. When the incident light interacts with the sample, it excites the sample to a higher energy state (black arrow), there is a transient energy transfer which results in scattering radiation with identical frequency to the incident light (Rayleigh scattering, red arrow), lower frequency (Stokes scattering, green arrow) or higher frequency (anti-Stokes scattering, dark blue arrow). Modified from Vasakova (2011)

RS is a vibrational spectroscopy method which measures inelastic scattering (Stokes and anti-Stokes; Yorucu et al., 2016). However, as almost all the incident photons undergo elastic Rayleigh scattering when they interact with a sample, the Raman effect is very weak because it only measures the relatively low inelastic scattering, (1 in 10^{10} of all scattered light), (Talari et al., 2015, Bumbrah and Sharma, 2016). Therefore, RS needs highly sensitive spectrometers in order to detect these minimal shifts in light.

RS spectral data is presented as the difference in energy intensity between the incident and the inelastic scattered radiation in the Y-axis, and the wavelength shift in the X-axis (Bumbrah and Sharma, 2016). Raman shift (ΔW) can be understood as the difference in frequency between incident $\left(\frac{1}{\lambda 0}\right)$ and Raman scattered light $\left(\frac{1}{\lambda 1}\right)$, and it is normally measured in 1/cm, that is, in wavenumbers (W; Talari et al., 2015):

$$\Delta W = \frac{1}{\lambda 0\ nm} - \frac{1}{\lambda 1\ nm}\ x\ \frac{10^7 nm}{cm}$$

For most organic molecules, Raman spectra are recorded in the range of 3000-400 cm^{-1}.

The full Raman spectrum is then separated into regions to analyse particular biological macromolecules such as proteins and aminoacids (amide, aminoacids and fingerprint region), lipids and nucleic acids (high wavenumber regions). This more detailed analysis enables to gain insight into the differences in chemical composition and molecular structure between different samples (Choo-Smith et al., 2002).

2.1.3. **Advantages of Raman spectroscopy**

Although inelastic scattering, known as the Raman Effect, was discovered in 1927, it was not until the 1980s with the development of advanced instrumentation and bioinformatics that the potential of RS as an analytical technique caught the attention of the industrial and scientific sectors (Gala and Chauhan, 2015). Ever since then, the potential scope of RS applications has continued to grow. RS has shown promise for a series of *in vivo* applications and real-time clinical interventions including continuous non-invasive glucose monitoring, guidance for biopsy excision during surgical procedures and faster sample analysis which may replace more invasive histopathological techniques (Choo-Smith et al., 2002, Bumbrah and Sharma, 2016, Lundsgaard-Nielsen et al., 2018, Lazaro-Pacheco et al., 2019).

In particular for the study of human biofluids, RS has become an attractive research tool (Sikirzhytskaya et al., 2012, Talari et al., 2015, Yorucu et al., 2016) because:

1. RS reveals a unique vibrational signature which allows the discrimination of biomarkers.
2. Samples are not destroyed during RS and therefore, they can be further interrogated with other techniques.
3. Only a minimum amount of the sample is needed for RS analysis. This can be as low as a few picolitres or femtolitres.
4. Most samples can be easily analysed even if they are dissolved in water as the interference from water is minimal (due to its low Raman activity).
5. RS data collection is quick and relatively inexpensive, and multidimensional analysis of the data has been dramatically facilitated by advanced software packages.
6. Some Raman spectrometers have already been developed as portable devices which make them ideal for potential bedside tools in the clinical setting.

2.1.4. **Raman spectroscopic signature of cervicovaginal fluid**

In the last few years, RS has found increasing popularity in the field of forensic science, thanks to its potential to identify and characterise traces of biofluids at crime scenes (Virkler and Lednev,

2009). As a consequence, human saliva, semen and blood have been extensively studied with RS. However, only one pilot study has ever interrogated the CVF of non-pregnant women with RS (Sikirzhytskaya et al., 2012). Despite having a small sample size (n=7), this preliminary study managed to describe the first spectroscopic signature of CVF in non-pregnant women (Table 2.1).

Table 2.1. Assignment of Raman bands in dried CVF spectral components, (Sikirzhytskaya et al., 2012)

Raman band (cm^{-1})	**Assignment**	**Origin**
481	NCO bending	Urea
855-850	CH_3	Lactate
940-930	CC	Acetic acid
1002	Aromatic ring breathing/ NCN	Phenylalanine/ Urea
1045	C-O, C-CO_2, C-CH_3	Lactic acid
1082	C-O, C-COH	Lactic acid
1125	C-CH_3, NH_2	Lactic acid/ Urea
1260-1250	CH, amide III	Proteins
1333-1330	CH, amide III	Proteins
1455-1445	CH_3	Lactic acid
1610	CO_2^-	Lactic acid
1655	COO^-	Lactic acid

C: carbo, CVF: cervicovaginal fluid, H: hydrogen, N: nitrogen

2.2. Aims and objectives

2.2.1. **Aims and hypothesis**

The aim of this study was to assess the predictive value of RS analysis of CVF for sPTB in the clinical setting.

2.2.2. **Objectives**

- To test whether CVF from pregnant women can be assessed with RS
- To standardise HVS collection and CVF processing for RS analysis
- To compare the mid-gestation RS spectra of CVF in a cohort of asymptomatic women deemed at high risk of sPTB (AHR), and in women presenting with symptoms of threatened preterm labour (SYMP) based on delivery outcomes
- To determine the accuracy of RS for predicting sPTB when used on mid- and third trimester CVF samples from AHR and SYMP women
- To inform sample size calculation for future clinical trials

2.3. Materials and methods

2.3.1. **Study population and sample collection**

CVF was obtained from pregnant women attending antenatal clinic and Triage delivery suites at the Jessop Wing (Sheffield NHS Teaching Hospitals Trust, UK). Based on their obstetric history and presenting complaints, study participants were recruited into two different arms: (1) pregnant women deemed at high risk of PTB, i.e. with previous obstetric history of PTB or late miscarriage or an incidental short cervix at their 20 week scan but with no symptoms of preterm labour, who attended antenatal clinic during their second trimester (AHR), and (2) pregnant women attending Triage between 20^{+0} and 36^{+6} weeks of gestation with symptoms of threatened PTB but not yet in established labour or advanced cervical dilation (less than four cm dilated and no more than one contraction every ten minutes) and intact membranes (SYMP). Further samples from asymptomatic patients considered to be at low risk for PTB were collected in order to characterise the baseline spectral fingerprint of dried CVF in pregnancy.

Following written consent, a pair of high vaginal swabs was obtained from the posterior fornix of the vagina prior to performing any vaginal examination using dry polystyrene Dacron high-vaginal swabs (Delta lab Eurotubo 300263, Fisher Scientific). Women who had abnormal cervical cytology within the previous year, were already receiving antibiotic treatment for confirmed vaginal infection or tocolytic agents such as oxytocin inhibitors (Atosiban®) and indomethacin at the time of sampling, had multiple gestations or held a diagnosis of prelabour premature rupture of membranes (PPROM) were excluded from the study.

At the time of sample collection, most participants' risk of PTB was also assessed by standard clinical methods including quantitative measurement of fFN and TVU CL. After collection, the samples were labelled and immediately stored at -80^{o}C and processed within five days. Medical records were subsequently followed up to ascertain delivery outcomes.

The study was conducted with approval from the Yorkshire & Humber Committee of the UK National Research Ethics Service (Research Ethics Committee Number 13/YH/0167).

2.3.2. **Sample size justification and statistical analysis of demographic and clinical data**

Given the preliminary nature of the work proposed, no formal sample size calculation was performed as one of the aims of the study was to generate enough data to inform sample size for future trials (Billingham et al., 2013). However, we aimed to include a minimum of 7-10 patients for each arm of the study as a growing body of evidence suggested that at least seven biological

replicates should be assessed when performing spectroscopic-based multivariate analysis (Baker et al., 2016, Ali et al., 2018).

Demographic and clinical data was first inspected with Shapiro-Wilk normality tests to assess distribution and select the most appropriate statistical hypothesis test. In cases in which a normal distribution was confirmed, unpaired Student *t*-tests were used to compare clinical data based on birth outcomes. For non-normally distributed data, non-parametric tests such as Mann-Whitney U tests were employed instead. All statistical analyses were conducted using SPSS software (IBM, v25).

2.3.3. **Sample preparation for RS**

The tip of each swab, saturated with CVF, was cut off and placed into a 1.5 mL microfuge tube. Six hundred microliters of sterile Phosphate Buffered Saline (PBS) at pH 7.4 were then added to the tube, which was vortexed at 300 revolutions per minute (rpm) for 5 minutes. The processed samples were subsequently stored at -80^{o}C until analysed with RS.

For scanning with RS, a drop (~0.1 mL) of the vortexed sample was placed on a microscope slide wrapped in sterile aluminium foil which is known to have weak fluorescence in Raman and increase resonance of the sample signal (Liao and Stern, 1982). The drop was then smeared on the slide by a single operator and left to dry at room temperature for 15 minutes before being scanned with RS (Virkler and Lednev, 2008).

2.3.4. **RS measurements**

The technique to collect Raman spectra was first optimised and standardised to reduce background noise and artefacts which can adversely affect the weak Raman signals (Kerr et al., 2015). High-quality Raman spectra were recorded by scanning five random single points from each smeared sample using a DXR Raman Microscope (Thermo Scientific, USA) equipped with a 532 nm wavelength diode laser. All measurements were consistently collected using a light power of 9.2 mW, a 25 µm pinhole aperture and a 50x LWD objective NA 0.50 (Olympus LMPLFLN). Collection times were set to 10-second exposures for all samples (Butler et al., 2016).

2.3.5. **Analysis of RS data**

Spectra from all single points was collected with OMNIC (Thermo Scientific, USA) and analysed with Unscrambler X (CAMO, Norway). Data was first transformed with Savitzky-Golay smoothing to remove random noise, followed by standard normal variate (SNV) to reduce the

multiplicative interference of scatter and particle size, and baseline correction to minimise the fluorescence generated by the sample (Daszykowski et al., 2008, Chen et al., 2018). Spectral features such as peak intensity, band position and frequency shift were analysed for the whole spectra, that is the general region (GR), as well as for individual components: fingerprint (FP), amide (A), aminoacids (AA) and high wavenumber (HWN) regions. Once processed, the data was subsequently analysed with unsupervised and supervised chemometric techniques namely Principal Component Analysis (PCA) and computational modelling construction with Linear Discriminant Analysis (LDA) respectively. PCA is a useful technique for analysing complex information from biological samples. It displays trends and patterns by transforming and geometrically projecting high-dimensional data into fewer dimensions, thus reducing the error rate associated with multiple test correction. Unlike LDA, no prior knowledge on sample classification or outcome is required (Lever et al., 2017). LDA, on the other hand, relies on a series of reference observations to classify unlabelled data (Izenman, 2008).

Based on LDA, the performance of RS to predict PTB in AHR and SYMP and delivery within two weeks of sampling was tested (Parikh *et al.*, 2008) using parameters such as:

- Sensitivity: understood as the ability of RS to identify those who delivered PTB and calculated as $\frac{True\ Positive}{True\ Positive + False\ Negative}$
- Specificity: defined as the ability of RS to correctly identify those women who had a term delivery and expressed as $\frac{True\ Negative}{True\ Negative + False\ Positive}$
- PPV: the probability of a patient with a positive result having a PTB, calculated as $\frac{True\ Positive}{True\ Positive+False\ Positive}$
- NPV: the probability of a pregnant woman with a negative result having a term delivery, calculated as $\frac{True\ Negative}{True\ Negative+False\ Negative}$

Most prominent spectral peaks were assigned a chemical significance based on existing literature (Sikirzhytskaya et al., 2012, Talari et al., 2015). For example, RS values at 480 and 1002 cm^{-1} were associated with urea, whereas peaks at 930 and 1460 cm^{-1} were linked to acetate instead (Sikirzhytskaya *et al.*, 2012).

2.3.6. **Measurement of fetal fibronectin (fFN), transvaginal cervical length (TVU CL) and vaginal bacterial infection**

CVF fFN levels was analysed with the FFN analyser (Hologic®), whereas CL and the presence of funnelling and intra-amniotic sludge were measured by transvaginal ultrasound (ALOKA ProSound Alpha 6).

After RS swabs had been retrieved, an extra high-vaginal sterile charcoal swab was taken from the posterior fornix and sent to the Sheffield NHS Teaching Hospital Clinical Microbiology Department to test for BV, Group β Streptococcus, *Candida*, *Ureaplasma*, *Trichomonas*, and *Mycoplasma* spp. *Candida* is prevalent in pregnancy (30-40% colonisation) but colonisation is likely to be asymptomatic and not require any treatment as per the British Association for Sexual Health and HIV (BASHH) guideline. Therefore, a decision was made to treat only *Candida* positive women who presented with symptoms of vulvovaginitis at the time of the study visit. Positive microbiological swabs for other species were managed according to local protocols and excluded from the RS analysis.

2.4. Results

2.4.1. **Optimisation of Raman analysis of CVF**

I first optimised the technique for studying CVF with RS by testing two different surfaces in order to avoid fluorescent signals arising from the glass slide impurities which could overlap with the Raman signal (Kerr *et al.*, 2015). The same CVF sample (n=5) was smeared on two types of microscope slides: anti-reflective calcium fluoride and aluminium-wrapped conventional glass, and subsequently scanned using a DXR Raman spectrometer. As only minimal differences were seen between the two spectra (Figure 2.4), all following samples were scanned on glass slides wrapped in aluminium to minimise consumable costs.

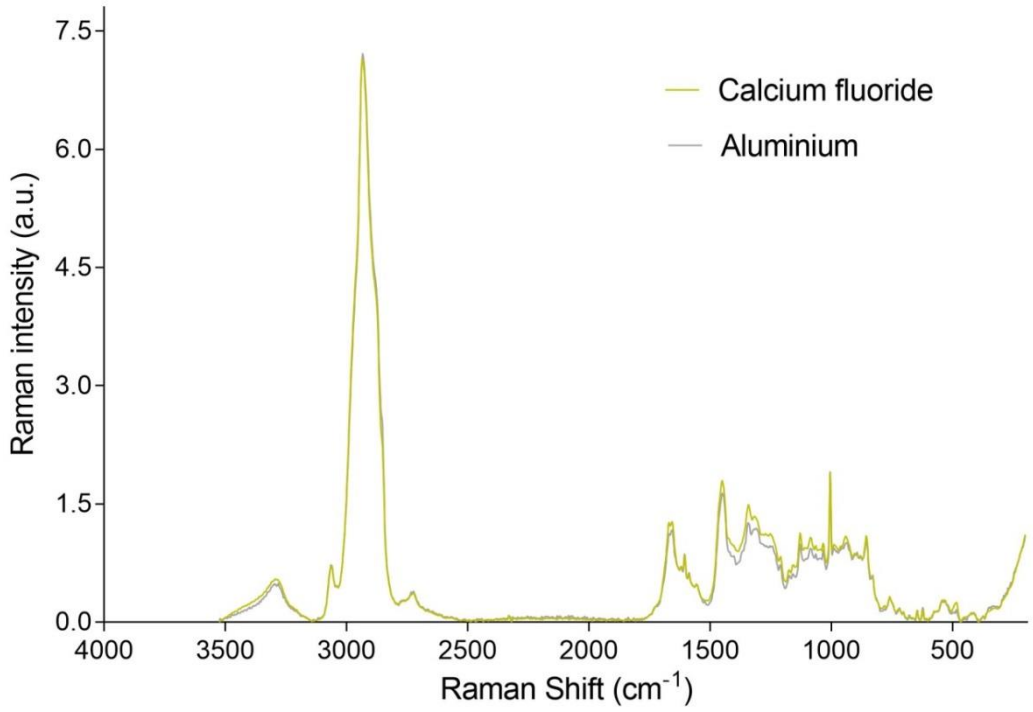

Figure 2.4. Full spectra were obtained from the same CVF sample scanned first on calcium fluoride substrate and subsequently on an aluminium-wrapped microscopic slide. The procedure was repeated on five different samples.

2.4.2. **Participants' demographic and clinical data**

Vaginal swabs were obtained from 21 asymptomatic women at high risk of sPTB between 20^{+0}-28^{+0} weeks (AHR), and from 25 symptomatic women presenting to Labour Ward between 20^{+0}-36^{+6} weeks in threatened preterm labour (SYMP) as per the inclusion and exclusion criteria listed on section 2.31. Demographic and clinical characteristics are summarised in Table 2.2. Except for fFN,

comparisons between birth outcomes within each cohort were carried out employing unpaired Student's *t*-test. For fFN, a Shapiro-Silk test ($p<0.001$) confirmed the data was not normally distributed and thus, Mann-Whitney U test was employed instead. For discrete variables such as smoking status, chi-square tests with a significance level of 0.05 were used.

Patient recruitment was performed in an untreated cohort of patients before the inception of the local Preterm Birth Clinic in September 2017, and samples were selected aiming to achieve relatively similar number of index cases and controls in each arm of the study. This may explain the relatively higher incidence of PTB seen in this pilot study which is not necessarily representative of the local incidence in the unit.

Within the AHR cohort, 47.62% of the women (n=10) delivered prematurely with a mean pregnancy duration of 225.80 ± 34.21 days. Out of the ten women who delivered early, two (9.52% of the total AHR population) had a delivery before 28^{+0} weeks of gestation, two (9.52%) between 28^{+0} and 32^{+0} weeks, and the remaining six (28.57%) between 32^{+0} and 36^{+6} weeks. Similarly, within the SYMP group, 48% of women (n=12) delivered before 37 weeks, with a mean duration of 217.00 ± 24.26 days. Of the twelve premature births recorded in this group, three (12% of all SYMP women) occurred before 28^{+0} weeks of gestation, four (16%) between 28^{+0} and 32^{+0} weeks and five (20%) between 32^{+0} and 36^{+6} weeks. Eight (32%) symptomatic women delivered within two weeks of presenting with symptoms suggestive of preterm labour. Time to delivery from the moment CVF samples were collected was significantly shorter in AHR and SYMP women who delivered prematurely ($p<0.01$).

In the AHR group, no statistically significant difference was seen for BMI or maternal age between women who had a sPTB and those who had a term delivery ($p=0.97$ and $p=0.48$ respectively). Similarly, the difference in smoking status was found not to be statistically significant (30% vs 18%, $p=0.4$) nor the gestational age at time of scanning ($p=0.17$, Appendix A: Figures A.1 and A.2). In the SYMP group, even when all ages were within normal range, those who delivered preterm were significantly older than those who had at term delivery ($p=0.04$). Similar to the AHR group, no statistically significant difference was seen for BMI ($p=0.53$), or smoking status ($p=0.70$).

Regarding fFN and CL, no statistically significant difference was seen within the AHR group (with *p*-values of 0.43 and 0.44 respectively). In the SYMP cohort, fFN levels were significantly higher in women who delivered prematurely ($p=0.03$). On the contrary, CL in the SYMP cohort did not yield any statistically significant difference based on birth outcome ($p=0.063$; Table 2.2).

The Clinical Microbiology Department at Sheffield NHS Teaching hospital only reported the presence of *Candida* spp in two charcoal swabs, both of which were retrieved from AHR women who delivered at term. As none of these patients complained of vulvovaginal candidiasis symptoms

at the time of the visit, the results were interpreted as a colonisation rather than an infection and did not prompt antibiotic treatment. No other microorganisms were isolated in any of the remaining swabs.

Table 2.2. Demographic and clinical data for the AHR and SYMP groups

Characteristics	**AHR** (n=21)		**SYMP** (n=25)	
	sPTB (n=10)	**Term** (n=11)	**sPTB** (n=12)	**Term** (n=13)
BMI (kg/m^2)	27.12 ± 7.33 (n=10)	27.27 ± 7.56 (n=11)	29.04 ± 12.09 (n= 11)	26.67 ± 5.60 (n= 10)
Maternal age (years)	30.7 ± 4.02 (n=10)	32.18 ± 5.31 (n=11)	32.08* ± 8.31 (n=12)	26.08 ± 6.24 (n=13)
fFN (ng/mL)	87.50 ± 164.47 (n=8)	24.29 ± 29.21 (n=7)	188.00** ± 208.82 (n=6)	11.00 ± 16.02 (n=8)
TVU CL (mm)	27.22 ± 15.03 (n=9)	31.36 ± 7.96 (n=11)	22.44 ± 13.17 (n=9)	34.17 ± 5.85 (n=6)
Gestational age at presentation (days)	151.9 ± 27.17 (n=10)	134.45 ± 29.09 (n=11)	201.42 ± 20.49 (n=12)	200.73 ± 35.71 (n=13)
Gestational age at delivery (days)	225.80## ± 34.21 (n=10)	272.64 ± 9.84 (n=11)	217.00***± 24.26 (n=12)	277.45 ± 7.06 (n=11)
Time to delivery from presentation (days)	73.90## ± 37.61 <2 weeks (n=2) 10-12 weeks (n=4) >12 weeks (n=4)	138.18 ± 25.64 >12 weeks (n=11)	14.62**** ± 13.63 <2weeks (n=8) 2-4 weeks (n=1) >4weeks (n=3)	76.73 ± 32.24 <2 weeks (n=0) 2-4 weeks (n=1) >4 weeks (n=10)
Ethnicity group White British Black African Asian	 80% (n=8) 20% (n=2) -	 82% (n=9) 9% (n=1) 9% (n=1)	 83.3% (n=10) 8.3% (n=1) 8.3% (n=1)	 69.2% (n=9) 15.4% (n=2) 15.4% (n=2)
Smoker	30% (n=3)	18% (n=2)	16.6% (n=2)	23% (n=3)

All data is presented as mean ± SD, BMI: body mass index, n= number of women for whom data is available
p=0.04 vs SYMP Term, **p=0.03 vs SYMP Term, *** p=0.03 vs SYMP Term,** p<0.01 vs SYMP Term,## p<0.01 vs AHR Term*

2.4.3. **Raman spectral profile of CVF in pregnancy**

Three swabs obtained from asymptomatic low-risk women in their mid-trimester were first analysed with RS as proof of concept. The average spectral profile obtained after analysing five

random points from their CVF samples was consistent with the data available on the spectroscopic signature of vaginal fluid in non-pregnant women reported in the literature (Figure 2.5; Sikirzhytskaya et al., 2012). In parallel, three sterile (unused) swabs were processed in PBS and prepared following the same experimental procedure to be used as negative controls. Smeared dried sterile PBS did not show any Raman activity thus no background control signal had to be subtracted from CVF RS data (data not presented).

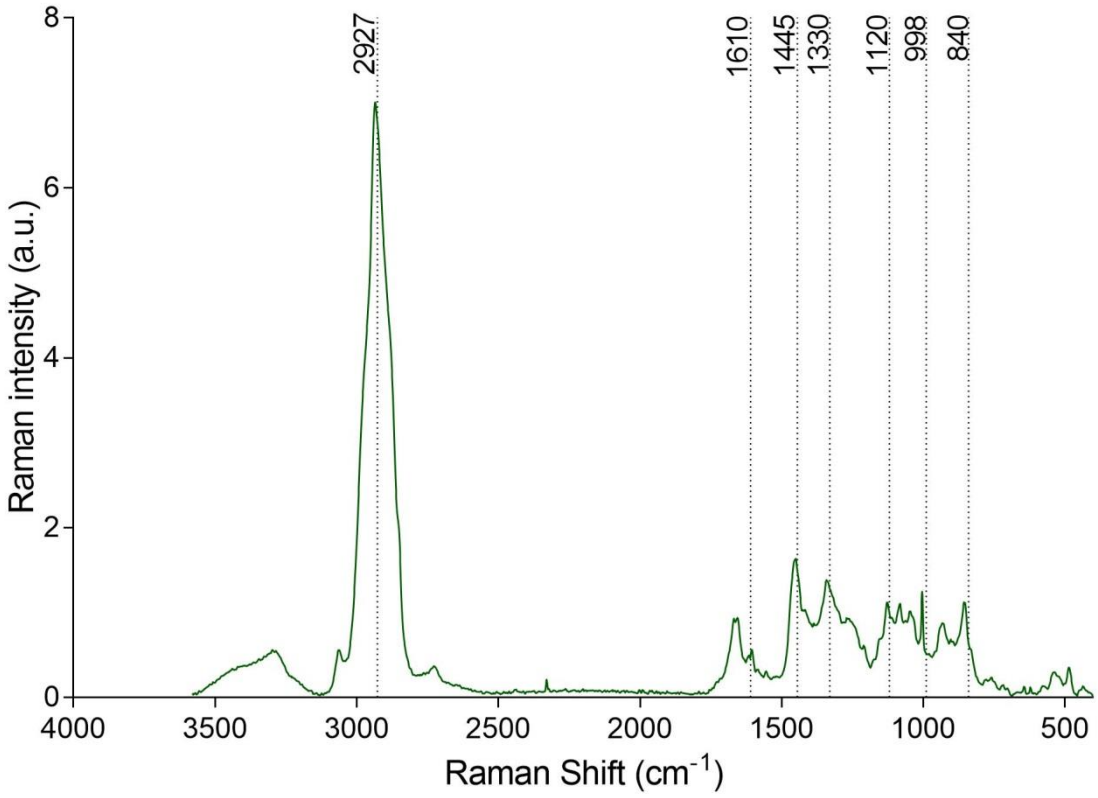

Figure 2.5. CVF spectral profile of low-risk asymptomatic pregnant women

Expanding upon these initial findings, I then processed and analysed all AHR and SYMP samples. I first analysed spectral differences based on the time to delivery and then assessed each region of the spectra separately to gain insight into the differences in CVF composition based on birth outcome.

2.4.4. **AHR: spectral differences based on time interval to delivery**

The general region within the AHR cohort was assessed based on the time interval between the gestational age at which the CVF was obtained and the gestational age at which birth occurred. Samples were grouped in three categories: delivery < 2 weeks (n=2), delivery within 10-12 weeks (n=4) and delivery > 12 weeks (n=15) as illustrated in Table 2.2.

Despite the small number of AHR women who delivered within two weeks of assessment (n=2), the high wavenumber and fingerprint spectral region were noted to significantly differ when compared to those who had a longer interval to delivery (Figure 2.6). Qualitatively, signals appeared to be lower for peaks at 2930, 1655 and 1338 cm^{-1} tentatively assigned to phospholipids and collagen respectively (Talari et al., 2015). On the contrary, bands at 1082, 1002, 930 and 850 cm^{-1}, normally associated with carbohydrate residues of collagen, phenylalanine, acetate and polysaccharides/disaccharides seemed to increase as the interval to delivery shortened, with the highest signals identified in women who delivered within two weeks of presentation (Ghartey et al., 2015, Talari et al., 2015, Amabebe et al., 2016a).

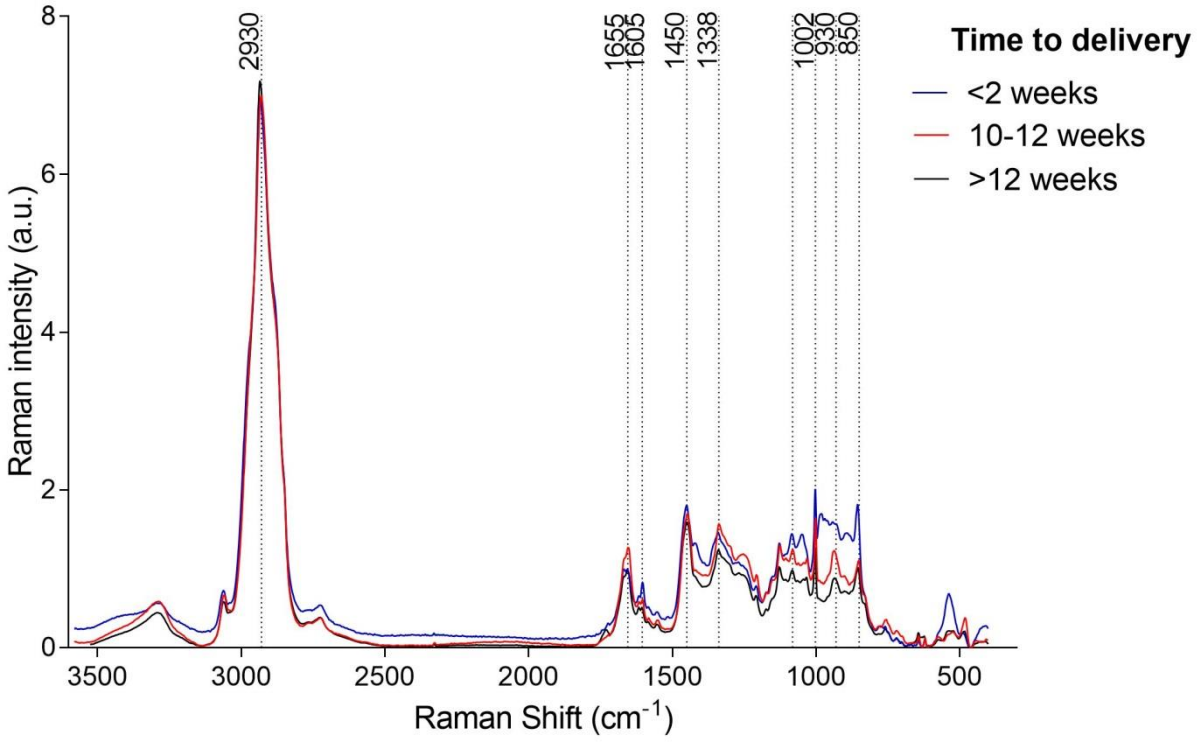

Figure 2.6. Comparison of the AHR general region spectra based on time to delivery from the moment of sampling

These qualitative differences were analysed in more depth using PCA. PC-1, which explained 40% of the variance seen across sample categories, did not enable full separation of the samples. The measurements from women who delivered within two weeks of presentation were considerably scattered in the right upper quadrant, with half of the points falling outside the Hotelling's ellipse (95% CI). These outliers corresponded to the only patient who delivered within a week of sampling and had an extreme PTB (Figure 2.7a).

The main differences in PC-1 were identified at bands 2930, 1730, 1330, 1002 and 635 cm^{-1} (Sikirzhytskaya et al., 2012, Talari et al., 2015, Amabebe et al., 2017). These findings suggested than women who had a shorter interval to delivery had higher signals for methionine and guanine, and lower for glutamic acids and CH_3 asymmetric stretch of lipids in their CVF compared to those who had a longer time to deliver (Figure 2.7b).

(a)

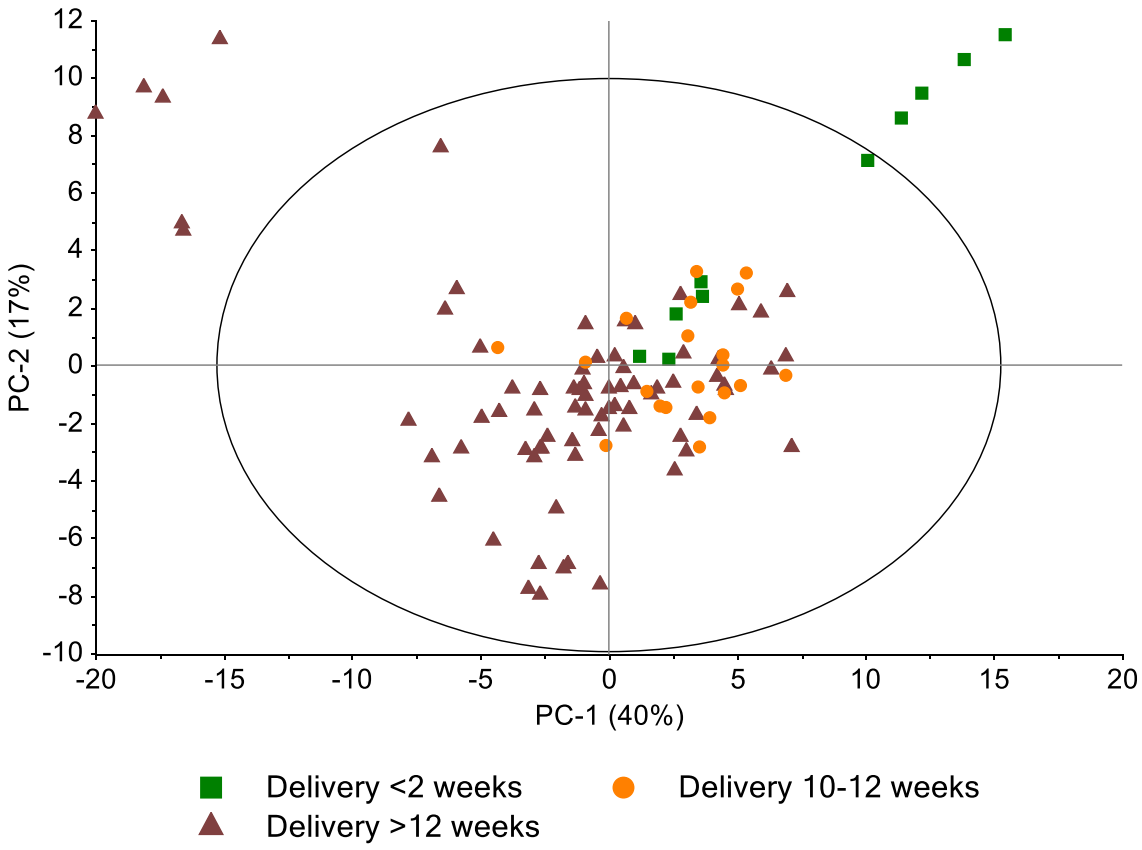

(b)

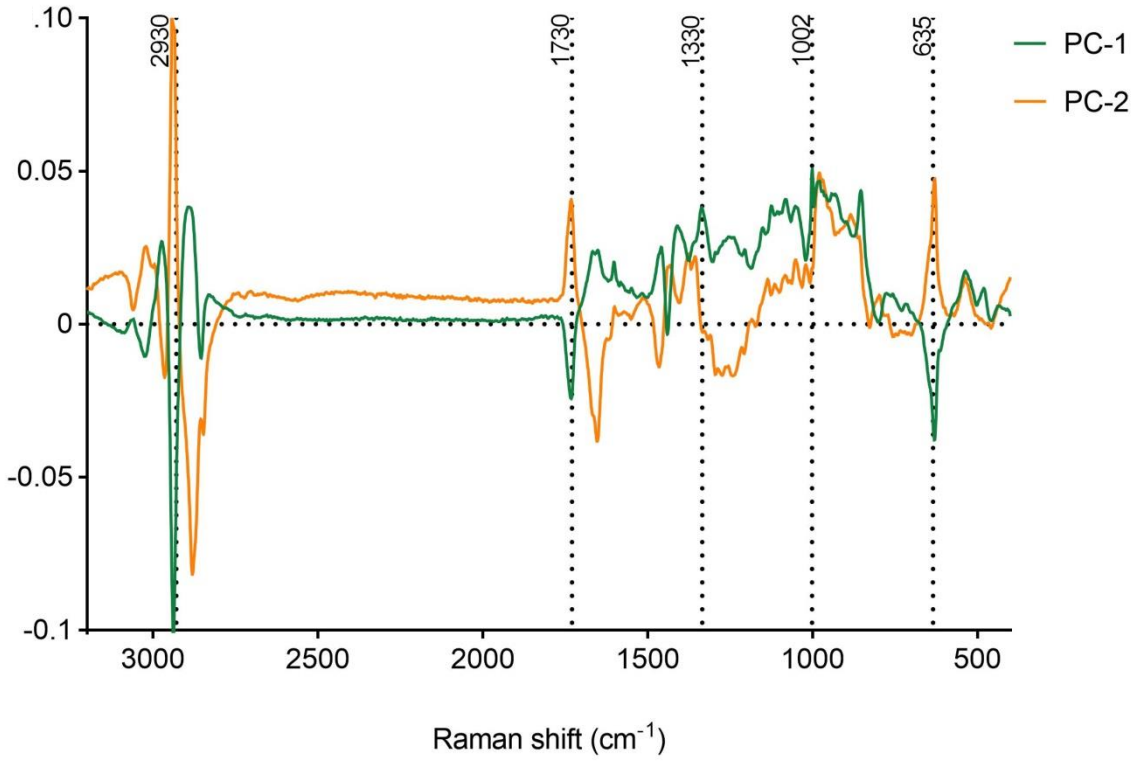

Figure 2.7. (a) A two-dimensional principal component analysis score plot of the general region of CVF in AHR women who delivered within two weeks, between 10-12 weeks and >12 weeks from presentation, and **(b)** loading plots of the general region representing principal components PC-1 (green) and PC-2 (yellow). *Values outside the ellipse in (a) represent outliers (Hotelling's T2, 95% CI).*

2.4.5. **SYMP: spectral differences based on time interval to delivery**

Similarly to AHR, the general region of the SYMP spectra was assessed based on the time interval between sampling and delivery. Samples were grouped in three categories: delivery within 2 weeks of assessment (n=8), delivery between 2-4 weeks of presentation (n=2) and delivery > 4 weeks (n=13) as represented in Figure 2.8.

Similarly to what was observed within the AHR cohort, signal intensity in the fingerprint region (1847-1400 cm^{-1}) appeared to be inversely proportional to the time interval to delivery. Qualitatively, women who delivered within two weeks of presentation appeared to have more prominent peaks at 1440 and 1330 cm^{-1}, tentatively assigned to proteins such as fibronectin, and also at 1002, 855 and 750 cm^{-1} linked to urea and aminoacids (Sikirzhytskaya et al., 2012); and lower signals identified at 1650-1640 cm^{-1} normally associated with collagen (Talari et al., 2015).

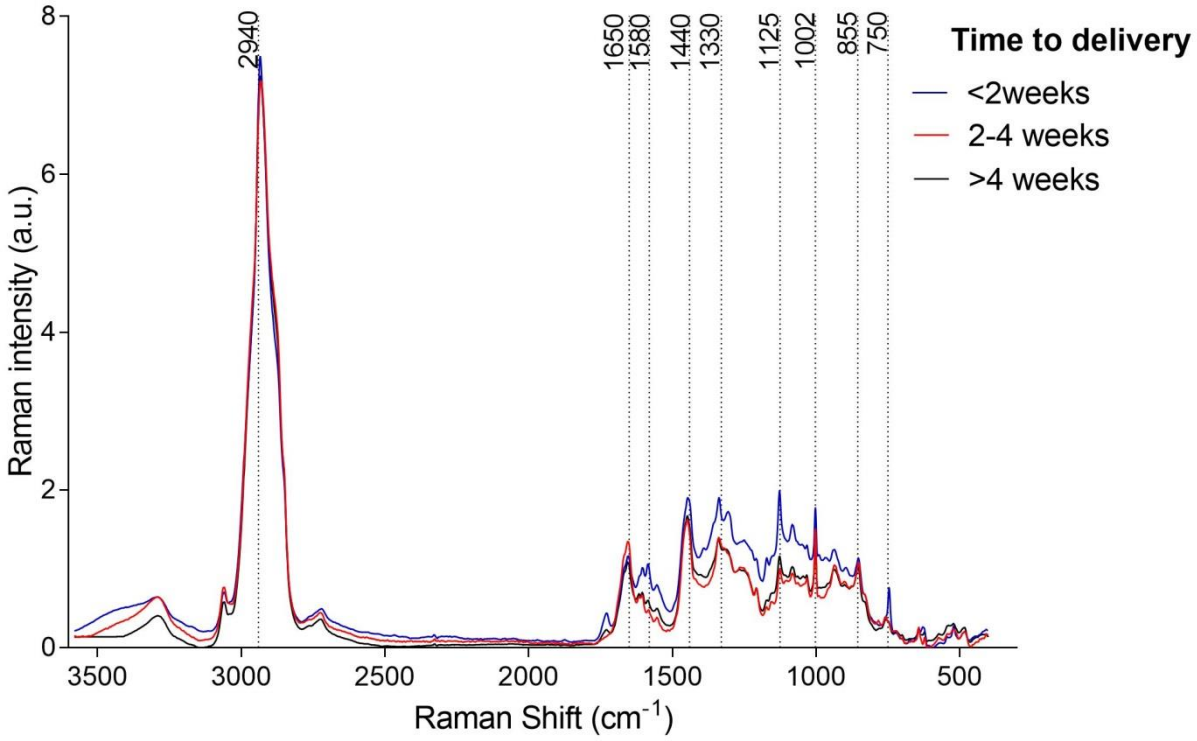

Figure 2.8. Comparison of the SYMP general region spectra based on time to delivery from the moment of sampling

The PCA revealed partial aggrupation of samples based on time to delivery (Figure 2.9). PC-1, responsible for 67% of the variance across the three different groups, showed most samples from women who delivered within two weeks clustered in the lower quadrants whereas women who delivered >4 weeks from presentation tended to be in the upper quadrants. The main differences between groups were noted at peaks 2940, 1580, 1002 and 855 cm^{-1} which may represent changes

in the symmetric stretching of lipids as well as in proteins like fibronectin and other components such as lactic acid, urea and aminoacids respectively (Sikirzhytskaya et al., 2012, Talari et al., 2015).

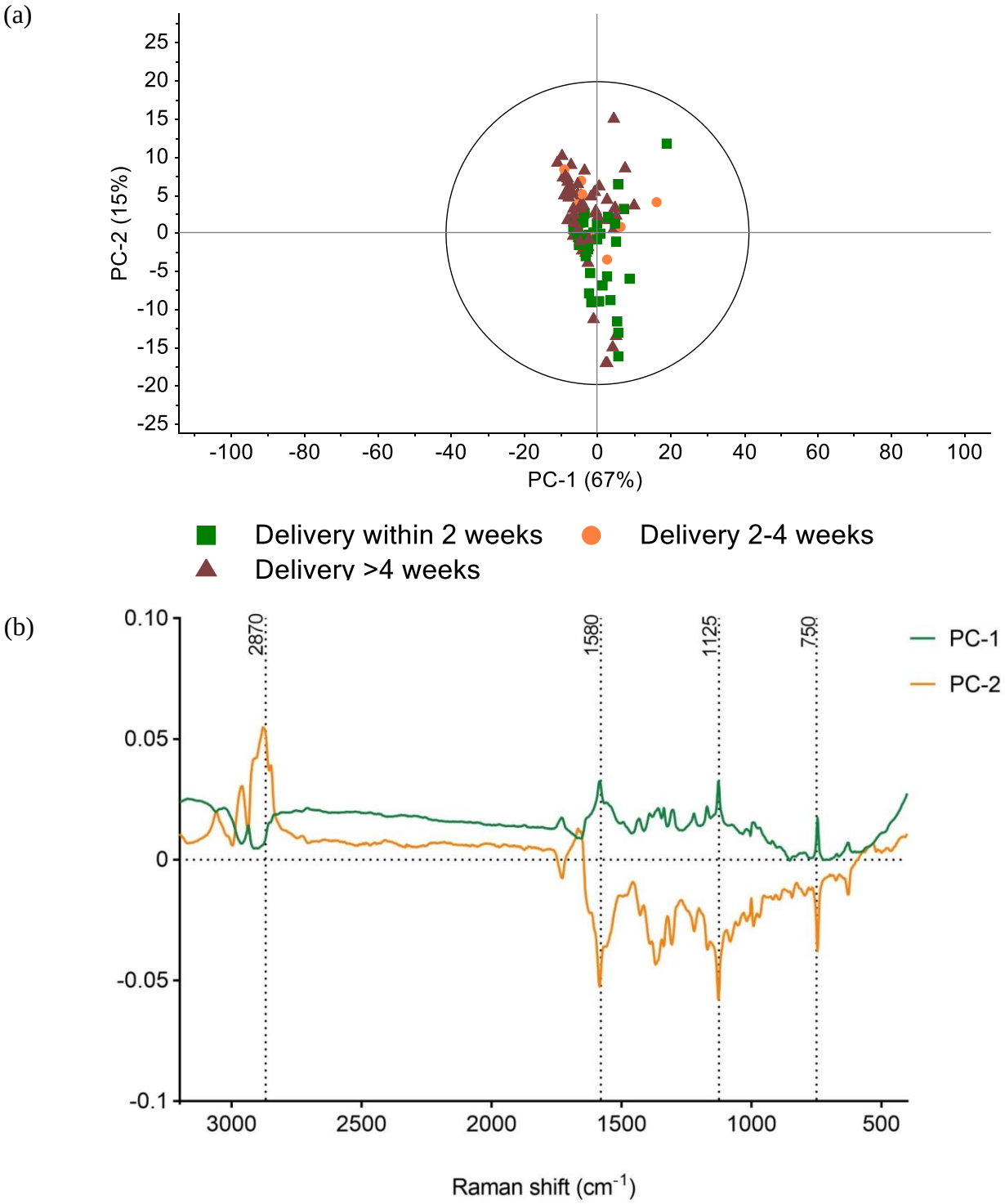

Figure 2.9. (a) A two-dimensional principal component analysis score plot of the general region of CVF in SYMP women who delivered within two weeks, between 2-4 weeks and >4 weeks from presentation, and **(b)** loading plots of the general region representing principal components PC-1 (green) and PC-2 (yellow). *Values outside the ellipse in (a) represent outliers (Hotelling's T2, 95% CI).*

2.4.6. **AHR group: spectral differences in the General region (GR)**

Following time to delivery analysis, AHR spectra were assessed based on delivery outcomes. The qualitative analysis of the whole Raman spectra (3300-400 cm^{-1}) in the AHR group showed that the most prominent peaks were located in the middle (1660-800 cm^{-1}) and higher wavenumber regions (3300-2800 cm^{-1}). These peaks were mainly due to stretching vibrations in the regions of proteins, nucleic acids, lipids and fatty acids (Sikirzhytskaya et al., 2012, Ramos et al., 2017). When the spectra were averaged and plotted per birth outcome, only minimal differences in peak intensities and peak shifts were identified (Figure 2.10).

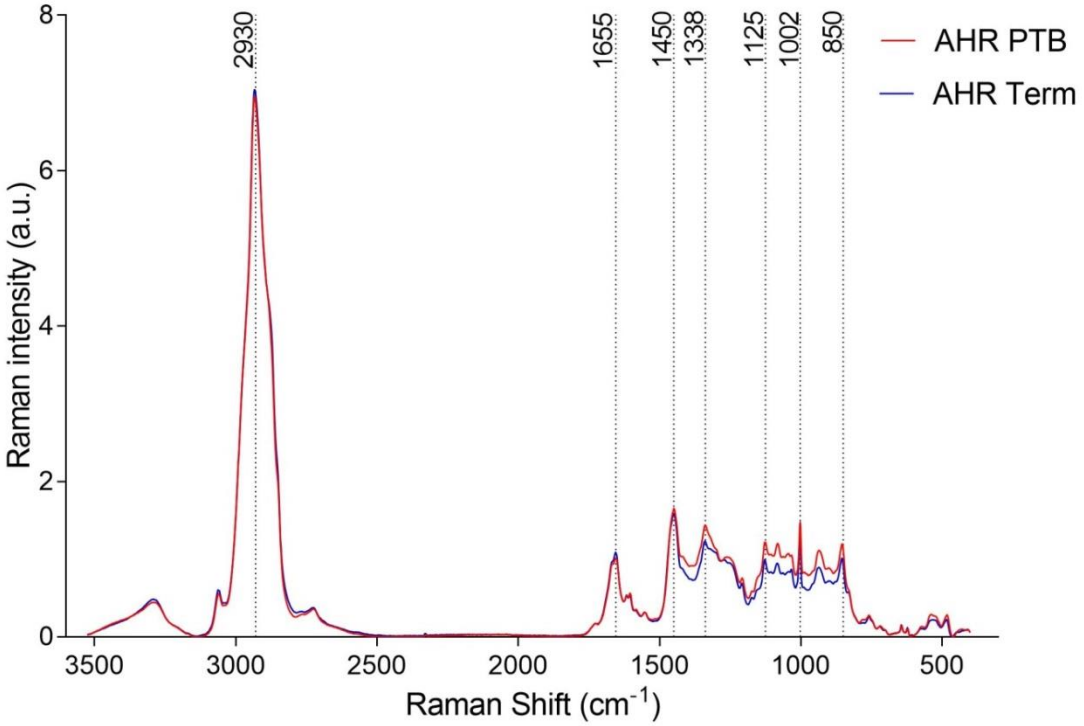

Figure 2.10. Comparison of the full mean spectra between AHR women who delivered preterm (red) and those who delivered at term (blue)

A multivariate approach using PCA was subsequently employed to reliably identify and quantify these minimal spectral differences between AHR women who delivered preterm and those who had a term delivery. Consistent with the qualitative findings, PCA only enabled partial aggrupation of samples. The first principal component (PC-1) was responsible for 42% of the variance seen in the general region. Based on the loading graph for PC-1, the main differences between women who delivered prematurely and those who delivered at term were located in wavelengths 2930, 1655, 1450, 1338, 1002 and 850-840 cm^{-1}. These observations suggested that CVF of women with a sPTB had higher RS signals for the regions belonging to total lactic acid,

proteins, acetate and urea in their mid-trimester CVF compared to their term counterparts (Figure 2.11).

(a)

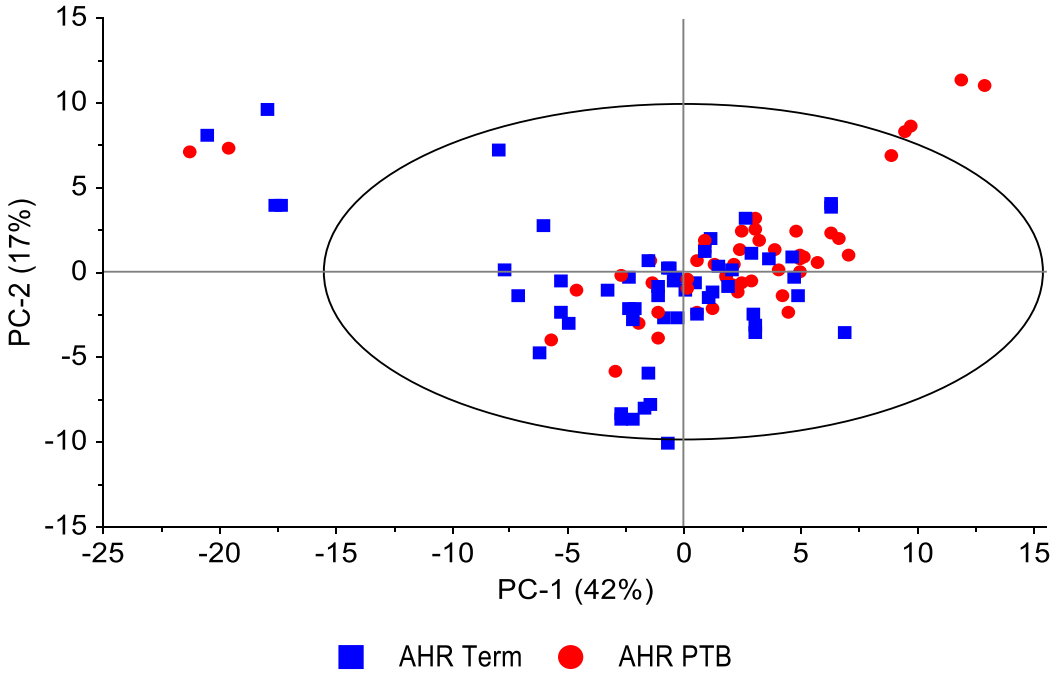

(b)

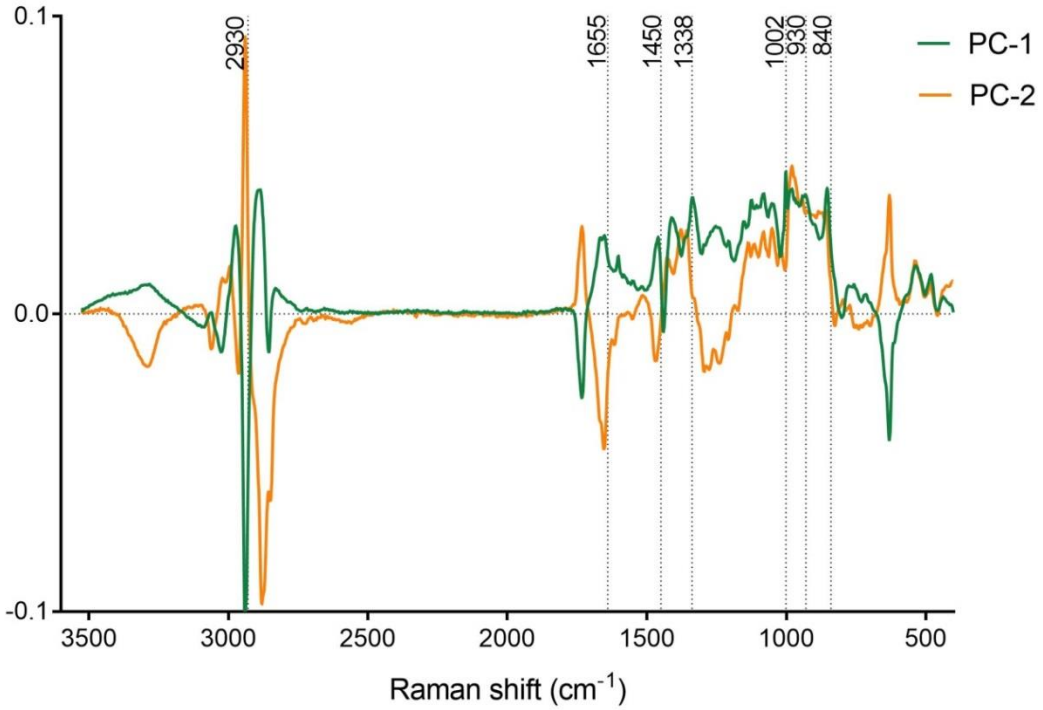

Figure 2.11. **(a)** A two-dimensional principal component analysis score plot of the general region of CVF in sPTB (red) and term (blue) AHR women, and **(b)** loading plots of the general region representing principal components PC-1 (green) and PC-2 (yellow). *Values outside the ellipse in (a) represent outliers (Hotelling's T2, 95% CI).*

2.4.7. **AHR group: spectral differences in the Fingerprint region (FP)**

Consistent with the findings in the general region, relatively higher peaks were seen in the fingerprint region (1847-400 cm^{-1}) of women who had a sPTB; this is the region with the more substance-specific pattern of the spectrum (Figure 2.12).

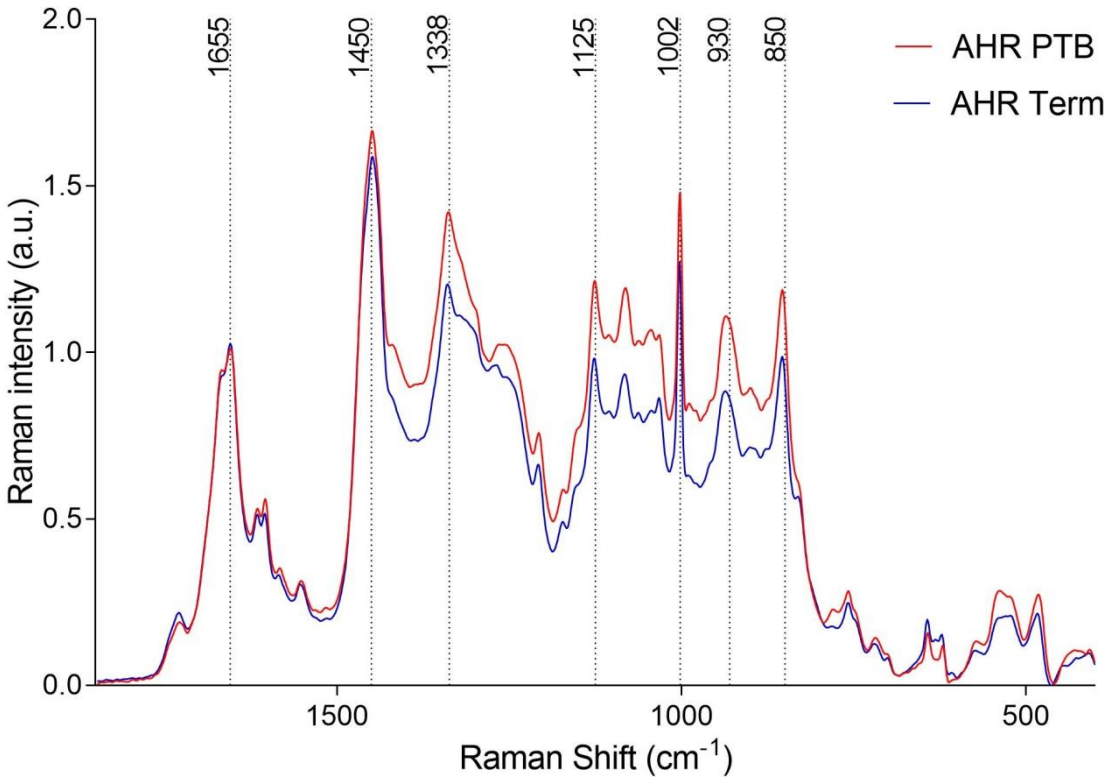

Figure 2.12. Comparison of the fingerprint spectra between AHR women who delivered preterm (red) and those who delivered at term (blue)

A subsequent principal component analysis of the FP region allowed better aggregation of samples between birth outcomes than the general region, with PC-1 being capable of explaining 54% of variance between the two groups (Figure 2.13). The major differences were seen in peaks at 1655, 1450, 1125 and 850 cm^{-1} but also at 1337, 1082 and 930 cm^{-1}. These peaks are normally associated with CH_2 twisting and CH_3 stretching of lipids, NCN stretching in urea and CC aromatic ring stretching of phenylalanine, CH_3 deformation in short-chain fatty acids (such as lactate) and amide I of α-helices of proteins collectively. All in all, women who delivered prematurely seemed to have higher values of conformational changes in proteins, total lactate, acetate and urea than those who delivered at term.

(a)

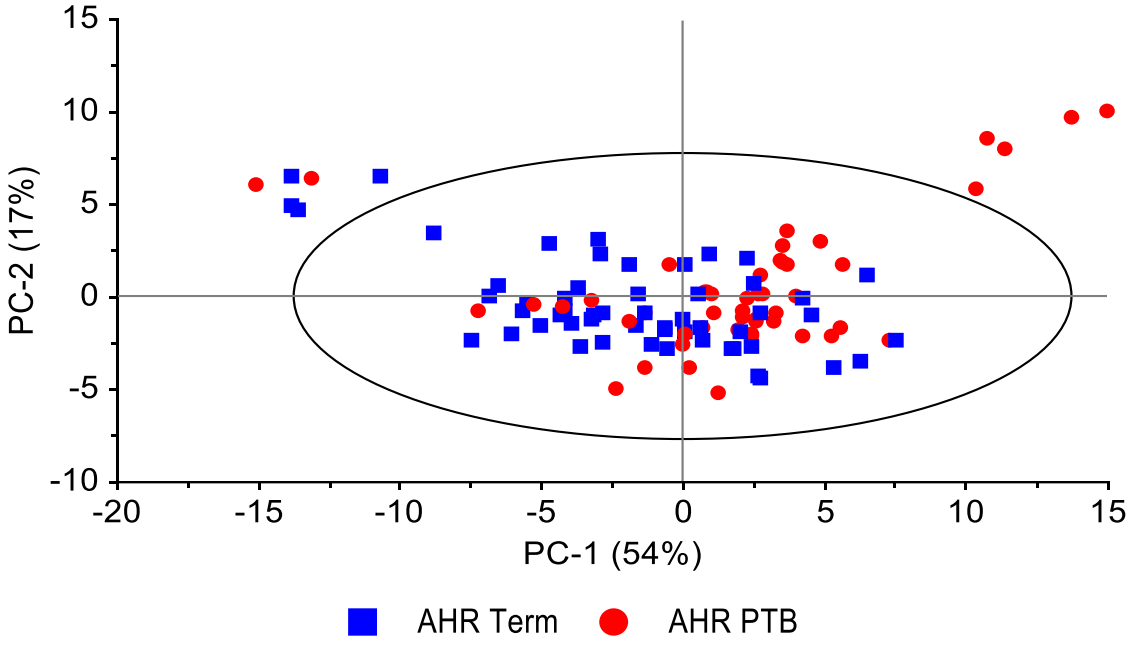

(b)

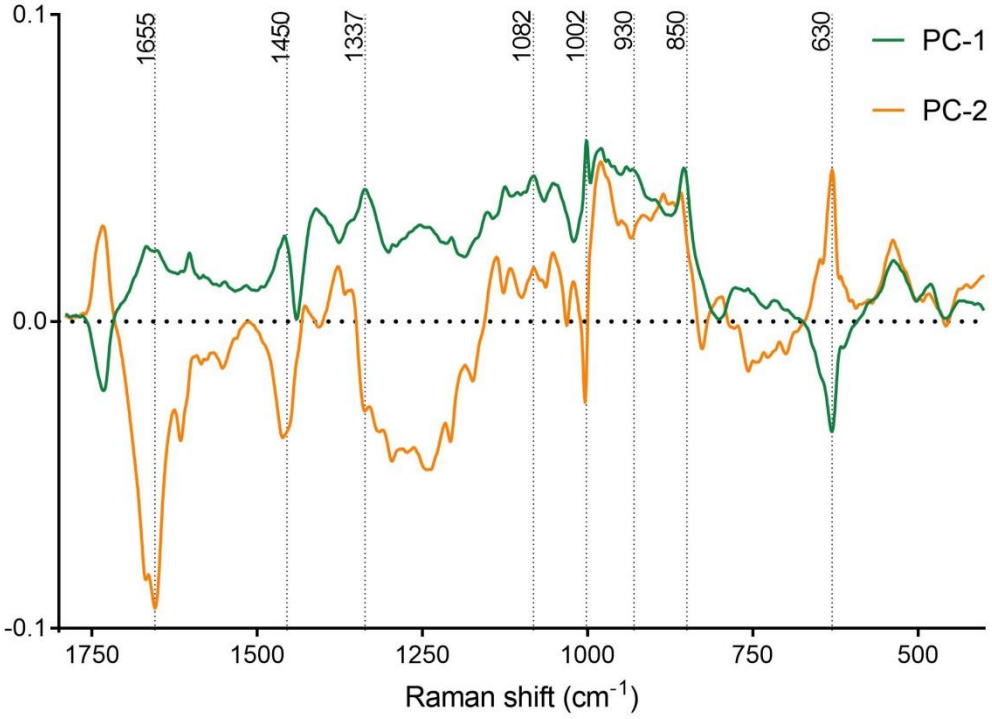

Figure 2.13. (a) A two-dimensional principal component analysis score plot of the fingerprint region of CVF in sPTB (red) and term (blue) AHR women, and **(b)** loading plots of the fingerprint region representing principal components PC-1 (green) and PC-2 (yellow). *Values outside the ellipse in (a) represent outliers (Hotelling's T2, 95% CI).*

2.4.8. **AHR group: spectral differences in the Amide region (A)**

When the amide spectra (1799-1099 cm^{-1}) was averaged and plotted per birth outcome, the profiles did not completely overlap which suggested certain differences between the two groups (Figure 2.14). Overall, the intensity of the peaks seemed higher in women who delivered preterm compared to those who delivered at term.

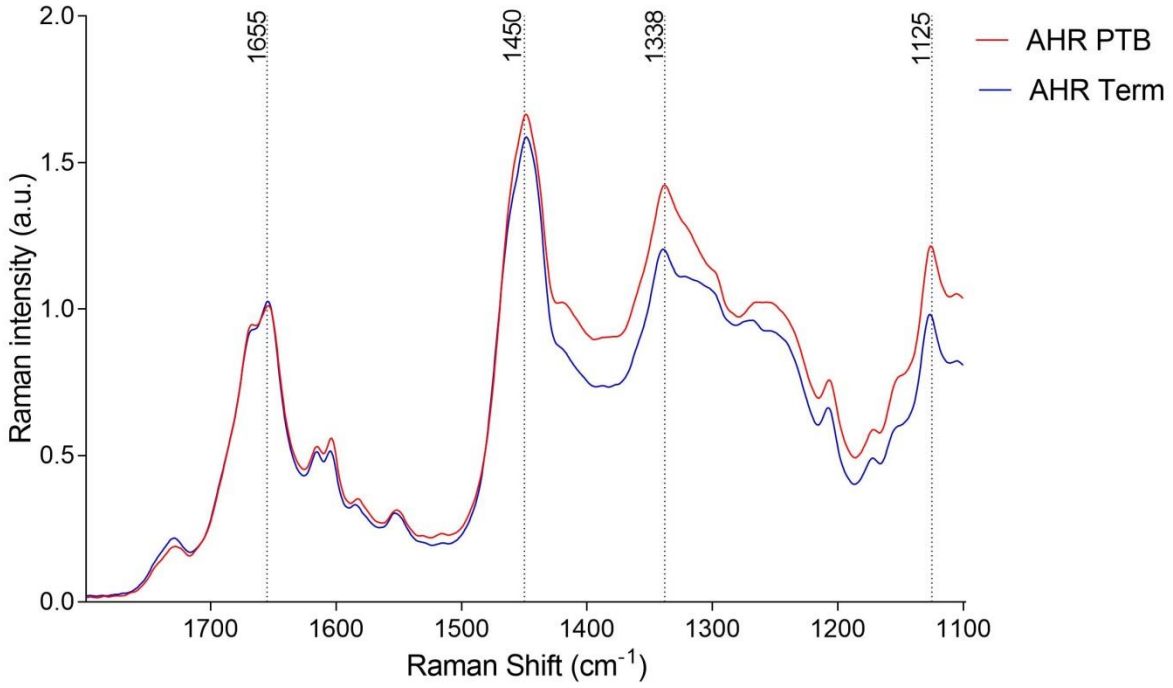

Figure 2.14. Comparison of the amide region spectra between AHR women who delivered preterm (red) and those who delivered at term (blue)

PC-1, which was capable of explaining 60% of the variation in the data, clearly separated samples based on birth outcomes (Figure 2.15). The main differences were seen at wavelengths 1655, 1445-1455, 1330-1337 cm-1 and 1120-1125 cm^{-1}, which are characteristically assigned to $\nu_{as}COO^-$ of lactic acid, $\delta_{as}CH_3$ and δCH of proteins, and $\nu C\text{-}CH_3$ of lactate, respectively (Berjot et al., 1987, Sikirzhytskaya et al., 2012). Overall, short-chain fatty acids and secondary conformation of the proteins in the samples seemed to significantly differ based on the time of delivery.

(a)

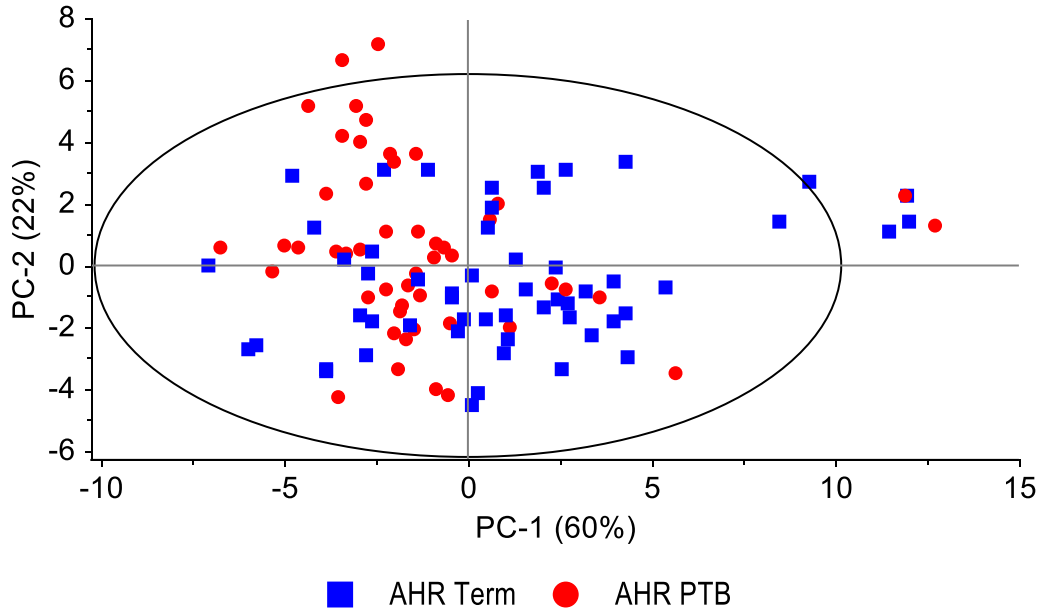

(b)

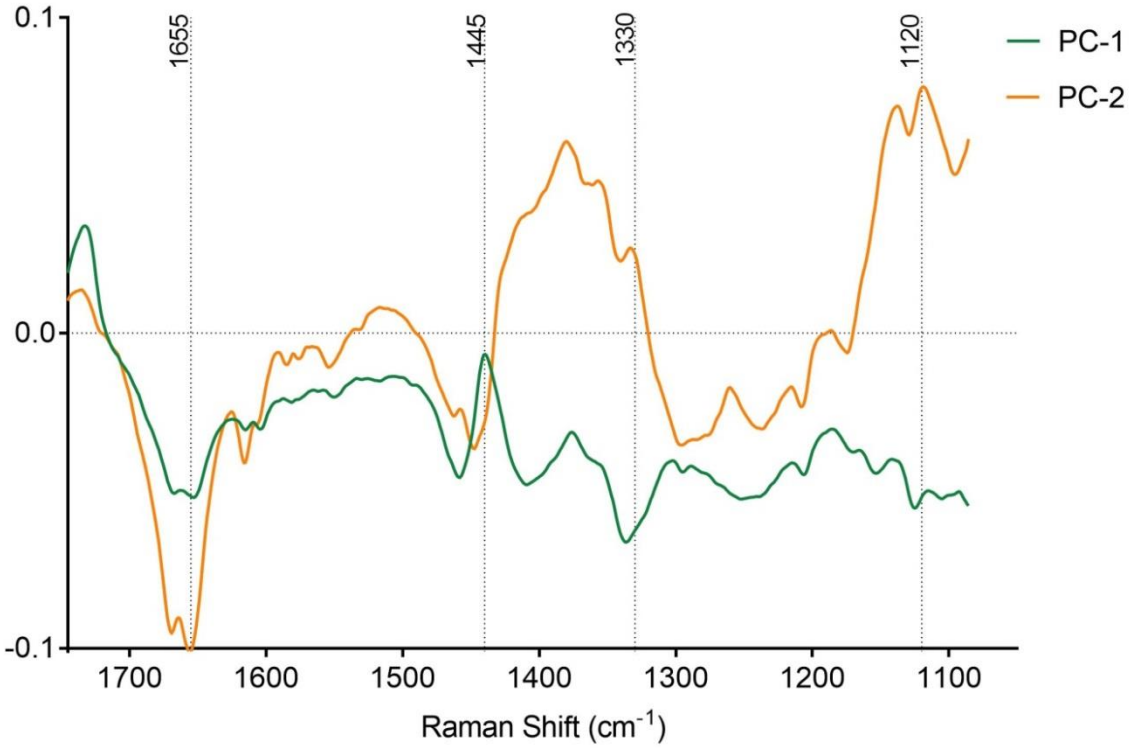

Figure 2.15. (a) A two-dimensional principal component analysis score plot of the amide region of CVF in sPTB (red) and term (blue) AHR women, and **(b)** loading plots of the amide region representing principal components PC-1 (green) and PC-2 (yellow). *Values outside the ellipse in (a) represent outliers (Hotelling's T2, 95% CI).*

2.4.9. **AHR group: spectral differences in the Amide I region (A1)**

Within the amide spectral profile, amide band I (1799-1487 cm^{-1}) was specifically looked at in an attempt to identify differences linked to secondary conformation of proteins (β-sheet and α-helix structure) based on birth outcomes (Movasaghi et al., 2007). When the average spectra were plotted for each delivery outcome, higher intensity peaks were seen at 1670-1655 cm^{-1} in those who delivered at term. However, these differences appeared to be minimal (Figure 2.16).

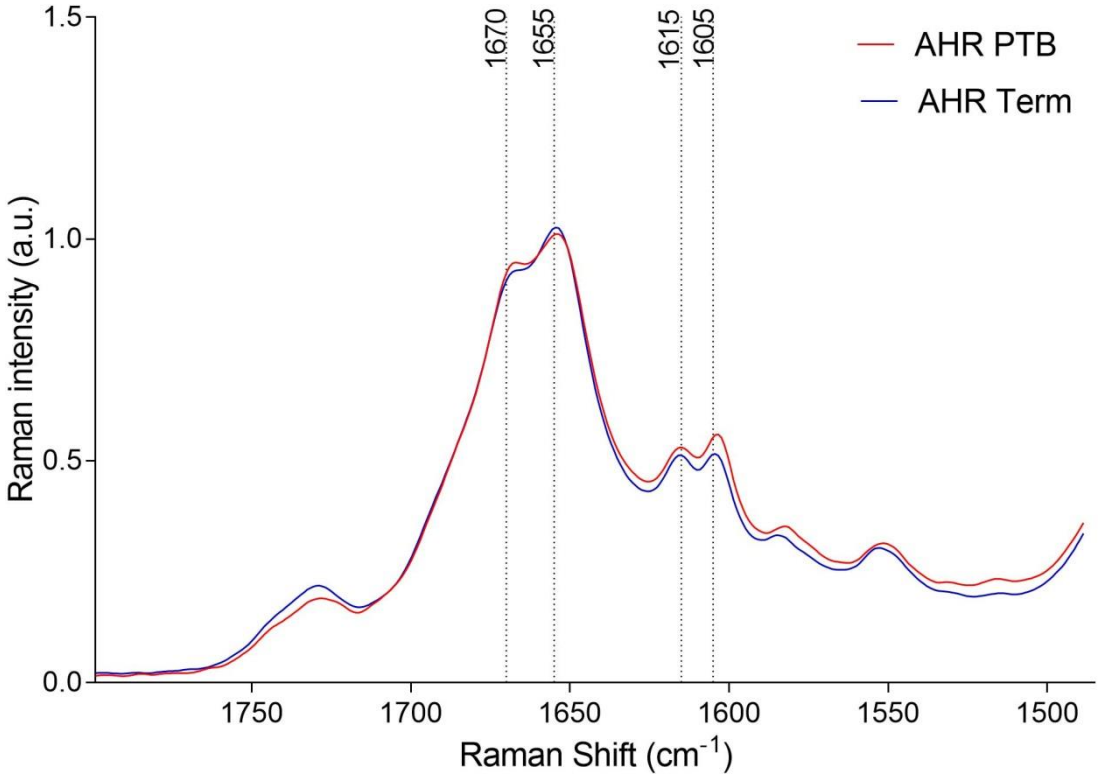

Figure 2.16. Comparison of the amide I region spectra between AHR women who delivered preterm (red) and those who delivered at term (blue)

Consistently, PCA of this region failed to produce a well-defined aggrupation pattern for AHR samples based on delivery outcomes (Figure 2.17). PC-1, responsible for 67% of the variation, enabled only partial separation of samples. As with the preliminary qualitative analysis, main differences were seen at 1660-1650 cm^{-1}, normally assigned to C=O stretch of α-helix proteins and νNH_2 of urea (Ngarize et al., 2004, Sikirzhytskaya et al., 2012).

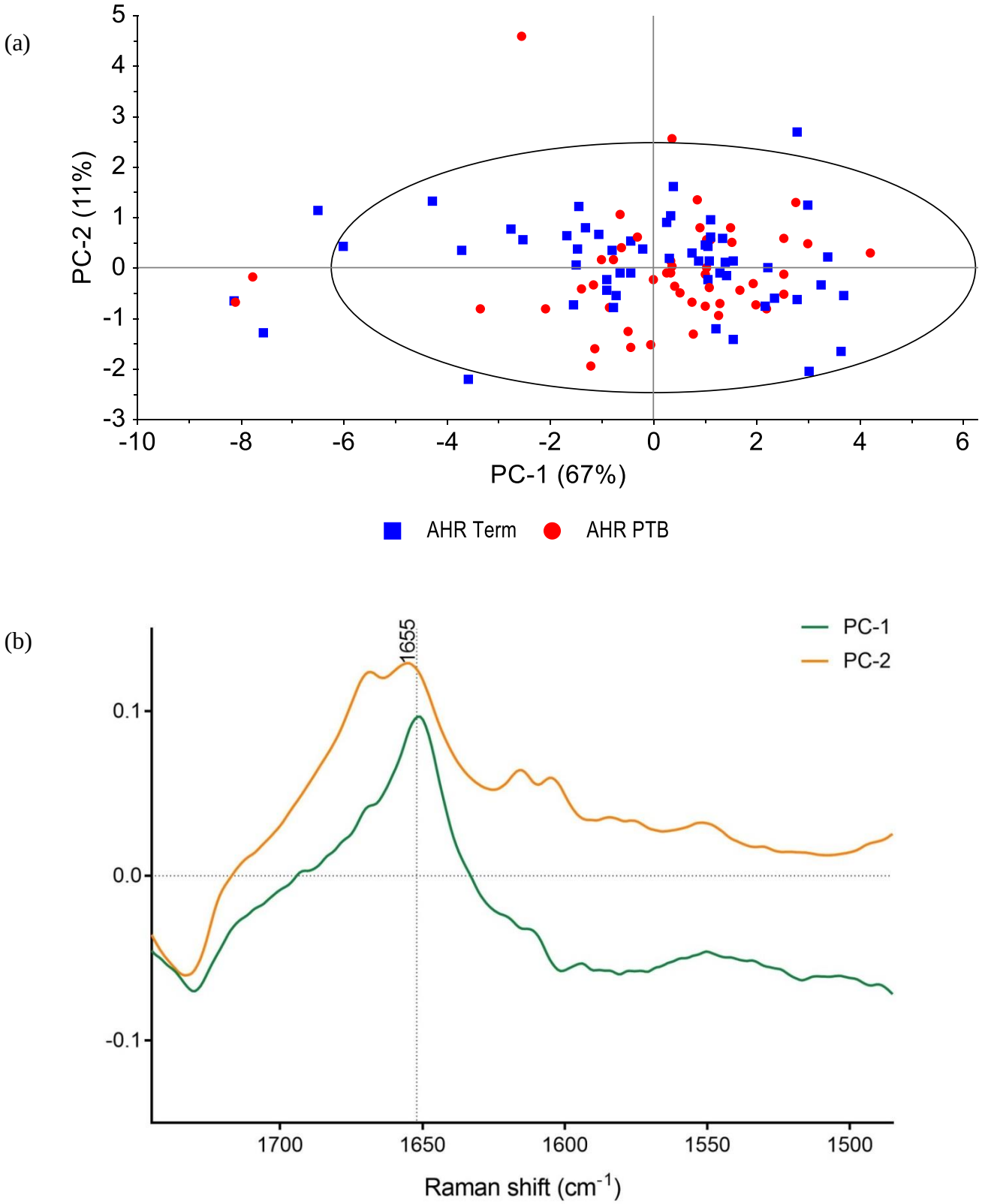

Figure 2.17. (a) A two-dimensional principal component analysis score plot of the amide I region of CVF sPTB (red) and term (blue) AHR women, and **(b)** loading plots of the amide I region representing principal components PC-1 (green) and PC-2 (yellow). *Values outside the ellipse in (a) represent outliers (Hotelling's T2, 95% CI).*

2.4.10. **AHR group: spectral differences in the Amide II region (A2)**

Continuing the in-depth analysis of the amide region, the amide II band (1487-1358 cm^{-1}) was assessed next. When the average spectra were plotted based on birth outcome, profiles almost seemed to mirror each other, with only minimal differences seen in intensity (Figure 2.18).

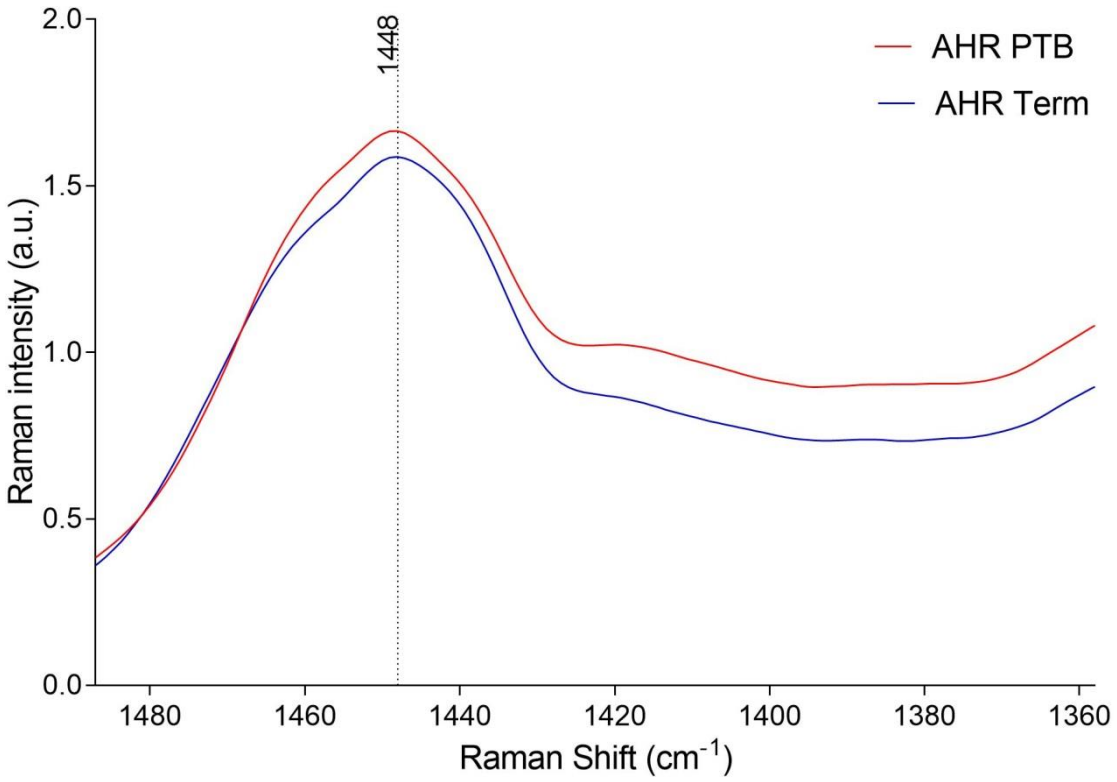

Figure 2.18. Comparison of the amide II region spectra between AHR women who delivered preterm (red) and those who delivered at term (blue)

Nonetheless, when this region was analysed in more detail with PCA, samples were better grouped than in amide I. PC-1 was capable of explaining 73% of the variation seen in the specimens, with main differences identified at 1450-1440 cm^{-1}, which is normally assigned to $\delta_{as}CH_3$ in short-chain fatty acids (Figure 2.19).

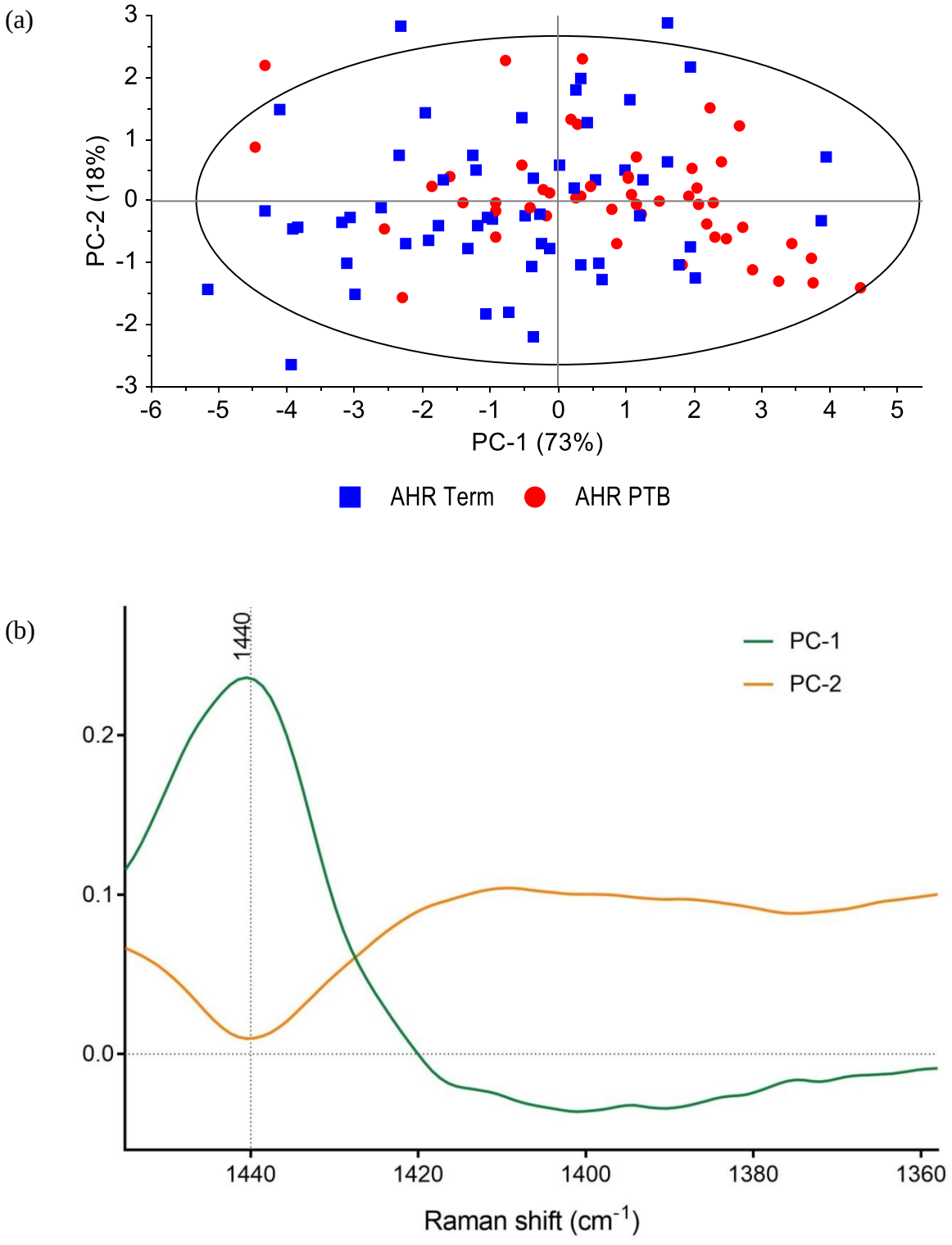

Figure 2.19. (a) A two-dimensional principal component analysis score plot of the amide II region of CVF in sPTB (red) and term (blue) AHR women, and **(b)** loading plots of the amide II region representing principal components PC-1 (green) and PC-2 (yellow). *Values outside the ellipse in (a) represent outliers (Hotelling's T2, 95% CI).*

2.4.11. **AHR group: spectral differences in the Amide III region (A3)**

When the amide band III (1358-1099 cm^{-1}) was analysed within the AHR cohort, some differences in intensity and frequency shift were noted between delivery outcomes. With the exception of a few bands between 1300 and 1250 cm^{-1}, peaks seemed to be noticeably higher in women who delivered prematurely (Figure 2.20).

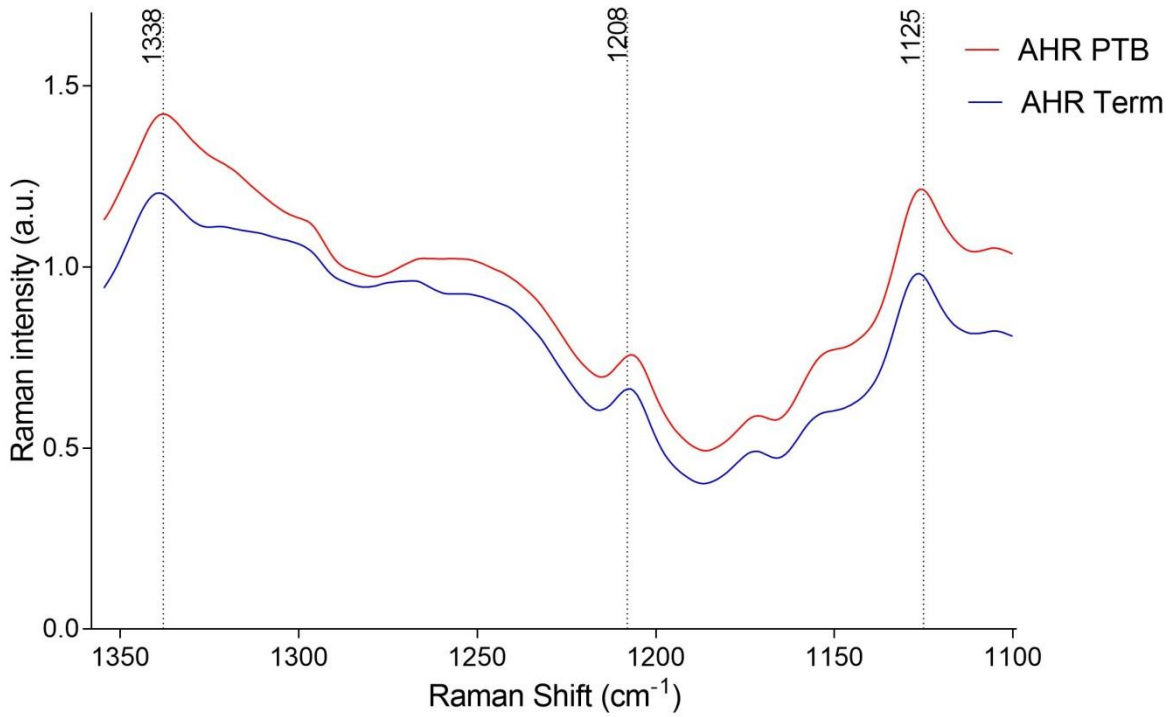

Figure 2.20. Comparison of the amide III region spectra between AHR women who delivered preterm (red) and those who delivered at term (blue)

Consistent with these preliminary qualitative findings, PCA of the amide III region displayed significant aggrupation of AHR samples based on birth outcome, with PC-1 being able to explain 76% of the variance seen in the samples (Figure 2.21). Higher signals were identified at 1125 cm^{-1}, a Raman band which is typically assigned to δCH in proteins, νC-CH_3 in lactic acid and ρNH_2 in urea (Figure 2.17; Movasaghi et al., 2007, Sikirzhytskaya et al., 2012, Talari et al., 2015).

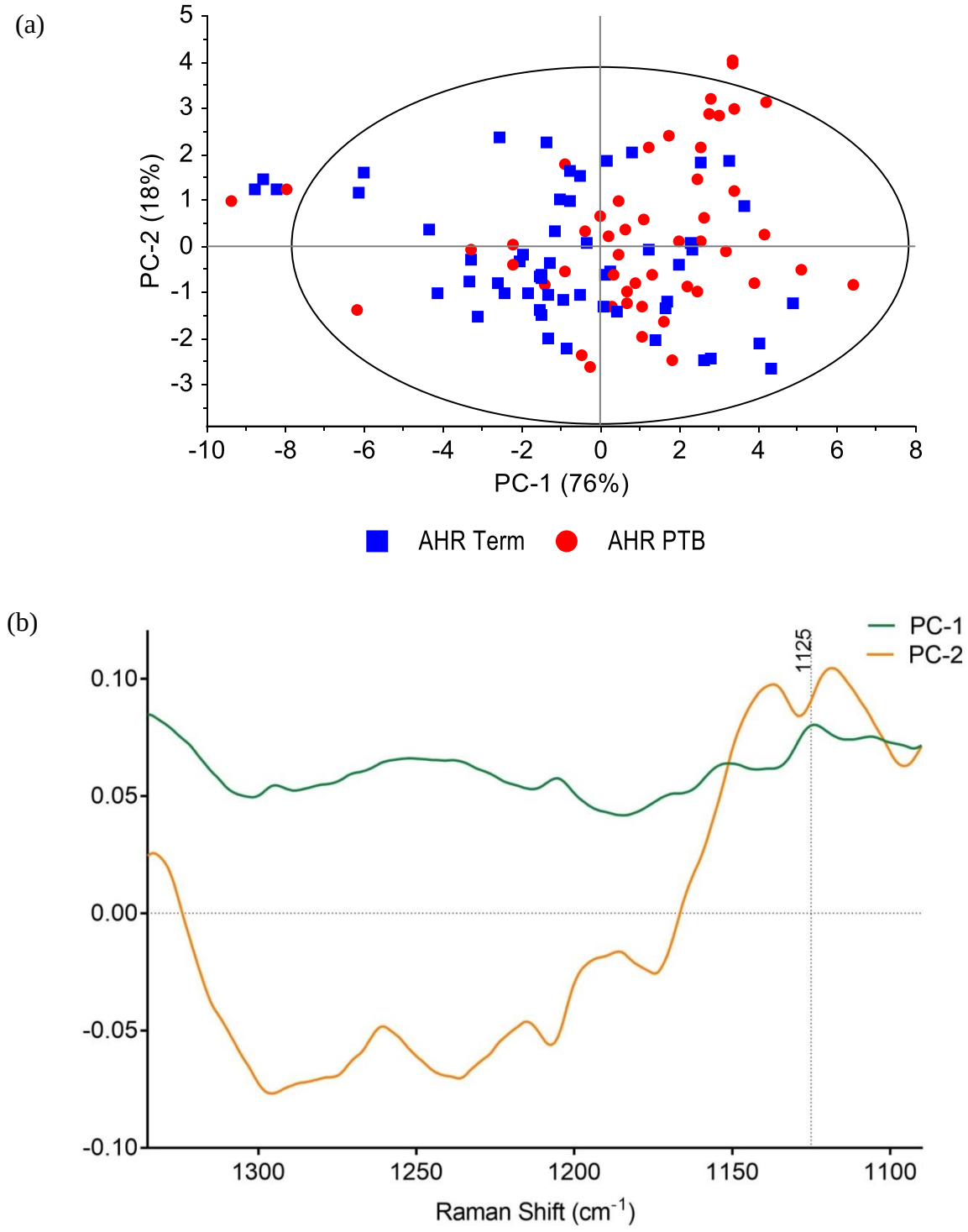

Figure 2.21. (a) A two-dimensional principal component analysis score plot of the amide III region of CVF in sPTB (red) and term (blue) AHR women, and **(b)** loading plots of the amide III region representing principal components PC-1 (green) and PC-2 (yellow). *Values outside the ellipse in (a) represent outliers (Hotelling's T2, 95% CI).*

2.4.12. **AHR group: spectral differences in the Aminoacids region (AA)**

The spectral region associated with aminoacids (878-480 cm^{-1}) also enabled partial differentiation of the AHR samples between birth outcomes (Figure 2.22).

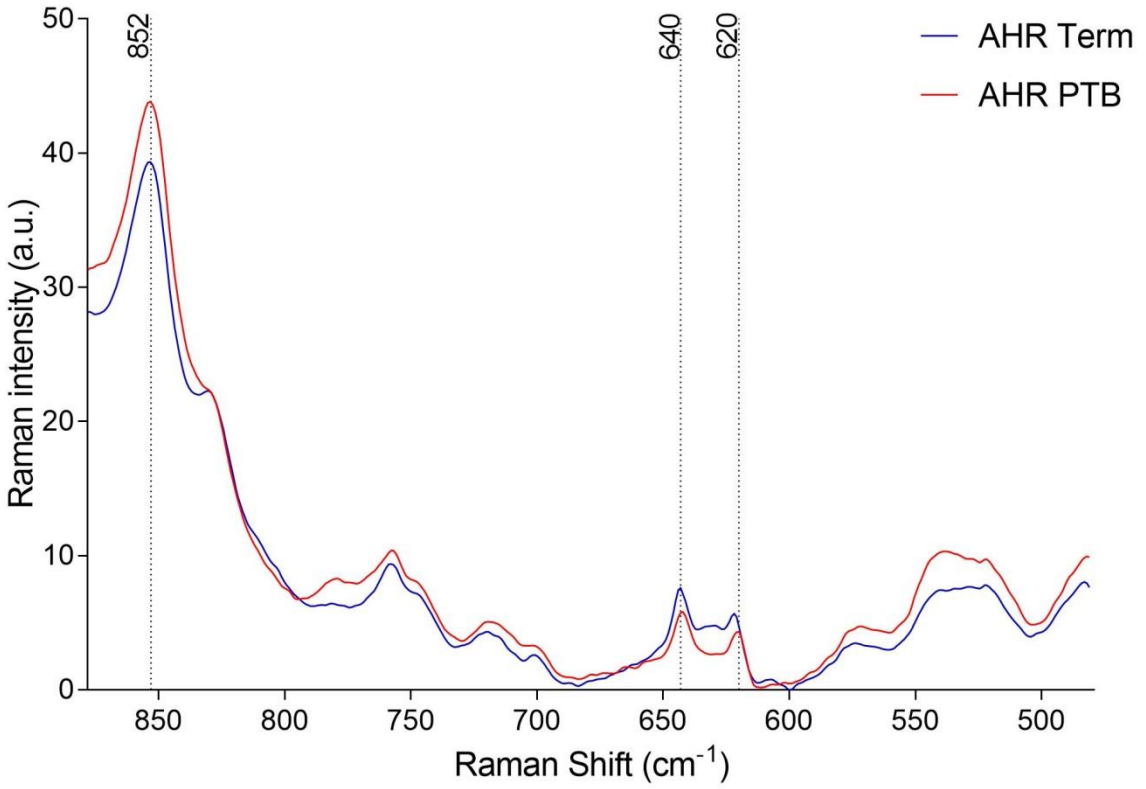

Figure 2.22. Comparison of the AA region spectra between AHR women who delivered preterm (red) and those who delivered at term (blue)

When PCA was applied, PC-1 was responsible for 60% of the variance seen. Women who delivered prematurely had higher values at 850 cm^{-1} and lower peaks at 640-630 cm^{-1} than their term counterparts. These bands have previously been linked to stretching vibrations of tyrosine and valine, and ν(C-S) vibration of methionine respectively (Sikirzhytskaya et al., 2012, Talari et al., 2015). These initial observations suggest the CVF of women who delivered prematurely may have different concentrations of some essential aminoacids when compared to those who had a term delivery (Figure 2.23).

(a)

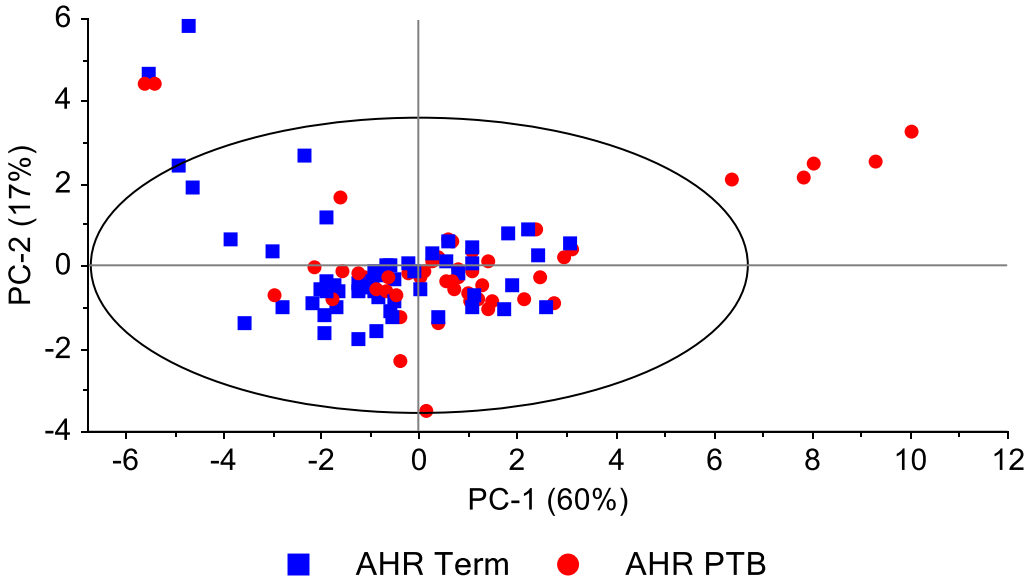

(b)

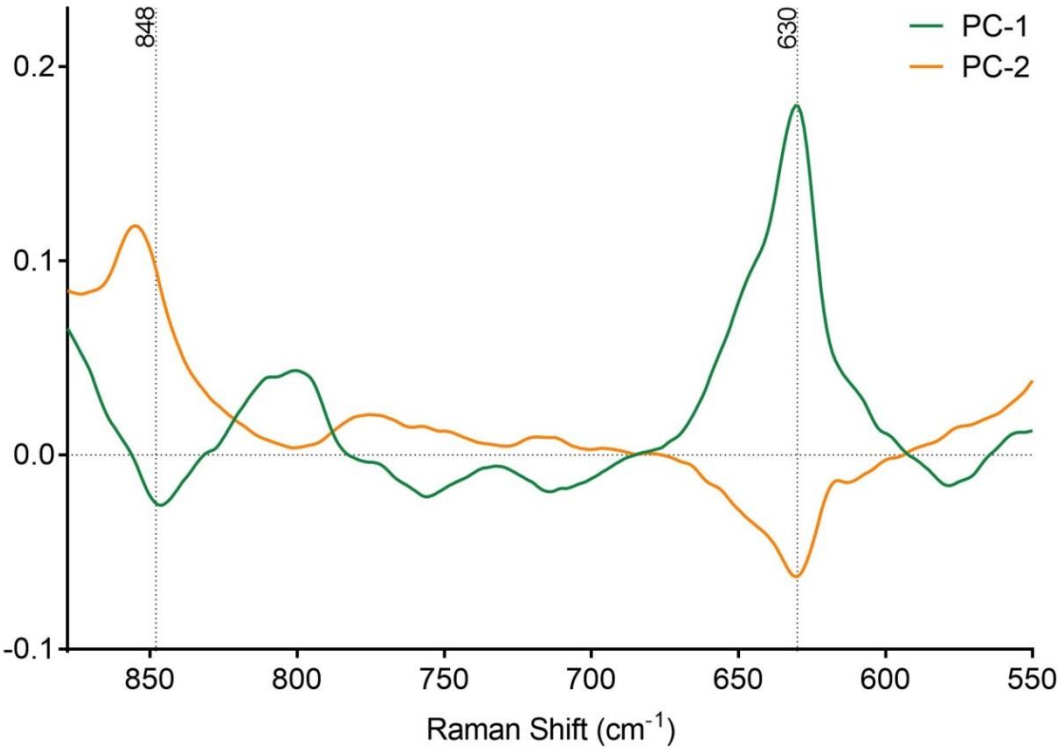

Figure 2.23. (a) A two-dimensional principal component analysis score plot of the aminoacids region of CVF in sPTB (red) and term (blue) AHR women, and **(b)** loading plots of the aminoacids region representing principal components PC-1 (green) and PC-2 (yellow). *Values outside the ellipse in (a) represent outliers (Hotelling's T2, 95% CI).*

2.4.13. **AHR group: spectral differences in the High wavenumber region (HWN)**

When the HWN region spectra (3300-2600 cm^{-1}) were averaged and plotted per birth outcome, minimal differences were identified between the two groups (Figure 2.24). Only at 2940-2930 cm^{-1} were higher signals seen for women who delivered at term. These peaks have been linked to the CH_2 stretching of the methylene groups of lipids in the vaginal mucosa (Orphanou et al., 2015).

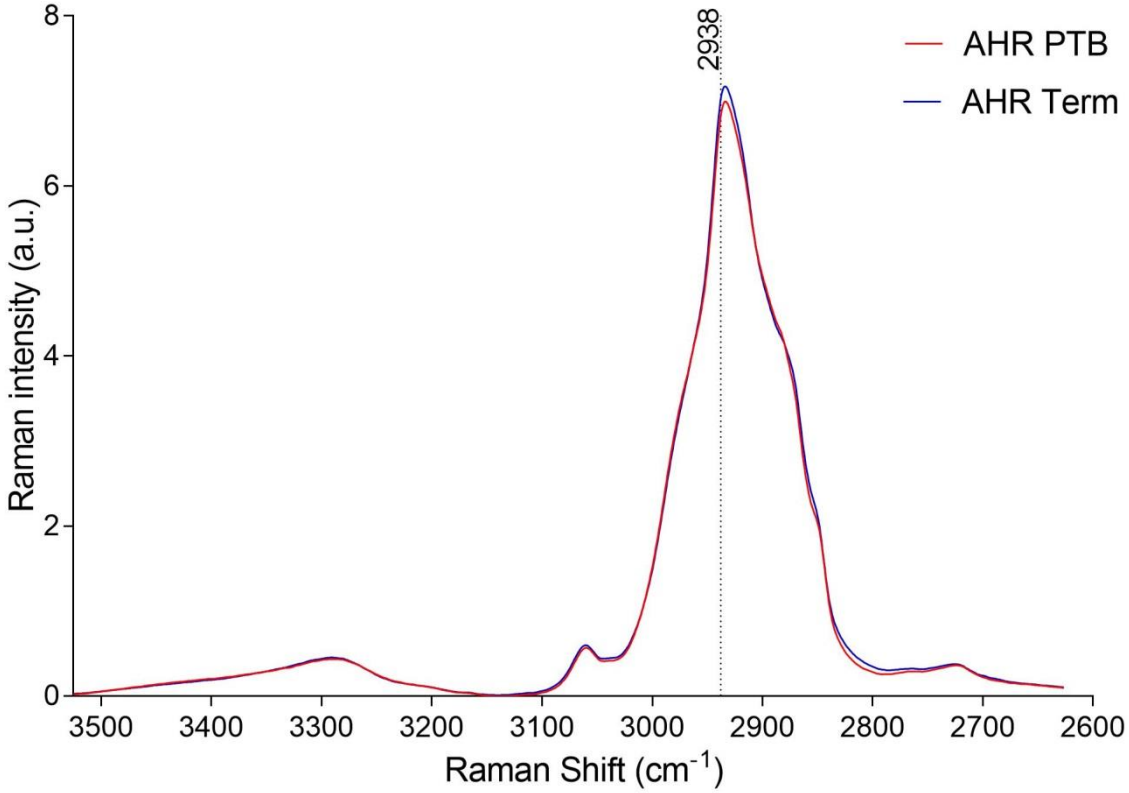

Figure 2.24. Comparison of the high wavenumber region spectra between AHR women who delivered preterm (red) and those who delivered at term (blue)

PC-1 (56%) enabled partial grouping of AHR samples based on delivery outcomes as seen in Figure 2.25. Main differences were seen at 2940-2930 and 2855-2850 cm^{-1} which have been previously assigned to the chain-end CH_3 bands of proteins and lipids, and the CH_2 symmetric stretch of lipids respectively.

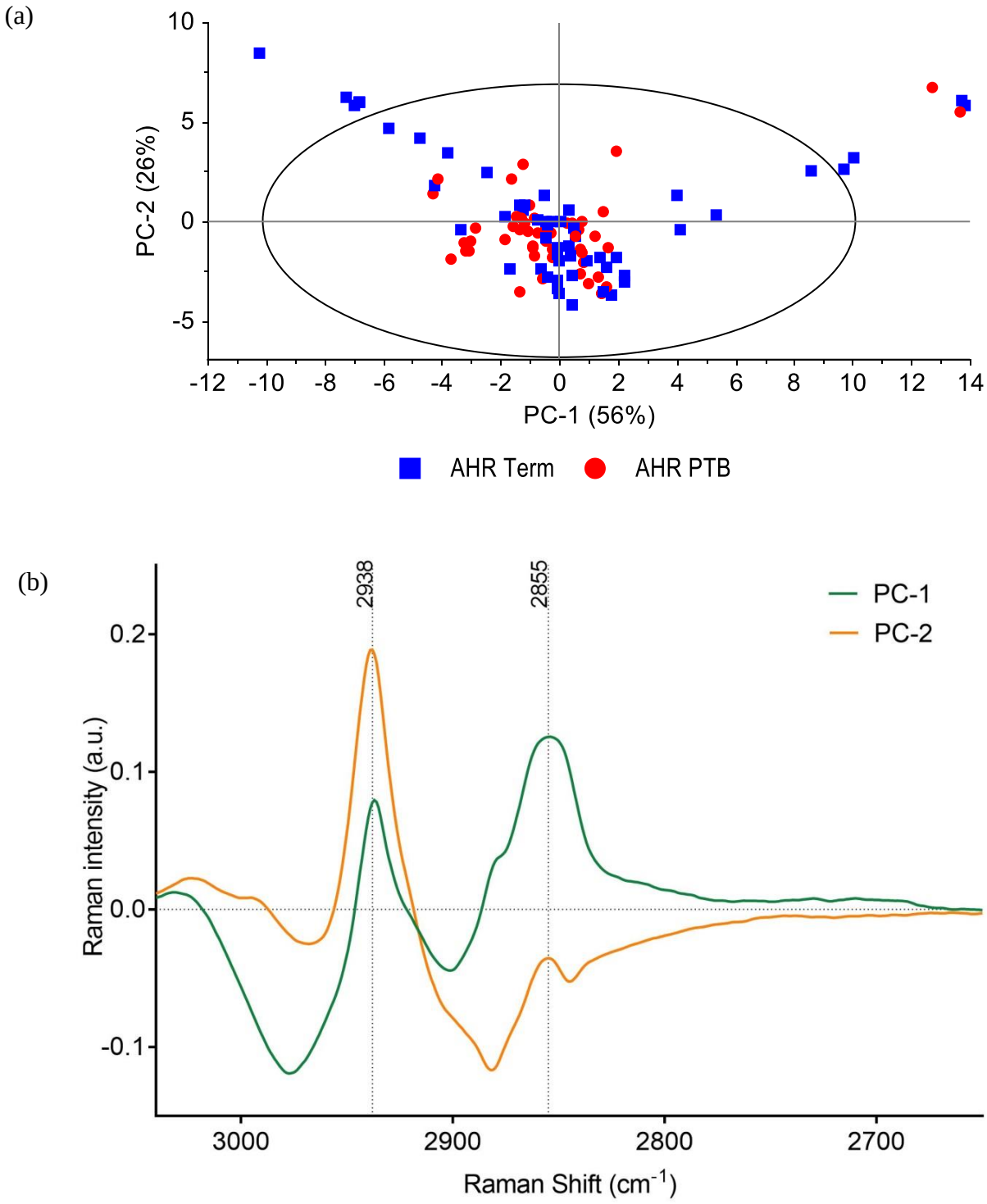

Figure 2.25. (a) A two-dimensional principal component analysis score plot of the high wavenumber region of CVF in sPTB (red) and term (blue) AHR women, and **(b)** loading plots of the high wavenumber region representing principal components PC-1 (green) and PC-2 (yellow). *Values outside the ellipse in (a) represent outliers (Hotelling's T2, 95% CI).*

2.4.14. **SYMP group: spectral differences in the General region (GR)**

Similarly to the findings in the AHR group, when the whole Raman spectra (3300-400 cm^{-1}) was analysed in the SYMP cohort, the most prominent peaks were identified in bands between 1660-800 cm^{-1} and 3300-2800 cm^{-1}. These bands are normally assigned to stretching and bending vibrations in nucleic acids, fatty acids, lipids and proteins (Sikirzhytskaya et al., 2012). Compared to AHR, spectral differences in the SYMP group between birth outcomes were more evident, with higher Raman peaks seen in women who delivered prematurely (Figure 2.26).

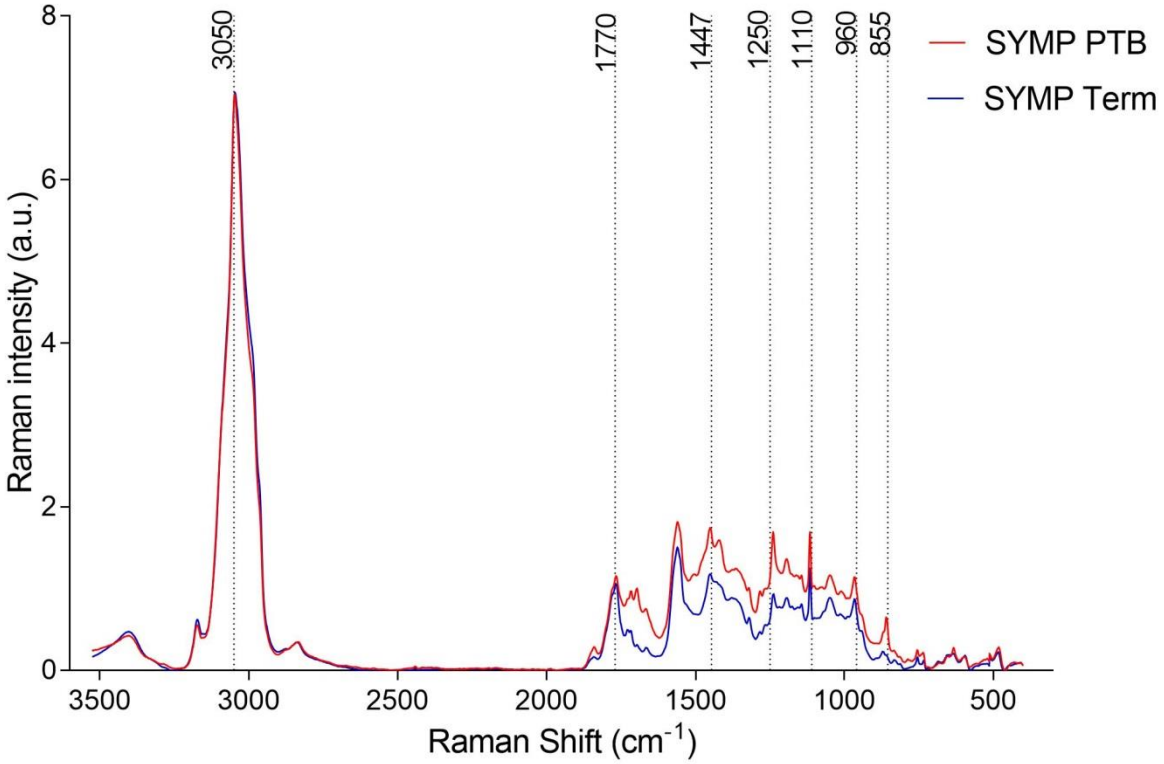

Figure 2.26. Comparison of the full mean spectra between SYMP women who delivered preterm (red) and those who a term delivery (blue)

When these spectral differences were further analysed with PCA, good sample separation was achieved in PC-1 (responsible for 51% of the variance). While term samples clustered more closely together, sPTB specimens appeared more scattered with a higher number of outliers (Figure 2.27). Women who had a sPTB seemed to display higher peaks at 1590, 1147, 1338 and 1130 cm^{-1}, normally linked to lactic acid, urea and proteins, and lower peaks at 3050 and 2930 cm^{-1}, previously associated with lipids (Movasaghi et al., 2007).

(a)

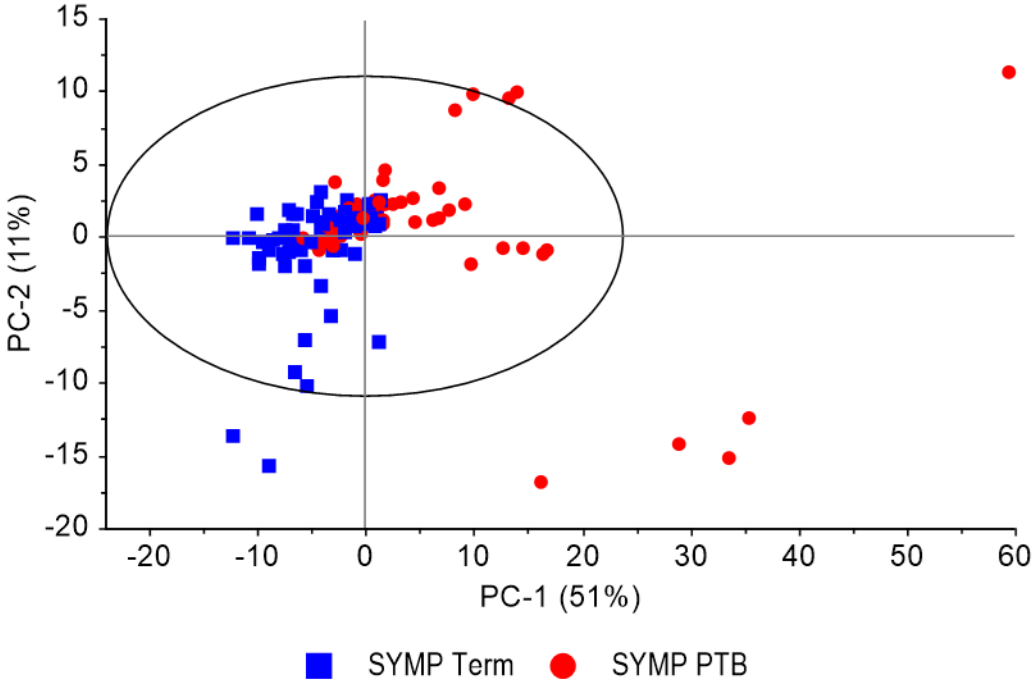

(b)

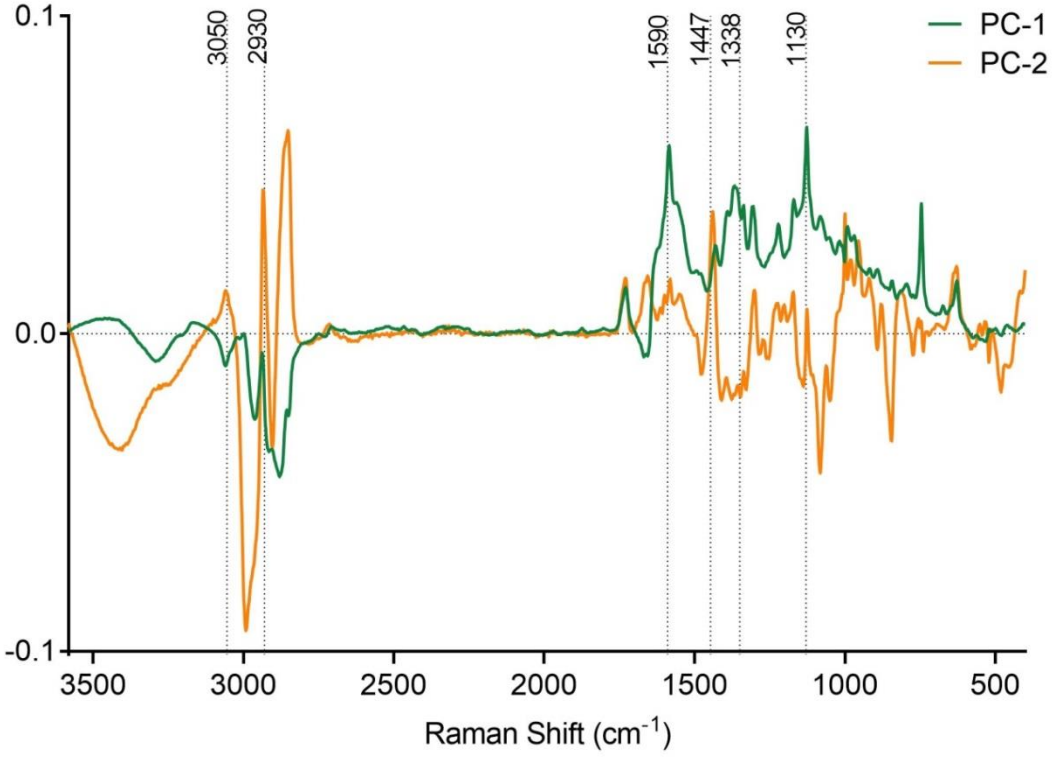

Figure 2.27. (a) A two-dimensional principal component analysis score plot of the general region of CVF in sPTB (red) and term (blue) SYMP women, and **(b)** loading plots of the general region representing principal components PC-1 (green) and PC-2 (yellow). *Values outside the ellipse in (a) represent outliers (Hotelling's T2, 95% CI).*

2.4.15. **SYMP group: spectral differences in the Fingerprint region (FP)**

When the FP region was analysed in more detail (1847–400 cm^{-1}), clear differences were seen based on birth outcomes (Figure 2.28). Even though both spectra mirrored each other, peaks were consistently higher on women who went on to have a PTB except for a small sub-region between 1800 and 1500 cm^{-1}.

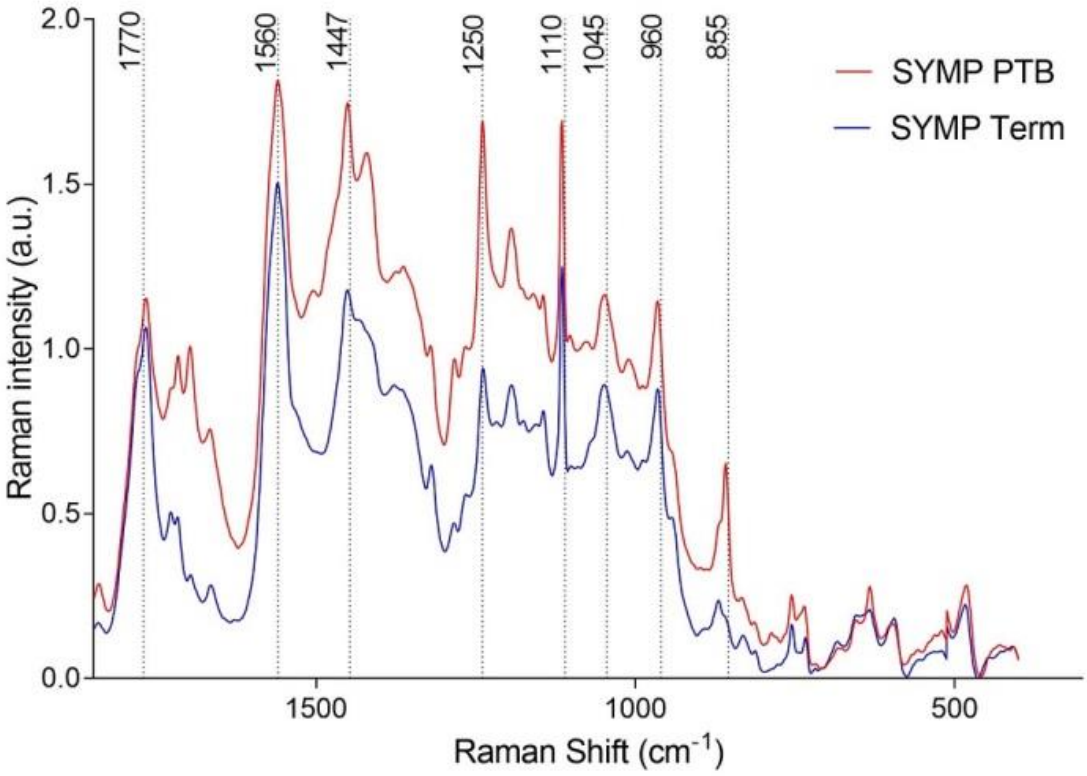

Figure 2.28. Comparison of the fingerprint spectra between SYMP women who delivered preterm (red) and those who had a term delivery (blue)

As evidenced in Figure 2.29, PC-1 which captured 63% variance enabled partial segregation of the samples. Most of these differences were seen at 1590, 1370, 1125 and 745 cm^{-1}, normally associated with νCO_2 of lactic acid and νCN and ρNH_2 of urea. Overall, women who presented in threatened preterm labour and went on to deliver prematurely seemed to have higher levels of metabolites such as urea than their term counterparts (Sikirzhytskaya et al., 2012, Talari et al., 2015).

(a)

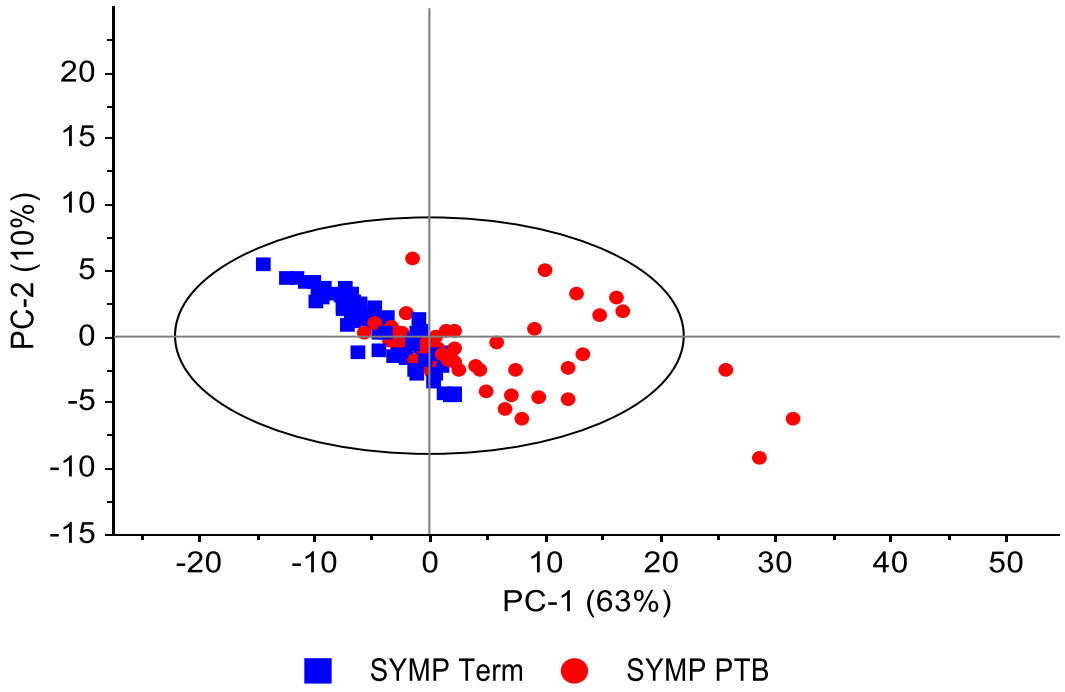

(b)

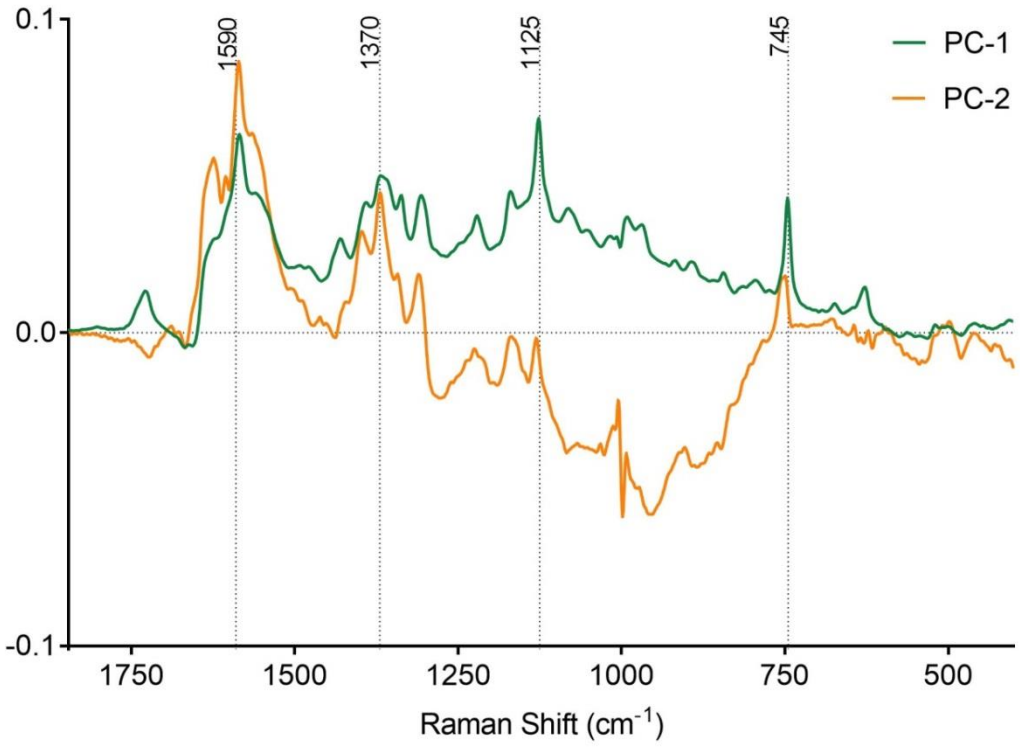

Figure 2.29. (a) A two-dimensional principal component analysis score plot of the fingerprint region of CVF in sPTB (red) and term (blue) SYMP women, and **(b)** loading plots of the fingerprint region representing principal components PC-1 (green) and PC-2 (yellow). *Values outside the ellipse in (a) represent outliers (Hotelling's T2, 95% CI).*

2.4.16. **SYMP group: spectral differences in the Amide region (A1)**

Within the amide profile (1799-1099 cm^{-1}), the highest peaks were identified at 1560, 1450, 1420, 1245 and 1115 cm^{-1} which have previously been assigned to urea, short-chain fatty acids and secondary structure of proteins. In alignment with the GR and FP findings, all the peaks within the amide region were consistently higher in women who delivered prematurely (Figure 2.30).

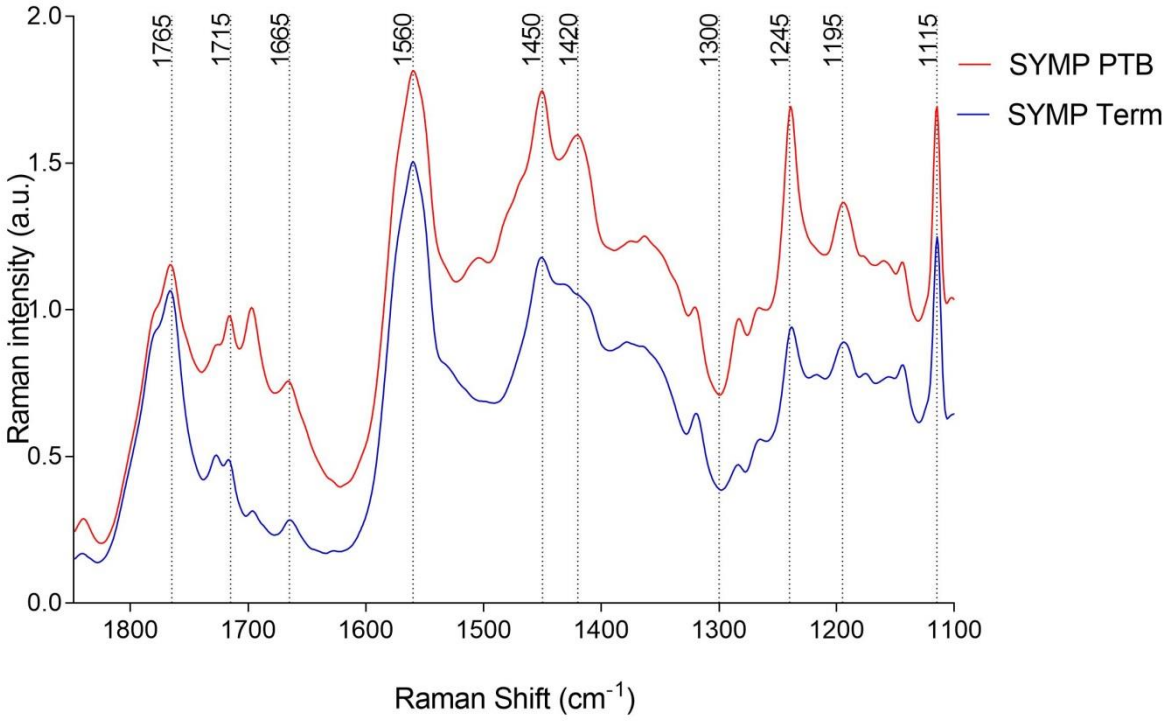

Figure 2.30. Comparison of the amide region spectra between SYMP women who delivered preterm (red) and those who had a term delivery (blue)

PC-1 was capable of explaining 77% of the variance. Despite some overlapping seen between sPTB and term samples in the left-hand quadrants of the plot, a clear separation between birth outcomes was achieved (Figure 2.31). The main peaks responsible for the variance in PC-1 were located at 1540, 1330 and 1260 cm^{-1} associated with C=O and δCH vibrations of proteins respectively (Talari et al., 2015).

(a)

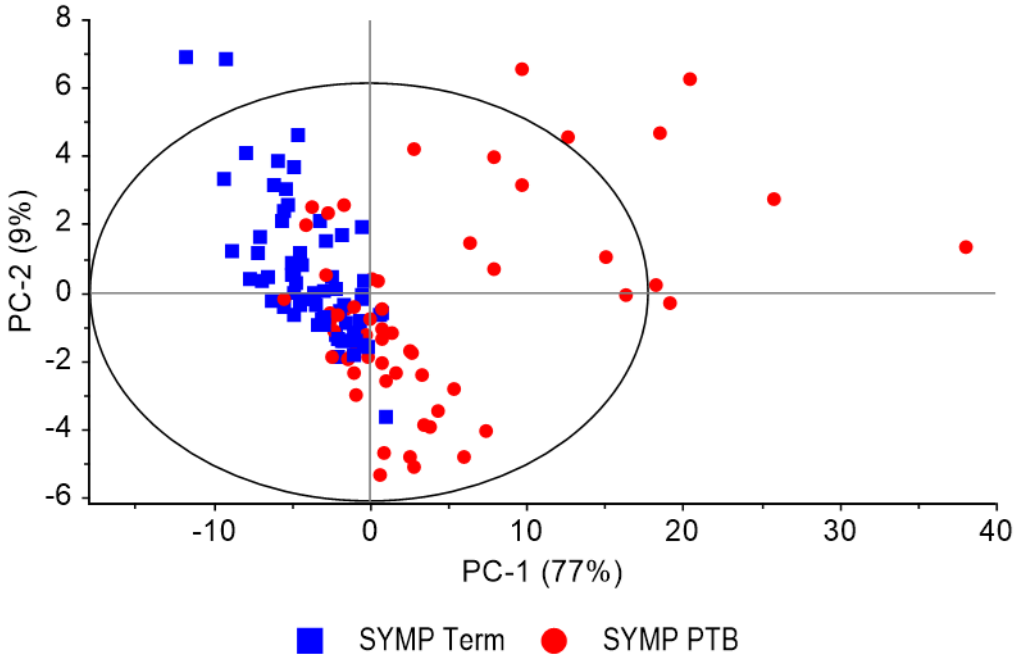

(b)

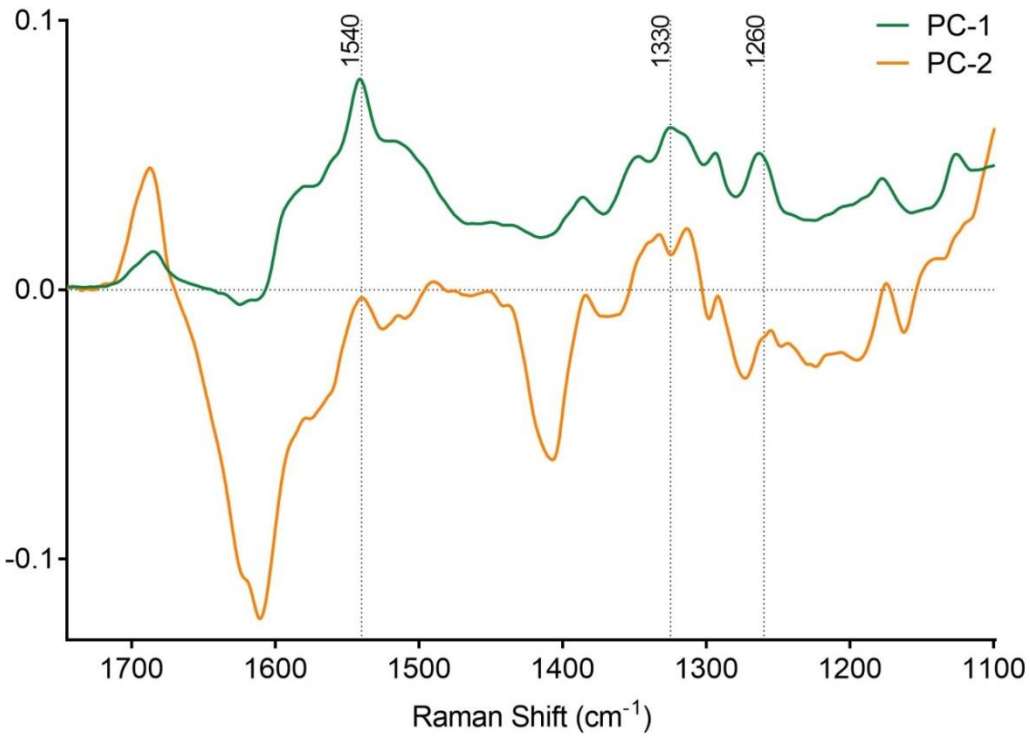

Figure 2.31. (a) A two-dimensional principal component analysis score plot of the amide region of CVF in sPTB (red) and term (blue) SYMP women, and **(b)** loading plots of the amide region representing principal components PC-1 (green) and PC-2 (yellow). *Values outside the ellipse in (a) represent outliers (Hotelling's T2, 95% CI).*

2.4.17. **SYMP group: spectral differences in the Amide I region (A1)**

Differences between birth outcomes were particularly accentuated for the amide I region (1799-1487 cm^{-1}). Higher peaks at 1765, 1715, 1697, 1665 and 1560 cm^{-1} were noted in women who delivered prematurely, which suggested a larger amount of proteins in the CVF of SYMP women who went on to deliver prematurely (Figure 2.32).

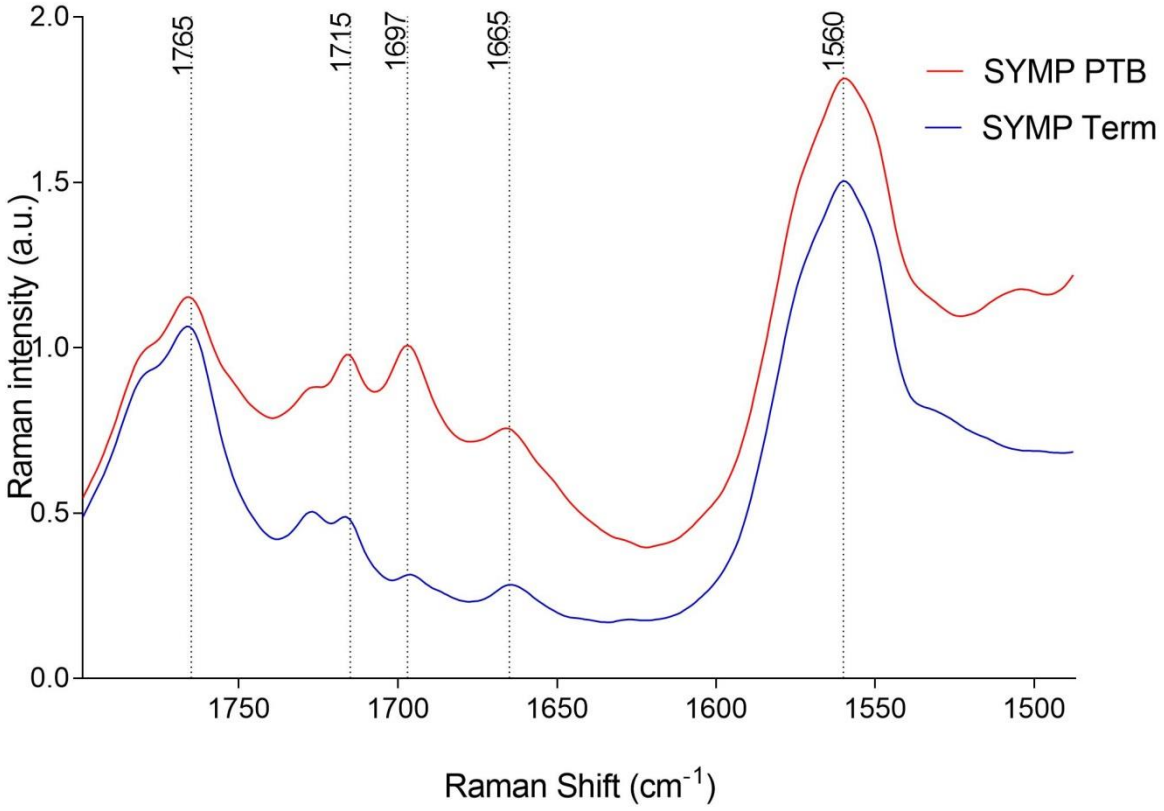

Figure 2.32. Comparison of the amide I region spectra between SYMP women who delivered preterm (red) and those who had a term delivery (blue)

PC-1, responsible for 79% of the variance, enabled partial separation of the specimens based on birth outcome. Similar to the general region (section 2.4.12), samples from term SYMP women seemed more closely grouped together in the A1 region than those from women who delivered prematurely (Figure 2.33). The highest peak was registered at 1590 cm^{-1}, normally assigned to νCO2 of lactic acid and some aromatic aminoacids such as tyrosine (Sikirzhytskaya et al., 2012).

(a)

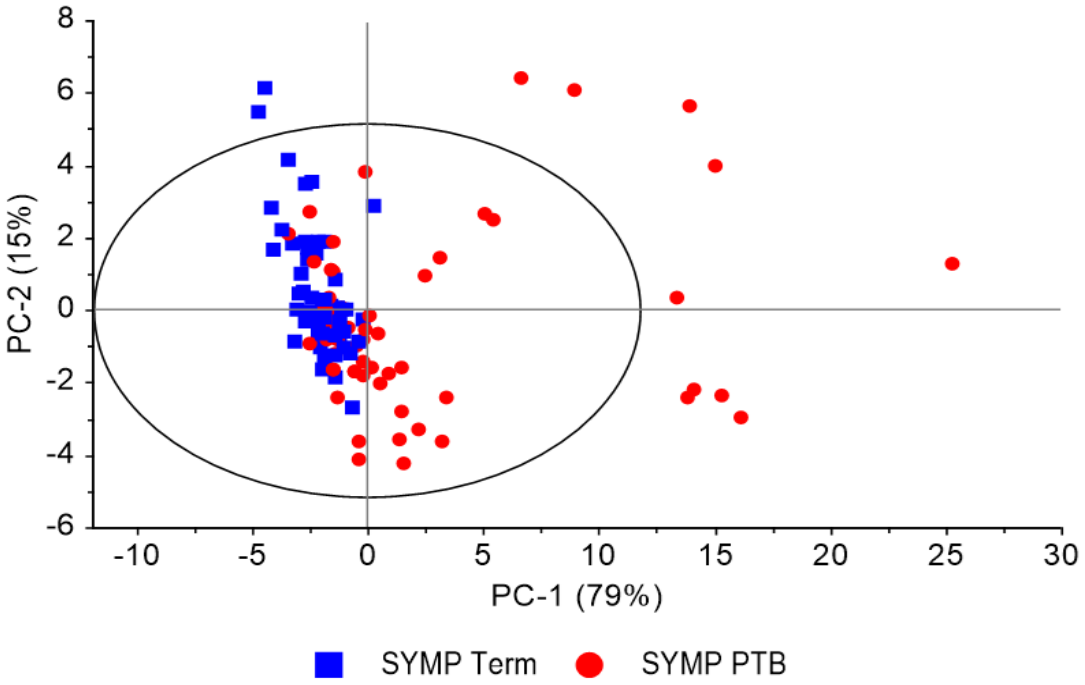

(b)

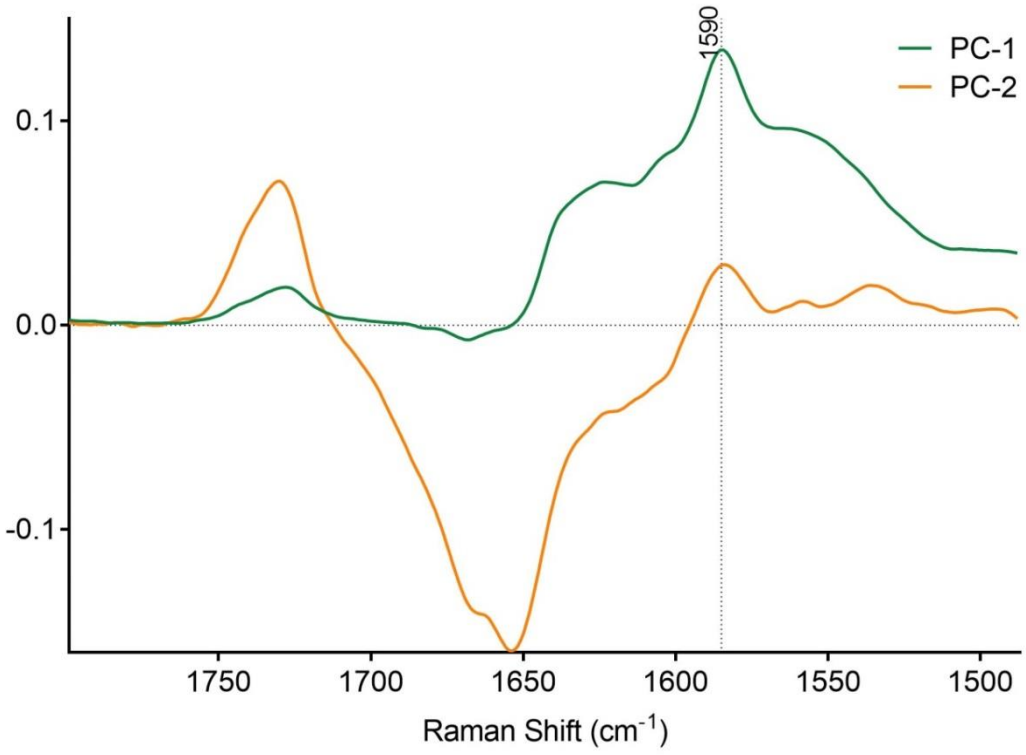

Figure 2.33. (a) A two-dimensional principal component analysis score plot of the amide I region of CVF in sPTB (red) and term (blue) SYMP women, and **(b)** loading plots of the amide I region representing principal components PC-1 (green) and PC-2 (yellow). *Values outside the ellipse in (a) represent outliers (Hotelling's T2, 95% CI).*

2.4.18. **SYMP group: spectral differences in the Amide II region (A2)**

The spectral profile of the amide II region (1487-1358 cm^{-1}) was quite similar in frequency shift between SYMP women who delivered prematurely and those who delivered at term. However, there was a clear distinction in intensity with higher levels recorded in the CVF of women who had a sPTB (Figure 2.34).

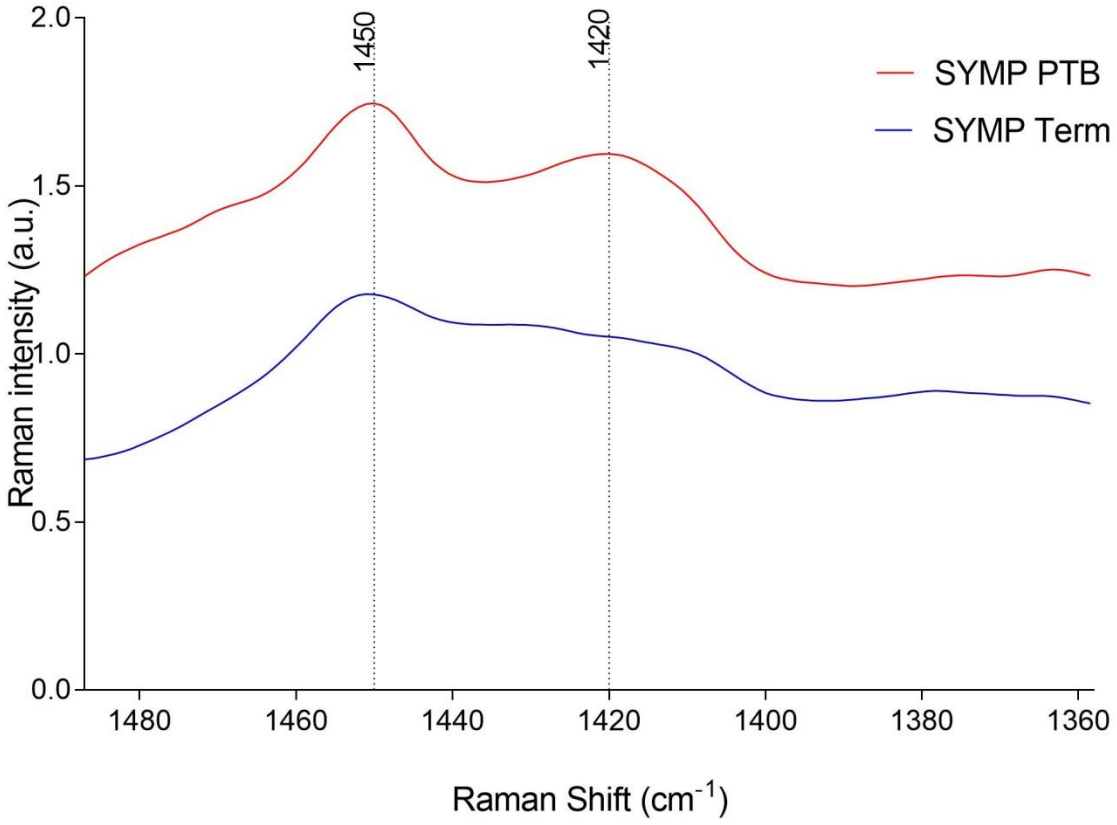

Figure 2.34. Comparison of the amide II region spectra between SYMP women who delivered preterm (red) and those who had a term delivery (blue)

When the amide II region was analysed with PCA, it was possible to partially separate the SYMP samples based on birth outcomes (Figure 2.31). PC-1 was responsible for 78% of the variance in the samples, whereas PC-2 was only accountable for 12% (Figure 2.35a). Nonetheless, only one dip was identified in the loading plots (Figure 2.35b), specifically at 1440 cm^{-1} in PC-1. This band has been previously associated with the $\delta_{as}CH_3$ of lactic acid which suggests a differential metabolite expression in the CVF of SYMP women based on birth outcomes (Sikirzhytskaya et al., 2012).

(a)

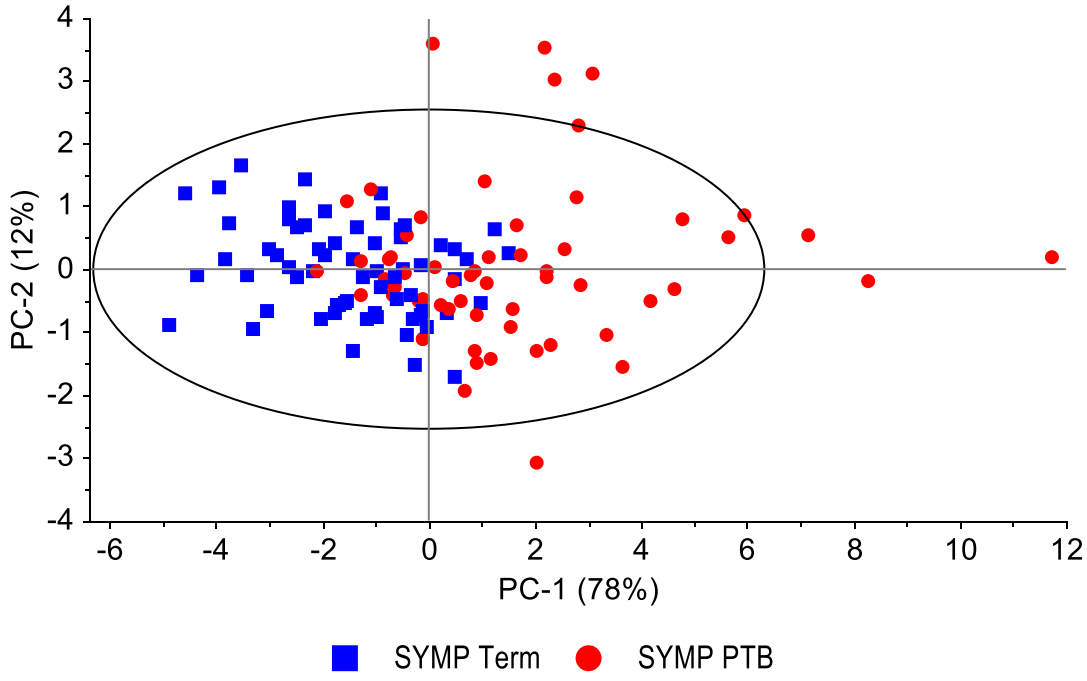

(b)

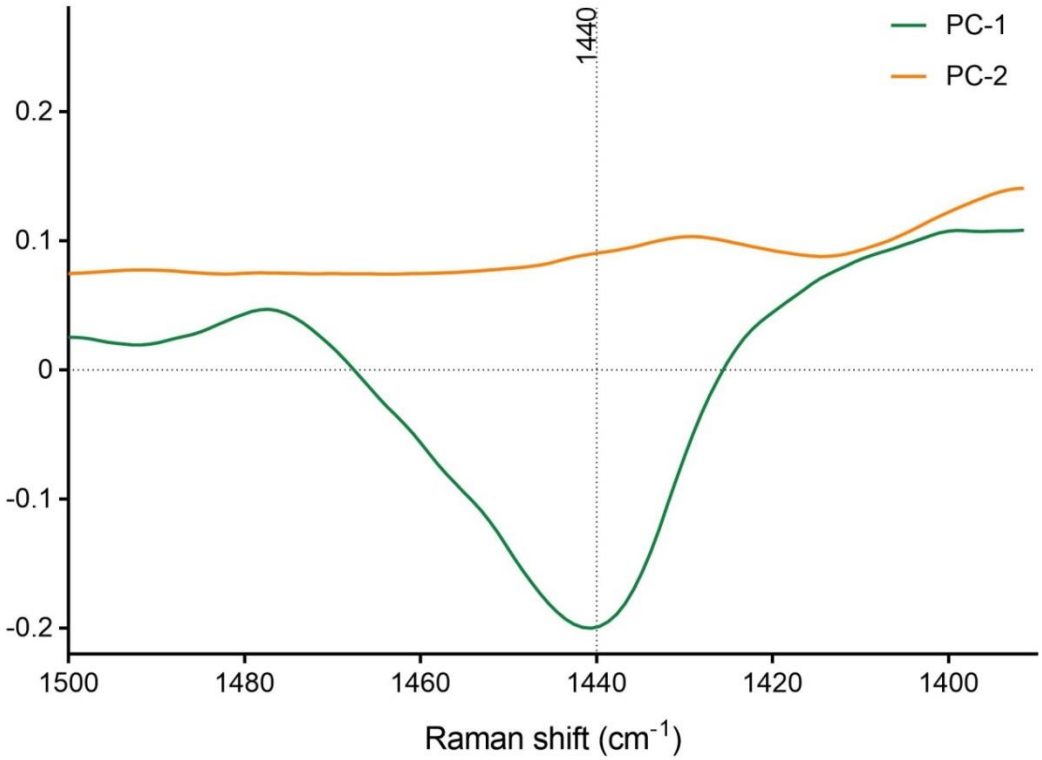

Figure 2.35. (a) A two-dimensional principal component analysis score plot of the amide II region of CVF in sPTB (red) and term (blue) SYMP women, and **(b)** loading plots of the amide II region representing principal components PC-1 (green) and PC-2 (yellow). *Values outside the ellipse in (a) represent outliers (Hotelling's T2, 95% CI).*

2.4.19. **SYMP group: spectral differences in the Amide III region (A3)**

In the amide III region, spectra were quite similar between birth outcomes, almost mirroring each other but at different intensities (Figure 2.36). The main peaks were registered at 1320, 1240, 1195, 1145 and 1115 cm^{-1} which are associated with lactic acid, proteins and urea.

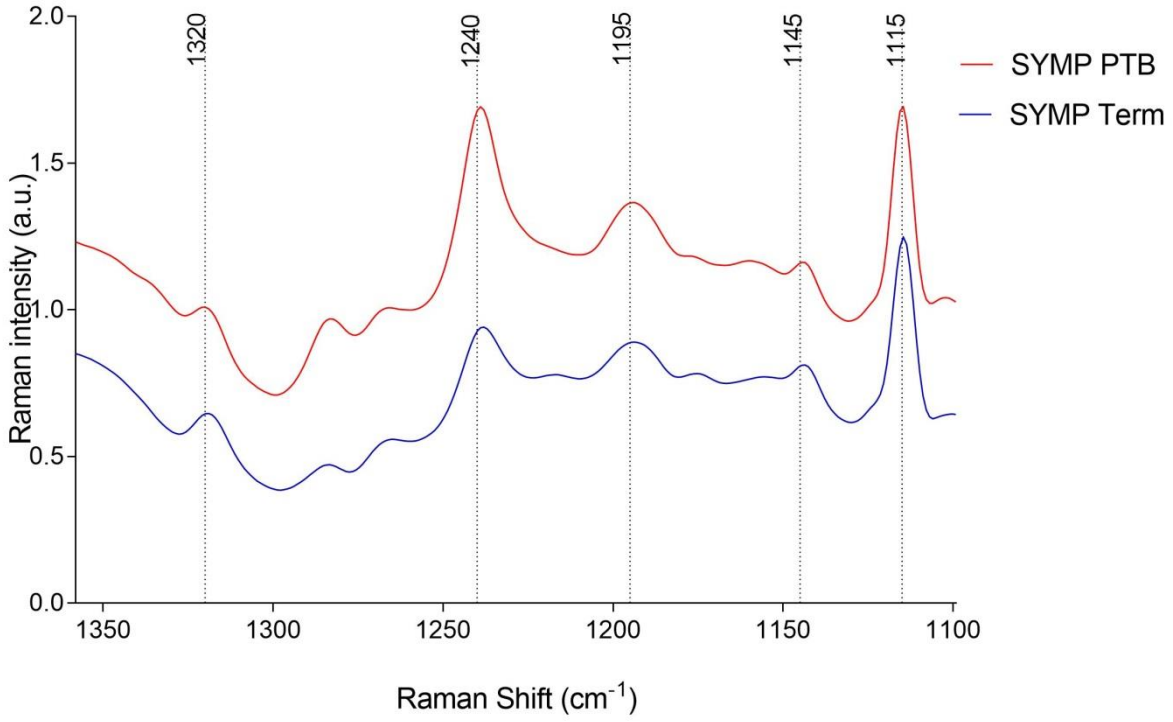

Figure 2.36. Comparison of the amide III region spectra between SYMP women who delivered preterm (red) and those who had a term delivery (blue)

PC-1 was capable of explaining 88% of the variance in the samples. However, it did not yield a full separation of the samples as some overlapping was noted on the low quadrants of the PCA plot (Figure 2.37). The main differences between birth outcome were identified at 1338, 1305 and 1125 cm^{-1}, which have been previously linked to δCH in proteins and νC-CH_3 in lactic acid (Movasaghi et al., 2007).

(a)

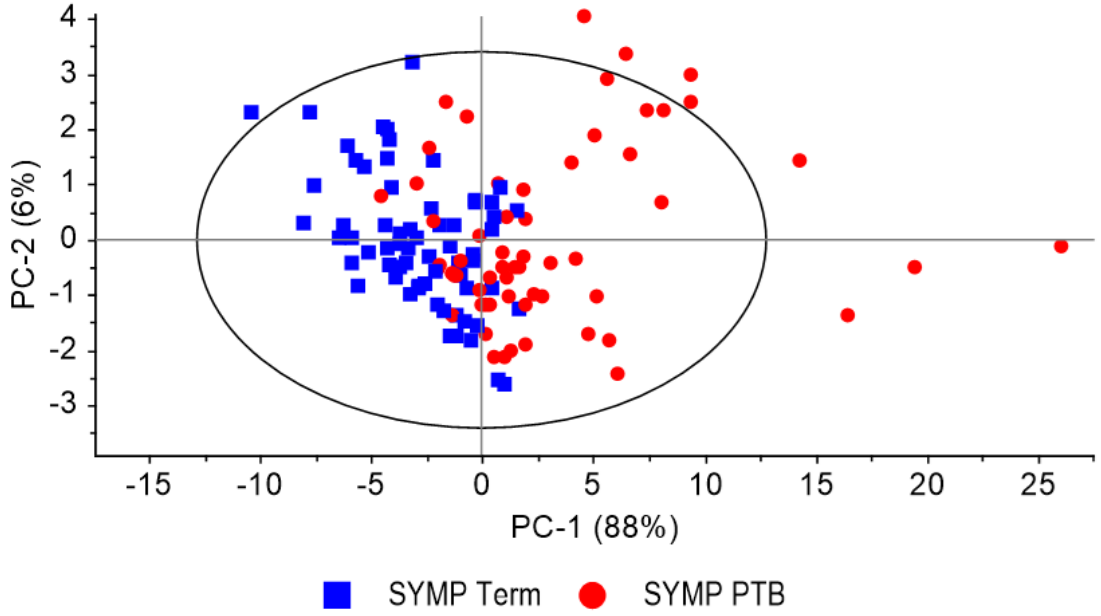

(b)

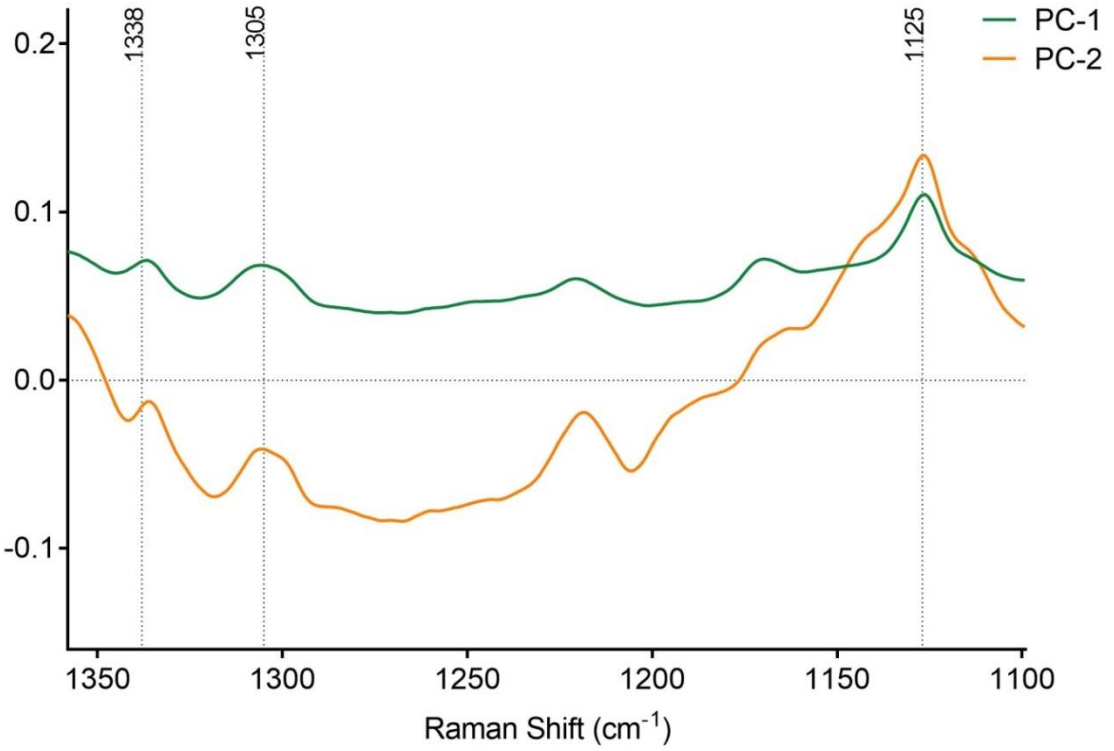

Figure 2.37. (a) A two-dimensional principal component analysis score plot of the amide III region of CVF in sPTB (red) and term (blue) SYMP women, and **(b)** loading plots of the amide III region representing principal components PC-1 (green) and PC-2 (yellow). *Values outside the ellipse in (a) represent outliers (Hotelling's T2, 95% CI)*.

2.4.20. **SYMP group: spectral differences in the Aminoacids region (AA)**

Within the aminoacids region (878-480 cm^{-1}), the main peaks were identified at 855 cm^{-1} (urea), 750-745 cm^{-1} (tryptophan), 633 cm^{-1} (tyrosine, proline, hydroxyproline), 595 cm^{-1} (phosphatidylinositol) and 481 cm^{-1} (urea). When the spectra were compared between birth outcomes, significant differences were noted in peak intensity and shift frequency (Figure 2.38). Consistent with previous SYMP chemometric analysis, women who delivered prematurely had consistently higher values in the most prominent Raman bands of the AA region.

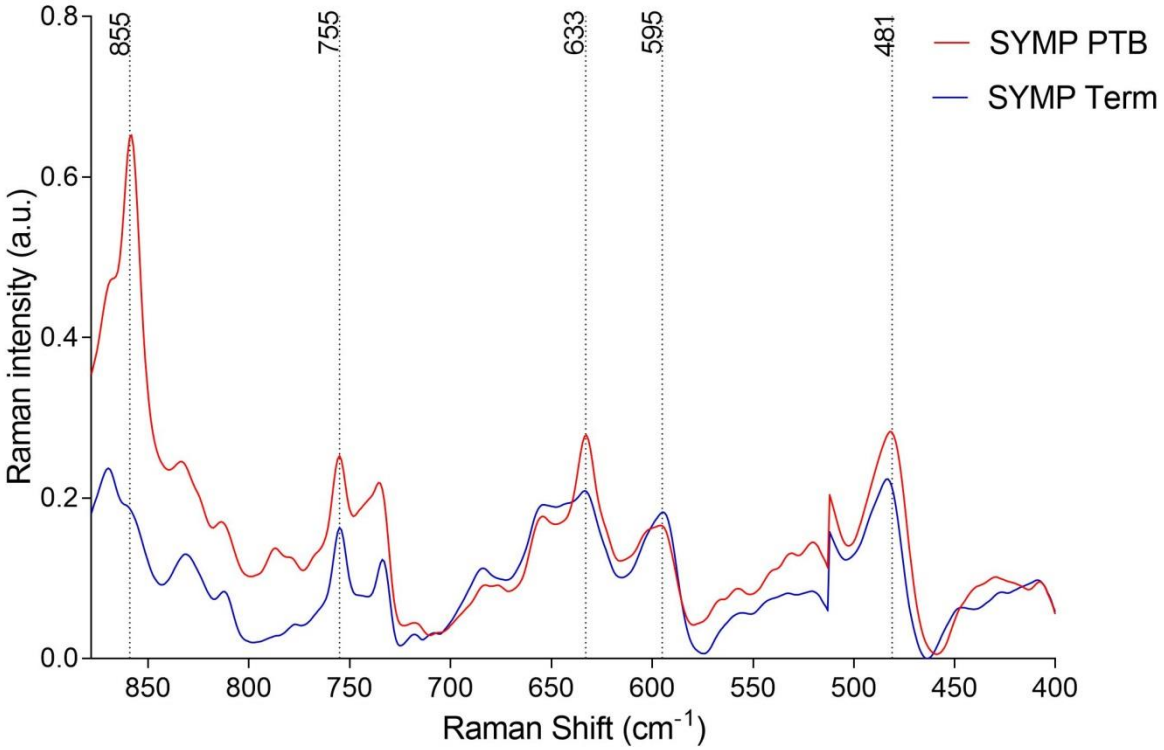

Figure 2.38. Comparison of the aminoacids region spectra between SYMP women who delivered preterm (red) and those with a term delivery (blue)

PCA was unable to show clear separation of samples based on birth outcome; some overlapping of the PTB and term samples was noted in the upper quadrants of PC-1 (Figure 2.39a). Most of the variance was explained by differences in peak intensity at 745 and 633 cm^{-1} linked to lactic acid, tryptophan, methionine, valine and tyrosine molecular vibrations (Movasaghi et al., 2007, Talari et al., 2015).

(a)

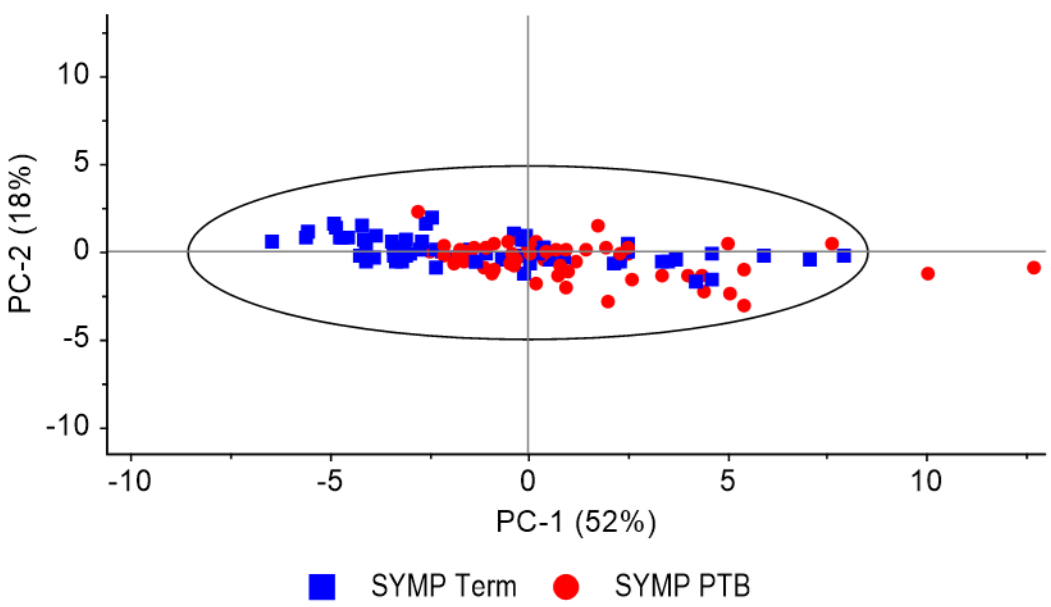

(b)

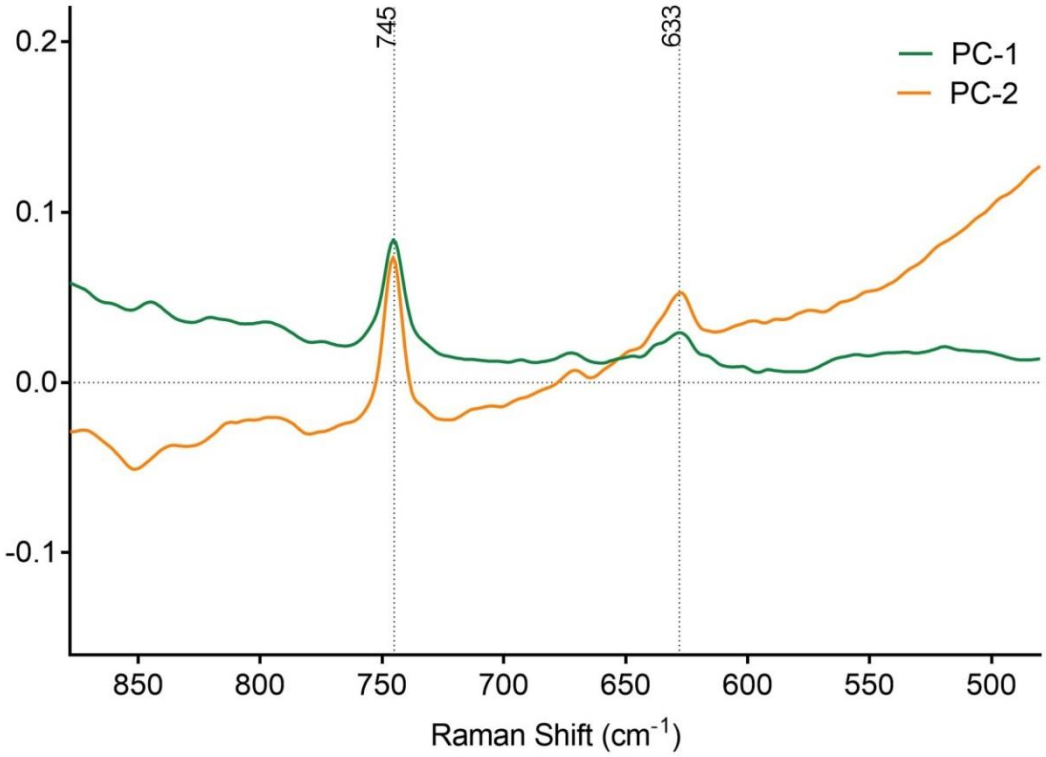

Figure 2.39. (a) A two-dimensional principal component analysis score plot of the aminoacids region of CVF in sPTB (red) and term (blue) SYMP women, and **(b)** loading plots of the aminoacids region representing principal components PC-1 (green) and PC-2 (yellow). *Values outside the ellipse in (a) represent outliers (Hotelling's T2, 95% CI).*

2.4.21. **SYMP group: differences in the High wavenumber region (HWN)**

When the HWN region in the SYMP spectra was assessed based on birth outcome, the two average profiles almost completely overlapped (Figure 2.40). Only one peak was identified at 3050 cm^{-1}, normally associated with stretching vibrations of lipids (Talari et al., 2015).

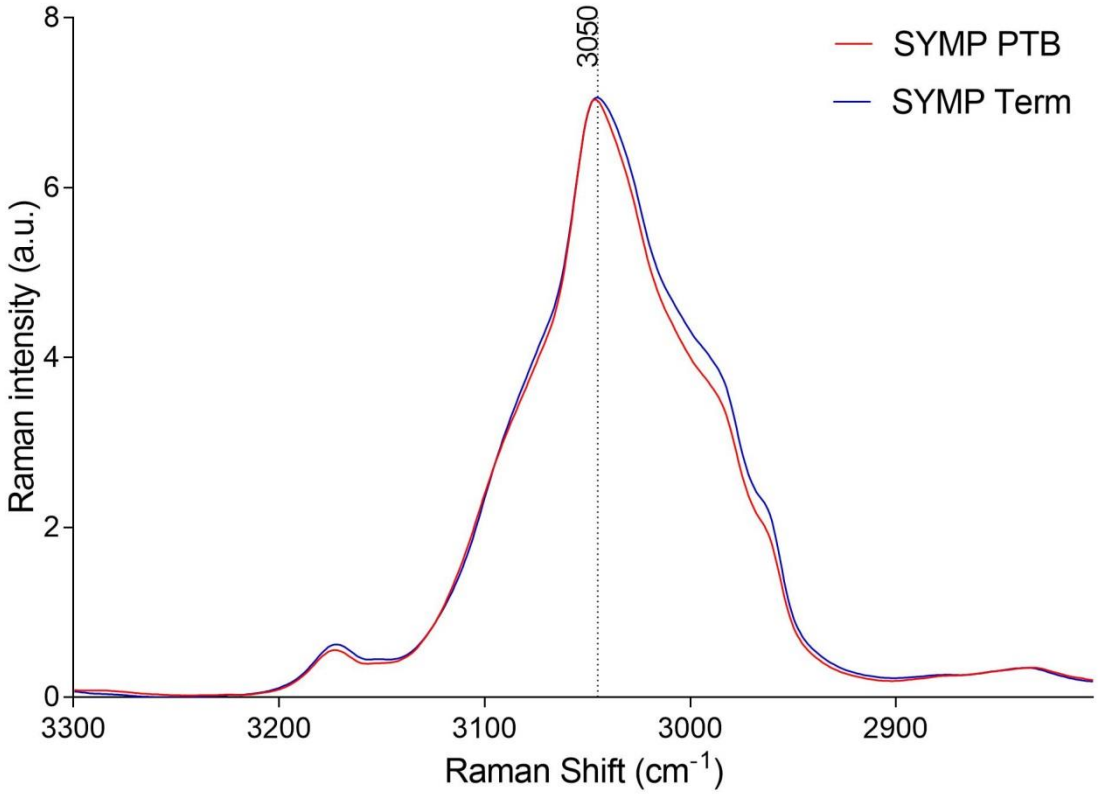

Figure 2.40. Comparison of the high wavenumber region spectra between SYMP women who delivered preterm (red) and those who had a term delivery (blue)

PCA failed to clearly differentiate samples based on birth outcomes with evident overlapping in the left quadrants (Figure 2.41). The main peaks and dips to explain variance in PC-1 (46%) were located at 2930 and 2880 cm^{-1}, which are normally associated with CH_2 asymmetric stretch of lipids and proteins (Talari et al., 2015).

(a)

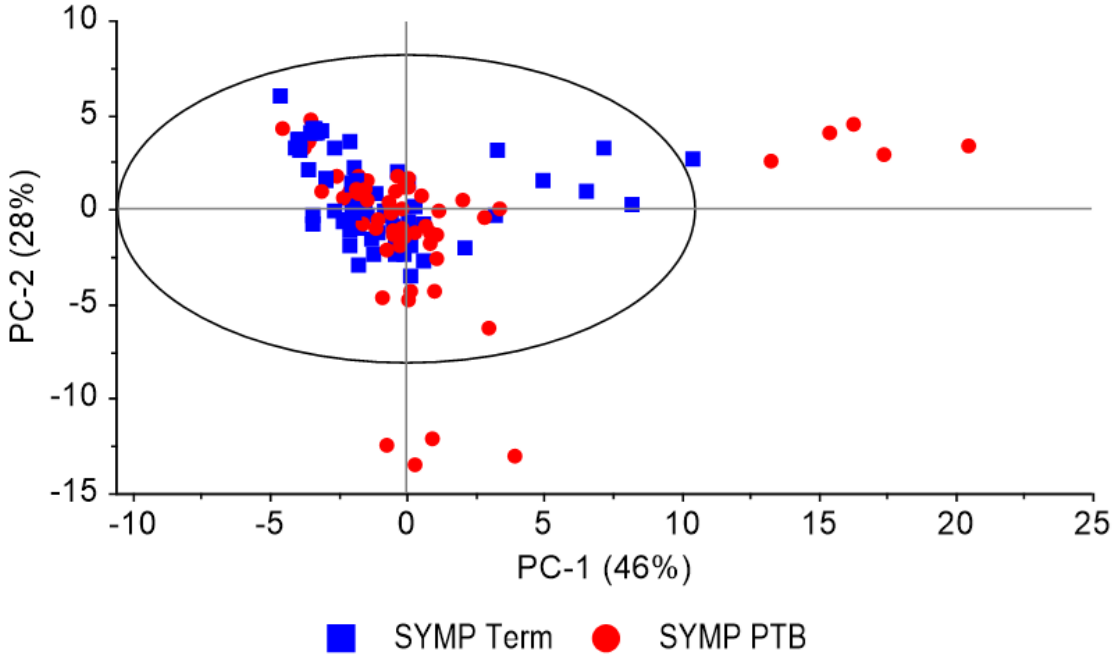

(b)

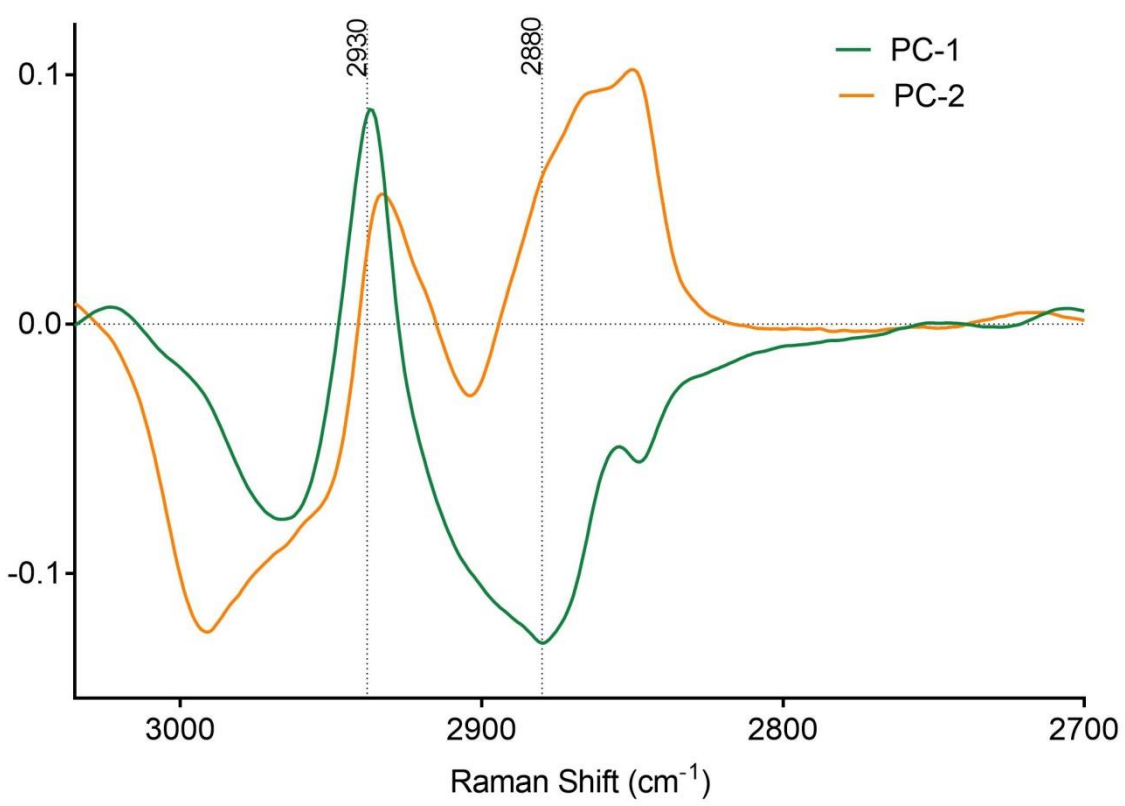

Figure 2.41. (a) A two-dimensional principal component analysis score plot of the high wavenumber region of CVF sPTB (red) and term (blue) SYMP women, and **(b)** loading plots of the high wavenumber region representing principal components PC-1 (green) and PC-2 (yellow). *Values outside the ellipse in (a) represent outliers (Hotelling's T2, 95% CI).*

2.4.22. **RS analysis of CVF: diagnostic value for sPTB**

Multiple points from each sample were scanned with RS to experimentally assess intra-sample reproducibility. These single-point spectra were then employed as training and testing data to build predictive models for sPTB both in the AHR and in the SYMP groups using a PCA-LDA approach based on the spectral general region. The model had an accuracy of 83.7% for AHR and 81.25% for SYMP.

The classifier models based on RS data enabled prediction of sPTB with a sensitivity of 88.64% and a specificity of 71.88% in AHR women assessed between 20^{+0}-28^{+0} weeks, and a sensitivity of 93.75% and a specificity of 67.24% for SYMP women presenting in threatened preterm labour between 20^{+0}-36^{+6} weeks.

Predictive values were also calculated for fFN and CL with cut-offs of 50 ng/mL and 25 mm respectively (Tables 2.3 and 2.4). For both cohorts, RS appeared to have higher sensitivity and NPV than CL and fFN.

Table 2.3. RS, CL and fFN test performance for the AHR group (95% CI)

	RS	CL (<25 mm)	fFN (>50 ng/ml)
Sensitivity (95% CI)	88.64% (75.44-96.21)	22.2% (2.81-60.01)	25% (3.19-65.09)
Specificity (95% CI)	71.88% (59.24-82.40)	90.91% (58.72-99.77)	85.71% (42.13-99.64)
Positive predictive value (95% CI)	68.42% (59.09-76.47)	66.67% (17.66-94.61)	66.67% (18.51-94.63)
Negative predictive value (95% CI)	90.20% (79.9-95.52)	58.82% (49.02-67.98)	50% (37.72-62.28)

CI: confidence interval, CL: cervical length, fFN: fetal fibronectin, RS: Raman spectroscopy

Table 2.4. RS, CL and fFN test performance for the SYMP group (95% CI)

	RS	CL (<25 mm)	fFN (>50 ng/ml)
Sensitivity (95% CI)	93.75% (84.76-98.27)	55.56% (21.20-86.3)	80% (28.36-99.49)
Specificity (95% CI)	67.24% (53.66-78.99)	100% (54.09-100)	80% (44.39-97.48)
Positive predictive value (95% CI)	75.95% (68.48-82.11)	100% (-)	66.67% (34.94-88.16)
Negative predictive value (95% CI)	90.70% (78.78-96.24)	63.64% (45.74-78.42)	88.89% (57.42-97.94)

CI: confidence interval, CL: cervical length, fFN: fetal fibronectin, RS: Raman spectroscopy

2.4.23. **RS analysis of CVF: diagnostic value for prediction of delivery within two weeks of presentation**

Training and testing data was also employed to create LDA models capable of assessing the performance of RS for prediction of delivery within two weeks of CVF sampling. It is worth noticing that only two AHR women gave birth within two weeks of assessment and therefore results should be interpreted with caution. For AHR women, the model had an accuracy of 95.79%, and enabled identification of delivery within two weeks with a sensitivity of 50% and a specificity of 98.88% (Table 2.5). For SYMP women, the model was 84.85% accurate and had a sensitivity of 96.97% and a specificity of 77.27% (Table 2.6).

Table 2.5. RS, CL and fFN test performance for prediction of birth within two weeks for the AHR group (95% CI)

	RS	CL (<25 mm)	fFN (>50 ng/ml)
Sensitivity (95% CI)	50% (11.81-88.19)	100% (15.81-100)	50% (1.26-98.74)
Specificity (95% CI)	98.88% (93.90-99.97)	89.47% (66.86-98.70)	85.71% (57.19-98.22)
Positive predictive value (95% CI)	75% (26.76-96.10)	50% (21.23-78.73)	33.33% (7.03-76.77)
Negative predictive value (95% CI)	96.70% (92.94-98.49)	100% (-)	92.31% (54.35-95.75)

CI: confidence interval, CL: cervical length, fFN: fetal fibronectin, RS: Raman spectroscopy

Table 2.6. RS, CL and fFN test performance for prediction of birth within two weeks for the SYMP group (95% CI)

	RS	CL (<25 mm)	fFN (>50 ng/ml)
Sensitivity (95% CI)	96.97% (84.24-99.92)	28.57% (3.67-70.96)	40% (5.27-85.34)
Specificity (95% CI)	77.27% (65.30-86.69)	62.50% (24.49-91.48)	75% (34.91-96.81)
Positive predictive value (95% CI)	68.09% (57.66-76.97)	40% (13.25-74.43)	50% (16.55-83.35)
Negative predictive value (95% CI)	98.08% (85.05-99.72)	50% (32.90-67.10)	66.67% (46.83-8195)

CI: confidence interval, CL: cervical length, fFN: fetal fibronectin, RS: Raman spectroscopy

2.5. Discussion and interpretation

2.5.1. **Main findings**

In this chapter, I employed Raman spectroscopy, a technique which is based on the inelastic scattering of low-intensity monochromatic light, to characterise the CVF in pregnant women and assess its predictive value for sPTB. I speculated that RS would be capable of generating unique molecular signatures from the CVF of pregnant women at mid-gestation, which could then be used to accurately predict delivery outcomes. In order to test this hypothesis, I conducted a pilot study on the two groups of women who currently get screened for PTB in the NHS (section 1.3.1): asymptomatic high-risk women, and symptomatic patients presenting in threatened preterm labour but not yet in established labour. This approach enabled to compare RS with the predictive tools currently available in the clinical setting since study participants were also offered TVU CL and fFN as part of their clinical assessment.

As RS had never been attempted on CVF of pregnant women before, I first optimised the technique for collecting, processing and scanning swabs guided by previous research using ^{1}H-NMR and vibrational spectroscopy on CVF (Sikirzhytskaya et al., 2012, Amabebe et al., 2016b). I dissolved CVF samples in PBS to maximise sample volume, employed aluminium foil as substrate for all Raman scanning to reduce fluorescence and background noise; and smoothed, normalised and baseline-corrected all spectra to facilitate comparison based on birth outcomes within each cohort.

CVF samples were compared based on time to delivery and delivery outcomes, and the spectral differences were quantified and employed to construct predictive models for PTB. For the AHR group, the predictive model had 88.64% sensitivity (95% CI: 75.44-96.21) and 71.88% specificity (95% CI: 59.24-82.40) for sPTB, whereas for the SYMP group, the model yielded 93.75% sensitivity (95% CI: 84.76-98.27) and 67.24% specificity (95% CI: 53.66-78.99). When spectral differences were assessed against the time interval to delivery, the AHR model had 50% sensitivity (95% CI: 11.81-88.19) and 98.88% specificity (95% CI: 93.90-99.97) to predict birth within two weeks of sampling whereas the SYMP was 96.97% sensitive (95% CI: 84.24-99.92) and 77.27% specific (95% CI: 65.30-86.64).

Despite the small sample size, these results were highly promising as RS was capable of predicting sPTB and delivery within two weeks of sampling with similar and/or better accuracy than fFN and CL. Women who delivered preterm were found to have higher fFN values and shorter TVU CL values than their term counterparts. However, none of these differences proved to be

statistically significant, most likely due to the limited number of samples. The exception was fFN in the SYMP group which was significantly higher in women who delivered prematurely and yielded high NPV for delivery within two weeks of assessment (section 2.4.2). In these women, higher intensity levels were also noted in fibronectin-related CH_3 and CH_2 deformation modes as well as in amide I peaks which suggest RS signals positively correlated with fFN values (Osterlund, 1988, Strehle et al., 2004). Therefore, and not surprisingly, RS behaved similar to fFN for prediction of PTB with high NPV but relatively modest PPV.

The main spectral changes between women who delivered term and those who delivered prematurely were largely seen in spectral peaks associated with lipids, protein conformation (Amide I and III) and aminoacids, lactic acid and acetate. These were also the molecular groups which seemed to vary based on the time interval to delivery. Spectral findings overlapped between both analyses as all women who delivered within two weeks of sampling had a sPTB. When samples were assessed based on the time interval between sampling and delivery, spectral differences were noted to gradually increase the closer to birth. We hypothesised these differences could reflect the gradual cervical remodelling process which begins early in pregnancy and culminates at the time of delivery from a molecular perspective (Read et al., 2007, Elovitz et al., 2014, Cook et al., 2019).

In particular, mid-trimester CVF from women who went on to have a sPTB was found to display consistently higher signals in bands assigned to collagen residues, glucose, fibronectin and tyrosine, and lower signals for bands normally associated with glutamic acid and lipids. Ghartey et al. (2015) had previously reported that GC-MS analysis of CVF was capable of identifying differences in aminoacids and peptide metabolism between women who delivered prematurely and those who delivered at term, and they speculated these changes were a reflection of shifts in the vaginal microbiota. Further studies subsequently explored this hypothesis and found that metabolites from branched aminoacids such as leucine, valine and valine, were relatively higher in cases of vaginal dysbiosis, and correlated positively with genital inflammation and inversely with flora diversity and Lactobacilli abundance (Ilhan et al., 2019).

In our study, AHR and SYMP women who delivered prematurely were found to have lower lipid intensities, which we hypothesised could be due to lipid oxidation (Narice et al., 2018). As previously described in Section 1.5.1, lipid degradation is likely to play a key role in the pathogenesis of PTB by producing pro-inflammatory ROS which may lead to prostaglandin production and break down of the cervical stroma (Scholl and Stein, 2001, Ferguson et al., 2017).

CVF from women who went on to deliver prematurely also displayed lower level of glutamic acid and increased acetate, which have previously been proposed as metabolic signatures of PTB-related bacterial dysbiosis and/ or subclinical infection such as BV (Srinivasan et al., 2015,

Amabebe et al., 2016a, Amabebe et al., 2019). Even though none of our participants tested positive for genital infections of known clinical significance, no formal in-depth analysis of the vaginal microbiota was conducted. Therefore, subtle shifts in the relative abundance of microbial species in the vaginal milieu, which may increase susceptibility to PTB, were not available for further correlation with metabolomics data (Ravel et al., 2011, Stafford et al., 2017).

Overall, the findings from preliminary study support the hypothesis that mid-trimester CVF metabolite and proteomic differential expression may hold predictive value for sPTB and delivery within two weeks of presentation, and that RS may enable the identification of potential biomarkers of sPTB pending further validation with targeted –omics techniques (Baker et al., 2016).

2.5.2. **Strengths**

To the best of my knowledge, this is the first study to analyse CVF in pregnant women using RS and to report its predictive value for sPTB. Previous ^{1}H-NMR and enzyme-based spectrophotometry research has shown that the metabolite profile of the CVF of women who delivered prematurely significantly differs from that with a term delivery. However, ^{1}H-NMR has been rather cumbersome and expensive to be successfully translated into the clinical setting (Amabebe et al., 2016b). RS, on the other hand, may be more suitable as a bedside CVF screening test as evidenced by the proof-of-concept data presented in this chapter. However, larger clinical studies are still needed to better understand the clinical utility of RS for prediction of sPTB.

RS has already been proposed for the *in vivo* study of cervical remodelling as an endoscopic probe (Vargis et al., 2012), and recent experimental work both on mice models and pregnant women has concluded that RS has the capability to identify key biochemical changes in cervical remodelling with potential predictive value for sPTB (Chapter 4; O'Brien et al., 2018, O'Brien et al., 2019). Our RS project represents an interesting alternative to the study of cervical tissue for prediction of sPTB as CVF samples are easily collectable and pose minimal discomfort for patients. Once collected, swabs can be rapidly analysed with almost no previous sample preparation using compact bedside Raman spectrometer (Ramos et al., 2017). Furthermore, the large and comprehensive amounts of -omics data produced by RS can be analysed with a multivariate approach using user-friendly software (Pieters et al., 2013).While other metabolomics techniques are only capable of targeting one type of metabolite at a time with modestly expensive analysers, RS is not restricted to a specific protein, nucleic acid or metabolite, and can provide an overall signature of the molecular composition of the CVF (Baker et al., 2016, Ramos et al., 2017).

2.5.3. **Limitations**

However, our pilot RS study did not come without some methodological limitations regarding:

(1) Sample size: given the pilot nature of this work, there were not enough participants to perform subgroup analysis based on ethnicity which is known to affect the vaginal microbiome and thus the metabolic signature of CVF (Fettweis et al., 2014). Additionally, no patients who were receiving treatment such as vaginal progesterone or cerclage were included. Larger statistically-powered clinical studies are therefore needed to further validate this technique and demonstrate the predictive accuracy for sPTB in the clinical setting when such confounding factors are accounted for. It is also worth noticing that in our untreated cohorts, incidence of sPTB was ~50% which is significantly higher than the expected rate in high-risk groups (~25%). Whereas the modelled sensitivity and specificity presented in this chapter should be unaffected by this higher incidence, positive and negative predictive values should be interpreted with caution until further trials are performed (Parikh et al., 2008). We aimed to include a relatively similar number of index and control cases for each arm which explains the relatively higher incidence of sPTB in our study. Furthermore, we employed strict inclusion criteria which limited selection to untreated women, and excluded those receiving antibiotics or tocolysis at the moment of sampling. It is worth noticing that the RS study was performed before the introduction of a specialised preterm birth clinic in our unit. The impact of our preterm birth clinic on neonatal outcomes is currently being formally analysed but preliminary findings suggest there has been a reduction in the rate of PTB thanks to more timely and better targeting of interventions.

(2) CVF smear for RS scanning: even though the smearing of the samples on the slide was always performed by the same operator, there was no guarantee that the sample would always be homogenously and reproducibly distributed on the microscope slide. Unequal distribution of the sample could potentially lead to systematic error as previously described for the spectroscopic analysis of biofluids by drop deposit (Baker et al., 2016). Depending on the nature of the surface and the contact angle, the macromolecules of the solution may migrate to the periphery of the drop producing the characteristic coffee ring effect. As a result, the spectra from the same specimen may significantly vary depending on the area scanned (Deegan et al., 1997, Esmonde-White et al., 2014). In order to address this potential intra-sample variability, the smear technique was standardised: a similar volume was taken from each microtube, smeared in the same direction and on a similar surface always by the same operator. Additionally, random points were scanned from each smeared sample and analysed to assess intra- and inter-sample variability. The development of a method to automatically standardise the smearing in future collections may reduce this systematic error.

(3) Reduced specificity: the large datasets produced by RS and the potential physiological variability that exists between individuals might have increased the risk of false positives and measurement error. In an attempt to minimise this bias, the process of sample collection and spectral acquisition was standardised. Larger trials with adequate control of variables and confounding factors should enhance precision and thus specificity of the test (Baker et al., 2016).

(4) Lack of low-risk pregnant participants: I purposely tested RS on AHR and SYMP women and not on asymptomatic low-risk women for pragmatic reasons. AHR women have the highest incidence of PTB, and are usually referred to preterm birth clinic in our hospital for counselling, screening and prophylactic interventions. Equally, women who present with symptoms of preterm labour are offered clinical assessment to best time prophylactic intervention which may reduce PTB-associated morbidity and mortality. This arrangement enabled prospective AHR and SYMP participants to be opportunistically recruited when they attended for their routine care without adding any extra clinical commitment. Furthermore, given the higher incidence of PTB in the AHR and SYMP groups, a relatively smaller sample was needed to achieve enough index cases (birth<37 weeks) to characterise the RS spectra.

On the contrary, asymptomatic low-risk women were anticipated to have a lower incidence of PTB (~5-8%), and to be less likely to attend the maternity unit during their second trimester. Therefore, a decision was made not to test RS on unscreened low-risk asymptomatic women during this pilot study as it would not have been possible to recruit enough index cases within the limited time and resources available for the study. However, these women represent an important group to study in the future in which at least two thirds of sPTB are thought to occur and for which there are currently no effective screening techniques available (Campbell, 2018).

2.5.4. **Future research**

RS seems useful for accurately discriminating CVF samples based on the time interval to delivery and birth outcomes by detecting key molecular changes which may hold predictive value for sPTB. Our findings support larger prospective clinical trials to further assess the vibrational spectral profile of CVF across gestation and the predictive value of RS for sPTB in both singleton and multiple pregnancies. Future studies may benefit from correlating RS spectral findings with placental histology in order to gain a deeper understanding of the mechanistic pathway of inflammation and infection which underlies PTB. RS evidence of increased CVF lipid peroxidation, for example, may be associated with acute funisitis and villitis normally associated with PTB (Faye-Petersen, 2008). Sample size calculation for future studies is provided in chapter 5.

Chapter 3

Polarisation-sensitive optical coherence tomography (PS-OCT) as a potentially non-invasive technique to assess collagen in the human cervix to predict preterm birth

3.1. Introduction and background

3.1.1. **Pathological cervical remodelling**

During a normal pregnancy, as the uterus expands to accommodate the growing fetus, the cervix remains closed but it eventually softens, effaces and dilates for delivery. However, rather than being a circumscribed event that happens towards the end of pregnancy, cervical remodelling is thought to be a continuous, evolving process which commences soon after conception at a microscopic level and continues all the way through pregnancy reaching the most dramatic point prior to delivery (Read et al., 2007).

The preferential orientation the cervical collagen exhibits in non-pregnant women is thought to be lost during pregnancy (Aspden, 1988, Kirby et al., 1988). As birth approaches collagen fibres in the cervix have been reported to become more soluble, thicker, and disorganised leaving larger gaps amongst them (Read et al., 2007, Akins et al., 2010, Timmons et al., 2010). The disorganisation of collagen fibres affects its mechanical function and impacts on the ability of the cervix to maintain the pregnancy until term (House et al., 2009). Unfortunately, most techniques which are capable of properly assessing the morphology of collagen are either invasive or can only be performed *in vitro* (Feltovich et al., 2012, Vargis et al., 2012). If this microscopic rearrangement of cervical collagen fibres could be detected using potentially non-invasive affordable imaging techniques at early stages of the remodelling process, it might be possible to better predict and more appropriately manage the onset of premature labour. New light-based techniques derived from conventional optical coherence tomography (OCT) may be able to meet this demand.

3.1.2. **Fundamentals of OCT**

OCT is a 3D optical imaging method which provides cross-sectional images of the tissue of interest with a spatial resolution of 10 μm or less and a depth of penetration of 0.5-1 mm. Its mode of operation is analogous to ultrasound imaging but instead of sound, OCT uses light to measure the time delay of the light reflected from the different layers of the sample in order to build a 3D map (Fujimoto et al., 2000, Popescu et al., 2011).

Because the speed of light is much higher than that of sound, direct measurement of *echo* time delay of backscattered light waves is not possible so OCT relies on low-coherence interferometry to measure time delay indirectly (Fujimoto et al., 2000). The basic arrangement of the interferometers is the Michaelson configuration in which low coherence near-infrared light from a source is split by a beam splitter/coupler into two paths known as the reference and the target arms of the

interferometer (Figure 3.1). The light is then directed towards a reference mirror and the sample of interest, and after interaction with these, it is reflected back to the coupler along the same arms. If the distance travelled by the backscattered light along the reference and target arms is equal, a phenomenon known as interference occurs and the beams recombine at the coupler; these interference effects are then recorded by the OCT photodetector (Popescu et al., 2011). By moving the reference mirror in a controlled manner, OCT produces spectral interference signals which provide the depth profile of the sample (Pircher et al., 2011).

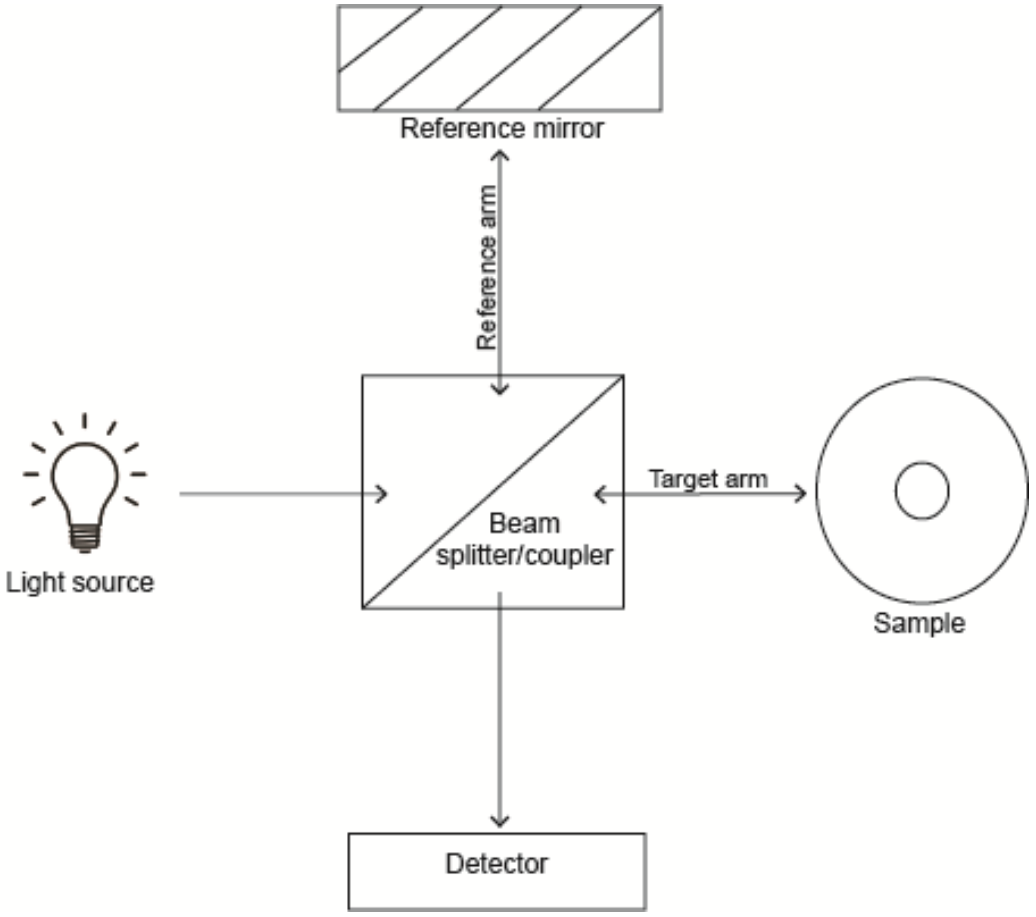

Figure 3.1. Michaelson arrangement of an OCT-type of interferometer. Adapted from Jansz et al. (2014) CC BY License 4.0.

Thanks to its ability to provide real-time and in-situ imaging of biological tissues with better resolution than ultrasound, OCT has become an increasingly popular technique in the clinical setting, especially for the *in vivo* study of the human retina (Bijlsma and Stilma, 2005). Specifically within the field of ophthalmology, OCT is currently employed to discriminate between genuine macular holes and simulating lesions, quantify macular oedema and measure retinal nerve fibre layer thickness in the context of glaucomatous eyes (Jaffe and Caprioli, 2004). But the applications of OCT go beyond its ability to assess the morphological changes seen in progressive pathologic diseases such as glaucoma. Recent *in vitro* work by Xin *et al.* (2016) on the aqueous outflow system

in the eye has shown that the information provided by OCT enables inference about the mechanical properties of the tissue of interest such as compliance and stiffness.

3.1.3. **OCT to assess the cervix**

Outside the field of ophthalmology, some recent *in vitro* work has demonstrated that OCT may also hold the potential to assess the directionality and alignment of collagen fibres in the human cervix. Using cross-sections from non-pregnant and pregnant women undergoing a hysterectomy or a cesarean hysterectomy respectively, Yao *et al*. (2016) were able to infer the preferential orientation of collagen fibres in the upper cervix (section 1.5.2) using OCT and a new pixel-wise fiber orientation algorithm.

Despite its many advantages and potential applications, the application of OCT to study human disease, and cervical remodelling in particular, has been limited by its failure to accurately and clearly discriminate between tissues (Pircher *et al.*, 2011), its low penetration depth and the presence of imaging artefacts (Jaffe and Caprioli, 2004). In an attempt to overcome some of these limitations, I proposed the use of Polarisation-sensitive optical coherence tomography (PS-OCT), a recently-developed functional extension of OCT, to evaluate collagen fibres in the human cervix.

3.1.4. **Fundamentals of PS-OCT**

Some materials are capable of altering the polarisation state of the light that passes through them, a phenomenon known as birefringence. PS-OCT is particularly sensitive to birefringence, and relies on the polarisation state of the backscattered light to improve OCT depth resolution (Matcher, 2009). Only a few anisotropic biological structures in the human body exhibit this optical behaviour (Burns *et al.*, 2011). These structures include the highly-organised type I and III collagen fibres. I therefore hypothesised that the human cervix, which is abundant in collagen bundles, would be well-suited to PS-OCT imaging. If PS-OCT was shown to be capable of reliably assessing the orientation of human cervical collagen *in vitro*, *in vivo* probes could be developed to study cervical remodelling during pregnancy (Le *et al.*, 2015).

For uniaxial birefringent structures such as collagen, PS-OCT can provide quantitative information about the tissue:

(1) Reflectivity (R): a property which PS-OCT shares with OCT, which represents the total power backscattered by the sample at a specific position. Differences in refractive index within a sample are displayed in the “structural OCT” image (Matcher, 2009, Al-Mujaini et al., 2013).

(2) Linear birefringence(Δn): anisotropic structures exhibit a different refractive index for each polarisation state of the incident light. As a result, the polarised light propagates at different speeds through the tissue. The polarisation direction with the higher refractive index is called slow axis (SA), whereas the axis along which the polarised light moves faster is referred to as fast axis (FA). The difference between these two axes is called linear birefringence (de Boer et al., 1997, Matcher, 2009).

(3) Phase retardation (δ): refers to the phase shifting between the two polarisation states of the incident light. This phase difference $(d\delta_s)$ is then used to calculate Δn at a specific position (z) as illustrated in the following equation, in which (λ_0) represents the light wavelength in vacuum (Matcher, 2009):

$$\Delta n = \frac{\lambda_0}{2\pi}\frac{d\delta_s(z)}{dz}$$

It is worth mentioning that PS-OCT does not strictly quantify the intrinsic birefringence of the tissue but rather the "apparent" birefringence. Apparent birefringence is dependent not only on the intrinsic anisotropy of the tissue but also on the orientation of the optic axis relative to the direction of the incident light. If the incident light is parallel to the optic axis of the tissue, no birefringence will be seen regardless of whether there is any anisotropy in the sample. On the other hand, if the incident light shines at 90^o to the optic axis, apparent birefringence will reach its maximum value. In collagen fibres, it is normally assumed that the optic axis corresponds to the long axis of the fibres. Therefore, if collagen fibres are arranged perpendicular to the incident light, maximum birefringence is displayed; whereas if collagen fibres are parallel to the light, no birefringence is seen. Hence, a lack of apparent birefringence in a sample could either suggest a parallel arrangement of collagen fibres to the incident light or an absence of collagen fibres in the area being scanned (Ugryumova et al., 2009).

3.2. Aims and objectives

3.2.1. **Aims and hypothesis**

The aim of this project was to determine whether PS-OCT is capable of measuring, reliably and non-destructively, the arrangement of collagen fibres in the *ex vivo* human cervix.

3.2.2. **Objectives**

- To assess the apparent birefringence properties of the cervix in non-pregnant women using PS-OCT
- To determine collagen fibre arrangement in the human non-pregnant uterus employing the apparent birefringence of the cervical tissue obtained with PS-OCT
- To characterise the distribution of collagen fibres in the human cervix based on parity, age, menopausal status and BMI
- To correlate PS-OCT findings on cervical collagen fibre orientation with H&E and Masson's Trichrome staining

3.3. Materials and methods

3.3.1. **Study population and sample size**

Cervical samples were obtained from women undergoing vaginal, total abdominal or laparoscopic-assisted hysterectomy for benign conditions such as menorrhagia, prolapse or endometriosis, and who understood English so were able and willing to give consent. No age, parity or menopausal status restriction was applied. Patients with known gynaecological cancer, abnormal or outdated smear tests, previous history of LLETZ or other cervical surgery, and recently confirmed cervicovaginal infection were excluded from the study.

The sample size for this project was determined based on previous studies which had employed SHG and X-ray diffraction to assess cervical collagen orientation and had reported statistically significant differences in samples size ranging from 8 to 18 specimens (Aspden, 1988, Narice et al., 2016). Therefore, and given the exploratory nature of the project which aimed to replicate some of these findings with an alternative technique such as PS-OCT, it was agreed that a minimum of 20 samples should be sufficient to draw a robust conclusion about the potential ability of PS-OCT to assess the alignment of collagen in the human cervix.

The study was granted approval by the Yorkshire & Humber Committee of the UK National Research Ethics Service (Research Ethics Committee Number 08/H1310/35) and the University of Sheffield (Registration number 160268520).

3.3.2. **Participant recruitment and sample collection**

Patients were approached during their pre-operative anaesthetic review. The study was explained, and printed material was provided. If they decided to participate, written consent was sought and obtained before surgery. All patient clinical and demographic data was coded and anonymised, and only the research team had access to it in accordance to the Data Protection Act (Data Protection Act, 1998) and more recently the EU General Data Protection Regulation (GDPR).

Soon after the uterus and the cervix were removed in theatre at the Royal Hallamshire Hospital (Sheffield Teaching Hospitals NHS Trust), whole cross-sections of the ectocervix (n=20) were further excised. I obtained all the samples, which were approximately 2 cm long x 2 cm high x 2 cm deep (Figure 3.2).

Histopathologists were notified about the patient's participation in the study and the approximate dimensions of the cervical area excised to facilitate the analysis of the remaining uterine specimen.

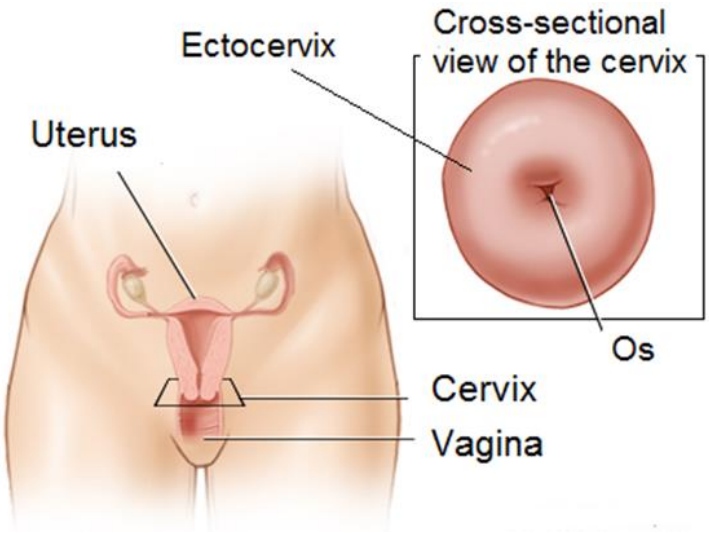

Figure 3.2. Anatomical and cross-sectional view of the human cervix. Adapted from Healthwise©

3.3.3. **Cervical sample preparation for PS-OCT**

After cervical cross-sections were excised from the uterine specimen, synthetic absorbable monofilament sutures (PDS®-polydioxanone) were used to orientate the sample so that the ectocervix could be easily identified from the ECM (Patel and Jenkins, 2016). The samples were then labelled and immediately stored in PBS with antibiotics: 0.1 mg/mL streptomycin, 0.25 µg/mL amphotericin B and 100 IU/mL penicillin at -20^{o}C on Human Tissue Authority (HTA) licensed premises until processing with PS-OCT could be performed.

Before being scanned with PS-OCT, the samples were thawed in sterile PBS at room temperature. For PS-OCT scanning of the cervical regions, samples were placed inside Ibidi® bottom µ-Dish (dish diameter 35 mm, glass area 21mm, volume 2 mm) and sealed with Parafilm®.

3.3.4. **PS-OCT instrumentation**

Cervical samples were scanned using our in-house PS-OCT prototype at the University of Sheffield (Figure 3.3), which was developed from an in-house source swept (SS) OCT, and modified so that it could detect the horizontal and vertical polarisation states of the backscattered light using two different orthogonal polarisation channels (Lu *et al.*, 2011).

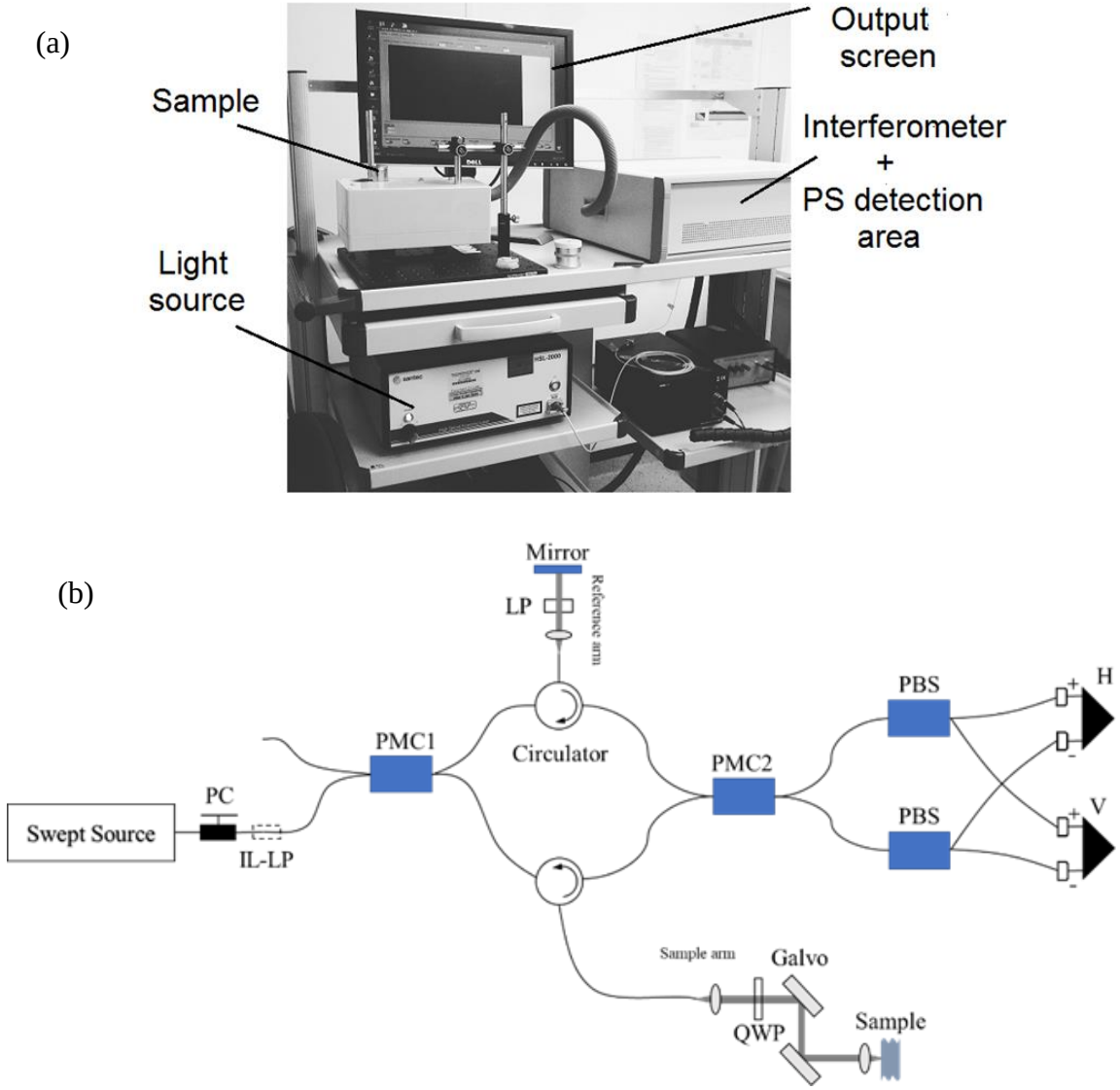

Figure 3.3. (a) PS-OCT machine at University of Sheffield, **(b)** simplified schematic of the PS-OCT system. PC: polarisation controllers. Il-LP: in-line linear polariser. PMC1: polarisation-maintaining coupler 1. LP: linear polariser. QWP: quarter wave plate. Galvo: galvanometer system. PMC2: polarisation-maintaining coupler 2. PBS: polarisation beam splitter. H: horizontal. V: vertical. Adapted from Lu et al (2011), CC License

Partly based on a Michaelson interferometer and arranged in a similar fashion to the one described by Al-Qaisi and Akkin (2010), the system comprised a swept laser source (HSL-200-10-

MDL, SANTEC, Japan) with a wavelength of 1315 nm, a full width at half maximum of 128 nm, a wavelength scanning rate of 10 kHz and a duty cycle of 60% which supplied an output power of 10 mW to the system. The light emitted from the light source was firstly polarised and then modulated by passing through a polarisation controller (PC) and an in-line linear polariser (Il-LP). This linearly polarised light then entered a polarisation-maintaining fibre (PMF) based Mach-Zender interferometer, where it was split into two beams by a 2 x 2 polarisation-maintaining coupler (PMC1) which had been aligned to couple only with the slow axis of the PMF (PMC1, OLCPLP-22-131-10-90-FA, Opto-Link Corporation Ltd, China). Ten percent of the light was coupled to the reference arm, whereas the remaining 90% was directed to the sample arm through two three-port polarisation-maintaining circulators (Opto-Link Corporation Ltd, China).

In the reference arm, the light acquired a polarizing angle of 45° to the slow axis of PMF by passing through a linear polariser (LP) positioned at 45° to the slow axis of the PMF. After interacting with a plane static reference mirror, it was reflected back to the circulator. In the sample arm, the light first travelled through a quarter wave plate (QWP, Edmund Optics, US) oriented at 45° to the slow axis of PMF and became circularly polarised. This circularly polarised light then sequentially transited a galvanometer scanning system (Cambridge Technology, US) and OCT scanning lens with an effective focal length of 36 mm (Thorlabs LSM03) before being scattered by the sample. The galvanometer system allowed both volumetric and B-scanning to be performed whereas the scanning lens enabled the light to be focused with a 25 μm-diameter light spot in the focal plane.

After interacting with the reference mirror and the sample respectively, both beams re-combined and interfered with each other at another 2 x 2 polarisation-maintaining coupler (PMC2, Opto-Link Corporation Ltd, China). The light was then separated into horizontal and vertical polarised signals by two identical polarisation beam splitters (PBS, Nova Wave Technologies, US). These signals were then detected and amplified by two balanced detectors (New Focus, US) and recorded by a 14-bit transient recorder (M2i. 4022, Spectrum GmbH, Germany) at 20 MS/s (Al-Qaisi and Akkin, 2008, 2010; Wang *et al.*, 2010; Lu *et al.*, 2011).

3.3.5. **PS-OCT scanning of the cervix**

Given the presumed preferential orientation exhibited by collagen fibres in the cervix, (Figure 3.4; Aspden, 1988), the surface of the ectocervix was divided into three equal circumferential regions for scanning purposes: centre area (around the endocervical canal), middle area and outer area also referred to as edge (Figure 3.4a).

Cervical samples were scanned from the centre to the edge region with the laser aimed perpendicularly to the surface. As illustrated in Figure 3.4b, each sample (n=20) was scanned 9 times at different points, 3 from each cervical region, (that is 3 from the centre, 3 from the middle and 3 from the edge). From each scanning point, 1000 B-mode scans were combined using LabVIEW (US, 2017) to produce a 3D (volumetric) image with a size of 4 x 4 x ~2.15 mm (Figure 3.4c).

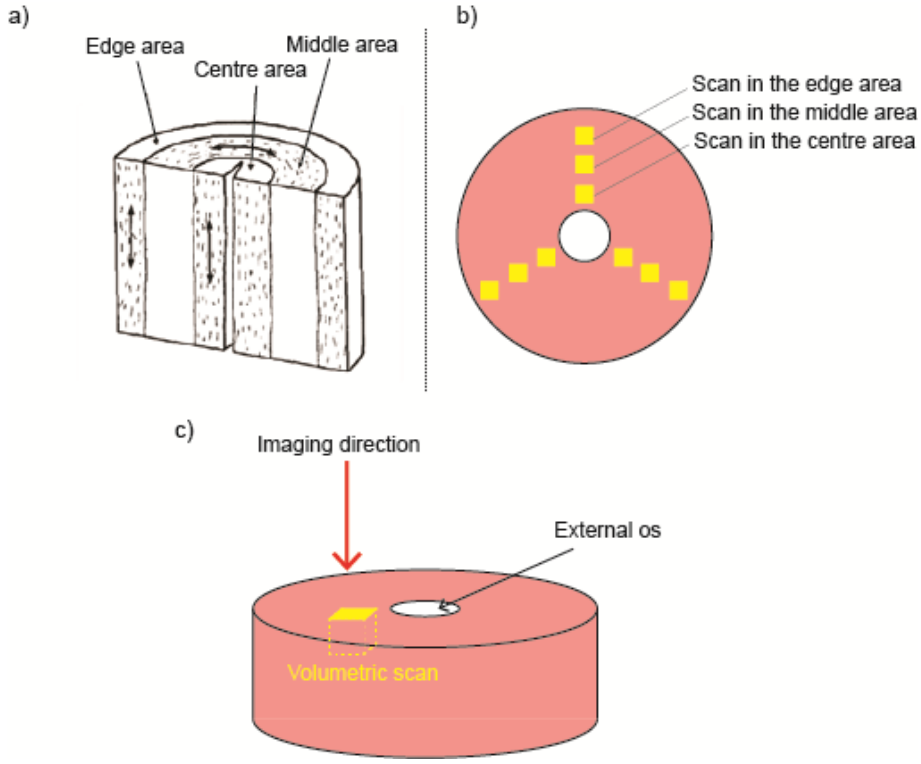

Figure 3.4. Schematic representation of the PS-OCT shows scanning strategy employed. (**a)** Preferential collagen orientation in the human cervix as seen with X-ray diffraction. Collagen fibres in the centre and edge appear more longitudinally aligned, whereas in the middle region they seem to be predominantly circumferential. Adapted from Aspden (1988) and Li et al. (2019), (**b)** PS-OCT scanning points on the cervical sample, **(c)** PS-OCT scanning direction of the cervix

3.3.6. **PS-OCT imaging processing**

The raw data was exported from LabVIEW for offline analysis with MATLAB (Mathworks, Natick, MA, 2017). The retardance $(\delta_s(z))$ image was computed as:

$$\delta_s(z) = arctan\left(\frac{A_{0;V}(z)}{A_{0;H}(z)}\right)$$

where $A_{0;V}(z)$ and $A_{0;H}(z)$ are amplitudes of the vertical and horizontal polarisation signals respectively.

The phase retardance of 100 x 100 A-scans were then averaged at each depth of the tissue (Figure 3.5a), and plotted as a function of depth. As seen in Figure 3.5b, a linear fitting method was subsequently applied to this gradient of retardance to obtain the retardance slope of the birefringent tissue $(d\delta_s)$, needed to calculate the apparent birefringence (Δn) as per:

$$\Delta n = \frac{\lambda_0}{2\pi}\frac{d\delta_s(z)}{dz}$$

where z represents the physical depth into sample; λ_0, the centre wavelength of the light source; and Δn, the refractive index difference between the specimen (n) and the ordinary beam (n_o). Birefringence is therefore the unit-less ratio of change in retardance per propagation distance travelled by light (in this case, depth).

(a)

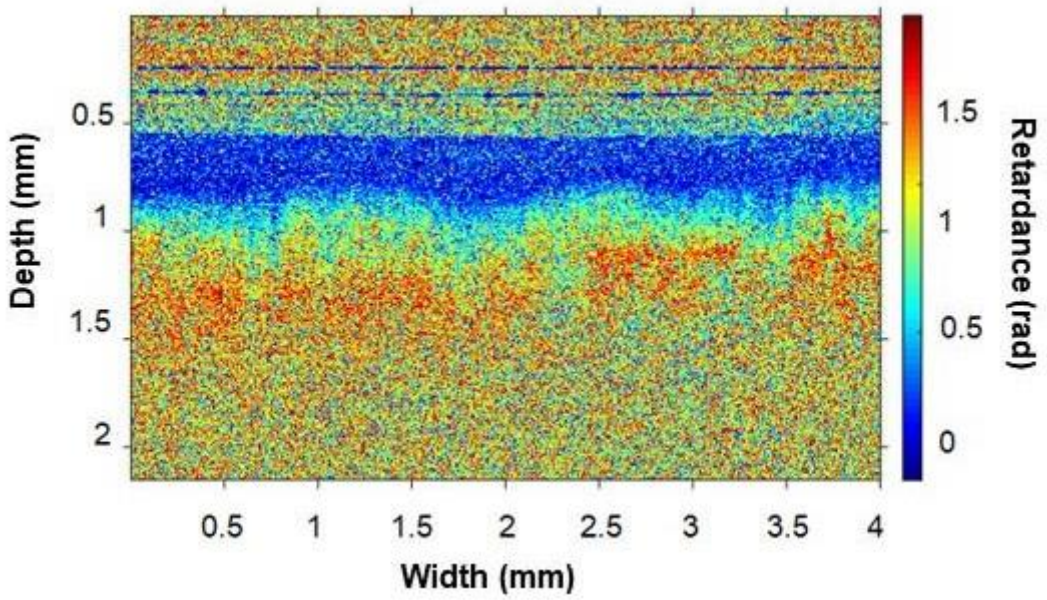

(b)

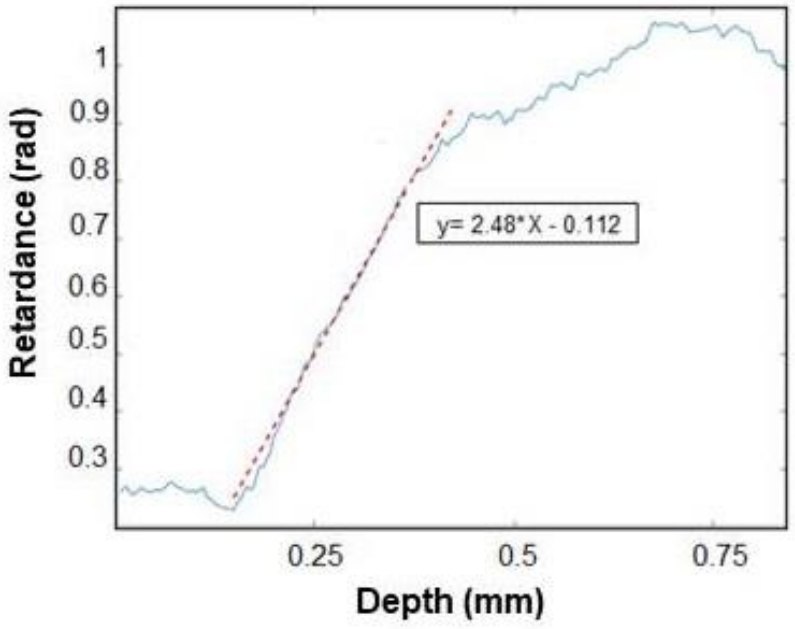

Figure 3.5. (a) Phase-retardance image per depth. The blue band represents the cervical epithelium whereas the red-yellow oscillation underneath belongs to the collagen stroma. Note that the colour oscillation seen on top of the epithelium is an artefact as the rapid change of retardance between noise and sample surface can generate false birefringence signal, **(b)** Retardance as function of depth. The red dashed line illustrates the linear regression necessary to calculate apparent birefringence based on the retardance gradient represented with an asterisk (*) in the equation.

3.3.7. **Statistical analysis**

Apparent birefringence from each sample was then compared within and amongst specimens using ANOVA when the assumption of equality of variances was met, and the non-parametric

Kruskal-Wallis when the Shapiro-Wilk test was significant (IBM, v25). The threshold for *p*-values was set at 0.05. Collagen birefringence was also correlated with age and BMI using Pearson's correlation coefficient, and differences based on parity and menopausal status were assessed with ANOVA or Kruskal-Wallis depending on whether the assumption of equality of variances was met.

3.3.8. **Preparation of histological slides**

Histology was used as a control technique for PS-OCT for assessment of collagen fibres arrangement. Three cervical samples, previously scanned with PS-OCT, were selected for histological analysis. These samples, which had been frozen after PS-OCT scanning, were left to defrost at room temperature for 60 minutes. Given the sample thickness, each cross-section was fixed in formaldehyde 3.7% (w/v) for seven days at room temperature and then cut in half to expose the area of interest whilst trying to minimise the introduction of mechanical artefacts (Chatterjee, 2014). The samples were then processed at the University of Sheffield Medical School Core Facilities following the protocols summarised in Table 3.1.

Table 3.1. Breakdown of steps used to prepare histology slides

Step	Solution	Immersion time (hours)
1	70% IMS	1
2	70% IMS	1
3	80% IMS	1.5
4	85% IMS	1.5
5	90% IMS	1.5
6	95% IMS	1.5
7	100% IMS	1.5
8	100 % IMS	1.5
9	Xylene	1.5
10	Xylene	1.5
11	Paraffin wax	2
12	Paraffin wax	2

IMS= Industrial Methylated Spirit

Once solidified, the rectangular wax blocks were sliced in a coronal orientation, and the 5µm-thick slices were then transferred to a water bath set to 38^{o}C before being mounted on the surface of ThermoFisher® glass slides for further staining and analysis. For each sample, 18 slides were prepared (six each for centre, middle and edge area).

3.3.9. **Masson's trichrome and H&E staining techniques**

To assess the overall histological architecture of the cervix, the specimens were processed with a modified H&E staining technique. Steps with the corresponding reagents are described in Table 3.2. Haematoxylin rendered the nuclei dark blue, whereas eosin stained cytoplasmic structures in a pink-orange range (NSH, July 2001).

Table 3.2. Modified H&E staining protocol used for human cervical samples

Step	Stage	Solution	Immersion time (minutes)
1	De-waxing	Xylene I	5-10
2	De-waxing	Xylene II	5
3	Re-hydration	100% alcohol	3
4	Re-hydration	100% alcohol	3
5	Re-hydration	95% alcohol	3
6	Re-hydration	90% alcohol	3
7	Re-hydration	70% alcohol	3
8	Rinse	Tap water	1
9	Staining	Gill's haematoxylin	2
10	Rinse	Tap water (running)	5
11	Re-hydration	70% alcohol	3
12	Re-hydration	50% alcohol	3
13	Staining	1% Eosin /95% alcohol	0.5-1
14	De-hydration	100% alcohol	0.5
15	De-hydration	100% alcohol	0.5
16	De-hydration	100% alcohol	0.5
17	Mounting	Xylene I	5
18	Mounting	Xylene II	5
19	Mounting	DPX mountant	-

DPX: a mixture of distyrene, pasticiser and xylene

A modified Masson's trichrome stain technique was also performed to better visualise and characterise collagen arrangement in the cervical specimens (Table 3.3). Collagen fibres were stained green with this technique (Burack et al., 1941).

Table 3.3. Modified Masson's trichrome stain technique step by step

Step	Stage	Solution	Immersion time (minutes)
1	De-waxing	Xylene	10
2	Re-hydrate	100% alcohol	2
3	Re-hydrate	70% alcohol	2
4	Rinse	Distilled water	2
5	Pre-staining fixation	Bouin's solution	60-120
6	Rinse	Tap water (running)	2
7	Staining	Weigert's haematoxylin	10
8	Wash	Scott's tap water	0.5
9	Rinse	Tap water (running)	2
10	Staining	Ponceau-Fuchsin	10
11	Rinse	Distilled water	2
12	Staining	Phosphomolybdic acid (PPM acid)	2
13	Brief rinse	Distilled water	*quick dip
14	Staining	Light Green	8
15	De-hydrate	70>100% alcohol	*4 dips in each
16	Mounting	Xylene I	5
17	Mounting	Xylene II	5
18	Mounting	DPX mountant	-

3.3.10. **Qualitative analysis of collagen fibre orientation in histologically processed samples**

After the samples were processed histologically, 16 images from the different cervical regions were selected for analysis, and subsequently reviewed and compared qualitatively by a group of scientists and staff members of the University of Sheffield with no prior knowledge of the project (n=8). Based on the degree of parallelism of the collagen fibres, the assessors were asked to classify the pictures into two groups: 1) samples with well-aligned collagen fibres running parallel and 2) samples with more disorganised fibres, arranged in bundles. Sensitivity and specificity (± 95% CI) were calculated to report their ability to accurately discriminate between the two groups.

3.3.11. **Quantitative analysis of collagen fibres orientation in histologically processed sample**

Images were selected from the histological slides for post-processing and quantitative analysis (10X, LEICA DM750). Based on a 2D Fourier transformation analysis using the Directionality plug-in in FIJI®, the mean fibre direction of cervical collagen was calculated (Narice et al., 2016). For each image, the fibre orientation was estimated by applying second derivatives of a 2D Gaussian function and displayed as a histogram with the peak indicative of the dominant orientation (Figure 3.6; Liu, 1991). The standard deviation of the Gaussian distribution was then used as a proxy of fibre arrangement (with higher values suggesting more disorganised collagen fibres, and lower values implying a more parallel arrangement of fibres). The difference in dispersion was then compared within and amongst samples using Student *t*-tests and ANOVA (SPSS v25), with *p*-values<0.05 considered to be statistically significant.

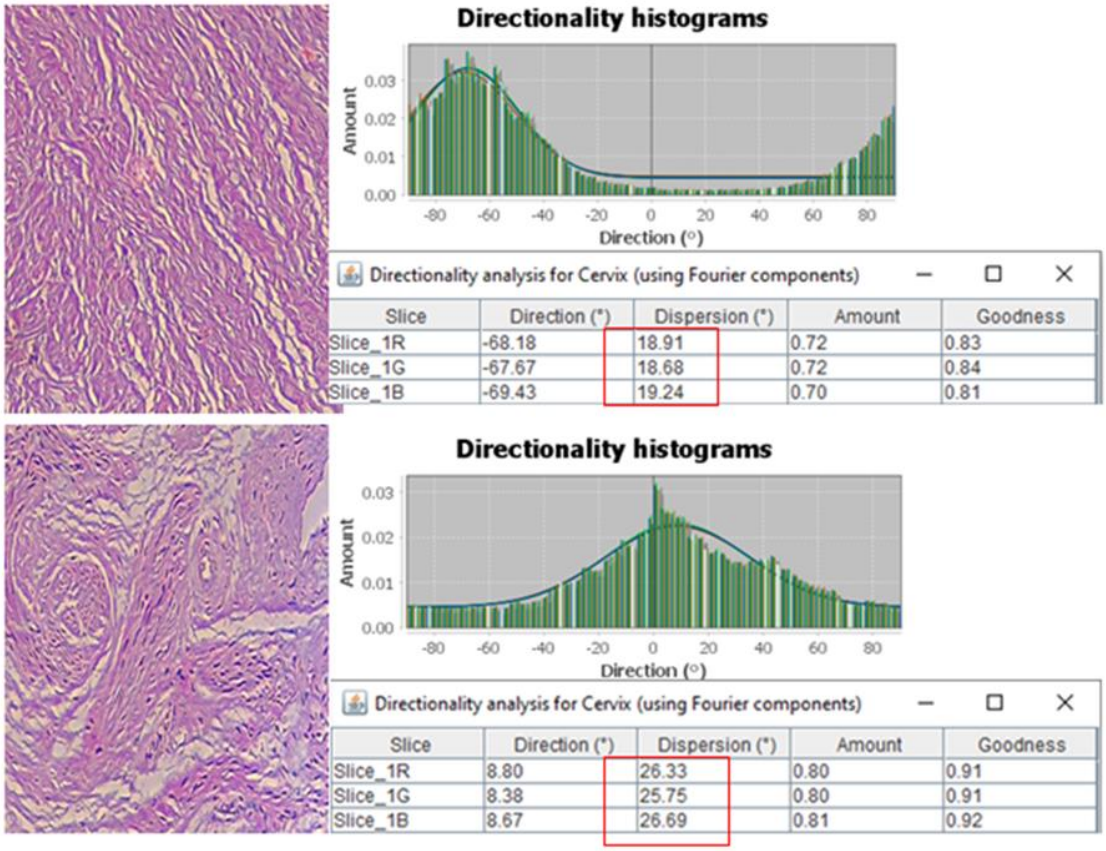

Figure 3.6. The directionality of collagen fibres in histological images of the human cervix were analysed with Fiji®. A histogram with the peak indicative of the dominant orientation was produced for each image, and the standard deviation was used as a surrogate for collagen fibre dispersion (values in red-squares).

3.3.12. **Correlation between PS-OCT and histological findings**

In order to validate any PS-OCT findings regarding the arrangement of collagen in the human cervix, the apparent birefringence was compared with the degree of dispersion of the collagen fibres using Pearson's correlation.

3.4. Results

I performed preliminary testing of an in-house PS-OCT on the non-gravid cervix of pre-, peri- and postmenopausal women to evaluate changes in birefringence and map the distribution of collagen fibres in the human cervix.

3.4.1. **Participants' demographic and clinical data**

Twenty participants were recruited for the study. Their demographic and clinical data is summarised in Table 3.4 and presented per menopausal status. Twenty-five percent (n=5) of the women recruited were premenopausal, 15% (n=3) perimenopausal -defined as any woman over the age of 45 with 3-11 months of amenorrhea and increased menstrual irregularity (Brambilla et al., 1994), and 60% (n=12) were postmenopausal.

As expected, premenopausal women were significantly younger than perimenopausal, who in turn, were younger than their postmenopausal counterparts ($p<0.001$). The indication and type of surgery was different among the three menopausal groups ($p<0.05$), while no significant difference was seen for BMI ($p=0.58$), parity ($p=0.71$), previous mode of delivery ($p=0.21$) or hormonal treatment ($p=0.31$).

Table 3.4. Demographic and clinical characteristics of PS-OCT participants

Parameters		**Premenopausal (n=5)**	**Perimenopausal (n=3)**	**Postmenopausal (n=12)**
Age (years)		38.80 (6.80)*	49.67 (1.15)*	68.33 (8.59)*
BMI (kg/m^2)		25.39 (3.6)	26.67 (4.72)	28.07 (5.29)
Parity	0	20% (n=1)	-	-
	1	20% (n=1)	-	16.67% (n=2)
	2	40% (n=2)	66.67% (n=2)	41.67% (n=5)
	3	20% (n=1)	33.33% (n=1)	25% (n=3)
	4	-		16.67% (n=2)
Previous mode of delivery	VB	60% (n=3)	100% (n=3)	91.67% (n=11)
	Instrumental	20% (n=1)	-	-
	Instrumental + VB	20% (n=1)	-	-
	VB + CS	-	-	8.33% (n=1)
Indication for surgery	Pain	40% (n=2)	33.33% (n=1)	-
	Prolapse	20% (n=1)$^{\#}$	33.33% (n=1)$^{\#}$	100% (n=12)$^{\#}$
	HMB	40% (n=2)	33.33% (n=1)	-
Type of surgery	TAH	40% (n=2)$^{\#}$	-	-
	VH	60% (n=3)$^{\#}$	66.67% (n=2)$^{\#}$	100% (n=12)$^{\#}$
	TLH	-	33.33% (n=1)$^{\#}$	-
Hormonal treatment	GnRH	20% (n=1)	33.33% (n=1)	-
	Estriol 0.1%	-	-	16.67% (n=2)

*Mean ± SD, *ANOVA p<0.001, # Chi-square p<0.05, CS: caesarean section, GnRH: gonadotrophin releasing hormones, HMB heavy menstrual bleeding, TAH: total abdominal hysterectomy, TLH: total laparoscopic hysterectomy, VB: vaginal birth, VH: vaginal hysterectomy*

3.4.2. **PS-OCT qualitative analysis of retardance**

The cervical cross-sections from all participants (n=20) were scanned progressively in a circumferential fashion from the endocervical canal to the edge. On the lid of the Petri dish three circumferential areas of equal size were drawn to facilitate orientation during scanning (central -C-, middle -M- and edge -E-), and each of these regions was then scanned three times at randomly selected sub-areas of 4 x 4 x 2 mm using the in-house PS-OCT.

As a result, nine sets of 1000 B-scans were obtained from each of the 20 samples (180 sets in total). The intensity and retardance scans in each set were then qualitatively and quantitatively assessed both in an axial and sagittal view (Figure 3.7a).

Within the retardance images, the blue colour indicated lower refractive index components, whereas the areas with a red-deep orange oscillation denoted the presence of birefringent structures and the more yellow-light orange pixels were associated with noise. As expected, in all sagittal views we identified a broad blue band at the superior end, evidencing the presence of a relatively poor birefringent cervical epithelium. Underneath the epithelium, a deeper orange line was seen in some of the regions, indicating the birefringent collagenous content of the stroma arranged perpendicular to the incident light (Figure 3.7b).

(a)

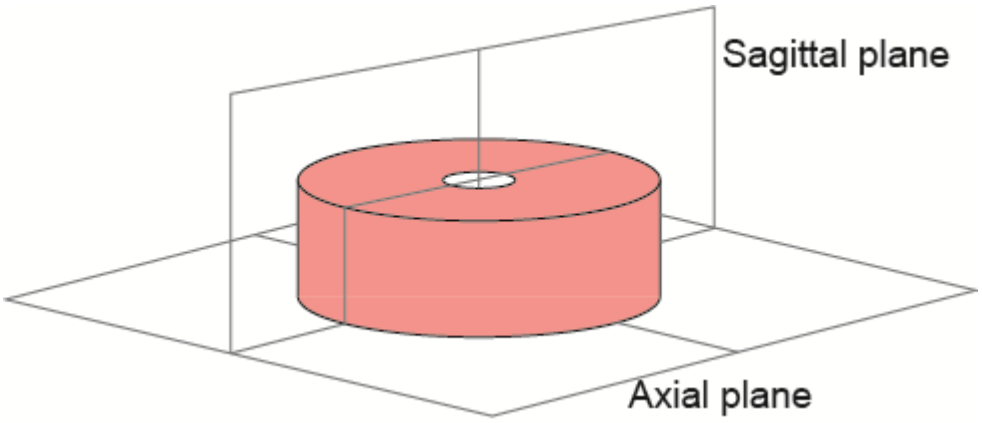

(b)

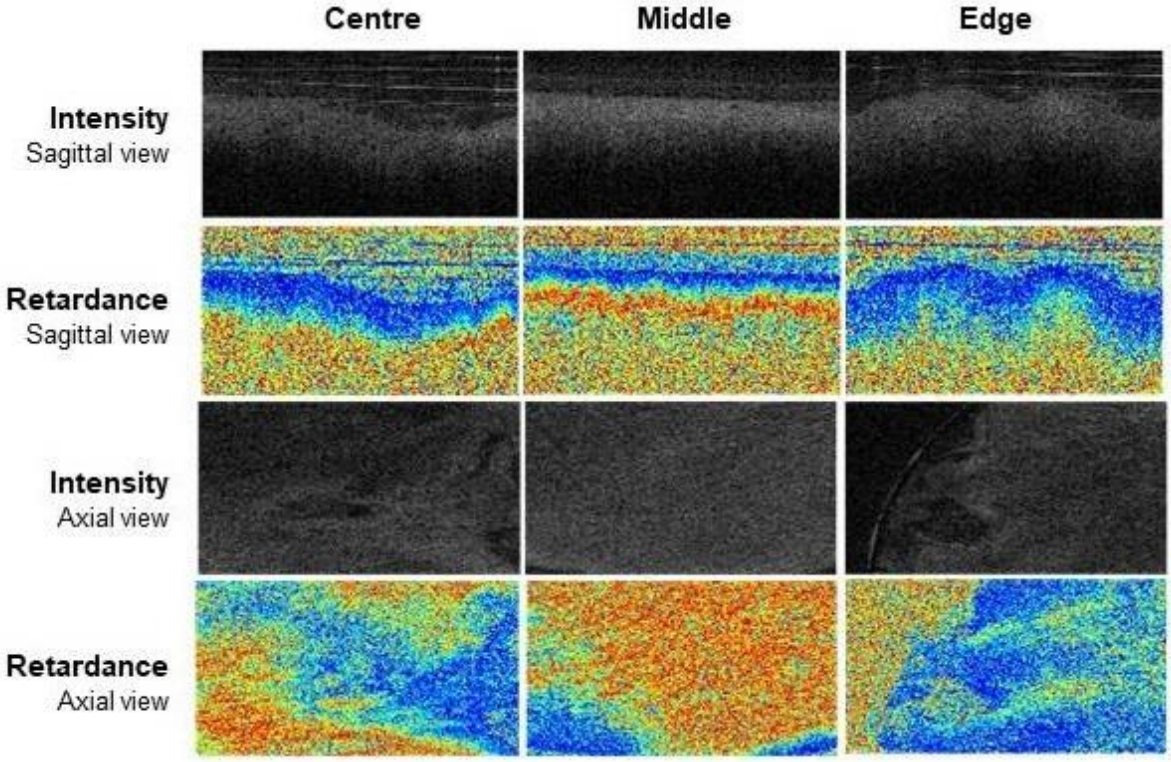

Figure 3.7. (a) Schematic of cervical planes, **(b)** PS-OCT views of cervical intensity and retardance from a sagittal and an axial view, and displayed by cervical region

When the retardation images in sagittal plane were grouped per region, the colour oscillation was noted to be distinctively stronger in the middle area compared to the centre or the edge. The middle region consistently had a more continuous red-orange line underneath the blue upper band, while the centre and the edge displayed a fainter red line or no line at all, or in some occasions, an interrupted line (Figure 3.8).

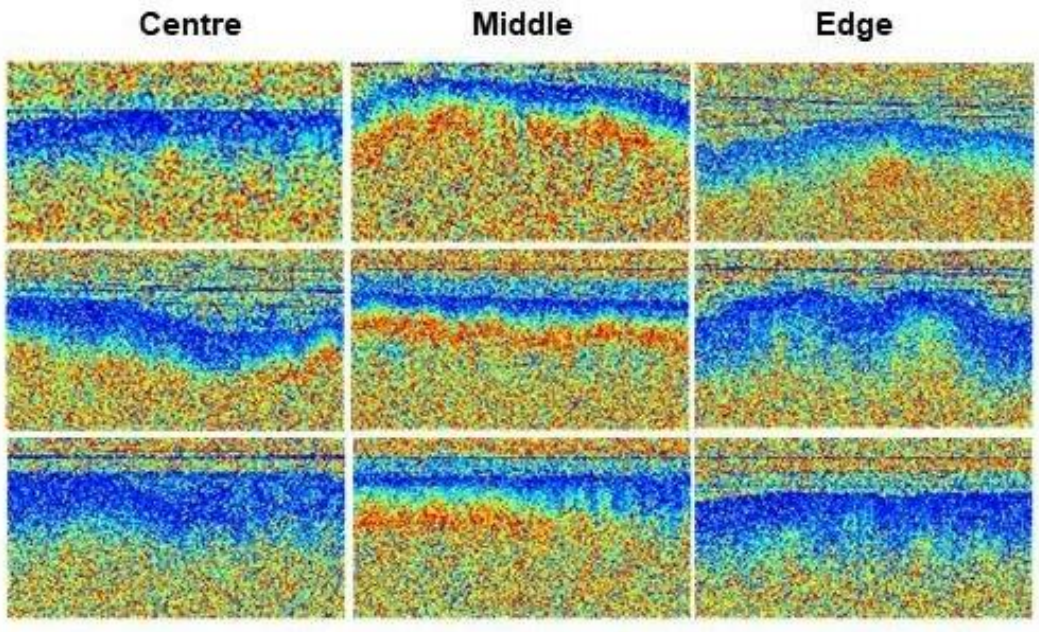

Figure 3.8. PS-OCT retardance displayed by cervical region in sagittal view

3.4.3. **PS-OCT differences in birefringence by cervical region**

Plotted in a split histogram, the apparent birefringence looked reasonably normally distributed for the middle and edge cervical regions but positively skewed for the centre area (Figure 3.9). The three histograms also appeared equally wide (with the exception of a few outliers), implying similar variances for all three regions. These initial assumptions were further corroborated with descriptive and analytical statistics. A non-significant Levene's test (=0.09) supported the equality of variances. The middle area had a mean apparent birefringence of $6.29 \times 10^{-3} \pm 4.01 \times 10^{-3}$, whereas the centre and edge regions had a mean birefringence of $2.75 \times 10^{-3} \pm 8.32 \times 10^{-4}$ and $2.59 \times 10^{-3} \pm 0.12 \times 10^{-3}$ respectively (Table 3.5; Figure 3.10).

The null hypothesis that all regions within the cervix would display a similar mean apparent birefringence was rejected ($p<0.001$). Post-hoc comparisons using the Bonferroni test showed significantly higher values for the middle area compared to the edge or the centre regions with an effect size of 33.4% (Table 3.5).

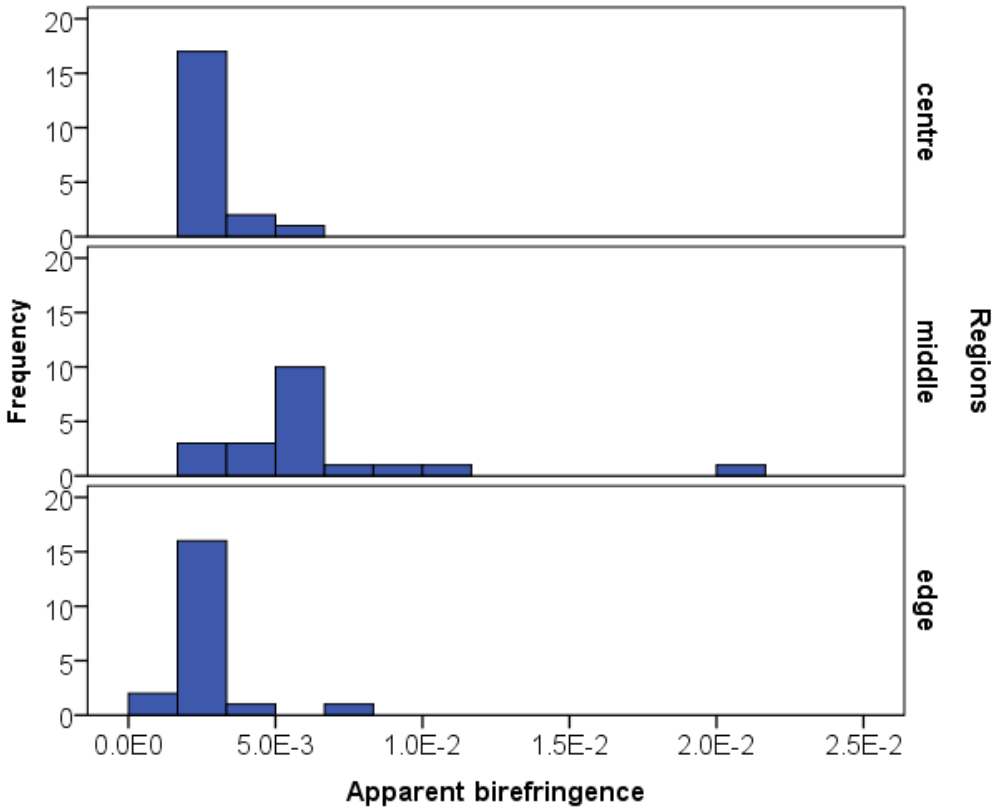

Figure 3.9. Distribution of apparent birefringence by cervical regions: centre, middle and edge

Table 3.5. Mean apparent birefringence per region. Bonferroni-adjusted one-way ANOVA

	Regions		
	Centre	**Middle**	**Edge**
n	20	20	20
Mean	2.75×10^{-3} *	6.29×10^{-3}	2.59×10^{-3}*
SD	8.32×10^{-4}	4.01×10^{-3}	0.12×10^{-3}

** p<0.05 versus middle region, n=number of samples, SD: standard deviation*

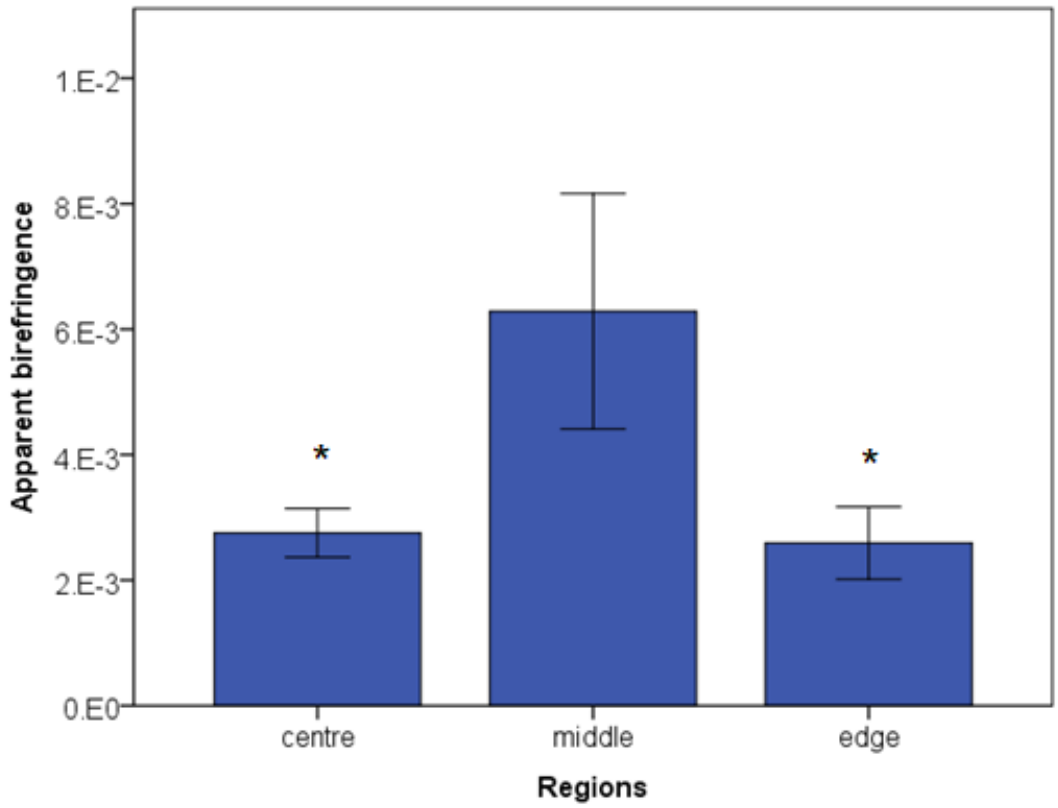

Figure 3.10. Average means of apparent birefringence per cervical region. Error bars indicate 95% CI interval confidence for the mean apparent birefringence. **p-value<0.05 versus middle region*

3.4.4. **PS-OCT differences in birefringence by parity**

Participants' parity ranged from zero to four. When the distribution of apparent birefringence was plotted against parity, all regions met the assumption of equal variances except for the edge (Levene's test, p=0.004). Therefore, for the centre and the middle region, one-way ANOVA was used whereas for the edge area, the non-parametric Kruskal-Wallis test was employed instead. The apparent birefringence of none of the three cervical regions seemed to significantly differ based on parity (centre, p=0.98; middle, p=0.55; edge, p=0.30).

3.4.5. **PS-OCT differences in birefringence by age**

The apparent birefringence was subsequently assessed against the age of the participants using a 2-tailed Pearson's correlation. In the middle region, apparent birefringence seemed to significantly increase with age (p<0.01). On the other hand, the correlations for the central and edge area were not statistically significant (p=0.08 and p=0.62 respectively; Figure 3.11).

(a)

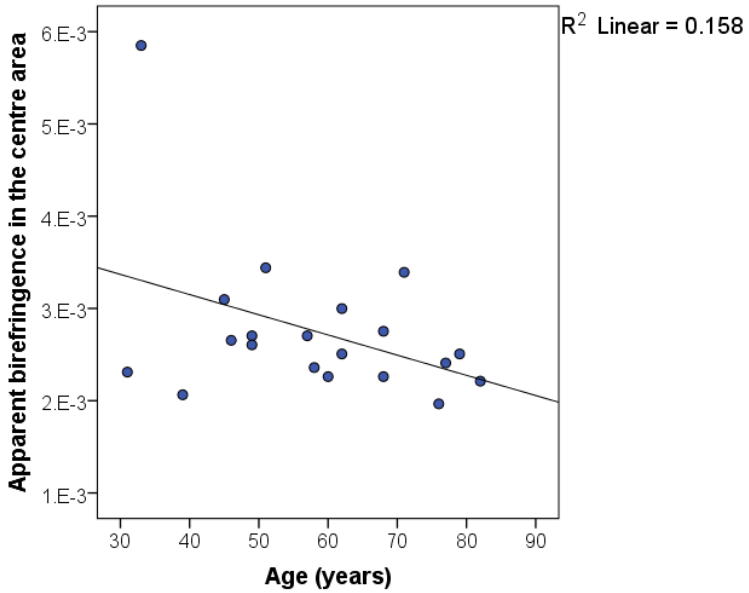

(b)

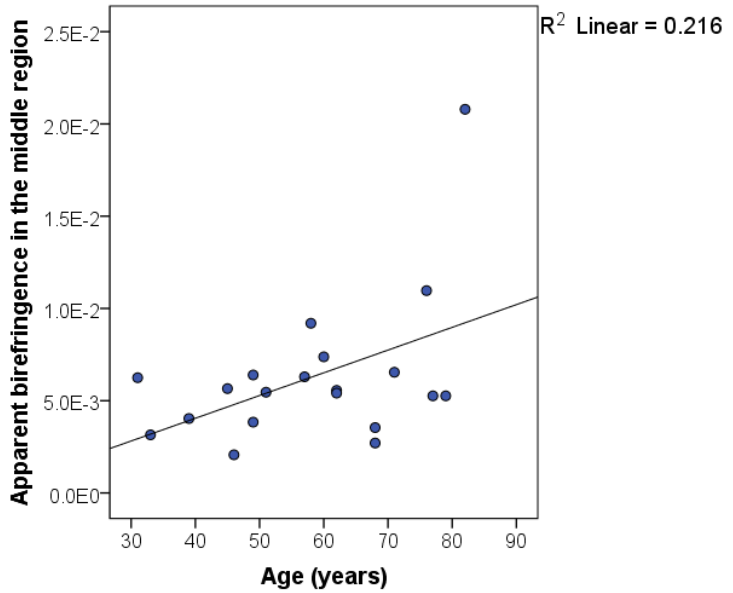

(c)

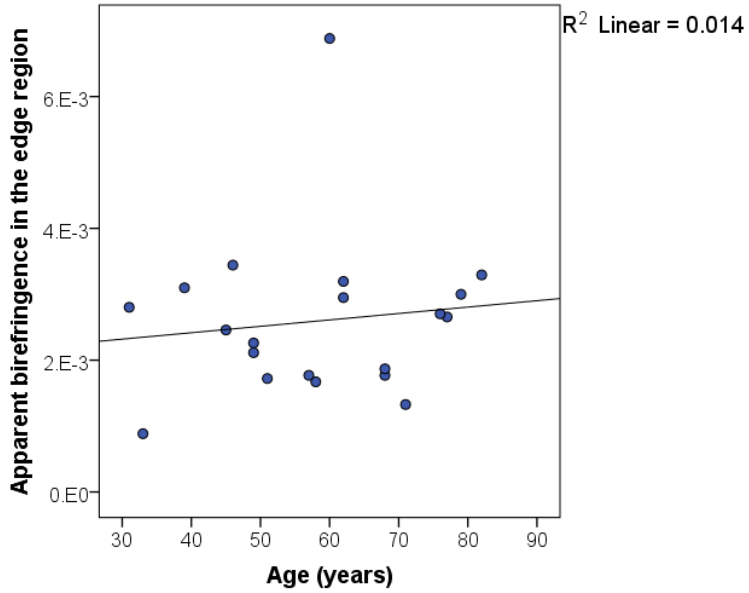

Figure 3.11. Association between apparent birefringence and age for each of the cervical regions: **(a)** centre, **(b)** middle and **(c)** edge. Age positively correlated with birefringence in the middle region ($p<0.01$)

3.4.6. **PS-OCT differences in birefringence by menstrual status**

In all women, regardless of their menopausal status, the apparent birefringence of the middle area was higher than the centre and edge areas (Figure 3.12, Table 3.6). However, when the mean apparent birefringence from each cervical region was compared across the different menopausal groups, no statistically significant differences were found (centre region, p=0.37 with Kruskal-Wallis; and middle and edge regions, p=0.31 and p=0.69 respectively with one-way ANOVA).

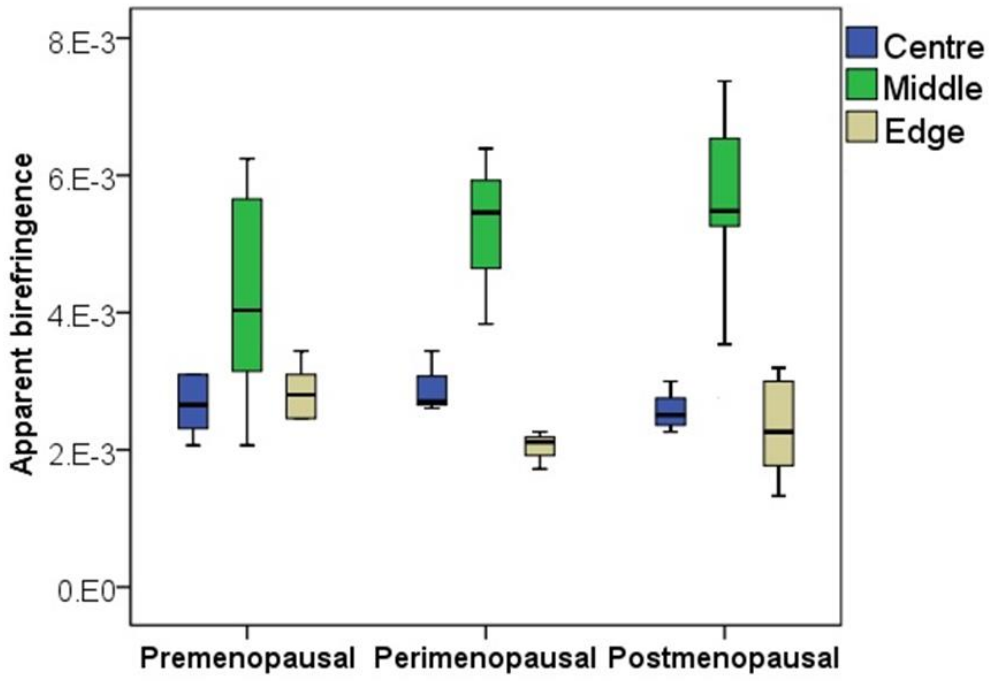

Figure 3.12. Mean differences in apparent birefringence presented by menopausal group. *Error bars ± 95% CI*

Table 3.6 Mean apparent birefringence in each cervical region based on menopausal status

	Regions (Mean ± SD)		
	Centre	**Middle**	**Edge**
Premenopausal (n=5)	$3.20 \times 10^{-3} \pm 1.53 \times 10^{-3}$	$4.23 \times 10^{-3} \pm 1.71 \times 10^{-3}$	$2.54 \times 10^{-3} \pm 9.92 \times 10^{-4}$
Perimenopausal (n=3)	$2.91 \times 10^{-3} \pm 4.57 \times 10^{-4}$	$5.23 \times 10^{-3} \pm 1.29 \times 10^{-3}$	$2.03 \times 10^{-3} \pm 2.70 \times 10^{-3}$
Postmenopausal (n=12)	$2.53 \times 10^{-3} \pm 3.87 \times 10^{-4}$	$7.41 \times 10^{-3} \pm 4.77 \times 10^{-3}$	$2.76 \times 10^{-3} \pm 1.46 \times 10^{-3}$

SD: standard deviation

3.4.7. **PS-OCT differences in birefringence by BMI**

Apparent birefringence did not significantly correlate with BMI for any of the three cervical areas proposed, (centre p=0.18, middle p=0.92 and edge p=0.65). As illustrated in Figure 3.13, the coefficients of determination (R^2) in all groups were close to 0 suggesting that the two variables do not fluctuate in tandem.

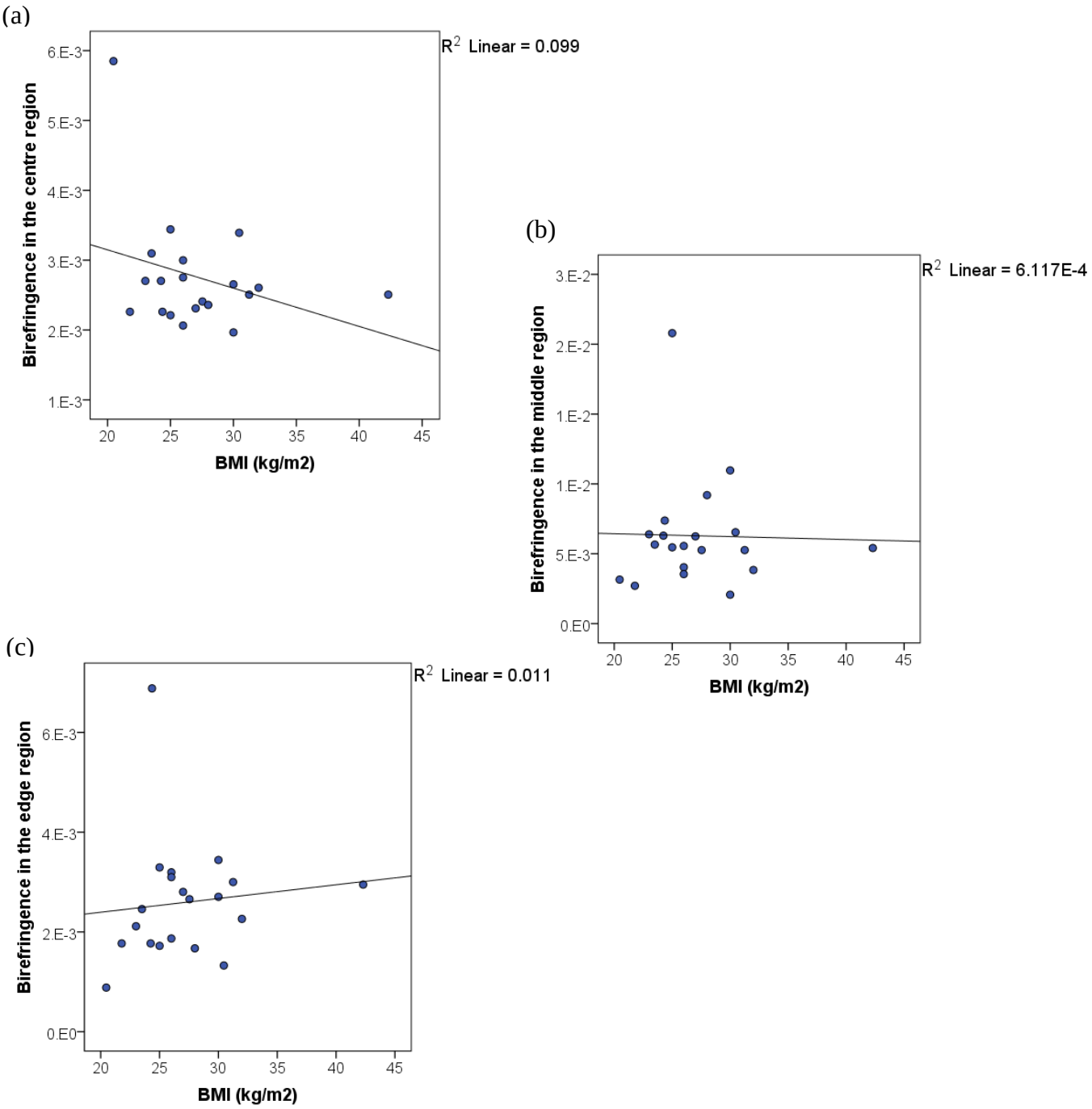

Figure 3.13. The association between apparent birefringence and BMI in the **(a)** centre, **(b)** middle, and **(c)** edge regions was not statistically significant.

3.4.8. **H&E and Masson's histology: qualitative analysis of cervical collagen orientation**

Collagen fibres appeared better aligned and more parallel in the middle region compared to the edge or the centre regions when either H&E or Masson's Trichrome were employed as the staining technique to qualitatively assess the histologically-processed cervical specimens (Figure 3.14). This initial observation was further validated by independent blinded assessors who managed to identify the most aligned samples, that is, those images corresponding to the middle area (n=6) within a pool of 16 images with a sensitivity of 94.53% (89.06%-97.77%), and a specificity of 100%.

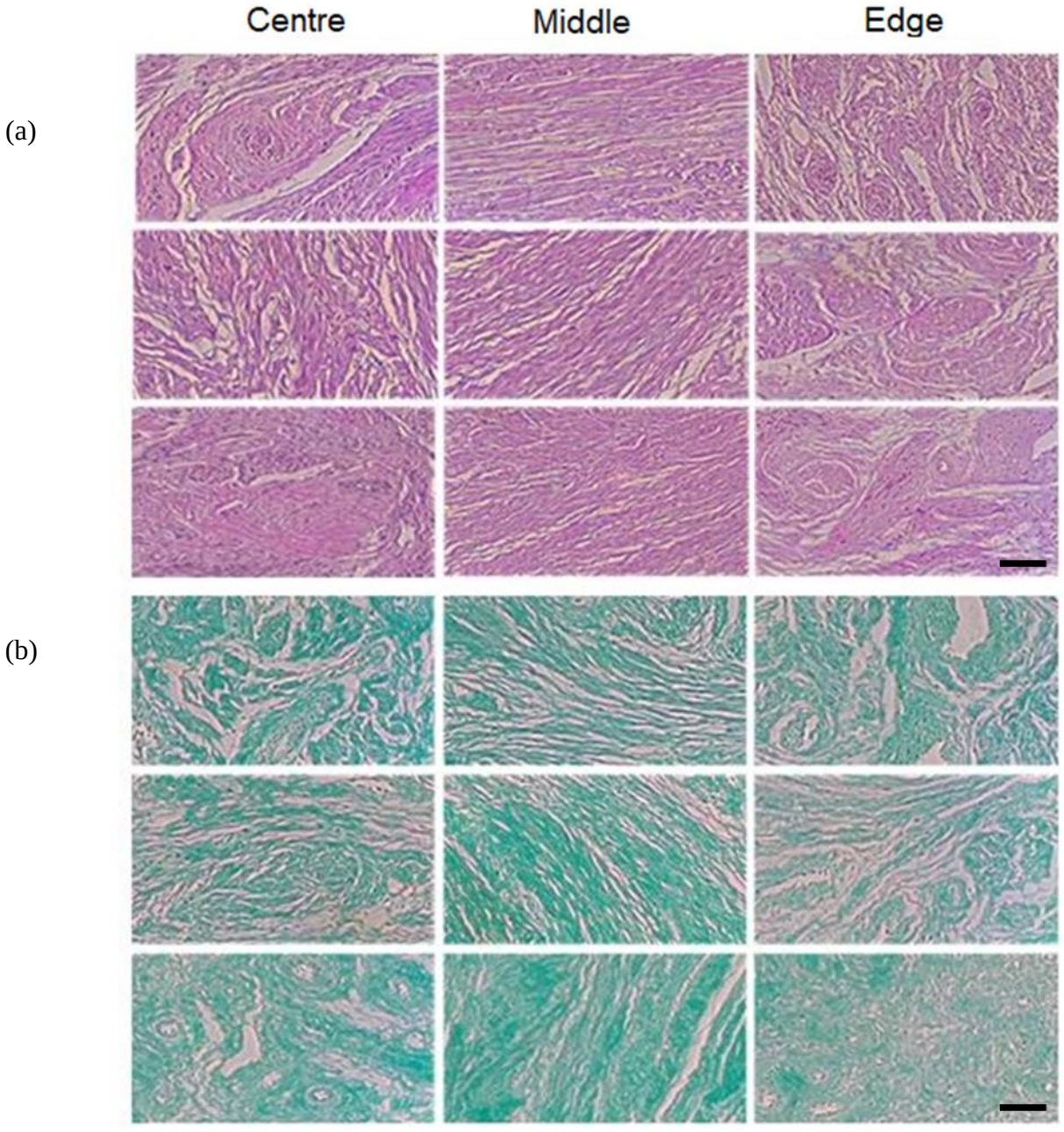

Figure 3.14. Cervical regions stained with **(a)** H&E or **(b)** Masson's trichrome technique displayed per cervical region. *Scale bar=100 μm*

3.4.9. **H&E and Masson's histology: quantitative analysis of cervical collagen orientation**

Plotted in a split histogram, the dispersion of the collagen fibres appeared only normally distributed for the centre and the edge regions, but not for the middle area (Figure 3.15).

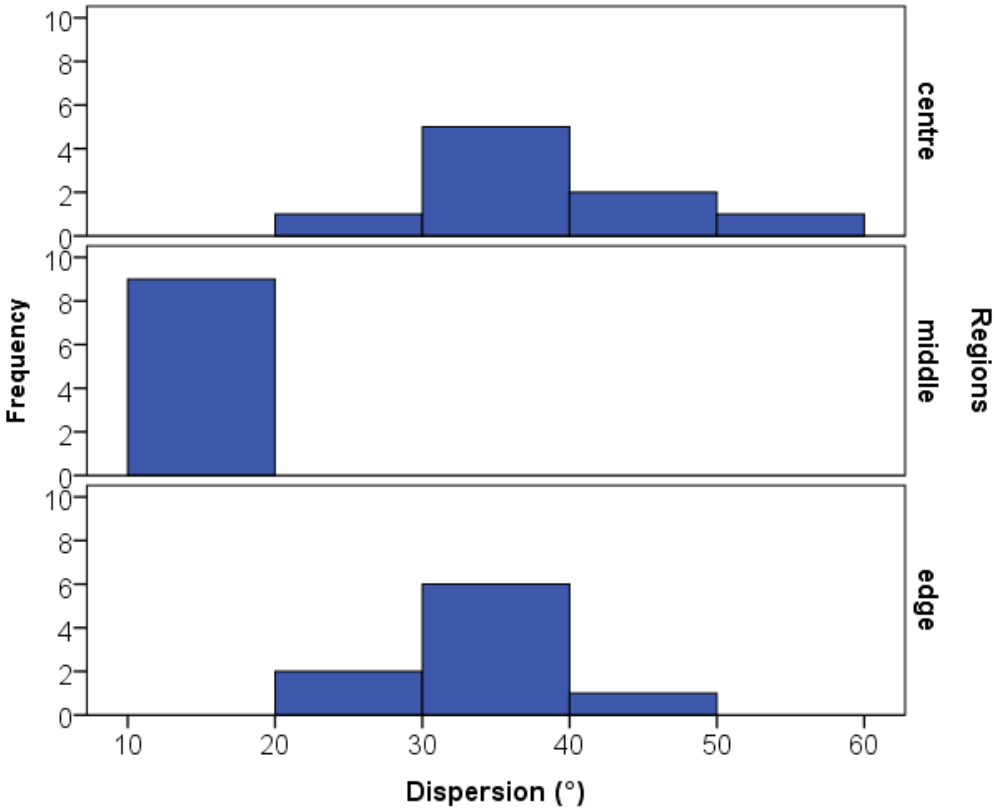

Figure 3.15. Distribution of collagen fibre dispersion represented for each cervical area

This finding was quantitatively confirmed with the Levene's test for equality of variance ($p<0.001$). As a result, the non-parametric Kruskal-Wallis test was employed instead of ANOVA to compare the dispersion in the alignment of collagen fibres amongst the different cervical regions. Consistent with the qualitative observations, the test showed that the collagen fibres in the middle area were significantly less dispersed and therefore, more parallel arranged than in the centre and edge regions ($p<0.001$; Figure 3.16, Table 3.7).

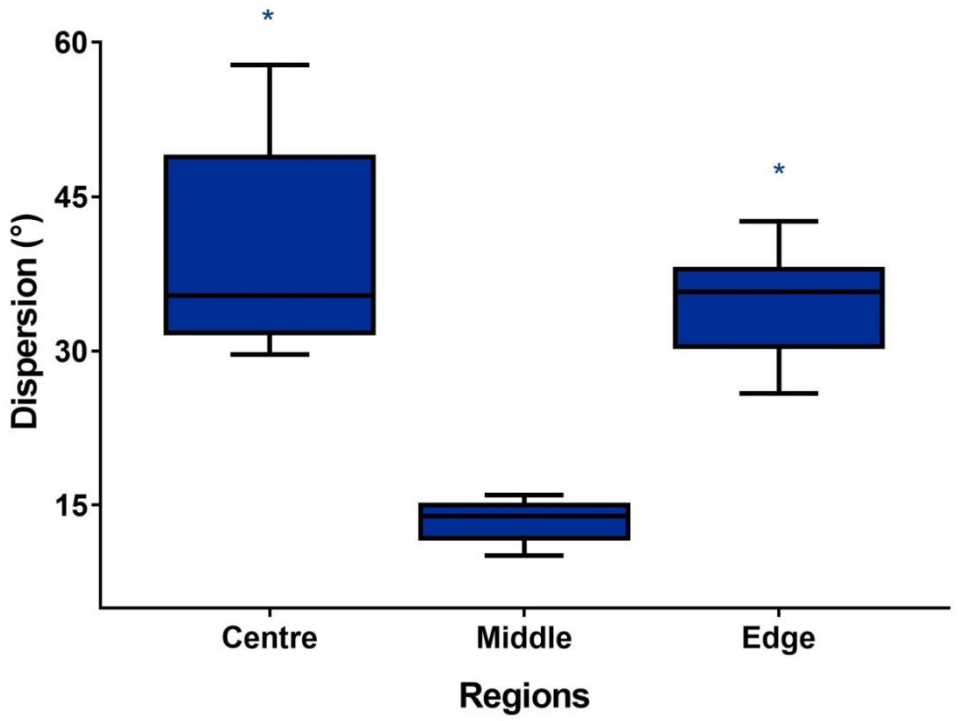

Figure 3.16. Median dispersion for collagen fibres in each cervical region. Boxes represent the interquartile range (25-75thquartile), whereas the whiskers indicate minimum-maximum values.
*p-value<0.05 versus middle region

Table 3.7. Median and interquartile range dispersion of collagen fibre alignment per region using non-parametric Kruskal-Wallis

	Regions		
	Centre (n=9)	**Middle (n=9)**	**Edge (n=9)**
Median (°)	35.36*	13.90	35.74*
Interquartile range (°)	17.56	3.70	7.94

** p<0.05 versus middle region*

3.4.10. **Correlation between PS-OCT and histological findings**

The degree of dispersion of collagen fibres negatively correlated with the apparent birefringence ($p<0.001$), as fibres orientated perpendicular to the light were more uniformly aligned in the histological specimens (Figure 3.17). Contrarily, fibres orientated oblique or parallel to the light, that is, fibres with lower birefringence seemed more disorganised as cross-sections of the collagen bundles became more apparent (Figures 3.14 and 3.17).

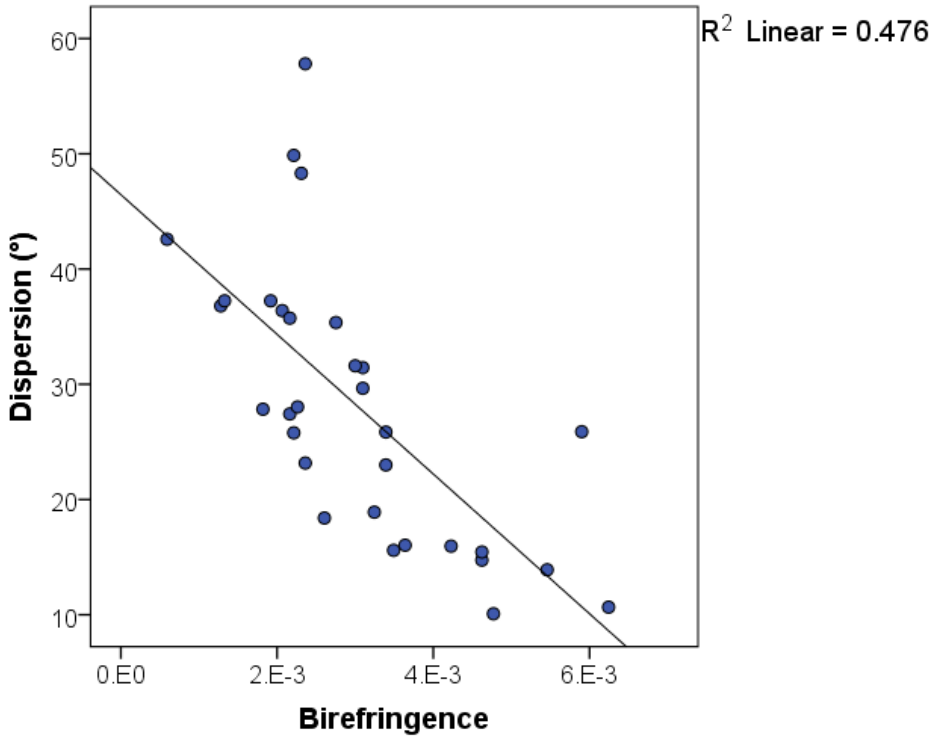

Figure 3.17. Correlation between histology and PS-OCT findings. The degree of dispersion assessed in the histological specimens negatively correlated with the apparent birefringence, ($p<0.001$).

3.5. Discussion and interpretation

3.5.1. **Main findings**

In this chapter, PS-OCT was used on cervical samples to identify whether it could reliably detect changes in the collagen arrangement. In collaboration with the Department of Materials Science and Engineering at the University of Sheffield, we interrogated 20 cross-sections from the ectocervix of women who had undergone hysterectomy for benign reasons with our in-house PS-OCT prototype. After systematically scanning the samples and computing the data, we were able to accurately determine the phase retardation and birefringence of the cervical collagen. By mapping out the birefringence of each cervical area, we were then able to estimate the distribution of collagen fibres in the cervix.

Regardless of parity, age, menopausal status or BMI, significantly higher birefringence values were identified in the middle region of all cervical samples, which suggests that collagen fibres located in this area are arranged more perpendicular to the incident light (90°) than those situated closer to the edge or the endocervical canal ($p<0.001$). It appears, therefore, consistent with previous X-ray diffraction findings (Aspden, 1988), that collagen fibres around the endocervical canal and in the outermost region are preferentially arranged in a longitudinal or oblique fashion, whereas those in the middle area are predominantly circumferential.

After characterising the distribution of birefringence in the cervical samples, I explored whether this preferential arrangement of collagen fibres varied depending on parity, age, menopausal status or BMI. Similarly to what Yao et al. (2016) reported in their OCT study, no significant difference in birefringence was found based on parity (centre, $p=0.98$; middle, $p=0.55$; edge, $p=0.30$). However, when anisotropy was analysed against age, birefringence was shown to positively correlate with age for the middle cervical region ($p<0.01$). Collagen fibres in the middle region appeared more circumferentially aligned in older women. This observation is consistent with my previous SHG work in which we showed that in postmenopausal women cervical collagen fibres in the middle region are more parallel-aligned than in their premenopausal counterparts (Narice et al., 2016). Since the orientation of collagen fibres determines the direction in which the cervix can best withstand tensile strain, we hypothesised that cervical remodelling, far from being confined to pregnancy, is a continuous and gradual process which extends beyond the reproductive years (Aspden, 1988, Bauer et al., 2007, Myers et al., 2015). As the function of the cervix evolves with age, the cervical collagen network will continue to reorganise itself to reflect these changes.

Currently, no imaging techniques can assess the *in vivo* remodelling of the cervix in pregnancy and throughout life at a microscopic level. After the early experiments performed with X-ray diffraction, at least four other research imaging modalities have been tested to assess, with some success, the preferential orientation of collagen fibres in the cervix including magnetic resonance diffusion tensor imaging (MRDTI), SHG, conventional OCT and full-field Mueller Matrix polarimetry (Weiss et al., 2006, Akins et al., 2010, Lau et al., 2013, Yao et al., 2016, Liang et al., 2018). Two cervical areas with distinctive collagen arrangement have been identified with MRDTI: an outer region with circumferentially-positioned collagen and an inner region with collagen fibres running more vertically (Weiss et al., 2006). SHG has also identified differences in collagen alignment in the human cervix, but given the technique's high resolution of approximately 2μm, the analysis on directionality has been at fibril-level rather at histological level (Feltovich et al., 2012, Narice et al., 2016). OCT has also managed to partly recreate *in vitro* the three radial zone model described by Aspden (1988) in the upper portion of the human cervix known as *portio supravaginalis* both in pregnant and non-pregnant women (Feltovich et al., 2012, Yao et al., 2016). *In vivo* experimental Mueller Matrix polarimetry has also been capable of identifying changes in the circumferential orientation of collagen fibres close to the cervical os between non-pregnant and pregnant women (Chue-Sang et al., 2017, Chue-Sang et al., 2018). However, limitations inherent to these imaging techniques such as slow real-time processing (MRDTI), limited imaging speed (SHG), lack of tissue-specific contrast and depth-resolved changes in tissue phase retardance and birefringence (OCT and Mueller matrix polarimetry respectively) have affected their translatability into the clinical setting. Hence, there remains a need to develop more accurate and precise non-invasive imaging techniques which can better support clinical practice.

As shown in this chapter, PS-OCT may have the potential to meet this need. On top of sharing OCT high resolution and high 3D speed imaging, PS-OCT has the advantage of being able to measure the polarisation state of the backscattered optical light when it interacts with anisotropic structures such as collagen (Pircher et al., 2011, Gan et al., 2014). This feature is of particular relevance in the study of the human cervix which, unlike the rest of the muscular uterus, is predominantly comprised of a collagen-rich, and therefore highly anisotropic connective tissue (Danforth, 1983; Strasswimmer *et al.*, 2004). To the best of our knowledge, the use of PS-OCT on the cervix has only been reported by one previous study. Lee *et al.* (2008) employed a PS-OCT prototype specifically to detect cervical intraepithelial cancer (CIN) on human cervical biopsies, for which they reported a sensitivity of 94.7% and a specificity of 71.2%.

3.5.2. **Strengths**

The strength of this study relies mainly on its relevance, innovation and design robustness. Accurate and acceptable ways to assess cervical remodelling *in vivo* are lacking. Insight into these changes in human beings has been gleaned by limited invasive biopsy studies and conventional microscopic techniques. Characterising these changes using techniques that may lend themselves to future non-invasive applications remains a major challenge. Our proof-of-concept study has demonstrated for the first time the ability of PS-OCT to characterise the arrangement of the collagen network in the *in vitro* human cervix, and supports the potential development of an *in vivo* probe for collagen monitoring during cervical remodelling in pregnancy. PS-OCT is particularly suitable for integration into an endoscope or hand-held probe as evidenced by the many OCT probes which are already used in the clinical setting for eye and skin disorders (Fujimoto and Swanson, 2016).

There are currently no techniques capable of identifying women who are at higher risk of going into premature labour, a condition that affects approximately 10.6% of all births and 14.8 million infants worldwide every year (Lee et al., 2019). If changes in the arrangement of cervical collagen were shown to be predictive of PTB, PS-OCT could be developed into a portable and non-invasive point-of-care device to screen for PTB during pregnancy all around the world. Interventions such as administration of antenatal steroids to accelerate fetal lung maturation, admission for ongoing inpatient care or *in utero* transfer to appropriate neonatal treatment facilities could be better targeted to women who screen positive for sPTB.

One of the main pillars of the present study was the robustness of its design: a detailed protocol was developed and subjected to internal and external peer review prior to commencing experiments. All PS-OCT data was analysed by two independent assessors. In case of disagreement, an agreement was reached with input from a third senior assessor. PS-OCT findings on collagen fibres directionality were correlated with conventional histology. For the qualitative analysis of collagen fibres orientation, we selected assessors who had no previous knowledge of the study and who were blinded to region classification and outcomes to minimise bias.

3.5.3. **Limitations**

The present study supports the potential of PS-OCT as a clinically-applicable imaging technique to assess the cervix. However, it does not come without a series of limitations which should be addressed in future analyses.

The experiments were performed *in vitro* on cervical specimens harvested from non-pregnant women given the exploratory nature of the study which aimed to generate proof-of-concept data for the ability of PS-OCT to reliably assess collagen orientation in the cervix. Consequently, our findings do not reflect the dynamic and complex process of cervical remodelling in pregnancy. However, they demonstrate that PS-OCT is able to characterise collagen orientation in the *in vitro* human cervix with accuracy and precision when compared to conventional histology, thus setting the foundation for further *in vivo* studies pending the development of a hand-held probe.

Previous *in vitro* studies using OCT have focused on the collagen network at the *portio supravaginalis* of the cervix rather than the *portio vaginalis* (Yao et al., 2016), as there is evidence to support that the upper section of the cervix plays an instrumental role in maintaining the integrity of the cervix during pregnancy (Myers et al., 2015). Some studies have even suggested that the internal os may behave as an occlusive muscular structure (Nott et al., 2016), even though it is not clear whether such muscular bundles are actually functional (Rorie and Newton, 1967, Vink and Feltovich, 2016). Not surprisingly, early changes identified at the internal os such cervical funnelling have been linked with cervical insufficiency and a higher risk of chorionamnionitis, PPROM and PTB (Stolz et al., 2017). However, in order to capture the behaviour and morphology of the upper cervix at a microscopic level with high resolution, a non-invasive imaging technique with a high-frequency wavelength would be needed at the expense of limiting the depth penetration. Poor depth penetration would render the technique not suitable to study the internal os *in vivo* which is located at least 3-4 cm away from the ectocervix, the furthest point a probe can interact with in the vagina. As a consequence, we purposely decided to scan the ectocervix and its underlying stroma rather than the upper region of the cervix as this would realistically be the area targeted by a non-invasive transvaginal PS-OCT probe.

For this PS-OCT pilot study, the main focus has been on the microstructural arrangement of the collagen network in the human cervix. Previous studies have reported that cervical collagen fibres arranged in a circumferential fashion tend to prevent dilation of the cervix, whereas those organised longitudinally are thought to resist cervical effacement (Nott et al., 2016). Even though there is strong evidence to support a close link between structure and function, neither the mechanical function of the collagen fibres nor the correlation between mechanical and morphological findings has been directly tested in this study (Myers et al., 2015).

Given the pilot nature of the study, no formal sample size calculation was performed but based on previous studies, a target size of 20 samples was agreed (Narice et al., 2016). Despite the small number of samples tested, it was possible to establish a statistically significant association between age and birefringence. A similar result was expected for menopausal status and birefringence as

menopause and age tend to positively correlate. However, the null hypothesis could not be confidently rejected ($p>0.05$) most likely due to the sample being underpowered for this outcome. Further research is therefore encouraged before firm associations can be made between clinical parameters and bioptical properties of the cervix.

Regarding the control technique, electron microscopy (EM) and its variants have been proposed as the gold-standard imaging technique for assessing the ultrastructure of the collagen fibres at the nanometre level (Bancelin et al., 2014). However, given its high cost and demanding sample preparation protocol, we purposely selected transmitted-light microscopy as the control technique to validate PS-OCT findings on cervical collagen fibre orientation. Despite its lower resolution, optical microscopy offers a wider field of view than EM which enables better visualisation of the overall cervical extracellular matrix. To improve visualisation and characterisation of the cervical collagen content, cervical samples were not only stained with H&E but also with Masson's trichrome technique which is more collagen-specific (Flint et al., 1975, Kershaw et al., 2007).

Finally, by interrogating the cervical surface with an incident light at 90°, the PS-OCT strategy described in this chapter was able to partly recreate the complex 3D collagenous scaffolding of the human cervix by measuring apparent birefringence. However, as previously mentioned, apparent birefringence does not only depend on the intrinsic optical anisotropy of the collagen fibres but also on the orientation of the optic axis. Even though our study does not specifically measure intrinsic birefringence, it has set the foundations for follow-on research with an alternative PS-OCT scanning strategy known as conical scanning PS-OCT (CS-PS-OCT). This technique involves scanning a conical surface of a sample which is normally placed at 45° to the incident light in order to calculate the fast axis and the "brush" direction of fibres in complex 3D biological tissues (Lu et al., 2014).

3.5.4. **Future research**

PS-OCT has the potential to help us better understand cervical remodelling prior to birth. Given the extensive experience of our research group in developing engineering techniques for clinical application, we plan to develop a hand-held PS-OCT prototype which could be used for *in vivo* assessment of cervical collagen and epithelium depth. Such a technique could then become the ideal complement of bioimpedance techniques such as EIS or MIS for real-time study of cervical remodelling in pregnancy.

Future work could explore the possibility of subjecting the cervical samples to dynamic shear analysis using oscillatory deformation under compression to obtain additional information about mechanical integrity and its correlation with structural changes (Feltovich et al., 2012).

Furthermore, the 3D structural orientation of collagen fibres and intrinsic birefringence of the cervix could be further explored with the conical bean scanning PS-OCT. The information provided by successive azimuthal rotations of 0-360° could then be used to compare the alignment of collagen between different cervical regions and cohorts of patients (Li et al., 2019).

Chapter 4

Magnetic induction spectroscopy as a potential technique for non-invasive assessment of electrical biomarkers in the human cervix for the prediction of spontaneous preterm birth

4.1. Introduction and background

The electrical properties of a biological tissue are greatly dependent on its complex cellular and stromal architecture, any anatomical variation may therefore impact on the tissue's electrical behaviour. Cervical remodelling prior to sPTB is no exception. At early stages of the process, when structural changes of the cervix may be too small to be identified by current imaging techniques, subtle yet measurable variations in cervical dielectric properties may serve a diagnostic purpose for sPTB.

Building on recent work performed at the University of Sheffield using Electrical impedance spectroscopy (EIS), I hypothesised that Magnetic induction spectroscopy (MIS) may be able to accurately and reliably gauge the electrical properties of the cervix during pregnancy which might provide enough contrast to discriminate between women who deliver prematurely from those who deliver at term. Therefore, in this chapter, I aimed to test the technical and clinical performance of a specifically designed magnetic induction spectroscopic probe and explore its diagnostic potential for sPTB by sensing the electrical properties of the *in vitro* and *in vivo* human cervix.

4.1.1. **Spectroscopy techniques for cervical remodelling**

In the last few decades, there has been a growing interest in developing spectroscopic techniques which are capable of non-invasively assessing and monitoring cervical remodelling as potential predictive tools for PTB. In order to assess the scope of these studies and identify areas for future technology development and improvement, I conducted a comprehensive systematic review (Narice et al., 2018). All primary research which reported on the *in vivo* assessment of cervical remodelling with spectroscopic techniques that may hold potential for prediction of PTB was included. Studies were searched from Medline, Web of Science and Scopus from 1946, 1864 and 1960 respectively until July 2019 regardless of language or country of origin. The search terms used included "diagnosis", "preterm birth", "spectroscopy" and "cervical remodelling" as well as alternative keywords such as "cervical ripening", "prematurity", "screening" and "spectral analysis" (Appendix B). References from all the shortlisted articles were manually searched for additional studies.

The online database search yielded 107 studies (n=64 from Medline, n=29 from Web of Science and n=14 from Scopus), 15 of which were excluded for duplication. Twelve studies were retrieved from the citation search adding to a total of 104 articles. The titles and abstracts of these papers were assessed for eligibility, as a result of which 75 further studies were excluded. The full text of the remaining 29 papers was read in depth, out of which six studies were excluded for being

reviews or for not employing *in vivo* techniques. Overall, 23 primary research studies were included in the final review (Figure 4.1; Table 4.1).

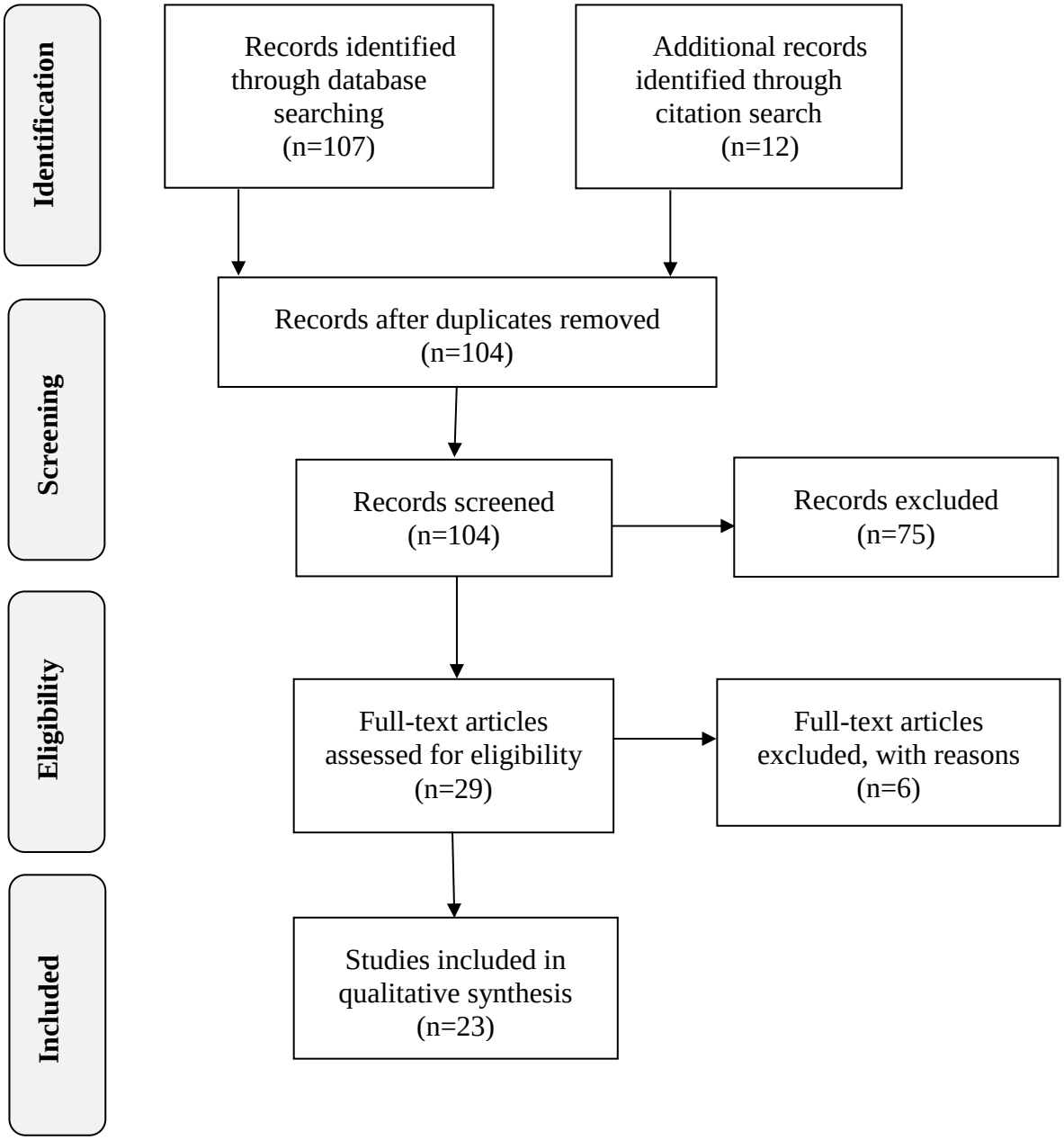

Figure 4.1. Preferred Reporting Items for Systematic Reviews and Meta-Analysis (PRISMA) flow chart showing the methodology for the selection of spectroscopic studies on *in vivo* cervical remodelling

Table 4.1. Summary of the studies included. Adapted from Narice et al. (2018)

Authors	Journal	Year	Subject	Technique
Glassman et al.	*Am J Obstet Gynecol*	1995	Mice	LIF
Glassman et al.	*SPIE Proceedings*	1997	Mice	LIF
Maul et al.	*Am J Obstet Gynecol*	2003	Human	LIF
Schlemback et al.	*Am J Obstet Gynecol*	2003	Human	LIF
Fittkow et al.	*Eur J Obstet Gynecol Reprod Biol*	2005	Human	LIF
Kuon et al.	*Am J Obstet Gynecol*	2011	Mice	LIF
Baños et al.	*Lasers in Surgery and Medicine*	2007	Human	FD-NIRS
Matzinger et al.	*Lasers in Medical Science*	2009	Human	FD-NIRS
Hornung et al.	*Lasers in Medical Science*	2011	Human	FD-NIRS
Vargis et al.	*Annals of Biomedical Engineering*	2012	Mice	RS
O'Brien et al.	*Nature Scientific Reports*	2017	Mice	RS
O'Brien et al.	*Am J Obstet Gynecol*	2018	Human	RS
O'Brien et al.	*J of Biophotonics*	2019	Human	RS
Qu et al.	*J of Biomedical Optics*	2018	Human	PANIR
Yan et al.	*IEEE International Ultrasonics Symposium*	2018	Mice	Spectroscopic PA
O'Connell et al.	*BJOG*	2000	Human	EIS
O'Connell et al.	*J Matern Fetal Neonatol Med*	2003	Human	EIS
Gandhi et al.	*Biomed Eng Online*	2006	Human	EIS
Gandhi et al.	*Eur J Obstet Gynecol Reprod Biol*	2006	Human	EIS
Jokhi et al.	*BMC Pregnancy Childbirth*	2009	Human	EIS
Jokhi et al.	*Biomed Eng Online*	2009	Human	EIS
Etemandi et al.	*IEEE Transaction on Biomedical Engineering*	2013	Human	EIS/LIF
Stern et al.	*BJOG*	2016	Human	EIS

EIS: electrical impedance spectroscopy, FD-NRS: frequency domain-near infrared spectroscopy, LIF: Light-induced fluorescence spectroscopy, PA: photoacoustic, PANIR: photoacoustic infrared

The selected studies can be divided into five categories based on the spectroscopic technique used namely light-induced fluorescence -also known as collascope-, frequency domain-near

infrared spectroscopy, different variants of photoacoustic spectroscopy, RS and bioimpedance spectroscopic techniques:

- Light-induced fluorescence spectroscopy

Light-induced fluorescence spectroscopy (LIF) relies on the native fluorescence generated by intrinsic fluorophores present in cells and tissue. The collagen-abundant cervix is particularly suited to this technique due to the high amount of fluorescent pyridinoline in its type I and III collagen crosslinking (Glassman et al., 1995). Early studies in non-pregnant and pregnant rats showed an inversely proportional relationship between LIF and gestational age. As term approached, fluorescence significantly decreased ($p<0.01$). Similarly, LIF was dramatically reduced if the cervix was treated with anti-progesterone agents, suggesting a change in collagen maturation prior to birth (Glassman et al., 1997, Shi et al., 1999). These findings were then validated in pregnant women in whom a significant decrease in cervical LIF was noted after treatment with prostaglandins (Fittkow et al., 2005, Kuon et al., 2011). LIF was also noted to be significantly lower in women with signs of labour who delivered within 24 hours compared to those who took longer to give birth (Maul et al., 2003), and in women who had been diagnosed with cervical insufficiency (Schlembach et al., 2003).

- Frequency domain-near infrared spectroscopy

Frequency domain near-infrared spectroscopy (FD-NRS), a non-invasive spectroscopic technique capable of assessing light scattering and absorbing structures in the cervix, showed a significant reduction in the cervical concentration of haemoglobin after the administration of prostaglandins in women who were undergoing termination of pregnancy in their first trimester. It was postulated this could be due to increased hydration (Baños et al., 2007). However, when FD-NRS was applied on non-pregnant women to assess cervical softening during menstrual bleeding, no changes in the total concentration of haemoglobin or water were seen, suggesting an alternative physiological cervical remodelling process during the regular endometrial cycle (Matzinger et al., 2009). Similarly, no significant changes were seen in water content throughout an uncomplicated pregnancy when tested with FD-NRS (Hornung et al., 2011).

- Photoacoustic spectroscopy

Photoacoustic spectroscopy (PA) has been combined with transvaginal cervical length (TVU CL) and ultrasound viscoelasticity to assess cervical hydration and oxygenation on rodent models with promising results (Yan et al., 2018). A variant which incorporates near-infrared spectroscopy

and endoscopic technology known as photoacoustic near-infrared (PANIR) has shown that water concentration in the human cervix seems to significantly increase as pregnancy progresses (Qu et al., 2018). These findings support the need for larger pre-clinical studies to assess the potential predictive value of PA and PANIR for PTB.

- Raman spectroscopy

When RS was employed to characterise *in vivo* cervical remodelling in rodents, significant spectral changes were noted in the peaks for fatty acids, aminoacids and collagen just before birth consistent with increased cervical compliance and ECM disorganisation (Vargis et al., 2012). These same peaks appeared with significant delay in mice with impaired cervical remodelling (cyclooxygenase-1 deletion) when compared to the wild type (O'Brien et al., 2017). Since then, *in vivo* RS has also been tested on the human cervix. Preliminary studies on healthy pregnant volunteers showed that blood-related Raman peaks significantly increased throughout pregnancy whereas those assigned to ECM proteins decreased ($p<0.05$; O'Brien et al., 2018). The recent development of a visually-guided RS probe which can be used without the need for a speculum portends higher patients' satisfaction in the clinical setting and sets the foundation for further clinical trials which are currently underway (O'Brien et al., 2019).

- Bioimpedance spectroscopy

Bioimpedance spectroscopy was first proposed in the late 1960s to measure body fluid volume by transmitting electric current in low frequencies through a specific tissue (Merhametsiz et al., 2015). It was subsequently employed to help differentiate between normal and cancerous tissue in breast, cervix, skin, and bladder (Halter et al., 2007). The way a biological tissue responds to electrical current depends on its physiological and physiochemical structure as well as on the frequency of the signal used. By combining tissue responses to electrical stimuli at multiple frequencies, unique information about the tissue anatomy and composition can be retrieved thus enabling differentiation between healthy and pathological samples (Dean et al., 2008, Bera, 2014).

By the early 2000s, a series of studies had already showed the potential of EIS to assess the electrical properties of the cervix in non-pregnant women and had opened up promising lines of research for EIS in pregnancy. Brown et al. (2000) reported that *in vivo* EIS measurements of the cervix correlated well with histopathological results for the prediction of precancerous cervical lesions (CIN2/3) with an AuROC of 0.92, and Predanic (2002) showed that *in vitro* impedance measurements were consistent with the traditional assessment of the cervix by palpation and could

be used to objectively characterise the consistency of the non-pregnant cervix into soft, moderate and firm ($p<0.0001$). A pilot study in pregnancy (O'Connell et al., 2000) also showed that cervical impedance values between pregnant women at term and non-pregnant women were significantly different ($p<0.001$) and postulated that EIS might be capable of predicting the onset of labour by characterising the cervical remodelling process which precedes labour. Since then, further studies have optimised the technique (Gandhi et al., 2006a, Gandhi et al., 2006b, Jokhi et al., 2009a, Jokhi et al., 2009b, Etemadi et al., 2013) and shown that EIS is capable of detecting significant changes in the cervix between women who deliver preterm and those who deliver at term (resistivity of 2.90 versus 3.5 ohm respectively, $p<0.0001$; Stern et al., 2016)

In women at high risk of sPTB, cervical impedance measured with EIS between 20-28 weeks of gestation in pilot studies has also been reported to show promise for predicting delivery<37 weeks with a sensitivity of 76% ($p<0.01$), higher than that obtained with CL or fFN (Figure 4.2; Anumba et al., 2018). A further randomised prospective multicentre study would enable validation of the clinical utility of EIS for predicting sPTB compared to routine care.

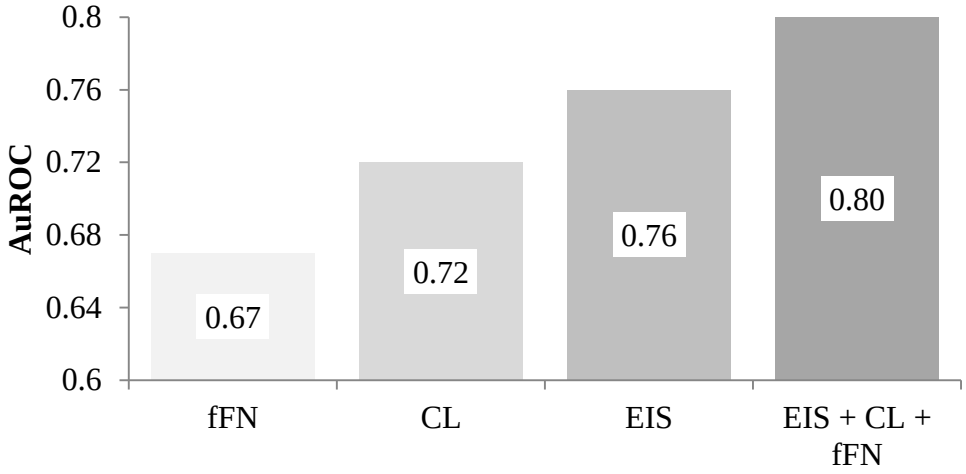

Figure 4.2. EIS test performance as a stand-alone technique and in combination with fFN and CL. *AuROC: area under the receiver operating characteristic curve, CL: cervical length, EIS electrical impedance spectroscopy, fFN: fetal fibronectin*. Adapted with permission from Anumba et al. (2018)

In this chapter, I proposed the use of a new bioimpedance spectroscopic technique known as Magnetic induction spectroscopy (MIS), which builds on the foundations of EIS, to assess cervical remodelling both *in vitro* and *in vivo*, and explore its potential role in the prediction of sPTB.

4.1.2. **Bioimpedance -fundamentals of EIS**

The flow of electrical current (I) relies on voltage (V) and resistance (R). Current is the charge flowing per unit time, voltage is the driving force exerted on the electrons to move along the wire,

and resistance is the degree of opposition experienced by the electrons when they flow (Fish and Geddes, 2009). In ideal circumstances, these three properties follow Ohm's law, which defines resistance (R) as the ratio between voltage (V) and current (I) at a given time (t):

$$R\ (t) = \frac{V\ (t)}{I\ (t)}$$

Resistance applies to both direct current (DC) and alternating current (AC) systems, and is independent of frequency, as a resistor cannot store energy and therefore, the current is always in phase with the voltage regardless of the frequency (Figure 4.3; Szulcek et al., 2014). In addition, electrical circuits can have a capacitor that store energy as an electrical charge. This property is called capacitance (C) and it is only applicable to AC circuits, as direct current cannot flow through a capacitor (Avis et al., 1996).

Ideal circuits can be applied to understand how an electrical field interacts with biological systems, which can inform on the structure and contents of a tissue. Cells, for example, have bilayer membranes which are capable of storing an electrical charge, thus acting as capacitors. When the current is flowing, the capacitor needs to rearrange the polar regions between the plates (dielectric material) in order to store energy. As this process takes some time to build up, the voltage lags the electrical current by 90^{o} (Saggio, 2014). This inertia produced by capacitors is called capacitive reactance and unlike resistance, it varies inversely with the frequency of the current (Khalil et al., 2014).

In theory, as both resistance and reactance represent opposition of a system to the flow of an electrical current, they can be measured and expressed together in ohms (Ω) as impedance (Z). However, as these two components are out-of-phase with each other, impedance is not the simple algebraic sum of resistance and reactance, but rather the vector addition of these two phenomena (Szulcek et al., 2014).

When cells are modelled as electrical circuits, the extracellular and intracellular spaces behave like resistors whereas the membrane acts as a capacitor (Figure 4.3). At low frequencies, the electrical current is kept out of the cell by the membrane high capacitive reactance and only flows through the extracellular space. As frequency increases, however, current flows into the intracellular space because the capacitive reactance of the membrane decreases. In short, when frequency approaches zero, the membranes act as an open circuit (voltage drop with no current) whereas when frequency tends to infinity, the membrane acts as a short circuit (current with no voltage drop). As a result, at low frequencies, all current flows through the extracellular resistance whereas at very high frequencies, current splits through the extracellular and intracellular space (De Lorenzo et al., 1997, Khalil et al., 2014).

In EIS, AC current over a wide range of frequencies is applied to a biological system by an array of electrodes (Clemente, 2012). As a result, the current flows through the tissue layers with different impedances depending on the structure encountered and the frequency used. EIS uses these changes in impedance to characterise the electrical behaviour of the tissue (Brown et al., 1994).

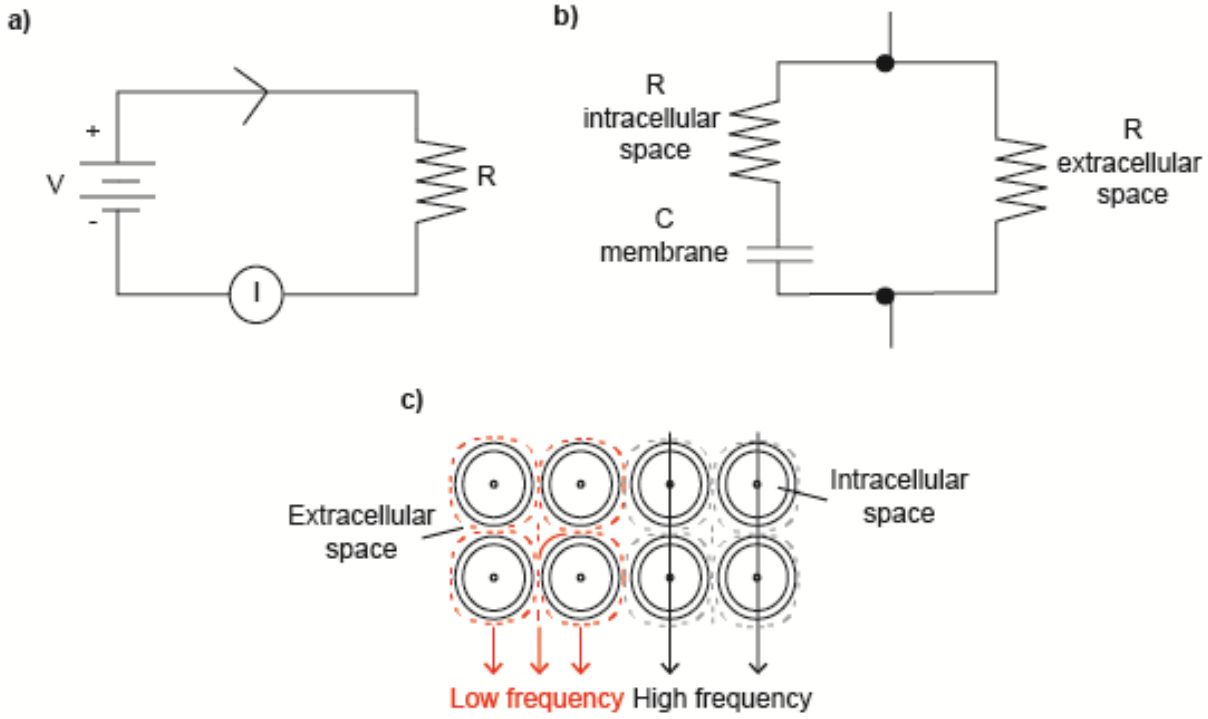

Figure 4.3. (a) Ideal electrical circuit with voltage (V), current (I) and resistance (R). Adapted from Brown et al. (1994), **(b)** equivalent electrical system in the cell with intracellular and extracellular resistance and membrane capacitance -C-, **(c)** response of the tissue to different frequencies. At low frequency, the cell membranes prevent current from reaching the intracellular space. At high frequencies, the membranes capacitive reactance is negligible, and the current flows across the cell. Adapted with permission from De Lorenzo et al. (1997).

4.1.3. **Advantages and limitations of EIS in Obstetrics and Gynaecology**

In the last few decades, EIS has rapidly gained popularity as a biomedical research tool for the study of human conditions (Dean et al., 2008) as it is a non-invasive, label-free method capable of providing real-time quantitative information about the electrical properties of a tissue (Åberg et al., 2003, Gu and Zhao, 2010). EIS has now been developed into relatively affordable portable devices that make it an ideal technique to better manage patients in the clinical setting. Such is the case of the ZedScan®, an EIS device which was developed at the University of Sheffield to examine the non-pregnant cervix, and which has already been validated as a clinical adjunct to colposcopy for the screening of cervical cancer (Brown et al., 2000, Macdonald et al., 2017). When this new EIS

technology was compared to routine care using a cost-effectiveness analysis, EIS showed similar sensitivity and specificity as routine care but lower total costs justifying its clinical adoption in the National Health Service (NICE, 2015b).

While a growing body of literature suggests that EIS might be a technique which is capable of detecting key changes in the cervical remodelling process in pregnancy with a high level of accuracy, it does not come without a series of shortcomings that may limit its clinical application for prediction of PTB and which call for further optimisation of the technique. The main disadvantages noted when using EIS is the need for contact between the sample and electrodes: impedance values seem to vary significantly depending on how much pressure is exerted on the probe when collecting data. Additionally, computational analysis has also suggested that the presence of mucus on the cervical surface can introduce error into impedance measurements by adding an extra layer over the epithelium thereby increasing membrane reactance (Gonzalez-Correa et al., 2005, Wang et al., 2017).

4.1.4. **Magnetic induction spectroscopy for the prediction of PTB**

Magnetic induction spectroscopy (MIS), a technique which allows the non-destructive measurement of bioimpedance properties without the need for electrodes to be in contact with the tissue, may be able to overcome EIS drawbacks (Barai et al., 2012, O'Toole et al., 2015, Wang et al., 2017). Instead of electrodes, the MIS device comprises a series of encased coils capable of producing small magnetic fields which induce currents within the tissue (Figure 4.6). These induced currents produce a second magnetic field that is captured by the MIS device and transformed into measureable data (Wang et al., 2017). Therefore, unlike EIS, the MIS device does not need to be in contact with the tissue of interest and it can bypass the potential influence of pressure and probe positioning on the cervix.

Pilot studies have tested the potential of different MIS probes to discriminate between normal and malignant prostate cancer (Halter et al., 2007) and to measure brain oedema (Netz et al., 1993, Merwa et al., 2004), thoracic conductivity (Guardo et al., 1997) and breathing patterns in patients with sleep apnoea (Richer and Adler, 2005). The studies have led to the development of a working MIS prototype which can be applied *in vivo* to assess the cervix in pregnant women (Wang et al., 2017).

4.1.5. **Fundamentals of MIS**

Different methods have been used to achieve non-contact inductive coupling between the sensors and the sample including modulation and gradiometer systems (Xiang et al., 2018). In the MIS prototype proposed in this chapter, two sensing coils were arranged equidistantly to a driving coil; the sensing coil located at the top was then placed in proximity to the cervix (Figure 4.4; Wang et al., 2017).

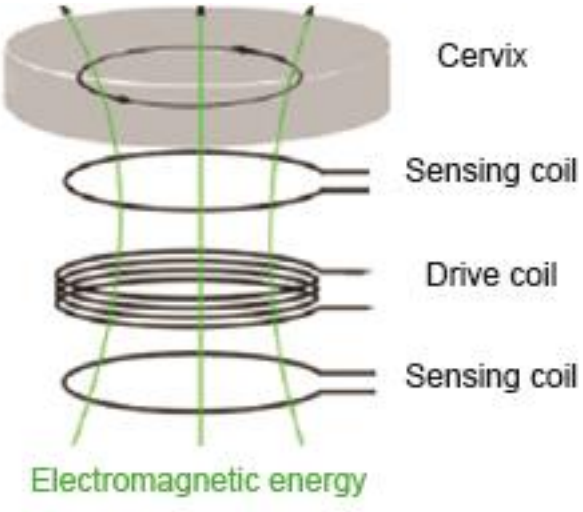

Figure 4.4. Schematic diagram of the axial gradiometer of the MIS device. Adapted with permission from Wang et al. (2017).

In our MIS prototype, a drive voltage applied to the drive coil generates an alternating current (0°), which in turn creates an in-phase magnetic field known as primary magnetic field. The primary magnetic field induces an electromotive force (e.m.f.) in the sensing coils which is -90° to the drive current and proportional to frequency as described by Faraday's law: $\varepsilon\ (e.m.f.) = \frac{\Delta\varphi}{\Delta t}$ in which $\Delta\varphi$ represents the difference in magnetic flux at a given time (Δt). As long as the gradiometer coils are positioned equidistant to the drive coil and connected in antiphase, this output voltage is cancelled out.

The drive current also creates an electric field in the tissue of interest. Similarly to the e.m.f. elicited in the detector coils, this electric field is out of phase to the drive current (-90°) and proportional to frequency. Within the tissue, this electric field causes a current to flow (eddy current) which in turn generates a secondary magnetic field. The secondary magnetic field then induces out-of-phase voltages in the sensing coils which are -180° with respect to the drive current and proportional to frequency squared as they have been double-induced by a magnetic field. As the sensing coils are positioned at different distances to the target sample, it is the ratio between these

double-induced voltages (ΔV) that provide a unique electromagnetic signature of the tissue and is what the MIS system described in this chapter measures as transresistance.

Overall, even though the MIS work presented in this chapter expands upon previous EIS studies, EIS and MIS are fundamentally two different techniques. Whereas EIS relies on the movement of electrical current through electrodes, MIS can sense electrical conductivity through non-contacting inductive coupling (Halter et al., 2007, Jokhi et al., 2009a, Wang et al., 2017). Understanding how MIS differs from EIS in measuring frequency-dependent electrical properties is therefore essential to better contextualise and interpret the findings reported in the present study.

4.2. Aims and objectives

4.2.1. **Aims**

The aim of this study was to develop and test an optimised prototype of a transvaginal MIS clinical probe which could measure, accurately and consistently, cervical transresistance both *in vitro* and *in vivo* as a potential predictive tool for sPTB**.**

4.2.2. **Objectives**

- To support the technical team in the optimisation of a clinical grade MIS probe capable of generating, capturing and displaying *in vitro* and *in vivo* measurements of cervical transresistance
- To assess the repeatability of the optimised MIS probe for cervical transresistance in the *in vitro* human cervix and in pregnant women
- To compare transresistance profiles for the stromal and the epithelial surfaces in the *in vitro* human cervix
- To compare cervical transresistance in asymptomatic pregnant women deemed at high risk of PTB (AHR) between 20-22 and between 26-28 weeks, and pregnant women with symptoms for preterm labour (SYMP) between 20-34^{+6} weeks
- To examine whether cervical transresistance may hold any predictive value for sPTB in AHR and SYMP women

4.3. Materials and methods

4.3.1. **Refinement of the probe**

The work presented in this chapter was performed using a prototype magnetic induction spectroscopy gradiometer probe specifically designed for measuring bioimpedance parameters of the human cervix over the range of a few kHz to about 1MHz.

This new MIS device was developed as a working and optimised version of the Mark I prototype, a ferrite-cored coaxial gradiometer probe previously built as a proof of concept to assess the dielectric properties of the cervix *in vivo* (Figure 4.5; Wang et al., 2017). A small feasibility study funded by the National Institute for Health Research (NIHR) Invention for Innovation (i4i) grant (II-ES-0511-21004) had promisingly shown Mark I was capable of measuring transresistance on 10 healthy pregnant volunteers at term. However, this preliminary study had also highlighted a series of limitations arising from the probe design which were affecting its performance *in vivo* and its potential translatability into the clinical setting.

As a result, key upgrades were introduced to Mark I with the aim to increase the system sensitivity, reduce thermal perturbation, and improve repeatability and patients' acceptability. The new probe was renamed Mark II after its predecessor.

Mark II retained the original ferrite-cored gradiometer structure from Mark I which comprises a pair of field sensing coils positioned on a vertical axis and equidistant to the drive coil. The ferrite core behaves as a magnetic concentrator, and it is therefore a key component in the MIS system to increase the sensitivity to the small magnetic field arising from the tissue of interest. There is also a ferrite cylinder surrounding the coils which works as an electrically insulating packing to help reduce the magnetic field in the adjacent tissue. Electric field shielding is also necessary because the drive voltage the MIS requires to induce the primary magnetic field is much larger than the induced signals it captures from the tissue of interest. As a result, the engineering team (Dr Jill Tozer and Dr Jamie Healey) aimed to design the system in a way in which it was sensitive mainly to magnetic field perturbations rather than electric field changes (Wang et al., 2017).

The optimisation of the ferrite core and outer cylindrical ferrite case significantly helped increase the sensitivity of the Mark II probe to small voltage changes as low as 15 microvolts created by the eddy currents flowing within the cervix, while reducing the interference from the vaginal wall and the electric field.

The thermal stability of the MIS probe was also optimised. Thermally-stable materials were used to reduce the thermal drift caused by the electrical current flowing through the drive coil. The

power dissipated in the drive coil can cause thermal expansion which may alter the symmetry of the sensing coils and affect the proper functioning of the system. The two sensing coils must be identical and perfectly aligned with the drive coil to cancel out the primary magnetic field so that only the differential voltage resulting from the tissue-induced magnetic field is recorded. The Mark II probe was therefore equipped with copper wire coils wound on borosilicate glass (Pyrex®), a material which is stable at 4.0 x 10^{-6}/K. Furthermore, spacing washers made of MACOR®, a ceramic glass with an expansion coefficient of 8.1 x 10^{-6}/K, were also added to separate the coils from each other and the outer casing; and core and shields with low thermal expansion coefficient were chosen (7.0-10.0 x 10^{-6}/K).

The thermal drift was further minimised by modifying the circuitry so that it could operate on a reduced power supply voltage. Additionally, a detailed standard operating procedure (SOP) was developed by the clinical team in conjunction with the engineers to minimise abrupt changes in temperature when the probe was being operated. It was agreed that the probe would be switched on at least 30 minutes before any scanning to enable all parts of the device to reach thermal equilibrium in air. Letting the probe warm up allowed it to be above room temperature so at the time of vaginal insertion the difference with the body temperature was smaller than if it had not been turned on in advance. It was further agreed that each cervical measurement would be repeated at least three times and the signal would be "chopped" to facilitate thermal drift tracking in the raw data at the time of analysis.

Further modifications in the MIS system involved replacing the previous digital-to-analogue interface (NI DAQ 6366, National Instruments) and converter (NI-USB 6366) with a field-programmable gate array (FPGA) controlled system. This allowed the analogue-to-digital conversion to be in the probe itself which removed the movement artefacts that were a significant problem with Mark I. Digital-matched filter techniques were also developed which reduced the background noise and improved clinical measurement time.

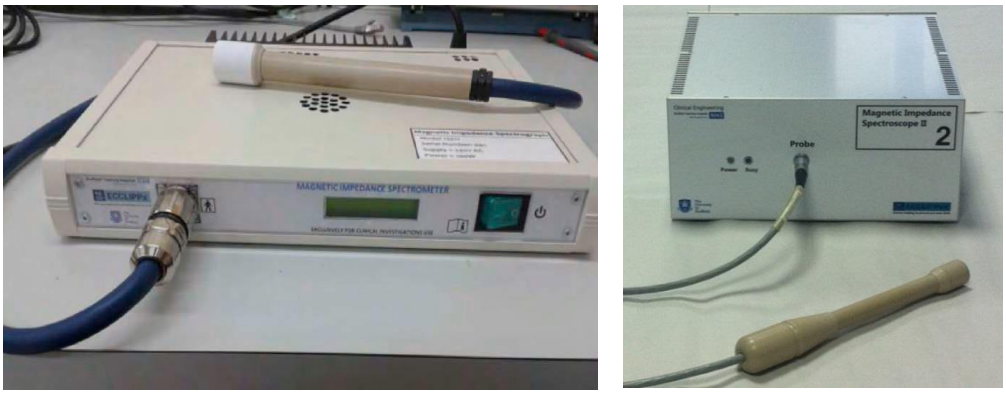

Figure 4.5. (a) Mark I probe attached to a spectrometer, **(b)** Mark II probe connected to an optimised spectrometer

Other ways of improving the system efficiency included assessing different geometries and sizes of the probe which would allow better fitting in the vagina and proximity to the cervical surface. A series of plastic shield models with gradiometers angled at 0° and 30° were 3D printed and tested *in vitro* with and without speculum on the synthetic cervix (SynDaver® uterus) before the probe was assembled together (Figure 4.6).

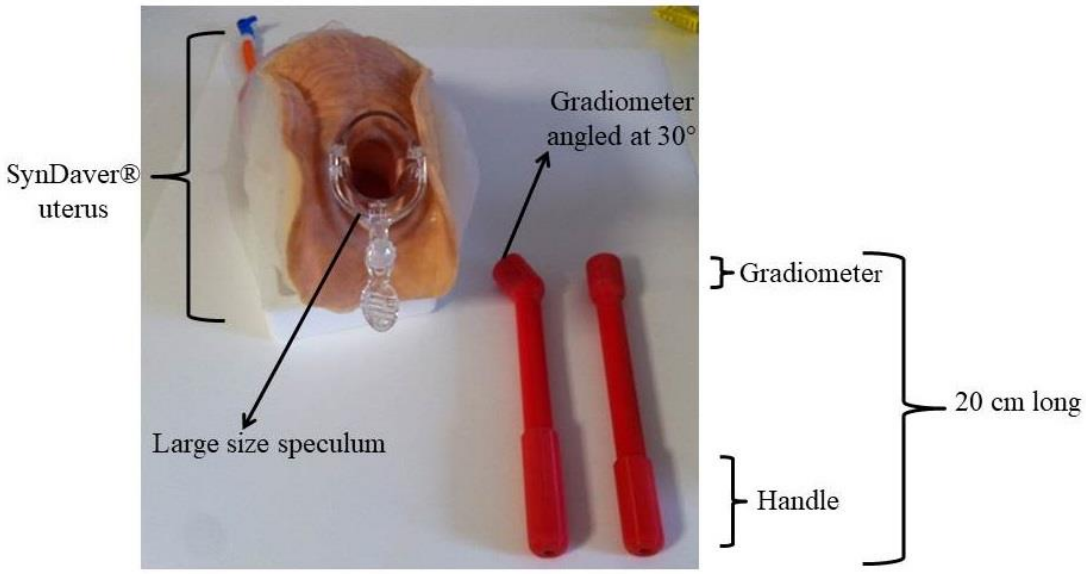

Figure 4.6. Shield models for the MIS probe were 3D printed at different angles and tested on the SynDaver® uterus

Given the anatomical variations associated with the cervical position and the relatively axial position adopted by the gravid uterus from 20 weeks of gestation, I concluded, after these experiments, that a probe with a straight gradiometer on a speculum would be the most useful as it could be used on the most number of patients (Figure 4.7). After trying it on the synthetic uterus, I

also requested a longer and flatter handle to facilitate probe manipulation during scanning. Furthermore, in order to improve patients' comfort and acceptability, the probe head diameter was further reduced from 29 mm (as seen in Mark I) to 27.5 mm.

Many of these upgrades were first explored computationally on COMSOL Multiphysics® (USA, 2017) before being tested experimentally *in vitro* and *in vivo*. I provided the engineering team with access to different transvaginal probes and speculum sizes to build a realistic model of a probe which would be acceptable in the clinical setting. Fine element analysis was used to simulate how different probe dimensions and shapes would affect the sensitivity of the system at different depths of the tissue being sampled. Physiological variants such as the presence of air or mucus on the cervical surface were also modelled at this early exploratory period to predict how the probe would behave in real conditions.

All these technical upgrades were carried out giving careful consideration to safety. I conducted an extensive review of the cervix innervation to inform the engineering team about the risks of neural stimulation (Prospero registration interim ID: 173778, Appendix B). The systematic review highlighted the limited evidence available on cervical neural stimulation. The innervation of the cervix, which arises mainly from the hypogastric plexuses, is thought to be confined to the endocervix and deep ectocervix while it spares most of the distal region of the cervix, that is, the portio vaginalis (Berkley et al., 1993). Direct electrical stimulation of the cervix in pregnant rats has not been found to alter delivery times nor cause damage to the cervix or affect birthweight when compared to control groups. However, in low frequencies (10 Hz), it has been shown to cause cervical softening and ripening (Fang et al., 2015). As a result, the system was designed for higher frequencies (above 20 kHz), and a specific absorption rate (SAR) of 3.6 mW/kg, well below the maximum value established by the International Commission on Non-Ionizing Radiation Protection (ICNIRP) which is 80 mW/kg (ICNIRP, 1998) so that it could not cause neural stimulation or tissue heating. Rigorous safety testing was undertaken by the Hospital Medical Physics Department at the Royal Hallamshire Hospital, and the prototype passed all safety checks before the clinical pilot study was commenced.

Figure 4.7. Mark II Magnetic induction spectrometry (MIS) probe. A ruler is shown for scale.

4.3.2. *In vitro* studies on human cervical tissue

The MIS prototype was tested on human cervical specimens selected from our HTA approved biorepository. The cervical samples were harvested from non-pregnant women undergoing hysterectomy for benign reasons at the Royal Hallamshire Hospital, and stored at -80°C for around 4-6 months (REC 08/H1310/83). Each cervical cross-section was approximately 2 cm long, 2 cm high and 2 cm deep, and included the ectocervix (stratified squamous epithelium) on one side and a stromal surface on the other.

Samples were allowed to thaw at room temperature for 60 minutes before being scanned with the Mark II MIS probe. For each measurement, the probe was covered with a sheath and positioned just a few millimetres away from the ectocervix; and real-time transresistance data was recorded holding the probe in place for approximately three seconds. The probe was then removed to a distance of approximately 1-2 cm before being reapplied in the same position for a second cervical measurement. This procedure was repeated three times for each sample. After the ectocervix had been scanned, the cervical cross-sections were turned over to expose the stromal surface, from which a single MIS measurement was obtained.

The three consecutive MIS measurements from the ectocervix were employed to assess intra-observer variability (as described in section 4.3.4), and differences in transresistance between the ectocervix and the stromal surface were calculated by comparing the measurements from both cervical surfaces using ANOVA and Kruskal Wallis tests as applicable.

4.3.3. *In vivo* studies on pregnant women

After the Mark II MIS probe was manufactured and tested *in vitro*, a prospective pilot clinical study, the ECCLIPPx II (**E**le**C**tri**C**a**L** **I**mpedance **P**rediction of **P**reterm Birth by Spectroscopy of the **c**ervi**X** II), was conducted over a period of 14 months to assess *in vivo* repeatability, characterise cervical transresistance in a small cohort of high-risk and symptomatic pregnancies and explore its predictive value for sPTB.

❖ Setting for clinical trial

The studies were undertaken at the Jessop Wing Maternity Unit of the Royal Hallamshire Hospital, a tertiary referral unit with a birth rate of nearly 7,000 deliveries per annum, which is well-suited for the care of women at high risk of premature delivery. The Jessop Wing not only runs a weekly specialised antenatal service which provides care to women at high risk of PTB but it also houses the regional neonatal intensive care unit with high-dependency care facilities equipped to deal with extremely premature births, including those born at gestational ages borderline for viability (between 23-26 weeks) thereby receiving *in utero* transfers from other hospitals in South Yorkshire including Rotherham, Doncaster, Bassetlaw, Barnsley and Chesterfield.

❖ Participants: inclusion and exclusion criteria

Cervical transresistance was assessed on a cohort of asymptomatic women deemed at high risk of PTB (AHR) who were attending the specialised PTB clinic for pregnancy care, and on a second cohort of pregnant women who presented to Labour Ward between 20-34^{+6} weeks with symptoms suggestive of preterm labour (SYMP; Figure 4.8):

- AHR cohort: participants were judged to be at high risk of PTB based on their previous obstetric history (one or more premature births<37 weeks or one or more late miscarriages). Or alternatively, they were included if they had an incidental short cervix (<25 mm) before 20-22 weeks.
- SYMP cohort: participants were women admitted to the Labour Ward or the Triage assessment unit with symptoms suggestive of sPTB (more than one regular contraction every 10 minutes) but not yet in established labour (cervical dilation less than 4 cm) and with intact membranes.

Women with signs of cervical infection, abnormal cervical smear within the previous year, multiple pregnancy and known fetal anomaly were excluded from the study as these conditions are known to be independent risk factors for sPTB.

❖ Recruitment of prospective participants

AHR participants were approached at their booking antenatal visit at Jessop Wing. The study was explained and study materials were provided including the Patient information leaflet (PIL). If they wished to participate in the study, women were scheduled to attend Fetomaternal Unit for their MIS measurement between 20-22 weeks and later on between 26-28 weeks. I would obtain written consent on the first study visit and review it during their follow-up appointment to confirm patients were still willing to remain in the study. As these MIS appointments were performed on the same day patients were already scheduled to attend PTB clinic, participating in the study did not increase their number of clinical appointments. This, we think, translated into higher compliance with lower drop-out rates.

Symptomatic women, on the other hand, were approached when they attended Labour Ward or the Triage unit in threatened preterm labour. Patients were provided with specifically designed study materials, and were asked to contact the research staff directly if they wanted to participate in the trial. If they agreed to take part in the study, I would secure written informed consent after a minimum "cooling" period of 30 minutes to allow the patient to read the material and discuss any doubts. I would then conduct the study visit at either the Fetomaternal unit or directly on the delivery suite depending on patients' and clinical staff preference, severity of symptoms and ongoing care in place. All symptomatic participants receiving intravenous magnesium sulphate, for example, were assessed on Labour Ward as transferring them to Fetomaternal unit would have interfered with the intravenous infusion.

The daily screening of eligible patients, including those with whom the study was discussed but they declined to participate, was recorded in bespoke screening logs which allowed me to audit the recruitment process and implement alternative strategies to reach the target sample.

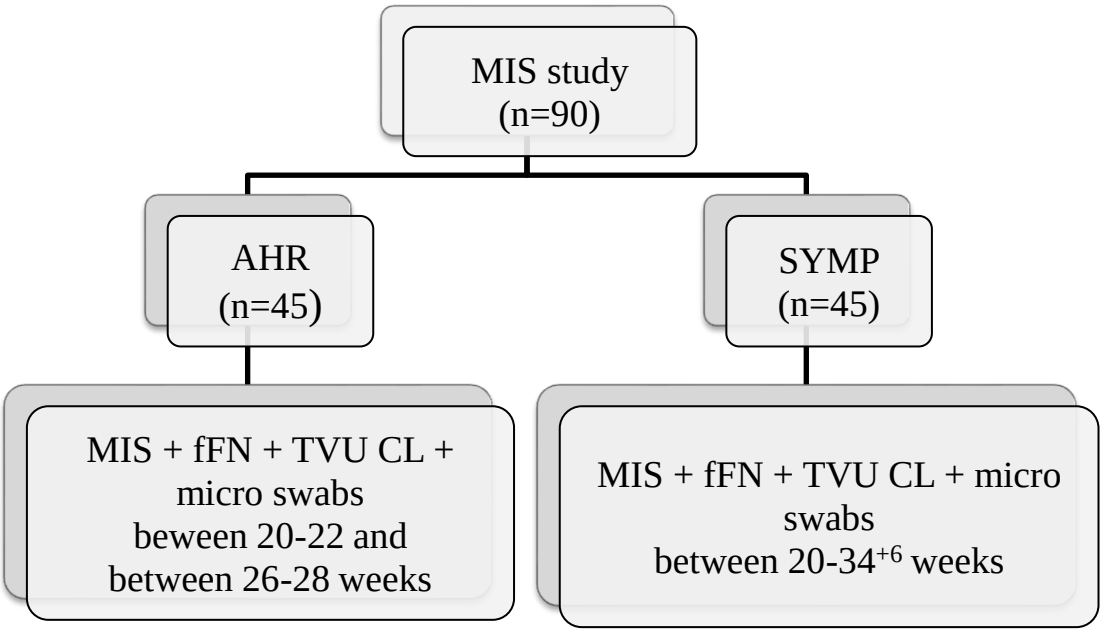

Figure 4.8. Flow diagram of the MIS clinical trial: asymptomatic high risk (AHR) group and symptomatic (SYMP) group. *fFN*: fetal fibronectin, *MIS*: magnetic impedance spectroscopy, *TVU CL*: transvaginal ultrasound

❖ **Ethical considerations and informed consent**

The ethical issues raised by this study were considered minimal as the new probe Mark II was an optimisation of the Mark I device which had already been shown to be safe in pregnant women during a small repeatability study (Wang et al., 2017). The magnetic field used in MIS for inducing electrical current is significantly smaller (>10 fold smaller) than the one used for clinical MRI. The frequencies at which the device operates start at 20 kHz, which is well above the frequencies associated with neural stimulation. All the experiments were carried out following the guidance for magnetic exposure provided by the Health Protection Agency (HPA) and the International Commission on Non-Ionising Radiation Protection Guidelines (ICNIRP), (ICNIRP, 1998)

Written consent was sought from all research participants, who were entitled to withdraw from the study at any point and for any reason or no reason at all without any penalty.

Research participants' health records were accessed in accordance with the Data Protection Act (Data Protection Act, 1998), and this clinical information along with the experimental data was recorded on a specifically designated case report form (CRF) for entry into an encrypted and anonymised database. As only anonymised data was used for analysis and interpretation, it was not possible to identify any individual participants from the final results.

The CRFs along with the consent forms were stored in a locked cabinet in approved research premises in agreement with the code of confidentiality and data protection which operates within

the Sheffield Teaching Hospitals NHS Trust. Forms were also prepared to facilitate detection, evaluation and reporting of potential adverse events which were defined as any unexpected medical occurrence, disease or injury, or untoward clinical signs in participants or users related to the use of investigational medical devices (BS EN ISO 14155:2011). Examples of serious effects included but were not limited to vaginal bleeding, severe pain, injury to the cervix and PPROM/delivery while performing the procedure or immediately after. In the case of serious adverse events (SAE), such as maternal death or idiopathic intrauterine fetal death, a plan to inform the Research Ethics Committee (REC) was agreed on.

Ethical and Research Governance approvals were sought before commencing any biological work while the probe was still being manufactured. PILs and written consent forms were prepared with input from members of the Jessop Wing Preterm Birth Patient and Public Involvement (PPI) group.

- **Sample size for the *in vivo* predictive study**

Based on the previous performance of EIS for prediction of PTB between 20-22 weeks of gestation, I hypothesised that MIS would predict sPTB with an AuROC of 0.8 (Anumba et al., 2018). Similarly, using previous microbiome and EIS studies carried out in Jessop Wing (Amabebe et al., 2016a), it was estimated that approximately 20% of all AHR women and 17% of all SYMP patients recruited would deliver prematurely, with an expected ratio of negative (delivered at term) to positive (delivered prematurely) cases of 4:1.

With a power of 80% (type II error of 20%), a type I error of 5%, a ratio of -/+ cases of 4:1 and a hypothesised AuROC of 0.8, the sample size for the *in vivo* predictive study was calculated using MedCalc® (Belgium, 2015). A sample size of 45 women was shown to be required, with at least 9 women delivering prematurely in each arm. However, in order to cover for women dropping out of the study at some point, the sample size needed to assess the effectiveness of MIS was agreed to be closer to 50 women per group (which would allow five women to withdraw at any point without compromising the study outcomes).

Regarding recruitment timelines, and based on previous EIS studies in which almost 400 pregnant women were recruited over 36 months at a rate of 11 women per month, it was estimated that I would be able to recruit at least five AHR and five SYMP women on average every month at Jessop Wing, which would allow the target numbers to be attained within 12-14 months of the start of the study (Stern et al., 2016).

- **Data collection**

For all AHR and SYMP women, the study visits were conducted in a similar fashion by a single operator. After securing written consent, a full history was taken, and all pertinent clinical and demographic data was retrieved and recorded in CRFs.

The MIS device was switched on at least 30 minutes before the actual measurements were taken to allow the system to warm up and reach a stable temperature before being used on the patient. Just prior to covering the probe with a disposable condom, measurements were taken from a ferrite calibrator and in air to enable subsequent phase-reference and calibration of the MIS data (section 4.3.4).

Patients were then asked to empty their bladder and position themselves in lithotomy before a disposable clear crystal plastic speculum was inserted to visualise the cervix (Robinson Healthcare®, 119 mm long with a tip width of 33mm). In order to reduce patients discomfort but minimise interference in subsequent fFN measurement and metabolites quantification, the speculum was lubricated with sterile water. Once the cervix was identified and the speculum was secured in place, four swabs were taken from the posterior vaginal wall: one for fFN analysis, two Dacron swabs for metabolomics studies (Delta lab Eurotubo 300263, Fisher Scientific) and one charcoal swab for clinical microbiology analysis at the maternity unit.

Without removing the speculum, the MIS probe was then inserted in close proximity to the cervix and the first measurement was taken by pressing the footswitch. At the beginning of the trial, a second operator had to attend each study visit to press the *capture* button on the laptop while the main operator kept the speculum and probe in place during measurements. However, in order to enable independent study visits by a single operator, a footswitch feature was added (Figure 4.9).

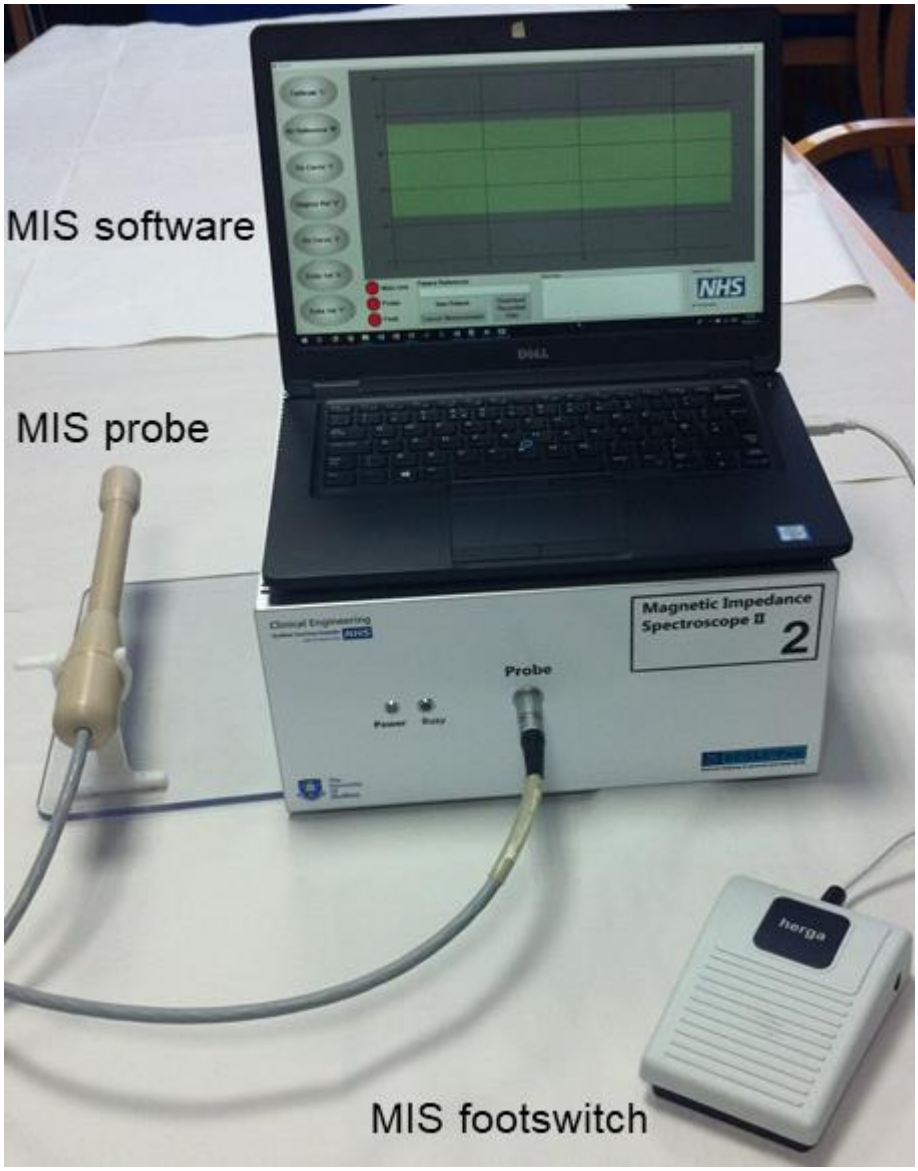

Figure 4.9. MIS device with added footswitch

Three cervical readings were obtained from each patient by steadily holding the probe in place for 3-5 seconds (sometimes less if the patient could not tolerate the procedure). In between these three cervical measurements, the probe would be withdrawn 5-10 mm (without removing it from the vagina) and measurements of the vaginal environment would be taken. Overall for each study visit, there were eight measurements taken: first with the ferrite calibrator, then in air, followed by six alternating cervical and vaginal measurements.

After MIS measurements were recorded, the probe and the speculum were gently removed. A TVU was then performed to assess CL followed by a transabdominal scan to check viability +/- growth if applicable.

After completing each visit, the disposable condom covering the probe was removed and discarded, and the device was subjected to high-level decontamination. Similar to the transvaginal

probes used for scanning CL, the MIS probe was classified as a semi-critical instrument given the added risk of coming into contact with non-intact skin or mucous membrane despite being encased in a disposable probe cover (Abramowicz et al., 2017). Therefore, before and after each use, the probe head and ferrite calibrator were cleaned with a chloride dioxide based decontaminant, Tristel Duo® foam, which has proven efficacy against most spores, mycobacteria, viruses, fungi, and bacteria including Human Immunodeficiency virus, Human Papilloma virus, and Hepatitis B and C viruses as well as *Candida* and BV-associated *Gardnerella vaginalis* (Coates, 2001, Hitchcock et al., 2016).

- **Cervical length measurement**

After patients were scanned with the MIS device, they were asked to remain in lithotomy with their legs partly abducted. The TVU probe (Hitachi Aloka ProSound Alpha 7) was covered by a disposable sheath and lubricated before being gently introduced in the vagina. Once a long view of the cervix was achieved, the probe was slightly repositioned until the external os, internal os and whole length of the endocervical canal could be confidently identified. Taking care not to compress the cervix which could falsely elongate the CL, the image was magnified until the cervix occupied ¾ of the field. Once this image was obtained, callipers were placed on the screen at the internal and external os, and the CL was measured in a straight line. The procedure was repeated three times, and the shortest CL measurement was recorded. Any dynamic changes as well as the presence of cervical sludge or funnelling were recorded as added independent risk factors of PTB (Kagan and Sonek, 2015).

- **Fetal fibronectin measurement**

As per manufacturers' instructions, the fFN was the first swab to be collected to avoid sample contamination. After retrieving the sample from the posterior vaginal fornix, the tip of the swab was immersed in buffer, before being checked with the bedside Rapid fFN Hologic® Perilynx system which yielded quantitative results measured in ng/mL.

- **Storage of triple swabs and pH readings**

Dacron swabs for metabolomics studies were immediately stored at 4°C in clinic at Jessop Wing before they could be transferred for long-term storage at -80°C at the University of Sheffield. Microbiology swabs were sent to Royal Hallamshire Hospital laboratory facilities.

Vaginal pH was measured with Fisherbrand^{TM} narrow range pH indicator paper strips (3.6-6.1) placed on the tip of the speculum after being withdrawn from the vagina.

Microbiology and pH data were comprehensively analysed in the context of further metabolomics studies and delivery outcomes (Chapter 5).

❖ **Disclosure of results and clinical management**

All participants were advised on their CL and fFN results at the time of the visit. Their risk of sPTB was also computed using the Quantitative Innovation in Predicting Preterm birth app, QUiPP® (Watson et al., 2017).

Patients with a short CL, a positive fFN result or deemed at high risk of delivery within seven days were offered appropriate management as per local and national guidelines including admission, referral to our specialised Preterm Birth Clinic, consideration of cerclage or progesterone and/or administration of antenatal steroids and magnesium sulphate, and neonatal counselling (NICE, 2015a).

4.3.4. **MIS data analysis**

All demographic, clinical and experimental data was coded in SPSS (IBM, USA) and analysed employing descriptive and inferential statistics. Categorical data such as birth<37 weeks was analysed with Chi-square tests whereas continuous data was compared using parametric (e.g. Student's *t*-test or ANOVA) and non-parametric tests (e.g. Mann-Whitney U and Kruskal Wallis tests).

The MIS device measured transresistance at 15 different frequencies: 21, 42, 56, 72, 86, 100, 202, 302, 402, 502, 604, 704, 804, 904 and 1013 kHz. The raw data was first calibrated by subtracting the measurement taken while holding the probe in air and then phase-referenced using the ferrite measurement values. The real part of the transresistance was subsequently divided by squared frequency (in kHz) and recorded as Henries^2/frequency^2 (H^2/ohm). Given its double-induced nature, MIS transresistance measurements are directly proportional to conductivity unlike EIS impedance measurements which are inversely proportional to electrical conductivity (Wang et al., 2017). The relationship each technique has with regards to conductivity constituted the basis for the comparison between MIS and EIS findings discussed in this chapter.

Intra-observer variability measures, namely intra-class correlation coefficients (ICC) and their 95% intervals, were derived for each of the 15 frequencies studied in order to check whether the cervical measurements obtained from the same sample or patient were consistent (Jokhi et al.,

2009b). As MIS cervical readings were quite small (in the range of 10^{-7}), transresistance measurements were first multiplied by 10^8 to increase the magnitude of the variance and allow calculation of the ICCs in SPSS v25.

An initial Shapiro-Wilk test was performed to confirm the data was normally distributed, and a logarithmic or cube root transformation was applied when this assumption was not met to facilitate further analysis. A two-way mixed-effects method was selected to assess intra-observer reliability as suggested by Shrout and Fleiss (1979) for studies in which there are multiple scores obtained by the same observer. Furthermore, a model with absolute agreement was chosen to address potential variability arising from repeated measurements, (Koo and Li, 2016). Reliability was considered excellent if ICC values were>0.75, fair to good if ICC were ≥0.4 and ≤0.75, and poor if<0.4 (Jokhi et al., 2009b).

The agreement between MIS cervical readings was also quantified using the differences between repeats at each frequency. Based on these differences between measurements, the 95% limits of agreement (LOA) were calculated as mean difference ± 1.96 SD of the difference, and displayed in Bland-Altman plots (Bland and Altman, 1986, Bland and Altman, 1999). Each plot provided an interval in which 95% of all the differences between two specific cervical measurements were expected to fall: the wider the interval, the larger the variability (Bland and Altman, 1999). The analysis was independently performed for both the *in vitro* as well as the *in vivo* data.

The primary outcome for the *in vivo* study was prediction of sPTB <37 weeks. AuROCs were constructed for fFN, TVU CL and MIS at different frequencies by plotting sensitivity against 1-specificity in MedCalc® V19.0.7. The AuROC provided an estimate of the overall predictive performance of the tests for the MIS cohort. Any model with an AuROC of 1.0 was considered ideal (100% sensitivity, 100% specificity), highly accurate if the AuROC was greater than 0.9, moderately accurate if the model yielded an AuROC between 0.7-0.9, poorly accurate for AuROCs between 0.5-0.7 and no discriminatory power if the AuROC was equal or lower than 0.5 (Akobeng, 2007).

Clinical parameters including AuROC, sensitivity, specificity, PPV, NPV, and positive and negative likelihood ratio (+/-LR) were computed for MIS as a stand-alone technique as well as combined with other routine predictive tools. Any difference with a *p*-value of less than 0.05 was deemed statistically significant. All the results were reported and presented in agreement with STARD (STAndards for the Reporting of Diagnostic accuracy studies) with estimates of accuracy and precision (95% CI; Bossuyt et al., 2015)

4.3.5. **Patient and public involvement and dissemination**

To maximise pathways to impact, the opinion from patients and the public was actively sought at all stages of the study. Service users and members of the Preterm Birth PPI group were regularly consulted on the project (April and December 2017, July 2018 and February 2019). This PPI group was set up in 2012 to support PTB-related research in the unit; since then, it has grown from four mothers to a current membership of approximately 15 women and partners. Most members have either experienced PTB first hand or have actively contributed to the care of families who have suffered from a late pregnancy loss or an early premature delivery. Throughout the ECCLIPPx II study, the PPI group has played an essential role at helping word the lay summary, PILs and consent sheets, as well as developing recruitment strategy and disseminating the study at the Mobile Festival (September 2017) and the Festival of the Mind (September 2018).

4.4. Results

I first tested the Mark II probe *in vitro* to assess feasibility and repeatability of transresistance measurements, and ensure it was appropriate for further *in vivo* testing. I then proceeded to evaluate MIS *in vivo* repeatability and explore its predictive capacity for sPTB in pregnant women.

4.4.1. *In vitro* MIS demographics

Seven cervical samples harvested from non-pregnant women undergoing hysterectomy for benign conditions at the Royal Hallamshire Hospital were scanned with the Mark II MIS probe. Indications for surgery included endometriosis (42.88%, n=3) and uterine prolapse (57.12%, n=4). None of the patients had a history of cervical surgery or gynaecological cancer. The age of the participants ranged from 31 to 76 years with a mean of 56.29 ± 14.97 years. All cervical samples were retrieved from multiparous women with an average BMI of 29.24 ± 6.17 kg/m^2. Only two patients were receiving hormonal therapy (GnRH) at the time of the surgery (28.57%, n=2).

4.4.2. *In vitro* MIS repeatability

The epithelial surface of the cervical samples was consecutively scanned three times (C1, C2, and C3), allowing 3-4 seconds in between measurements. A Shapiro-Wilk test confirmed these values were normally distributed (p>0.0.5) and therefore, parametric tests such as *t*-Student, ANOVA, ICCs and Bland-Altman were applied.

Reliability was first calculated for all three cervical measurements together (C1-C2-C3), and was subsequently assessed between the first and the second (C1-C2), the second and the third (C2-C3), and the first and the third measurements (C1-C3).

When the three cervical measurements were compared to one another, intra-observer variability was good at most frequencies (ICC>0.65). The highest ICCs with narrower 95% CI were identified at mid-frequencies between 202 and 402 kHz, whereas the lowest ICCs were seen at 56 and 72 kHz (Table 4.2). At most frequencies, however, the CIs were noted to be quite wide which may in part be explained by the small sample size (n=7), the variation between cervical samples as well as the potential thermal shock experienced by the probe when it came in contact with the relatively cold samples.

Table 4.2. Repeatability of all *in vitro* cervical measurements (C1-C2-C3) calculated at each frequency (n=7).

Frequency (KHz)	REPEATABILITY		
	ICC	95% CI	
21	**0.702**	0.189	0.936
42	**0.749**	0.278	0.936
56	**0.660**	0.165	0.924
72	**0.690**	0.239	0.931
86	**0.702**	0.235	0.935
100	**0.709**	0.266	0.936
202	**0.820**	0.504	0.963
302	**0.790**	0.452	0.955
402	**0.764**	0.401	0.949
502	**0.734**	0.342	0.941
604	**0.725**	0.315	0.939
704	**0.729**	0.307	0.941
804	**0.734**	0.304	0.942
904	**0.749**	0.320	0.946
1013	**0.759**	0.333	0.949

CI: confidence interval, ICC: intra-class correlation coefficient

When only C1-C2 were considered, intra-observer repeatability was excellent at almost all frequencies (ICCs>0.75) with the exception of 21 kHz which yielded an ICC of 0.623 (Table 4.3). The highest ICC was identified at 202 kHz, and the narrowest CI at 86 kHz. However, and similarly to what was reported for C1-C2-C3, CIs at all frequencies were quite wide especially at 21 kHz and between 402 and 1013 kHz.

Table 4.3. Repeatability between the first and the second *in vitro* cervical measurements (C1-C2) calculated at each frequency (n=7).

Frequency (kHz)	**REPEATABILITY**		
	ICC	**95% CI**	
21	**0.623**	-0.112	0.926
42	**0.830**	0.252	0.969
56	**0.874**	0.432	0.977
72	**0.891**	0.459	0.981
86	**0.896**	0.502	0.981
100	**0.890**	0.480	0.980
202	**0.913**	0.385	0.986
302	**0.850**	0.008	0.976
402	**0.820**	-0.059	0.972
502	**0.796**	-0.067	0.969
604	**0.795**	-0.055	0.969
704	**0.808**	-0.045	0.972
804	**0.822**	-0.037	0.975
904	**0.842**	-0.033	0.978
1013	**0.853**	-0.039	0.980

CI: confidence interval, ICC: intra-class correlation coefficient

Contrary to C1-C2, when the intra-observer variability between C2-C3 was assessed, the highest concordance was noted at 21 kHz with an ICC of 0.915 (Table 4.4). With the exception of 42 and 56 kHz, ICCs seemed to gradually improve as frequency increased reaching values over 0.75 in the range 202-1013 kHz.

Table 4.4. Repeatability between the second and the third *in vitro* cervical measurements (C2-C3) calculated at each frequency (n=7).

Frequency (kHz)	**REPEATABILITY**		
	ICC	**95% CI**	
21	**0.915**	0.585	0.985
42	**0.663**	-0.101	0.939
56	**0.579**	-0.112	0.915
72	**0.621**	-0.113	0.926
86	**0.635**	-0.109	0.931
100	**0.651**	-0.106	0.933
202	**0.788**	0.108	0.961
302	**0.798**	0.251	0.962
402	**0.796**	0.276	0.961
502	**0.791**	0.232	0.960
604	**0.796**	0.196	0.962
704	**0.806**	0.193	0.964
804	**0.809**	0.197	0.965
904	**0.816**	0.234	0.966
1013	**0.828**	0.286	0.968

CI: confidence interval, ICC: intra-class correlation coefficient

The maximum disagreement between cervical measurements, however, was noted when the first and third *in vitro* cervical measurements were compared (C1-C3) with ICCs ranging from 0.579 at 704 kHz to 0.774 at 42 kHz (Table 4.5).

Table 4.5. Repeatability between the first and the third *in vitro* cervical measurements (C1-C3) calculated at each frequency (n=7).

Frequency (kHz)	**REPEATABILITY**		
	ICC	**95% CI**	
21	**0.601**	-0.117	0.920
42	**0.774**	0.191	0.956
56	**0.606**	-0.069	0.918
72	**0.607**	-0.047	0.915
86	**0.622**	-0.035	0.919
100	**0.627**	-0.025	0.921
202	**0.761**	0.130	0.954
302	**0.715**	-0.033	0.945
402	**0.669**	-0.031	0.933
502	**0.609**	-0.066	0.917
604	**0.587**	-0.071	0.910
704	**0.579**	-0.078	0.907
804	**0.583**	-0.081	0.909
904	**0.598**	-0.076	0.914
1013	**0.607**	-0.071	0.916

CI: confidence interval, ICC: intra-class correlation coefficient

Overall, when all the cervical pairs were taken into account, the greatest agreement was noted between the first and the second measurements (C1-C2), and the lowest concordance was seen between the first and the third measurements (C1-C3) as illustrated in Figure 4.9. ICCs appeared to be higher at the mid-frequencies, particularly at 202 kHz, and lower at both extremes of the frequency range except for 21 kHz in C2-C3 (Figure 4.10).

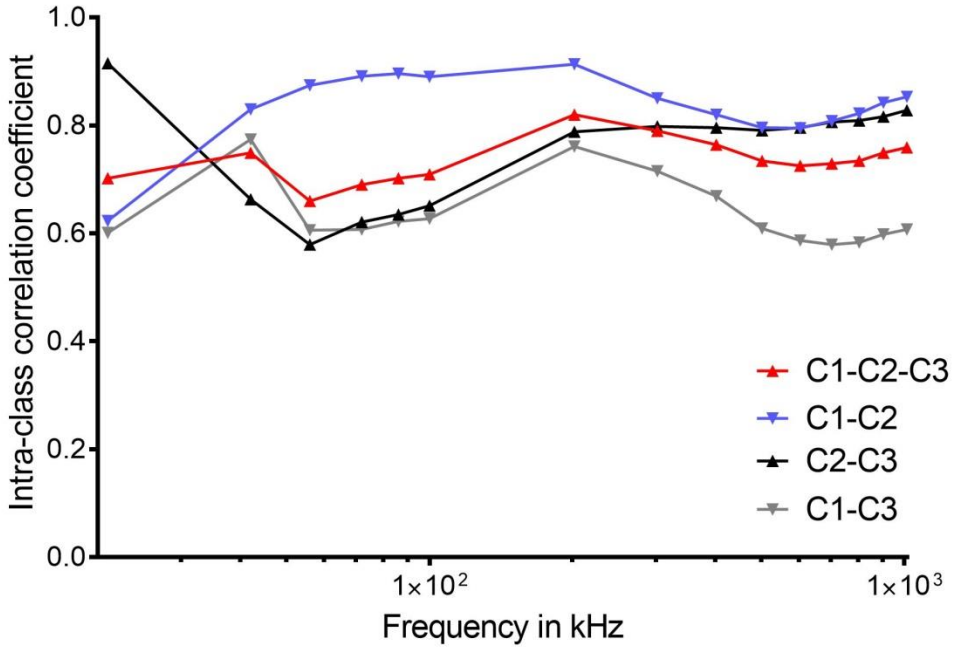

Figure 4.10. ICCs are compared between *in vitro* cervical measurements: C1-C2-C3, C1-C2, C2-C3, and C1-C3 taken at 15 different frequencies. *X-axis is in logarithmic scale.*

The agreement between MIS cervical measurements was graphically assessed with the construction of sequential Bland-Altman plots at each of the 15 frequencies studied for C1-C2, C2-C3 and C1-C3 respectively. The difference between two specific measurements was plotted against the mean of these two paired values which, given the lack of reference values for MIS, was regarded as the best estimate of what the true transresistance value would be at a particular frequency. The farther the mean difference (black dotted line) was from zero, the greater the measurement bias.

In most Bland-Altman plots, *in vitro* MIS data was noted to be randomly scattered without any evidence of proportional bias which supported the assumption that the data was homoscedastic as variability did not seem to be affected by the magnitude of the measurements (Figures 4.11 and 4.12; Appendix C: Figure C.1-C.4). The mean and the standard deviation (SD) of these differences were subsequently employed to construct limits of agreements (LOA) with 95% interval estimates (red dotted lines). The limits of agreement enabled to predict where 95% of the difference between cervical measurements would fall (Table 4.6; Appendix C: Tables C.1 and C.2).

In vitro repeatability C1-C2

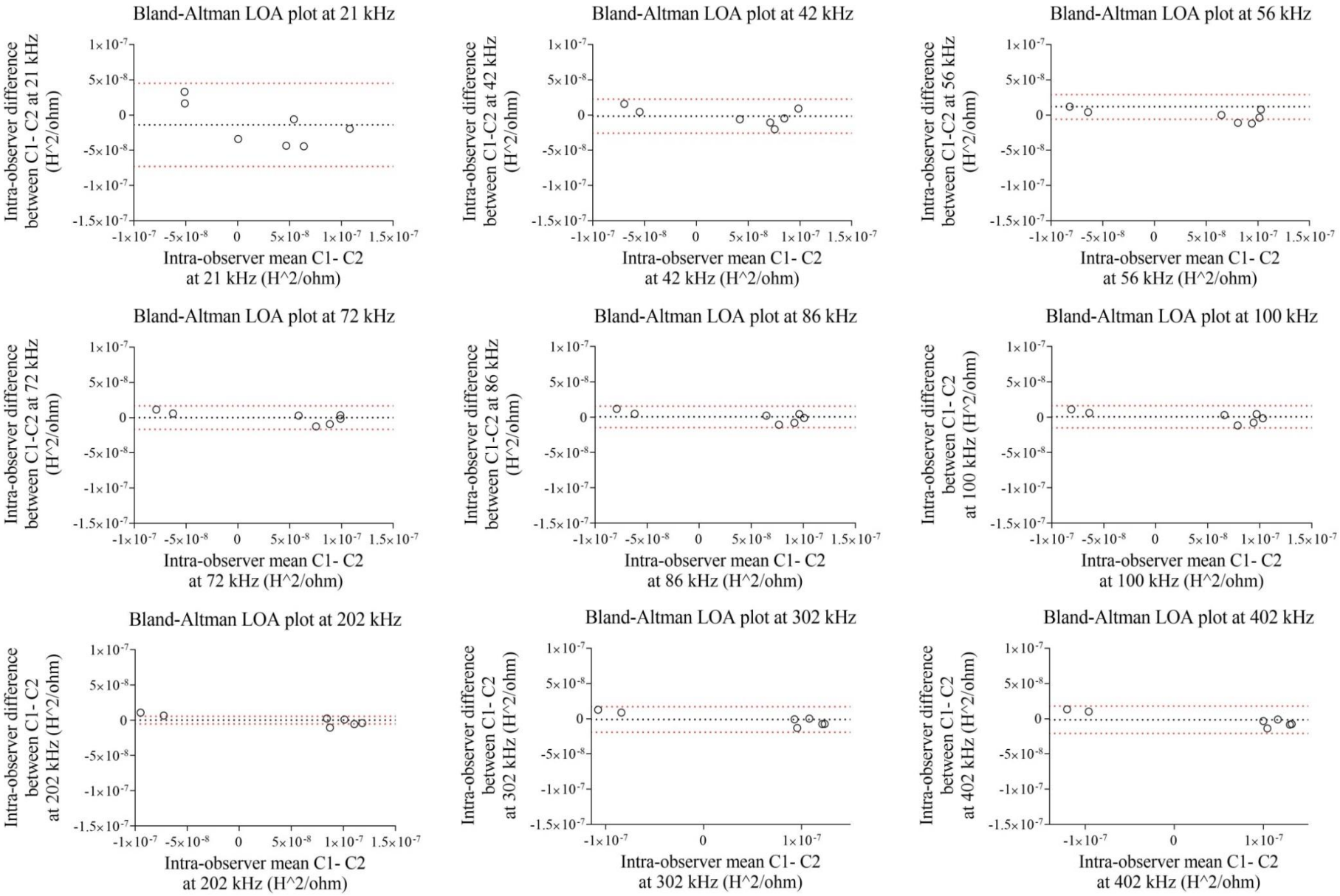

Figure 4.11. Bland-Altman plots for MIS *in vitro* C1-C2 data at 21-402 kHz. Intra-observer repeatability (n=7)
C1: first cervical measurement, C2: second cervical measurement, LOA: limits of agreement

In vitro repeatability C1-C2

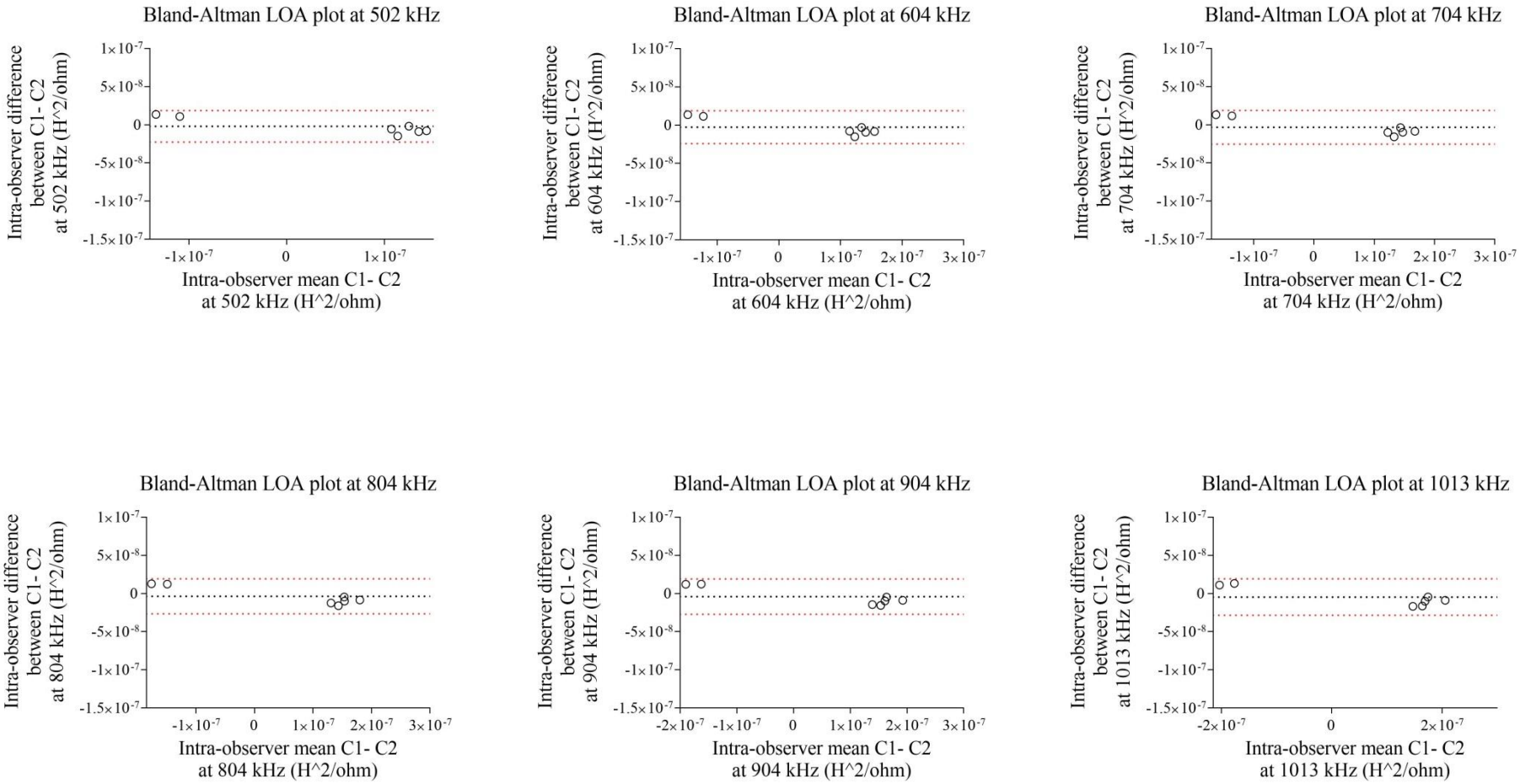

Figure 4.12. Bland-Altman plots for MIS *in vitro* C1-C2 data at 502-1013 kHz. Intra-observer repeatability (n=7)
C1: first cervical measurement, C2: second cervical measurement, LOA: limits of agreement

Limited systematic bias was noted for all paired combinations of MIS measurements as most mean differences were found to lie close to zero especially at low-mid frequencies (72-202 kHz). With the exception of C2-C3 which had the narrowest LOA at 21 kHz, limits of agreement were also narrower at mid-frequencies, and wider at both ends of the frequency range (Figure 4.10 and 4.11; Appendix C: Figures C.1-C.4). For C1-C2, the narrower LOA was noted at 202 kHz and the wider LOA at 21 kHz. This meant that for about 95% of the measurements taken at 202 kHz; C1 was expected to be $1.45E^{-8}$ H^2/ohm below or $1.45E^{-8}$ H^2/ohm above C2, whereas at 21 kHz, most C1 would be $7.29E^{-8}$ H^2/ohm lower or $4.51E^{-8}$ H^2/ohm higher than C2.

Table 4.6. Mean differences and limits of agreement on *in vitro* C1-C2 transresistance measurements (H^2/ ohm). Intra-observer reliability, n=7.

Frequency (kHz)	Mean Difference (C1-C2)	SD	Lower 95% CI of mean	Upper 95% CI of mean	Lower limit of agreement	Upper limit of agreement
21	**$-1.39\ E^{-8}$**	$3.01E^{-8}$	$-4.17E^{-8}$	$1.39E^{-8}$	$-7.29E^{-8}$	$4.51E^{-8}$
42	**$-1.64\ E^{-9}$**	$1.23E^{-8}$	$-1.30E^{-8}$	$9.74E^{-9}$	$-2.57E^{-8}$	$2.25E^{-8}$
56	**$1.19E^{-9}$**	$9.07E^{-9}$	$-3.16E^{-8}$	$1.16E^{-7}$	$-5.88E^{-9}$	$2.9E^{-8}$
72	**$1.60E^{-10}$**	$8.48E^{-9}$	$-7.68E^{-9}$	$8.01E^{-9}$	$-1.65E^{-8}$	$1.68E^{-8}$
86	**$4.57E^{-10}$**	$7.75E^{-9}$	$-6.71E^{-9}$	$7.63E^{-9}$	$-1.47E^{-8}$	$1.56E^{-8}$
100	**$4.61E^{-10}$**	$7.98E^{-9}$	$-6.92E^{-9}$	$7.84E^{-9}$	$-1.52E^{-8}$	$1.61E^{-8}$
202	**$5.22E^{-11}$**	$7.36E^{-9}$	$-6.75E^{-9}$	$6.86E^{-9}$	$-1.45E^{-8}$	$1.45E^{-8}$
302	**$-9.32E^{-10}$**	$9.26E^{-9}$	$-9.4E^{-9}$	$7.63E^{-9}$	$-1.91E^{-8}$	$1.72E^{-8}$
402	**$-1.38E^{-9}$**	$9.93E^{-9}$	$-1.05E^{-8}$	$7.81E^{-9}$	$-2.08E^{-8}$	$1.81E^{-8}$
502	**$-2.01E^{-9}$**	$1.05E^{-8}$	$-1.17E^{-8}$	$7.73E^{-9}$	$-2.26E^{-8}$	$1.86E^{-8}$
604	**$-2.61E^{-9}$**	$1.09E^{-8}$	$-1.28E^{-8}$	$7.55E^{-9}$	$-2.40E^{-8}$	$1.88E^{-8}$
704	**$-3.20E^{-9}$**	$1.13E^{-8}$	$-1.37E^{-8}$	$7.25E^{-9}$	$-2.53E^{-8}$	$1.89E^{-8}$
804	**$-3.71E^{-9}$**	$1.17E^{-8}$	$-1.45E^{-8}$	$7.13E^{-9}$	$-2.66E^{-8}$	$1.92E^{-8}$
904	**$-4.09E^{-9}$**	$1.18E^{-8}$	$-1.50E^{-8}$	$6.83E^{-9}$	$-2.72E^{-8}$	$1.90E^{-8}$
1013	**$-4.6E^{-9}$**	$1.22E^{-8}$	$-1.59E^{-8}$	$6.73E^{-9}$	$-2.85E^{-8}$	$1.93E^{-8}$

C1: first cervical measurement, C2: second cervical measurement, CI: confidence interval, SD: standard deviation, SE: standard error

In conclusion, similarly to what was observed with ICCs, Bland-Altman plots suggested that the highest *in vitro* repeatability was between the first and second cervical measurements at the lower mid-frequencies.

4.4.3. *In vitro* MIS transresistance: epithelial versus stromal surfaces

The epithelial and stromal surfaces of each cervical cross-section were scanned with the Mark II MIS probe. The difference in their transresistance values was then assessed using a one-way ANOVA adjusted with Bonferroni post-hoc tests after a Shapiro-Wilk test confirmed a normal distribution of the data at all 15 frequencies studied.

The three transresistance measurements of the epithelial surface (C1-C2-C3) were compared against the stromal surface measurement, both individually as well as collectively using their mean value. However, particular emphasis was given to C3 as it was hypothesised that the variability observed between C3 and the stroma surface was less likely to be affected by thermal shock given that the measurements had only been taken three seconds apart and that the probe temperature had already stabilised after being in contact with the sample during the first two measurements.

When the stromal surface was compared to C3, transresistance was significantly higher at frequencies 56 and 86 kHz and above ($p<0.05$), (Figure 4.13). The largest differences were identified at 1013 kHz (mean difference $4.60E^{-8}$ H^2/ohm, SD: $1.10E^{-8}$, $p<0.01$) and 202 kHz (mean difference $4.56E^{-8}$ H^2/ohm, SD: $8.83E^{-9}$, $p<0.01$), exemplified in Figure 4.13.

When C1 measurements were individually compared to the stromal surface, there were not statistically significant differences at the lower frequencies whereas it was significantly different for the mid- and higher frequencies (302-1013 kHz). These are the frequencies which yielded maximum reliability in the repeatability analysis. Similarly, when C2 and the mean of C1-C2-C3 were compared to stromal surface, differences in transresistance were significant only at mid- and high frequencies, that is, at 202-1013 kHz and 502-1013 kHz respectively ($p<0.05$) but not at the lower end.

No statistically significant difference was seen in transresistance between C1, C2 and C3 measurements of the epithelial surface ($p>0.05$).

(a)

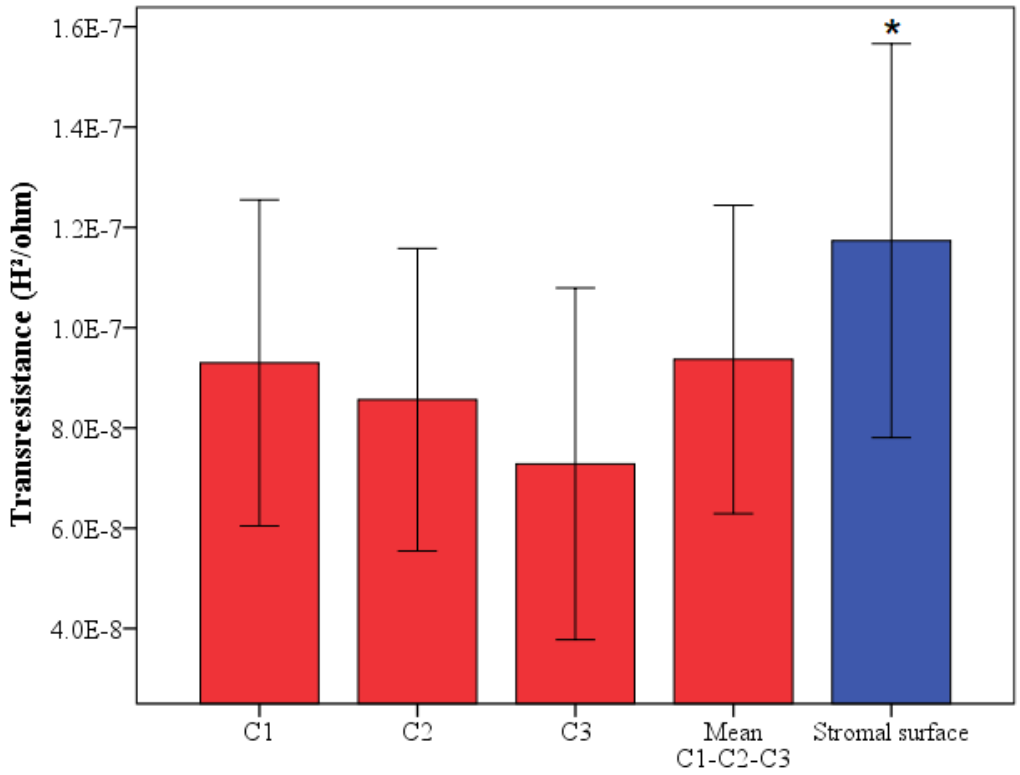

(b)

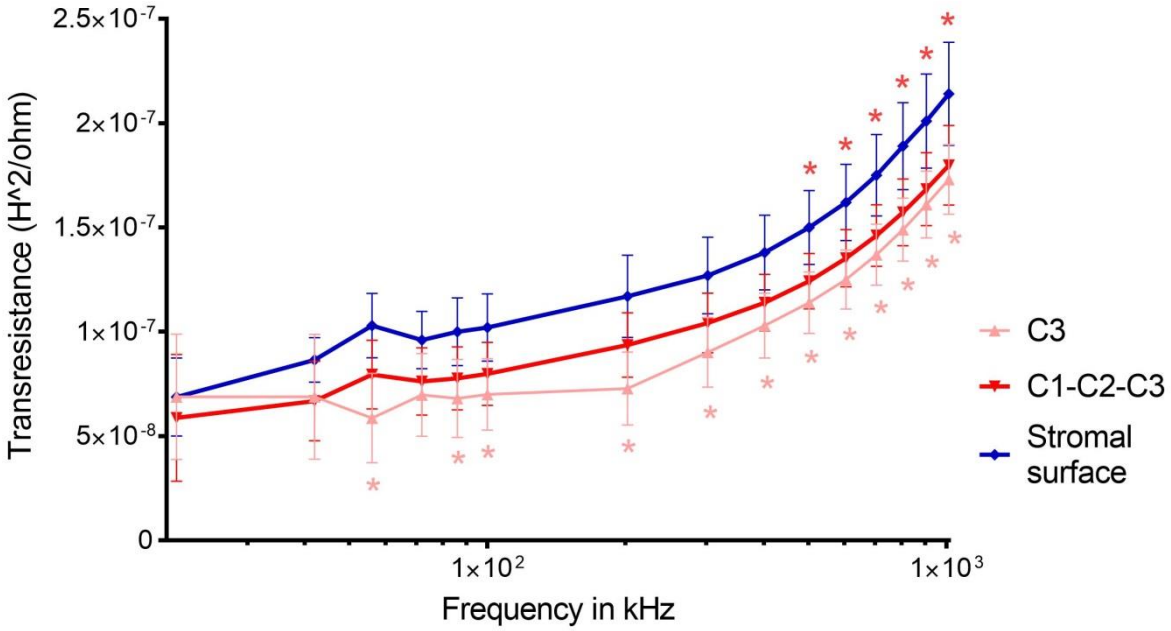

Figure 4.13. Epithelial versus stromal cervical surfaces, **(a)** transresistance mean values are displayed for the first (C1), second (C2) and third (C3) measurements of the epithelial surface, their mean (C1-C2-C3) and the stromal surface at 202 kHz; **(b)** Transresistance of the ectocervix (C3 and C1-C2-C3) and the stromal surface has been plotted against frequency (21-1013 kHz). Red asterisks mark significant differences between the stromal surface and the mean of C1-C2-C3, and pink asterisks mark significant differences between the stromal surface and C3 ($p<0.05$). Frequencies are logarithmically spaced in the X-axis. Error bars represent standard deviations.

4.4.4. *In vivo* MIS demographics

A clinical study was conducted with Human Research Authority approval by the Yorkshire & the Humber Research Ethics Committee (17/YH0179) in alignment with Sheffield Teaching Hospitals NHS Trust regulations (Registration number STH 19385). Between May 15th 2018 and August 1st 2019, 98 pregnant women were recruited into the study: 49 deemed at high risk of PTB (50%) who attended two visits between 20-22 and later on between 26-28 weeks, and 49 (50%) with symptoms of premature labour. Demographics and clinical data of all the patients recruited for the MIS study until August 2019 is displayed per delivery outcome in Tables 4.7 and 4.8. Whereas Table 4.7 includes all preterm deliveries regardless of whether they were spontaneous or induced after PPROM, Table 4.8 further breaks down the PTB information into those who experienced PPROM or sPTB. The rationale behind such a subgroup analysis relies on the assumption that PPROM and sPTB may not necessarily respond to the same pathophysiological process and hence they may not be effectively screened in the same way.

A series of Shapiro-Wilk tests confirmed demographic and clinical data per delivery outcome was well-modelled by a normal distribution ($p>0.05$). As a result, comparisons were performed using parametric methods such as Student's *t*-test or ANOVA tests, and the data was presented as mean +/- SD.

Within the AHR cohort, 17 women delivered before 37 completed weeks of gestation (34.69%) with a mean gestational delivery of 227.94 ± 28.28 days. Out of these 17 women, 13 (76.47%) experienced spontaneous preterm deliveries whereas the remaining four were induced after PPROM. Of the 13 AHR participants who spontaneously delivered prematurely, three (23.08%) had an extreme preterm (<28 weeks) thus only 46 women returned for a follow-up visit between 26-28 weeks, two (15.38%) delivered between 28^{+0} and 32^{+0}, and eight (61.54%) had a late PTB between 32^{+0} and 36^{+6}. The mean gestational age for sPTB was very similar to that seen for all PTB at 227.62 ± 29.80 days, both significantly lower than that for term deliveries (Tables 4.7 and 4.8).

Within the SYMP cohort, 13 women delivered prematurely (26.53%); out of whom eight had a sPTB (61.54%; Table 4.8). Of the eight women who experienced sPTB, one (12.5%) gave birth before 28^{+0} weeks, four (50%) delivered between 28^{+0} and 32^{+0} weeks, and three (37.5%) had a late sPTB. The gestational age of women who were induced prematurely for PPROM tended to be higher than those with a sPTB, but this difference was not statistically significant (Table 4.8). This result fits with expectations as women who suffer premature rupture of membranes but do not go into labour are normally managed conservatively until at least 34-37 weeks unless there are added obstetric complications such as signs of infection or slow fetal growth (Thomson et al., 2019).

In the AHR group, no statistically significant difference was seen in maternal age, BMI, smoking status or history of LLETZ based on delivery outcomes (Tables 4.7 and 4.8). The majority of AHR participants (>80%) were Caucasians followed by a small percentage of Asian, African and Hispanic women. Most AHR Asian women who participated in the study delivered prematurely (n=3, 75%). Similarly, within the SYMP cohort, groups per delivery outcome seemed to be well-matched as no statistically significant differences were seen in maternal age, BMI, previous LLETZ or percentage of smokers. Most SYMP women were also Caucasian (>75%), and in keeping with what was observed for AHR participants, half of all Asian SYMP patients (n=2, 50%) delivered prematurely.

Regarding fFN and CL, no statistically significant differences were seen for the AHR women either between 20-22 weeks or later between 26-28 weeks. At their follow-up, AHR women had consistently shorter cervices compared to their first visit. Even though these differences were not statistically significant, they support the hypothesis that the cervix naturally shortens as pregnancy progresses (Souka et al., 2011). For the SYMP cohort, fFN was significantly higher in women who delivered prematurely, both in women who experienced PPROM as well as in those who had a sPTB (Table 4.8). This result is consistent with previous studies which suggest that fFN is particularly discriminatory in the SYMP cohort given their higher pre-test probability of PTB (Section 1.3.2). On the other hand, CL did not vary significantly between women who had a preterm and a term delivery.

Finally, whereas only three AHR women were receiving vaginal progesterone in their first visit, the number had doubled by the second visit. However, no statistical difference was seen based on delivery outcome (Table 4.7). No SYMP woman had a cerclage or was on progesterone treatment at the time of the study visit.

Table 4.7. Demographic and clinical data of all MIS study participants displayed per PTB versus term delivery outcomes

Characteristics		AHR 1st visit 20-22 weeks (n=49)		AHR 2nd visit 26-28 weeks (n=46)		Symptomatic 20-34+6 weeks (n=49)	
		PTB (n=17)	Term (n=32)	PTB (n=14)	Term (n=32)	PTB (n=13)	Term (n=36)
Maternal age (years)		28.76 ± 6.09	31.47 ± 6.04	29.71 ± 5.84	31.47 ± 6.04	29.38 ± 5.03	28.50 ± 4.92
Ethnicity	**Caucasian**	82.35% (n=14)	84.38% (n=27)	85.71% (n=12)	84.38% (n=27)	76.92% (n=10)	78.95% (n=29)
	African		3.12% (n=1)		3.12% (n=1)		13.16% (n=5)
	Asian	17.65% (n=3)	9.37% (n=3)	14.29% (n=2)	9.37% (n=3)	15.38% (n=2)	5.26% (n=2)
	West Indies					7.69% (n=1)	2.63% (n=1)
	Hispanic		3.12% (n=1)		3.12% (n=1)		
BMI (kg/m^2)		26.18 ± 4.68	27.50 ± 6.31	26.94 ± 4.05	27.50 ± 6.31	25.45 ± 1.35	28.23 ± 6.61
Smoker		6.25% (n=1)	25% (n=8)	7.14% (n=1)	25% (n=8)	30.76% (n=4)	13.89% (n=5)
History of LLETZ		17.65% (n=3)	21.88% (n=7)	21.43% (n=3)	21.88% (n=7)	15.38% (n=2)	8.33% (n=3)
fFN (ng/mL)		4.35 ± 0.93	4.06 ± 1.76	3.29 ± 1.64	3.66 ± 1.38	69.38 ± 100.25*****	5.78 ± 9.16
CL (mm)		34.06 ± 5.94	35.25 ± 5.97	32.71 ± 5.43	32.66 ± 5.89	26.54 ± 9.35	31.94 ± 8.72
Prophylactic treatment	**Progesterone**	6.25% (n=1)	3.12% (n=1)	14.29% (n=2)	6.25% (n=2)		
	Progesterone and cerclage		3.12% (n=1)[#]		6.25% (n=2)		
Gestational age at presentation (days)		140.29 ± 6.55	145.69 ± 7.89	182.93 ± 9.12	186.53 ± 6.72	193.08 ± 36.27	205.67 ± 27.56
Gestational age at delivery (days)		227.94 ± 28.28[+]	273.16 ± 8.34	233.5 ± 21.49[++]	273.16 ± 8.34	218.69 ± 29.81*****	272.61 ± 11.92

[+]*p<0.05 versus AHR 1st visit term,* [++]*p<0.05 versus AHR 2nd visit term, *p<0.05 vs SYMP term*
[#]*Transabdominal cerclage, sPTB: spontaneous preterm birth*

Table 4.8. Demographic and clinical data of all MIS study participants displayed per PPROM and sPTB versus term delivery outcomes

Characteristics		AHR 1st visit 20-22 weeks (n=49)			AHR 2nd visit 26-28 weeks (n=46)			Symptomatic 20- 34+6 weeks (n=49)		
		PPROM (n=4)	sPTB (n=13)	Term (n=32)	PPROM (n=3)	sPTB (n=11)	Term (n=32)	PPROM (n=5)	sPTB (n=8)	Term (n=36)
Maternal age (years)		28.75 ± 8.66	28.77 ± 5.54	31.47 ± 6.04	28 ± 10.44	30.18 ± 4.62	31.47 ± 6.04	31.40 ± 3.78	28.13 ± 5.51	28.50 ± 4.92
Ethnicity	**Caucasian**	100% (n=4)	76.92% (n=10)	84.38% (n=27)	100% (n=3)	81.82% (n=9)	84.38% (n=27)	60% (n=3)	87.5% (n=7)	80.56% (n=29)
	African			3.12% (n=1)			3.12% (n=1)			13.88% (n=5)
	Asian		23.08% (n=3)	9.37% (n=1)		18.18% (n=2)	9.37% (n=3)	20% (n=1)	12.5% (n=1)	2.78% (n=1)
	West Indies							20% (n=1)		2.78% (n=1)
	Hispanic			3.12% (n=1)			3.12% (n=1)			
BMI (kg/m^2)		27.70 ± 1.70	25.71 ± 5.24	27.50 ± 6.31	27.67 ± 2.08	26.75 ± 4.50	27.50 ± 6.31	26.97 ± 3.32	24.51 ± 5.64	28.23 ± 6.61
Smoker		25% (n=1)		25% (n=8)	33.33% (n=1)		25% (n=8)	20% (n=1)	37.5% (n=2)	13.89% (n=5)
History of LLETZ			23.08% (n=3)	21.88% (n=7)		27.27% (n=3)	21.88% (n=7)	20% (n=1)	12.5% (n=1)	8.33% (n=3)
fFN (ng/mL)		4.0 ± 1.41	4.46 ± 0.78	4.06 ± 1.76	2.33 ± 1.53	3.55 ± 1.63	3.66 ± 1.38	87.8 ± 117.03*	57.88 ± 94.91*	5.78 ± 9.16
CL (mm)		37.75 ± 5.32	32.92 ± 5.83	35.25 ± 5.97	32.33 ± 4.51	32.82 ± 5.84	32.66 ± 5.89	23.20 ± 12.38	28.63 ± 7.09	31.94 ± 8.72
Prophylactic treatment	**Progesterone**		7.69% (n=1)	3.12% (n=1)		18.18% (n=2)	6.25% (n=2)			
	Progesterone and cerclage			3.12% (n=1)#			6.25% (n=2)			
Gestational age at presentation (days)		140 ± 7.12	140.38 ± 6.68	145.69 ± 7.89	182 ± 8.72	183.18 ± 9.62	186.53 ± 6.72	207.4 ± 41.37	184.16 ± 32.25	205.67 ± 27.56
Gestational age at delivery (days)		229 ± 26.70+	227.62 ± 29.80+	273.16 ± 8.34	220.67 ± 25.54++	237.00 ± 20.16++	273.16 ± 8.34	233 ± 24.36*	209.75 ± 30.76*	272.61 ± 11.92

+ *p<0.05 versus AHR 1st visit term,* ++ *p<0.05 versus AHR 2nd visit term, *p<0.05 vs SYMP term*

Transabdominal cerclage, PPROM: prelabour premature rupture of membranes, sPTB: spontaneous preterm birth

4.4.5. *In vivo* MIS data

An MIS file was created at each study visit to record cervical transresistance values at 15 pre-established frequencies. At the time of writing this chapter (September 2019), no serious event had been identified, 98 women had completed the study, and there were 144 CRF datasets available with known delivery outcomes. Forty-nine of these files were generated when AHR women attended their first study visit and 46 when they came to their follow-up appointments (three patients failed to attend the 2nd visit as they delivered before 26-28 weeks of gestation). A similar number of files was produced from the SYMP cohort (n=49). However, it was not possible to include all these datasets in the final analysis as a series of software and hardware upgrades needed during the trial affected signal processing in acquisition and rendered some of the data non-comparable.

Three months into the clinical study, the software used to capture and process the MIS data was found to record the measurements with some time inaccuracies which did not allow confident interpretation of the data. As a result, all the datasets retrieved until then were excluded from the final analysis (SYMP n=17, AHR 1st visit n=15, AHR 2nd visit n=10).

Similarly, replacement of the probe during the trial adversely impacted on the final sample size. The majority of the MIS measurements were performed with a working prototype MIS probe named A. However, in February 2019, probe A had to be replaced due to some structural damage noticed to the cable where it entered the probe. Study visits were then conducted by a similar probe referred to as C. Both probes captured MIS transresistance values quite effectively. However, parallel *in vitro* work by the engineering team identified that each probe had a different response to the surrounding electric field which could potentially affect the comparability of the data retrieved. After a series of attempts at generating a scale factor which could account for the wide and complex range of electric field variation with mixed results, a decision was made to analyse the output from each probe individually. As a result, final analyses were performed independently for each probe employing 77 datasets for probe A (SYMP=24, AHR 1st visit=27 and AHR 2nd visit=26), and 30 for probe C (SYMP=8, AHR 1st visit=9 and AHR 2nd visit=13).

Splitting data by probe significantly reduced the sample size of each cohort thus increasing the risk of type II error for any of the statistical inferential tests applied. In an attempt to compensate for these smaller sample sizes and compare results from each probe, emphasis was placed on describing trends and gradients. Whenever possible, a linear equation was calculated for each variable. The relationship between different outcomes namely PTB/Term in the SYMP and AHR cohorts was

then displayed as a ratio of their gradients. These ratios were then compared between probes to assess any trend consistency.

In view of the reduced sample size, demographics and clinical data were reassessed to ensure cohorts were adequately matched by delivery outcome (Table 4.9). Shapiro-Wilk tests confirmed variables were normally distributed per birth outcome both in the AHR and SYMP cohorts ($p>0.05$). Despite the reduced number of participants, the statistical significance reported for fFN in the SYMP group and for gestational age at delivery for both AHR and SYMP participants in Table 4.8 was retained. However, precision was reduced as suggested by the considerably larger standard deviations (Table 4.9).

Within the smaller AHR cohort, no statistically significant differences were seen in maternal age, BMI, history of LLETZ and smoking status based on delivery outcome (Table 4.9), which is similar to what was reported in Tables 4.7 and 4.8 for all the MIS patients. Comparison of CL and fFN did not yield any statistical significance either, and like in the complete dataset, AHR women in this smaller group all seemed to have shortened CL at 26-28 weeks when compared to their first MIS visit.

For the SYMP smaller cohort, women were also adequately-matched for maternal age, BMI, smoking status and history of LLETZ based on delivery outcome. Regarding CL and fFN, fFN was significantly higher in women who delivered prematurely, both spontaneously and iatrogenically following PPROM ($p<0.05$; Table 4.9).

Table 4.9. Demographic and clinical data of the MIS study participants whose cervical transresistance measurements were included in the final analysis.

Characteristics		AHR 1st visit 20-22 weeks (n=34)			AHR 2nd visit 26-28 weeks (n=37)			Symptomatic 20- 34+6 weeks (n=32)		
		PPROM (n=3)	sPTB (n=8)	Term (n=23)	PPROM (n=3)	sPTB (n=9)	Term (n=25)	PPROM (n=3)	sPTB (n=5)	Term (n=24)
Maternal age (years)		31.33 ± 8.51	31 ± 5.16	30.30 ± 6.07	28 ± 10.44	30.33 ± 5.15	30.72 ± 6.02	32.67 ± 4.04	26.6 ± 6.38	28.71 ± 5.35
Ethnicity	**Caucasian**	100% (n=3)	87.5% (n=7)	86.96% (n=20)	100% (n=3)	88.89% (n=8)	84% (n=21)	33.33% (n=1)	80% (n=4)	75% (n=18)
	African									16.67% (n=4)
	Asian		12.5% (n=1)	8.70% (n=2)		11.11% (n=1)	12% (n=3)	33.33% (n=1)	20% (n=1)	4.17% (n=1)
	West Indies							33.33% (n=1)		4.17% (n=1)
	Hispanic			4.34% (n=1)			4% (n=1)			
BMI (kg/m^2)		26.93 ± 0.90	25.40 ± 4.28	25.64 ± 5.88	27.67 ± 2.08	26.30 ± 4.83	25.93 ± 5.80	27.77 ± 3.45	27.63 ± 4.12	28.51 ± 6.45
Smoker		33.33% (n=1)		21.74% (n=5)	33.33% (n=1)		20% (n=5)	33.33% (n=1)	20% (n=1)	16.67% (n=4)
History of LLETZ			25% (n=2)	26.09% (n= 6)		22.22% (n=2)	24% (n=6)			8.33% (n=2)
fFN (ng/mL)		4.00 ± 1.73	4.25 ± 0.89	4.09 ± 1.5	2.33 ± 1.53	3.89 ± 1.54	3.56 ± 1.5	143.00 ± 126.35*	48.00 ± 101.76*	4.13 ± 2.19
CL (mm)		39.67 ± 4.5	33.13 ± 4.5	35.48 ± 6.04	32.33 ± 4.51	32.33 ± 5.95	33.52 ± 5.93	18.33 ± 14.57	27.60 ± 4.28	30.54 ± 9.38
Prophylactic treatment	**Progesterone**		12.5% (n=1)	4.35% (n=1)		22.22% (n=2)	8% (n=2)			
	Progesterone and cerclage			4.35% (n=1)#			4% (n=1)			
Gestational age at presentation (days)		138.67 ± 8.08	142 ± 6.99	145.35 ± 8.01	184.73 ± 7.91	182 ± 8.72	186.08 ± 6.87	188.67 ± 45.76	178.60 ± 38.68	202.92 ± 29.43
Gestational age at delivery (days)		225.00 ± 31.19+	233.25 ± 22.49+	274.57 ± 8.59	220.67 ± 25.54++	235.67 ± 22.25++	273.88 ± 8.56	219.33 ± 22.01*	198 ± 31.15	272.83 ± 12.68*

+ *p<0.05 versus AHR 1st visit term,* ++ *p<0.05 versus AHR 2nd visit term, *p<0.05 vs SYMP term*

Transabdominal cerclage, PPROM: prelabour premature rupture of membranes, sPTB: spontaneous preterm birth

4.4.6. *In vivo* MIS repeatability

During each study visit, an attempt was made to scan the cervix at least three times. However, on a few occasions, it was not possible to record all measurements due to patient discomfort or technical difficulties during the procedure. Like the *in vitro* MIS study, the consecutive cervical measurements were named C1, C2 and C3, and were used for the repeatability study. A total of 32 datasets from a combination of AHR 1st and 2nd visits conducted with probe A were employed to assess intra-observer reliability through the calculation of ICCs and construction of Bland-Altman plots. The closeness of agreement was first calculated between all three cervical measurements and subsequently assessed between C1-C2, C2-C3, and C1-C3.

Histogram representation of transresistance measurements demonstrated that the data was positively skewed at most frequencies. A subsequent Shapiro-Wilk test confirmed that the data was not normally distributed ($p<0.05$). The datasets were then normalised to facilitate subsequent statistical analyses such as ICC and Bland-Altman which require that the assumption of normality is met. Logarithmic and fractional rank transformation methods were initially explored but as they failed to normalise the data at the lower frequencies, preference was given to cube root transformation which significantly reduced data skewedness.

When the three cervical measurements were considered together (C1-C2-C3), intra-observer variability was excellent at the low mid-frequencies (86 and 202 kHz) with ICCs ranging from 0.912 to 0.935. For transresistance measurements taken at the higher frequencies, reliability was noted to be fair to good with the smallest ICC identified at 804 kHz with a value of 0.681 (Table 4.10). Confidence intervals were consistently wider at frequencies with lower ICCs, and narrower at those with higher measurement agreement such as 100 kHz.

Table 4.10. Repeatability of cube root transformed *in vivo* cervical measurements (C1-C2-C3) calculated at each frequency (n=32).

Frequency (kHz)	REPEATABILITY		
	ICC	95% CI	
21	**0.847**	0.717	0.921
42	**0.857**	0.744	0.925
56	**0.889**	0.808	0.941
72	**0.912**	0.847	0.953
86	**0.917**	0.856	0.955
100	**0.935**	0.887	0.965
202	**0.917**	0.858	0.956
302	**0.886**	0.807	0.938
402	**0.773**	0.636	0.872
502	**0.815**	0.697	0.897
604	**0.720**	0.565	0.839
704	**0.699**	0.535	0.826
804	**0.681**	0.511	0.814
904	**0.746**	0.599	0.855
1013	**0.808**	0.688	0.893

CI: confidence interval, ICC: intra-class correlation coefficient

When the first and second cervical measurements were compared (C1-C2), the highest reliability was noted at the low-mid frequencies (42-202 kHz) with ICCs ranging from 0.889 to 0.935. The lowest agreement, on the other hand, was identified at the mid-/mid-high frequency range (502-804 kHz) with ICCs between 0.486 and 0.703 (fair to good). Concordance seemed to once again slightly improve towards the highest frequencies (904-1013 kHz) but without reaching the same values as those seen at the lowest frequencies (Table 4.11, Figure 4.13).

Table 4.11. Repeatability of cube root transformed *in vivo* cervical measurements (C1-C2) calculated at each frequency (n=32).

Frequency (kHz)	**REPEATABILITY**		
	ICC	**95% CI**	
21	**0.940**	0.873	0.971
42	**0.885**	0.772	0.943
56	**0.949**	0.899	0.975
72	**0.940**	0.881	0.970
86	**0.937**	0.876	0.969
100	**0.947**	0.895	0.974
202	**0.916**	0.836	0.958
302	**0.899**	0.803	0.949
402	**0.762**	0.570	0.876
502	**0.677**	0.438	0.827
604	**0.494**	0.194	0.717
704	**0.486**	0.181	0.709
804	**0.532**	0.239	0.739
904	**0.703**	0.478	0.843
1013	**0.753**	0.555	0.871

CI: confidence interval, ICC: intra-class correlation coefficient

For C2-C3, ICCs were excellent at all frequencies with values ranging from 0.814 at 904 kHz (95% CI: 0.656-0.904) to 0.974 at 202 kHz (0.947-0.987). Similarly to C1-C2, higher ICCs and consistently narrower confidence intervals were noted at the low mid-frequencies (72-302 kHz) which suggested greater agreement between cervical measurements at that specific frequency range (Table 4.12).

Table 4.12. Repeatability of cube root transformed *in vivo* cervical measurements (C2-C3) calculated at each frequency (n=32).

Frequency (kHz)	**REPEATABILITY**		
	ICC	**95% CI**	
21	**0.873**	0.704	0.942
42	**0.921**	0.824	0.963
56	**0.908**	0.808	0.956
72	**0.947**	0.892	0.974
86	**0.953**	0.902	0.977
100	**0.963**	0.926	0.982
202	**0.974**	0.947	0.987
302	**0.941**	0.884	0.971
402	**0.870**	0.752	0.934
502	**0.971**	0.941	0.986
604	**0.973**	0.945	0.987
704	**0.944**	0.888	0.972
804	**0.829**	0.680	0.912
904	**0.814**	0.656	0.904
1013	**0.867**	0.747	0.933

CI: confidence interval, ICC: intra-class correlation coefficient

Sample concordance between the first and the third cervical measurements (C1-C3) seemed to follow a similar pattern to the one described for C1-C2 and C2-C3 with the highest ICCs values identified at low-mid frequencies (72-302 kHz) and the lowest at the higher frequency range (604-904 kHz). However, the discordance between C1 and C3 appeared to be more marked than for any other pair combination as illustrated by the relatively lower ICCs and wider CIs (Table 4.13). Despite this increased variability, intra-observer reliability for C1-C3 was still excellent at low-mid frequencies, and fair to good at the high/ mid-high frequencies (Table 4.13).

Table 4.13. Repeatability of cube root transformed *in vivo* cervical measurements (C1-C3) calculated at each frequency (n=32).

Frequency (kHz)	**REPEATABILITY**		
	ICC	**95% CI**	
21	**0.748**	0.465	0.880
42	**0.761**	0.505	0.884
56	**0.813**	0.640	0.906
72	**0.847**	0.700	0.924
86	**0.856**	0.726	0.927
100	**0.890**	0.788	0.944
202	**0.853**	0.722	0.925
302	**0.805**	0.638	0.900
402	**0.652**	0.398	0.814
502	**0.717**	0.499	0.851
604	**0.522**	0.226	0.732
704	**0.510**	0.210	0.724
804	**0.606**	0.337	0.785
904	**0.698**	0.466	0.840
1013	**0.791**	0.617	0.892

CI: confidence interval, ICC: intra-class correlation coefficient

Overall, when all pair combinations were considered, C2-C3 measurements appeared to be closer in agreement than C1-C2 and C1-C3 (Figure 4.14). However, repeatability values at all frequencies and for all pair combinations were found to yield acceptable ICCs (good to excellent) suggesting that MIS measurements are highly repeatable especially at the low mid-frequencies.

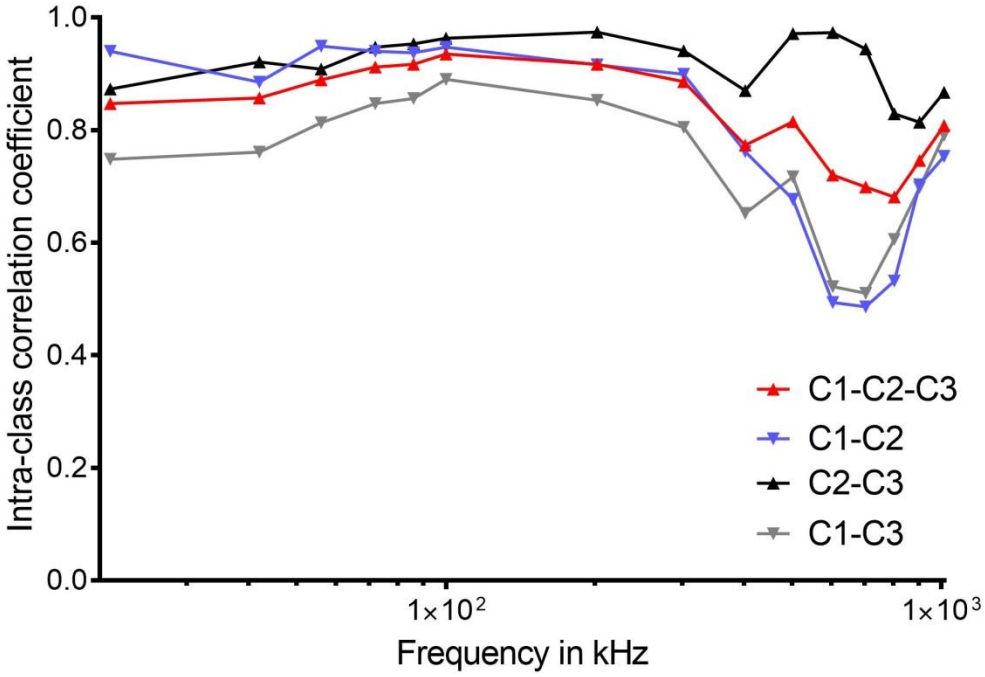

Figure 4.14. ICCs are compared between *in vivo* cervical measurements: C1-C2-C3, C1-C2, C2-C3, and C1-C3 taken at 15 different frequencies. *X-axis is in logarithmic scale*.

Similarly to the *in vitro* experiments, sequential Bland-Altman plots were constructed to better display the discrepancy between *in vivo* cervical measurements at increasing frequencies. The results for C2-C3 are presented in Table 4.14 and exemplified in Figures 4.15 and 4.16, while C1-C2 and C2-C3 are summarised in Appendix C (Tables C.3 and C.4; Figures C.5-C.8).

Visual inspection of the plots revealed that mean differences between cervical measurements at all frequencies were close to zero suggesting limited systematic error, especially at low-mid frequencies (72-302 kHz; Figures 4.15 and 4.16). Compared to the *in vitro* repeatability observations, the *in vivo* data aggregated more closely together and some points overlapped more frequently. However, unlike the *in vitro* data, the presence of outliers at the higher end frequencies gave the false impression of proportional bias in the range 804-1013 kHz whereas for low and mid-frequency the data appeared clearly homoscedastic. Consistent with ICCs, the limits of agreements seemed to be wider at the higher frequencies and narrower at mid-low frequencies particularly for the pair C2-C3 (Table 4.14; Appendix C: Tables C.3 and C.4).

Table 4.14. Mean differences and limits of agreement on cube root transformed *in vivo* transresistance measurements for C2-C3 measured in H^2/ohm. Intra-observer reliability (n=32).

Frequency (kHz)	Mean Difference (C2-C3)	SD	Lower 95% CI of mean	Upper 95% CI of mean	Lower limit of agreement	Upper limit of agreement
21	**-8.26E^{-4}**	1.55E^{-3}	-1.38E^{-3}	-2.70E^{-4}	**-3.86E^{-3}**	**2.21E^{-3}**
42	**-5.38E^{-4}**	1.16E^{-3}	-9.58E^{-4}	-1.17E^{-4}	**-2.89E^{-3}**	**1.74E^{-3}**
56	**-5.13E^{-4}**	1.27E^{-4}	-9.73E^{-4}	-5.23E^{-5}	**-3.00E^{-3}**	**1.98E^{-3}**
72	**-3.28E^{-4}**	9.79E^{-4}	-6.81E^{-4}	2.25E^{-5}	**-2.25E^{-3}**	**1.59E^{-3}**
86	**-3.19E^{-4}**	9.24E^{-4}	-6.53E^{-4}	1.132E^{-5}	**-2.13E^{-3}**	**1.49E^{-3}**
100	**-1.91E^{-4}**	8.40E^{-4}	-4.94E^{-4}	1.12E^{-4}	**-1.84E^{-3}**	**1.46E^{-3}**
202	**9.37E^{-5}**	6.77E^{-4}	-1.50E^{-4}	3.38E^{-4}	**-1.23E^{-3}**	**1.42E^{-3}**
302	**1.47E^{-4}**	9.81E^{-4}	-2.07E^{-4}	5.01E^{-4}	**-1.78E^{-3}**	**2.07E^{-3}**
402	**3.05E^{-4}**	1.31E^{-3}	-1.69E^{-4}	7.79E^{-4}	**-2.26E^{-3}**	**2.87E^{-3}**
502	**4.55E^{-4}**	5.84E^{-4}	-1.65E^{-4}	2.56E^{-4}	**-1.10E^{-3}**	**1.19E^{-3}**
604	**-4.75E^{-4}**	5.56E^{-4}	-2.05E^{-4}	1.96E^{-4}	**-1.09E^{-3}**	**1.09E^{-3}**
704	**-1.08E^{-4}**	8.02E^{-4}	-3.97E^{-4}	1.81E^{-4}	**-1.68E^{-3}**	**1.46E^{-3}**
804	**-2.63E^{-4}**	1.45E^{-3}	-7.87E^{-4}	2.62E^{-4}	**-3.11E^{-3}**	**2.58E^{-3}**
904	**-2.84E^{-4}**	1.58E^{-3}	-8.55E^{-4}	2.86E^{-4}	**-3.38E^{-3}**	**2.81E^{-3}**
1013	**-1.86E^{-4}**	1.45E^{-3}	-7.11E^{-4}	3.38E^{-4}	**-3.03E^{-3}**	**2.66E^{-3}**

C2: second cervical measurement, C3: third cervical measurement, CI: confidence interval, SD: standard deviation, SE: standard error

Cube root transformed *in vivo* repeatability data C2-C3

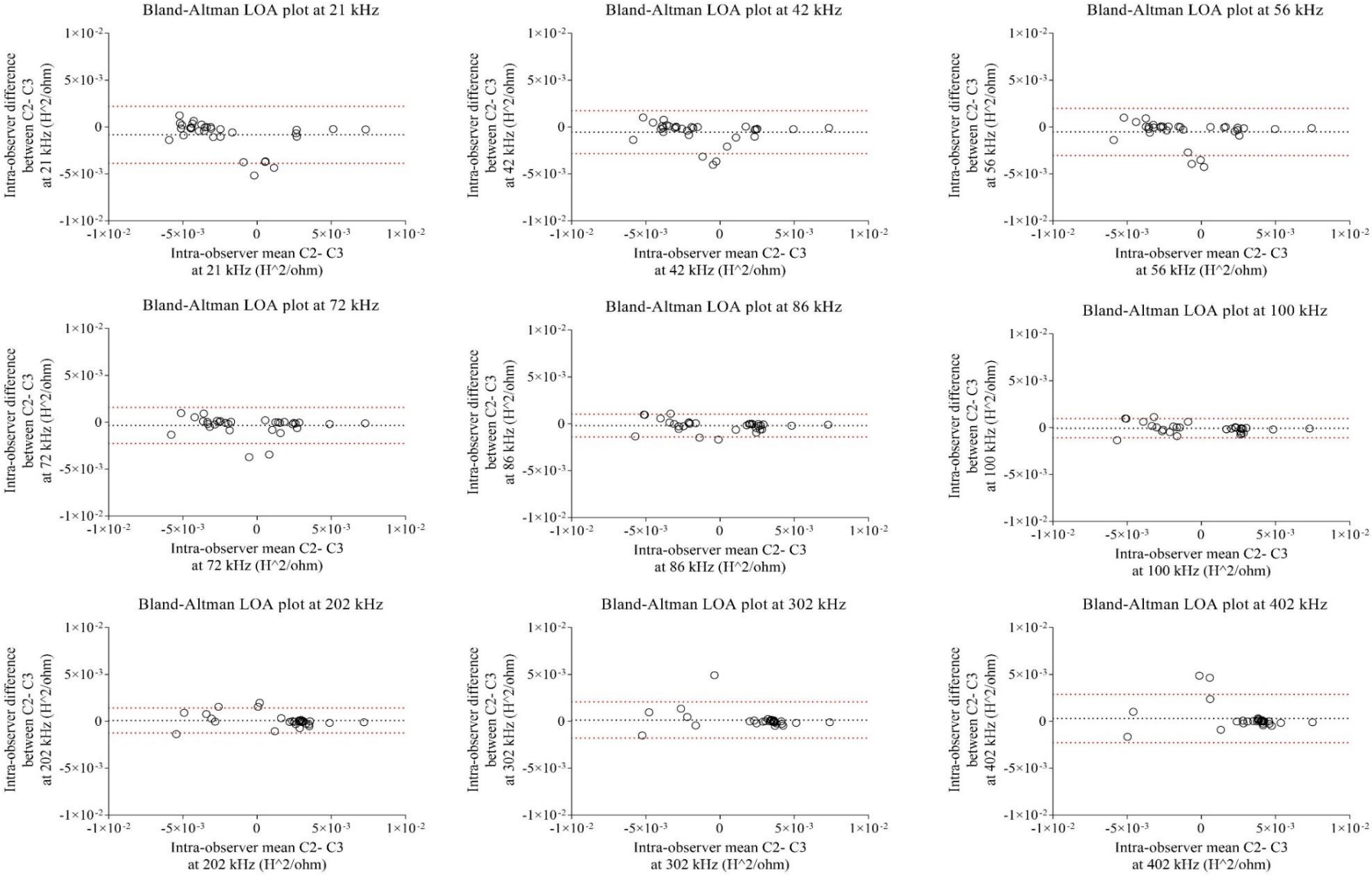

Figure 4.15. Bland-Altman plots for MIS *in vivo* C2-C3 data at 21-402 kHz. Intra-observer repeatability (n=32). The central black dotted line represents the mean difference whereas the two red dotted lines represent the upper and lower LOAs.

C2: second cervical measurement, C3: third cervical measurement, LOA: limits of agreement

Cube root transformed *in vivo* repeatability data C2-C3

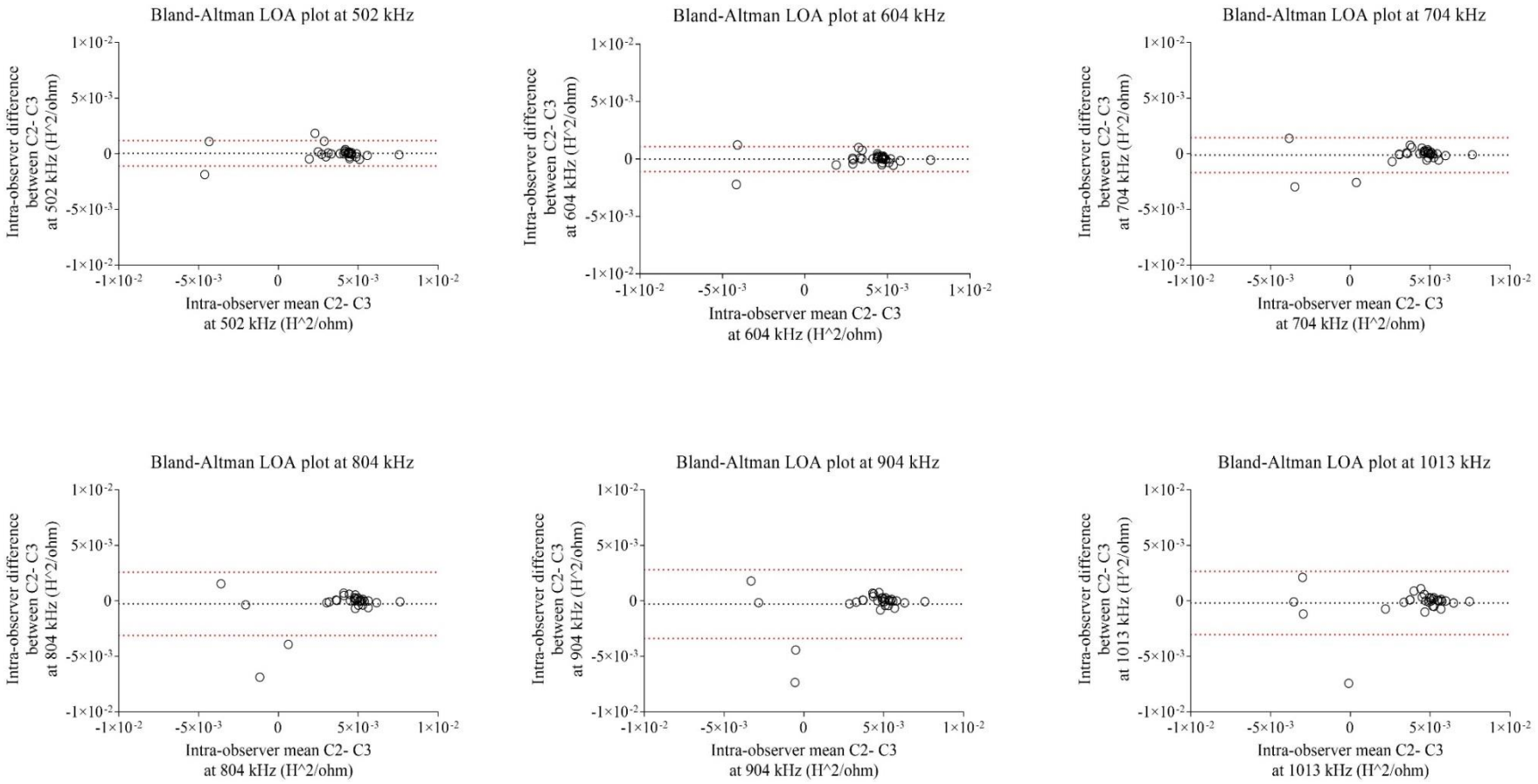

Figure 4.16. Bland-Altman plots for MIS *in vivo* C2-C3 data at 502-1013 kHz. Intra-observer repeatability (n=32). The central black dotted line represents the mean difference whereas the two red dotted lines represent the upper and lower LOAs

C2: second cervical measurement, C3: third cervical measurement, LOA: limits of agreement

For the preliminary study on MIS clinical performance (section 4.4.3), a decision was made to use the measurement with the largest signal at 502 kHz regardless of whether it was C1, C2 or C3. The rationale behind this approach is that the closer the probe is to the tissue of interest, the higher the signals are expected to be. Therefore, larger signals suggest better positioning of the probe during scanning. Furthermore, using the measurements with the largest signals at 502 kHz yielded the highest and most statistically significant AuROC (Appendix D), and they included more index cases than individual repeats as it was not always possible to retrieve complete datasets with three repeats for every participant.

4.4.7. *In vivo* MIS data based on birth outcome: PTB vs Term

Transresistance measurements based on birth outcome were normally distributed (Shapiro-Wilk test, $p>0.05$). As a result, comparisons amongst different groups were performed with ANOVA and/ or Student's *t*-test, and displayed as mean ± SD.

The first approach was to analyse all AHR and SYMP data captured with probe A that was matched for gestational age at the time of the visit. When AHR 1st visit and SYMP (≤160 days) data was considered together, probe A transresistance was noted to be significantly lower between 402-704 kHz in women who had a PTB (n=10) when compared to those with a term delivery (n=20; Figure 4.17a). When the PTB data was further assessed for women who had a spontaneous PTB (n=6) and those who were induced prematurely after experiencing PPROM (n=4), transresistance in these sub-groups tended to be lower than in those who had a term delivery even though these differences were not statistically significant (Figure 4.17b).

When AHR 2nd visit and SYMP (>160 days) data was considered instead (n=47), transresistance values at the lower frequencies also tended to be higher for women who had a term delivery (n=33) when compared to those with a PTB (n=14) even though the difference was not statistically significant. At mid- and high-frequencies, however, the curves appeared to approximate (Figure 4.17c). When PTB was sub-classified into PPROM (n=5) and sPTB (n=9), those who were induced after PPROM tended to display higher transresistance than those who went into labour spontaneously even though these differences were not supported by statistical significance ($p>0.05$; Figure 4.17d)

A similar approach was applied to transresistance values measured with probe C. When AHR 2nd visit and gestational-matched SYMP data was analysed together, women who delivered spontaneously (n=4) tended to have lower transresistance than those with a term delivery (n=12), especially at low and mid-low frequencies ($p>0.05$; Figure 4.18). It was not possible to compare

transresistance values for the AHR 1st visit and SYMP (≤160 days) or for women who experienced PPROM between probe A and C as there were not enough index cases measured with probe C (PTB, n<3).

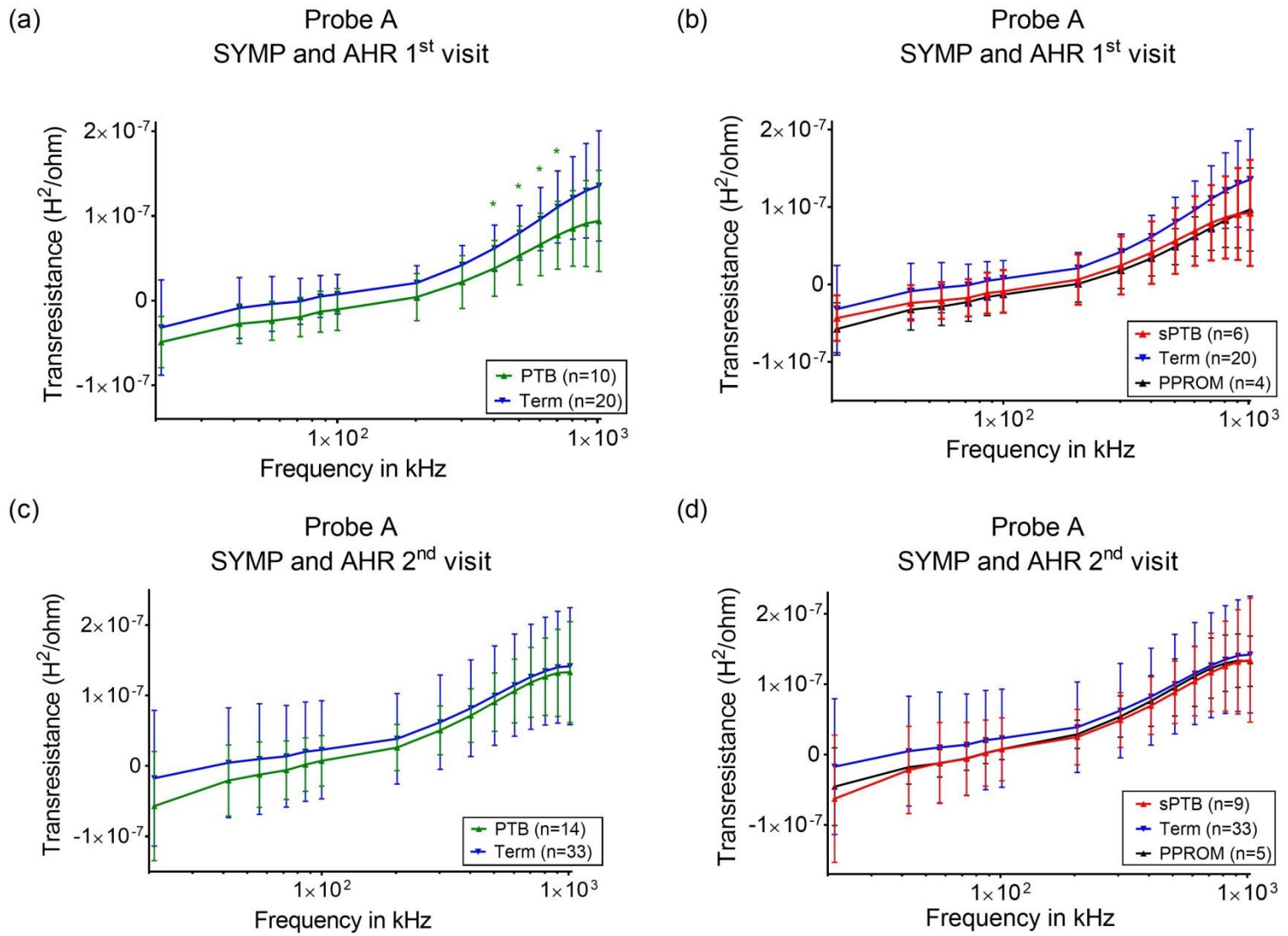

Figure 4.17. Mean transresistance +/- SD is displayed for gestationally-matched SYMP and AHR 1st visit based on **(a)** PTB and term, and **(b)** sPTB, term and PPROM. Transresistance data is also presented for gestationally-matched SYMP and AHR 2nd visit data for **(c)** PTB and term and **(d)** sPTB, term and PPROM. *X-axis is in logarithmic scale. Error bars represent standard deviations from the mean. Green asterisks mark significant differences between term and PTB ($p<0.05$). AHR: asymptomatic high risk, PPROM: prelabour premature rupture of membrane, PTB: preterm birth, sPTB: spontaneous preterm birth, SYMP: symptomatic*

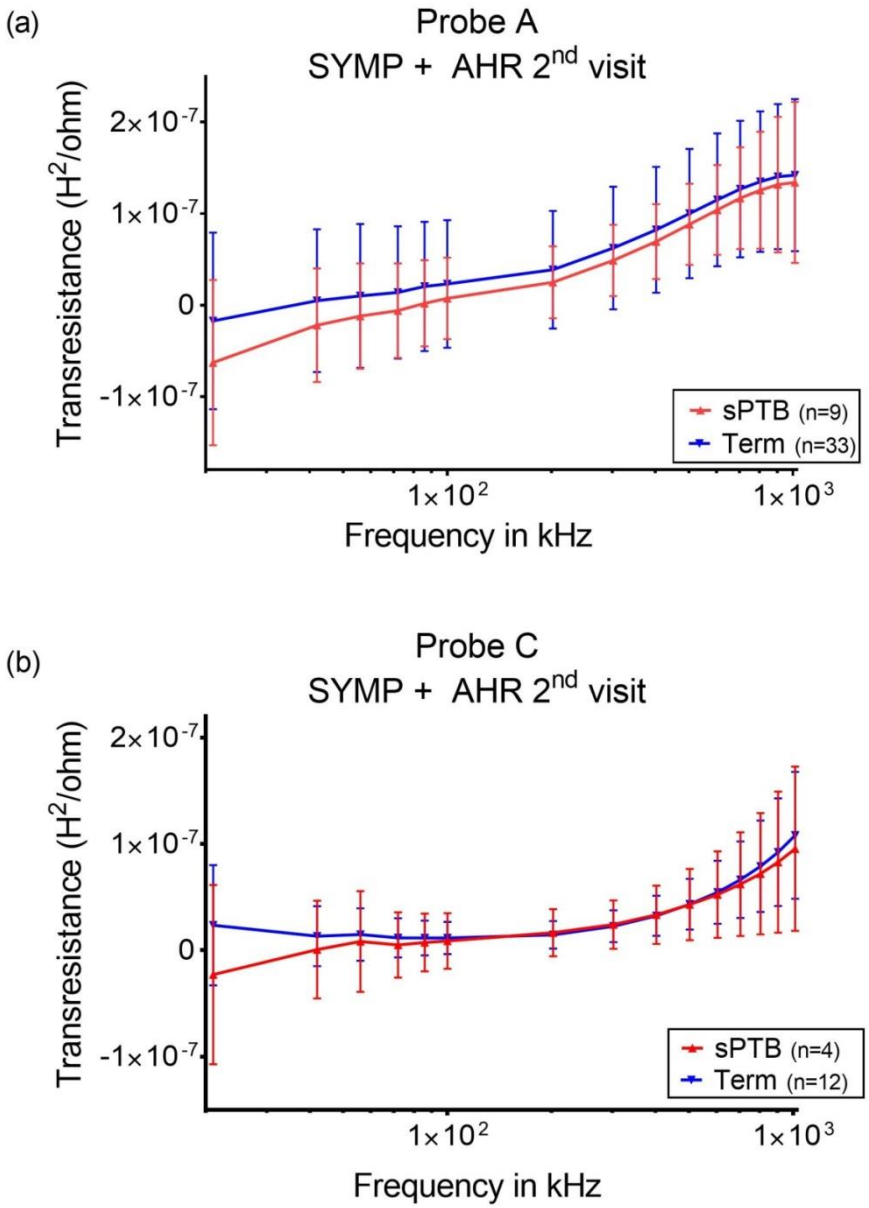

Figure 4.18. Mean transresistance +/- SD for gestationally-matched SYMP and AHR 2nd visit data based on sPTB and term deliveries for **(a)** probe A and **(b)** probe C. *X-axis is in logarithmic scale. Error bars represent standard deviations from the mean.*
AHR: asymptomatic high risk, sPTB: spontaneous preterm birth, SYMP: symptomatic women

In order to assess how comparable the data from each probe was, the relationship between transresistance and frequency was modelled with linear regression, and a data-fitting equation was produced for each delivery outcome. The difference in gradients (slope) between sPTB and term for all the spectra was assessed, and its ratio was then compared between probes.

The ratio of gradients between sPTB and term was noted to be quite similar between probes A and C when gestationally-matched SYMP and AHR 2nd visit data was combined together (probe

A=1.09 versus probe C=1.06). Steeper gradients were noted for those who delivered prematurely even though these differences were not statistically significant (Table 4.15).

Table 4.15. The relationship between transresistance and frequency for AHR 2nd visit and SYMP>160 days is displayed as a linear equation per each delivery outcome, and the gradients (in bold) in ratios.

Probe	sPTB	Term	Ratio sPTB/ Term	*p*-value
A	$y = \mathbf{1.79E^{-10}}\,x - 1.95E^{-8}$	$y = \mathbf{1.64E^{-10}}\,x - 7.7E^{-9}$	$\frac{1.79^{-10}}{1.64^{-10}} = 1.09$	0.39
C	$y = \mathbf{9.75E^{-11}}\,x - 5.18E^{-9}$	$y = \mathbf{9.16^{-11}}\,x + 4.47E^{-9}$	$\frac{9.75^{-11}}{9.16^{-11}} = 1.06$	0.46

4.4.8. *In vivo* MIS data: SYMP and AHR cohorts

Transresistance values were subsequently analysed for each cohort independently. When only probe A data from AHR 1st visit was considered (term n=18, sPTB n=6, PPROM n=3), transresistance values tended to be consistently higher in women who delivered at term compared to those who either had a sPTB or PPROM but the differences were not statistically significant. Mean transresistance values between sPTB and PPROM were quite similar at all frequencies except at 21 kHz (Figure 4.19).

When probe A data from the AHR 2nd visit was assessed instead (term n=17, sPTB=6, PPROM n=3), transresistance at low and mid-frequencies tended to be higher in women who had a term delivery. Unlike AHR 1st visit, women who experienced PPROM tended to have lower cervical transresistance values than their term and sPTB counterparts, even though none of these differences were statistically significant (Figure 4.19).

In the SYMP cohort, transresistance values measured with probe A followed a similar tendency to the one seen in AHR patients, but in this case the trend was supported by statistical significance. Women who had a term delivery (n=18) had significantly higher transresistance values than their counterparts in the frequency range between 202-502 kHz ($p<0.05$; Table 4.19). Contrary to AHR 2nd visit, women who experienced PPROM (n=3) tended to have higher transresistance than those who had a sPTB (n=3), but this observation was not statistically significant (Figure 4.19).

Only AHR 2nd visit data retrieved with probe C was assessed comparing delivery outcomes as there were insufficient index cases (sPTB<3) in the AHR 1st visit and SYMP cohorts to perform statistical analyses. Transresistance values measured from AHR women at 26-28 weeks were significantly higher at the lowest frequency end ($p<0.05$) in those who went on to deliver at term (n=7) compared to those who had a sPTB (n=3), (Figure 4.19). Both in A probe and C probe data,

the gradient in transresistance tended to be steeper for women who delivered prematurely compared to those who had a term delivery. This difference between delivery outcomes was statistically significant for probe A ($p<0.003$; Table 4.16).

Table 4.16. The relationship between AHR 2nd visit transresistance and frequency is displayed as a linear equation per each delivery outcome, and the gradients (in bold) in ratios.

Probe	sPTB	Term	Ratio sPTB/ Term	*p*-value
A	$y = \mathbf{1.79E^{-10}}\,x - 6.96E^{-9}$	$y = \mathbf{1.34E^{-10}}\,x + 1.51E^{-8}$	$\frac{1.79^{-10}}{1.34^{-10}} = 1.33$	0.003
C	$y = \mathbf{9.75E^{-11}}\,x - 1.95E^{-8}$	$y = \mathbf{8.93E^{-11}}\,x + 6.6E^{-9}$	$\frac{9.57^{-11}}{8.93^{-11}} = 1.09$	0.54

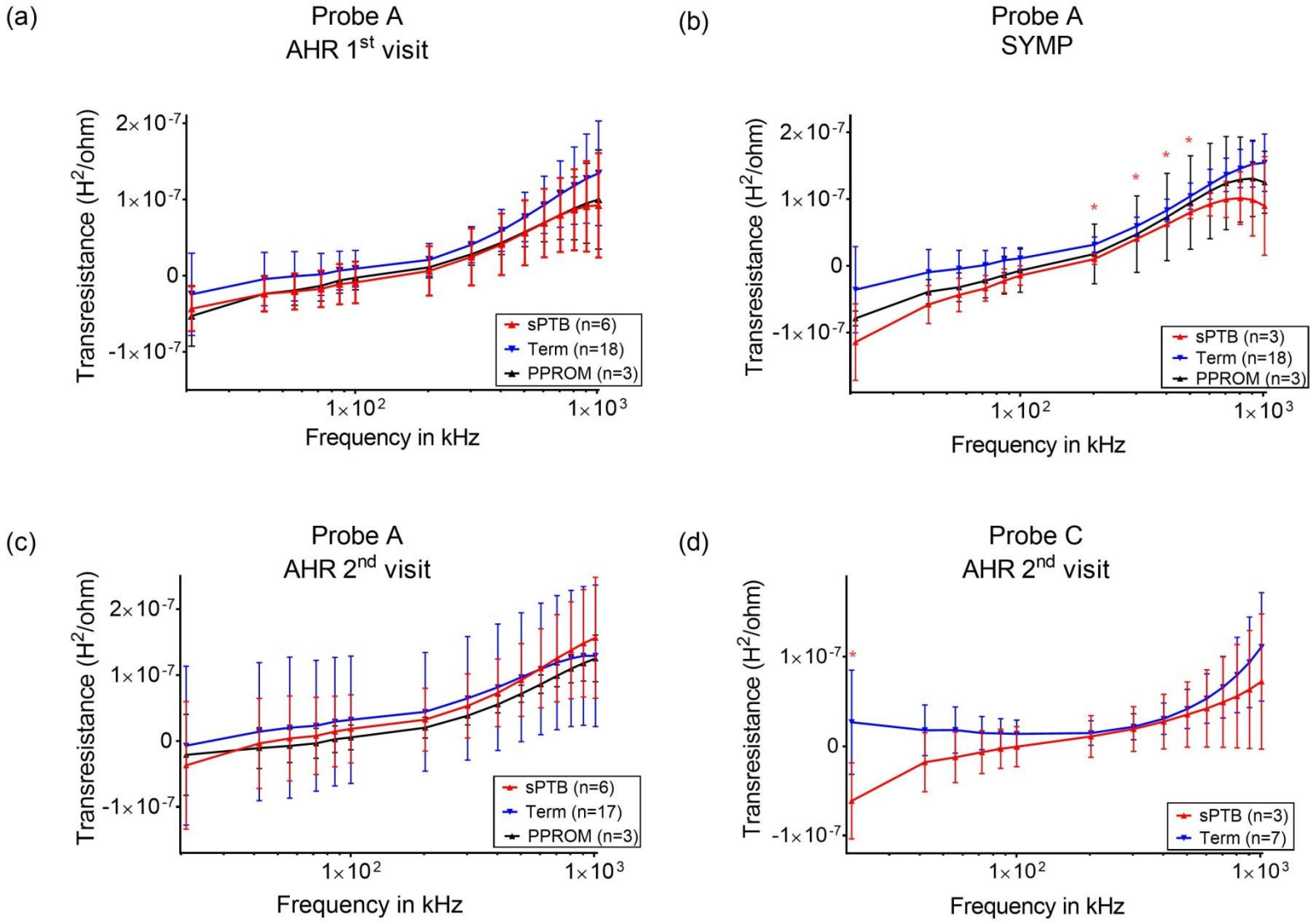

Figure 4.19. Probe A mean transresistance data is displayed per delivery outcome (red: sPTB, blue: term, black: PPROM) for **(a)** AHR patients at 1st visit, **(b)** SYMP patients and **(c)** AHR women at their 2nd visit . Probe C mean transresistance data is also displayed for **(d)** AHR women at their 2nd visit. *X-axis is in logarithmic scale. Error bars represent standard deviations from the mean. Red asterisks mark significant differences between term and sPTB ($p<0.05$). AHR: asymptomatic high risk, PPROM: prelabour premature rupture of membranes, sPTB: spontaneous preterm birth, SYMP: symptomatic*

4.4.9. *In vivo* MIS: cervical transresistance based on time to delivery

The relationship between cervical transresistance and time interval to delivery in the AHR and SYMP cohorts was subsequently assessed using Pearson's correlation. No statistically significant linear relationship was noted between the two variables. As suggested by the low coefficient of determination (R^2), changes in transresistance measurements did not seem to be accounted by time to delivery (Appendix E).

4.4.10. Predictive value of MIS for sPTB: selecting the best frequency for each cohort with probe A

The predictive capacity of MIS for sPTB was determined through the construction of receiver operating characteristic curves (AuROC) based on the transresistance measurements taken from probe A. The AuROC was calculated at 15 different pre-established frequencies (21 kHz-1013 kHz) for measurements taken from AHR women at their 1st and 2nd study visits as well as from SYMP participants during their single appointment. Each AuROC ± 95% CI was then compared to the null hypothesis of an AuROC of 0.5. Small *p*-values (<0.05) were regarded as evidence that MIS could distinguish between women who had a sPTB from those who went on to have a term delivery. PPROM cases were excluded as it still remains unclear whether they respond to the same pathophysiology as sPTB (section 1.2). Further analysis of MIS performance against current predictive tools was carried out in section 4.4.6-4.4.7.

For AHR women scanned between 20-22 weeks (AHR 1st visit, sPTB=6, term=18), transresistance measured at 42 kHz yielded the highest AuROC with a value of 0.73 (95% CI: 0.51-0.89), and was found to reject the null hypothesis with a *p*-value of 0.03 (Figure 4.20a). On the contrary, AuROCs at the remaining frequencies were non-statistically significant, with values ranging from 0.62 at 202 kHz to 0.71 at 72 kHz (Table 4.17).

Table 4.17. Predictive capacity of MIS for sPTB in AHR women scanned between 20-22 weeks (n=24)

Frequency (kHz)	AuROC	95% Confidence Interval	*p*-value
21	0.67	0.45-0.85	0.20
42	0.73	0.51-0.89	0.03
56	0.70	0.48-0.87	0.09
72	0.71	0.49-0.88	0.06
86	0.67	0.45-0.84	0.22
100	0.69	0.47-0.86	0.15
202	0.62	0.40-0.80	0.44
302	0.62	0.40-0.80	0.46
402	0.62	0.40-0.80	0.45
502	0.64	0.42-0.82	0.36
604	0.68	0.46-0.85	0.27
704	0.67	0.45-0.84	0.21
804	0.70	0.48-0.87	0.08
904	0.70	0.48-0.87	0.74
1013	0.67	0.45-0.85	0.15

AuROC: area under the receiver operating characteristic curve

At the follow-up appointment (AHR 2nd visit), transresistance values from AHR women failed to produce any AuROC curves with significant *p*-values (Table 4.18). The general performance of MIS to discriminate between women with a sPTB (n=6) and a term delivery (n=17) was relatively poor compared to the first visit. However, and consistent with what was reported for AHR 1st visit, the highest AuROCs were produced at the lower end of the frequency range namely at 21 and 42 kHz with values of 0.64 (95% CI: 0.41-0.83) and 0.60 (95% CI: 0.38-0.80) respectively (Figure 4.20b). On the other hand, the lowest performance was recorded at mid- and higher frequencies with AuROCs ranging from 0.50 (95% CI: 0.29-0.71) at 202 and 302 kHz to 0.59 (95% CI: 0.37-0.79) at 1013 kHz.

Table 4.18. Predictive capacity of MIS for sPTB in AHR women scanned between 26-28 weeks (n=23).

Frequency (kHz)	AuROC	95% Confidence Interval	*p*-value
21	0.64	0.41-0.83	0.36
42	0.60	0.38-0.80	0.49
56	0.58	0.36-0.78	0.58
72	0.58	0.36-0.78	0.59
86	0.53	0.31-0.74	0.84
100	0.51	0.29-0.71	0.97
202	0.50	0.29-0.71	1.00
302	0.50	0.29-0.71	1.00
402	0.51	0.30-0.73	0.92
502	0.54	0.33-0.75	0.76
604	0.54	0.33-0.75	0.76
704	0.56	0.34-0.76	0.68
804	0.56	0.33-0.76	0.71
904	0.57	0.35-0.77	0.64
1013	0.59	0.37-0.79	0.52

AuROC: area under the receiver operating characteristic curve

For SYMP women (term=18, sPTB=3), MIS transresistance values gave significant AuROCs at all frequencies with the exception of 1013 kHz (Table 4.19). The highest AuROC was recorded at 302 kHz with a value of 1.00 (95% CI: 0.84-1.00). But AuROCs were equally significant and high from 42 to 402 kHz ranging from 0.89 to 0.96. The lowest AuROCs, on the other hand, were identified at both extremes of the frequency range namely at 21 and 1013 kHz.

Table 4.19. Predictive capacity of MIS for sPTB in SYMP women (n=21).

Frequency (kHz)	AuROC	95% Confidence Interval	*p*-value
21	0.82	0.59-0.95	0.03
42	0.91	0.70-0.99	<0.01
56	0.89	0.68- 0.98	<0.01
72	0.91	0.70-0.99	<0.01
86	0.91	0.70-0.99	<0.01
100	0.91	0.70-0.99	<0.01
202	0.96	0.78-1.00	<0.01
302	1.00	0.84-1.00	<0.01
402	0.91	0.70-0.99	<0.01
502	0.85	0.63-0.97	<0.01
604	0.87	0.65-0.98	<0.01
704	0.87	0.65-0.98	<0.01
804	0.89	0.68-0.98	<0.01
904	0.83	0.61-0.96	<0.01
1013	0.80	0.57-0.94	0.10

AuROC: area under the receiver operating characteristic curve

Overall, in AHR women scanned between 20-22 weeks MIS transresistance measurements taken at 42 kHz seemed to have better predictive value than at any other frequency. The measurements recorded at their follow-up between 26-28 weeks of gestation failed to produce significant AuROCs, with the largest value identified at 21 kHz. Finally, for symptomatic participants, the greatest predictive capacity was observed for MIS measurements at 302 kHz (Figure 4.20c). These are the frequencies which were considered for further comparison with fFN and CL in sections 4.4.11-4.4.12.

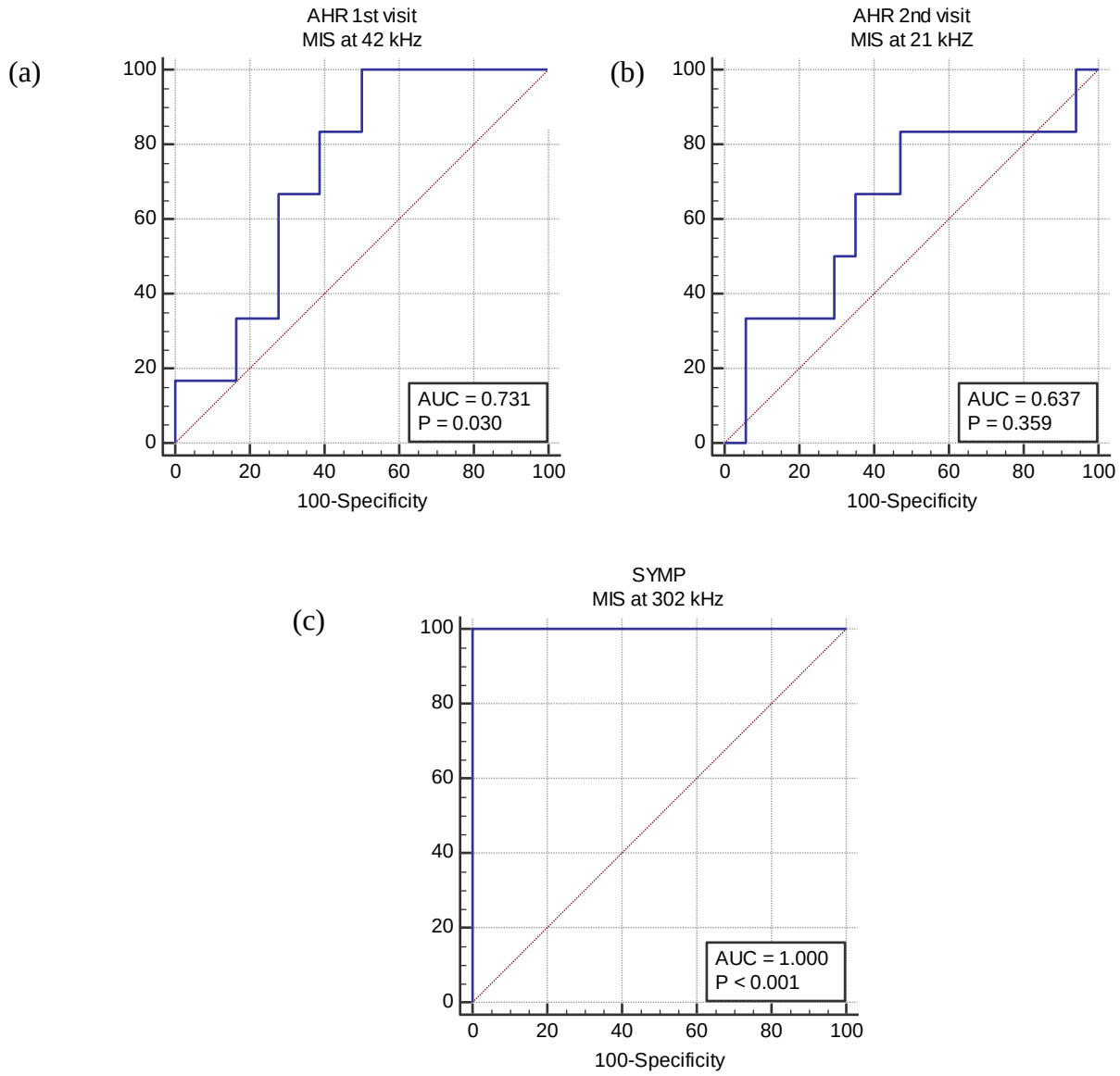

Figure 4.20. AuROC analysis of MIS at 42 kHz, 21 kHz and 302 kHz for prediction of sPTB in **(a)** AHR women at their 1st and **(b)** 2nd visits, and **(c)** SYMP women at their only visit respectively; *p*-values correspond to comparison with the null hypothesis of an AuROC of 0.5. *AuROC: area under the receiver operating characteristic curve*

4.4.11. **Predictive value of MIS for sPTB in the AHR cohorts**

After assessing the frequency at which MIS produced the highest AuROC for predicting sPTB in each cohort, the test performance of MIS was further assessed by calculating its sensitivity, specificity, PPV, NPV and positive and negative likelihood ratio (+/-LR) with its corresponding 95% CI (Table 4.20). Based on logistic regression, AuROC analysis was subsequently performed to compare MIS to current predictive tools such as fFN and CL either as a stand-alone technique or combined with other tests.

For AHR women scanned at their first visit, MIS at 42 kHz alone was better at predicting sPTB than CL and fFN (Table 4.20). MIS tended to have better sensitivity and NPV than CL and higher

specificity and PPV than fFN. These differences in predictive capacity, however, were not statically significant (Table 4.21).

CL tended to have a better performance than fFN with an AuROC of 0.65 (95% CI: 0.43-0.83) compared to 0.52 (95% CI: 0.31-0.73) but these differences were not statistically significant (p=0.46, Table 4.21). Furthermore, combining fFN with CL failed to improve the predictive performance of CL alone, and produced a model with lower sensitivity and NPV than that obtained for CL alone (Figure 4.21). Similarly, when fFN and MIS were combined, the resulting AuROC was lower than that seen for MIS alone which suggested no improvement in MIS predictive capacity when fFN was added. However, when MIS transresistance was combined with CL, the performance of these tests tended to improve and produce a model with a greater AuROC at 0.76 (95% CI: 0.54-0.91), and higher specificity, PPV and +LR than MIS alone (Figure 4.21).

Finally, when all three tests were combined, AuROC was lower than MIS alone, even if there was a slight improvement in specificity and PPV. Compared to the null-hypothesis, this AuROC value was noted to be statistically significant (p=0.04) but not when it was assessed against any of the individual tests (Table 4.21).

Table 4.20. Predictive performance of MIS, CL and fFN for sPTB in AHR women scanned between 20-22 weeks; *p*-values correspond to comparison with the null hypothesis of an AuROC of 0.5.

Technique	AuROC (95% CI)	Sens (%) (95% CI)	Spec (%) (95% CI)	PPV (%) (95% CI)	NPV (%) (95% CI)	+LR (95% CI)	-LR (95% CI)	*p*-value
MIS at 42 kHz	0.73 (0.51-0.89)	100.0 (54.1-100.0)	50.0 (26.0-74.0)	40.0 (29.58-51.41)	100.0	2.0 (1.3-3.2)	0.0	0.03*
CL	0.65 (0.43-0.83)	66.7 (22.3-95.7)	66.7 (41.0-86.70)	40.0 (21.93-61.27)	85.71 (64.88-95.15)	2.0 (0.8-4.7)	0.5 (0.2-2.3)	0.25
fFN	0.52 (0.31-0.73)	100.0 (54.1-100.0)	16.7 (3.6-41.4)	28.57 (24.55-32.97)	100.0	1.2 (1.0-1.5)	0.0	0.88
CL+ fFN	0.63 (0.41-0.82)	50.0 (18.0-88.2)	83.3 (58.6-96.4)	50.0 (21.3-78.7)	83.33 (68.63-91.95)	3.0 (0.8-11.1)	0.6 (0.3-1.4)	0.37
MIS + CL	0.76 (0.54-0.91)	100.0 (54.1-100.0)	66.67 (41.0-86.)	50.0 (34.22-65.78)	100.0	3.0 (1.6-5.8)	0.0	<0.01*
MIS + fFN	0.69 (0.47-0.86)	100.0 (54.1-100.0)	50.0 (26.0-74.0)	40.0 (29.58-51.41)	100.0	2.0 (1.3-3.2)	0.0	0.08
MIS + CL + fFN	0.72 (0.50-0.88)	100.0 (54.1-100.0)	55.56 (30.0-78.5)	42.86 (30.91-55.70)	100.0	2.25 (1.3-3.8)	0.0	0.04*

*+LR: positive likelihood ratio, -LR: negative likelihood ratio, AuROC: area under the receiver operating characteristic curve, CL: cervical length, fFN: fetal fibronectin, MIS: magnetic induction spectroscopy, NPV: negative predictive value, PPV: positive predictive value, sens: sensitivity, spec: specificity, *significant p-value<0.05*

Table 4.21. Comparison of AuROCs of predictive tools for sPTB in AHR women scanned between 20-22 weeks.

AuROC curve comparison	*p*-value
MIS vs CL	0.63
MIS vs fFN	0.17
MIS vs fFN + CL	0.57
CL vs fFN	0.46

AuROC: area under the receiver operating characteristic curve, CL: cervical length, fFN: fetal fibronectin MIS: magnetic impedance spectroscopy

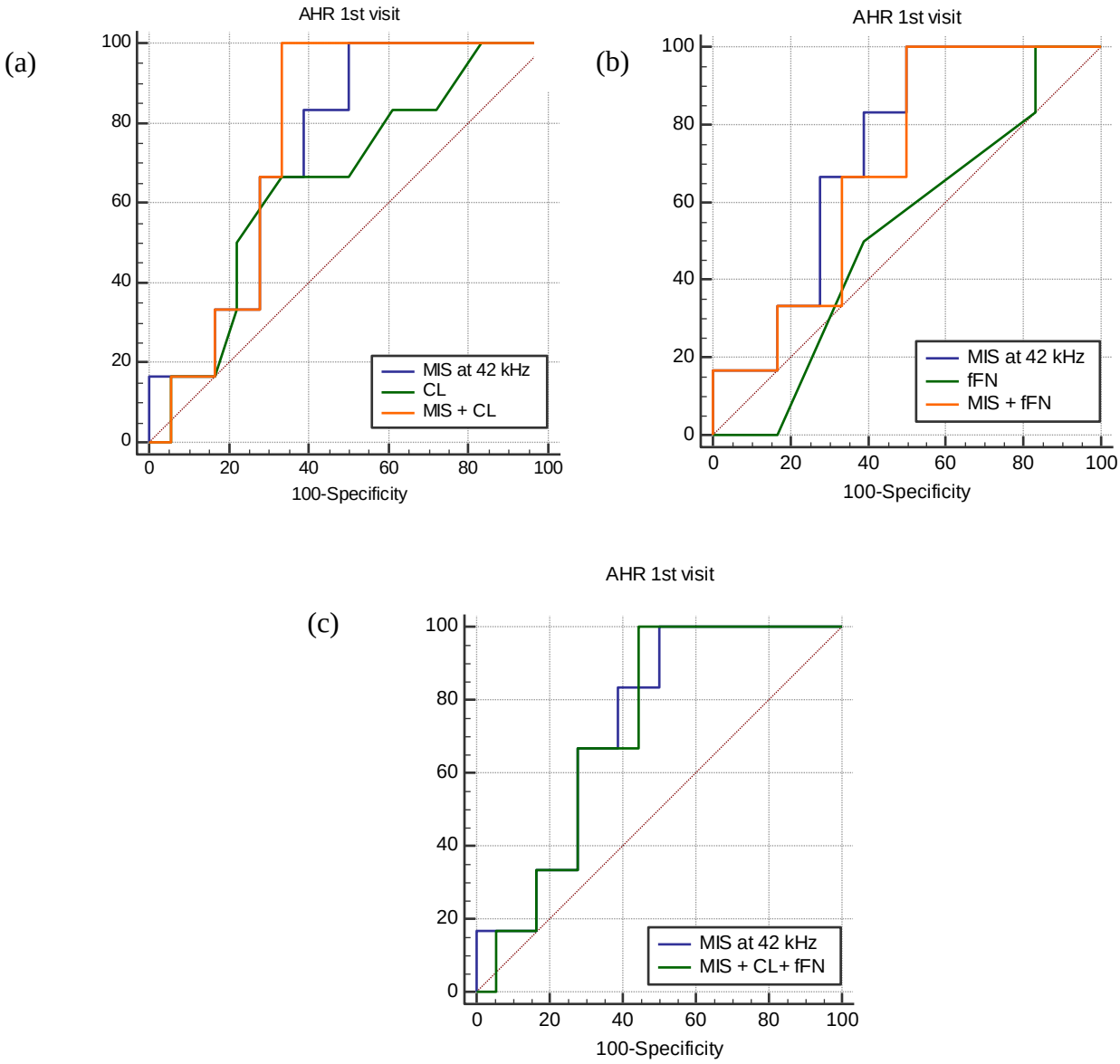

Figure 4.21. AuROC analysis of MIS at 42 kHz for prediction of sPTB in AHR women at their 1st visit compared and combined with **(a)** CL, **(b)** fFN, and **(c)** CL and fFN. *AuROC: area under the receiver operating characteristic curve, CL: cervical length, fFN: fetal fibronectin, MIS: magnetic induction spectroscopy*

When AHR patients were followed up at 26-28 weeks, MIS at 21 kHz did to produce a significant AuROC either alone or combined with any of the routine tests ($p>0.05$, Table 4.22). Regarding CL and fFN, their AuROCs were quite similar, even though fFN displayed a much higher NPV and +LR as expected (section 1.3.2).

When CL and fFN were added together, their overall performance was almost similar to MIS with just slightly higher specificity, PPV and NPV. However, when MIS was combined with fFN and CL either individually or collectively, the predictive capacity of MIS did not improve and actually saw a reduction from its original AuROC of 0.64 (95% CI: 0.41-0.82) to a resulting AuROC of 0.61 (95% CI: 0.38-0.80; Figure 4.22). None of these tests was statistically significantly different from one another (Table 4.23).

Table 4.22. Predictive performance of MIS, CL and fFN for sPTB in AHR women scanned between 26-28 weeks; *p*-values correspond to comparison with the null hypothesis of an AuROC of 0.5.

Technique	AuROC (95% CI)	Sens (%) (95% CI)	Spec (%) (95% CI)	PPV (%) (95% CI)	NPV (%) (95% CI)	+LR (95% CI)	-LR (95% CI)	*p*-value
MIS at 21 kHz	0.64 (0.41-0.82)	83.33 (35.9-99.6)	52.94 (27.8-77.0)	38.46 (25.19-53.70)	90.0 (58.73-98.27)	1.77 (1- 3.3)	0.31 (0.05-2.0)	0.36
CL	0.55 (0.33-0.76)	66.7 (22.3-95.7)	58.8 (32.9-81.6)	36.36 (20.4-56.03)	83.3 (25.19-53.70)	1.62 (0.7-3.6)	0.57 (0.2-1.9)	0.72
fFN	0.56 (0.37-0.79)	33.3 (4.3-77.7)	94.1 (71.3-99.9)	66.67 (17.95-94.81)	80.0 (67.17-87.70)	5.67 (0.6-51.8)	0.71 (0.4-1.3)	0.88
CL + fFN	0.64 (0.42-0.83)	83.33 (35.9-99.6)	58.52 (32.9-81.6)	41.67 (26.74-58.30)	90.91 (61.53-98.43)	2.02 (1.0-4.0)	0.28 (0.05-1.80)	0.32
MIS + CL	0.63 (0.40-0.82)	83.3 (35.9-99.6)	47.06 (23.0-72.2)	35.71 (23.84-49.64)	88.89 (55.49-98.09)	1.57 (0.9-2.8)	0.35 (0.06-2.5)	0.40
MIS + fFN	0.61 (0.38-0.80)	83.3 (35.9-99.6)	47.06 (23.0-72.2)	35.71 (23.84-49.64)	88.89 (55.49-98.09)	1.57 (0.9-2.8)	0.71 (0.2-2.4)	0.48
MIS + CL + fFN	0.61 (0.38-0.80)	83.3 (35.9-99.6)	47.06 (23.0-72.2)	35.71 (23.84-49.64)	88.89 (55.49-98.09)	1.57 (0.9-2.8)	0.35 (0.06-2.5)	0.47

+LR: positive likelihood ratio, -LR: negative likelihood ratio, AuROC: area under the receiver operating characteristic curve, CL cervical length, fFN: fetal fibronectin, MIS: magnetic induction spectroscopy; NPV: negative predictive value, PPV: positive predictive value, sens: sensitivity, spec: specificity

Table 4.23. Comparison of AuROCs of predictive tools for sPTB in AHR women between 26-28 weeks.

AuROC curve comparison	*p*-value
MIS vs CL	0.73
MIS vs fFN	0.80
MIS vs fFN + CL	0.98
CL vs fFN	0.90

AuROC: area under the receiver operating characteristic curve, CL: cervical length, fFN: fetal fibronectin, MIS: magnetic impedance spectroscopy

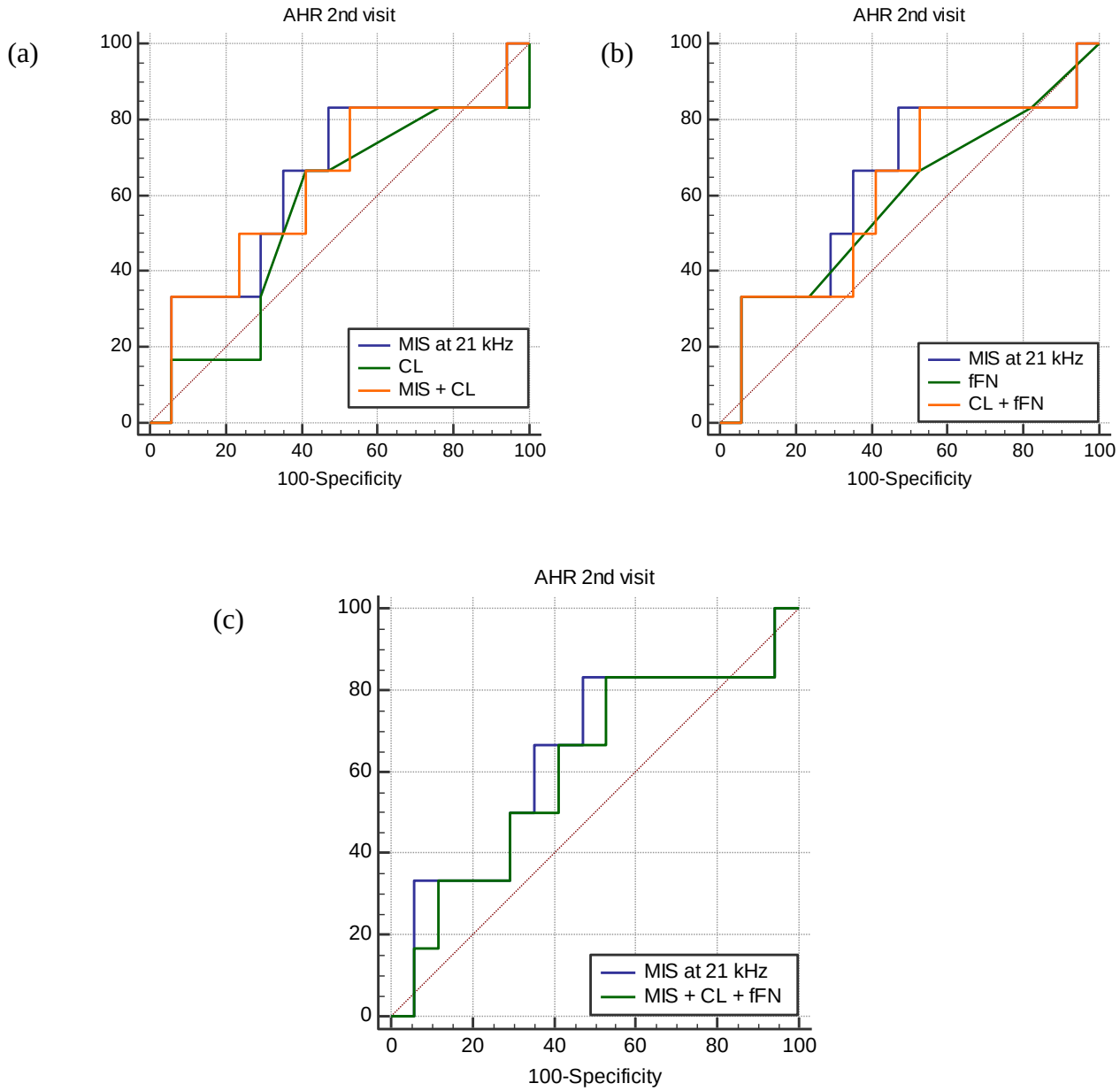

Figure 4.22. AuROC analysis of MIS at 42 kHz for prediction of sPTB in AHR women at their 2nd visit compared and combined with **(a)** CL, **(b)** fFN, and **(c)** CL and fFN. *AuROC: area under the receiver operating characteristic curve, CL: cervical length, fFN: fetal fibronectin, MIS: magnetic induction spectroscopy*

4.4.12. **Predictive value of MIS for sPTB in the SYMP cohort**

In the symptomatic cohort, MIS transresistance measured at 302 kHz produced the model with the highest predictive performance for sPTB with a sensitivity and specificity of 100% (Table 4.24). The AuROC for MIS with a value of 1.00 (95% CI: 0.84-1.00) was significantly different not only from the null hypothesis of non-discriminating power (AUR=0.5) but also from that generated by CL (0.51, 95% CI: 0.29-0.73) with a *p*-value lower than 0.001, (Table 4.25; Figure 4.23).

Contrary to what was reported for AHR women in their first visit, CL in the SYMP cohort tended to have lower sensitivity, specificity, NPV and PPV than fFN, but these differences were not

considered statistically significant (Table 4.24). When CL was combined with fFN, the resulting AuROC tended to increase from the 0.51 and 0.58 seen for CL and fFN respectively to 0.59 along with a modest improvement in specificity, PPV, NPV and +LR (Table 4.24). On the other hand, combining MIS with either CL or fFN or both did not add any benefit to MIS alone which had accurately discriminated all women who delivered at term (n=18) from those who had a sPTB (n=3).

Table 4.24. Predictive performance of MIS, CL and fFN for sPTB in SYMP women; *p*-values correspond to comparison with the null hypothesis of an AuROC of 0.5

Technique	**AuROC (95% CI)**	**Sens (%) (95% CI)**	**Spec (%) (95% CI)**	**PPV (%) (95% CI)**	**NPV (%) (95% CI)**	**+LR (95% CI)**	**-LR (95% CI)**	***p*-value**
MIS at 302 kHz	1.00 (0.84-1.00)	100.0 (29.2-100.2)	100.0 (81.5-100.0)	100.0	100.0	-	0.0	<0.001*
CL	0.51 (0.29-0.73)	0.0 (0.0-70.76)	55.56 (30.8-78.5)	0.00	76.92 (68.80-83.44)	1.5 (0.6-3.9)	0.6 (0.1-3.1)	0.95
fFN	0.58 (0.35-0.79)	66.67 (9.4-99.2)	83.3 (58.6-96.4)	40.00 (15.29-71.12)	93.75 (74.92-98.69)	4.0 (1.1-14.8)	0.4 (0.08-2.00)	0.78
CL + fFN	0.59 (0.36-0.80)	66.67 (9.4-99.2)	88.90 (65.3-98.6)	50.0 (17.70-82.23)	94.12 (76.20-98.76)	6.0 (1.3-27.8)	0.38 (0.08-1.00)	0.76
MIS + CL	1.00 (0.84-1.00)	100.0 (29.2-100.0)	100.0 (81.5-100)	100.0	100.0	-	0.0	<0.001*
MIS + fFN	1.00 (0.84-1.00)	100.0 (29.2-100.0)	100.0 (81.5-100)	100.0	100.0	-	0.0	<0.001*
MIS + CL + fFN	1.00 (0.84-1.00)	100.0 (29.2-100.0)	100.0 (81.5-100)	100.0	100.0	-	0.0	<0.001*

*+LR: positive likelihood ratio, -LR: negative likelihood ratio, AuROC: area under the receiver operating characteristic curve, CL cervical length, fFN: fetal fibronectin, MIS: magnetic induction spectroscopy; NPV: negative predictive value, PPV: positive predictive value, sens: sensitivity, spec: specificity, *significant p-value<0.05*

Table 4.25. Comparison of AuROCs of predictive tools for sPTB in SYMP women

AuROC curve comparison	*p*-value
MIS vs CL	<0.001*
MIS vs fFN	0.16
MIS vs fFN + CL	0.17
CL vs fFN	0.83

*AuROC: area under the receiver operating characteristic curve, CL: cervical length, fFN: fetal fibronectin, MIS: magnetic impedance spectroscopy,*significant p-value<0.05*

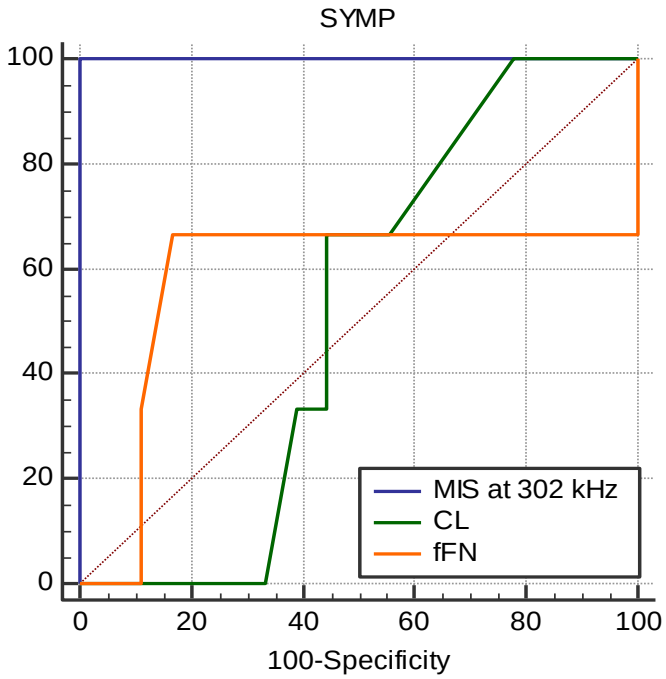

Figure 4.23. AuROC analysis of MIS at 302 kHz, CL and fFN for prediction of sPTB in SYMP women.
AuROC: area under the receiver operating characteristic curve, CL: cervical length, fFN: fetal fibronectin MIS: magnetic induction spectroscopy

4.5. Discussion and interpretation

4.5.1. **Main findings**

This study has shown that MIS is capable of accurately and reliably measuring the electrical properties of the human cervix and may hold potential for early discrimination between women who deliver prematurely from those who have a term delivery.

The *in vitro* repeatability data demonstrated good within-observer repeatability especially at low and low-mid frequencies (86-302 kHz). The higher concordance in cervical repeats was noted between first and second measurements (C1-C2) which displayed the lowest measurement bias and narrowest limits of agreement. The poorest agreement, on the other hand, was seen between the first and third measurements (C1-C3) which had lower ICCs and wider confidence intervals. This larger bias noted between C1-C3 measurements was thought to be partly due to the thermal shock experienced by the MIS probe when it came in contact with the cervical samples. Despite being left to thaw for one hour at room temperature, it is likely that the cervical samples may have still been cold at the time of MIS scanning given their thickness. As the difference in temperature between the probe and the samples reduced over successive measurements, the thermal influence is likely to have played a smaller role in the variability of the measurements taken. This assumption, along with that of thermal drift, would help explain why cervical measurements taken closer in time, namely C1-C2 and C2-C3, displayed better agreement than those taken further apart such as C1-C3.

Similar to the *in vitro* experiments, the *in vivo* repeatability study also showed good intra-observer reliability in the low and low-mid frequency range (72-303 kHz). All combinations of cervical measurements yielded acceptable reliability but the highest concordance was seen between C2–C3 and the lowest between C1-C3. Compared to the *in vitro* study, *in vivo* repeatability was higher. As ICCs are particularly susceptible to small sample sizes (Mehta et al., 2018), the improved agreement seen between *in vivo* cervical measurements may be explained by the larger number of participants and the lower within-subject variation as all datasets were obtained from the same cohort of women. For the *in vitro* study, on the contrary, datasets were retrieved from a much smaller and heterogeneous pool of samples with different post-excision measurement times which may all have contributed to the greater variation seen (Haemmerich et al., 2009).

The increased reliability seen between 72 and 302 kHz for both *in vitro* and *in vivo* MIS cervical measurements seems to fit in with previous EIS pilot studies in which the highest concordance between cervical repeats was identified between 9.7 and 312 kHz (Anumba et al., 2011, Anumba et al., 2018). On the other hand, the decreased agreement seen at both extremes of the frequency range,

that is, 21 and 1013 kHz, could be due to increased susceptibility to noise as previously described for an earlier EIS transvaginal probe (Gandhi et al., 2006a).

After establishing acceptable *in vitro* repeatability for MIS, the cervical samples were further probed to ascertain any difference in transresistance between the epithelial (ectocervix) and stromal surfaces. Regardless of age, menopausal status or indication for surgery, transresistance of the stromal surface was significantly higher than that of the ectocervix at most mid- and high frequencies ($p<0.05$). Stromal tissue has been found to be more conductive than the epithelium before. For example, previous studies on the human prostate by Halter et al. (2011) also showed that stromal-dominant regions seemed to exhibit lower impedance and larger conductivity than the more densely cellular and glandular tissues. They hypothesised that the increased number of cell membranes in the epithelial areas would provide greater permittivity and therefore greater capacitance which would account for the differences seen in impedance (Halter et al., 2009a, Halter et al., 2011).

Following the *in vitro* studies, MIS was tested on both asymptomatic women deemed at high risk of sPTB (AHR) and symptomatic women presenting in threatened preterm labour (SYMP) during their second and third trimester. Cervical transresistance was measured at multiple frequencies in an attempt to assess whether it would provide enough contrast to differentiate between those who would have a spontaneous premature delivery from those who would go on to deliver at term or experience premature rupture of membranes without going into labour (PPROM).

When all pregnant women were considered together regardless of their previous risk factors or symptoms, cervical transresistance was consistently higher in women who had a term delivery compared to their sPTB counterparts especially at low and mid-low frequencies (<303 kHz). This difference was statistically significant ($p<0.05$) when AHR 1st visit and gestationally-matched SYMP data from probe A was combined.

When the data was further analysed for each cohort or probe independently, a similar trend in transresistance per delivery outcome was identified. However, these differences were non-statistically significant. It is worth mentioning, however, that the initial sample calculation for our MIS study had not been powered for subgroup analysis, and this was only performed when the introduction of a new probe half-way through the study rendered some of the data non-comparable. Therefore, failure to find statistically significant differences for delivery endpoint in these groups may have been due to insufficient sample sizes. This necessitates a larger study using an optimised probe configuration that would be robust enough to ensure that different probes gave highly identical transresistance measurements.

When linear regression was subsequently applied to compare trends in probe A and probe C, the ratio of gradients between women who had a sPTB or a term delivery was not statistically different and had a similar trend. These observations support the preliminary hypothesis that cervical transresistance may hold enough discriminating power to differentiate women who have a term delivery from those with a sPTB regardless of the probe being used (Wang et al., 2017).

For women who experienced PPROM, cervical transresistance appeared to be relatively lower than for those who had a term delivery similarly to what was reported for sPTB. But when all women who had a premature delivery were considered together, no clear difference was seen between those who went into spontaneous labour from those who were induced following PPROM. An insufficient number of index cases did not allow a detailed comparison of cervical transresistance in women with PPROM based on cohort or probe.

Overall, women who delivered prematurely appeared to have lower mid-trimester cervical transresistance than those who had a term delivery when scanned with the optimised MIS probe. At first glance, this finding may seem to contradict previous EIS studies which suggested mid-trimester cervical conductivity was higher in women destined to deliver prematurely (Anumba et al., 2011, Anumba et al., 2018). However, unlike EIS which has limited depth penetration, MIS is capable of assessing the electrical properties of not only the ectocervix but also of a considerable amount of the underlying ECM. As a result, MIS and EIS findings are not expected to necessarily match. Interestingly, previous attempts to measure gestation-dependent electrical changes beyond the ectocervix with an alternative tetrapolar EIS prototype which had higher penetrance found that pregnant women in their last trimester had significantly lower conductivity (that is, higher impedance) than at earlier gestations (Gandhi et al., 2006a). The authors proposed that the reduction seen in cervical conductivity could be due to an increased stromal cellular infiltration and changes in the density and quantity of soluble collagen in preparation for cervical ripening. Based on this assumption and on previous studies which have shown a significant leukocyte infiltrate in the cervix during cervical remodelling, we hypothesised that the lower MIS transresistance (which equates to lower conductivity and higher impedance, section 4.3.4) seen in women who delivered prematurely could be equally attributed to collagen rearrangement and an increase in the cellular density of the ECM prior to sPTB (Timmons et al., 2009).

In order to assess whether these variations in cervical transresistance could provide enough contrast to accurately differentiate between women who had a sPTB from those with a term delivery in our study, AuROC curves were constructed at multiple frequencies for each cohort. For AHR women scanned between 20-22 weeks, transresistance measured at 42 kHz was found to provide the most discriminating power with an AuROC of 0.73 ($p=0.03$). These findings are in

keeping with previous EIS studies which reported that the optimal test performance for prediction of sPTB was at 39 kHz (Anumba et al., 2011).

For AHR women scanned between 26-28 weeks, none of the AuROC was statistically significantly. Similarly to what has been reported for CL, the clinical efficacy of MIS for prediction of sPTB seemed to reduce with increasing gestational age (Jafari-Dehkordi et al., 2015). We hypothesised that the loss of discriminatory power in our model as pregnancy progresses could be due to (1) the cases of extreme PTB registered before the follow-up visit (n=3) which reduced the skewedness of the dataset by removing the participants with the most dramatic cervical changes and (2) the natural shortening of the cervix which is expected to occur with advancing gestational age and which makes cervical transresistance changes more subtle between control and index cases.

The utility of MIS for prediction of sPTB was subsequently compared to that of TVU CL and fFN. Of the 24 AHR women scanned at 20-22 weeks, the six (25%) who had sPTB were better predicted by cervical MIS than TVU CL and fFN alone (Table 4.20). MIS and TVU CL was the only combination of tests which seemed to improve prediction of sPTB (AuROC 0.76, 95% CI: 0.54-0.91) even though the PPV was still modest and similar to that of CL + fFN combined (50%, 95% CI: 34.22-65.78; Table 4.20).

For AHR women scanned at 26- 28 weeks, the clinical efficacy of MIS was less certain with an AuROC of 0.64 (95% CI: 0.41-0.82), higher than that seen for TVU CL and fFN alone and similar to the one achieved for fFN and CL combined (Table 4.22). Finally, for the SYMP cohort (n=21), even though modelling was limited by the reduced number of index cases (sPTB, n=3), MIS was capable of better identifying women who had a sPTB (n=3) with a sensitivity and specificity of 100%, significantly higher than that seen for CL alone ($p<0.001$; Table 4.25). Overall, MIS performed clinically better than CL and fFN for predicting sPTB in AHR and SYMP women. However, given the small sample size available, results should be interpreted with caution and validated with larger follow-on studies.

4.5.2. **Strengths**

For the present study, we have designed, constructed and tested an optimised magnetic induction spectrometer for measuring the electrical transresistance spectra of the human cervix in the frequency range of 20 kHz to 1 MHz.

MIS had only been previously tested once before as proof of concept on a small number of pregnant women at term (n=10) using an earlier prototype developed by our engineering team at the University of Sheffield (Wang et al., 2017). Expanding upon these results, we hypothesised that the

electrical properties of the cervix measured by MIS in pregnancy would provide enough contrast to predict delivery outcomes. To be fit for purpose, the design of the MIS probe had to be significantly modified. Extensive work was carried out by the University of Sheffield clinical engineering team to increase signal sensitivity and reduce thermal drift and potential confounding influence of the vaginal electrical field in the optimised MIS probe. Upgrades included but were not limited to removal of measurement artefacts, addition of magnetic shielding, reduction of power dissipation by better choice of materials and coil assembly, minimisation of the probe diameter and standardisation of the protocol for clinical use in order to improve patient acceptability and measurement repeatability respectively. The introduction of these changes greatly improved the signal-to-noise ratio and the electrical performance of the device compared to its predecessor, and enabled the development of a clinical device which conformed to the harmonised standards expected for any applicable Directive and Clinical Engineering Quality Management System. Future changes to improve calibration across probes may include slight changes to the device geometry and electrical shielding, and the introduction of a sensor to provide auto-feedback to the operator regarding proximity of the probe to the cervix.

The refined MIS probe was shown to produce highly repeatable cervical measurements both *in vitro* and *in vivo* (Tables 4.3 and 4.12), and to be able to discriminate between women who had a sPTB from those who delivered at term in our study with improved accuracy compared to current screening tests. A logical future step, therefore, would be to try to replicate these findings in larger and adequately-powered clinical trials, and assess reproducibility across devices in a multicentre study informed by MHRA. If MIS were to be developed to the point it can identify women at high risk of sPTB, better decisions could be made to prevent or delay sPTB and enable patients to make informed decisions. Women who were deemed to be at high risk of PTB with MIS (as a "rule-in" test) would then be offered more timely care including infection screening, progesterone therapy, or cervical cerclage. MIS assessment may well prove useful for recommending one intervention over another for which there is currently scarce evidence. On the other hand, if MIS could better identify women who are not at true risk of PTB despite their previous obstetric history or symptoms (as a "rule-out" test), monitoring of women at low risk may be de-escalated, and unnecessary therapy such as tocolytics and steroids treatments could be avoided. By prolonging the duration of the pregnancy, MIS-based evaluation could thereby reduce the short and long-term complications associated with sPTB and optimise antenatal provision of care (Suff et al., 2019).

The ECCLIPPx II study also aimed to explore service-user acceptability of the MIS device to inform future device iteration and patients' satisfaction. Previous research prioritisation exercises which involved people affected by PTB and healthcare professionals in the UK and Republic of

Ireland had reported that the top research priority for the public is to identify the most effective treatments and diagnostic tools to predict and prevent PTB (Oliver et al., 2019) The acceptability work, which is beyond the scope of this thesis, is currently being conducted by the research midwifery team at Sheffield NHS Teaching Hospital who have adopted a mixed-method approach based on the previous ECCLIPPx I study which had reported high acceptability for EIS. Twenty participants (10 AHR, 10 SYMP) have been asked to complete validated questionnaires (visual analogue scales, Stait-Trait anxiety inventory, EQ-5D-5L instruments for overall health outcomes) and attend semi-structured qualitative interviews in an attempt to capture and assess participants' expectations, experience of intervention, comfortableness, anxiety and/or embarrassment during procedure capable of informing future device iterations and follow-on studies.

Given the complexity of clinically translating MIS technology from the bench to the bedside, one of the main pillars of the study has been the interdisciplinary work. World authorities in bioimpedance from the University of Sheffield and Cardiff provided regular advisory input into the development of an optimised clinical grade MIS probe for cervical assessment to predict sPTB. Equally important have been the contributions made by members of the general public and maternity service users from the Jessop Wing Preterm Birth PPI group who have provided key feedback at all stages of the study from its design to Ethics approval, recruitment and data dissemination.

4.5.3. **Limitations**

Given the preliminary nature of our study and the limited resources available, MIS was tested only on women considered to be at higher risk of sPTB either because of their previous obstetric history or because of their symptoms at presentation. The low-risk population, which is responsible for more than 50% of sPTB, was purposely not sampled because the lower incidence (and therefore pre-test probability) meant that larger samples would have been needed to reach enough index cases to assess the ability of MIS to predict sPTB. The requirement of a larger target sample could not be met with the allocated time and funding for the study. However, the promising results seen for MIS in our pilot research emphasised the need for future multicentre clinical trials which would allow the testing of MIS on all pregnant women regardless of their baseline risk for sPTB.

Another limitation in our study was the small number of MIS datasets available for adequately powered statistical analysis. Even though the target sample of patients for each arm was achieved (n=45) with enough index cases (PTB, n=9), not all MIS datasets were available for final analysis due to technical challenges with device manufacture which rendered some of the data non-

comparable. However, an exhaustive descriptive analysis of gradients and trends was performed to check for consistency between subgroups. Our findings seem to suggest similar transresistance patterns in all cohorts namely increased cervical transresistance in women who had a term delivery compared to those who delivered prematurely. However, larger studies are required to conclusively show the predictive capacity of MIS.

Based on this pilot study and local statistics (20% PTB), sample size calculation for future studies were conducted using MedCalc® (Belgium, 2015). Assuming that a minimum of 12-15% of AHR women deliver prematurely as reported in the literature (and confirmed by our pilot study with over 25% PTB rate), we hypothesised that 146-178 AHR women (with 19 index cases) would have to be studied to achieve an AuROC of 70% with a power of 80% and significance level of 0.05. Ideally, a larger number of AHR women should be approached in order to compensate for potential drop-outs after the first visit. However, it is worth mentioning that our pilot study had 100% follow-up retention rate and the only three AHR patients who did not attend their second visit failed to do so because they had already delivered.

After adjusting the predicted ratio of negative to positive cases and AuROC to 75%, similar sample size calculations were carried out to determine the target number of SYMP as well as low-risk pregnant women who would be needed in future studies. We concluded that a minimum of 92 SYMP women (80 term and 12 sPTB), and 162 low-risk participants (150 term and 12 sPTB) would have to be studied to accurately assess the clinical efficacy of MIS for sPTB.

Finally, comparisons between *in vivo* and *in vitro* findings in our study should be interpreted with caution as electrical properties are known to significantly differ after a tissue is devascularised (Halter et al., 2009a). For example, previous studies in animal models reported a decrease in liver conductivity of up to 53% after the organ had been removed (Haemmerich et al., 2002). As an explanation for this phenomenon, it was hypothesised that the increased cellular swelling seen in devascularisation would reduce the extracellular fluid volume thus decreasing conductivity (Halter et al., 2009a, Halter et al., 2009b). The main reason for conducting the studies on extirpated cervical tissue was to determine the *ex vivo* repeatability of the MIS measurements under controlled conditions prior to *in vivo* studies.

4.5.4. **Future research**

Mid-trimester cervical measurements using MIS seem to be more predictive for sPTB than current screening tests in singleton pregnancies in our limited dataset. Confirmation of these findings in larger and adequately-powered trials may help determine the suitability of MIS for

clinical use. Prospective studies may also assess the clinical efficacy of MIS for prediction of sPTB in multiple pregnancies, a population with a 12-fold increased risk of PTB for which there is currently no predictive test of value (Murray et al., 2018).

Chapter 5

Metabolomics analysis of cervicovaginal fluid with enzyme-based spectrophotometry for preterm birth prediction

5.1. Introduction and background

The shift from a *Lactobacillus* dominance in the vaginal microbiota to a more diverse and mixed bacterial community has been implicated in the pathophysiology of PTB (Stafford et al., 2017). The altered carbohydrate metabolism exhibited by the overgrowth of anaerobic bacteria is thought to leave distinctive metabolite fingerprints which may be detectable through enzyme-based spectrophotometric analysis of CVF (Amabebe et al., 2016a). This relatively easy-to-perform CVF metabolomics profiling may hold predictive value for PTB in the clinical setting.

5.1.1. **Untargeted and targeted metabolomics techniques for the study of CVF**

Metabolomics, which involves the systematic study of the metabolome, provides a unique insight into the metabolic state of an organism. By better reflecting what has been encoded by the genome and modified by the diet and the environment, metabolic profiling may provide a closer approximation to an individual's overall health at a functional level (Deidda et al., 2015, Beger et al., 2016). Metabolomics approaches can discriminate between normal and pathophysiological states by identifying the specific metabolic pathways altered in the context of disease. Additionally, some techniques can also quantify metabolic products thus better characterising the chemical composition of a sample (Bracewell-Milnes et al., 2017).

There are at least two analytical approaches for metabolomics studies: untargeted and targeted methods (Li et al., 2018). Untargeted metabolomics techniques aim to simultaneously measure as many metabolites as possible in an attempt to discover candidate biomarkers of disease (Gorrochategui et al., 2016). No previous knowledge of specific metabolites within the sample is needed as many of the potential biomarkers arise from previously unknown compounds (Roberts et al., 2012). The large datasets produced by untargeted experiments usually require highly-extensive processing and complex data analysis. Examples of untargeted methods for the prediction of sPTB include RS analysis of CVF (Chapter 2). Targeted methods, on the other hand, focus on a smaller and well-characterised set of metabolites for which biological importance has already been defined. Quantification of these metabolites is performed through the construction of calibration curves using chemical standards, and yields greater sensitivity and specificity than untargeted methods. Furthermore, results from targeted techniques are relatively easier to interpret than those from untargeted methods (Menni et al., 2017). The enzyme-based spectrophotometry analysis of CVF for the prediction of PTB proposed in this chapter constitutes an example of a targeted metabolomics technique (Amabebe and Anumba, 2017).

5.1.2. **Fundamentals of enzyme-based spectrophotometry**

Spectrophotometry is an analytical technique which is capable of quantifying the concentration of analytes in a sample based on their ability to transmit or absorb light at a certain wavelength. In the spectrophotometer, a lamp provides the source of light. The beam strikes the diffraction grating which behaves like a prism separating the light into its component wavelengths. As the grating rotates, only light of a specific wavelength passes through the slit to interact with the sample. The photodetector then measures transmittance and absorbance of the sample. The signal is subsequently amplified, recorded and displayed as digital data in a recorder or computer (Figure 5.1; Mavrodineanu and Hughes, 1968).

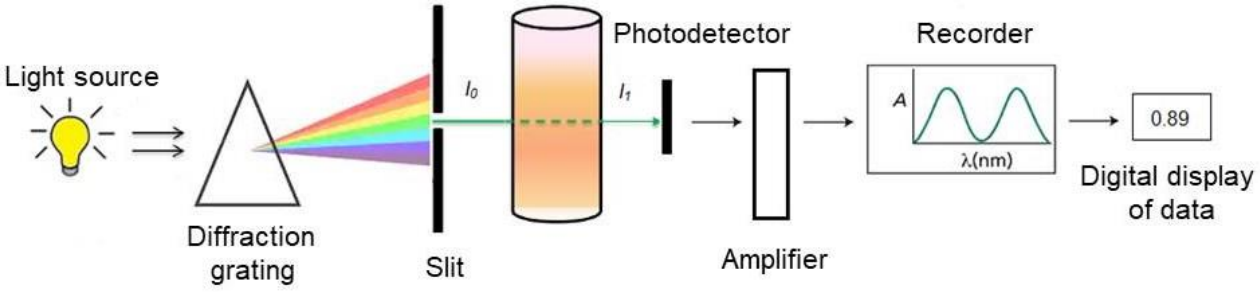

Figure 5.1. Schematic of the essential components of a spectrophotometer
I_0 and I_1: intensity of the light beam before and after passing through the sample, respectively

Concentrations of metabolites in a sample can thus be measured using the Beer-Lambert law which states that "the absorbance (A) of a given sample is directly proportional to its concentration(c)", as illustrated by the following equation:

$$A = \varepsilon \, x \, b \, x \, c,$$

where ε refers to the wavelength-dependent absorptivity coefficient which is unique for each molecule, and b stands for the path length or distance travelled by the light through the solution which normally depends on the width of the cuvette (Ball, 2006).

In enzyme-based spectrophotometry, spectrophotometry is used to determine the efficiency rate of enzyme-catalysed reactions normally based on the oxidative status of cofactors such as nicotinamide adenine dinucleotide (NAD^+) and nicotinamide adenine dinucleotide phosphate ($NADP^+$) which can absorb light at 340 nm in their reduced but not oxidised forms (Boeckx et al., 2017). As a result, substrates or products involved in reactions which change the oxidative state of these coenzymes can be objectively quantified. Ideally, the detector should be highly sensitive and stable in order to detect subtle changes in light absorbance, and reduce noise and fluorescence.

Automated devices have the added benefit of minimising measurement bias while increasing time efficiency and speed of analysis.

5.1.3. **Enzyme-based spectrophotometry for the prediction of sPTB**

The feasibility of commercial enzyme-based spectrophotometry assays for assessing candidate biomarkers of sPTB in the CVF has already been demonstrated in previous studies (Section 1.5.1; Amabebe et al., 2016a, Stafford et al., 2017). Amabebe et al. (2016a) showed that CVF acetate measured with this technique was significantly higher in untreated symptomatic women who delivered prematurely ($p<0.05$). Wood (2018) also found that the combinations of CVF pyruvate, lactate and urea measured with enzyme-based spectrophotometry could improve the diagnostic performance of TVU CL and fFN for sPTB in symptomatic as well as in high-risk women in the ECCLIPPx I study (Table 5.1).

Table 5.1. Predictive capacity of CVF metabolites in symptomatic and high-risk women compared to standard screening techniques (Wood, 2018)

	Symptomatic women AuROC (95% CI)	**High-risk women AuROC (95% CI)**
CL	0.75 (0.59-0.88)	0.76 (0.67-0.83)
fFN	0.84 (0.68-0.94)	0.69 (0.59-0.77)
CFLUP	0.90 (0.75-0.98)	0.78 (0.69-0.86)

AuROC: area under the receiver operating characteristic curve, CFLUP: cervical length + fetal fibronectin + lactate + urea + pyruvate, CI: confidence interval, CL: cervical length, fFN: fetal fibronectin

5.2. Aims and objectives

5.2.1. **Aims**

The aim of this study was to assess whether the quantification of CVF metabolites in pregnancy using enzyme-based spectrophotometry could improve the predictive capacity for sPTB in the ECCLIPPx II study.

5.2.2. **Objectives**

- To assess the differential CVF metabolite concentrations based on concomitant vaginal bacterial and fungal infection and/ or colonisation
- To quantify CVF acetate, urea, D- and L-lactate in women deemed at high risk of sPTB (AHR) as well as in women presenting in threatened preterm labour (SYMP) using enzyme-based spectrophotometry assays
- To evaluate the prognostic capacity of CVF metabolite profiling for sPTB in AHR and SYMP women
- To compare the predictive value of CVF metabolites for sPTB with current screening and research techniques such as CL and fFN, and MIS respectively

5.3. Materials and methods

5.3.1. **Study population and sample size**

The experiments presented in this chapter were nested within the MIS study described in Chapter 4. For every patient who consented to the MIS study, two CVF samples were obtained at each appointment and stored for subsequent metabolite profiling.

CVF metabolites were quantified and analysed for both MIS cohorts: asymptomatic women deemed at high risk of sPTB based on their previous obstetric history or an incidentally short cervix on transvaginal ultrasound at 20 weeks (AHR), and symptomatic women presenting in threatened preterm labour but without advanced cervical dilation (SYMP). Women diagnosed with PPROM, multiple gestations, abnormal cervical cytology within the previous year or established genital infections immediately prior to the study visit were excluded.

Sample size calculations were conducted using MedCalc® software based on local birth statistics and published studies which reported an AuROC of around 0.80-0.84 for sPTB prediction using CVF metabolite profiling (Amabebe et al., 2016a, Amabebe et al., 2016b). Given an estimated prevalence of sPTB in the range of 25% for the proposed cohorts, the expected ratio of negative (term-delivered) to positive cases (preterm delivered) was set at 4:1. Assuming a power of 80%, a type I error of 5% and a null hypothesis of AuROC=0.5, a sample size of 35-45 women was determined for each arm. However, further sample size calculations employing MetaboAnalyst® software recommended a minimum of 60 participants and a maximum of 1000 to achieve adequate accuracy when testing CVF biomarkers for PTB prediction (Wood, 2018).

5.3.2. **Recruitment and CVF sample collection**

Women were recruited at the Jessop Wing Maternity Unit of the Royal Hallamshire Hospital in Sheffield (UK) from May 2018-August 2019 as a subgroup of the MIS ECCLIPPx II study (Chapter 4).

At each MIS study visit, CVF was collected from the vaginal posterior fornix using dry polystyrene Dacron swabs during the speculum examination (Section 4.3.3). For AHR women, CVF samples were first collected between 20-22 weeks, and then between 26-28 weeks, whereas for SYMP participants CVF samples were retrieved at just one point in time between 20-34^{+6} weeks upon presentation of symptoms suggestive of preterm labour. After sample collection, the swabs were stored at -80°C until further processing for metabolite analysis.

5.3.3. **Sample preparation for metabolomics**

CVF samples were processed as previously described (Amabebe et al., 2016a, Wood, 2018). The tip of the CVF-saturated swab was cut and placed in a 1.5 mL microfuge tube with 1 mL of sterile PBS (pH 7.4, Sigma-Aldrich D8537, UK). The tube was then vortexed at 300 rpm for five minutes to separate the CVF from the swab. Seven-hundred microliters of the solution were then transferred to a second Eppendorf tube and centrifuged for three minutes at 13,000 rpm thus enabling separation of the CVF from the swab particles. The supernatant was subsequently aspirated and transferred into a screw-cap sterile centrifuge tube which was stored at -80°C until metabolomics was performed.

5.3.4. **CVF metabolite quantification**

Acetate, urea, and D- and L-lactate levels in CVF were measured employing a set of end-point enzyme-based spectrophotometry assays which rely on absorbance of NADH and NADPH produced by chemical reactions specific to each metabolite (Megazyme®, Ireland). Because the amount of NADH/ NADPH formed or consumed in these assays is stoichiometric with the metabolite in the sample, absorbance changes enabled to indirectly estimate the metabolites absolute concentration (Amabebe et al., 2016a). Spectrophotometric reactions and measurements were performed using a ChemWell® 2910 auto-analyser (Awareness Technology Inc., Austria). These metabolites were selected on the basis of previous reports that suggested differences in acetate and lactate could reflect altered carbohydrate metabolism in the vaginal environment (Section 1.5.1; Amabebe et al., 2016a, Wood, 2018) whereas urea concentration could be affected by the presence of *Ureaplasma urealyticum*, a bacteria which has been linked to sPTB (Viscardi, 2010, Wood, 2018).

5.3.5. **Acetate in CVF**

Acetate concentrations were measured using the Megazyme® K-ACETGK 04/18 assay kit as per manufactures' instructions (detection limit 10 mg/L). The reaction mixture was prepared combining 30 µL of the sample with 200 µL of reagent 1 [distilled water, buffer at pH 7.4, acetate kinase (AK), phosphotransacetylase (PTA), adenosine-5'-diphosphate-glucokinase (ADP-GK), and glucose-6-phosphate dehydrogenase (G6P-DH)], and 20 µL of reagent 2 [NAD+ (reduced nicotinamide adenine dinucleotide), ATP (adenosine triphosphate), D-glucose, coenzyme-A (CoA), and polyvinylpyrrolidone (PVP)].

The method involved a four-step "positive" enzymatic reaction for five minutes at 37^{o}C that resulted in an increase in absorbance at 340 nm (NADH). These absorbance changes were used to determine acetate concentration in the CVF samples. The reactions are as follows:

Acetic acid in the sample is first phosphorylated to acetyl-phosphate and ADP by AK:

(1) Acetic acid + ATP $\xrightarrow{\text{AK}}$ acetyl-phosphate + ADP

Acetyl-phosphate is quickly converted into acetyl-CoA and inorganic phosphate in the presence of CoA by PTA, as follows:

(2) Acetyl-phosphate + CoA $\xrightarrow{\text{PTA}}$ acetyl-CoA + Pi

The ADP from (1) is then transformed into adenosine-5'-monophosphate (AMP) by ADP-GK, while D-glucose is simultaneously converted into glucose-6-phosphate:

(3) ADP + D-glucose $\xrightarrow{\text{ADP- GK}}$ glucose-6-phosphate + AMP

Finally, the glucose-6-phosphate from the previous step is oxidised to gluconate-6-phosphate by G6P-DH with the resulting formation of NADH:

(4) Glucose-6-phosphate + NAD^{+} $\xrightarrow{\text{G6P-DH}}$ 6-phosphogluconate + NADH+ H^{+}

A calibration curve was generated with 0, 0.45, 0.9 and 1.8 g/L acetate solutions, and was subsequently used to determine the concentration of acetic acid present in the sample based on NADH absorbance (Figure 5.2).

The samples were also run against a blank in which the sample was substituted by distilled water to assess the baseline absorbance of the reagent solution, and a negative control using the solution obtained from a sterile swab processed in a similar way to the CVF samples to assess for potential confounding variables such as contamination or procedural artefact. Samples were run in duplicates, and mean concentrations were employed to inform statistical analyses.

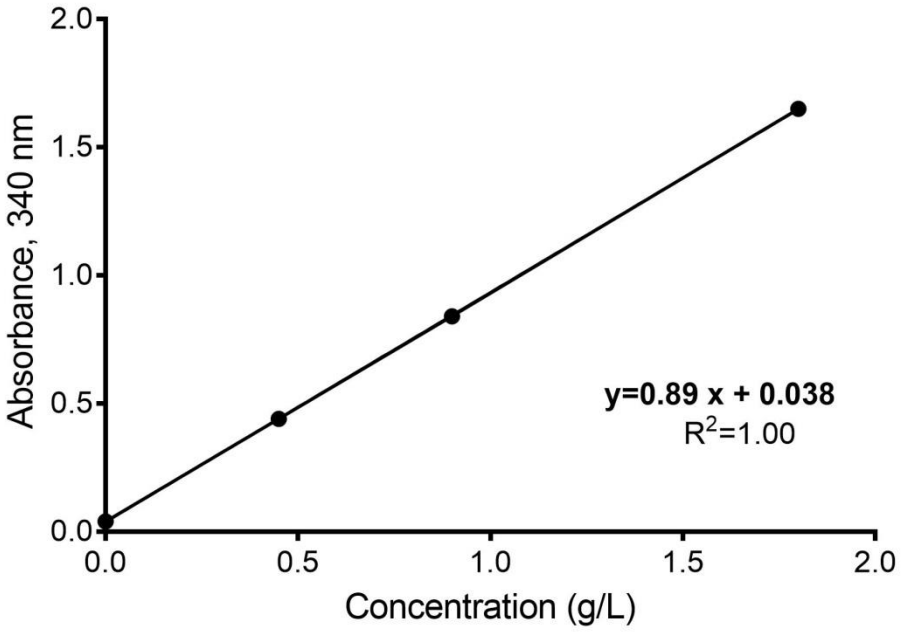

Figure 5.2. Calibration curve correlates acetate concentration to absorbance at 340 nm (NADH).

5.3.6. **Urea in CVF**

Urea concentration in CVF was measured using the Urea/ Ammonia Rapid Assay kit (K-URAMR 10/18, Megazyme®). Reagents and standards were employed and stored as per manufacturers' instructions. A reaction mixture with a final volume of 260 µL was prepared for each sample containing 10 µL of sample, 200 µL of reagent 1 (NADPH, buffer at pH 8.0 and distilled water), 25 µL of reagent 2 [glutamate dehydrogenase (GIDH) and distilled water] and 25 µL of reagent 3 (urease and distilled water).

Similar to the acetic acid kit, the urea K-URAMR is an end-point type of assay but unlike the acetic acid assay, urea is quantified on the basis of consumed NADPH (rather than NADH produced) during the reaction. The method relies on a two-step "negative" enzymatic reaction as follows:

Urea in the sample is first hydrolysed to ammonia (NH_3) and carbon dioxide by urease. This reaction involves mixing reagent 1 and 2 with the sample for five minutes at 37^{o}C.

(1) $\text{Urea} + H_2O \xrightarrow{\text{Urease}} 2NH_3 + CO_2$

The next step involves adding reagent 3 with which ammonia, in the presence of NADPH and GIDH, reacts with 2-oxoglutarate to form L-glutamic acid and $NADP^+$ for six minutes at 37^{o}C.

(2) $\text{2-oxoglutarate} + \text{NADPH} + NH_4^+ \xrightarrow{\text{GIDH}} \text{L-glutamic acid} + NADP^+ + H_2O$

NADPH consumption is measured as a decrease in absorbance at 340 nm and used as a proxy to determine urea concentration in the sample (detection limit: 0.13 mg/L).

A calibration curve was constructed with 0 (distilled water), 0.025, 0.05 and 0.1 g/L of urea (Figure 5.3). Similarly to the acetic acid assay, samples were run against a blank control containing only distilled water and a negative control obtained from a sterile Dacron swab. Samples were processed in duplicates, and the mean concentration was used for statistical analyses.

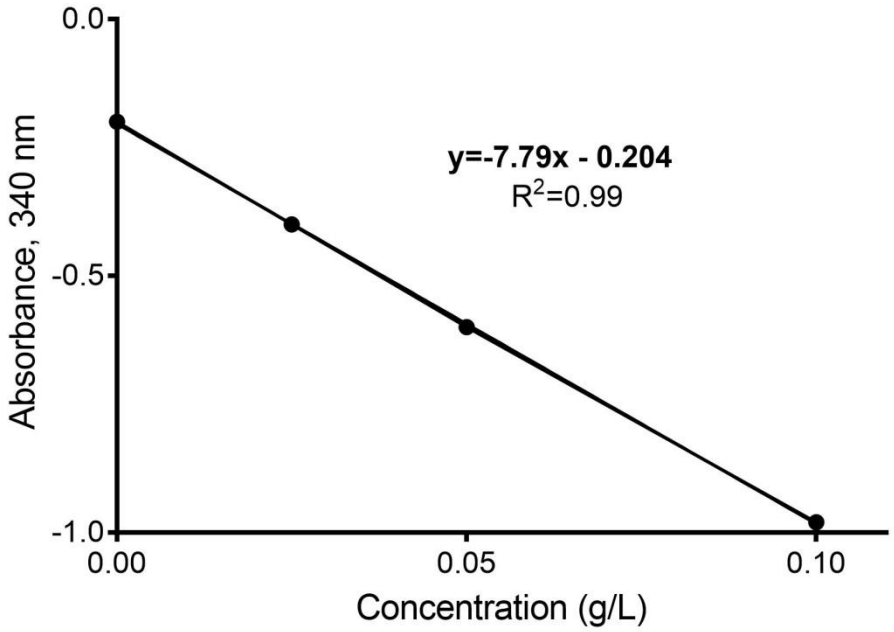

Figure 5.3. Calibration curve negatively correlates urea concentration to absorbance at 340 nm (NADPH)

5.3.7. **D-lactate and L-lactate in CVF**

D-lactate and L-lactate levels in CVF were measured independently using the K-DATE 08/18 and K-LATE 06/18 Megazyme® Rapid Assay Kits, and subsequently combined to estimate the total amount of lactate in the samples. Similarly to acetate, these end-point assays showed positive linearity by measuring an increase in absorbance at 340 nm (NADH).

For D-lactate, a reaction mixture was prepared containing 10 µ of sample, 200 µL of reagent 1 [distilled water, buffer, NAD^+ and D-glutamate-pyruvate transaminase suspension (D-GPT)] and 25 µL of reagent 2 [distilled water and D-lactate dehydrogenase (D-LDH)], with a final volume of 235 µL.

For L-lactate, the reaction mixture was the same except for a substitution of D-LDH in reagent 1 for L- lactate dehydrogenase (L-LDH) to ensure isomer specificity in the measurements.

D-lactate and L-lactate quantification requires a two-step enzymatic reaction that is as follows:

In the first reaction, D-lactate and L-lactate are oxidised to pyruvate in the presence of NAD^+ by D-LDH or L-LDH respectively.

(1) D-/ L-lactate + NAD^+ $\xleftrightarrow{\text{D-/ L-LDH}}$ pyruvate + NADH + H^+

Because the equilibrium of the reaction favours D-/ L-lactate and NAD^+ over pyruvate, a further step is necessary to minimise the reverse reaction. That extra step involves the conversion of pyruvate to D-alanine and 2-oxoglutarate by D-GPT:

(2) Pyruvate + D-glutamate $\xrightarrow{\text{D-GPT}}$ D-alanine + 2-oxoglutarate

D- / L-lactate is stoichiometric with the amount of NADH generated in reaction (1).

Similarly to acetic acid and urea, calibrations curves were constructed for D- and L-lactate using D- and L-lactic acid standards of known concentrations at 0, 0.25, 0.5 and 1.0 g/L respectively (Figure 5.4). The samples were also run in duplicates against a blank control and negative control. Once the concentrations of both isomers were determined, the ratio of L- to D-lactate was calculated for each sample. Furthermore, D- and L-lactate were added to calculate total lactate concentration.

(a)

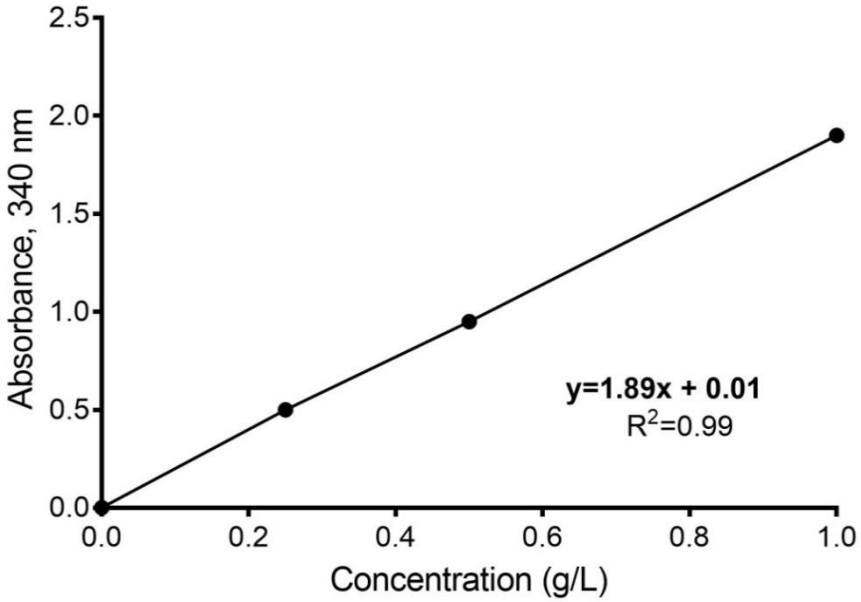

(b)

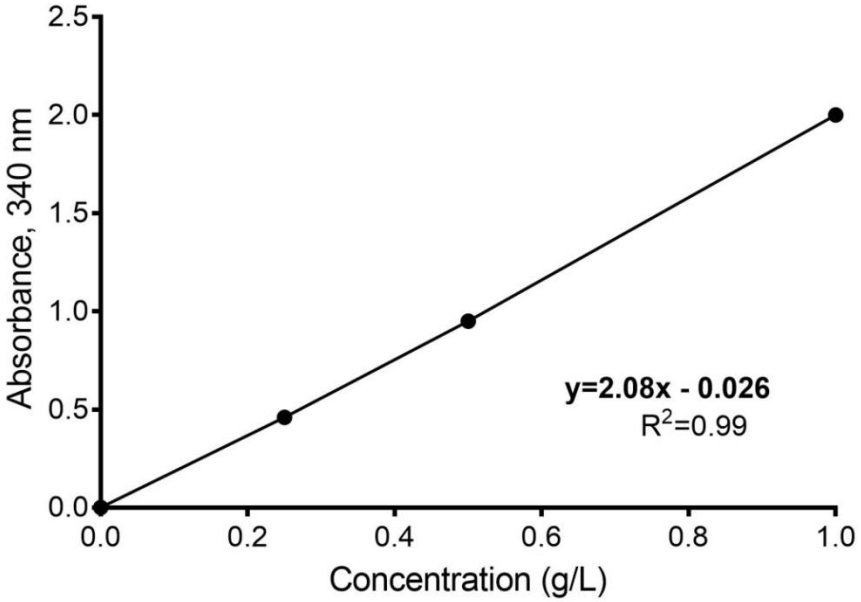

Figure 5.4. Calibration curves correlate **(a)** D-lactate and **(b)** L-lactate with absorbance at 340 nm (NADH)

5.3.8. **pH, CL, and fFN**

As enumerated in chapter 4, when MIS participants attended their study visits, CL and quantitative fFN was simultaneously ascertained. During CVF collection, vaginal pH was also determined by smearing a high-quality narrow pH range paper (Fisherbrand^{TM}) on the speculum (pH 3.6-6.1).

5.3.9. **Vaginal microbiology analysis**

In addition to CVF collection for metabolite profiling, an extra swab was retrieved from the vaginal vault and posterior fornix for screening of vaginal infections. Samples were placed in Amies charcoal transport medium for microbiology analysis at Sheffield NHS Teaching Hospitals. These high vaginal swabs were assessed for organisms which have been linked to vaginal infection (and potential adverse neonatal outcomes) such as *Trichomonas vaginalis*, yeast, streptococci, coliforms and other anaerobic bacteria.

Candida spp detection was reported as mild, moderate or heavy depending on the degree of overgrowth. However, given the high prevalence of *Candida* in pregnancy, candidiasis was only treated if there were concomitant signs or symptoms of cervicovaginitis.

Swabs were also assessed for BV-associated bacteria such as *Gardnerella vaginalis*, *Prevotella* and *Mobiluncus* spp, and for the presence of clue cells using acridine orange (Nugent et al., 1991, Money, 2005). Patients who tested positive for clue cells and/or met other Amsel criteria such as pH>4.5 and grey-white discharge were offered antimicrobial treatment (Mohammadzadeh et al., 2014).

When swab cultures confirmed the presence of Lancefield group B streptococci (GBS), carriers were offered intrapartum antibiotic prophylaxis in alignment with national guidelines in the UK (RCOG, 2017).

5.3.10. **Statistical analysis**

The distribution of the data was assessed with Shapiro-Wilk normality tests. If the assumption of normality was met, demographic and clinical information was subsequently interrogated with parametric tests such as unpaired Student's *t*-test and ANOVA and presented as mean +/- SD. On the other hand, if the data was found to be non-normally distributed, non-parametric tests such as Mann-Whitney U and Kruskal-Wallis tests were employed instead, and the data was summarised using median as a measure of centrality and the interquartile range (IQR) as a measure of dispersion. Chi-square tests were also used to establish relationships between categorical data.

Furthermore, metabolites concentrations were evaluated within the context of the vaginal pH (Pearson's correlation) and microbiological cultures (unpaired Student *t*-test) in an attempt to better determine the metabolic signature of vaginal infections and/ or colonisation; *p*-values<0.05 were considered statistically significant.

The concentration of CVF was assessed based on time to delivery and subsequently, between birth outcomes. The primary outcome for all statistical analyses was the prediction of delivery prior to 37 weeks of gestation. For the SYMP cohort, prediction of sPTB within two weeks of presentation was also assessed. Clinical efficacy of CVF metabolic profiling was evaluated through the construction of AuROCs. Logistic regression models were used to test the predictive capacity of all metabolites combinations as well as in conjunction with CL, fFN and MIS. All AuROCs were compared to the null hypothesis of AuROC=0.5 (no effect).

Statistical analyses were performed in SPSS v25 and MedCalc®, and curves and graphs were designed with GraphPrism® 7 software.

5.4. Results

5.4.1. **Participants' demographic and clinical data**

This study was approved by the Yorkshire & the Humber Committee of the UK National Research Ethics Service (Research Ethics Committee 17/YH0179).

As described in Section 4.4.4, a total of 144 pairs of swabs were obtained for CVF analysis from AHR women seen between 20-22 weeks (n=49) and later on between 26-28 weeks (n=46), and SYMP women between 20-34^{+6} (n=49).

Within the AHR cohort, four patients (8.16%) were induced prematurely after experiencing PPROM, 13 (26.53%) went into spontaneous preterm labour, and 32 (65.31%) had a term delivery. No statistically significant differences were seen in maternal age, BMI, history of LLETZ and smoking status between delivery outcomes (Table 4.8). Three women had an extreme sPTB (<28^{+0} weeks) before their follow-up visit which accounts for the difference seen in the number of women between the first and second visit (n=49 vs n=46; Section 4.4.4).

Within the SYMP group, five participants (10.20%) were iatrogenically induced before 37 weeks due to PPROM, eight (16.33%) spontaneously delivered preterm and 36 (73.47%) went on to deliver at term (Table 4.8). Three women (6.12%) delivered within two weeks of presenting with preterm labour symptoms. Like in the findings for the AHR cohort, SYMP women with a term and a preterm birth appeared to be adequately matched for maternal age, LLETZ, smoking status and BMI (Chapter 4, Table 4.8).

SYMP women who delivered prematurely has significantly higher CVF fFN than their term counterparts ($p<0.05$; Table 4.8). No other variables significantly differed between cohorts or delivery outcomes.

When all MIS participants were considered together, CL and fFN negatively correlated: the shorter the cervix, the higher the CVF fFN concentration ($p<0.001$; Figure 5.5).

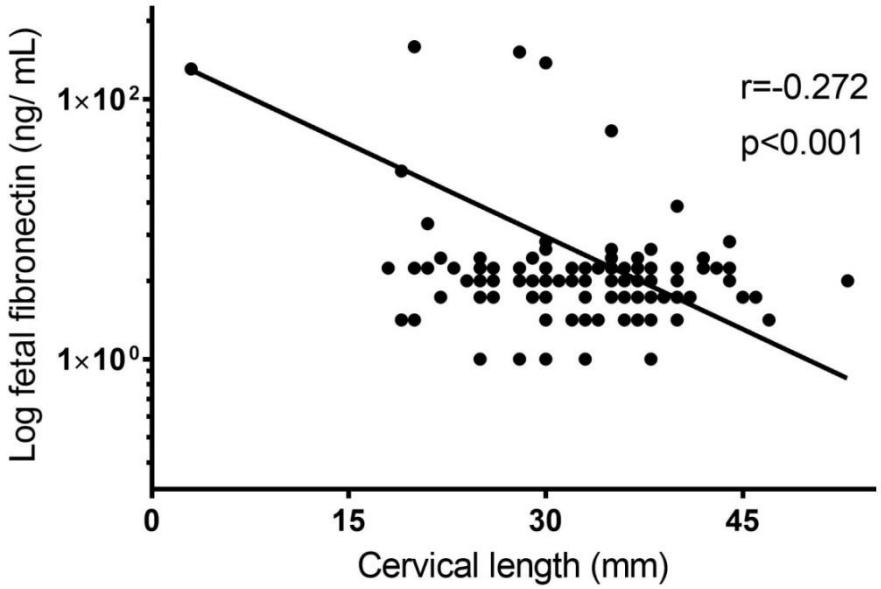

Figure 5.5. Cervical length negatively correlated with fetal fibronectin (n=144). Pregnant women with a shorter cervix were found to have higher CVF concentration of fetal fibronectin (p<0.001). *fFn in the y-axis is in logarithmic scale.*

5.4.2. **Correlation between CVF metabolites and pH**

When the association between CVF metabolite concentration and vaginal acidity was assessed, total lactate concentration negatively correlated with vaginal pH: the higher the concentration of total lactate, the lower the pH (p<0.01; Figure 5.6).

When lactate isomers were further assessed independently against vaginal pH, L- but not D-lactate was also found to significantly correlate with vaginal acidity. Similarly to what was reported for total lactate, women with higher concentrations of L-lactate in their CVF had significantly lower vaginal pH (p<0.01).

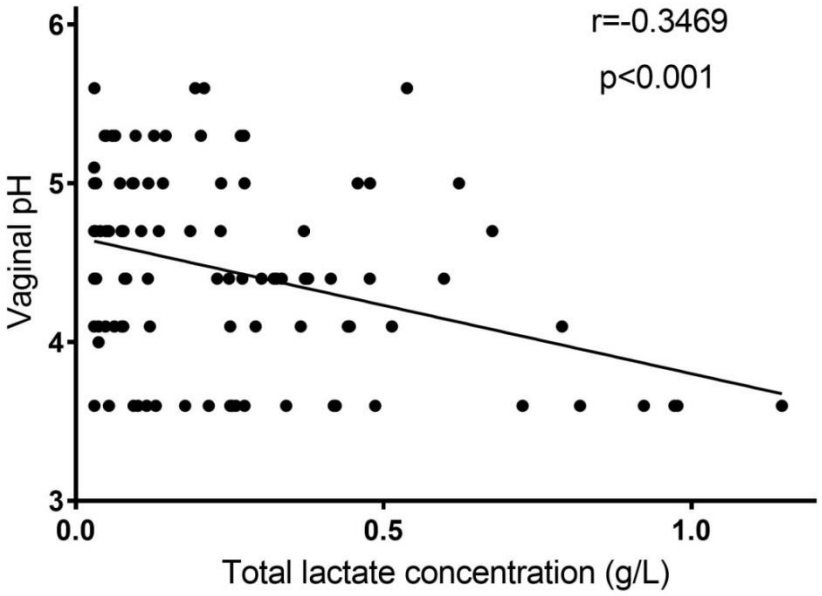

Figure 5.6. Total lactate concentration negatively correlated with vaginal pH (n=134; p<0.001).

5.4.3. **High-vaginal swabs microbiology**

The analysis of 144 pairs of high-vaginal swabs (HVS) performed by the Clinical Microbiology Department at Sheffield NHS Teaching Hospitals identified fungal and bacterial colonisation +/- infection on 42 occasions: 14 (33.34%) in AHR women attending their first visit (between 20-22 weeks), 12 (28.57%) during their follow-up between 26-28 weeks, and 16 (38.09%) in SYMP women between 20-34^{+6} (Table 5.2).

Table 5.2. HVS microbiology by cohort, (number of cases, % within each cohort)

		AHR 1st visit	AHR 2nd visit	SYMP	Total
Negative swab		35 (71.43%)	34 (73.91%)	33 (67.35%)	102
Candida	**Light growth**	3 (6.12%)	3 (6.52%)	3 (6.12%)	9
	Moderate growth	5 (10.20%)	0	2 (4.08%)	7
	Heavy growth	2 (4.08%)	0	4 (8.16%)	6
Ureaplasma urealyticum		0	0	1 (2.04%)	1
Bacterial vaginosis		1 (2.04%)	3 (6.52%)	2 (4.08%)	6
Group B *Streptococcus*		3 (6.12%)	6 (13.04%)	4 (8.16%)	13
Total		49 (100%)	46 (100%)	49 (100%)	144

AHR: asymptomatic high-risk cohort, HVS: high-vaginal swab, SYMP: symptomatic cohort

All patients who tested positive for BV and *Ureaplasma urealyticum* received a short course of metronidazole and erythromycin respectively to minimise the risk of sPTB. Follow-up swabs ("cure test") to ensure the dysbiosis had effectively been treated were performed only in women who were still symptomatic. Because antibiotic treatment is likely to have significantly altered the metabolite profiling in these women, swabs from women who went on to receive antimicrobial therapy for *Ureaplasma* spp and BV were excluded from the overall metabolite profiling analysis based on birth outcomes, and analysed independently.

On the other hand, all swabs in which *Candida* spp and Group B Streptococcus colonisation was identified were included because none of these women received antibiotic treatment during their pregnancy. Patients who tested positive for *Candida* spp did not report any symptoms of vulvovaginitis during their study visits which required treatment. Similarly, those diagnosed with Group B Streptococcus colonisation did not receive antibiotic therapy until they were in established labour. Intravenous Benzylpenicillin (Penicillin G) was offered to GBS positive women during labour to minimise the infection risk of the newborn when passing through the birth canal.

The majority of women diagnosed with fungal and Group B Streptococcus colonisations (n=35, 100%) delivered at term (n=27, 77.14%), with a few experiencing PPROM (n=3, 8.57%) or a sPTB (n=5, 14.29%). However, no significant association was found between vaginal colonisation and delivery outcomes (Fisher's exact test, p=0.48; Table 5.3). When confirmed cases of vaginal infection, namely *Ureaplasma* spp and BV, were analysed by delivery outcome, women who went

to experience PPROM had the highest proportion of positive swabs (n=2, 16.67%) compared to those who had a term (n=4, 4%) or sPTB (n=1, 3.12%). However, these differences were not statistically significant (Fisher's exact test, p=0.42; Table 5.3).

Table 5.3. HVS microbiology by delivery outcome, (number of cases, % within each delivery outcome)

		PPROM	sPTB	Term	Total
Negative swab		7 (58.34%)	26 (81.25%)	69 (69%)	102
Candida	**Light growth**	0	1 (3.13%)	8 (8%)	9
	Moderate growth	1 (8.33%)	1 (3.13%)	5 (5%)	7
	Heavy growth	0	1 (3.13%)	5 (5%)	6
Ureaplasma urealyticum		1 (8.33%)	0	0	1
Bacterial vaginosis		1 (8.33%)	1 (3.13%)	4 (4%)	6
Group B *Streptococcus*		2 (16.67%)	2 (6.25%)	9 (9%)	13
Total		12 (100%)	32 (100%)	100 (100%)	144

HVS: high-vaginal swab, PPROM: prelabour premature rupture of membranes, sPTB: spontaneous preterm birth

5.4.4. **CVF metabolite profile based on high-vaginal swabs microbiology results**

The vaginal pH was positively skewed in women who had a negative HVS (n=77). This sub-group was not normally distributed (Shapiro-Wilk, $p<0.05$) and therefore, non-parametric tests were employed to assess the relationship between vaginal pH and microbiology results.

The median pH for all swabs was 4.4 (IQR: 0.90). Even though no statistically significant difference was seen in vaginal pH based on microbiology results, women who tested positive for BV tended to have relatively higher median pH than any other group (Table 5.4).

Table 5.4. Vaginal pH displayed per microbiology results

		Median pH	IQR	Number of cases
Negative swab		4.4	0.95	77
Candida	**Light growth**	4.4	0.6	9
	Moderate growth	4.1	(-)	3
	Heavy growth	4.4	1.18	6
Ureaplasma urealyticum		3.6	(-)	1
Bacterial vaginosis		5	1.02	5
Group B *Streptococcus*		4.4	0.45	9
Total		4.4	0.90	110

IQR: interquartile range

CVF metabolites concentrations namely acetate, urea, D- and L-lactate, and total lactate results were normally distributed when they were analysed by clinical microbiology results (Shapiro-Wilk test, $p>0.05$). Therefore, statistical comparisons were conducted using parametric tests, and results were presented as mean +/- SD.

All swabs that were positive for *Candida* colonisation were analysed together. Acetate was significantly higher in women who had a diagnosis of BV ($p=0.015$; Table 5.5). Other metabolites did not significantly differ by microbiology result.

Table 5.5. CVF metabolite concentrations compared by microbiology results with one-way ANOVA (mean ± SD, n=number of cases)

	Acetate (g/L)	**Urea (g/L)**	**D-lactate (g/L)**	**L-lactate (g/L)**	**Total lactate (g/L)**	**Ratio L-/D-lactate**
Negative swab	0.103 ± 0.046 (n=89)	0.003 ± 0.003 (n=101)	0.03 ± 0.004 (n=96)	0.20 ± 0.25 (n=96)	0.23 ± 0.25 (n=96)	5.70 ± 7.19 (n=96)
Candida	0.103 ± 0.041 (n=20)	0.032 ± 0.003 (n=22)	0.032 ± 0.004 (n=22)	0.22 ± 0.22 (n=21)	0.25 ± 0.22 (n=21)	6.6 ± 6.86 (n=21)
Ureaplasma urealyticum	0.06 (n=1)	0.004 (n=1)	0.03 (n=1)	-	0.03 (n=1)	-
Bacterial vaginosis	0.21 ± 0.15* (n=5)	0.005 ± 0.002 (n=5)	0.035 ± 0.007 (n=6)	0.33 ± 0.29 (n=3)	0.37 ± 0.29 (n=3)	9.52 ± 7.93 (n=3)
Group B *Streptococcus*	0.12 ± 0.99 (n=13)	0.003 ± 0.002 (n=13)	0.031 ± 0.002 (n=12)	0.14 ± 0.14 (n=12)	0.17 ± 0.14 (n=12)	4.27 ± 4.23 (n=12)

**p-value<0.05, SD: standard deviation*

5.4.5. **CVF metabolites based on time to delivery**

CVF metabolites were subsequently analysed within the AHR and the SYMP cohorts based on time to delivery (Appendix F). None of the CVF metabolites was found to significantly correlate with time interval to delivery ($p>0.05$). Furthermore, the low coefficients of determination (R^2) obtained when the data was modelled as linear regressions (Figures E.1-E.2) suggested that time to delivery cannot explain the variability seen in metabolic concentration across samples.

The differential concentration of CVF metabolites was further analysed based on delivery outcome.

5.4.6. **Metabolites in the AHR cohort by birth outcomes**

Excluding swabs which were positive for BV or *Ureaplasma* spp, CVF samples obtained from AHR women between 20-22 weeks and between 26-28 weeks of gestation were assessed for acetate, urea, D- and L-lactate, total lactate concentration and L-/D-lactate ratio and sorted by birth outcome. Discrepancies between the numbers of samples analysed for each metabolite were due to fluorescence artefact or problems with the enzyme kit which rendered some results unreadable. Metabolite data was non-normally distributed (Shapiro-Wilk test, $p<0.05$) for both AHR 1st and 2nd visits.

For AHR 1st visit, no differences were seen in metabolite expression between women who delivered preterm (either iatrogenic or spontaneously) and term (Table 5.6). Metabolite profiles are further displayed for PPROM and sPTB in Table 5.7.

Table 5.6. CVF metabolite quantification in AHR women between 20-22 weeks displayed as all PTB versus term deliveries, median (IQR), n=number of cases.

Metabolites	PTB	Term	*p*-value
Acetate (g/L)	0.10 (0.09) n=17	0.084 (0.02) n=29	0.28
Urea (g/L)	0.002 (0.003) n=17	0.003 (0.003) n=32	0.41
D-lactate (g/L)	0.031 (0.005) n=17	0.030 (0.003) n=32	0.43
L-lactate (g/L)	0.08 (0.22) n=17	0.09 (0.25) n=29	0.62
Total lactate (g/L)	0.11 (0.22) n=17	0.12 (0.25) n=29	0.68
L-/D- lactate ratio	2.48 (5.71) n=17	2.92 (7.34) n=29	0.71

IQR: interquartile range, PTB: preterm birth. Comparisons were made with Mann-Whitney U test.

Table 5.7. CVF metabolite quantification in AHR women between 20-22 weeks displayed as PPROM and sPTB versus term deliveries, median (IQR), n=number of cases.

Metabolites	PPROM	sPTB	Term	*p*-value
Acetate (g/L)	0.12 (0.09) n=4	0.08 (0.023) n=13	0.084 (0.02) n=29	0.07
Urea (g/L)	0.002 (0.003) n=4	0.003 (0.003) n=13	0.003 (0.003) n=32	0.72
D-lactate (g/L)	0.030 (0.003) n=4	0.032 (0.006) n=13	0.03 (0.003) n=32	0.30
L-lactate (g/L)	0.087 (0.19) n=4	0.078 (0.30) n=13	0.09 (0.25) n=29	0.76
Total lactate (g/L)	0.12 (0.19) n=4	0.11 (0.30) n=13	0.12 (0.25) n=29	0.82
L-/D- lactate ratio	2.9 (5.56) n=4	2.48 (7.74) n=13	2.92 (7.34) n=29	0.82

IQR: interquartile range, PPROM: pre-labour premature rupture of membranes, sPTB: spontaneous preterm birth. A Kruskal-Wallis test was performed for statistical analysis among groups.

Similarly, the analysis of CVF metabolite concentrations between 26-28 weeks of gestation (AHR 2nd visit) did not significantly differ between women who had a PTB and those who had a term delivery, even when preterm births were further assessed into sPTB and PPROM (Tables 5.8 and 5.9).

Table 5.8. CVF metabolites quantification in AHR women between 26-28 weeks displayed as all PTB versus term deliveries, median (IQR), n=number of cases.

Metabolites	PTB	Term	*p*-value
Acetate (g/L)	0.09 (0.05) n=11	0.08 (0.04) n=25	0.79
Urea (g/L)	0.002 (0.004) n=12	0.003(0.003) n=30	0.37
D-lactate (g/L)	0.030 (0.006) n=12	0.030 (0.002) n=30	0.79
L-lactate (g/L)	0.06 (0.23) n=10	0.17 (0.32) n=28	0.39
Total lactate (g/L)	0.09 (0.23) n=10	0.20 (0.33) n=28	0.37
L-/D- lactate ratio	1.77 (6.20) n=10	5.18 (10.37) n=28	0.33

PTB: preterm birth. Comparisons were made with Mann-Whitney U test.

Table 5.9. CVF metabolite quantification in AHR women between 26-28 weeks displayed as PPROM and sPTB versus term deliveries, median (IQR), n=number of cases.

Metabolites	PPROM	sPTB	Term	*p*-value
Acetate (g/L)	0.09 (-) n=2	0.09 (0.05) n=9	0.08 (0.04) n=25	0.78
Urea (g/L)	0.003 (-) n=2	0.002 (0.004) n=10	0.003(0.003) n=30	0.61
D-lactate (g/L)	0.03 (-) n=2	0.03 (0.005) n=10	0.03 (0.002) n=30	0.84
L-lactate (g/L)	0.16 (-) n=1	0.04 (0.24) n=9	0.17 (0.32) n=28	0.63
Total lactate (g/L)	0.19 (-) n=1	0.07 (0.25) n=9	0.20 (0.33) n=28	0.63
L-/D- lactate ratio	5.2 (-) n=1	1.31 (6.62) n=9	5.18 (10.37) n=28	0.57

IQR: interquartile range, PPROM: pre-labour premature rupture of membranes, sPTB: spontaneous preterm birth. A Kruskal-Wallis test was performed for statistical analysis among groups.

CVF metabolite concentrations in AHR women did not significantly differ between their first and second visits when analysed by delivery outcome (Table 5.10).

Table 5.10. CVF metabolites in AHR women comparing between 1st and 2nd visit by delivery outcome, median (IQR), n=number of cases.

Metabolites	Delivery outcome	1st visit	2nd visit	*p*-value
Acetate (g/L)	Term n=24	0.09 (0.03)	0.08 (0.04)	0.66
	PTB n=11	0.09 (0.04)	0.09 (0.05)	0.58
Urea (g/L)	Term n=29	0.003 (0.003)	0.003 (0.003)	0.28
	PTB n=12	0.002 (0.003)	0.002 (0.004)	0.53
D-lactate (g/L)	Term n=29	0.030 (0.002)	0.030 (0.002)	0.30
	PTB n=12	0.032 (0.005)	0.030 (0.006)	0.89
L-lactate (g/L)	Term n=26	0.09 (0.25)	0.13 (0.31)	0.41
	PTB n=9	0.08 (0.19)	0.07 (0.24)	0.86
Total lactate (g/L)	Term n=26	0.12 (0.25)	0.16 (0.32)	0.41
	PTB n=9	0.11 (0.20)	0.10 (0.25)	0.86
L-/D- lactate ratio	Term n=26	2.62 (7.30)	4.08 (8.40)	0.32
	PTB n=9	2.13 (2.11)	2.23 (6.50)	0.52

IQR: interquartile range, PTB: preterm birth. Wilcoxon signed-rank test was performed for statistical analysis.

5.4.7. **Metabolites in the SYMP cohort by birth outcomes**

CVF samples collected from SYMP women between 20-34^{+6} weeks were also assessed for acetate, urea, D- and L-lactate concentrations using enzyme-based spectrophotometry. Metabolite concentrations in SYMP participants were not normally distributed (Shapiro-Wilk test, $p<0.05$).

In women who delivered prematurely (either spontaneously or induced), median L-lactate was significantly lower than in women who had a term delivery ($p<0.05$). Total lactate concentration and the L-/D-lactate ratio were also significantly lower in women who had a sPTB (Table 5.11). When PTB data was further analysed into sPTB and PPROM, total lactate and the L-/D-ratio also tended to be lower in women who delivered prematurely, but these differences were not statistically significant ($p=0.05$; Table 5.12).

Table 5.11. CVF metabolite quantification in SYMP women displayed as all PTB versus term deliveries, median (IQR), n=number of cases.

Metabolites	PTB	Term	*p*-value
Acetate (g/L)	0.14 (0.08) n=12	0.11 (0.07) n=29	0.81
Urea (g/L)	0.004 (0.002) n=12	0.003 (0.002) n=34	0.37
D-lactate (g/L)	0.03 (0.001) n=12	0.03 (0.003) n=34	0.16
L-lactate (g/L)	0.03 (0.14) n=11	0.16 (0.34) n=34	0.01*
Total lactate (g/L)	0.06 (0.14) n=11	0.19 (0.35) n=34	0.01*
L-/D- lactate ratio	1.0 (4.39) n=11	4.88 (9.28) n=34	0.01*

PTB: preterm birth. Comparisons were made with Mann-Whitney U test, *significant *p*-values<0.05

Table 5.12. CVF metabolites quantification in SYMP women displayed as PPROM and sPTB versus term deliveries, median (IQR), n=number of cases.

Metabolites	PPROM	sPTB	Term	*p*-value
Acetate (g/L)	0.14 (0.07) n=4	0.14 (0.08) n=8	0.11 (0.07) n=29	0.97
Urea (g/L)	0.003 (0.003) n=4	0.004 (0.002) n=8	0.003 (0.002) n=34	0.66
D-lactate (g/L)	0.03 (0.005) n=4	0.03 (0.001) n=8	0.03 (0.003) n=34	0.16
L-lactate (g/L)	0.09 (-) n=3	0.03 (0.17) n=8	0.16 (0.34) n=34	0.05
Total lactate (g/L)	0.12 (-) n=3	0.06 (0.17) n=8	0.19 (0.35) n=34	0.05
L-/D- lactate ratio	2.39 (-) n=3	1.0 (5.46) n=8	4.88 (9.28) n=34	0.05

IQR: interquartile range, PPROM: pre-labour premature rupture of membranes, sPTB: spontaneous preterm birth. Kruskal-Wallis was performed for statistical analysis among groups.

5.4.8. **Predictive capacity of CVF metabolites in the AHR cohort**

Even though the concentration of urea, acetate and lactate in CVF of AHR participants at 20-22 weeks or later on at 26-28 weeks did not significantly differ based on delivery outcomes, AuROCs were constructed to assess the predictive capacity for PTB of individual and/ or combined CVF metabolites.

When the predictive capacity of CVF metabolites was individually assessed in AHR women between 20-22 weeks, no differences were found against the null hypothesis of AuROC of 0.5 (Table 5.13). However, when total lactate, urea and acetate (LUA) were combined, the predictive capacity for PTB (either sPTB or PPROM) significantly increased to an AuROC of 0.69 (p=0.03;

Figure 5.7). Similarly, when metabolites were assessed for prediction of PPROM in AHR women during the first visit, acetate had significant predictive capacity either alone or combined with urea and lactate (LUA; Table 5.14; Figure 5.7). Conversely, no other individual or combined CVF metabolite was shown to significantly improve sPTB prediction (Tables 5.13 and 5.14).

Table 5.13. Predictive capacity of CVF metabolites for PTB (both PPROM and sPTB) in AHR patients between 20-22 weeks

CVF metabolite	PTB		
	AuROC	95% Confidence Interval	*p*-value
Acetate	0.60	0.44-0.74	0.32
Urea	0.57	0.42-0.71	0.40
D-lactate	0.55	0.41-0.70	0.54
L-lactate	0.52	0.38-0.67	0.76
Total lactate	0.53	0.38-0.68	0.70
L-/D- lactate ratio	0.53	0.38-0.68	0.53
LUA	0.69	0.53-0.82	0.03*

*AuROC: area under the receiver operating characteristic curve, LUA: total lactate, urea and acetate combined, *significant p-values<0.05*

Table 5.14. Predictive capacity of CVF metabolites for sPTB and PPROM in AHR patients between 20-22 weeks

CVF metabolite	sPTB		PPROM	
	AuROC (95% CI)	*p*-value	AuROC (95% CI)	*p*-value
Acetate	0.51 (0.35-0.67)	0.91	0.87 (0.73-0.98)	<0.001*
Urea	0.57 (0.41-0.72)	0.45	0.56 (0.37-0.74)	0.61
D-lactate	0.62 (0.46-0.76)	0.25	0.64 (0.44-0.81)	0.33
L-lactate	0.57 (0.41-0.72)	0.49	0.55 (0.36-0.73)	0.84
Total lactate	0.56 (0.40-0.71)	0.55	0.54 (0.37-0.74)	0.70
L-/D- lactate ratio	0.55 (0.39-0.71)	0.58	0.54 (0.37-0.74)	0.78
LUA	0.66 (0.49-0.80)	0.08	0.92 (0.76-0.99)	<0.001*

AuROC: area under the receiver operating characteristic curve, PPROM: prelabour premature rupture of membranes, sPTB: spontaneous preterm birth, LUA: total lactate, urea and acetate combined, significant p-values<0.05*

(a)

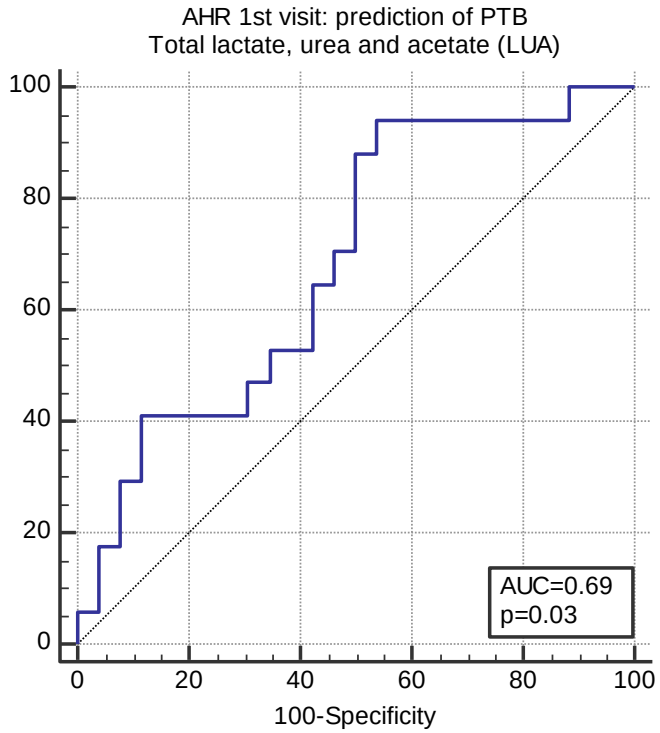

(b)

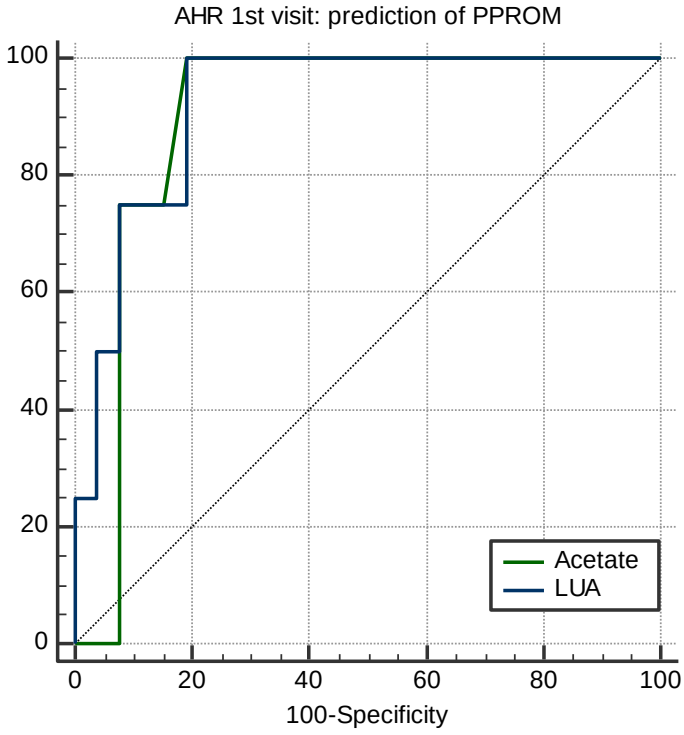

Figure 5.7. AuROC analysis of CVF metabolites for prediction of **(a)** PTB combining total lactate, urea and acetate (LUA), and **(b)** PPROM using acetate or LUA. *AuROC: area under the receiver operating characteristic curve, PPROM: prelabour premature rupture of membrane, PTB: preterm birth*

The predictive performance of CVF metabolites was subsequently compared with that of CL, fFN and MIS at 42 kHz either when used as a stand-alone technique or combined. It is worth

mentioning that models which included MIS had a considerably smaller sample size compared to other techniques due to technical difficulties experienced when capturing and processing data (Section 4.4.1). It is likely that some of these models are not sufficiently powered to make comparisons.

For sPTB prediction, neither CL nor fFN measured between 20-22 weeks had a statistically significant AuROC (Table 5.15). The combination of CL and fFN tended to slightly increase the AuROC (0.63, 95% CI: 0.47-0.76), however this was still not statistically significant (p=0.17). MIS, on the other hand, not only produced a statistically significant AuROC but it also showed the highest sensitivity and NPV for prediction of sPTB (p=0.03, Table 5.15). Nonetheless, the comparison between MIS alone and CL and fFN combined was not statistically significant (p=0.64, Table 5.16).

When CL and fFN were combined with total lactate, urea and acetate (LUA), the resulting AuROC was significantly better than the null hypothesis with a value of 0.70 (p=0.03). This combination tended to modestly improve specificity and NPV when compared to CL and fFN alone, but these differences were not statistically significant (p=0.08; Table 5.16). When MIS was combined with metabolites, the model had a statistically significant AuROC (p=0.01) and a relatively higher PPV for prediction of sPTB. Adding CL and fFN to this model (LUA + MIS + CL + fFN) was shown to significantly improve the performance of fFN alone (p=0.01; Table 5.16, Figure 5.8), even though PPV remained modestly low at 50% (95% CI: 30.6-69.4, Table 5.15).

Table 5.15. Predictive performance of metabolites, CL, fFN and MIS for sPTB in AHR women scanned between 20-22 weeks; *p*-values correspond to comparison with the null hypothesis of an AuROC of 0.5

Technique (+/- cases)	**AuROC (95% CI)**	**Sens (%) (95% CI)**	**Spec (%) (95% CI)**	**PPV (%) (95% CI)**	**NPV (%) (95% CI)**	**+LR (95% CI)**	**-LR (95% CI)**	***p*-value**
CL (13/32)	0.61 (0.46-0.76)	84.62 (54.55-98.08)	37.5 (23.77-53.46)	28.21 (23.11-35.22)	89.47 (69.24-96.98)	1.36 (0.98-1.88)	0.41 (0.11-0.15)	0.22
fFN (13/32)	0.60 (0.45-0.75)	61.5 (31.58-86.14)	65.6 (50.45-80.43)	36.36 (23.75-51.17)	84.85 (73.16-92)	1.85 (1.01-3.39)	0.58 (0.28-1.19)	0.22
CL + fFN (13/32)	0.63 (0.47-0.76)	76.9 (46.19-94.96	53.1 (37.87-68.34)	32.26 (23.62-42.30)	88.89 (74.08-95.73)	1.65 (1.07-2.54)	0.43 (0.15-1.21)	0.17
MIS (6/18)	0.73 (0.51-0.89)	100.0 (54.1-100.0	50.0 (26.0-74.0)	40.0 (29.58-51.41)	100.0	2.0 (1.3- 3.2)	0.0	0.03*
LUA (13/26)	0.66 (0.49-0.80)	76.9 (46.19-94.96)	57.7 (42.10-74.43)	38.46 (27.89-50.25)	88.46 (73.31-95.54)	1.88 (1.16-3.03)	0.39 (0.14-1.09)	0.08
LUA + CL + fFN (13/26)	0.70 (0.53-0.84)	76.9 (46.19-94.96)	61.5 (44.62-76.64)	40.0 (28.87-52.27)	88.89 (74.20-95.70)	2.0 (1.22-3.29)	0.37 (0.13-1.04)	0.03*
LUA + MIS (6/17)	0.77 (0.55-0.92)	83.3 (35.88-99.58)	70.6 (44.04-89.69)	50.0 (30.6-69.4)	92.31 (66.14-98.66)	2.83 (1.25-6.43)	0.24 (0.04-1.45)	0.01*
LUA + MIS + CL + fFN (6/17)	0.80 (0.58-0.94)	83.3 (35.88-99.58)	70.6 (44.04-89.69)	50.0 (30.6-69.4)	92.31 (66.14-98.66)	2.83 (1.25-6.43)	0.24 (0.04-1.45)	0.002*

*+LR: positive likelihood ratio, -LR: negative likelihood ratio, AuROC: area under the receiver operating characteristic curve, CL cervical length, fFN: fetal fibronectin, LUA: total lactate, urea and acetate, MIS: magnetic induction spectroscopy NPV: negative predictive value, PPV: positive predictive value, sens: sensitivity, spec: specificity,*significant AuROC with p-values<0.05*

Table 5.16. Comparison of AuROCs of predictive tools for sPTB in AHR women between 20-22 weeks.

AuROC comparisons	*p*-value
CL vs fFN	0.93
CL + fFN vs CL + fFN + LUA	0.08
MIS vs CL + fFN	0.67
MIS vs MIS + LUA	0.90
MIS + LUA vs CL + fFN	0.64
MIS + LUA + CL + fFN versus CL	0.33
MIS + LUA + CL + fFN versus fFN	0.01*
MIS + LUA + CL + fFN versus CL/fFN	0.28

*AuROC: area under the receiver operating characteristic curve, CL: cervical length, fFN: fetal fibronectin, LUA: total lactate, urea and acetate, MIS: magnetic induction spectroscopy, *significant p-values<0.05*

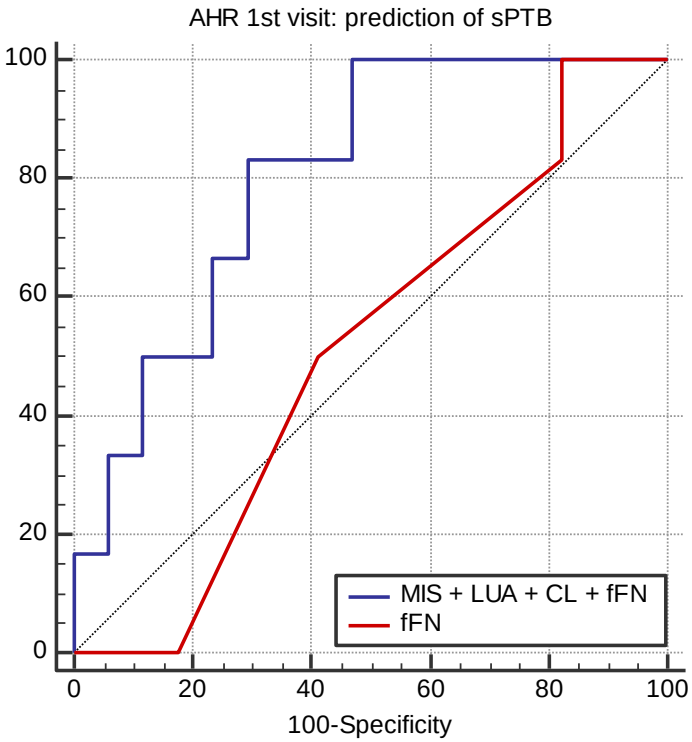

Figure 5.8. Comparison of AuROCs between fFN alone (red line) and when it is combined with CVF metabolites (LUA), MIS and CL (blue line) for prediction of sPTB in AHR women between 20-22 weeks (p=0.01). *AuROC: area under the receiver operating characteristic curve, CL: cervical length, fFN: fetal fibronectin, LUA: total lactate, urea and acetate, MIS: magnetic induction spectroscopy, sPTB: spontaneous preterm birth*

When the predictive capacity for PTB of CVF metabolites was assessed in AHR women attending clinic between 26-28 weeks, none of the metabolites, either singly or combined, predicted PTB better than chance alone (p>0.05; Table 5.17). Even when PTB cases were analysed separately as either PPROM or sPTB, AuROCs were not statistically significant (Table 5.18).

Table 5.17. Predictive capacity of CVF metabolites for PTB (both PPROM and sPTB) in AHR patients between 26-28 weeks

CVF metabolite	PTB		
	AuROC	95% Confidence Interval	*p*-value
Acetate	0.53	0.36-0.70	0.80
Urea	0.59	0.43-0.74	0.36
D-lactate	0.54	0.38-0.69	0.71
L-lactate	0.59	0.42-0.75	0.37
Total lactate	0.59	0.42-0.75	0.38
L-/D- lactate ratio	0.61	0.44-0.76	0.30
LUA	0.63	0.45-0.80	0.27
D-lactate/urea	0.67	0.51-0.81	0.07

AuROC: area under the receiver operating characteristic curve, LUA: total lactate, urea and acetate

Table 5.18. Predictive capacity of CVF metabolites for sPTB and PPROM in AHR participants between 26-28 weeks

CVF metabolite	sPTB		PPROM	
	AuROC (95% CI)	*p*-value	AuROC (95% CI)	*p*-value
Acetate	0.50 (0.32-0.68)	1.00	0.66 (0.45-0.83)	0.55
Urea	0.60 (0.44-0.75)	0.35	0.52 (0.34-0.70)	0.90
D-lactate	0.52 (0.36-0.68)	0.83	0.61 (0.42-0.78)	0.74
L-lactate	0.61 (0.43-0.76)	0.35	#	#
Total lactate	0.60 (0.43-0.76)	0.36	#	#
L-/D-lactate ratio	0.62 (0.44-0.77)	0.27	#	#
LUA	0.62 (0.43-0.79)	0.37	#	#
D-lactate/urea	0.65 (0.49-0.80)	0.14	0.71 (0.52-0.86)	0.43

AuROC: area under the receiver operating characteristic curve, LUA: total lactate, urea and acetate, PPROM: prelabour premature rupture of membranes, sPTB: spontaneous preterm birth, #not enough cases for inferential statistics

Similarly to what was reported for AHR 1st visit, both CL and fFN performed poorly for prediction of sPTB between 26-28 weeks with AuROCs not significantly different from the null hypothesis (*p*-values of 0.92 and 0.81, respectively; Table 5.19).

CL tended to have higher specificity and PPV, and lower sensitivity than fFN. The NPV of fFN was noted to be unusually low which suggested a high rate of false negative results. Combining CL with fFN did not significantly improve the AuROC nor did MIS at 21 kHz (Table 5.19).

When fFN and CL were combined with D-lactate and urea, the AuROC increased from 0.55 (95% 0.39-0.71) to 0.66 (95% 0.49-0.80), but except for a modest improvement in specificity the clinical performance did not significantly improve (p=0.81; Table 5.20). Similarly, MIS predictive capacity did not significantly improve when D-lactate and urea were added (AuROC remained quite static from 0.64 to 0.65, p=0.35, Tables 5.19 and 5.20).

Total lactate, urea and acetate (LUA), which had previously performed well between 20-22 weeks of gestation, was not significantly predictive of sPTB between 26-28 weeks. When combined with fFN and CL, the model tended to produce the largest AuROC (p=0.09) with the highest PPV (Table 5.19), however this increase was still not statistically significant when compared to fFN and CL either singly or combined (Table 5.20).

Table 5.19. Predictive performance of metabolites, CL, fFN and MIS for sPTB in AHR women scanned between 26-28 weeks; *p*-values correspond to comparison with the null hypothesis of an AuROC of 0.5

Technique (+/- cases)	AuROC (95% CI)	Sens (%) (95% CI)	Spec (%) (95% CI)	PPV (%) (95% CI)	NPV (%) (95% CI)	+LR (95% CI)	-LR (95% CI)	*p*-value
CL (10/31)	0.52 (0.35-0.67)	30.0 (6.7-65.2)	51.61 (33.1-69.8)	16.67 (6.76-35.54)	69.57 (57.36-79.52)	0.62 (0.2-1.7)	1.36 (0.8-2.3)	0.89
fFN (10/31)	0.56 (0.40-0.72)	80.0 (44.4-97.5)	3.20 (0.08-16.7)	21.05 (16.26-26.79)	33.33 (4.81-83.19)	0.83 (0.6-1.1)	6.20 (0.6-61.4)	0.50
CL + fFN (10/31)	0.55 (0.39-0.71)	40.0 (12.2-73.8)	83.9 (66.3-94.5)	44.44 (20.95-70.72)	81.25 (71.35-88.03)	2.48 (0.8-7.5)	0.72 (0.4-1.2)	0.64
MIS (6/17)	0.64 (0.41-0.82)	83.33 (35.9-99.6)	52.94 (27.8-77.0)	38.46 (25.19-53.70)	90.0 (58.73-98.27)	1.77 (1- 3.3)	0.31 (0.05-2.0)	0.36
DU (10/30)	0.64 (0.47-0.79)	60.0 (26.5-87.8)	70.0 (50.6-85.3)	40.0 (24.04-58.40)	84.00 (70.35-92.08)	2.00 (0.9-4.2)	0.57 (0.3-1.3)	0.18
DU + CL + fFN (10/30)	0.66 (0.49-0.80)	70.0 (34.8-93.3)	66.7 (47.2-82.7)	41.18 (26.79-57.25)	86.96 (71.45-94.67)	2.10 (1.1-4.0)	0.45 (0.2-1.2)	0.45
DU + MIS (6/17)	0.65 (0.42-0.83)	83.3 (35.88-99.58)	64.7 (38.33-85.79)	45.45 (28.52-63.51)	91.67 (63.98-98.55)	2.36 (1.1-4.9)	0.26 (0.04-1.6)	0.33
DU + MIS + CL + fFN (6/17)	0.61 (0.39-0.80)	83.3 (35.88-99.58)	58.8 (32.92-81.56)	41.67 (26.74-58.30)	90.91 (61.53-98.43)	2.02 (1.0-4.0)	0.28 (0.05-1.8)	0.46
LUA + CL + fFN (8/23)	0.71 (0.52-0.86)	75.0 (34.91-96.81)	78.26 (56.30-92.54)	54.55 (33.40-74.17)	90.0 (72.67-96.82)	3.45 (1.4-8.3)	0.32 (0.09-1.1)	0.09
LUA + MIS (5/16)	0.55 (0.32-0.77)	80.0 (28.36-99.49)	43.7 (19.75-70.12)	30.77 (19.37-45.13)	87.50 (52.67-97.78)	1.42 (0.8-2.6)	0.46 (0.07-2.9)	0.76
LUA + MIS + CL + fFN (5/16)	0.65 (0.41-0.84)	80.0 (28.36-99.49)	68.7 (41.34-88.98)	44.44 (25.51-65.15)	91.67 (64.88-95.50)	2.56 (1.1-6)	0.29 (0.05-1.7)	0.37

+LR: positive likelihood ratio, -LR: negative likelihood ratio, AuROC: area under the receiver operating characteristic curve, CL cervical length, DU: D-lactate and urea, fFN: fetal fibronectin, LUA: total lactate, urea and acetate, MIS: magnetic induction spectroscopy, NPV: negative predictive value, PPV: positive predictive value, sens: sensitivity, spec: specificity.

Table 5.20. Comparison of AuROCs of predictive tools for sPTB in AHR women between 26-28 weeks.

AuROC comparisons	*p*-value
CL vs fFN	0.46
CL + fFN vs CL + fFN + DU	0.81
MIS vs MIS + DU	0.35
CL+ fFN + DU vs CL	1.00
CL+ fFN + DU vs fFN	0.59
CL + fFN vs CL + fFN + LUA	0.95
MIS vs MIS + LUA	0.70
CL + fFN + LUA vs CL	0.64
CL + fFN + LUA vs fFN	0.53

AuROC: area under the receiver operating characteristic curve, CL: cervical length, fFN: fetal fibronectin, DU: D-lactate and urea, LUA: total lactate, urea and acetate, MIS: magnetic induction spectroscopy

5.4.9. **Predictive capacity of CVF metabolites in the SYMP cohort**

The predictive value of CVF metabolites for PTB prediction in the SYMP cohort was also assessed with the construction of AuROCs. Contrary to the findings reported for AHR, when metabolites were individually assessed, L-lactate as well as total lactate and the L-/D-lactate ratio were significantly predictive of PTB ($p<0.01$; Table 5.21). On the other hand, models solely based on D-lactate, urea or acetate were not statistically significant ($p>0.05$).

Further metabolite profiling analysis in SYMP women who went on to have sPTB and PPROM also revealed significant predictive capacity for L-lactate, total lactate and L-/D- lactate (Table 5.22). D-lactate was also found to produce significant AuROCs for women who had sPTB ($p=0.004$) but not for those who experienced PPROM ($p=0.94$; Table 5.22).

AuROCs based on logistic regression were subsequently created to assess the predictive performance of combined CVF metabolites. Similarly to what was reported for AHR women between 20-22 weeks, when total lactate, urea and acetate were combined together (LUA), not only did the model become statistically significant for prediction of all PTB as well as for PPROM and sPTB ($p<0.01$) but it also produced the largest AuROC (Tables 5.21 and 5.22).

Table 5.21. Predictive capacity of CVF metabolites for PTB (both PPROM and sPTB) in SYMP patients

CVF metabolite	PTB		
	AuROC	95% Confidence Interval	*p*-value
Acetate	0.56	0.40-0.72	0.55
Urea	0.58	0.43-0.72	0.34
D-lactate	0.64	0.49-0.78	0.08
L-lactate	0.80	0.62-0.88	<0.01*
Total lactate	0.77	0.62-0.88	<0.01*
L-/D- lactate ratio	0.77	0.62-0.88	<0.01*
LUA	0.87	0.73-0.96	<0.01*

*AuROC: area under the receiver operating characteristic curve, LUA: total lactate, urea and acetate combined,*significant p-values<0.05*

Table 5.22. Predictive capacity of CVF metabolites for sPTB and PPROM in SYMP participants

CVF metabolite	sPTB		PPROM	
	AuROC (95% CI)	*p*-value	AuROC (95% CI)	*p*-value
Acetate	0.54 (0.37-0.71)	0.74	0.61 (0.42-0.77)	0.44
Urea	0.60 (0.57-0.85)	0.30	0.57 (0.42-0.73)	0.55
D-lactate	0.72 (0.57-0.85)	0.004*	0.51 (0.34-0.68)	0.94
L-lactate	0.74 (0.59-0.87)	0.004*	0.79 (0.62-0.91)	0.01*
Total lactate	0.75 (0.59-0.87)	0.004*	0.77 (0.61-0.0.89)	0.01*
L-/D- lactate ratio	0.74 (0.59-0.87)	0.006*	0.79 (0.63-0.91)	0.01*
LUA	0.87 (0.71-0.97)	<0.001*	0.88 (0.71-0.97)	0.01*

*AuROC: area under the receiver operating characteristic curve, LUA: total lactate, urea and acetate, PPROM: prelabour premature rupture of membranes, sPTB; spontaneous preterm birth,*significant p-values<0.05*

The predictive value of CVF metabolites for sPTB was further assessed both as a stand-alone technique and in combination with other screening tools. Even though MIS had been showed to have excellent predictive performance for sPTB within the SYMP cohort (Section 4.4.8), it was purposely omitted in the comparative analysis with CVF metabolites given the relatively small number of index cases (sPTB, n=3).

Similarly to what was reported for AHR women between 20-22 weeks and between 26-28 weeks, CL and fFN alone did not produce statistically significant AuROCs in the SYMP cohort (Table 5.23). When CL and fFN were individually compared with CVF metabolites, LUA was actually significantly better at predicting sPTB than CL (p=0.02, Table 5.24, Figure 5.9). Combining CL and fFN did not significantly improve the AuROC of CL and fFN alone (p=0.11; Table 5.23). On the other hand, when CL and fFN were further combined with CVF metabolites (LUA), the AuROC did not only achieve statistical significance (p<0.01) but it also produced the model with the highest sensitivity and +LR for sPTB prediction (Table 5.23). This model was significantly better at predicting sPTB than CL and fFN singly or combined (p<0.05; Table 5.24; Figure 5.9), despite having lower PPV than CL + fFN combined (100% versus 63.64%, Table 5.23).

Table 5.23. Predictive performance of metabolites, CL, fFN and CVF metabolites for sPTB in SYMP women; *p*-values correspond to comparison with the null hypothesis of an AuROC of 0.5

Technique (+/- cases)	**AuROC (95% CI)**	**Sens (%) (95% CI)**	**Spec (%) (95% CI)**	**PPV (%) (95% CI)**	**NPV (%) (95% CI)**	**+LR (95% CI)**	**-LR (95% CI)**	***p*-value**
CL (8/34)	0.62 (0.46-0.77)	87.5 (46.0-0.77)	47.1 (29.8-64.9)	28.0 (20.5-36.97)	94.12 (71.19-99.04)	1.65 (1.1-2.5)	0.27 (0.04-1.7)	0.23
fFN (8/34)	0.60 (0.44-0.75)	50.0 (15.70-84.30)	88.2 (72.5-96.7)	50.0 (24.01-75.99)	88.24 (78.77-93.81)	4.25 (1.3-13.5)	0.57 (0.3-1.1)	0.53
CL + fFN (8/34)	0.69 (0.53-0.82)	37.5 (8.52-75.51)	100.0 (89.7-100.0)	100.0	87.18 (79.90-92.08)	-	0.63 (0.4-1.1)	0.11
LUA (8/29)	0.87 (0.71-0.96)	100.0 (63.06-100.0)	68.97 (49.2-84.7)	47.06 (34.07-60.46)	100.0	3.22 (1.9-5.5)	0.0	<0.01*
LUA + CL + fFN (8/29)	0.91 (0.77-0.98)	87.5 (47.35-99.68)	86.2 (68.3-96.1)	63.64 (40.44-81.85)	96.15 (79.89-99.37)	6.34 (2.5-16.4)	0.15 (0.02-0.9)	<0.01*

*+LR: positive likelihood ratio, -LR: negative likelihood ratio, AuROC: area under the receiver operating characteristic curve, CL cervical length, DU: D-lactate and urea, fFN: fetal fibronectin, LUA: total lactate, urea and acetate, MIS: magnetic induction spectroscopy, NPV: negative predictive value, PPV: positive predictive value, sens: sensitivity, spec: specificity, *significant p-values<0.05*

Table 5.24. Comparison of AuROCs of predictive tools for sPTB in SYMP women

AuROC comparisons	***p*-value**
CL vs fFN	0.86
LUA vs CL	0.02*
LUA vs fFN	0.12
LUA + CL + fFN vs CL + fFN	0.03*
LUA + CL + fFN versus CL	<0.01*
LUA + CL + fFN versus fFN	0.03*

*AuROC: area under the receiver operating characteristic curve, CL: cervical length, fFN: fetal fibronectin, LUA: total lactate, urea and acetate, *significant p-values<0.05*

(a)

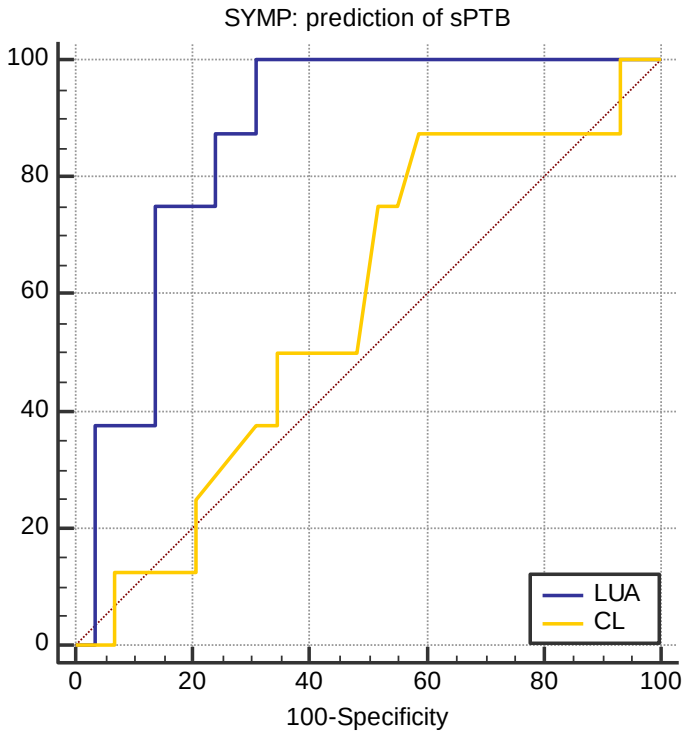

(b)

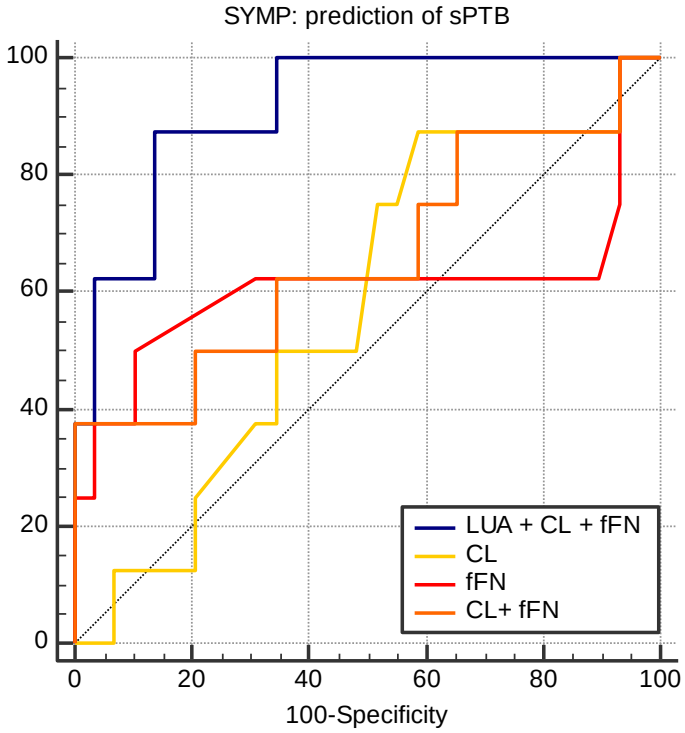

Figure 5.9. AuROC analysis of predictive tools for sPTB in symptomatic women; **(a)** CL versus CVF LUA (p=0.01), and **(b)** CVF LUA + CL + fFN versus CL and fFN singly and/or combined (p<0.05). *AuROC: area under the receiver operating characteristic curve, LUA: total lactate, urea and acetate, CL: cervical length, sPTB: spontaneous preterm birth*

5.4.8. Predictive capacity of CVF metabolites in the SYMP cohort for sPTB within two weeks of presentation

Within the SYMP group (n=49), three women delivered within two weeks of presenting with symptoms of preterm labour, (n=3, 6.12%). CVF metabolite profiling revealed that D- and L-lactate, individually or collectively, were significantly predictive of sPTB in those cases. Furthermore, combining total lactate with acetate (LA) produced the largest AuROC with values over 0.8 ($p<0.01$; Table 5.25).

Table 5.25. Predictive capacity of CVF metabolites for sPTB within two weeks of presentation in SYMP patients.

CVF metabolite	sPTB		
	AuROC	95% Confidence Interval	*p*-value
Acetate	0.66	0.49-0.81	0.33
Urea	0.57	0.42-0.73	0.54
D-lactate	0.79	0.64-0.90	<0.01*
L-lactate	0.71	0.56-0.84	<0.01*
Total lactate	0.73	0.57-0.85	<0.05*
L/D- lactate ratio	0.71	0.55-0.84	<0.05*
LA	0.83	0.67-0.93	<0.01*

*AuROC: area under the receiver operating characteristic curve, LA: total lactate and acetate combined, *significant p-values<0.05*

For this subgroup of SYMP women, neither CL nor fFN produced statistically significant AuROCs (Table 5.26). Even though the AuROC tended to increase when CL and fFN were combined, the model was still not significantly better than the null hypothesis (AuROC=0.5). CVF metabolites, on the other hand, produced a statistically significant model with 100% sensitivity and 62.9% specificity for predicting SYMP who would go on to deliver spontaneously within 14 days of presenting with symptoms. This model was significantly better than CL alone ($p=0.02$; Table 5.27). Furthermore, when CVF metabolites were combined with CL and fFN, the resulting model had the highest clinical performance, significantly superior to that of CL alone and capable of confidently identifying all the index cases, ($p<0.01$; Table 5.27).

Table 5.26. Predictive performance of metabolites, CL, fFN and CVF metabolites for sPTB within two weeks of presentation in SYMP women; *p*-values correspond to comparison with the null hypothesis of an AuROC of 0.5

Technique (+/- cases)	**AuROC (95% CI)**	**Sens (%) (95% CI)**	**Spec (%) (95% CI)**	**PPV (%) (95% CI)**	**NPV (%) (95% CI)**	**+LR (95% CI)**	**-LR (95% CI)**	***p*-value**
CL (3/41)	0.55 (0.4-0.7)	100.0 (29.2-100.0)	48.8 (32.9-64.9)	12.5 (9.58-16.15)	100.0	1.95 (1.4-2.6)	0.00	0.53
fFN (3/41)	0.70 (0.55-0.83)	66.7 (9.4-99.2)	100.0 (91.4-100.0)	100.0	97.62 (89.22-99.51)	-	0.33 (0.07-1.7)	0.49
CL + fFN (3/41)	0.81 (0.67-0.91)	66.7 (9.4-99.2)	100.0 (91.4-100.0)	100.0	97.62 (89.22-99.51)	-	0.33 (0.07-1.7)	0.1
LA (3/35)	0.83 (0.67-0.93)	100.0 (29.2-100.0)	62.9 (44.9-78.5)	18.75 (13.4-26.20)	100.0	2.69 (1.7-4.1)	0.00	<0.01*
LA + CL + fFN (3/35)	1.00 (0.91-1.00)	100.0 (29.2-100.0)	100.0 (91.4-100.0)	100.0	100.0	-	0.00	<0.01*

*+LR: positive likelihood ratio, -LR: negative likelihood ratio, AuROC: area under the receiver operating characteristic curve, CL cervical length, DU: D-lactate and urea, fFN: fetal fibronectin, LA: total lactate and acetate, NPV: negative predictive value, PPV: positive predictive value, sens: sensitivity, spec: specificity,*significant p-values<0.05*

Table 5.27. Comparison of AuROCs of predictive tools for sPTB within two weeks of presentation in SYMP women

AuROC comparisons	***p*-value**
CL vs fFN	0.49
LA vs CL	0.02*
LA vs fFN	0.76
LA + CL + fFN vs CL + fFN	0.32
LA + CL + fFN versus CL	<0.01*
LA + CL + fFN versus fFN	0.32

*AuROC: Area under the receiver operating characteristic curve, CL: cervical length, fFN: fetal fibronectin, LA: total lactate and acetate, *significant p-values<0.05*

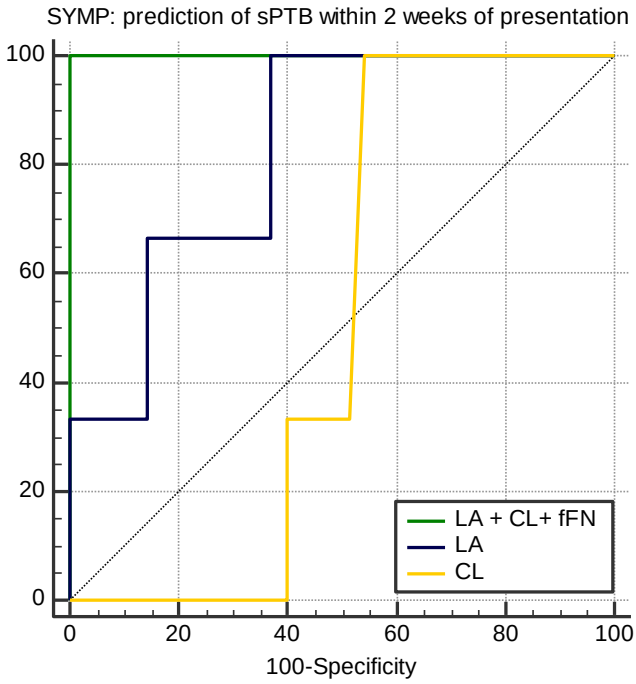

Figure 5.10. AuROC analysis of predictive tools for sPTB within two weeks of presentation in symptomatic women. *AuROC: area under the receiver operating characteristic curve, LA: total lactate and acetate, CL: cervical length, sPTB: spontaneous preterm birth*

5.5. Discussion and interpretation

5.5.1. **Main findings**

In this chapter, I assessed whether the differential CVF metabolite concentration in the AHR and SYMP cohorts within the MIS study hold any predictive value for sPTB both as a stand-alone technique and when used in conjunction with current clinical screening tools. Additionally, I explored whether vaginal infections and/or colonisations of confirmed clinical significance had distinctive CVF metabolic signatures which could potentially facilitate identification, management and response to treatment.

The comparative analysis of CVF metabolites based on birth outcomes demonstrated that SYMP women who had a sPTB or experienced PPROM had significantly lower concentration of total lactate, in particular L-lactate, and lower L-/D-lactate ratio than their term counterparts (<0.001). Previous studies have shown that vaginal communities dominated by *Streptococcus*, *Gardnerella* and *Enterococcus* as well as certain species of *Lactobacillus* had significantly lower median of L-lactate concentration than their eubiotic counterparts (Witkin et al., 2013b, Aldunate et al., 2015). A recent pilot study by Stafford et al. (2017) reported that *L. jensenii*-dominated vaginal microbiotas, for example, had significantly lower CVF lactate and correlated with higher risk of PTB when compared to those with predominance of *L. crispatus* and *L. gasseri* ($p<0.01$).

There is a large body of *in vitro* evidence to support that lactic acid produced by the vaginal microbiota has an important antimicrobial and antiviral role by acidifying the vaginal milieu, enhancing bacteriocins and hydrogen peroxide, and inhibiting the binding of opportunistic bacteria to epithelial cells by secreting anti-adhesive molecules (Linhares et al., 2011, Tachedjian et al., 2017, Stafford et al., 2017, Amabebe and Anumba, 2018). Research also suggests that vaginal lactate may be involved in immunomodulating the symbiotic relationship between the host and the commensal microbial community which if altered may contribute to ascending genital tract infections (Al-Mushrif et al., 2000, Witkin et al., 2013a, Aldunate et al., 2015). Based on this assumption, lactate supplements have been explored as an alternative to manage vaginal dysbiosis by helping re-establish the lactobacilli flora and counteracting the release of pro-inflammatory cytokines induced by BV-secreted SCFAs (Andersch et al., 1990, Mirmonsef et al., 2011, Verstraelen et al., 2016). Oral and vaginal administration of *Lactobacillus rhamnosus GR-1/ reuteri RC-14*) have been shown to reduce the recurrence of bacterial vaginosis and promote an acidic vaginal pH (Bodean et al., 2013, Romero et al., 2014b, Dhanasekar et al., 2019). If enzyme-based spectrophotometric quantification of CVF lactate was developed into a point-of-care diagnostic test

for dysbiosis, interventions capable of restoring the dominance of lactobacilli such as maternal probiotic supplementation could be better targeted (Witkin et al., 2019).

In addition to changes in CVF lactate concentrations, potentially PTB-related perturbations to the vaginal microbiota may manifest as an increase in SCFA concentration (Section 1.4.1). MIS women who tested positive for BV had higher acetate concentrations when compared to patients with negative or other microbiology swab results ($p<0.05$). This association further supports the measurement of SCFAs as surrogate biomarkers of vaginal dysbiosis and increased susceptibility to PTB (Aldunate et al., 2015).

In our study, all patients who were diagnosed with BV were actively treated with antibiotic therapy which is likely to have altered their delivery outcome (Hillier et al., 1995a, Manns-James, 2011, Shimaoka et al., 2019). For this reason, swabs which tested positive for BV or *Ureaplasma* spp were excluded from the predictive analysis of CVF. *In vivo* work in untreated cohorts may prove challenging for ethical reasons but further *in vitro* work and observational studies may unravel the potential causality between BV and PTB.

Consistent with previous studies, a correlation was found between total lactate concentration and pH ($p<0.05$; Amabebe et al., 2016a, Wood, 2018, O'Hanlon et al., 2019). Furthermore, women who tested positive for BV tended to have higher pH than any other participant with a median value of five in keeping with Amsel diagnostic criteria for BV (Mohammadzadeh et al., 2014).

Within the AHR cohorts, CVF metabolites did not significantly differ between delivery outcomes. These findings were consistent with previous studies by Thomas et al. (2015), Amabebe et al. (2016b) and Wood (2018).

For AHR 1st visit (20-22 weeks), predictive models for PTB based only on individual metabolites, or CL and fFN did not have AuROCs different from the null hypothesis. Nonetheless, when total lactate, urea and acetate (LUA) were combined, the resulting model significantly improved the prediction for all PTB ($p=0.03$). For prediction of sPTB in particular, however, the largest AuROC was obtained when CVF LUA was further combined with fFN, CL and MIS which produced an AuROC significantly larger than that for fFN alone ($p<0.01$; Figure 5.8). These findings were consistent with previous studies which also reported that the addition of CVF metabolite profiling to current screening tools such as CL and fFN might have a synergistic effect on the predictive capacity of the models for sPTB (Amabebe et al., 2016a, Wood, 2018)

For AHR 2nd visit (26-28 weeks), none of the individual or combined CVF metabolites predicted sPTB. CL and fFN also showed poor performance for prediction of sPTB. Similarly to what was reported for AHR 1st visit, the largest AuROC was identified when CVF metabolites were

combined with CL and fFN but the difference was not statistically significant (p=0.09) which may be partly due to the reduced sample size (type II error).

For SYMP women, models based on individual total lactate or L-lactate were capable of accurately predicting sPTB and PPROM with a mean AuROC of 0.80 (95% CI: 0.62-0.88; p<0.01). When CVF lactate was further combined with urea and acetate (LUA), the AuROC improved from 0.80 to 0.87 and showed better performance than CL alone (p<0.01; Table 5.21). The best clinical performance, however, was achieved when CVF metabolites were further combined with CL and fFN (Table 5.23). CVF metabolites were also significantly better at predicting sPTB in SYMP women within two weeks of presentation when compared to CL alone (p=0.02; Table 5.27). The combination of CVF total lactate and acetate with fFN and CL produced a predictive model with excellent performance capable of accurately identifying all index cases (AuROC=1.00, Table 5.26).

Overall, the use of current screening techniques for sPTB, namely CL and fFN, were sub-optimal both in the AHR and SYMP cohorts. Combining CVF metabolites with CL and fFN improved the accuracy and clinical performance of the models for sPTB prediction (p<0.05). This finding further supports the development of a multiple bed-side CVF biomarker test to accommodate for the numerous pathways implicated in sPTB (Goldenberg et al., 2001, Heng et al., 2015b).

5.5.2. **Strengths**

The experiments were nested within the larger MIS study (Chapter 4) which enabled to assess the prognostic capacity of CVF metabolites not just as a stand-alone technique but also combined with current clinical and research techniques (CL, fFN and MIS). CVF metabolites were shown to significantly enhance the predictive value of CL and fFN which supports their clinical application as a point-of-care testing for prediction of sPTB. Furthermore, as previously shown by Amabebe et al. (2016a) and Wood (2018), the technique and protocol employed in this study was relatively easy to perform and fast enough to be transferable to the clinical setting pending the development of a portable device. Additionally, the automated quantification of CVF metabolites by ChemWell® and the use of duplicates had the advantage of reducing human error thus increasing the measurements accuracy (Fernie et al., 2011).

5.5.3. **Limitations**

Limitations in this study included the small sample size in some groups, a lack of formal assessment of the vaginal bacterial taxa, a methodological error when measuring vaginal pH and the exclusion of asymptomatic low-risk women for PTB.

CVF metabolite experiments were nested within the larger MIS study which had not been originally designed for the outcomes proposed in this chapter. As a result, the sample size is likely to have not been sufficiently powered to attain statistical significance and/or precision for certain delivery outcomes (Ngo et al., 2017). Larger clinical studies would therefore allow drawing conclusion about the clinical use of CVF metabolites.

CVF samples were assessed by the Clinical Microbiology Department at the Royal Hallamshire Hospital only for vaginal colonisation and/or infections with recognised clinical significance. However, there is growing evidence to support that some subclinical infections and dysbiosis which are not routinely tested for may also be implicated in the pathogenesis of PTB (Section 1.5.1). An in-depth analysis of the vaginal microbial composition including identification and quantification of lactobacilli community state types and Nugent score for confirmed cases of BV would enable a better understanding of the relationship between vaginal microbiota and CVF metabolite profile (Ravel et al., 2011, Stafford et al., 2017, van der Veer et al., 2019).

High-vaginal swabs, except for those which tested positive for BV and *Ureaplasma Urealyticum*, had a median pH between 4.0 and 4.5. These values were within the normal range but slightly higher than expected (Boskey et al., 1999, Hemalatha et al., 2013). For example, healthy Lactobacillus-dominated vaginal microbiotas are known to have a relatively lower mean pH of 3.5 ± 0.2 when measured in ideal conditions namely within the hypoxic and hypercapnic vaginal environment (O'Hanlon et al., 2013). However, the exposure of CVF to air is known to skew pH measurements upwards as certain *Lactobacillus* strains consume rather than produce lactic acid in aerobic conditions (Murphy et al., 1985). Therefore, even though in this study the vaginal pH was measured from the tip of the speculum immediately after it was withdrawn from the vagina, exposure to air might have contributed to higher pH. Because all samples were taken in the same way, deviations in pH measurements are likely to be similar in magnitude and direction. Therefore, the expected relative differences are unlikely to be affected. Women with confirmed BV, for example, still had higher median pH values than their negative counterparts (pH 5.0 versus 4.4). Previous studies had already questioned the accuracy of commercial pH papers for evaluating the vaginal environment (Heinze et al., 1989, Khandalavala and Van Geem, 1999) favouring the use of

more expensive devices such as the hand-held digital pH meter and micro-electrode (De Los Santos and Zuniga, 2004, O'Hanlon et al., 2013).

Because CVF experiments were nested within the MIS study, only CVF from asymptomatic women deemed at high risk and symptomatic patients presenting in threatened preterm labour was assessed. However, the majority of PTB still occur in low-risk women for whom there is no appropriate screening test. As a result, larger clinical studies could assess whether targeted CVF metabolomics techniques are effective for PTB prediction in the low-risk population (Newnham et al., 2017).

5.5.4. **Future research**

CVF metabolite profiling appears to enhance the predictive capacity of current screening techniques for PTB both in high-risk and symptomatic women with singleton pregnancies. These preliminary findings are promising and call for larger clinical trials with higher statistical power that include low-risk asymptomatic populations as well as women with multiple pregnancies for whom there is currently no effective way of predicting the risk of PTB.

Furthermore, prospective metabolomics studies should be complemented with formal analysis of vaginal bacterial, fungal and viral taxa to determine the predominant species as well as any changes in particular microorganisms within the total microbiota which may increase susceptibility to PTB (Nunn and Forney, 2016, Stafford et al., 2017). Differential CVF metabolite abundance within and between ethnic groups should also be addressed in future research as it may help better stratify PTB risk in women who have less protective vaginal environments (Ravel et al., 2011, Pendharkar et al., 2013).

Finally, the measurement of inflammatory cytokines within CVF samples should also be considered in future studies as it may help better understand how certain products of bacterial metabolism such as SCFA may impact on the host immune system (Amabebe et al., 2018).

Chapter 6

General conclusions

Accurate prediction of PTB remains an obstetric challenge. Current predictive techniques are suboptimal partly because they oversimplify the multi-causality of PTB, and partly because they are not cost-effective on a global scale (Goldenberg et al., 2001, Moutquin, 2003, Suff et al., 2019). As a result, there is a need for novel and more practical technology which can account for PTB multifactorial nature and help better stratify the risk for PTB. Earlier and more accurate identification of women at higher risk of delivering prematurely would enable to target interventions more adequately which in turn would improve neonatal outcomes (Behrman and Butler, 2007). This unmet medical need was the impetus for these studies in which I tested the feasibility of new techniques which could improve the overall predictive capacity for PTB.

I purposely explored techniques which had the potential to be integrated together to simultaneously analyse multiple pathways associated with PTB from a joint biochemical, biomechanical and bioelectrical perspective (Feltovich et al., 2012, Heng et al., 2015a). All the techniques proposed in this thesis, namely Raman spectroscopy (RS), Polarisation-sensitive optical coherence tomography (PS-OCT), Magnetic induction spectroscopy (MIS) and Enzyme-based spectrophotometry, rely on the interaction between electromagnetic radiation and matter (Halter et al., 2007, Matcher, 2009, Zumdahl and Zumdahl, 2013, Talari et al., 2015). RS, PS-OCT and MIS do not involve destruction or modification of the sample, and are particularly suited for *in vivo* use (Narice et al., 2018). These technologies, which operate on minimal light or electricity, already exist or have the potential to be developed into endoscopic probes or bed-side portable devices adequate for point-of-care testing. Their relative ease of use, low costs, and high reproducibility and acceptability are some of the attractive features which position these new technologies as potential cost-effective alternatives to the more subjective cervical length measurement, expensive fFN assay, cumbersome mass spectrometry or ^{1}H-NMR.

At a biochemical level, I first examined the cervicovaginal fluid (CVF) in asymptomatic high-risk women (AHR) and in women with symptoms of preterm labour (SYMP) using untargeted spectroscopic techniques (Chapter 2). To the best of my knowledge, this is the first time Raman spectroscopy has been tested on pregnant women CVF. I deliberately examined CVF samples from AHR and SYMP women because there is already a surveillance pathway in the NHS for the two cohorts. Therefore, selecting these patients enabled to compare the predictive performance of the proposed techniques against the clinically validated CL and fFN. Additionally, because PTB incidence is significantly higher in AHR and SYMP women than in asymptomatic low-risk women, it was possible to achieve enough index cases to run statistical inferential tests within the time and resources available.

RS was capable of identifying differences in the CVF spectra based on the time to delivery and between delivery outcomes both within AHR and SYMP cohorts. We showed that various peaks of Raman spectra, mainly those corresponding to protein configuration, fatty acids, lipid peroxidation and collagen metabolism, gradually changed the closer to birth, and significantly differed based on birth outcomes. Vargis et al. (2012) had previously reported on similar findings when probing the vibrational modes of cervical tissue in gravid murine models, and had suggested that these changes could reflect collagen disorganisation and birth-related inflammation at a molecular level. RS analysis of CVF could provide a more cost-effective and acceptable alternative to indirectly assess cervical remodelling at a microstructural level, compared to the more invasive and potentially less acceptable transvaginal RS, which is currently being translated into a clinical working probe (O'Brien et al., 2019).

Upon the chemical differences identified based on the time to delivery and birth outcomes, predictive models for PTB were constructed for each cohort. Subsequent comparative analyses against CL and fFN showed that RS had higher sensitivity and NPV for prediction of PTB than current screening techniques. We hypothesised that the better performance of RS over TVU CL for prediction of sPTB could be due to its ability to identify cervical remodelling from earlier stages, whereas TVU CL sensitivity is limited to macroscopic changes in the cervical anatomy which may occur later in pregnancy when birth is already imminent. In SYMP patient, RS had a better PPV but relatively similar NPV than fFN which may be due to RS ability to measure fFN as evidenced by the increasing peaks in amide I closer to birth (section 2.5.1). However, and contrary to other -omics techniques, RS does not only focus on fibronectin, or one specific metabolite or nucleic acid at a time, but rather provides an overall chemical signature of the CVF. This may explain why in our study RS performed better than single biomarker-based techniques such as TVU CL or qfFN.

Based on these preliminary findings and building on previous work by Aldunate et al. (2015), Amabebe et al. (2016b) and Wood (2018), the differential CVF metabolite abundance of AHR and SYMP women within the ECCLIPPx II study was further assessed with enzyme-based spectrophotometry, a targeted spectroscopic technique (Chapter 5). Specific metabolites, which are thought to reflect dysbiotic changes in the vaginal microbiota, were measured including urea, acetate, and D- and L-lactate (Amabebe et al., 2016b). Women with confirmed bacterial vaginosis infections (BV) had higher amount of CVF acetate amount and pH compared to those with a negative vaginal swab or other microbial infection or colonisation, and SYMP participants who delivered prematurely had significantly lower concentration of CVF lactate (section 5.5.1). These observations suggest that enzyme-based spectrophotometric measurement of acetate and lactate may have the potential to be developed into a point-of-contact diagnostic test for vaginal dysbiosis

which would enable better targeting and response evaluation of delivery-modifying interventions such as antimicrobial and probiotic therapy without the need to perform more time-consuming and costly techniques such as microbiology cultures (Nelson et al., 2009, Yang et al., 2015). Furthermore, the quantitative analysis of combined rather than single CVF lactate, urea and acetate was shown to enhance the accuracy of CL and fFN for prediction of sPTB. These results highlighted two interesting points: firstly, that shifts in the vaginal microbiota which are associated with increased susceptibility to PTB are likely to leave traceable biochemical signatures in the CVF (O'Hanlon et al., 2013, Stafford et al., 2017), and secondly, that the development of a multiple-marker test for CVF rather than the assessment of one single metabolite may prove more useful for prediction of sPTB (Goldenberg et al., 2001, Amabebe et al., 2016b).

In addition to analysing CVF in pregnant women, I also assessed two novel spectroscopic techniques, PS-OCT and MIS, which have the potential to assess *in vivo* cervical remodelling from a biomechanical and bioelectrical perspective respectively. The motivation was that CVF analysis alone may not be enough to accurately predict sPTB. While RS spectral analysis, enzyme-based spectrophotometric measurements of metabolites and/or ELISA detection and quantification of fibronectin in the CVF may be capable of better identifying infection and inflammation-related PTB, it may fail to recognise other underlying mechanisms linked to preterm labour such as uterine overdistension or cervical insufficiency (Section 1.2). I therefore hypothesised that regardless of whatever triggers PTB, the cervix has to efface, soften and dilate for birth to occur, and changes in collagen alignment as well as an increase in cervical elasticity and variations in cellular organisation and density (and thus hydration) may play a key role (Read et al., 2007, Timmons et al., 2010, Feltovich et al., 2012, Mahendroo, 2012).

In collaboration with the Department of Materials and Engineering at the University of Sheffield, I designed and conducted a pilot study to explore whether PS-OCT was capable of assessing the preferential arrangement of collagen fibres in the *ex vivo* human cervix (Chapter 3; Matcher, 2009). Twenty cervical cross-sections were systematically scanned with an in-house PS-OCT prototype and later on dissected and analysed with conventional histopathology techniques to correlate findings. PS-OCT could confidently characterise the distinctive pattern of collagen organisation previously reported with X-ray diffraction in non-pregnant women by Aspden (1988). Furthermore, PS-OCT findings significantly correlated with histology (Li et al., 2019), further supporting the potential of PS-OCT for *in vivo* assessment of cervical collagen alignment pending the development of an endoscopic probe. Interestingly, collagen fibres in the middle region of the cervix were found to be more circumferentially aligned in older women, a finding which is supported by previous studies employing SHG (Narice et al., 2016). As hypothesised in section

3.5.1, the change in collagen arrangement seen in elderly women may reflect a physiological adaptation of the tensile response of the cervix to age. In premenopausal women, the disorganised cervical collagen increases tissue compliance which is needed for cervical remodelling during the regular menstrual period and parturition. However, this compliance is no longer required after menopause during which the higher incidence of pelvic organ prolapse and lower level of oestrogen are thought to lead to a re-arrangement of the cervical collagen fibres (Nallasamy et al., 2017b, Rosado-Mendez et al., 2018).

The microstructure of the cervix during pregnancy was further assessed *in vitro* and *in vivo* using a new technology, MIS, which is capable of accurately and consistently measuring cervical electrical properties (Chapter 4). Contrary to Electrical impedance spectroscopy (EIS), MIS does not require physical contact between the probe and the sample, thereby minimising the influence of pressure and probe positioning on measurement accuracy and repeatability (Anumba et al., 2011, Wang et al., 2017, Anumba et al., 2018). In the ECCLIPPx II study, mid-trimester cervical transresistance had enough contrast within the AHR and SYMP cohorts to differentiate between women who went on to deliver prematurely from those who had a term delivery. In women who delivered prematurely, average transresistance of the cervix (and thus conductivity) was consistently lower than in women who delivered at term. We hypothesised that the decrease in cervical conductivity could be due to a more disorganised collagen arrangement in the stroma as well as an increase in the cellular density of the extracellular matrix prior to sPTB (Halter et al., 2007, Timmons et al., 2009, Timmons et al., 2010). Despite the relatively small sample size available, MIS was found to significantly improve sPTB prediction even when CL and fFN did not. Similarly to fFN, MIS had high NPV and relatively low PPV (Section 4.4.10), which suggests that MIS behaves more like a "rule-out" than a "rule-in" predictive technique for sPTB, and that not all increases in cervical transresistance are likely to translate into premature labour. The next logical step to further assess the clinical utility of MIS would be to improve inter-device reliability so that larger and adequately-powered trials can be conducted to confirm the predictive value of MIS in the clinical setting.

In conclusion, I have conducted a series of pilot studies to explore novel and potentially non-invasive spectroscopic and light-based approaches which may hold predictive value for PTB in the clinical setting. These small-scale tests showed that (1) RS can accurately detect key molecular differences in the CVF of pregnant women based on the time to delivery and birth outcome, (2) specific quantification of some of these metabolic differences in CVF using enzyme-based spectrophotometry may enhance the predictive capacity for sPTB of fFN and CL when combined, and may better reflect the presence of underlying vaginal dysbiosis, (3) PS-OCT is capable of

assessing the distinctive arrangement of collagen fibers in the *in vitro* human cervix which is thought to be lost prior to birth, and (4) mid-trimester cervical transresistance measured by MIS may accurately predict sPTB. Even though these pilot studies have shown that the spectroscopic techniques here proposed are feasible and may be capable of providing a better understanding of the molecular processes that underlie the pathogenesis of PTB such as inflammation and infection (RS/ enzyme-based spectrophotometry), and collagen disorganisation and cervical hydration (RS/PS-OCT/ MIS), larger population studies are required to expand these findings and assess their clinical applicability for PTB prediction (Feltovich et al., 2012, Horne et al., 2018).

Future research may benefit from including asymptomatic low-risk women and patients with multiple pregnancies for whom there is currently no predictive tool available for PTB. Specifically for RS, it would be worth studying how the molecular CVF signature naturally changes as pregnancy progresses by conducting longitudinal prospective studies, and complementing the finding of potential novel biomarkers of cervical remodeling with targeted –omics techniques such as GC-/LC-MS and ^{1}H-NMR. This improved knowledge about how CVF changes prior to labour could allow us to understand the processes leading up to birth better and help identify signs that predict more accurately when labour and preterm labour might start. As RS is likely to detect inflammatory and infection-related cervical remodeling changes at early stages (sections 2.5.1 and 2.5.4), CVF molecular signatures should also be correlated with specific and non-specific placental markers of infection and inflammation such as histological evidence of chorioamnionitis, funisitis and villitis (Faye-Petersen, 2008), and microbiological analysis of CVF.

A similar approach may be needed for future CVF enzyme-based spectrophotometric studies in pregnancy as formal assessment of vaginal microbiota will help better characterise the metabolic signature of vaginal dysbiosis likely to be implicated in PTB, and further guide and evaluate response to antimicrobial and probiotic treatment. High-vaginal swabs, for example, could be analysed before and after administration of antibiotics for vaginal infections, and metabolite concentrations could be correlated with the host immune response via quantification of CVF cytokines (Section 5.5.4; Stafford et al., 2017).

PS-OCT has been shown to non-destructively measure cervical collagen arrangement *in vitro*. Given the close relationship between collagen structure and functionality, future studies may further benefit from correlating PS-OCT findings with mechanical tests such as dynamic shear analysis to understand how changes in collagen alignment may affect tissue stiffness and compliance prior to birth and PTB (Section 3.5.4). As described in Section 1.5.2, there have already been attempts to improve the predictive value for PTB by combining cervical optical imaging techniques such TVU CL with biomechanical techniques like strain elastography. Pending the development of an *in vivo*

transvaginal probe, PS-OCT may also be suitable for a combined approach with elastography or cervical consistency index techniques (Parra-Saavedra et al., 2011, Feltovich et al., 2012, Swiatkowska-Freund and Preis, 2017).

The ECCLIPPx II study has allowed the development of a clinical grade device capable of reliably interrogating the cervix for transresistance measurements with potential predictive value for PTB. The pilot data, though limited in size, has showed promise for clinical use but it has also identified a series of technical issues and areas for improvement which need to be addressed in future device iterations before MHRA approval for a multicentre trial is sought. Better electrical shielding is likely to improve inter-device reliability and allow changes in the probe geometry so that it can be used without speculum thus increasing acceptability.

References

ABBOTT, D. S., RADFORD, S. K., SEED, P. T., TRIBE, R. M. & SHENNAN, A. H. 2013. Evaluation of a quantitative fetal fibronectin test for spontaneous preterm birth in symptomatic women. *American Journal of Obstetrics & Gynecology,* 208**,** 122.e1-122.e6.

ABDEL-ALEEM, H., SHAABAN, O. M. & ABDEL-ALEEM, M. A. 2013. Cervical pessary for preventing preterm birth. *Cochrane Database Syst Rev***,** Cd007873.

ÅBERG, P., NICANDER, I., HOLMGREN, U., GELADI, P. & OLLMAR, S. 2003. Assessment of skin lesions and skin cancer using simple electrical impedance indices. *Skin Research and Technology,* 9**,** 257-261.

ABRAMOWICZ, J. S., EVANS, D. H., FOWLKES, J. B., MARŠAL, K. & TERHAAR, G. 2017. Guidelines for Cleaning Transvaginal Ultrasound Transducers Between Patients. *Ultrasound in Medicine and Biology,* 43**,** 1076-1079.

ACOG 2001. ACOG Practice Bulletin No. 31: Assessment of Risk Factors for Preterm Birth. *Obstetrics & Gynecology,* 98**,** 709-716.

ADAMS WALDORF, K. M., SINGH, N., MOHAN, A. R., YOUNG, R. C., NGO, L., DAS, A., TSAI, J., BANSAL, A., PAOLELLA, L., HERBERT, B. R., SOORANNA, S. R., GOUGH, G. M., ASTLEY, C., VOGEL, K., BALDESSARI, A. E., BAMMLER, T. K., MACDONALD, J., GRAVETT, M. G., RAJAGOPAL, L. & JOHNSON, M. R. 2015. Uterine overdistention induces preterm labor mediated by inflammation: observations in pregnant women and nonhuman primates. *American journal of obstetrics and gynecology,* 213**,** 830.e1-830.e19.

AGRAWAL, V. & HIRSCH, E. 2012. Intrauterine infection and preterm labor. *Semin Fetal Neonatal Med,* 17**,** 12-9.

AKINS, M. L., LUBY-PHELPS, K. & MAHENDROO, M. 2010. Second harmonic generation imaging as a potential tool for staging pregnancy and predicting preterm birth. *J Biomed Opt,* 15**,** 026020.

AKOBENG, A. K. 2007. Understanding diagnostic tests 3: Receiver operating characteristic curves. *Acta Paediatr,* 96**,** 644-7.

AL-MUJAINI, A., WALI, U. K. & AZEEM, S. 2013. Optical coherence tomography: clinical applications in medical practice. *Oman medical journal,* 28**,** 86-91.

AL-MUSHRIF, S., ELEY, A. & JONES, B. M. 2000. Inhibition of chemotaxis by organic acids from anaerobes may prevent a purulent response in bacterial vaginosis. *J Med Microbiol,* 49**,** 1023-30.

AL-QAISI, M. K. & AKKIN, T. 2010. Swept-source polarization-sensitive optical coherence tomography based on polarization-maintaining fiber. *Optics Express,* 18**,** 3392-3403.

ALDUNATE, M., SRBINOVSKI, D., HEARPS, A. C., LATHAM, C. F., RAMSLAND, P. A., GUGASYAN, R., CONE, R. A. & TACHEDJIAN, G. 2015. Antimicrobial and immune modulatory effects of lactic acid and short chain fatty acids produced by vaginal microbiota associated with eubiosis and bacterial vaginosis. *Front Physiol,* 6**,** 164.

ALFIREVIC, Z., STAMPALIJA, T. & MEDLEY, N. 2017. Cervical stitch (cerclage) for preventing preterm birth in singleton pregnancy. *Cochrane Database of Systematic Reviews*.

ALI, N., GIRNUS, S., ROSCH, P., POPP, J. & BOCKLITZ, T. 2018. Sample-Size Planning for Multivariate Data: A Raman-Spectroscopy-Based Example. *Anal Chem,* 90**,** 12485-12492.

ALLEN-VERCOE, E. 2013. Bringing the gut microbiota into focus through microbial culture: recent progress and future perspective. *Curr Opin Microbiol,* 16**,** 625-9.

AMABEBE, E. & ANUMBA, D. 2017. A midtrimester combination of cervicovaginal fluid glutamate, acetate, and D ‐ lactate identified asymptomatic low ‐ risk women destined to deliver preterm: a prospective cohort study. *BJOG: An International Journal of Obstetrics & Gynaecology,* 126**,** 115-134.

AMABEBE, E. & ANUMBA, D. O. C. 2018. The Vaginal Microenvironment: The Physiologic Role of Lactobacilli. *Frontiers in Medicine,* 5.

AMABEBE, E., CHAPMAN, D. R., STERN, V. L., STAFFORD, G. & ANUMBA, D. O. C. 2018. Mid-gestational changes in cervicovaginal fluid cytokine levels in asymptomatic pregnant women are predictive markers of inflammation-associated spontaneous preterm birth. *Journal of reproductive immunology,* 126**,** 1-10.

AMABEBE, E., REYNOLDS, S., HE, X., WOOD, R., STERN, V. & ANUMBA, D. O. C. 2019. Infection/inflammation-associated preterm delivery within 14 days of presentation with symptoms of preterm labour: A multivariate predictive model. *PLOS ONE,* 14**,** e0222455.

AMABEBE, E., REYNOLDS, S., STERN, V., STAFFORD, G., PALEY, M. & ANUMBA, D. 2017. Prognostic utility of cervicovaginal fluid acetate-glutamate ratio for risk of preterm delivery within two weeks of presentation with symptoms of threatened preterm labour. *ISMRM 2017*.

AMABEBE, E., REYNOLDS, S., STERN, V., STAFFORD, G., PALEY, M. & ANUMBA, D. O. C. 2016a. Cervicovaginal Fluid Acetate: A Metabolite Marker of Preterm Birth in Symptomatic Pregnant Women. *Frontiers in medicine,* 3**,** 48-48.

AMABEBE, E., REYNOLDS, S., STERN, V. L., PARKER, J. L., STAFFORD, G. P., PALEY, M. N. & ANUMBA, D. O. C. 2016b. Identifying metabolite markers for preterm birth in cervicovaginal fluid by magnetic resonance spectroscopy. *Metabolomics : Official journal of the Metabolomic Society,* 12**,** 67-67.

ANDERSCH, B., LINDELL, D., DAHLEN, I. & BRANDBERG, A. 1990. Bacterial vaginosis and the effect of intermittent prophylactic treatment with an acid lactate gel. *Gynecol Obstet Invest,* 30**,** 114-9.

ANDRADE, K. C., BORTOLETTO, T. G., ALMEIDA, C. M., DANIEL, R. A., AVO, H., PACAGNELLA, R. C. & CECATTI, J. G. 2017. Reference Ranges for Ultrasonographic Measurements of the Uterine Cervix in Low-Risk Pregnant Women. *Revista Brasileira de Ginecologia e Obstetrícia,* 39**,** 443-452.

ANUMBA, D., STERN, V., HEALEY, T., LANG, Z.-Q. & BROWN, B. 2018. Cervical electrical impedance spectroscopy predicts preterm delivery in asymptomatic women - the ECCLIPPx (TM) studies. *BJOG: An International Journal of Obstetrics & Gynaecology,* 125**,** 12-14.

ANUMBA, D. O., JOKHI, R. P., GHULE, V., HEALEY, J. & BROWN, B. H. 2011. Cervical Electrical Impedance Spectroscopy May Predict Preterm Delivery in Women at Risk. *REPROD SCI,* 18**,** 301A-301A.

ARNTZEN, K. J., KJOLLESDAL, A. M., HALGUNSET, J., VATTEN, L. & AUSTGULEN, R. 1998. TNF, IL-1, IL-6, IL-8 and soluble TNF receptors in relation to chorioamnionitis and premature labor. *J Perinat Med,* 26**,** 17-26.

ASPDEN, R. M. 1988. Collagen Organisation in the Cervix and its Relation to Mechanical Function. *Collagen and Related Research,* 8**,** 103-112.

AURAY-BLAIS, C., RAICHE, E., GAGNON, R., BERTHIAUME, M. & PASQUIER, J.-C. 2011. Metabolomics and preterm birth: What biomarkers in cervicovaginal secretions are predictive of high-risk pregnant women? *International Journal of Mass Spectrometry,* 307**,** 33-38.

AVIS, N. J., LINDOW, S. W. & KLEINERMANN, F. 1996. In vitro multifrequency electrical impedance measurements and modelling of the cervix in late pregnancy. *Physiol Meas,* 17 Suppl 4A**,** A97-103.

BAKER, M. J., HUSSAIN, S. R., LOVERGNE, L., UNTEREINER, V., HUGHES, C., LUKASZEWSKI, R. A., THIÉFIN, G. & SOCKALINGUM, G. D. 2016. Developing and understanding biofluid vibrational spectroscopy: a critical review. *Chemical Society Reviews,* 45**,** 1803-1818.

BALIC, D., LATIFAGIC, A. & HUDIC, I. 2008. Insulin-like growth factor-binding protein-1 (IGFBP-1) in cervical secretions as a predictor of preterm delivery. *J Matern Fetal Neonatal Med,* 21**,** 297-300.

BALL, D. 2006. *Field guide to Spectroscopy* [Online]. SPIE Press. Available: https://spie.org/publications/fg08_p65_beers_law?SSO=1 [Accessed].

BALL, R. H., ADE, C. M., SCHOENBORN, J. A. & CRANE, J. P. 1996. The clinical significance of ultransonographically detected subchorionic hemorrhages. *Am J Obstet Gynecol,* 174**,** 996-1002.

BANCELIN, S., NAZAC, A., IBRAHIM, B. H., DOKLADAL, P., DECENCIERE, E., TEIG, B., HADDAD, H., FERNANDEZ, H., SCHANNE-KLEIN, M. C. & DE MARTINO, A. 2014. Determination of collagen fiber orientation in histological slides using Mueller microscopy and validation by second harmonic generation imaging. *Opt Express,* 22**,** 22561-74.

BAÑOS, A., WOLF, M., GRAWE, C., STAHEL, M., HAENSSE, D., FINK, D. & HORNUNG, R. 2007. Frequency domain near-infrared spectroscopy of the uterine cervix during cervical ripening. *Lasers in Surgery and Medicine,* 39**,** 641-646.

BARAI, A., WATSON, S., GRIFFITHS, H. & PATZ, R. 2012. Magnetic induction spectroscopy: non-contact measurement of the electrical conductivity spectra of biological samples. *Measurement Science and Technology,* 23**,** 085501.

BAUER, M., MAZZA, E., NAVA, A., ZECK, W., EDER, M., BAJKA, M., CACHO, F., LANG, U. & HOLZAPEFT, G. A. 2007. In Vivo Characterization of the Mechanics of Human Uterine Cervices. *Annals of the New York Academy of Sciences,* 1101**,** 186-202.

BEAUCHAMP, T. L. & CHILDRESS, J. F. 2001. Oxford University Press.

BEGER, R. D., DUNN, W., SCHMIDT, M. A., GROSS, S. S., KIRWAN, J. A., CASCANTE, M., BRENNAN, L., WISHART, D. S., ORESIC, M., HANKEMEIER, T., BROADHURST, D. I., LANE, A. N., SUHRE, K., KASTENMÜLLER, G., SUMNER, S. J., THIELE, I., FIEHN, O., KADDURAH-DAOUK, R., FOR "PRECISION, M. & PHARMACOMETABOLOMICS TASK GROUP"-METABOLOMICS SOCIETY, I. 2016. Metabolomics enables precision medicine: "A White Paper, Community Perspective". *Metabolomics,* 12**,** 149.

BEHRMAN, R. E. & BUTLER, A. S. 2007. The National Academies Collection: Reports funded by National Institutes of Health. Institute of Medicine Committee on Understanding Premature Birth and Assuring Healthy Outcomes. *In:* BEHRMAN, R. E. & BUTLER, A. S. (eds.) *Preterm Birth: Causes, Consequences, and Prevention.* Washington (DC): National Academies Press (US). National Academy of Sciences.

BERA, T. K. 2014. Bioelectrical Impedance Methods for Noninvasive Health Monitoring: A Review. *J Med Eng,* 2014**,** 381251.

BERGHELLA, V., BAXTER, J. K. & HENDRIX, N. W. 2009. Cervical assessment by ultrasound for preventing preterm delivery. *The Cochrane database of systematic reviews***,** CD007235-CD007235.

BERGHELLA, V., OWEN, J., MACPHERSON, C., YOST, N., SWAIN, M., DILDY, G. A., 3RD, MIODOVNIK, M., LANGER, O. & SIBAI, B. 2007. Natural history of cervical funneling in women at high risk for spontaneous preterm birth. *Obstet Gynecol,* 109**,** 863-9.

BERJOT, M., MARX, J. & ALIX, A. J. P. 1987. Determination of the secondary structure of proteins from the Raman amide I band: The reference intensity profiles method. *Journal of Raman Spectroscopy,* 18**,** 289-300.

BERKLEY, K. J., HUBSCHER, C. H. & WALL, P. D. 1993. Neuronal responses to stimulation of the cervix, uterus, colon, and skin in the rat spinal cord. *J Neurophysiol,* 69**,** 545-56.

BIJLSMA, W. R. & STILMA, J. S. 2005. [Optical coherence tomography, an important new tool in the investigation of the retina]. *Ned Tijdschr Geneeskd,* 149**,** 1884-91.

BILLINGHAM, S. A. M., WHITEHEAD, A. L. & JULIOUS, S. A. 2013. An audit of sample sizes for pilot and feasibility trials being undertaken in the United Kingdom registered in the United Kingdom Clinical Research Network database. *BMC Medical Research Methodology,* 13**,** 104.

BLAND, J. M. & ALTMAN, D. G. 1986. Statistical methods for assessing agreement between two methods of clinical measurement. *Lancet,* 1**,** 307-10.

BLAND, J. M. & ALTMAN, D. G. 1999. Measuring agreement in method comparison studies. *Stat Methods Med Res,* 8**,** 135-60.

BLENCOWE, H., COUSENS, S., CHOU, D., OESTERGAARD, M., SAY, L., MOLLER, A.-B., KINNEY, M., LAWN, J. & BORN TOO SOON PRETERM BIRTH ACTION, G. 2013. Born too soon: the global epidemiology of 15 million preterm births. *Reproductive health,* 10 Suppl 1**,** S2-S2.

BODE, M. 2002. *Characterization of type I and type III collagens in human tissues.* PhD Doctoral Dissertation, University of Oulu.

BODEAN, O., MUNTEANU, O., CIRSTOIU, C., SECARA, D. & CIRSTOIU, M. 2013. Probiotics--a helpful additional therapy for bacterial vaginosis. *J Med Life,* 6**,** 434-6.

BOECKX, J., HERTOG, M., GEERAERD, A. & NICOLAI, B. 2017. Kinetic modelling: an integrated approach to analyze enzyme activity assays. *Plant Methods,* 13**,** 69.

BOSKEY, E. R., TELSCH, K. M., WHALEY, K. J., MOENCH, T. R. & CONE, R. A. 1999. Acid production by vaginal flora in vitro is consistent with the rate and extent of vaginal acidification. *Infection and immunity,* 67**,** 5170-5175.

BOSSUYT, P. M., REITSMA, J. B., BRUNS, D. E., GATSONIS, C. A., GLASZIOU, P. P., IRWIG, L., LIJMER, J. G., MOHER, D., RENNIE, D., DE VET, H. C. W., KRESSEL, H. Y., RIFAI, N., GOLUB, R. M., ALTMAN, D. G., HOOFT, L., KOREVAAR, D. A. & COHEN, J. F. 2015. STARD 2015: an updated list of essential items for reporting diagnostic accuracy studies. *BMJ : British Medical Journal,* 351**,** h5527.

BRACEWELL-MILNES, T., SASO, S., ABDALLA, H., NIKOLAU, D., NORMAN-TAYLOR, J., JOHNSON, M., HOLMES, E. & THUM, M. Y. 2017. Metabolomics as a tool to identify biomarkers to predict and improve outcomes in reproductive medicine: a systematic review. *Hum Reprod Update,* 23**,** 723-736.

BRADFORD, C., SEVERINSEN, R., PUGMIRE, T., RASMUSSEN, M., STODDARD, K., UEMURA, Y., WHEELWRIGHT, S., MENTINOVA, M., CHELSKY, D., HUNSUCKER, S. W., KEARNEY, P., HICKOK, D., FLEISCHER, T. C., ICHETOVKIN, I., BONIFACE, J. J., CRITCHFIELD, G. C. & PELTIER, J. M. 2017. Analytical validation of protein biomarkers for risk of spontaneous preterm birth. *Clinical Mass Spectrometry,* 3**,** 25-38.

BRAMBILLA, D. J., MCKINLAY, S. M. & JOHANNES, C. B. 1994. Defining the perimenopause for application in epidemiologic investigations. *Am J Epidemiol,* 140**,** 1091-5.

BRAR, H. S., MEDEARIS, A. L., DEVORE, G. R. & PLATT, L. D. 1988. Maternal and fetal blood flow velocity waveforms in patients with preterm labor: prediction of successful tocolysis. *Am J Obstet Gynecol,* 159**,** 947-50.

BROCKLEHURST, P., GORDON, A., HEATLEY, E. & MILAN, S. J. 2013. Antibiotics for treating bacterial vaginosis in pregnancy. *Cochrane Database Syst Rev***,** Cd000262.

BROWN, B. H., BARBER, D. C., MORICE, A. H. & LEATHARD, A. D. 1994. Cardiac and respiratory related electrical impedance changes in the human thorax. *IEEE Trans Biomed Eng,* 41**,** 729-34.

BROWN, B. H., TIDY, J. A., BOSTON, K., BLACKETT, A. D., SMALLWOOD, R. H. & SHARP, F. 2000. Relation between tissue structure and imposed electrical current flow in cervical neoplasia. *Lancet,* 355**,** 892-5.

BRUIJN, M. M., HERMANS, F. J., VIS, J. Y., WILMS, F. F., OUDIJK, M. A., KWEE, A., PORATH, M. M., OEI, G., SCHEEPERS, H. C., SPAANDERMAN, M. E., BLOEMENKAMP, K. W., HAAK, M. C., BOLTE, A. C., VANDENBUSSCHE, F. P., WOISKI, M. D., BAX, C. J., CORNETTE, J. M., DUVEKOT, J. J., BIJVANK, B. W., VAN EYCK, J., FRANSSEN, M. T., SOLLIE, K. M., VAN DER POST, J. A., BOSSUYT, P. M., KOK, M., MOL, B. W. & VAN BAAREN, G. J. 2017. Which Factors Contribute to False-Positive, False-Negative, and Invalid Results in Fetal Fibronectin Testing in Women with Symptoms of Preterm Labor? *Am J Perinatol,* 34**,** 234-239.

BRUINSMA, F. J. & QUINN, M. A. 2011. The risk of preterm birth following treatment for precancerous changes in the cervix: a systematic review and meta-analysis. *Bjog,* 118**,** 1031-41.

BUMBRAH, G. S. & SHARMA, R. M. 2016. Raman spectroscopy – Basic principle, instrumentation and selected applications for the characterization of drugs of abuse. *Egyptian Journal of Forensic Sciences,* 6**,** 209-215.

BURACK, E., WOLFE, J. M., LANSING, W. & WRIGHT, A. W. 1941. The Effect of Age Upon the Connective Tissue of the Uterus, Cervix, and Vagina of the Rat. *Cancer Research,* 1**,** 227-235.

BUTLER, H. J., ASHTON, L., BIRD, B., CINQUE, G., CURTIS, K., DORNEY, J., ESMONDE-WHITE, K., FULLWOOD, N. J., GARDNER, B., MARTIN-HIRSCH, P. L., WALSH, M. J., MCAINSH, M. R., STONE, N. & MARTIN, F. L. 2016. Using Raman spectroscopy to characterize biological materials. *Nat Protoc,* 11**,** 664-87.

CABROL, D. 1991. Cervical distensibility changes in pregnancy, term, and preterm labor. *Semin Perinatol,* 15**,** 133-9.

CAMPBELL, S. 2018. Prevention of spontaneous preterm birth: universal cervical length assessment and vaginal progesterone in women with a short cervix: time for action! *American Journal of Obstetrics & Gynecology,* 218**,** 151-158.

CARTER, J., CATE, R., BRILEY, A. & POSTON, L. 2013. PL.55 Testing Saliva for the Prediction of Preterm Birth: How Acceptable is This Method to Women at Risk? *Archives of Disease in Childhood - Fetal and Neonatal Edition,* 98**,** A69-A70.

CARTER, J., HEZELGRAVE, N., SEED, P., TRIBE, R., DAVID, A., LACHELIN, G., SHENNAN, A. & POSTON, L. 2014. 8.5 Combined Fetal Fibronectin and Saliva Progesterone Measurement for Prediction of Spontaneous Preterm Birth. *Archives of Disease in Childhood - Fetal and Neonatal Edition,* 99**,** A12-A12.

CASERTA, D., MALLOZZI, M., MELDOLESI, C., BIANCHI, P. & MOSCARINI, M. 2014. Pregnancy in a unicornuate uterus: a case report. *Journal of medical case reports,* 8**,** 130-130.

CAUCI, S., MCGREGOR, J., THORSEN, P., GROVE, J. & GUASCHINO, S. 2005. Combination of vaginal pH with vaginal sialidase and prolidase activities for prediction of low birth weight and preterm birth. *Am J Obstet Gynecol,* 192**,** 489-96.

CAUGHEY, A. B., ROBINSON, J. N. & NORWITZ, E. R. 2008. Contemporary diagnosis and management of preterm premature rupture of membranes. *Reviews in obstetrics & gynecology,* 1**,** 11-22.

CAVAZOS-REHG, P. A., KRAUSS, M. J., SPITZNAGEL, E. L., BOMMARITO, K., MADDEN, T., OLSEN, M. A., SUBRAMANIAM, H., PEIPERT, J. F. & BIERUT, L. J. 2015. Maternal age and risk of labor and delivery complications. *Maternal and child health journal,* 19**,** 1202-1211.

CAVORETTO, P., CANDIANI, M., GIORGIONE, V., INVERSETTI, A., ABU-SABA, M. M., TIBERIO, F., SIGISMONDI, C. & FARINA, A. 2018. Risk of spontaneous preterm birth in singleton pregnancies conceived after IVF/ICSI treatment: meta-analysis of cohort studies. *Ultrasound in Obstetrics & Gynecology,* 51**,** 43-53.

CEKMEZ, Y., KIRAN, G., HABERAL, E. T. & DIZDAR, M. 2017. Use of cervicovaginal PAMG-1 protein as a predictor of delivery within seven days in pregnancies at risk of premature birth. *BMC Pregnancy Childbirth,* 17**,** 246.

CHANDIRAMANI, M., TRIBE, R. M. & SHENNAN, A. H. 2007. Preterm labour and prematurity. *Obstetrics, Gynaecology & Reproductive Medicine,* 17**,** 232-237.

CHATTERJEE, S. 2014. Artefacts in histopathology. *Journal of oral and maxillofacial pathology : JOMFP,* 18**,** S111-S116.

CHAWANPAIBOON, S., VOGEL, J. P., MOLLER, A. B., LUMBIGANON, P., PETZOLD, M., HOGAN, D., LANDOULSI, S., JAMPATHONG, N., KONGWATTANAKUL, K., LAOPAIBOON, M., LEWIS, C., RATTANAKANOKCHAI, S., TENG, D. N., THINKHAMROP, J., WATANANIRUN, K., ZHANG, J., ZHOU, W. & GULMEZOGLU, A. M. 2019. Global, regional, and national estimates of levels of preterm birth in 2014: a systematic review and modelling analysis. *Lancet Glob Health,* 7**,** e37-e46.

CHEN, H., XU, W. & BRODERICK, N. G. R. 2018. An Adaptive and Fully Automated Baseline Correction Method for Raman Spectroscopy Based on Morphological Operations and Mollification. *Applied Spectroscopy,* 73**,** 284-293.

CHERNEY, D. P., EKMAN, D. R., DIX, D. J. & COLLETTE, T. W. 2007. Raman spectroscopy-based metabolomics for differentiating exposures to triazole fungicides using rat urine. *Anal Chem,* 79**,** 7324-32.

CHOI, S.-J. 2017. Use of progesterone supplement therapy for prevention of preterm birth: review of literatures. *Obstetrics & gynecology science,* 60**,** 405-420.

CHOLLAT, C., SENTILHES, L. & MARRET, S. 2018. Fetal Neuroprotection by Magnesium Sulfate: From Translational Research to Clinical Application. *Frontiers in neurology,* 9**,** 247-247.

CHOO-SMITH, L. P., EDWARDS, H. G. M., ENDTZ, H. P., KROS, J. M., HEULE, F., BARR, H., ROBINSON JR, J. S., BRUINING, H. A. & PUPPELS, G. J. 2002. Medical applications of Raman spectroscopy: From proof of principle to clinical implementation. *Biopolymers,* 67**,** 1-9.

CHOW, L. & LYE, S. J. 1994. Expression of the gap junction protein connexin-43 is increased in the human myometrium toward term and with the onset of labor. *Am J Obstet Gynecol,* 170**,** 788-95.

CHUE-SANG, J., BAI, Y., STOFF, S., GONZALEZ, M., HOLNESS, N., GOMES, J., JUNG, R., GANDJBAKHCHE, A., CHERNOMORDIK, V. V. & RAMELLA-ROMAN, J. C. 2017.

Use of Mueller matrix polarimetry and optical coherence tomography in the characterization of cervical collagen anisotropy. *J Biomed Opt,* 22**,** 1-9.

CHUE-SANG, J., HOLNESS, N., GONZALEZ, M., GREAVES, J., SAYTASHEV, I., STOFF, S., GANDJBAKHCHE, A., CHERNOMORDIK, V. V., BURKETT, G. & RAMELLA-ROMAN, J. C. 2018. *Use of Mueller matrix colposcopy in the characterization of cervical collagen anisotropy*, SPIE.

CLEMENTE, F. Electrical impedance spectroscopy (EIS) measurement of human tissues. 2012 International Conference and Exposition on Electrical and Power Engineering, 25-27 Oct. 2012 2012. 1-2.

COATES, D. 2001. An evaluation of the use of chlorine dioxide (Tristel One-Shot) in an automated washer/disinfector (Medivator) fitted with a chlorine dioxide generator for decontamination of flexible endoscopes. *J Hosp Infect,* 48**,** 55-65.

COATES, J. 2006. Interpretation of Infrared Spectra, A Practical Approach. *Encyclopedia of Analytical Chemistry.*

CONNER, S. N., FREY, H. A., CAHILL, A. G., MACONES, G. A., COLDITZ, G. A. & TUULI, M. G. 2014. Loop electrosurgical excision procedure and risk of preterm birth: a systematic review and meta-analysis. *Obstet Gynecol,* 123**,** 752-61.

COOK, J., BENNETT, P. R., KIM, S. H., TEOH, T. G., SYKES, L., KINDINGER, L. M., GARRETT, A., BINKHAMIS, R., MACINTYRE, D. A. & TERZIDOU, V. 2019. First Trimester Circulating MicroRNA Biomarkers Predictive of Subsequent Preterm Delivery and Cervical Shortening. *Scientific reports,* 9**,** 5861-5861.

COOK, J. R., CHATFIELD, S., CHANDIRAMANI, M., KINDINGER, L., CACCIATORE, S., SYKES, L., TEOH, T., SHENNAN, A., TERZIDOU, V. & BENNETT, P. R. 2017. Cerclage position, cervical length and preterm delivery in women undergoing ultrasound indicated cervical cerclage: A retrospective cohort study. *PLOS ONE,* 12**,** e0178072.

COPPER, R. L., GOLDENBERG, R. L., DAVIS, R. O., CUTTER, G. R., DUBARD, M. B., CORLISS, D. K. & ANDREWS, J. B. 1990. Warning symptoms, uterine contractions, and cervical examination findings in women at risk of preterm delivery. *Am J Obstet Gynecol,* 162**,** 748-54.

CRANE, J. M. & HUTCHENS, D. 2011. Follow-up cervical length in asymptomatic high-risk women and the risk of spontaneous preterm birth. *J Perinatol,* 31**,** 318-23.

CRANE, J. M. G. & HUTCHENS, D. 2008. Transvaginal sonographic measurement of cervical length to predict preterm birth in asymptomatic women at increased risk: a systematic review. *Ultrasound in Obstetrics & Gynecology,* 31**,** 579-587.

CULHANE, J. F. & GOLDENBERG, R. L. 2011. Racial disparities in preterm birth. *Semin Perinatol,* 35**,** 234-9.

DAHLIN, S., GUNNERBECK, A., WIKSTRÖM, A.-K., CNATTINGIUS, S. & EDSTEDT BONAMY, A.-K. 2016. Maternal tobacco use and extremely premature birth – a population-based cohort study. *BJOG: An International Journal of Obstetrics & Gynaecology,* 123**,** 1938-1946.

DANFORTH, D. N. 1983. The morphology of the human cervix. *Clin Obstet Gynecol,* 26**,** 7-13.

DANFORTH, D. N. & BUCKINGHAM, J. C. 1964. CONNECTIVE TISSUE MECHANISMS AND THEIR RELATION TO PREGNANCY. *Obstet Gynecol Surv,* 19**,** 715-32.

DASARI, S., PEREIRA, L., REDDY, A. P., MICHAELS, J. E., LU, X., JACOB, T., THOMAS, A., RODLAND, M., ROBERTS, C. T., JR., GRAVETT, M. G. & NAGALLA, S. R. 2007. Comprehensive proteomic analysis of human cervical-vaginal fluid. *J Proteome Res,* 6**,** 1258-68.

DASZYKOWSKI, M., WROBEL, M. S., CZARNIK-MATUSEWICZ, H. & WALCZAK, B. 2008. Near-infrared reflectance spectroscopy and multivariate calibration techniques applied to modelling the crude protein, fibre and fat content in rapeseed meal. *Analyst,* 133**,** 1523-1531.

DE BOER, J. F., MILNER, T. E., VAN GEMERT, M. J. C. & NELSON, J. S. 1997. Two-dimensional birefringence imaging in biological tissue by polarization-sensitive optical coherence tomography. *Optics Letters,* 22**,** 934-936.

DE LORENZO, A., ANDREOLI, A., MATTHIE, J. & WITHERS, P. 1997. Predicting body cell mass with bioimpedance by using theoretical methods: a technological review. *J Appl Physiol (1985),* 82**,** 1542-58.

DE LOS SANTOS, G. E. & ZUNIGA, S. 2004. Comparison of pH measurement devices for determining vaginal pH in cynomolgus macaques. *Contemp Top Lab Anim Sci,* 43**,** 39-40.

DEAN, D. A., RAMANATHAN, T., MACHADO, D. & SUNDARARAJAN, R. 2008. Electrical Impedance Spectroscopy Study of Biological Tissues. *Journal of electrostatics,* 66**,** 165-177.

DEEGAN, R. D., BAKAJIN, O., DUPONT, T. F., HUBER, G., NAGEL, S. R. & WITTEN, T. A. 1997. Capillary flow as the cause of ring stains from dried liquid drops. *Nature,* 389**,** 827-829.

DEIDDA, M., PIRAS, C., DESSALVI, C. C., LOCCI, E., BARBERINI, L., TORRI, F., ASCEDU, F., ATZORI, L. & MERCURO, G. 2015. Metabolomic approach to profile functional and metabolic changes in heart failure. *Journal of translational medicine,* 13**,** 297-297.

DEKKER, G. A., LEE, S. Y., NORTH, R. A., MCCOWAN, L. M., SIMPSON, N. A. B. & ROBERTS, C. T. 2012. Risk Factors for Preterm Birth in an International Prospective Cohort of Nulliparous Women. *PLOS ONE,* 7**,** e39154.

DELOBEL-AYOUB, M., KAMINSKI, M., MARRET, S., BURGUET, A., MARCHAND, L., N'GUYEN, S., MATIS, J., THIRIEZ, G., FRESSON, J., ARNAUD, C., POHER, M. & LARROQUE, B. 2006. Behavioral outcome at 3 years of age in very preterm infants: the EPIPAGE study. *Pediatrics,* 117**,** 1996-2005.

DERRAIK, J. G. B., LUNDGREN, M., CUTFIELD, W. S. & AHLSSON, F. 2016. Maternal Height and Preterm Birth: A Study on 192,432 Swedish Women. *PloS one,* 11**,** e0154304-e0154304.

DHANASEKAR, K. R., SHILPA, B., GOMATHY, N. & KUNDAVI, S. 2019. Prenatal Probiotics: The Way Forward in Prevention of Preterm Birth. *Journal of Clinical Gynecology and Obstetrics; Vol. 8, No. 3, Sept 2019*.

DI QUINZIO, M. K. W., OLIVA, K., HOLDSWORTH, S. J., AYHAN, M., WALKER, S. P., RICE, G. E., GEORGIOU, H. M. & PERMEZEL, M. 2007. Proteomic analysis and characterisation of human cervico-vaginal fluid proteins. *Australian and New Zealand Journal of Obstetrics and Gynaecology,* 47**,** 9-15.

DI TOMMASO, M. & BERGHELLA, V. 2013. Cervical length for the prediction and prevention of preterm birth AU - Di Tommaso, Mariarosaria. *Expert Review of Obstetrics & Gynecology,* 8**,** 345-355.

DIMES, M. O. 2017. Premature birth report card. *March of Dimes*.

DODD, J. M. & CROWTHER, C. A. 2010. The role of progesterone in prevention of preterm birth. *International journal of women's health,* 1**,** 73-84.

DODD, J. M., JONES, L., FLENADY, V., CINCOTTA, R. & CROWTHER, C. A. 2013. Prenatal administration of progesterone for preventing preterm birth in women considered to be at risk of preterm birth. *Cochrane Database of Systematic Reviews*.

DOMINGUEZ, T. P. 2011. Adverse birth outcomes in African American women: the social context of persistent reproductive disadvantage. *Soc Work Public Health,* 26**,** 3-16.

DOS SANTOS, C. A. T., PÁSCOA, R. N. M. J. & LOPES, J. A. 2017. A review on the application of vibrational spectroscopy in the wine industry: From soil to bottle. *TrAC Trends in Analytical Chemistry,* 88**,** 100-118.

DOYLE, L. W., CROWTHER, C. A., MIDDLETON, P., MARRET, S. & ROUSE, D. 2009. Magnesium sulphate for women at risk of preterm birth for neuroprotection of the fetus. *Cochrane Database of Systematic Reviews*.

DRAPER, E. S., MANKTELOW, B., FIELD, D. J. & JAMES, D. 1999. Prediction of survival for preterm births by weight and gestational age: retrospective population based study. *BMJ (Clinical research ed.),* 319**,** 1093-1097.

EKMAN-ORDEBERG, G. & DUBICKE, A. 2012. Preterm Cervical Ripening in humans. *Facts, views & vision in ObGyn,* 4**,** 245-253.

EKMAN, G., MALMSTROM, A., ULDBJERG, N. & ULMSTEN, U. 1986. Cervical collagen: an important regulator of cervical function in term labor. *Obstet Gynecol,* 67**,** 633-6.

ELOVITZ, M. A., BROWN, A. G., ANTON, L., GILSTROP, M., HEISER, L. & BASTEK, J. 2014. Distinct cervical microRNA profiles are present in women destined to have a preterm birth. *Am J Obstet Gynecol,* 210**,** 221.e1-11.

ELOVITZ, M. A., WANG, Z., CHIEN, E. K., RYCHLIK, D. F. & PHILLIPPE, M. 2003. A new model for inflammation-induced preterm birth: the role of platelet-activating factor and Toll-like receptor-4. *The American journal of pathology,* 163**,** 2103-2111.

ESMONDE-WHITE, K. A., ESMONDE-WHITE, F. W. L., MORRIS, M. D. & ROESSLER, B. J. 2014. Characterization of biofluids prepared by sessile drop formation. *The Analyst,* 139**,** 2734-2741.

ETEMADI, M., CHUNG, P., HELLER, J. A., LIU, J. A., RAND, L. & ROY, S. 2013. Towards BirthAlert--A Clinical Device Intended for Early Preterm Birth Detection. *IEEE transactions on bio-medical engineering,* 60**,** 3484-3493.

FACCHINETTI, F., VENTURINI, P., BLASI, I. & GIANNELLA, L. 2005. Changes in the cervical competence in preterm labour. *BJOG: An International Journal of Obstetrics & Gynaecology,* 112**,** 23-27.

FANG, D., SHI, S. Q., SHI, L., YANG, J., LIU, H., XIA, H. & GARFIELD, R. E. 2015. Direct electrical stimulation softens the cervix in pregnant and nonpregnant rats. *Am J Obstet Gynecol,* 212**,** 786.e1-9.

FARAG, A. H., MOHAMMED, M. M., ELLAITHY, M. I. & SALAMA, H. A. 2015. Blind vaginal fetal fibronectin swab for prediction of preterm birth. *J Obstet Gynaecol Res,* 41**,** 1009-17.

FARON, G., BALEPA, L., PARRA, J., FILS, J.-F. & GUCCIARDO, L. 2018. The fetal fibronectin test: 25 years after its development, what is the evidence regarding its clinical utility? A systematic review and meta-analysis. *The Journal of Maternal-Fetal & Neonatal Medicine***,** 1-31.

FAYE-PETERSEN, O. M. 2008. The placenta in preterm birth. *J Clin Pathol,* 61**,** 1261-75.

FELTOVICH, H., HALL, T. J. & BERGHELLA, V. 2012. Beyond cervical length: emerging technologies for assessing the pregnant cervix. *Am J Obstet Gynecol,* 207**,** 345-54.

FERGUSON, K. K., MCELRATH, T. F., CHEN, Y. H., LOCH-CARUSO, R., MUKHERJEE, B. & MEEKER, J. D. 2015. Repeated measures of urinary oxidative stress biomarkers during pregnancy and preterm birth. *Am J Obstet Gynecol,* 212**,** 208.e1-8.

FERGUSON, K. K., MEEKER, J. D., MCELRATH, T. F., MUKHERJEE, B. & CANTONWINE, D. E. 2017. Repeated measures of inflammation and oxidative stress biomarkers in preeclamptic and normotensive pregnancies. *Am J Obstet Gynecol,* 216**,** 527.e1-527.e9.

FERNIE, A. R., AHARONI, A., WILLMITZER, L., STITT, M., TOHGE, T., KOPKA, J., CARROLL, A. J., SAITO, K., FRASER, P. D. & DELUCA, V. 2011. Recommendations for reporting metabolite data. *The Plant cell,* 23**,** 2477-2482.

FETTWEIS, J. M., BROOKS, J. P., SERRANO, M. G., SHETH, N. U., GIRERD, P. H., EDWARDS, D. J., STRAUSS, J. F., THE VAGINAL MICROBIOME, C., JEFFERSON, K. K. & BUCK, G. A. 2014. Differences in vaginal microbiome in African American women versus women of European ancestry. *Microbiology (Reading, England),* 160**,** 2272-2282.

FISH, R. M. & GEDDES, L. A. 2009. Conduction of electrical current to and through the human body: a review. *Eplasty,* 9**,** e44-e44.

FITTKOW, C. T., MAUL, H., OLSON, G., MARTIN, E., MACKAY, L. B., SAADE, G. R. & GARFIELD, R. E. 2005. Light-induced fluorescence of the human cervix decreases after prostaglandin application for induction of labor at term. *Eur J Obstet Gynecol Reprod Biol,* 123**,** 62-6.

FLENADY, V., HAWLEY, G., STOCK, O. M., KENYON, S. & BADAWI, N. 2013. Prophylactic antibiotics for inhibiting preterm labour with intact membranes. *Cochrane Database of Systematic Reviews*.

FLINT, M. H., LYONS, M. F., MEANEY, M. F. & WILLIAMS, D. E. 1975. The Masson staining of collagen — an explanation of an apparent paradox. *The Histochemical Journal,* 7**,** 529-546.

FLOOD, K. & MALONE, F. D. 2012. Prevention of preterm birth. *Seminars in Fetal and Neonatal Medicine,* 17**,** 58-63.

FOSTER, C. & SHENNAN, A. H. 2014. Fetal fibronectin as a biomarker of preterm labor: a review of the literature and advances in its clinical use. *Biomark Med,* 8**,** 471-84.

FUCHS, F., MONET, B., DUCRUET, T., CHAILLET, N. & AUDIBERT, F. 2018. Effect of maternal age on the risk of preterm birth: A large cohort study. *PloS one,* 13**,** e0191002-e0191002.

FUJIMOTO, J. & SWANSON, E. 2016. The Development, Commercialization, and Impact of Optical Coherence Tomography. *Investigative ophthalmology & visual science,* 57**,** OCT1-OCT13.

FUJIMOTO, J. G., PITRIS, C., BOPPART, S. A. & BREZINSKI, M. E. 2000. Optical coherence tomography: an emerging technology for biomedical imaging and optical biopsy. *Neoplasia,* 2**,** 9-25.

GALE, C., HAY, A., PHILIPP, C., KHAN, R., SANTHAKUMARAN, S. & RATNAVEL, N. 2012. In-utero transfer is too difficult: results from a prospective study. *Early Hum Dev,* 88**,** 147-50.

GAN, Y., YAO, W., MYERS, K. M. & HENDON, C. P. 2014. An automated 3D registration method for optical coherence tomography volumes. *Conf Proc IEEE Eng Med Biol Soc,* 2014**,** 3873-6.

GANDHI, S. V., WALKER, D., MILNES, P., MUKHERJEE, S., BROWN, B. H. & ANUMBA, D. O. 2006a. Electrical impedance spectroscopy of the cervix in non-pregnant and pregnant women. *Eur J Obstet Gynecol Reprod Biol,* 129**,** 145-9.

GANDHI, S. V., WALKER, D. C., BROWN, B. H. & ANUMBA, D. O. C. 2006b. Comparison of human uterine cervical electrical impedance measurements derived using two tetrapolar probes of different sizes. *Biomedical engineering online,* 5**,** 62-62.

GEORGIOU, H. M., DI QUINZIO, M. K. W., PERMEZEL, M. & BRENNECKE, S. P. 2015. Predicting Preterm Labour: Current Status and Future Prospects. *Disease Markers,* 2015**,** 9.

GHARTEY, J., BASTEK, J. A., BROWN, A. G., ANGLIM, L. & ELOVITZ, M. A. 2015. Women with preterm birth have a distinct cervicovaginal metabolome. *Am J Obstet Gynecol,* 212**,** 776.e1-776.e12.

GIBB, D. & SARIDOGAN, E. 2016. The role of transabdominal cervical cerclage techniques in maternity care. *The Obstetrician & Gynaecologist,* 18**,** 117-125.

GLASSMAN, W., BYAM-SMITH, M. & GARFIELD, R. E. 1995. Changes in rat cervical collagen during gestation and after antiprogesterone treatment as measured in vivo with light-induced autofluorescence. *Am J Obstet Gynecol,* 173**,** 1550-6.

GLASSMAN, W. S., LIAO, Q.-P., SHI, S.-Q., GOODRUM, L., OLSON, G., MARTIN, E., SAADE, G. & GARFIELD, R. E. 1997. *Fluorescence probe for cervical examination during various reproductive states,* SPIE.

GOLDENBERG, R. L., ANDREWS, W. W. & HAUTH, J. C. 2002. Choriodecidual infection and preterm birth. *Nutr Rev,* 60**,** S19-25.

GOLDENBERG, R. L., CULHANE, J. F., IAMS, J. D. & ROMERO, R. 2008. Epidemiology and causes of preterm birth. *Lancet,* 371**,** 75-84.

GOLDENBERG, R. L., IAMS, J. D., MERCER, B. M., MEIS, P. J., MOAWAD, A., DAS, A., MIODOVNIK, M., VANDORSTEN, P. J., CARITIS, S. N., THURNAU, G. & DOMBROWSKI, M. P. 2001. The Preterm Prediction Study: toward a multiple-marker test for spontaneous preterm birth. *Am J Obstet Gynecol,* 185**,** 643-51.

GOLDENBERG, R. L., MERCER, B. M., MEIS, P. J., COPPER, R. L., DAS, A. & MCNELLIS, D. 1996. The preterm prediction study: fetal fibronectin testing and spontaneous preterm birth. NICHD Maternal Fetal Medicine Units Network. *Obstet Gynecol,* 87**,** 643-8.

GOMEZ-LOPEZ, N., ROMERO, R., ARENAS-HERNANDEZ, M., PANAITESCU, B., GARCIA-FLORES, V., MIAL, T. N., SAHI, A. & HASSAN, S. S. 2018. Intra-amniotic administration of lipopolysaccharide induces spontaneous preterm labor and birth in the absence of a body temperature change. *The Journal of Maternal-Fetal & Neonatal Medicine,* 31**,** 439-446.

GONCALVES, L. F., CHAIWORAPONGSA, T. & ROMERO, R. 2002. Intrauterine infection and prematurity. *Ment Retard Dev Disabil Res Rev,* 8**,** 3-13.

GONZALEZ-CORREA, C. A., BROWN, B. H., SMALLWOOD, R. H., WALKER, D. C. & BARDHAN, K. D. 2005. Electrical bioimpedance readings increase with higher pressure applied to the measuring probe. *Physiol Meas,* 26**,** S39-47.

GORROCHATEGUI, E., JAUMOT, J., LACORTE, S. & TAULER, R. 2016. Data analysis strategies for targeted and untargeted LC-MS metabolomic studies: Overview and workflow. *TrAC Trends in Analytical Chemistry,* 82.

GOULDING, E. & LIM, B. 2014. McDonald transvaginal cervical cerclage since 1957: from its roots in Australia into worldwide contemporary practice. *BJOG: An International Journal of Obstetrics & Gynaecology,* 121**,** 1107-1107.

GRAVES, P. R. & HAYSTEAD, T. A. J. 2002. Molecular biologist's guide to proteomics. *Microbiology and molecular biology reviews : MMBR,* 66**,** 39-63.

GU, W. & ZHAO, Y. 2010. Cellular electrical impedance spectroscopy: an emerging technology of microscale biosensors. *Expert Review of Medical Devices,* 7**,** 767-779.

GUARDO, R., CHARRON, G., GOUSSARD, Y. & SAVARD, P. Contactless measurement of thoracic conductivity changes by magnetic induction. Proceedings of the 19th Annual International Conference of the IEEE Engineering in Medicine and Biology Society. 'Magnificent Milestones and Emerging Opportunities in Medical Engineering' (Cat. No.97CH36136), 30 Oct.-2 Nov. 1997 1997. 2450-2453 vol.6.

GUASCHINO, S., DE SETA, F., PICCOLI, M., MASO, G. & ALBERICO, S. 2006. Aetiology of preterm labour: bacterial vaginosis. *BJOG: An International Journal of Obstetrics & Gynaecology,* 113**,** 46-51.

GUZELOGLU-KAYISLI, O., KAYISLI, U. A., SEMERCI, N., BASAR, M., BUCHWALDER, L. F., BUHIMSCHI, C. S., BUHIMSCHI, I. A., ARCURI, F., LARSEN, K., HUANG, J. S., SCHATZ, F. & LOCKWOOD, C. J. 2015. Mechanisms of chorioamnionitis-associated preterm birth: interleukin-1beta inhibits progesterone receptor expression in decidual cells. *J Pathol,* 237**,** 423-34.

HAAS, D. M., CALDWELL, D. M., KIRKPATRICK, P., MCINTOSH, J. J. & WELTON, N. J. 2012. Tocolytic therapy for preterm delivery: systematic review and network meta-analysis. *BMJ : British Medical Journal,* 345**,** e6226.

HAAS, D. M., IMPERIALE, T. F., KIRKPATRICK, P. R., KLEIN, R. W., ZOLLINGER, T. W. & GOLICHOWSKI, A. M. 2009. Tocolytic Therapy: A Meta-Analysis and Decision Analysis. *Obstetrics & Gynecology,* 113**,** 585-594.

HAEMMERICH, D., OZKAN, R., TUNGJITKUSOLMUN, S., TSAI, J. Z., MAHVI, D. M., STAELIN, S. T. & WEBSTER, J. G. 2002. Changes in electrical resistivity of swine liver after occlusion and postmortem. *Med Biol Eng Comput,* 40**,** 29-33.

HAEMMERICH, D., SCHUTT, D. J., WRIGHT, A. W., WEBSTER, J. G. & MAHVI, D. M. 2009. Electrical conductivity measurement of excised human metastatic liver tumours before and after thermal ablation. *Physiol Meas,* 30**,** 459-66.

HALTER, R. J., HARTOV, A., HEANEY, J. A., PAULSEN, K. D. & SCHNED, A. R. 2007. Electrical impedance spectroscopy of the human prostate. *IEEE Trans Biomed Eng,* 54**,** 1321-7.

HALTER, R. J., SCHNED, A., HEANEY, J., HARTOV, A. & PAULSEN, K. D. 2009a. Electrical properties of prostatic tissues: I. Single frequency admittivity properties. *J Urol,* 182**,** 1600-7.

HALTER, R. J., SCHNED, A., HEANEY, J., HARTOV, A. & PAULSEN, K. D. 2009b. Electrical properties of prostatic tissues: II. Spectral admittivity properties. *J Urol,* 182**,** 1608-13.

HALTER, R. J., SCHNED, A. R., HEANEY, J. A. & HARTOV, A. 2011. Passive bioelectrical properties for assessing high- and low-grade prostate adenocarcinoma. *Prostate,* 71**,** 1759-67.

HARTMANN, K., THORP J.M., J., MCDONALDT, T. L., SAVITZ, D. A. & L., G. J. 1999. Cervical dimensions and risk of preterm birth. *Obstetrics and Gynecology,* 93**,** 504-509.

HEAZELL, A. E., BERNATAVICIUS, G., WARRANDER, L., BROWN, M. C. & DUNN, W. B. 2012. A metabolomic approach identifies differences in maternal serum in third trimester pregnancies that end in poor perinatal outcome. *Reprod Sci,* 19**,** 863-75.

HEINONEN, P. K. 1997. Unicornuate uterus and rudimentary horn. *Fertil Steril,* 68**,** 224-30.

HEINZE, T., RIEDEWALD, S. & SALING, E. 1989. Determination of vaginal pH by pH indicator strip and by pH micro electrode. *J Perinat Med,* 17**,** 477-9.

HEMALATHA, R., RAMALAXMI, B. A., SWETHA, E., BALAKRISHNA, N. & MASTROMARINO, P. 2013. Evaluation of vaginal pH for detection of bacterial vaginosis. *The Indian journal of medical research,* 138**,** 354-359.

HENG, Y. J., LIONG, S., PERMEZEL, M., RICE, G. E., DI QUINZIO, M. K. W. & GEORGIOU, H. M. 2015a. Human cervicovaginal fluid biomarkers to predict term and preterm labor. *Frontiers in Physiology,* 6.

HENG, Y. J., LIONG, S., PERMEZEL, M., RICE, G. E., DI QUINZIO, M. K. W. & GEORGIOU, H. M. 2015b. Human cervicovaginal fluid biomarkers to predict term and preterm labor. *Frontiers in physiology,* 6**,** 151-151.

HEZELGRAVE, N. L. & SHENNAN, A. H. 2016. Quantitative Fetal Fibronectin to Predict Spontaneous Preterm Birth: A Review. *Women's Health,* 12**,** 121-128.

HIBBARD, J. U., TART, M. & MOAWAD, A. H. 2000. Cervical length at 16-22 weeks' gestation and risk for preterm delivery. *Obstet Gynecol,* 96**,** 972-8.

HILLIER, S. L., NUGENT, R. P., ESCHENBACH, D. A., KROHN, M. A., GIBBS, R. S., MARTIN, D. H., COTCH, M. F., EDELMAN, R., PASTOREK, J. G., 2ND, RAO, A. V. & ET AL. 1995a. Association between bacterial vaginosis and preterm delivery of a low-birth-weight infant. The Vaginal Infections and Prematurity Study Group. *N Engl J Med,* 333**,** 1737-42.

HILLIER, S. L., NUGENT, R. P., ESCHENBACH, D. A., KROHN, M. A., GIBBS, R. S., MARTIN, D. H., COTCH, M. F., EDELMAN, R., PASTOREK, J. G., RAO, A. V., MCNELLIS, D., REGAN, J. A., CAREY, J. C. & KLEBANOFF, M. A. 1995b. Association between Bacterial Vaginosis and Preterm Delivery of a Low-Birth-Weight Infant. *New England Journal of Medicine,* 333**,** 1737-1742.

HITCHCOCK, B., MOYNAN, S., FRAMPTON, C., REUTHER, R., GILLING, P. & ROWE, F. 2016. A randomised, single-blind comparison of high-level disinfectants for flexible nasendoscopes. *J Laryngol Otol,* 130**,** 983-989.

HONEST, H., BACHMANN, L. M., COOMARASAMY, A., GUPTA, J. K., KLEIJNEN, J. & KHAN, K. S. 2003. Accuracy of cervical transvaginal sonography in predicting preterm birth: a systematic review. *Ultrasound Obstet Gynecol,* 22**,** 305-22.

HONEST, H., FORBES, C. A., DUREE, K. H., NORMAN, G., DUFFY, S. B., TSOURAPAS, A., ROBERTS, T. E., BARTON, P. M., JOWETT, S. M., HYDE, C. J. & KHAN, K. S. 2009. Screening to prevent spontaneous preterm birth: systematic reviews of accuracy and effectiveness literature with economic modelling. *Health Technol Assess,* 13**,** 1-627.

HOOVER, R. N., HYER, M., PFEIFFER, R. M., ADAM, E., BOND, B., CHEVILLE, A. L., COLTON, T., HARTGE, P., HATCH, E. E., HERBST, A. L., KARLAN, B. Y., KAUFMAN, R., NOLLER, K. L., PALMER, J. R., ROBBOY, S. J., SAAL, R. C., STROHSNITTER, W., TITUS-ERNSTOFF, L. & TROISI, R. 2011. Adverse Health Outcomes in Women Exposed In Utero to Diethylstilbestrol. *New England Journal of Medicine,* 365**,** 1304-1314.

HORGAN, R. P. & KENNY, L. C. 2011. 'Omic' technologies: genomics, transcriptomics, proteomics and metabolomics. *The Obstetrician & Gynaecologist,* 13**,** 189-195.

HORNE, E., LANCASTER, G. A., MATSON, R., COOPER, A., NESS, A. & LEARY, S. 2018. Pilot trials in physical activity journals: a review of reporting and editorial policy. *Pilot and Feasibility Studies,* 4**,** 125.

HORNUNG, R., SPICHTIG, S., BAÑOS, A., STAHEL, M., ZIMMERMANN, R. & WOLF, M. 2011. Frequency-domain near-infrared spectroscopy of the uterine cervix during regular pregnancies. *Lasers in Medical Science,* 26**,** 205-212.

HOUSE, M., KAPLAN, D. L. & SOCRATE, S. 2009. Relationships Between Mechanical Properties and Extracellular Matrix Constituents of the Cervical Stroma During Pregnancy. *Seminars in Perinatology,* 33**,** 300-307.

HUA, M., ODIBO, A. O., LONGMAN, R. E., MACONES, G. A., ROEHL, K. A. & CAHILL, A. G. 2011. Congenital uterine anomalies and adverse pregnancy outcomes. *Am J Obstet Gynecol,* 205**,** 558.e1-5.

IAMS, J. D., GOLDENBERG, R. L., MEIS, P. J., MERCER, B. M., MOAWAD, A., DAS, A., THOM, E., MCNELLIS, D., COPPER, R. L., JOHNSON, F. & ROBERTS, J. M. 1996. The length of the cervix and the risk of spontaneous premature delivery. National Institute of Child Health and Human Development Maternal Fetal Medicine Unit Network. *N Engl J Med,* 334**,** 567-72.

IAMS, J. D., GROBMAN, W. A., LOZITSKA, A., SPONG, C. Y., SAADE, G., MERCER, B. M., TITA, A. T., ROUSE, D. J., SOROKIN, Y., WAPNER, R. J., LEVENO, K. J., BLACKWELL, S. C., ESPLIN, M. S., TOLOSA, J. E., THORP, J. M., CARITIS, S. N., VAN DORSTEN, P. J., EUNICE KENNEDY SHRIVER NATIONAL INSTITUTE OF CHILD, H. & HUMAN DEVELOPMENT MATERNAL–FETAL MEDICINE UNITS, N. 2013. Adherence to criteria for transvaginal ultrasound imaging and measurement of cervical length. *American journal of obstetrics and gynecology,* 209**,** 365.e1-365.e3655.

IAMS, J. D., ROMERO, R., CULHANE, J. F. & GOLDENBERG, R. L. 2008. Primary, secondary, and tertiary interventions to reduce the morbidity and mortality of preterm birth. *Lancet,* 371**,** 164-75.

IBETO, L. A., CHANDIRAMANI, M., SYKES, L., CHATFIELD, S., COOK, J., ABBOTT, D., LOUDON, J., SIMCOX, R., JONES, B., SHENNAN, A. H., BNNETT, P. & TERZIDOU, V. 2012. The risk of preterm birth associated with uterine anomalies, and the clinical utility of serial measurement of cervical length. *Archives of Disease in Childhood - Fetal and Neonatal Edition,* 97**,** A115-A115.

ICNIRP. 1998. *International Commission on Non-Ionizing Radiation Protection* [Online]. Available: https://www.icnirp.org/cms/upload/publications/ICNIRPemfgdl.pdf [Accessed].

ILHAN, Z. E., ŁANIEWSKI, P., THOMAS, N., ROE, D. J., CHASE, D. M. & HERBST-KRALOVETZ, M. M. 2019. Deciphering the complex interplay between microbiota, HPV, inflammation and cancer through cervicovaginal metabolic profiling. *EBioMedicine,* 44**,** 675-690.

IZENMAN, A. 2008. *Modern Multivariate Statistical Techniques*, Springer.

JACQUES, S. L. 2013. Optical properties of biological tissues: a review. *Phys Med Biol,* 58**,** R37-61.

JAFARI-DEHKORDI, E., ADIBI, A. & SIRUS, M. 2015. Reference range of the weekly uterine cervical length at 8 to 38 weeks of gestation in the center of Iran. *Advanced biomedical research,* 4**,** 115-115.

JAFFE, G. J. & CAPRIOLI, J. 2004. Optical coherence tomography to detect and manage retinal disease and glaucoma. *Am J Ophthalmol,* 137**,** 156-69.

JANSZ, P. V., RICHARDSON, S., WILD, G. & HINCKLEY, S. 2014. Characterizing the resolvability of real superluminescent diode sources for application to optical coherence tomography using a low coherence interferometry model. *J Biomed Opt,* 19**,** 085003.

JARDE, A., LUTSIV, O., BEYENE, J. & MCDONALD, S. D. 2019. Vaginal progesterone, oral progesterone, 17-OHPC, cerclage, and pessary for preventing preterm birth in at-risk singleton pregnancies: an updated systematic review and network meta-analysis. *Bjog,* 126**,** 556-567.

JOKHI, R. P., BROWN, B. H. & ANUMBA, D. O. C. 2009a. The role of cervical Electrical Impedance Spectroscopy in the prediction of the course and outcome of induced labour. *BMC pregnancy and childbirth,* 9**,** 40-40.

JOKHI, R. P., GHULE, V. V., BROWN, B. H. & ANUMBA, D. O. 2009b. Reproducibility and repeatability of measuring the electrical impedance of the pregnant human cervix-the effect of probe size and applied pressure. *BioMedical Engineering OnLine,* 8**,** 10.

KAGAN, K. O. & SONEK, J. 2015. How to measure cervical length. *Ultrasound in Obstetrics & Gynecology,* 45**,** 358-362.

KEELAN, J. A. & NEWNHAM, J. P. 2017. Recent advances in the prevention of preterm birth. *F1000Research,* 6**,** F1000 Faculty Rev-1139.

KELLY, R., HOLZMAN, C., SENAGORE, P., WANG, J., TIAN, Y., RAHBAR, M. H. & CHUNG, H. 2009. Placental vascular pathology findings and pathways to preterm delivery. *American journal of epidemiology,* 170**,** 148-158.

KENYON, S., TAYLOR, D. J. & TARNOW-MORDI, W. O. 2002. ORACLE--antibiotics for preterm prelabour rupture of the membranes: short-term and long-term outcomes. *Acta Paediatr Suppl,* 91**,** 12-5.

KENYON, S. L., TAYLOR, D. J. & TARNOW-MORDI, W. 2001. Broad-spectrum antibiotics for spontaneous preterm labour: the ORACLE II randomised trial. ORACLE Collaborative Group. *Lancet,* 357**,** 989-94.

KERR, L. T., BYRNE, H. J. & HENNELLY, B. M. 2015. Optimal choice of sample substrate and laser wavelength for Raman spectroscopic analysis of biological specimen. *Analytical Methods,* 7**,** 5041-5052.

KERSHAW, C. M., SCARAMUZZI, R. J., MCGOWAN, M. R., WHEELER-JONES, C. P. & KHALID, M. 2007. The expression of prostaglandin endoperoxide synthase 2 messenger RNA and the proportion of smooth muscle and collagen in the sheep cervix during the estrous cycle. *Biol Reprod,* 76**,** 124-9.

KHALIL, M. R., THORSEN, P. & ULDBJERG, N. 2013. Cervical ultrasound elastography may hold potential to predict risk of preterm birth. *Dan Med J,* 60**,** A4570.

KHALIL, S. F., MOHKTAR, M. S. & IBRAHIM, F. 2014. The theory and fundamentals of bioimpedance analysis in clinical status monitoring and diagnosis of diseases. *Sensors (Basel, Switzerland),* 14**,** 10895-10928.

KHAMBAY, H., BOLT, L. A., CHANDIRAMANI, M., DE GREEFF, A., FILMER, J. E. & SHENNAN, A. H. 2012. The Actim Partus test to predict pre-term birth in asymptomatic high-risk women. *J Obstet Gynaecol,* 32**,** 132-4.

KHANDALAVALA, J. & VAN GEEM, T. A. 1999. Evaluating vaginal pH. Accuracy of two commercial pH papers in comparison to a hand-held digital pH meter. *J Reprod Med,* 44**,** 76-80.

KHANDELWAL, M. 2012. Vaginal progesterone in risk reduction of preterm birth in women with short cervix in the midtrimester of pregnancy. *Int J Womens Health,* 4**,** 481-90.

KHANDER, A., STERN, E., GERBER, R. S. & FOX, N. S. 2018. The association between obstetrical history and preterm birth in women with uterine anomalies. *J Matern Fetal Neonatal Med,* 31**,** 2550-2554.

KIEFER, D. G. & VINTZILEOS, A. M. 2008. The utility of fetal fibronectin in the prediction and prevention of spontaneous preterm birth. *Rev Obstet Gynecol,* 1**,** 106-12.

KIM, Y. M., CHAIWORAPONGSA, T., GOMEZ, R., BUJOLD, E., YOON, B. H., ROTMENSCH, S., THALER, H. T. & ROMERO, R. 2002. Failure of physiologic transformation of the spiral arteries in the placental bed in preterm premature rupture of membranes. *American Journal of Obstetrics & Gynecology,* 187**,** 1137-1142.

KINDINGER, L. M., BENNETT, P. R., LEE, Y. S., MARCHESI, J. R., SMITH, A., CACCIATORE, S., HOLMES, E., NICHOLSON, J. K., TEOH, T. G. & MACINTYRE, D. A. 2017. The interaction between vaginal microbiota, cervical length, and vaginal progesterone treatment for preterm birth risk. *Microbiome,* 5**,** 6-6.

KING, J. & FLENADY, V. 2002. Prophylactic antibiotics for inhibiting preterm labour with intact membranes. *Cochrane Database Syst Rev***,** Cd000246.

KIRBY, M. C., ASPDEN, R. M. & HUKINS, D. W. L. 1988. Determination of the orientation distribution function for collagen fibrils in a connective tissue site from a high-angle X-ray diffraction pattern. *Journal of Applied Crystallography,* 21**,** 929-934.

KIRILLIN, M. Y., MOTOVILOVA, T. & SHAKHOVA, N. M. 2017. Optical coherence tomography in gynecology: a narrative review. *Journal of Biomedical Optics,* 22**,** 1-9, 9.

KLEISSL, H. P., VAN DER REST, M., NAFTOLIN, F., GLORIEUX, F. H. & DE LEON, A. 1978. Collagen changes in the human uterine cervix at parturition. *American Journal of Obstetrics & Gynecology,* 130**,** 748-753.

KOO, T. K. & LI, M. Y. 2016. A Guideline of Selecting and Reporting Intraclass Correlation Coefficients for Reliability Research. *Journal of chiropractic medicine,* 15**,** 155-163.

KOSINSKA-KACZYNSKA, K., BOMBA-OPON, D., BOBROWSKA, K., KOZLOWSKI, S., BRAWURA-BISKUPSKI-SAMAHA, R., SZYMUSIK, I., WEGRZYN, P. & WIELGOS, M. 2015. Phosphorylated IGFBP-1 in predicting successful vaginal delivery in post-term pregnancy. *Archives of gynecology and obstetrics,* 292**,** 45-52.

KRAUSE, G., BRODHUN, B., ALTMANN, D., CLAUS, H. & BENZLER, J. 2006. Reliability of case definitions for public health surveillance assessed by Round-Robin test methodology. *BMC Public Health,* 6**,** 129.

KUCHARZ, E. 1992. *The Collagens: Biochemistry and Pathophysiology*, Springer.

KUON, R. J., SHI, S.-Q., MAUL, H., SOHN, C., BALDUCCI, J., SHI, L. & GARFIELD, R. E. 2011. A novel optical method to assess cervical changes during pregnancy and use to evaluate the effects of progestins on term and preterm labor. *American journal of obstetrics and gynecology,* 205**,** 82.e15-82.e8.2E20.

KYRGIOU, M., KOLIOPOULOS, G., MARTIN-HIRSCH, P., ARBYN, M., PRENDIVILLE, W. & PARASKEVAIDIS, E. 2006. Obstetric outcomes after conservative treatment for intraepithelial or early invasive cervical lesions: systematic review and meta-analysis. *Lancet,* 367**,** 489-98.

LACHELIN, G. C. L., MCGARRIGLE, H. H. G., SEED, P. T., BRILEY, A., SHENNAN, A. H. & POSTON, L. 2009. Low saliva progesterone concentrations are associated with spontaneous early preterm labour (before 34 weeks of gestation) in women at increased risk of preterm delivery. *BJOG: An International Journal of Obstetrics & Gynaecology,* 116**,** 1515-1519.

LARKIN, P. 2018. *Infrared and Raman Spectroscopy*, Elsevier.

LAU, T. Y., SANGHA, H. K., CHIEN, E. K., MCFARLIN, B. L., WAGONER JOHNSON, A. J. & TOUSSAINT, K. C., JR. 2013. Application of Fourier transform-second-harmonic generation imaging to the rat cervix. *J Microsc,* 251**,** 77-83.

LAZARO-PACHECO, D., SHAABAN, A. M., REHMAN, S. & REHMAN, I. 2019. Raman spectroscopy of breast cancer. *Applied Spectroscopy Reviews***,** 1-37.

LEE, A. C., KOZUKI, N., COUSENS, S., STEVENS, G. A., BLENCOWE, H., SILVEIRA, M. F., SANIA, A., ROSEN, H. E., SCHMIEGELOW, C., ADAIR, L. S., BAQUI, A. H., BARROS, F. C., BHUTTA, Z. A., CAULFIELD, L. E., CHRISTIAN, P., CLARKE, S. E., FAWZI, W., GONZALEZ, R., HUMPHREY, J., HUYBREGTS, L., KARIUKI, S., KOLSTEREN, P., LUSINGU, J., MANANDHAR, D., MONGKOLCHATI, A., MULLANY, L. C., NDYOMUGYENYI, R., NIEN, J. K., ROBERFROID, D., SAVILLE, N., TERLOUW, D. J., TIELSCH, J. M., VICTORA, C. G., VELAPHI, S. C., WATSON-JONES, D., WILLEY, B. A., EZZATI, M., LAWN, J. E., BLACK, R. E., KATZ, J. & GROUP, C. S.-F.-G.-A.-P. B. W. 2017. Estimates of burden and consequences of infants born small for gestational age

in low and middle income countries with INTERGROWTH-21(st) standard: analysis of CHERG datasets. *BMJ (Clinical research ed.),* 358**,** j3677-j3677.

LEE, A. C. C., BLENCOWE, H. & LAWN, J. E. 2019. Small babies, big numbers: global estimates of preterm birth. *The Lancet Global Health,* 7**,** e2-e3.

LEE, H. J., PARK, T. C. & NORWITZ, E. R. 2009. Management of pregnancies with cervical shortening: a very short cervix is a very big problem. *Reviews in obstetrics & gynecology,* 2**,** 107-115.

LEE, S. W., YOO, J. Y., KANG, J. H., KANG, M. S., JUNG, S. H., CHONG, Y., CHA, D. S., HAN, K. H. & KIM, B. M. 2008. Optical diagnosis of cervical intraepithelial neoplasm (CIN) using polarization-sensitive optical coherence tomography. *Opt Express,* 16**,** 2709-19.

LENGYEL, C. S., EHRLICH, S., IAMS, J. D., MUGLIA, L. J. & DEFRANCO, E. A. 2017. Effect of Modifiable Risk Factors on Preterm Birth: A Population Based-Cohort. *Matern Child Health J,* 21**,** 777-785.

LEPPERT, P. C. & YU, S. Y. 1991. Three-dimensional structures of uterine elastic fibers: scanning electron microscopic studies. *Connect Tissue Res,* 27**,** 15-31.

LEVER, J., KRZYWINSKI, M. & ALTMAN, N. 2017. Principal component analysis. *Nature Methods,* 14**,** 641.

LI, W., NARICE, B. F., ANUMBA, D. O. & MATCHER, S. J. 2019. Polarization-sensitive optical coherence tomography with a conical beam scan for the investigation of birefringence and collagen alignment in the human cervix. *Biomedical Optics Express,* 10**,** 4190-4206.

LI, Z., LU, Y., GUO, Y., CAO, H., WANG, Q. & SHUI, W. 2018. Comprehensive evaluation of untargeted metabolomics data processing software in feature detection, quantification and discriminating marker selection. *Anal Chim Acta,* 1029**,** 50-57.

LIANG, W., SAKULSAENGPRAPHA, V., LUBY-PHELPS, K., MAHENDROO, M. & LI, X. Quantitative Analyses of SHG Endomicroscopy Images of Cervical Collagen Network for Detecting Preterm Birth in Mouse Models. Biophotonics Congress: Biomedical Optics Congress 2018 (Microscopy/Translational/Brain/OTS), 2018/04/03 2018 Hollywood, Florida. Optical Society of America, CF1B.4.

LIAO, P. F. & STERN, M. B. 1982. Surface-enhanced Raman scattering on gold and aluminum particle arrays. *Optics Letters,* 7**,** 483-485.

LIM, E. S., RODRIGUEZ, C. & HOLTZ, L. R. 2018. Amniotic fluid from healthy term pregnancies does not harbor a detectable microbial community. *Microbiome,* 6**,** 87-87.

LINHARES, I. M., SUMMERS, P. R., LARSEN, B., GIRALDO, P. C. & WITKIN, S. S. 2011. Contemporary perspectives on vaginal pH and lactobacilli. *Am J Obstet Gynecol,* 204**,** 120.e1-5.

LIONG, S., DI QUINZIO, M. K., FLEMING, G., PERMEZEL, M., RICE, G. E. & GEORGIOU, H. M. 2015. New biomarkers for the prediction of spontaneous preterm labour in symptomatic pregnant women: a comparison with fetal fibronectin. *Bjog,* 122**,** 370-9.

LIU, L., OZA, S., HOGAN, D., CHU, Y., PERIN, J., ZHU, J., LAWN, J. E., COUSENS, S., MATHERS, C. & BLACK, R. E. 2016. Global, regional, and national causes of under-5 mortality in 2000-15: an updated systematic analysis with implications for the Sustainable Development Goals. *Lancet (London, England),* 388**,** 3027-3035.

LIU, Y., HONG, Z., TAN, G., DONG, X., YANG, G., ZHAO, L., CHEN, X., ZHU, Z., LOU, Z., QIAN, B., ZHANG, G. & CHAI, Y. 2014. NMR and LC/MS-based global metabolomics to identify serum biomarkers differentiating hepatocellular carcinoma from liver cirrhosis. *International Journal of Cancer,* 135**,** 658-668.

LIU, Z.-Q. 1991. Scale space approach to directional analysis of images. *Applied Optics,* 30**,** 1369-1373.

LU, Z., KASARAGOD, D. & MATCHER, S. J. 2014. Conical scan polarization-sensitive optical coherence tomography. *Biomedical optics express,* 5**,** 752-762.

LUNDSGAARD-NIELSEN, S. M., PORS, A., BANKE, S. O., HENRIKSEN, J. E., HEPP, D. K. & WEBER, A. 2018. Critical-depth Raman spectroscopy enables home-use non-invasive glucose monitoring. *PLOS ONE,* 13**,** e0197134.

MA, B., FORNEY, L. J. & RAVEL, J. 2012. Vaginal microbiome: rethinking health and disease. *Annu Rev Microbiol,* 66**,** 371-89.

MACAULAY, S., BUCHMANN, E. J., DUNGER, D. B. & NORRIS, S. A. 2019. Reliability and validity of last menstrual period for gestational age estimation in a low-to-middle-income setting. *Journal of Obstetrics and Gynaecology Research,* 45**,** 217-225.

MACDONALD, M. C., BROWN, B. H., LYON, R. E., HEALEY, T. J., PALMER, J. E. & TIDY, J. A. 2017. Influence of high risk HPV genotype on colposcopic performance: A large prospective study demonstrates improved detection of disease with ZedScan I, particularly in non-HPV 16 patients. *Eur J Obstet Gynecol Reprod Biol,* 211**,** 194-198.

MAHENDROO, M. 2012. Cervical remodeling in term and preterm birth: insights from an animal model. *Reproduction,* 143**,** 429-38.

MAILLOT, K. & ZIMMERMANN, B. K. 1976. The solubility of collagen of the uterine cervix during pregnancy and labour. *Arch. Gynak.,* 220**,** 275.

MAITRE, L., FTHENOU, E., ATHERSUCH, T., COEN, M., TOLEDANO, M. B., HOLMES, E., KOGEVINAS, M., CHATZI, L. & KEUN, H. C. 2014. Urinary metabolic profiles in early pregnancy are associated with preterm birth and fetal growth restriction in the Rhea mother–child cohort study. *BMC Medicine,* 12**,** 110.

MANABE, Y., MORI, T. & YOSHIDA, Y. 1984. Decidual morphology and F prostaglandin in amniotic fluid in stretch-induced abortion. *Obstet Gynecol,* 64**,** 661-5.

MANCUSO, M. S., SZYCHOWSKI, J. M., OWEN, J., HANKINS, G., IAMS, J. D., SHEFFIELD, J. S., PEREZ-DELBOY, A., BERGHELLA, V., WING, D. A. & GUZMAN, E. R. 2010. Cervical funneling: effect on gestational length and ultrasound-indicated cerclage in high-risk women. *Am J Obstet Gynecol,* 203**,** 259.e1-5.

MANNS-JAMES, L. 2011. Bacterial Vaginosis and Preterm Birth. *Journal of Midwifery & Women's Health,* 56**,** 575-583.

MARLOW, N. 2015. Keeping up with outcomes for infants born at extremely low gestational ages. *JAMA Pediatr,* 169**,** 207-8.

MARTIN, R. J. & FANAROFF, A. A. 2013. The Preterm Lung and Airway: Past, Present, and Future. *Pediatrics & Neonatology,* 54**,** 228-234.

MATCHER, S. J. 2009. A review of some recent developments in polarization-sensitive optical imaging techniques for the study of articular cartilage. *Journal of Applied Physics,* 105**,** 102041.

MATCHER, S. J. 2011. Practical aspects of OCT imaging in tissue engineering. *Methods Mol Biol,* 695**,** 261-80.

MATEI, A., SACCONE, G., VOGEL, J. P. & ARMSON, A. B. 2019. Primary and secondary prevention of preterm birth: a review of systematic reviews and ongoing randomized controlled trials. *Eur J Obstet Gynecol Reprod Biol,* 236**,** 224-239.

MATZINGER, B., WOLF, M., BAÑOS, A., FINK, D. & HORNUNG, R. 2009. Optical properties, physiologic parameters and tissue composition of the human uterine cervix as a function of hormonal status. *Lasers in Medical Science,* 24**,** 561-566.

MAUL, H., OLSON, G., FITTKOW, C. T., SAADE, G. R. & GARFIELD, R. E. 2003. Cervical light-induced fluorescence in humans decreases throughout gestation and before delivery: Preliminary observations. *American Journal of Obstetrics and Gynecology,* 188**,** 537-541.

MAVRODINEANU, R. & HUGHES, R. C. 1968. A multichannel spectrometer for simultaneous atomic absorption and flame emission analysis. *Appl Opt,* 7**,** 1281-5.

MEDLEY, N., VOGEL, J. P., CARE, A. & ALFIREVIC, Z. 2018. Interventions during pregnancy to prevent preterm birth: an overview of Cochrane systematic reviews. *Cochrane Database Syst Rev,* 11**,** Cd012505.

MEHTA, S., BASTERO-CABALLERO, R. F., SUN, Y., ZHU, R., MURPHY, D. K., HARDAS, B. & KOCH, G. 2018. Performance of intraclass correlation coefficient (ICC) as a reliability index under various distributions in scale reliability studies. *Statistics in medicine,* 37**,** 2734-2752.

MENNI, C., ZIERER, J., VALDES, A. M. & SPECTOR, T. D. 2017. Mixing omics: combining genetics and metabolomics to study rheumatic diseases. *Nat Rev Rheumatol,* 13**,** 174-181.

MENON, R., PEARCE, B., VELEZ, D. R., MERIALDI, M., WILLIAMS, S. M., FORTUNATO, S. J. & THORSEN, P. 2009. Racial disparity in pathophysiologic pathways of preterm birth based on genetic variants. *Reproductive biology and endocrinology : RB&E,* 7**,** 62-62.

MENON, R., TORLONI, M. R., VOLTOLINI, C., TORRICELLI, M., MERIALDI, M., BETRAN, A. P., WIDMER, M., ALLEN, T., DAVYDOVA, I., KHODJAEVA, Z., THORSEN, P., KACEROVSKY, M., TAMBOR, V., MASSINEN, T., NACE, J. & ARORA, C. 2011. Biomarkers of spontaneous preterm birth: an overview of the literature in the last four decades. *Reprod Sci,* 18**,** 1046-70.

MERCER, B. M., GOLDENBERG, R. L., MOAWAD, A. H., MEIS, P. J., IAMS, J. D., DAS, A. F., CARITIS, S. N., MIODOVNIK, M., MENARD, M. K., THURNAU, G. R., DOMBROWSKI, M. P., ROBERTS, J. M. & MCNELLIS, D. 1999. The preterm prediction study: effect of gestational age and cause of preterm birth on subsequent obstetric outcome. National Institute of Child Health and Human Development Maternal-Fetal Medicine Units Network. *Am J Obstet Gynecol,* 181**,** 1216-21.

MERHAMETSIZ, O., OGUZ, E. G., YAYAR, O., BEKTAN, B., CANBAKAN, B. & AYLI, D. 2015. Bioimpedance spectroscopy method to determine hypervolemia in maintenance hemodialysis patients. *Hippokratia,* 19**,** 324-331.

MERWA, R., HOLLAUS, K., BIRÓ, O. & SCHARFETTER, H. 2004. Detection of brain oedema using magnetic induction tomography: a feasibility study of the likely sensitivity and detectability. *Physiological Measurement,* 25**,** 347-354.

MILDVAN, A. S. 1987. Role of magnesium and other divalent cations in ATP-utilizing enzymes. *Magnesium,* 6**,** 28-33.

MINKOFF, H. 1983. Prematurity: infection as an etiologic factor. *Obstet Gynecol,* 62**,** 137-44.

MIRMONSEF, P., GILBERT, D., ZARIFFARD, M. R., HAMAKER, B. R., KAUR, A., LANDAY, A. L. & SPEAR, G. T. 2011. The effects of commensal bacteria on innate immune responses in the female genital tract. *Am J Reprod Immunol,* 65**,** 190-5.

MOHAMED, S. A., THOTA, C., BROWNE, P. C., DIAMOND, M. P. & AL-HENDY, A. 2014. Why is Preterm Birth Stubbornly Higher in African-Americans? *Obstetrics & gynecology international journal,* 1**,** 00019.

MOHAMMADZADEH, F., DOLATIAN, M., JORJANI, M. & ALAVI MAJD, H. 2014. Diagnostic value of Amsel's clinical criteria for diagnosis of bacterial vaginosis. *Global journal of health science,* 7**,** 8-14.

MOLINA, F. S., GOMEZ, L. F., FLORIDO, J., PADILLA, M. C. & NICOLAIDES, K. H. 2012. Quantification of cervical elastography: a reproducibility study. *Ultrasound Obstet Gynecol,* 39**,** 685-9.

MONEY, D. 2005. The laboratory diagnosis of bacterial vaginosis. *The Canadian journal of infectious diseases & medical microbiology = Journal canadien des maladies infectieuses et de la microbiologie medicale,* 16**,** 77-79.

MORGEN, C. S., BJØRK, C., ANDERSEN, P. K., MORTENSEN, L. H. & NYBO ANDERSEN, A.-M. 2008. Socioeconomic position and the risk of preterm birth—a study within the Danish National Birth Cohort. *International Journal of Epidemiology,* 37**,** 1109-1120.

MORTON, S. U. & BRODSKY, D. 2016. Fetal Physiology and the Transition to Extrauterine Life. *Clinics in perinatology,* 43**,** 395-407.

MOUTQUIN, J. M. 2003. Classification and heterogeneity of preterm birth. *Bjog,* 110 Suppl 20**,** 30-3.

MOVASAGHI, Z., REHMAN, S. & REHMAN, I. U. 2007. Raman Spectroscopy of Biological Tissues. *Applied Spectroscopy Reviews,* 42**,** 493-541.

MURPHY, M. G., O'CONNOR, L., WALSH, D. & CONDON, S. 1985. Oxygen dependent lactate utilization by Lactobacillus plantarum. *Arch Microbiol,* 141**,** 75-9.

MURRAY, S. R., STOCK, S. J., COWAN, S., COOPER, E. S. & NORMAN, J. E. 2018. Spontaneous preterm birth prevention in multiple pregnancy. *The Obstetrician & Gynaecologist,* 20**,** 57-63.

MUSILOVA, I., KACEROVSKY, M., TAMBOR, V. & TOSNER, J. 2011. [Proteomics and biomarkers for detection of preterm labor: a systematic review]. *Ceska Gynekol,* 76**,** 37-45.

MYERS, K., SOCRATE, S., TZERANIS, D. & HOUSE, M. 2009. Changes in the biochemical constituents and morphologic appearance of the human cervical stroma during pregnancy. *European Journal of Obstetrics & Gynecology and Reproductive Biology,* 144**,** S82-S89.

MYERS, K. M., FELTOVICH, H., MAZZA, E., VINK, J., BAJKA, M., WAPNER, R. J., HALL, T. J. & HOUSE, M. 2015. The mechanical role of the cervix in pregnancy. *Journal of biomechanics,* 48**,** 1511-1523.

NALLASAMY, S., AKINS, M., TETREAULT, B., LUBY-PHELPS, K. & MAHENDROO, M. 2017a. *Distinct reorganization of collagen architecture in lipopolysaccharide-mediated premature cervical remodeling<xref ref-type="fn" rid="fn01">[†]</xref>*, BIOONE.

NALLASAMY, S., YOSHIDA, K., AKINS, M., MYERS, K., IOZZO, R. & MAHENDROO, M. 2017b. Steroid Hormones Are Key Modulators of Tissue Mechanical Function via Regulation of Collagen and Elastic Fibers. *Endocrinology,* 158**,** 950-962.

NARICE, B. F., GREEN, N. H., MACNEIL, S. & ANUMBA, D. 2016. Second Harmonic Generation microscopy reveals collagen fibres are more organised in the cervix of postmenopausal women. *Reproductive Biology and Endocrinology,* 14**,** 70.

NARICE, B. F., MARTÍNEZ, M. A. G., AMABEBE, E., PACHECO, D. L., REHMAN, I. U. & ANUMBA, D. O. 2018. Spectroscopic techniques as potential screening tools for preterm birth: A review and an exploratory study. *Applied Spectroscopy Reviews***,** 1-20.

NEJAD, V. M. & SHAFAIE, S. 2008. The association of bacterial vaginosis and preterm labor. *J Pak Med Assoc,* 58**,** 104-6.

NELSON, D. B., HANLON, A., HASSAN, S., BRITTO, J., GEIFMAN-HOLTZMAN, O., HAGGERTY, C. & FREDRICKS, D. N. 2009. Preterm labor and bacterial vaginosis-associated bacteria among urban women. *Journal of perinatal medicine,* 37**,** 130-134.

NEMETH, E., MILLAR, L. K. & BRYANT-GREENWOOD, G. 2000. Fetal membrane distention: II. Differentially expressed genes regulated by acute distention in vitro. *Am J Obstet Gynecol,* 182**,** 60-7.

NETZ, J., FORNER, E. & HAAGEMANN, S. 1993. Contactless impedance measurement by magnetic induction--a possible method for investigation of brain impedance. *Physiol Meas,* 14**,** 463-71.

NEWNHAM, J. P., KEMP, M. W., WHITE, S. W., ARRESE, C. A., HART, R. J. & KEELAN, J. A. 2017. Applying Precision Public Health to Prevent Preterm Birth. *Frontiers in Public Health,* 5.

NGARIZE, S., HERMAN, H., ADAMS, A. & HOWELL, N. 2004. Comparison of changes in the secondary structure of unheated, heated, and high-pressure-treated beta-lactoglobulin and ovalbumin proteins using fourier transform raman spectroscopy and self-deconvolution. *J Agric Food Chem,* 52**,** 6470-7.

NGO, L. H., INOUYE, S. K., JONES, R. N., TRAVISON, T. G., LIBERMANN, T. A., DILLON, S. T., KUCHEL, G. A., VASUNILASHORN, S. M., ALSOP, D. C. & MARCANTONIO, E. R. 2017. Methodologic considerations in the design and analysis of nested case-control studies: association between cytokines and postoperative delirium. *BMC Medical Research Methodology,* 17**,** 88.

NGUYEN, S. L., GREENBERG, J. W., WANG, H., COLLAER, B. W., WANG, J. & PETROFF, M. G. 2019. Quantifying murine placental extracellular vesicles across gestation and in preterm birth data with tidyNano: A computational framework for analyzing and visualizing nanoparticle data in R. *PLOS ONE,* 14**,** e0218270.

NICE. 2015a. Preterm labour and birth | Guidance and guidelines. *National Institute for Health and Care Excellence* [Online], NG25. Available: https://www.nice.org.uk/guidance/ng25.

NICE. 2015b. *ZedScan edScan as an adjunct to colposcop colposcopy y in women with suspected cervical intr*. [Online]. Available: https://www.nice.org.uk/advice/mib20/chapter/evidence-review [Accessed].

NORMAN, K., PATTINSON, R. C., DE SOUZA, J., DE JONG, P., MOLLER, G. & KIRSTEN, G. 1994. Ampicillin and metronidazole treatment in preterm labour: a multicentre, randomised controlled trial. *Br J Obstet Gynaecol,* 101**,** 404-8.

NOTT, J. P., BONNEY, E. A., PICKERING, J. D. & SIMPSON, N. A. B. 2016. The structure and function of the cervix during pregnancy. *Translational Research in Anatomy,* 2**,** 1-7.

NSH July 2001. Guidelines for Hematoxylin & Eosin Staining. *In:* HISTOTECHNOLOGY, N. S. F. (ed.).

NUGENT, R. P., KROHN, M. A. & HILLIER, S. L. 1991. Reliability of diagnosing bacterial vaginosis is improved by a standardized method of gram stain interpretation. *J Clin Microbiol,* 29**,** 297-301.

NUNN, K. L. & FORNEY, L. J. 2016. Unraveling the Dynamics of the Human Vaginal Microbiome. *Yale J Biol Med,* 89**,** 331-337.

O'BRIEN, C. M., COCHRAN, K. J., MASSON, L. E., GOLDBERG, M., MARPLE, E., BENNETT, K. A., REESE, J., SLAUGHTER, J. C., NEWTON, J. M. & MAHADEVAN-JANSEN, A. 2019. Development of a visually guided Raman spectroscopy probe for cervical assessment during pregnancy. *Journal of Biophotonics,* 12**,** e201800138.

O'BRIEN, C. M., HERINGTON, J. L., BROWN, N., PENCE, I. J., PARIA, B. C., SLAUGHTER, J. C., REESE, J. & MAHADEVAN-JANSEN, A. 2017. In vivo Raman spectral analysis of impaired cervical remodeling in a mouse model of delayed parturition. *Sci Rep,* 7**,** 6835.

O'BRIEN, C. M., VARGIS, E., RUDIN, A., SLAUGHTER, J. C., THOMAS, G., NEWTON, J. M., REESE, J., BENNETT, K. A. & MAHADEVAN-JANSEN, A. 2018. In vivo Raman spectroscopy for biochemical monitoring of the human cervix throughout pregnancy. *American journal of obstetrics and gynecology,* 218**,** 528.e1-528.e18.

O'CONNELL, M. P., TIDY, J., WISHER, S. J., AVIS, N. J., BROWN, B. H. & LINDOW, S. W. 2000. An in vivo comparative study of the pregnant and nonpregnant cervix using electrical impedance measurements. *BJOG: An International Journal of Obstetrics & Gynaecology,* 107**,** 1040-1041.

O'HANLON, D. E., COME, R. A. & MOENCH, T. R. 2019. Vaginal pH measured in vivo: lactobacilli determine pH and lactic acid concentration. *BMC microbiology,* 19**,** 13-13.

O'HANLON, D. E., MOENCH, T. R. & CONE, R. A. 2013. Vaginal pH and microbicidal lactic acid when lactobacilli dominate the microbiota. *PloS one,* 8**,** e80074-e80074.

O'TOOLE, M. D., MARSH, L. A., DAVIDSON, J. L., TAN, Y. M., ARMITAGE, D. W. & PEYTON, A. J. 2015. Non-contact multi-frequency magnetic induction spectroscopy system for industrial-scale bio-impedance measurement. *Measurement Science and Technology,* 26**,** 035102.

OLÁH, K. S. J. 1994. The use of magnetic resonance imaging in the assessment of the cervical hydration state. *BJOG: An International Journal of Obstetrics & Gynaecology,* 101**,** 255-257.

OLAWUMI, T. 2015. *Ultra-low k dielectrics and plasma damage control for advanced technology nodes (10nm and below).*

OLIVER-WILLIAMS, C., FLEMING, M., WOOD, A. M. & SMITH, G. 2015. Previous miscarriage and the subsequent risk of preterm birth in Scotland, 1980-2008: a historical cohort study. *BJOG : an international journal of obstetrics and gynaecology,* 122**,** 1525-1534.

OLIVER, S., UHM, S., DULEY, L., CROWE, S., DAVID, A. L., JAMES, C. P., CHIVERS, Z., GYTE, G., GALE, C., TURNER, M., CHAMBERS, B., DOWLING, I., MCNEILL, J., ALDERDICE, F., SHENNAN, A. & DESHPANDE, S. 2019. Top research priorities for preterm birth: results of a prioritisation partnership between people affected by preterm birth and healthcare professionals. *BMC Pregnancy and Childbirth,* 19**,** 528.

ORPHANOU, C. M., WALTON-WILLIAMS, L., MOUNTAIN, H. & CASSELLA, J. 2015. The detection and discrimination of human body fluids using ATR FT-IR spectroscopy. *Forensic Sci Int,* 252**,** e10-6.

OSTERLUND, E. 1988. The secondary structure of human plasma fibronectin: conformational changes induced by acidic pH and elevated temperatures; a circular dichroic study. *Biochim Biophys Acta,* 955**,** 330-6.

OTA, E., MORI, R., MIDDLETON, P., TOBE‐GAI, R., MAHOMED, K., MIYAZAKI, C. & BHUTTA, Z. A. 2015. Zinc supplementation for improving pregnancy and infant outcome. *Cochrane Database of Systematic Reviews.*

OU, C. W., CHEN, Z. Q., QI, S. & LYE, S. J. 1998. Increased expression of the rat myometrial oxytocin receptor messenger ribonucleic acid during labor requires both mechanical and hormonal signals. *Biol Reprod,* 59**,** 1055-61.

OU, C. W., ORSINO, A. & LYE, S. J. 1997. Expression of connexin-43 and connexin-26 in the rat myometrium during pregnancy and labor is differentially regulated by mechanical and hormonal signals. *Endocrinology,* 138**,** 5398-407.

OXLUND, B. S., ORTOFT, G., BRUEL, A., DANIELSEN, C. C., BOR, P., OXLUND, H. & ULDBJERG, N. 2010a. Collagen concentration and biomechanical properties of samples from the lower uterine cervix in relation to age and parity in non-pregnant women. *Reprod Biol Endocrinol,* 8**,** 82.

OXLUND, B. S., ØRTOFT, G., BRÜEL, A., DANIELSEN, C. C., OXLUND, H. & ULDBJERG, N. 2010b. Cervical collagen and biomechanical strength in non-pregnant women with a history of cervical insufficiency. *Reproductive biology and endocrinology : RB&E,* 8**,** 92-92.

PARARAS, M. V., SKEVAKI, C. L. & KAFETZIS, D. A. 2006. Preterm birth due to maternal infection: Causative pathogens and modes of prevention. *Eur J Clin Microbiol Infect Dis,* 25**,** 562-9.

PARIKH, R., MATHAI, A., PARIKH, S., CHANDRA SEKHAR, G. & THOMAS, R. 2008. Understanding and using sensitivity, specificity and predictive values. *Indian journal of ophthalmology,* 56**,** 45-50.

PARRA-SAAVEDRA, M., GOMEZ, L., BARRERO, A., PARRA, G., VERGARA, F. & NAVARRO, E. 2011. Prediction of preterm birth using the cervical consistency index. *Ultrasound Obstet Gynecol,* 38**,** 44-51.

PELTIER, M. R. 2003. Immunology of term and preterm labor. *Reproductive biology and endocrinology : RB&E,* 1**,** 122-122.

PENDHARKAR, S., MAGOPANE, T., LARSSON, P. G., DE BRUYN, G., GRAY, G. E., HAMMARSTROM, L. & MARCOTTE, H. 2013. Identification and characterisation of vaginal lactobacilli from South African women. *BMC Infect Dis,* 13**,** 43.

PETRICEVIC, L., DOMIG, K. J., NIERSCHER, F. J., SANDHOFER, M. J., FIDESSER, M., KRONDORFER, I., HUSSLEIN, P., KNEIFEL, W. & KISS, H. 2014. Characterisation of the vaginal Lactobacillus microbiota associated with preterm delivery. *Sci Rep,* 4**,** 5136.

PETROU, S., YIU, H. H. & KWON, J. 2019. Economic consequences of preterm birth: a systematic review of the recent literature (2009–2017). *Archives of Disease in Childhood,* 104**,** 456.

PIETERS, S., VANDER HEYDEN, Y., ROGER, J. M., D'HONDT, M., HANSEN, L., PALAGOS, B., DE SPIEGELEER, B., REMON, J. P., VERVAET, C. & DE BEER, T. 2013. Raman spectroscopy and multivariate analysis for the rapid discrimination between native-like and non-native states in freeze-dried protein formulations. *Eur J Pharm Biopharm,* 85**,** 263-71.

PIRCHER, M., HITZENBERGER, C. K. & SCHMIDT-ERFURTH, U. 2011. Polarization sensitive optical coherence tomography in the human eye. *Prog Retin Eye Res,* 30**,** 431-51.

POPESCU, D. P., CHOO-SMITH, L.-P. I., FLUERARU, C., MAO, Y., CHANG, S., DISANO, J., SHERIF, S. & SOWA, M. G. 2011. Optical coherence tomography: fundamental principles, instrumental designs and biomedical applications. *Biophysical Reviews,* 3**,** 155.

PREDANIC, M. 2002. Evaluation of a device for objective determination of cervical consistency: a pilot study of device's validity on uterine specimens obtained by total abdominal hysterectomy for benign uterine disease. *J Perinat Med,* 30**,** 364-6.

PRIYA, B., MUSTAFA, M. D., GULERIA, K., VAID, N. B., BANERJEE, B. D. & AHMED, R. S. 2013. Salivary progesterone as a biochemical marker to predict early preterm birth in asymptomatic high-risk women. *Bjog,* 120**,** 1003-11.

PROCKOP, D. J. & KIVIRIKKO, K. I. 1995. Collagens: molecular biology, diseases, and potentials for therapy. *Annu Rev Biochem,* 64**,** 403-34.

QU, Y., HU, P., SHI, J., MASLOV, K., ZHAO, P., LI, C., MA, J., GARCIA-URIBE, A., MEYERS, K., DIVELEY, E., PIZZELLA, S., MUENCH, L., PUNYAMURTHY, N., GOLDSTEIN, N., ONWUMERE, O., ALISIO, M., MEYENBURG, K., MAYNARD, J., HELM, K., ALTIERI, E., SLAUGHTER, J., BARBER, S., BURGER, T., KRAMER, C., CHUBIZ, J., ANDERSON, M., MCCARTHY, R., ENGLAND, S. K., MACONES, G. A., M.D., M. J. S., TUULI, M. & WANG, L. V. 2018. In vivo characterization of connective tissue remodeling using infrared photoacoustic spectra. *Journal of Biomedical Optics,* 23**,** 1-6, 6.

QUINN, J.-A., MUNOZ, F. M., GONIK, B., FRAU, L., CUTLAND, C., MALLETT-MOORE, T., KISSOU, A., WITTKE, F., DAS, M., NUNES, T., PYE, S., WATSON, W., RAMOS, A.-M. A., CORDERO, J. F., HUANG, W.-T., KOCHHAR, S., BUTTERY, J. & BRIGHTON COLLABORATION PRETERM BIRTH WORKING, G. 2016. Preterm birth: Case definition & guidelines for data collection, analysis, and presentation of immunisation safety data. *Vaccine,* 34**,** 6047-6056.

RADFORD, S., ABBOTT, D., SEED, P., KEMP, J. & SHENNAN, A. 2012. Quantitative fetal fibronectin for the prediction of preterm birth in symptomatic women. *Archives of Disease in Childhood - Fetal and Neonatal Edition,* 97**,** A73.

RAFAEL, T. J., BERGHELLA, V. & ALFIREVIC, Z. 2014. Cervical stitch (cerclage) for preventing preterm birth in multiple pregnancy. *Cochrane Database Syst Rev***,** Cd009166.

RAJAEI, M., SULTANI, M. & ZARE, S. 2006. A randomized controlled trial of adjunctive erythromycin in women with idiopathic preterm labor. *J Matern Fetal Neonatal Med,* 19**,** 17-20.

RAMOS, I. R., LYNG, F. M., REHMAN, I. U., SHARRACK, B. & WOODROOFE, M. N. 2017. The use of vibrational spectroscopy to study the pathogenesis multiple sclerosis and other neurological conditions. *Applied Spectroscopy Reviews,* 52**,** 868-882.

RAVEL, J., GAJER, P., ABDO, Z., SCHNEIDER, G. M., KOENIG, S. S., MCCULLE, S. L., KARLEBACH, S., GORLE, R., RUSSELL, J., TACKET, C. O., BROTMAN, R. M., DAVIS, C. C., AULT, K., PERALTA, L. & FORNEY, L. J. 2011. Vaginal microbiome of reproductive-age women. *Proc Natl Acad Sci U S A,* 108 Suppl 1**,** 4680-7.

RCOG 2017. Prevention of Early-onset Neonatal Group B Streptococcal Disease. *BJOG: An International Journal of Obstetrics & Gynaecology,* 124**,** e280-e305.

READ, C. P., WORD, R. A., RUSCHEINSKY, M. A., TIMMONS, B. C. & MAHENDROO, M. S. 2007. Cervical remodeling during pregnancy and parturition: molecular characterization of the softening phase in mice. *Reproduction,* 134**,** 327-40.

REICH, O. & FRITSCH, H. 2014. The developmental origin of cervical and vaginal epithelium and their clinical consequences: a systematic review. *J Low Genit Tract Dis,* 18**,** 358-60.

RELMAN, D. A. 1999. The search for unrecognized pathogens. *Science,* 284**,** 1308-10.

RICE, G. E., GEORGIOU, H. M., AHMED, N., SHI, G. & KRUPPA, G. 2006. Translational Proteomics: Developing a Predictive Capacity – A Review. *Placenta,* 27**,** 76-86.

RICHARDS, L. B., LI, M., VAN ESCH, B. C. A. M., GARSSEN, J. & FOLKERTS, G. 2016. The effects of short-chain fatty acids on the cardiovascular system. *PharmaNutrition,* 4**,** 68-111.

RICHER, A. & ADLER, A. Eddy Current Based Flexible Sensor for Contactless Measurement of Breathing. 2005 IEEE Instrumentationand Measurement Technology Conference Proceedings, 16-19 May 2005 2005. 257-260.

ROBERTS, D., BROWN, J., MEDLEY, N. & DALZIEL, S. R. 2017. Antenatal corticosteroids for accelerating fetal lung maturation for women at risk of preterm birth. *Cochrane Database of Systematic Reviews*.

ROBERTS, L. D., SOUZA, A. L., GERSZTEN, R. E. & CLISH, C. B. 2012. Targeted Metabolomics. *Current Protocols in Molecular Biology,* 98**,** 30.2.1-30.2.24.

RODRIGUEZ-MARTINEZ, P., PALACIOS-GONZALEZ, B. & VADILLO-ORTEGA, F. 2017. Federation proceedings. *The FASEB Journal*.

ROMEJKO-WOLNIEWICZ, E., TELIGA-CZAJKOWSKA, J. & CZAJKOWSKI, K. 2014. Antenatal steroids: can we optimize the dose? *Current opinion in obstetrics & gynecology,* 26**,** 77-82.

ROMERO, R., ESPINOZA, J., EREZ, O. & HASSAN, S. 2006a. The role of cervical cerclage in obstetric practice: Can the patient who could benefit from this procedure be identified? *American Journal of Obstetrics and Gynecology,* 194**,** 1-9.

ROMERO, R., ESPINOZA, J., KUSANOVIC, J. P., GOTSCH, F., HASSAN, S., EREZ, O., CHAIWORAPONGSA, T. & MAZOR, M. 2006b. The preterm parturition syndrome. *Bjog,* 113 Suppl 3**,** 17-42.

ROMERO, R., HASSAN, S. S., GAJER, P., TARCA, A. L., FADROSH, D. W., BIEDA, J., CHAEMSAITHONG, P., MIRANDA, J., CHAIWORAPONGSA, T. & RAVEL, J. 2014a. The vaginal microbiota of pregnant women who subsequently have spontaneous preterm labor and delivery and those with a normal delivery at term. *Microbiome,* 2**,** 18.

ROMERO, R., HASSAN, S. S., GAJER, P., TARCA, A. L., FADROSH, D. W., NIKITA, L., GALUPPI, M., LAMONT, R. F., CHAEMSAITHONG, P., MIRANDA, J., CHAIWORAPONGSA, T. & RAVEL, J. 2014b. The composition and stability of the vaginal microbiota of normal pregnant women is different from that of non-pregnant women. *Microbiome,* 2**,** 4.

ROMERO, R., KUSANOVIC, J. P., CHAIWORAPONGSA, T. & HASSAN, S. S. 2011. Placental bed disorders in preterm labor, preterm PROM, spontaneous abortion and abruptio placentae. *Best practice & research. Clinical obstetrics & gynaecology,* 25**,** 313-327.

ROMERO, R., MAZAKI-TOVI, S., VAISBUCH, E., KUSANOVIC, J. P., CHAIWORAPONGSA, T., GOMEZ, R., NIEN, J. K., YOON, B. H., MAZOR, M., LUO, J., BANKS, D., RYALS, J. & BEECHER, C. 2010. Metabolomics in premature labor: a novel approach to identify patients at risk for preterm delivery. *J Matern Fetal Neonatal Med,* 23**,** 1344-59.

ROMERO, R., MAZOR, M., WU, Y. K., SIRTORI, M., OYARZUN, E., MITCHELL, M. D. & HOBBINS, J. C. 1988. Infection in the pathogenesis of preterm labor. *Semin Perinatol,* 12**,** 262-79.

RORIE, D. K. & NEWTON, M. 1967. Histologic and chemical studies of the smooth muscle in the human cervix and uterus. *American Journal of Obstetrics and Gynecology,* 99**,** 466-469.

ROSADO-MENDEZ, I. M., CARLSON, L. C., WOO, K. M., SANTOSO, A. P., GUERRERO, Q. W., PALMERI, M. L., FELTOVICH, H. & HALL, T. J. 2018. Quantitative assessment of cervical softening during pregnancy in the Rhesus macaque with shear wave elasticity imaging. *Physics in medicine and biology,* 63**,** 085016-085016.

ROSS, L. F., SAAL, H. M., DAVID, K. L. & ANDERSON, R. R. 2013. Technical report: ethical and policy issues in genetic testing and screening of children. *Genetics In Medicine,* 15**,** 234.

RUBENS, C. E., SADOVSKY, Y., MUGLIA, L., GRAVETT, M. G., LACKRITZ, E. & GRAVETT, C. 2014. Prevention of preterm birth: Harnessing science to address the global epidemic. *Science Translational Medicine,* 6**,** 262sr5-262sr5.

SAADE, G., BOGGESS, K., SULLIVAN, S., MARKENSON, G., IAMS, J., COONROD, D., PEREIRA, L., ESPLIN, M. S., COUSINS, L., LAM, G., HOFFMAN, M. K., FOX, A., BRADFORD, C., FLEISCHER, T., ICHETOVKIN, I., POLPITIYA, A., KEARNEY, P., BONIFACE, J. & HICKOK, D. 2016a. 17: Clinical validation of a two-protein test for

spontaneous preterm birth (sPTB) prediction in a large multicenter prospective study of asymptomatic women. *American Journal of Obstetrics & Gynecology,* 214**,** S12.

SAADE, G. R., BOGGESS, K. A., SULLIVAN, S. A., MARKENSON, G. R., IAMS, J. D., COONROD, D. V., PEREIRA, L. M., ESPLIN, M. S., COUSINS, L. M., LAM, G. K., HOFFMAN, M. K., SEVERINSEN, R. D., PUGMIRE, T., FLICK, J. S., FOX, A. C., LUETH, A. J., RUST, S. R., MAZZOLA, E., HSU, C., DUFFORD, M. T., BRADFORD, C. L., ICHETOVKIN, I. E., FLEISCHER, T. C., POLPITIYA, A. D., CRITCHFIELD, G. C., KEARNEY, P. E., BONIFACE, J. J. & HICKOK, D. E. 2016b. Development and validation of a spontaneous preterm delivery predictor in asymptomatic women. *Am J Obstet Gynecol,* 214**,** 633.e1-633.e24.

SAGGIO, G. 2014. *Principles of Analog Electronics*, CRC Press.

SAITO, S., KASAHARA, T., KATO, Y., ISHIHARA, Y. & ICHIJO, M. 1993. Elevation of amniotic fluid interleukin 6 (IL-6), IL-8 and granulocyte colony stimulating factor (G-CSF) in term and preterm parturition. *Cytokine,* 5**,** 81-8.

SANDALL, J., SOLTANI, H., GATES, S., SHENNAN, A. & DEVANE, D. 2016. Midwife ‐ led continuity models versus other models of care for childbearing women. *Cochrane Database of Systematic Reviews*.

SANGKOMKAMHANG, U. S., LUMBIGANON, P., PRASERTCHAROENSUK, W. & LAOPAIBOON, M. 2015. Antenatal lower genital tract infection screening and treatment programs for preventing preterm delivery. *Cochrane Database of Systematic Reviews*.

SASIENI, P., CASTANON, A., LANDY, R., KYRGIOU, M., KITCHENER, H., QUIGLEY, M., POON, L., SHENNAN, A., HOLLINGWORTH, A., SOUTTER, W. P., FREEMAN-WANG, T., PEEBLES, D., PRENDIVILLE, W. & PATNICK, J. 2016. Risk of preterm birth following surgical treatment for cervical disease: executive summary of a recent symposium. *BJOG : an international journal of obstetrics and gynaecology,* 123**,** 1426-1429.

SCHLEMBACH, D., MAUL, H., FITTKOW, C., OLSON, G., SAADE, G. & GARFIELD, R. 2003. Cross-linked collagen in the cervix of pregnant women with cervical insufficiency. *American Journal of Obstetrics and Gynecology,* 189**,** S70.

SCHOLL, T. O. & STEIN, T. P. 2001. Oxidant damage to DNA and pregnancy outcome. *J Matern Fetal Med,* 10**,** 182-5.

SHAH, N. M., LAI, P. F., IMAMI, N. & JOHNSON, M. R. 2019. Progesterone-Related Immune Modulation of Pregnancy and Labor. *Frontiers in Endocrinology,* 10.

SHANKAR, R., CULLINANE, F., BRENNECKE, S. P. & MOSES, E. K. 2004. Applications of proteomic methodologies to human pregnancy research: a growing gestation approaching delivery? *Proteomics,* 4**,** 1909-17.

SHARMA, B. S. M. & SUJATHA, N. Assessment of skin fibrosis using Mueller matrix polarimetry. 2018 3rd International Conference on Microwave and Photonics (ICMAP), 9-11 Feb. 2018 2018. 1-2.

SHARMA, P., KHAN, S., GHULE, M., SHIVKUMAR, V. B., DARGAN, R., SEED, P. T., SARKAR, A., MEHRA, S., SHIVKUMAR, P. V. & TRIBE, R. M. 2018. Rationale & design of the PROMISES study: a prospective assessment and validation study of salivary progesterone as a test for preterm birth in pregnant women from rural India. *Reprod Health,* 15**,** 215.

SHI, L., SHI, S. Q., SAADE, G. R., CHWALISZ, K. & GARFIELD, R. E. 1999. Changes in cervical resistance and collagen fluorescence during gestation in rats. *J Perinat Med,* 27**,** 188-94.

SHIMAOKA, M., YO, Y., DOH, K., KOTANI, Y., SUZUKI, A., TSUJI, I., MANDAI, M. & MATSUMURA, N. 2019. Association between preterm delivery and bacterial vaginosis with or without treatment. *Scientific reports,* 9**,** 509-509.

SHLOSSMAN, P. A., MANLEY, J. S., SCISCIONE, A. C. & COLMORGEN, G. H. 1997. An analysis of neonatal morbidity and mortality in maternal (in utero) and neonatal transports at 24-34 weeks' gestation. *Am J Perinatol,* 14**,** 449-56.

SHOULDERS, M. D. & RAINES, R. T. 2009. Collagen structure and stability. *Annu Rev Biochem,* 78**,** 929-58.

SHROUT, P. E. & FLEISS, J. L. 1979. Intraclass correlations: uses in assessing rater reliability. *Psychol Bull,* 86**,** 420-8.

SIBAI, B. M. 2006. Preeclampsia as a cause of preterm and late preterm (near-term) births. *Semin Perinatol,* 30**,** 16-9.

SIGNORE, C. C., SOOD, A. K. & RICHARDS, D. S. 1998. Second-trimester vaginal bleeding: correlation of ultrasonographic findings with perinatal outcome. *Am J Obstet Gynecol,* 178**,** 336-40.

SIKIRZHYTSKAYA, A., SIKIRZHYTSKI, V. & LEDNEV, I. K. 2012. Raman spectroscopic signature of vaginal fluid and its potential application in forensic body fluid identification. *Forensic Sci Int,* 216**,** 44-8.

SLADEK, S. M., WESTERHAUSEN-LARSON, A. & ROBERTS, J. M. 1999. Endogenous Nitric Oxide Suppresses Rat Myometrial Connexin 43 Gap Junction Protein Expression during Pregnancy1. *Biology of Reproduction,* 61**,** 8-13.

SMAILL, F. M. & VAZQUEZ, J. C. 2015. Antibiotics for asymptomatic bacteriuria in pregnancy. *Cochrane Database Syst Rev***,** Cd000490.

SMFM 2017. The choice of progestogen for the prevention of preterm birth in women with singleton pregnancy and prior preterm birth. *American Journal of Obstetrics & Gynecology,* 216**,** B11-B13.

SOTIRIADIS, A., PAPATHEODOROU, S., KAVVADIAS, A. & MAKRYDIMAS, G. 2010. Transvaginal cervical length measurement for prediction of preterm birth in women with threatened preterm labor: a meta-analysis. *Ultrasound Obstet Gynecol,* 35**,** 54-64.

SOUKA, A. P., PAPASTEFANOU, I., MICHALITSI, V., SALAMBASIS, K., CHRELIAS, C., SALAMALEKIS, G. & KASSANOS, D. 2011. Cervical length changes from the first to second trimester of pregnancy, and prediction of preterm birth by first-trimester sonographic cervical measurement. *J Ultrasound Med,* 30**,** 997-1002.

SOUKA, A. P. & PILALIS, A. 2019. Reproducibility of cervical length measurement throughout pregnancy. *The Journal of Maternal-Fetal & Neonatal Medicine***,** 1-7.

SRINIVASAN, S., MORGAN, M. T., FIEDLER, T. L., DJUKOVIC, D., HOFFMAN, N. G., RAFTERY, D., MARRAZZO, J. M. & FREDRICKS, D. N. 2015. Metabolic signatures of bacterial vaginosis. *MBio,* 6.

STAFFORD, G. P., PARKER, J. L., AMABEBE, E., KISTLER, J., REYNOLDS, S., STERN, V., PALEY, M. & ANUMBA, D. O. C. 2017. Spontaneous Preterm Birth Is Associated with Differential Expression of Vaginal Metabolites by Lactobacilli-Dominated Microflora. *Front Physiol,* 8**,** 615.

STERN, V. & ANUMBA, D. 2016. Prematurity. *In:* ANUMBA, D. & JIVRAJ, S. (eds.) *Antenatal Disorders for the MRCOG and Beyond.* 2 ed. Cambridge: Cambridge University Press.

STERN, V., HEALEY, J., BROWN, B. & ANUMBA, D. O. 2016. Blair Bell Research Society Annual Academic Meeting abstracts. *BJOG: An International Journal of Obstetrics & Gynaecology,* 123**,** e1-e14.

STOLZ, L. A., AMINI, R., SITU-LACASSE, E. H., SHAREEF, F., REED, H. A. & ADHIKARI, S. 2017. Cervical Funneling: Potential Pitfall of Point-of-Care Pelvic Ultrasound. *Cureus,* 9**,** e1649-e1649.

STORY, L., SIMPSON, N. A. B., DAVID, A. L., ALFIREVIC Z, Z., BENNETT, P. R., JOLLY, M. & SHENNAN, A. H. 2019. Reducing the impact of preterm birth: Preterm birth commissioning in the United Kingdom. *European Journal of Obstetrics & Gynecology and Reproductive Biology: X,* 3**,** 100018.

STREHLE, M. A., RÖSCH, P., PETRY, R., HAUCK, A., THULL, R., KIEFER, W. & POPP, J. 2004. A Raman spectroscopic study of the adsorption of fibronectin and fibrinogen on titanium dioxide nanoparticles. *Physical Chemistry Chemical Physics,* 6**,** 5232-5236.

SUFF, N., STORY, L. & SHENNAN, A. 2019. The prediction of preterm delivery: What is new? *Seminars in Fetal and Neonatal Medicine,* 24**,** 27-32.

SUNG, S. J., LEE, S. M., KIM, S., KIM, B. J., PARK, C. W., PARK, J. S. & JUN, J. K. 2018. The Risk of Spontaneous Preterm Birth according to Maternal Pre-pregnancy Body Mass Index in Twin Gestations. *J Korean Med Sci,* 33**,** e103.

SWIATKOWSKA-FREUND, M. & PREIS, K. 2017. Cervical elastography during pregnancy: clinical perspectives. *International journal of women's health,* 9**,** 245-254.

SWIATKOWSKA-FREUND, M., TRACZYK-LOS, A., PREIS, K., LUKASZUK, M. & ZIELINSKA, K. 2014. Prognostic value of elastography in predicting premature delivery. *Ginekol Pol,* 85**,** 204-7.

SZULCEK, R., BOGAARD, H. J. & VAN NIEUW AMERONGEN, G. P. 2014. Electric cell-substrate impedance sensing for the quantification of endothelial proliferation, barrier function, and motility. *J Vis Exp*.

TACHEDJIAN, G., ALDUNATE, M., BRADSHAW, C. S. & CONE, R. A. 2017. The role of lactic acid production by probiotic Lactobacillus species in vaginal health. *Research in Microbiology,* 168**,** 782-792.

TAIPALE, P. & HIILESMAA, V. 1998. Sonographic measurement of uterine cervix at 18-22 weeks' gestation and the risk of preterm delivery. *Obstet Gynecol,* 92**,** 902-7.

TALARI, A. C. S., MOVASAGHI, Z., REHMAN, S. & REHMAN, I. U. 2015. Raman Spectroscopy of Biological Tissues. *Applied Spectroscopy Reviews,* 50**,** 46-111.

THOMAS, M. M., SULEK, K., MCKENZIE, E. J., JONES, B., HAN, T.-L., VILLAS-BOAS, S. G., KENNY, L. C., MCCOWAN, L. M. E. & BAKER, P. N. 2015. Metabolite Profile of Cervicovaginal Fluids from Early Pregnancy Is Not Predictive of Spontaneous Preterm Birth. *International journal of molecular sciences,* 16**,** 27741-27748.

THOMSON, A. J., THE ROYAL COLLEGE OF, O. & GYNAECOLOGISTS 2019. Care of Women Presenting with Suspected Preterm Prelabour Rupture of Membranes from 24+0 Weeks of Gestation. *BJOG: An International Journal of Obstetrics & Gynaecology,* 126**,** e152-e166.

TIMMONS, B., AKINS, M. & MAHENDROO, M. 2010. Cervical remodeling during pregnancy and parturition. *Trends Endocrinol Metab,* 21**,** 353-61.

TIMMONS, B. C., FAIRHURST, A. M. & MAHENDROO, M. S. 2009. Temporal changes in myeloid cells in the cervix during pregnancy and parturition. *J Immunol,* 182**,** 2700-7.

TOLOSA, J. E., CHAITHONGWONGWATTHANA, S., DALY, S., MAW, W. W., GAITAN, H., LUMBIGANON, P., FESTIN, M., CHIPATO, T., SAUVARIN, J., GOLDENBERG, R. L., ANDREWS, W. W. & WHITNEY, C. G. 2006. The International Infections in Pregnancy (IIP) study: variations in the prevalence of bacterial vaginosis and distribution of

morphotypes in vaginal smears among pregnant women. *Am J Obstet Gynecol,* 195**,** 1198-204.

TRUMBO, T. A., SCHULTZ, E., BORLAND, M. G. & PUGH, M. E. 2013. Applied spectrophotometry: Analysis of a biochemical mixture. *Biochemistry and Molecular Biology Education,* 41**,** 242-250.

TSATSARIS, V., CABROL, D. & CARBONNE, B. 2004. Pharmacokinetics of tocolytic agents. *Clin Pharmacokinet,* 43**,** 833-44.

TSIARTAS, P., HOLST, R. M., WENNERHOLM, U. B., HAGBERG, H., HOUGAARD, D. M., SKOGSTRAND, K., PEARCE, B. D., THORSEN, P., KACEROVSKY, M. & JACOBSSON, B. 2012. Prediction of spontaneous preterm delivery in women with threatened preterm labour: a prospective cohort study of multiple proteins in maternal serum. *Bjog,* 119**,** 866-73.

UGRYUMOVA, N., JACOBS, J., BONESI, M. & MATCHER, S. J. 2009. Novel optical imaging technique to determine the 3-D orientation of collagen fibers in cartilage: variable-incidence angle polarization-sensitive optical coherence tomography. *Osteoarthritis and Cartilage,* 17**,** 33-42.

UK, G. 2017. Infectious diseases in pregnancy screening: programme overview. *Gov UK*.

ULDBJERG, N., EKMAN, G., MALMSTROM, A., OLSSON, K. & ULMSTEN, U. 1983. Ripening of the human uterine cervix related to changes in collagen, glycosaminoglycans, and collagenolytic activity. *Am J Obstet Gynecol,* 147**,** 662-6.

USMAN, S., FOO, L., TAY, J., BENNETT, P. R. & LEES, C. 2017. Use of magnesium sulfate in preterm deliveries for neuroprotection of the neonate. *The Obstetrician & Gynaecologist,* 19**,** 21-28.

VAN DER VEER, C., HERTZBERGER, R. Y., BRUISTEN, S. M., TYTGAT, H. L. P., SWANENBURG, J., DE KAT ANGELINO-BART, A., SCHUREN, F., MOLENAAR, D., REID, G., DE VRIES, H. & KORT, R. 2019. Comparative genomics of human Lactobacillus crispatus isolates reveals genes for glycosylation and glycogen degradation: implications for in vivo dominance of the vaginal microbiota. *Microbiome,* 7**,** 49.

VARGIS, E., BROWN, N., WILLIAMS, K., AL-HENDY, A., PARIA, B. C., REESE, J. & MAHADEVAN-JANSEN, A. 2012. Detecting biochemical changes in the rodent cervix during pregnancy using Raman spectroscopy. *Annals of biomedical engineering,* 40**,** 1814-1824.

VARLEY-CAMPBELL, J., MUJICA-MOTA, R., COELHO, H., OCEAN, N., BARNISH, M., PACKMAN, D., DODMAN, S., COOPER, C., SNOWSILL, T., KAY, T., LIVERSEDGE, N., PARR, M., KNIGHT, L., HYDE, C., SHENNAN, A. & HOYLE, M. 2019. Three biomarker tests to help diagnose preterm labour: a systematic review and economic evaluation. *Health Technol Assess,* 23**,** 1-226.

VASAKOVA, H. 2011. A powerful tool for material identification: Raman Spectroscopy. *Int. J. Math. Models Methods Appl. Sci.,* 7**,** 1205-1212.

VEENSTRA, T. D. 2012. Metabolomics: the final frontier? *Genome Medicine,* 4**,** 40.

VERSTRAELEN, H., VERVAET, C. & REMON, J. P. 2016. Rationale and Safety Assessment of a Novel Intravaginal Drug-Delivery System with Sustained DL-Lactic Acid Release, Intended for Long-Term Protection of the Vaginal Microbiome. *PLoS One,* 11**,** e0153441.

VINAGRE, L. E. D. F. & MARBA, S. T. M. 2010. Uso antenatal do corticosteroide e hemorragia peri-intraventricular. *Revista Paulista de Pediatria,* 28**,** 346-352.

VINK, J. & FELTOVICH, H. 2016. Cervical etiology of spontaneous preterm birth. *Seminars in fetal & neonatal medicine,* 21**,** 106-112.

VIRKLER, K. & LEDNEV, I. K. 2008. Raman spectroscopy offers great potential for the nondestructive confirmatory identification of body fluids. *Forensic Science International,* 181**,** e1-e5.

VIRKLER, K. & LEDNEV, I. K. 2009. Raman spectroscopic signature of semen and its potential application to forensic body fluid identification. *Forensic Sci Int,* 193**,** 56-62.

VISCARDI, R. M. 2010. Ureaplasma species: role in diseases of prematurity. *Clinics in perinatology,* 37**,** 393-409.

WALKER, D. C., BROWN, B. H., BLACKETT, A. D., TIDY, J. & SMALLWOOD, R. H. 2003. A study of the morphological parameters of cervical squamous epithelium. *Physiol Meas,* 24**,** 121-35.

WALKER, D. C., BROWN, B. H., SMALLWOOD, R. H., HOSE, D. R. & JONES, D. M. 2002. Modelled current distribution in cervical squamous tissue. *Physiol Meas,* 23**,** 159-68.

WANG, J. Y., HEALEY, T., BARKER, A., BROWN, B., MONK, C. & ANUMBA, D. 2017. Magnetic induction spectroscopy (MIS)-probe design for cervical tissue measurements. *Physiol Meas,* 38**,** 729-744.

WASSENAAR, T. M. & PANIGRAHI, P. 2014. Is a foetus developing in a sterile environment? *Lett Appl Microbiol,* 59**,** 572-9.

WATSON, H. A., CARLISLE, N., KUHRT, K., TRIBE, R. M., CARTER, J., SEED, P. & SHENNAN, A. H. 2019. EQUIPTT: The Evaluation of the QUiPP app for Triage and Transfer protocol for a cluster randomised trial to evaluate the impact of the QUiPP app on inappropriate management for threatened preterm labour. *BMC Pregnancy and Childbirth,* 19**,** 68.

WATSON, H. A., CARTER, J., SEED, P. T., TRIBE, R. M. & SHENNAN, A. H. 2017. The QUiPP App: a safe alternative to a treat-all strategy for threatened preterm labor. *Ultrasound Obstet Gynecol,* 50**,** 342-346.

WATSON, W. J., STEVENS, D., WELTER, S. & DAY, D. 1999. Observations on the sonographic measurement of cervical length and the risk of premature birth. *J Matern Fetal Med,* 8**,** 17-9.

WEISS, S., JAERMANN, T., SCHMID, P., STAEMPFLI, P., BOESIGER, P., NIEDERER, P., CADUFF, R. & BAJKA, M. 2006. Three-dimensional fiber architecture of the nonpregnant human uterus determined ex vivo using magnetic resonance diffusion tensor imaging. *The Anatomical Record Part A: Discoveries in Molecular, Cellular, and Evolutionary Biology,* 288A**,** 84-90.

WHO 2012. Born Too Soon: The Global Action Report on Preterm Birth.

WILLIAMS, T. C. & DRAKE, A. J. 2019. Preterm birth in evolutionary context: a predictive adaptive response? *Philos Trans R Soc Lond B Biol Sci,* 374**,** 20180121.

WILSON, J. 2004. Managing recurrent bacterial vaginosis. *Sexually transmitted infections,* 80**,** 8-11.

WITKIN, S. S., MENDES-SOARES, H., LINHARES, I. M., JAYARAM, A., LEDGER, W. J. & FORNEY, L. J. 2013a. Influence of Vaginal Bacteria and d- and l-Lactic Acid Isomers on Vaginal Extracellular Matrix Metalloproteinase Inducer: Implications for Protection against Upper Genital Tract Infections. *mBio,* 4**,** e00460-13.

WITKIN, S. S., MENDES-SOARES, H., LINHARES, I. M., JAYARAM, A., LEDGER, W. J. & FORNEY, L. J. 2013b. Influence of vaginal bacteria and D- and L-lactic acid isomers on vaginal extracellular matrix metalloproteinase inducer: implications for protection against upper genital tract infections. *MBio,* 4.

WITKIN, S. S., MORON, A. F., RIDENHOUR, B. J., MINIS, E., HATANAKA, A., SARMENTO, S. G. P., FRANCA, M. S., CARVALHO, F. H. C., HAMAMOTO, T. K., MATTAR, R., SABINO, E., LINHARES, I. M., RUDGE, M. V. C. & FORNEY, L. J. 2019. Vaginal Biomarkers That Predict Cervical Length and Dominant Bacteria in the Vaginal Microbiomes of Pregnant Women. *mBio,* 10**,** e02242-19.

WOOD, R. 2018. *Investigating the prognostic signifcance of cervicovaginal fluid pyruvate, lactate and urea for preterm birth in high-risk women.* MSc, University of Sheffield.

WOZNIAK, S., CZUCZWAR, P., SZKODZIAK, P., MILART, P., WOZNIAKOWSKA, E. & PASZKOWSKI, T. 2014. Elastography in predicting preterm delivery in asymptomatic, low-risk women: a prospective observational study. *BMC Pregnancy Childbirth,* 14**,** 238.

XIANG, J., XIONG, H. & DONG, Y. 2018. *Magnetic Induction Sensing with a Gradiometer Coil and Measurement Circuit.*

XIN, C., JOHNSTONE, M., WANG, N. & WANG, R. K. 2016. OCT Study of Mechanical Properties Associated with Trabecular Meshwork and Collector Channel Motion in Human Eyes. *PLOS ONE,* 11**,** e0162048.

YAN, Y., BASIJ, M., WANG, Z., SIDDIQUI, A., DONG, J., ALIJABBARI, N., HERNANDEZ-ANDRADE, E., GOMEZ-LOPEZ, N., HASSAN, S. & MEHRMOHAMMADI, M. Multi-parametric acoustic imaging of cervix for more accurate detection of patients at risk of preterm birth. 2018 IEEE International Ultrasonics Symposium (IUS), 22-25 Oct. 2018 2018. 1-4.

YANG, S., REID, G., CHALLIS, J. R. G., KIM, S. O., GLOOR, G. B. & BOCKING, A. D. 2015. Is there a role for probiotics in the prevention of preterm birth? *Frontiers in immunology,* 6**,** 62-62.

YAO, W., GAN, Y., MYERS, K. M., VINK, J. Y., WAPNER, R. J. & HENDON, C. P. 2016. Collagen Fiber Orientation and Dispersion in the Upper Cervix of Non-Pregnant and Pregnant Women. *PLOS ONE,* 11**,** e0166709.

YEOMAN, C. J., THOMAS, S. M., MILLER, M. E., ULANOV, A. V., TORRALBA, M., LUCAS, S., GILLIS, M., CREGGER, M., GOMEZ, A., HO, M., LEIGH, S. R., STUMPF, R., CREEDON, D. J., SMITH, M. A., WEISBAUM, J. S., NELSON, K. E., WILSON, B. A. & WHITE, B. A. 2013. A multi-omic systems-based approach reveals metabolic markers of bacterial vaginosis and insight into the disease. *PLoS One,* 8**,** e56111.

YORUCU, C., LAU, K., MITTAR, S., GREEN, N. H., RAZA, A., REHMAN, I. U. & MACNEIL, S. 2016. Raman spectroscopy detects melanoma and the tissue surrounding melanoma using tissue-engineered melanoma models AU - Yorucu, Ceyla. *Applied Spectroscopy Reviews,* 51**,** 263-277.

YOSHIDA, K., JIANG, H., KIM, M., VINK, J., CREMERS, S., PAIK, D., WAPNER, R., MAHENDROO, M. & MYERS, K. 2014. Quantitative Evaluation of Collagen Crosslinks and Corresponding Tensile Mechanical Properties in Mouse Cervical Tissue during Normal Pregnancy. *PLOS ONE,* 9**,** e112391.

ZEGELS, G., VAN RAEMDONCK, G. A., TJALMA, W. A. & VAN OSTADE, X. W. 2010. Use of cervicovaginal fluid for the identification of biomarkers for pathologies of the female genital tract. *Proteome science,* 8**,** 63-63.

ZIERER, J., MENNI, C., KASTENMULLER, G. & SPECTOR, T. D. 2015. Integration of 'omics' data in aging research: from biomarkers to systems biology. *Aging Cell,* 14**,** 933-44.

ZORK, N. M., MYERS, K. M., YOSHIDA, K., CREMERS, S., JIANG, H., ANANTH, C. V., WAPNER, R. J., KITAJEWSKI, J. & VINK, J. 2015. A systematic evaluation of collagen cross-links in the human cervix. *Am J Obstet Gynecol,* 212**,** 321.e1-8.

ZUMDAHL, S. & ZUMDAHL, S. 2013. *Chemistry*, Brooks Cole.

Appendix A

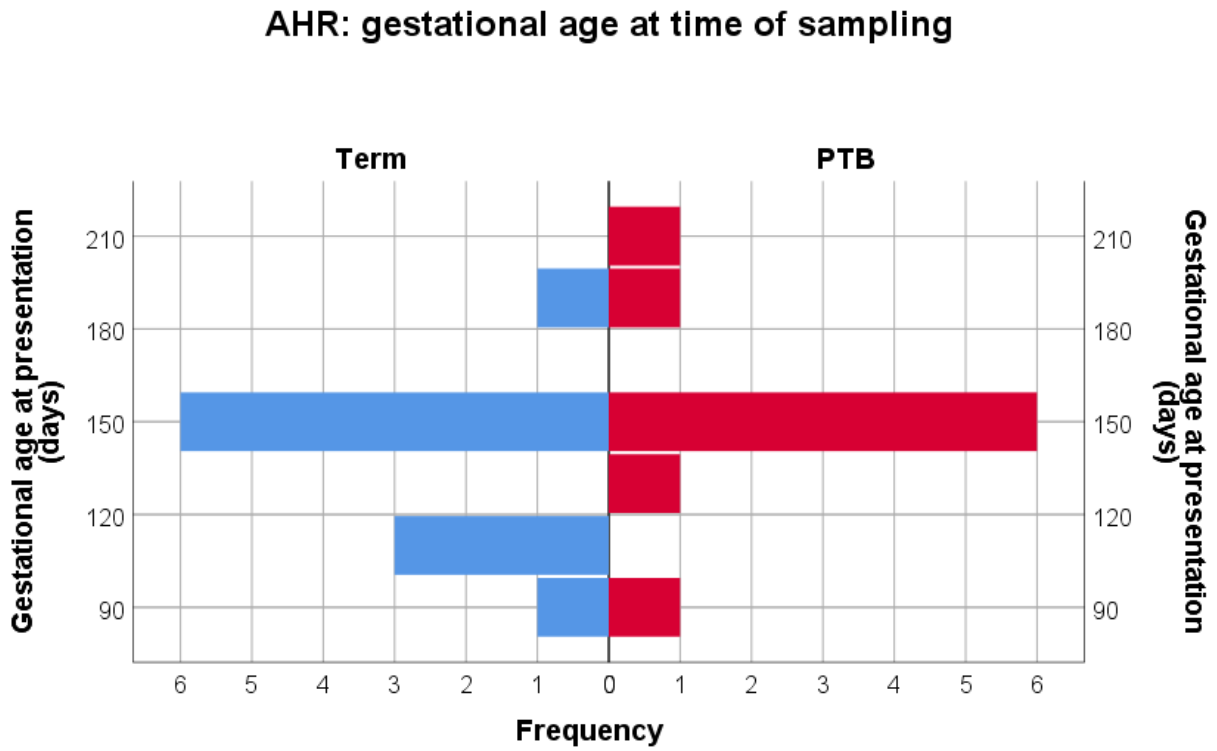

Figure A.1. Gestational age at time of sampling/ presentation in AHR women displayed per delivery outcomes in the RS study

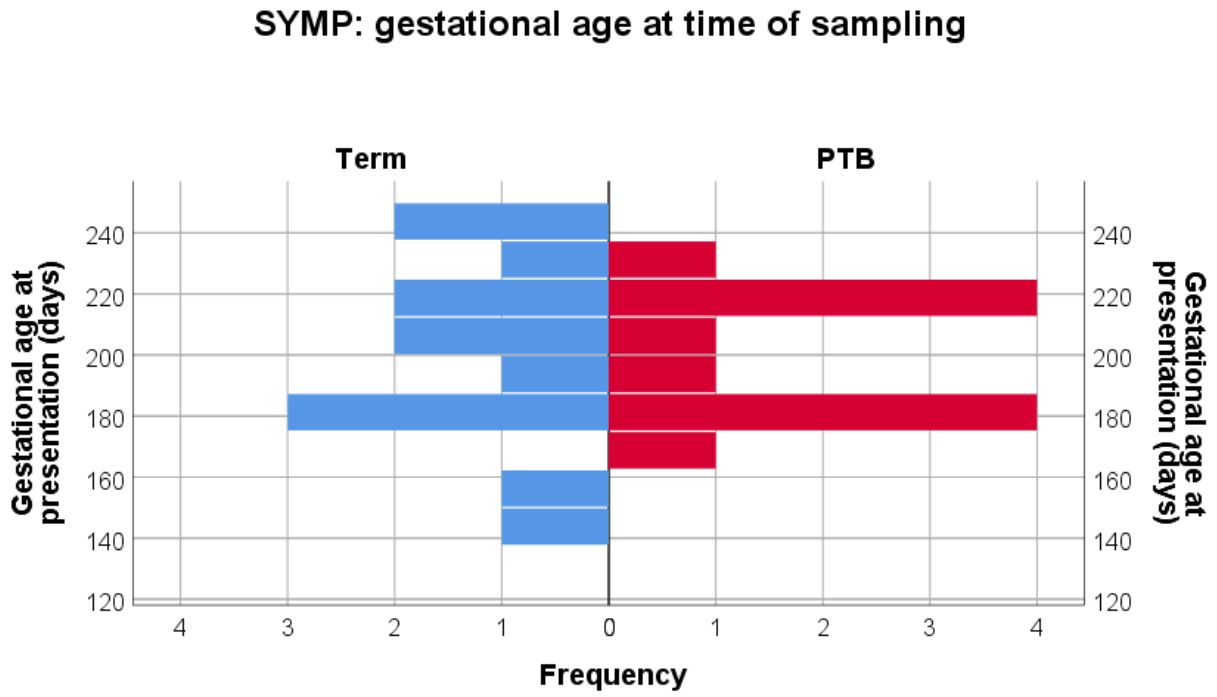

Figure A.2. Gestational age at time of sampling/ presentation in SYMP women displayed per delivery outcomes in the RS study

Appendix B

Search strategy for systematic review on spectroscopic techniques for assessing cervical remodelling *in vivo*

Database: **Ovid Medline**
<1946 to Present>
Search Strategy:

---

1. "preterm birth".mp. or exp Premature Birth/ (21765)
2. screening.mp. (567410)
3. prediction.mp. (229782)
4. exp Diagnosis/ or diagnosis.mp. (9568954)
5. 2 or 3 or 4 (9921654)
6. exp Obstetric Labor, Premature/ or prematurity.mp. or exp Premature Birth/ (45155)
7. 1 or 6 (52014)
8. spectroscopy.mp. or exp Spectrum Analysis/ (701192)
9. cervix.mp. or exp Cervix Uteri/ (66833)
10. exp Pregnancy, Animal/ or exp Cervical Ripening/ or exp Parturition/ or exp Obstetric Labor, Premature/ or exp Premature Birth/ or exp Pregnancy/ or exp Cervix Uteri/ or "cervical remodel*ing".mp. (887937)
11. exp CERVICAL RIPENING/ (1062)
12. 9 or 10 or 11 (922464)
13. 5 and 7 and 8 and 12 (64)

Total n=64

Database: **Scopus**
<1960 to Present>
Search Strategy:

("preterm birth" OR prematur*) AND (spectroscop* OR "spectrum analysis") AND (screening OR prediction OR diagnosis) AND (cervix OR "cervical remodel*" OR "cervical ripen*")

Total n=14

Database: **Web of Science**
<1864 to Present>
Search Strategy:

(*"preterm birth"* OR *prematur**) AND (*spectroscop** OR *"spectrum analysis"*) AND (*screening* OR *prediction* OR *diagnosis*) AND (*cervix* OR *"cervical remodel*"* OR *"cervical ripen*")*

Total n=29

Search strategy for systematic review on cervical neural stimulation with the use of bioimpedance spectroscopic technology

Database: **Ovid Medline**
<1946 to Present>
Search Strategy:
---
1. exp Cervix Uteri/ (27193)
2. exp Humans/ or exp Electromagnetic Fields/ or exp Animals/ (23027213)
3. exp Electric Stimulation/ (126260)
4. "adverse effect".mp. (31850)
5. *Equipment Safety/ or *Safety/ (13141)
6. 2 or 3 (23029081)
7. 4 or 5 (44976)
8. 1 and 6 and 7 (17)

Total n=17

Database: **Scopus**
<1960 to Present>
Search Strategy:
---
cervix AND (human OR animal) AND ("electromagnetic field" OR "electric stimulation" OR "neural stimulation") AND ("adverse effect" OR "safety")

Total n=15

Database: **Web of Science**
<1900 to Present>
Search Strategy:
---
cervix AND (human OR animal) AND (electromagnetic field OR electric stimulation OR neural stimulation) AND (adverse effect OR safety)

Total n=1

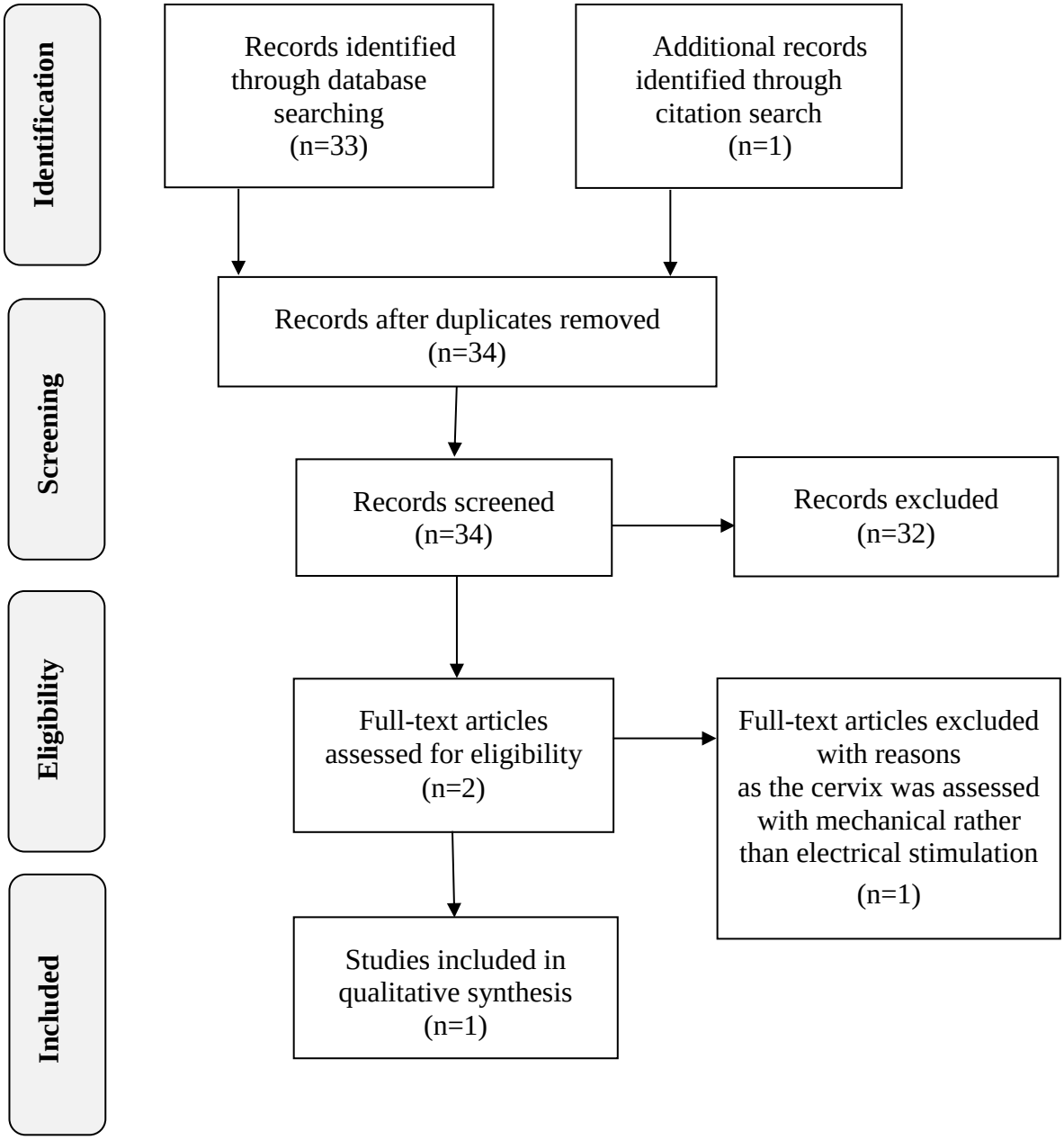

Figure B.1. Preferred Reporting Items for Systematic Reviews and Meta-Analysis (PRISMA) flow chart showing the methodology for the selection of on cervical neural stimulation with the use of bioimpedance spectroscopic technology

Table B.1. Summary of the studies included.

Author	Journal	Year	Subject	Technique	Outcome
Fang D et al.	*Am J Obstet Gynecol.*	2015	Pregnant and non-pregnant mice vs control (6-7/ group)	Different protocols of electrical stimulation of the cervix (0.1-0.2 mA, 10 Hz + LIF)	No altered delivery time, no changes in pup weight or damage to cervix between groups

Appendix C

Table C.1. Mean differences and limits of agreement for *in vitro* C2-C3 transresistance measurements (H^2/ ohm). Intra-observer reliability, n=7.

Frequency (kHz)	Mean difference (C2-C3)	SD	Lower 95% CI of mean	Upper 95% CI of mean	Lower limit of agreement	Upper limit of agreement
21	**-8.09E^{-9}**	1.01E^{-8}	-1.74E^{-8}	1.24E^{-9}	**-2.79E^{-8}**	**1.17E^{-8}**
42	**5.27E^{-9}**	1.92E^{-8}	-1.24E^{-8}	2.3E^{-8}	**-3.24E^{-8}**	**4.29E^{-8}**
56	**5.01E^{-9}**	2.06E^{-8}	-2.71E^{-8}	2.9E^{-8}	**-3.54E^{-8}**	**4.54E^{-8}**
72	**4.39E^{-9}**	1.84E^{-8}	-2.33E^{-8}	2.71E^{-8}	**-3.17E^{-8}**	**4.05E^{-8}**
86	**4.14E^{-9}**	1.66E^{-8}	-2.01E^{-8}	2.21E^{-8}	**-2.84E^{-8}**	**3.67E^{-8}**
100	**3.60E^{-9}**	1.63E^{-8}	-2.05E^{-8}	2.19E^{-8}	**-2.83E^{-8}**	**3.55E^{-8}**
202	**1.47E^{-9}**	1.8E^{-8}	-9.43E^{-9}	1.23E^{-8}	**-3.38E^{-8}**	**3.68E^{-8}**
302	**5.54E^{-10}**	1.07E^{-8}	-9.31E^{-9}	1.04E^{-8}	**-2.04E^{-8}**	**2.15E^{-8}**
402	**-4.29E^{-10}**	1.01E^{-8}	-1.61E^{-8}	9.24E^{-9}	**-2.02E^{-8}**	**1.94E^{-8}**
502	**-1.28E^{-9}**	9.82E^{-8}	-1.77E^{-8}	8.19E^{-9}	**-2.05E^{-8}**	**1.80E^{-8}**
604	**-2.10E^{-9}**	9.75E^{-9}	-1.92E^{-8}	7.95E^{-9}	**-2.12E^{-8}**	**1.70E^{-8}**
704	**-2.91E^{-9}**	9.79E^{-9}	-2.09E^{-8}	7.46E^{-9}	**-2.21E^{-8}**	**1.63E^{-8}**
804	**-3.84E^{-9}**	1.01E^{-8}	-2.28E^{-9}	6.61E^{-9}	**-2.36E^{-8}**	**1.60E^{-8}**
904	**-4.62E^{-9}**	1.03E^{-8}	-2.41E^{-8}	6.74E^{-9}	**-2.48E^{-8}**	**1.56E^{-8}**
1013	**-5.29E^{-9}**	1.04E^{-8}	-1.49E^{-8}	4.32E^{-9}	**-2.57E^{-8}**	**1.51E^{-8}**

SD: standard deviation, SE: standard error, CI: confidence interval, C2: second cervical measurement, C3: third cervical measurement

Table C.2. Mean differences and limits of agreement for *in vitro* C1-C3 transresistance measurements (H^2/ ohm). Intra-observer reliability, n=7

Frequency (kHz)	Mean difference (C1-C3)	SD	Lower 95% CI of mean	Upper 95% CI of mean	Lower limit of agreement	Upper limit of agreement
21	**-2.19E^{-8}**	2.69E^{-8}	-4.68E^{-8}	2.89E^{-9}	**-7.46E^{-8}**	**3.08E^{-8}**
42	**3.62E^{-9}**	1.58E^{-8}	-1.05E^{-8}	1.77E^{-8}	**-2.73E^{-8}**	**3.46E^{-8}**
56	**4.64E^{-8}**	1.86E^{-8}	-2.29E^{-8}	2.53E^{-8}	**-9.94E^{-9}**	**8.29E^{-8}**
72	**4.55E^{-9}**	1.73E^{-8}	-1.80E^{-8}	2.55E^{-8}	**-2.94E^{-8}**	**3.85E^{-8}**
86	**4.59E^{-9}**	1.57E^{-8}	-1.58E^{-8}	2.10E^{-8}	**-2.62E^{-8}**	**3.54E^{-8}**
100	**4.06E^{-9}**	1.57E^{-8}	-1.82E^{-8}	2.03E^{-8}	**-2.67E^{-8}**	**3.48E^{-8}**
202	**1.53E^{-9}**	1.20E^{-8}	-2.16E^{-8}	1.22E^{-8}	**-2.20E^{-8}**	**2.51E^{-8}**
302	**-3.77E^{-10}**	1.22E^{-8}	-2.70E^{-8}	9.41E^{-9}	**-3.99E^{-8}**	**2.35E^{-8}**
402	**-1.81E^{-9}**	1.27E^{-8}	-1.30E^{-8}	9.95E^{-9}	**-2.67E^{-8}**	**2.31E^{-8}**
502	**-3.29E^{-9}**	1.35E^{-8}	-3.2E^{-8}	7.51E^{-9}	**-2.98E^{-8}**	**2.32E^{-8}**
604	**-4.72E^{-9}**	1.44E^{-8}	-3.44E^{-8}	8.24E^{-9}	**-3.29E^{-8}**	**2.35E^{-8}**
704	**-6.11E^{-9}**	1.54E^{-8}	-2.03E^{-8}	8.10E^{-9}	**-3.63E^{-8}**	**2.41E^{-8}**
804	**-7.55E^{-9}**	1.64E^{-8}	-3.88E^{-8}	7.46E^{-9}	**-3.97E^{-8}**	**2.46E^{-8}**
904	**-8.71E^{-9}**	1.70E^{-8}	-3.95E^{-8}	6.64E^{-9}	**-4.20E^{-8}**	**2.46E^{-8}**
1013	**-9.89E^{-9}**	1.80E^{-8}	-2.66E^{-8}	6.78E^{-9}	**-4.52E^{-8}**	**2.54E^{-8}**

SD: standard deviation, SE: standard error, CI: confidence interval, C1: first cervical measurement, C3: third cervical measurement

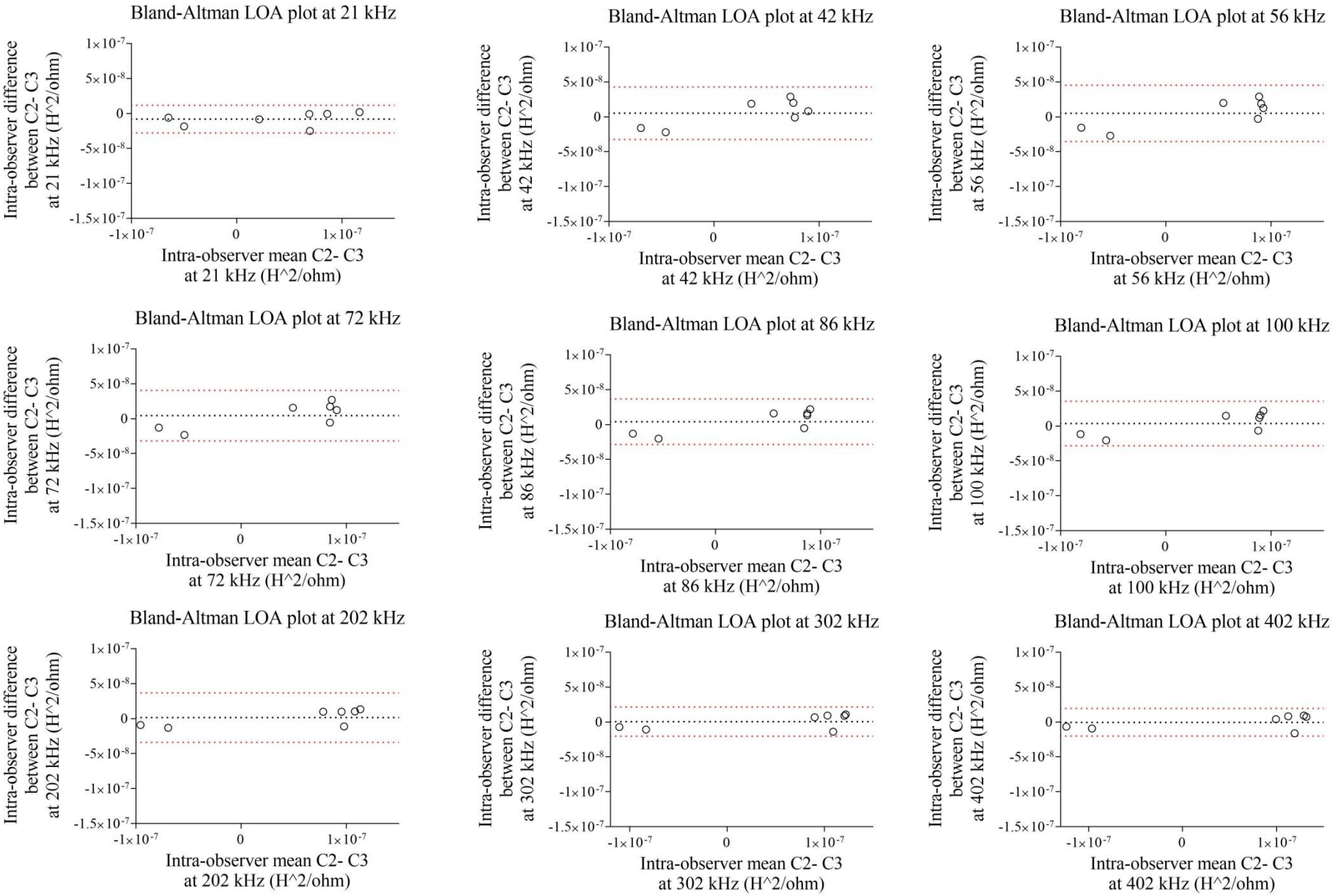

Figure C.1. Bland-Altman plots for MIS *in vitro* C2-C3 in the frequency range of 21-402 kHz. Within-observer repeatability (n= 7).

LOA: limits of agreement, C2: second cervical measurement, C3: third cervical measurement

In vitro repeatability C2-C3

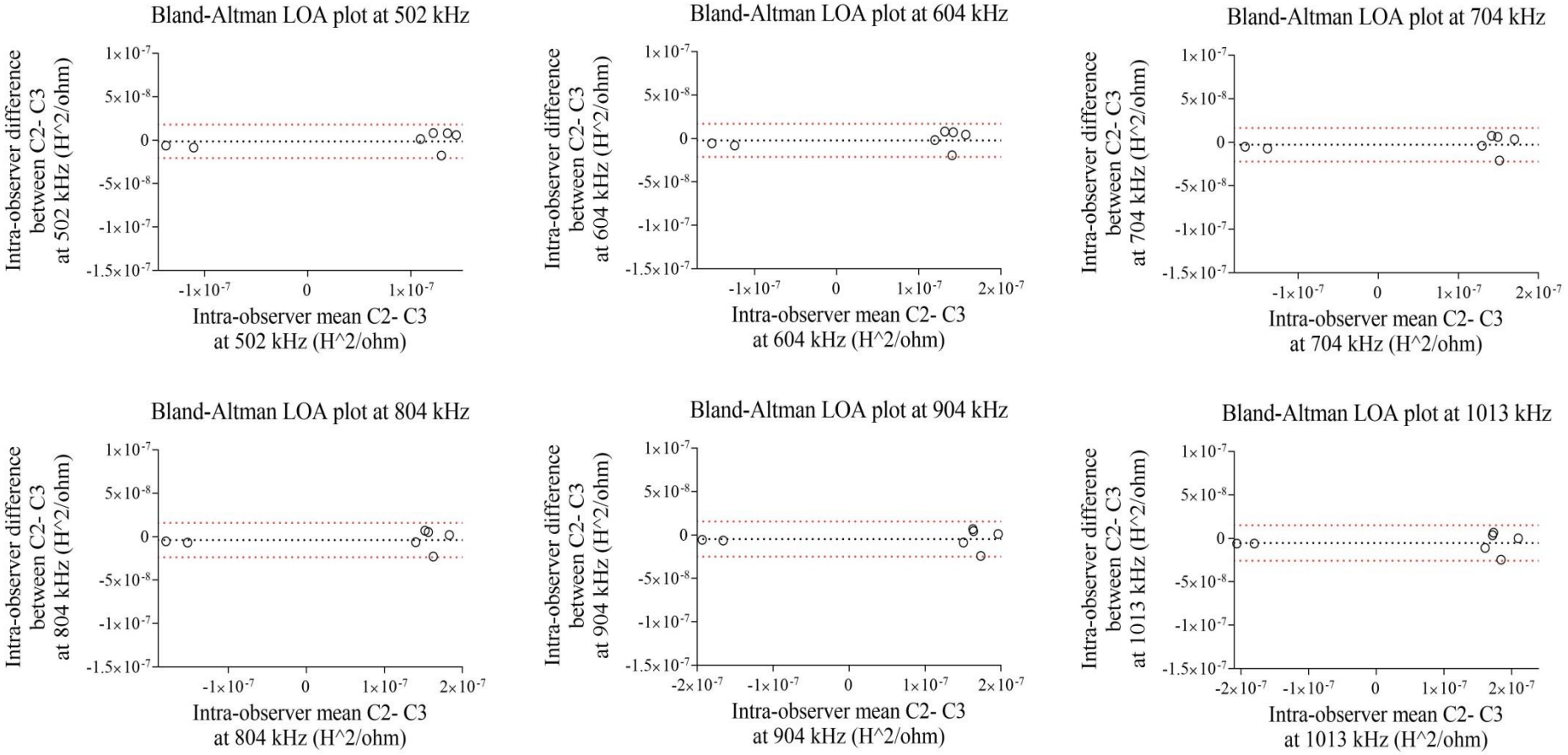

Figure C.2. Bland-Altman plots for MIS *in vitro* C2-C3 in the frequency range of 502-1013 kHz. Within-observer repeatability (n= 7).

LOA: limits of agreement, C2: second cervical measurement, C3: third cervical measurement

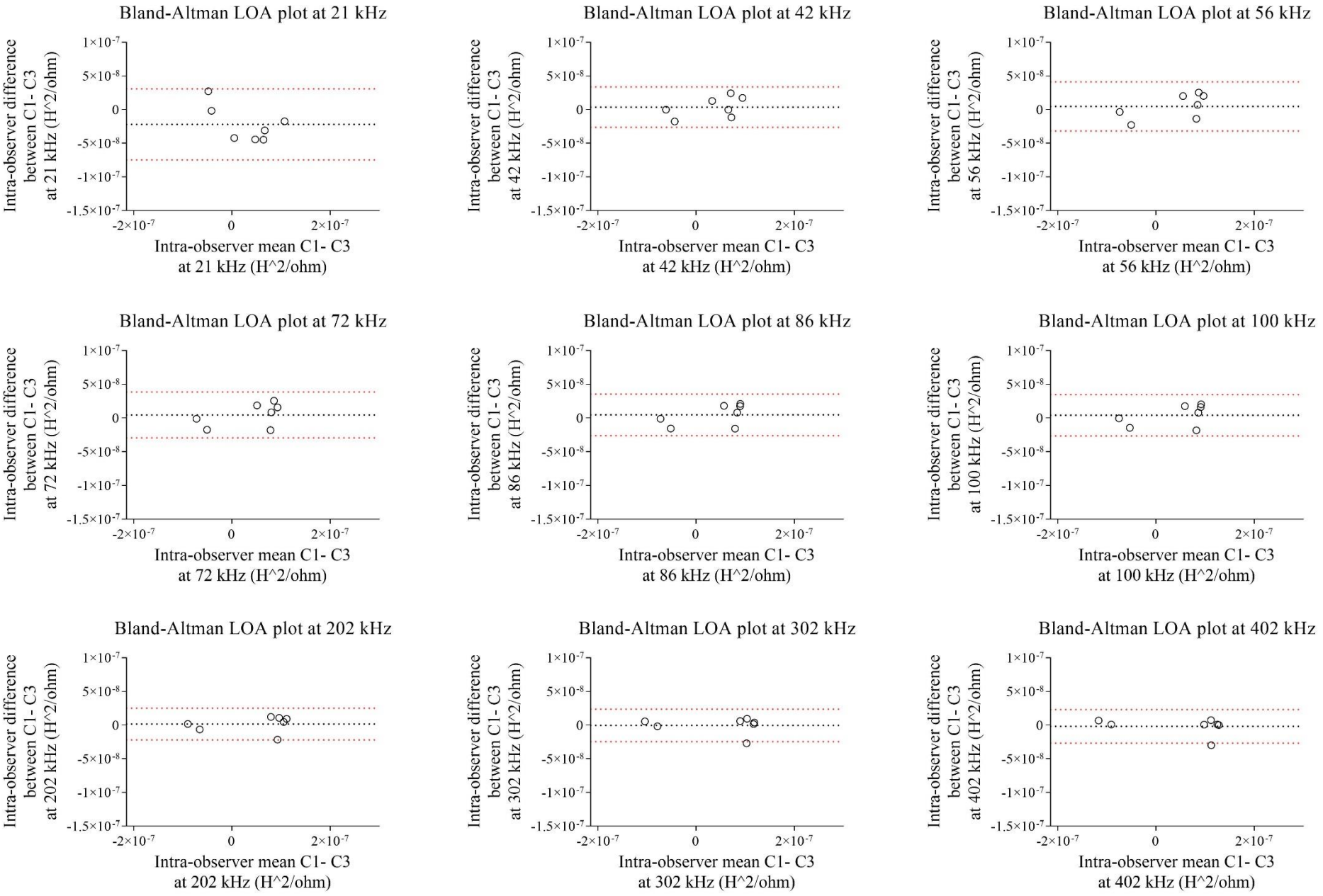

Figure C.3. Bland-Altman plots for MIS *in vitro* C1-C3 in the frequency range of 21-402 kHz. Within-observer repeatability (n= 7).

LOA: limits of agreement, C1: first cervical measurement, C3: third cervical measurement

In vitro repeatability C1-C3

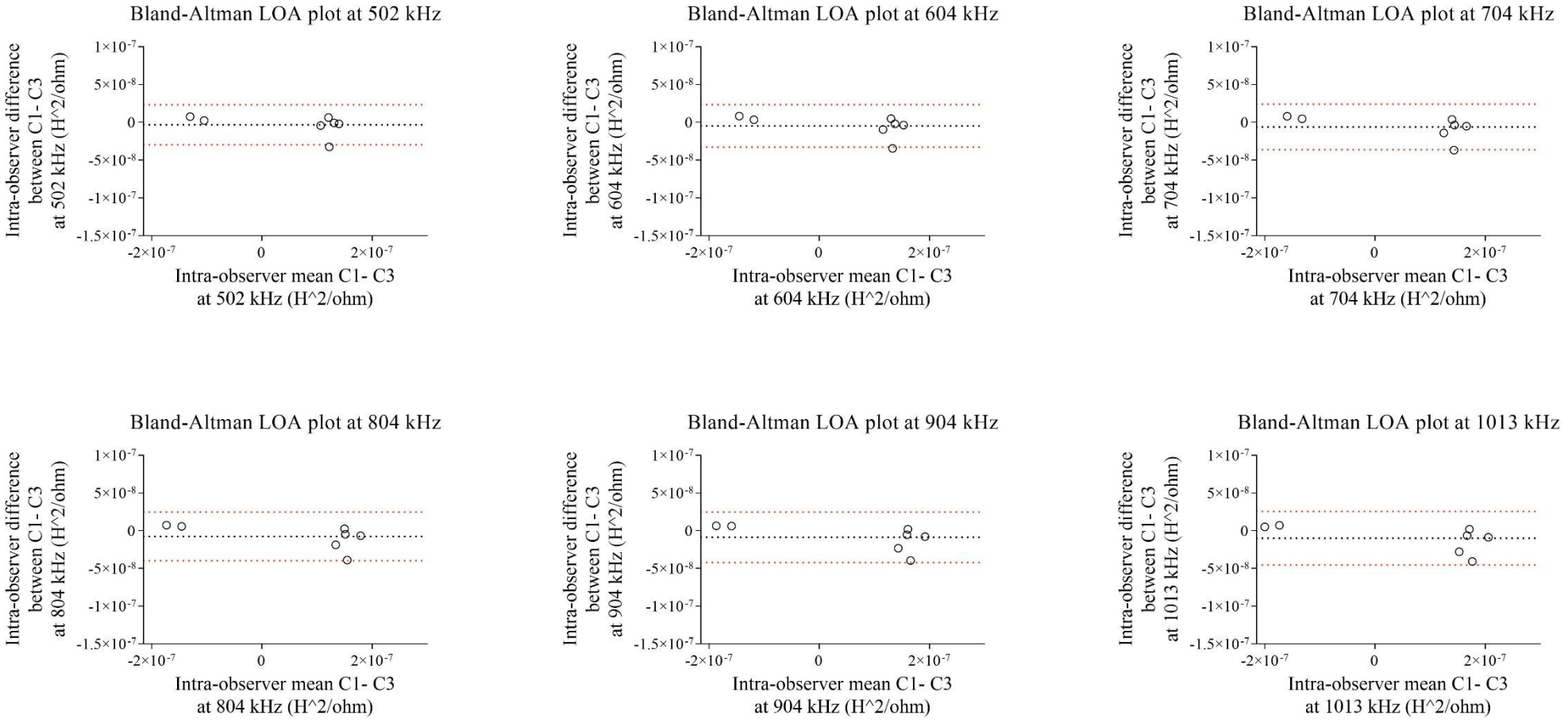

Figure C.4. Bland-Altman plots for MIS *in vitro* C1-C3 in the frequency range of 502-1013 kHz. Within-observer repeatability (n= 7).
LOA: limits of agreement, C1: first cervical measurement, C3: third cervical measurement

Table C.3. Mean differences and limits of agreement for *in vivo* C1-C2 transresistance measurements (H^2/ ohm). Intra-observer reliability, n=32.

Frequency (kHz)	Mean Difference (C1-C2)	SD	Lower 95% CI of mean	Upper 95% CI of mean	Lower Limit of Agreement	Upper Limit of Agreement
21	**-3.75E^{-4}**	9.88E^{-3}	-7.32E^{-4}	-1.91E^{-5}	**-1.97E^{-2}**	**1.90E^{-2}**
42	**-4.60E^{-4}**	1.34E^{-3}	-9.5E^{-4}	3.05E^{-5}	**-3.09E^{-3}**	**2.60E^{-3}**
56	**-1.46E^{-4}**	9.48E^{-4}	-4.94E^{-4}	2.02E^{-4}	**-2.02E^{-3}**	**1.69E^{-3}**
72	**-2.54E^{-4}**	1.10E^{-3}	-6.21E^{-4}	1.12E^{-4}	**-2.21E^{-3}**	**1.71E^{-3}**
86	**-1.19E^{-4}**	1.06E^{-3}	-5.08E^{-4}	2.70E^{-4}	**-2.20E^{-3}**	**1.96E^{-3}**
100	**-4.28E^{-5}**	9.69E^{-4}	-3.98E^{-4}	3.12E^{-4}	**-1.94E^{-3}**	**1.86E^{-3}**
202	**2.87E^{-4}**	1.07E^{-3}	-1.67E^{-4}	6.24E^{-4}	**-1.81E^{-3}**	**2.38E^{-3}**
302	**3.11E^{-4}**	1.08E^{-3}	-8.5E^{-5}	7.09E^{-4}	**-1.81E^{-3}**	**2.43E^{-3}**
402	**3.27E^{-4}**	1.40E^{-3}	-1.87E^{-4}	8.41E^{-5}	**-2.42E^{-3}**	**3.07E^{-3}**
502	**3.56E^{-4}**	1.57E^{-3}	-2.21E^{-4}	9.35E^{-4}	**-2.73E^{-3}**	**3.43E^{-3}**
604	**4.74E^{-4}**	1.85E^{-3}	-2.05E^{-4}	1.15E^{-3}	**-3.15E^{-3}**	**4.10E^{-3}**
704	**5.68E^{-4}**	1.94E^{-3}	-1.44E^{-4}	1.28E^{-3}	**-3.23E^{-3}**	**4.37E^{-3}**
804	**6.08E^{-4}**	2.01E^{-3}	-5.74E^{-5}	1.41E^{-3}	**-3.23E^{-3}**	**4.55E^{-3}**
904	**4.89E^{-4}**	1.83E^{-3}	-1.73E^{-4}	1.15E^{-3}	**-3.10E^{-3}**	**4.08E^{-3}**
1013	**5.03E^{-4}**	1.80E^{-3}	-1.59E^{-4}	1.16E^{-3}	**-3.03E^{-3}**	**4.13E^{-3}**

SD: standard deviation, SE: standard error, CI: confidence interval, C1: first cervical measurement, C2: second cervical measurement

Table C.4. Mean differences and limits of agreement for *in vivo* C1-C3 transresistance measurements (H^2/ ohm). Intra-observer reliability, n=32.

Frequency (kHz)	Mean Difference (C1-C3)	SD	Lower 95% CI of mean	Upper 95% CI of mean	Lower Limit of Agreement	Upper Limit of Agreement
21	**-1.20E^{-3}**	2.11E^{-3}	1.95E^{-3}	-4.40E^{-4}	**-5.34E^{-3}**	**2.94E^{-3}**
42	**-9.95E^{-4}**	1.89E^{-3}	-1.67E^{-3}	-3.15E^{-4}	**-4.70E^{-3}**	**2.71E^{-3}**
56	**-6.61E^{-4}**	1.76E^{-3}	-1.29E^{-3}	-2.58E^{-5}	**-4.11E^{-3}**	**2.79E^{-3}**
72	**-5.80E^{-4}**	1.57E^{-3}	-1.14E^{-3}	-1.45E^{-5}	**-3.66E^{-3}**	**2.50E^{-3}**
86	**-4.11E^{-4}**	1.56E^{-3}	-1.00E^{-3}	1.21E^{-4}	**-3.47E^{-3}**	**2.60E^{-3}**
100	**-2.38E^{-4}**	1.38E^{-3}	-7.36E^{-4}	2.60E^{-4}	**-2.94E^{-3}**	**2.47E^{-3}**
202	**3.10E^{-4}**	1.46E^{-3}	-2.16E^{-4}	8.37E^{-4}	**-2.55E^{-3}**	**3.17E^{-3}**
302	**4.44E^{-4}**	1.56E^{-3}	-1.20E^{-4}	1.01E^{-3}	**-2.60E^{-3}**	**3.50E^{-3}**
402	**6.15E^{-4}**	1.81E^{-3}	-3.79E^{-5}	1.26E^{-3}	**-2.93E^{-3}**	**4.16E^{-3}**
502	**3.84E^{-4}**	1.42E^{-3}	-1.28E^{-4}	8.97E^{-4}	**-2.40E^{-3}**	**3.16E^{-3}**
604	**4.46E^{-4}**	1.71E^{-3}	-1.72E^{-4}	1.07E^{-3}	**-2.91E^{-3}**	**3.80E^{-3}**
704	**4.34E^{-4}**	1.71E^{-3}	-1.80E^{-4}	1.04E^{-4}	**-2.92E^{-3}**	**3.96E^{-3}**
804	**3.86E^{-4}**	1.55E^{-3}	-1.75E^{-4}	9.48E^{-4}	**-2.65E^{-3}**	**3.42E^{-3}**
904	**2.05E^{-4}**	1.66E^{-3}	-3.92E^{-4}	8.02E^{-4}	**-3.05E^{-3}**	**3.46E^{-3}**
1013	**2.88E^{-4}**	1.55E^{-3}	-2.73E^{-4}	8.48E^{-4}	**-2.75E^{-3}**	**3.30E^{-3}**

SD: standard deviation, SE: standard error, CI: confidence interval, C1: first cervical measurement, C3: third cervical measurement

In vivo repeatability C1-C2

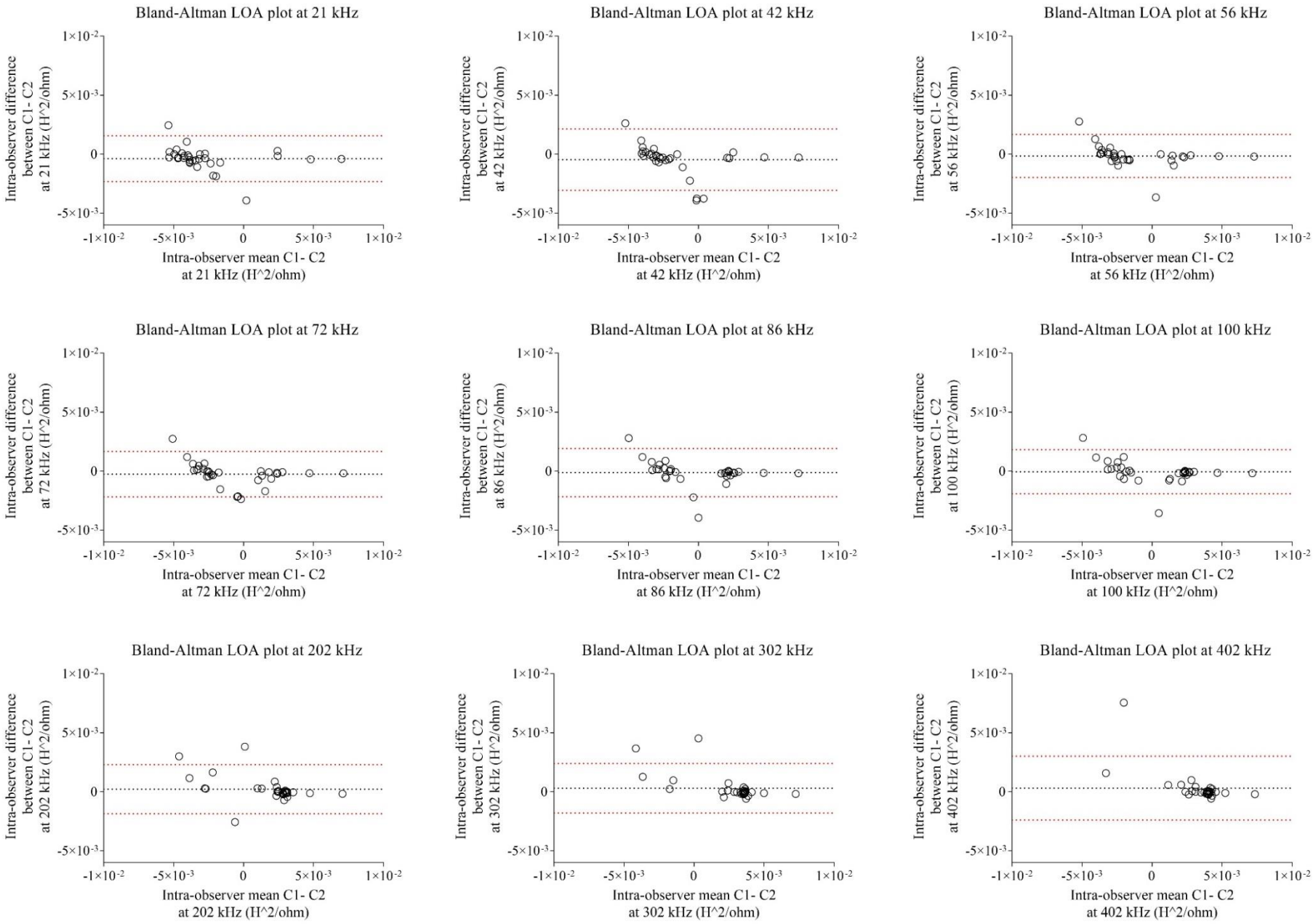

Figure C.5. Bland-Altman plots for MIS *in vivo* C1-C2 in the frequency range of 21-402 kHz. Within-observer repeatability (n=32).

LOA: limits of agreement, C1: first cervical measurement, C2: second cervical measurement

In vivo repeatability C1-C2

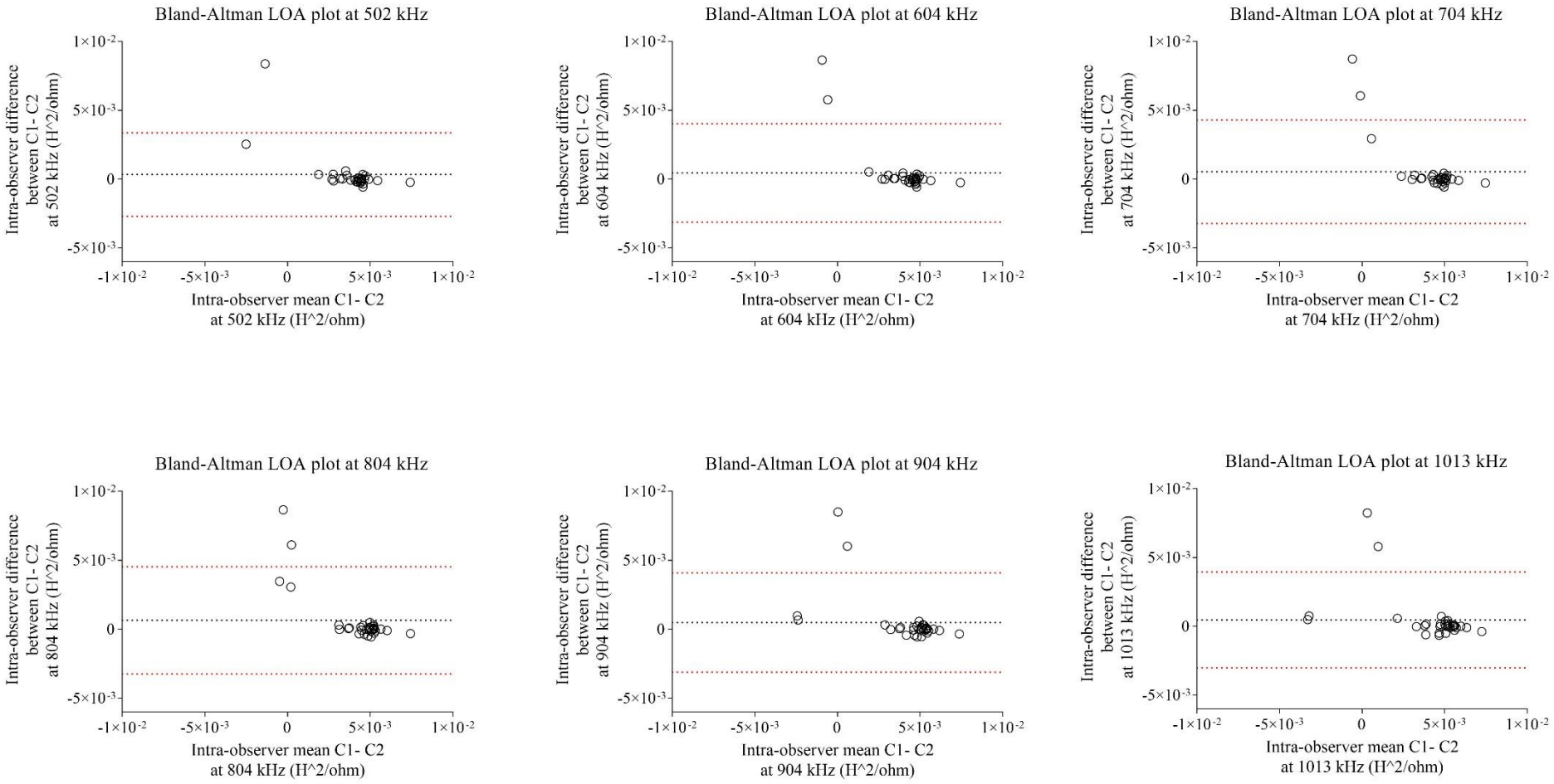

Figure C.6. Bland-Altman plots for MIS *in vivo* C1-C2 in the frequency range of 502-1013 kHz. Within-observer repeatability (n=32).
LOA: limits of agreement, C1: first cervical measurement, C2: second cervical measurement

In vivo repeatability C1-C3

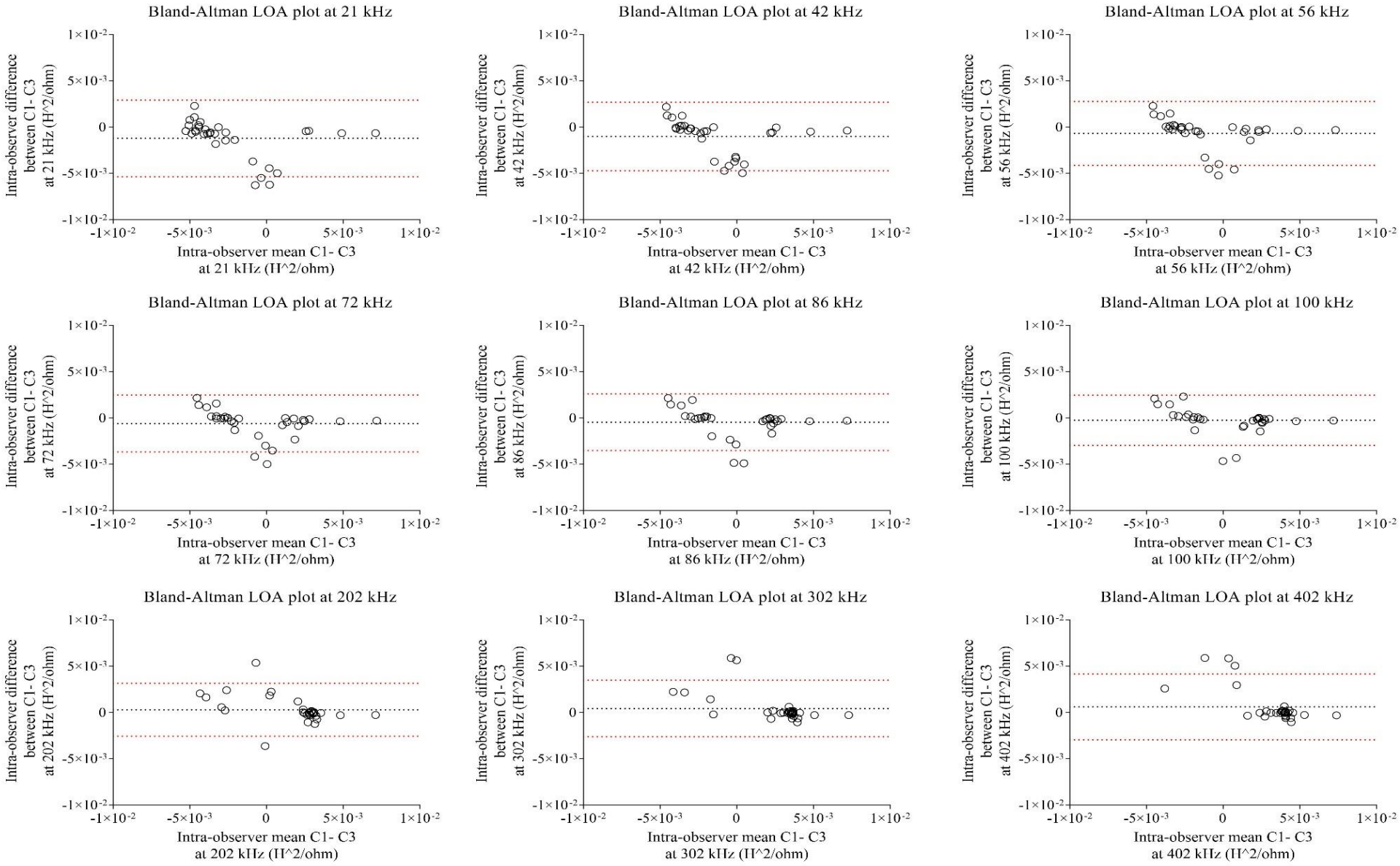

Figure C.7. Bland-Altman plots for MIS *in vivo* C1-C3 in the frequency range of 21-402 kHz. Within-observer repeatability (n=32).

LOA: limits of agreement, C1: first cervical measurement, C3: third cervical measurement

In vivo repeatability C1-C3

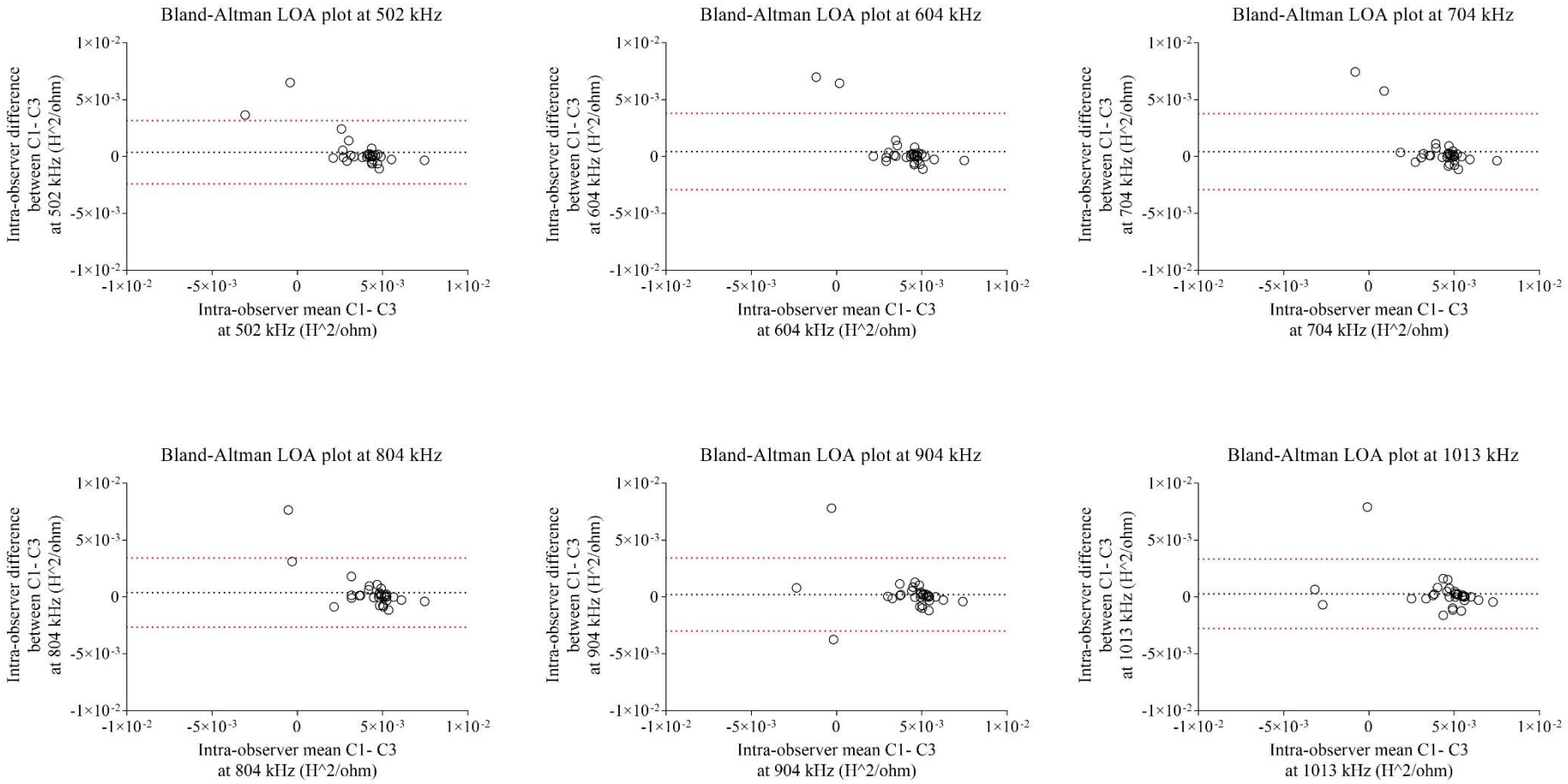

Figure C.8. Bland-Altman plots for MIS *in vivo* C1-C3 in the frequency range of 502-1013 kHz. Within-observer repeatability (n=32).
LOA: limits of agreement, C1: first cervical measurement, C3: third cervical measurement

Appendix D

Table D.1. Area under the receiver operating characteristic curve (95% CI) for prediction of PTB (PPROM + sPTB) for cervical measurements taken from AHR women during the first visit with probe A

Frequency	C1	C2	C3	Average C1-C2-C3	Largest signal at 500 kHz
21	0.72 (0.51-0.88)	0.61 (0.38-0.81)	0.66 (0.46-0.83)	0.68 (0.47-0.85)	0.68 (0.48-0.85)
42	0.67 (0.46-0.84)	0.65 (0.42-0.84)	0.66 (0.46-0.83)	0.72 (0.52-0.87)	0.73 (0.53-0.88)
56	0.68 (0.47-0.85)	0.65 (0.42-0.84)	0.64 (0.44-0.81)	0.71 (0.50-0.87)	0.73 (0.53-0.88)
72	0.69 (0.48-0.86)	0.62 (0.39-0.82)	0.66 (0.46 0.83)	0.69 (0.48-0.85)	0.72 (0.51-0.88)
86	0.67 (0.45-0.84)	0.55 (0.33-0.76)	0.63 (0.42-0.80)	0.67 (0.47-0.84)	0.69 (0.46-0.85)
100	0.64 (0.43-0.82)	0.56 (0.34-0.77)	0.65 (0.45-0.82)	0.69 (0.49-0.85)	0.71 (0.50-0.87)
202	0.62 (0.41-0.81)	0.53 (0.31-0.74)	0.61 (0.41-0.79)	0.63 (0.43-0.81)	0.65 (0.44-0.82)
302	0.61 (0.40-0.80)	0.52 (0.30-0.73)	0.63 (0.42-0.80)	0.62 (0.42-0.80)	0.65 (0.45-0.82)
402	0.57 (0.36-0.76)	0.55 (0.33-0.76)	0.63 (0.43-0.80)	0.62 (0.42-0.80)	0.62 (0.45-0.82)
502	0.57 (0.36-0.76)	0.61 (0.38-0.81)	0.63 (0.43-0.81)	0.64 (0.43-0.81)	0.65 (0.44-0.82)
604	0.56 (0.35-0.76)	0.63 (0.41-0.83)	0.64 (0.44-0.81)	0.62 (0.42-0.80)	0.68 (0.48-0.85)
704	0.57 (0.36-0.76)	0.65 (0.42-0.84)	0.63 (0.43-0.80)	0.64 (0.44-0.82)	0.68 (0.48-0.85)
804	0.57 (0.36-0.76)	0.66 (0.43-0.85)	0.66 (0.46-0.82)	0.67 (0.46-0.84)	0.68 (0.48-0.85)
904	0.59 (0.37-0.78)	0.67 (0.44-0.85)	0.65 (0.45-0.82)	0.67 (0.46-0.84)	0.70 (0.50-0.86)
1013	0.65 (0.43-0.83)	0.68 (0.45-0.86)	0.65 (0.45-0.82)	0.64 (0.44-0.82)	0.66 (0.45-0.83)

Cells are highlighted in grey to show $p<0.05$ compared to the null hypothesis of AuROC=0.5. C1: first cervical measurement, C2: second cervical measurement, C3: third cervical measurement.

Appendix E

AHR: probe A cervical transresistance based on time to delivery

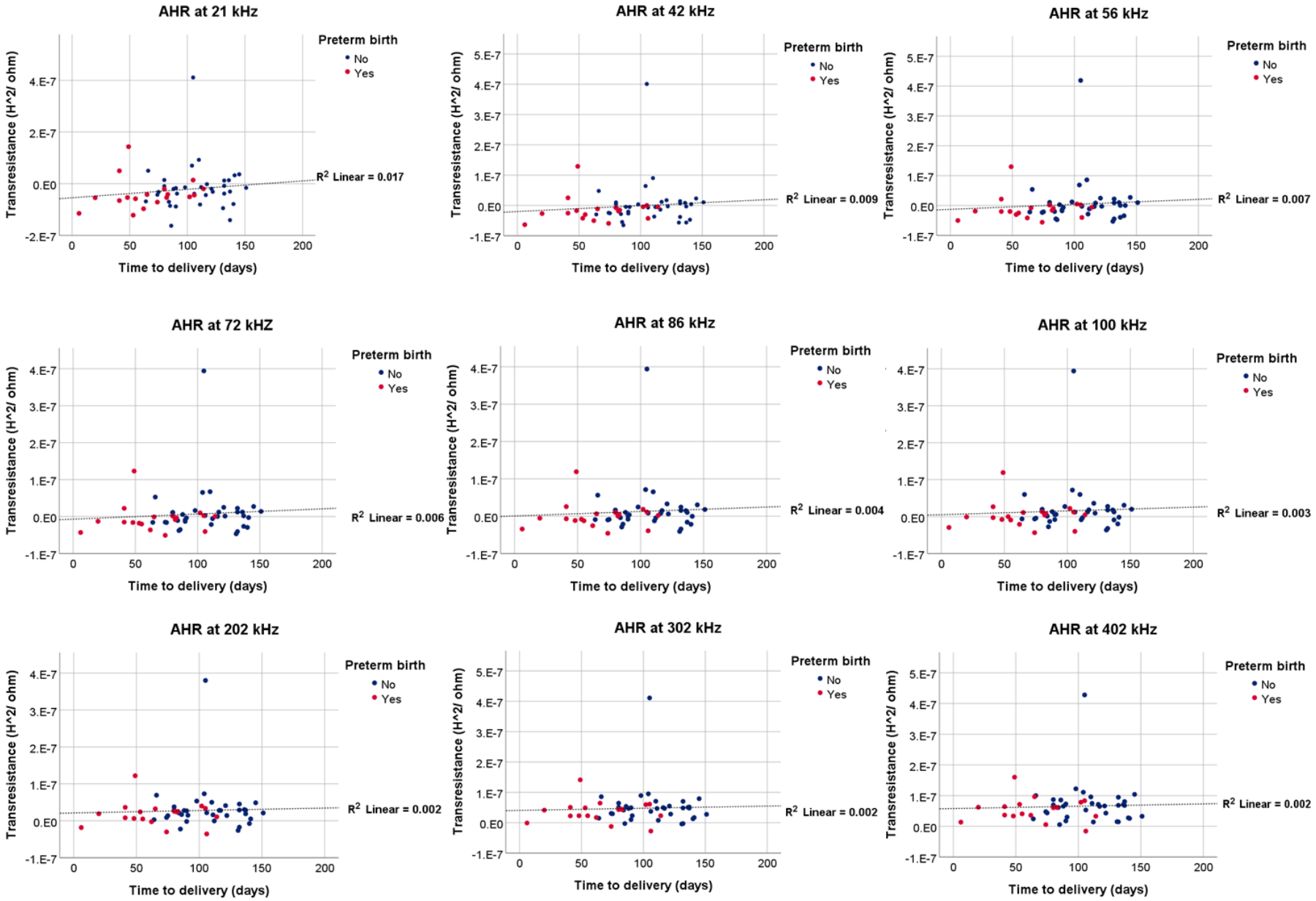

Figure E.1. AHR probe A cervical transresistance is plotted against time to delivery (days) and colour-coded based on delivery outcome (red=PTB, blue=term) for the range 21-402 kHz. *AHR: asymptomatic high risk*

AHR: probe A cervical transresistance based on time to delivery

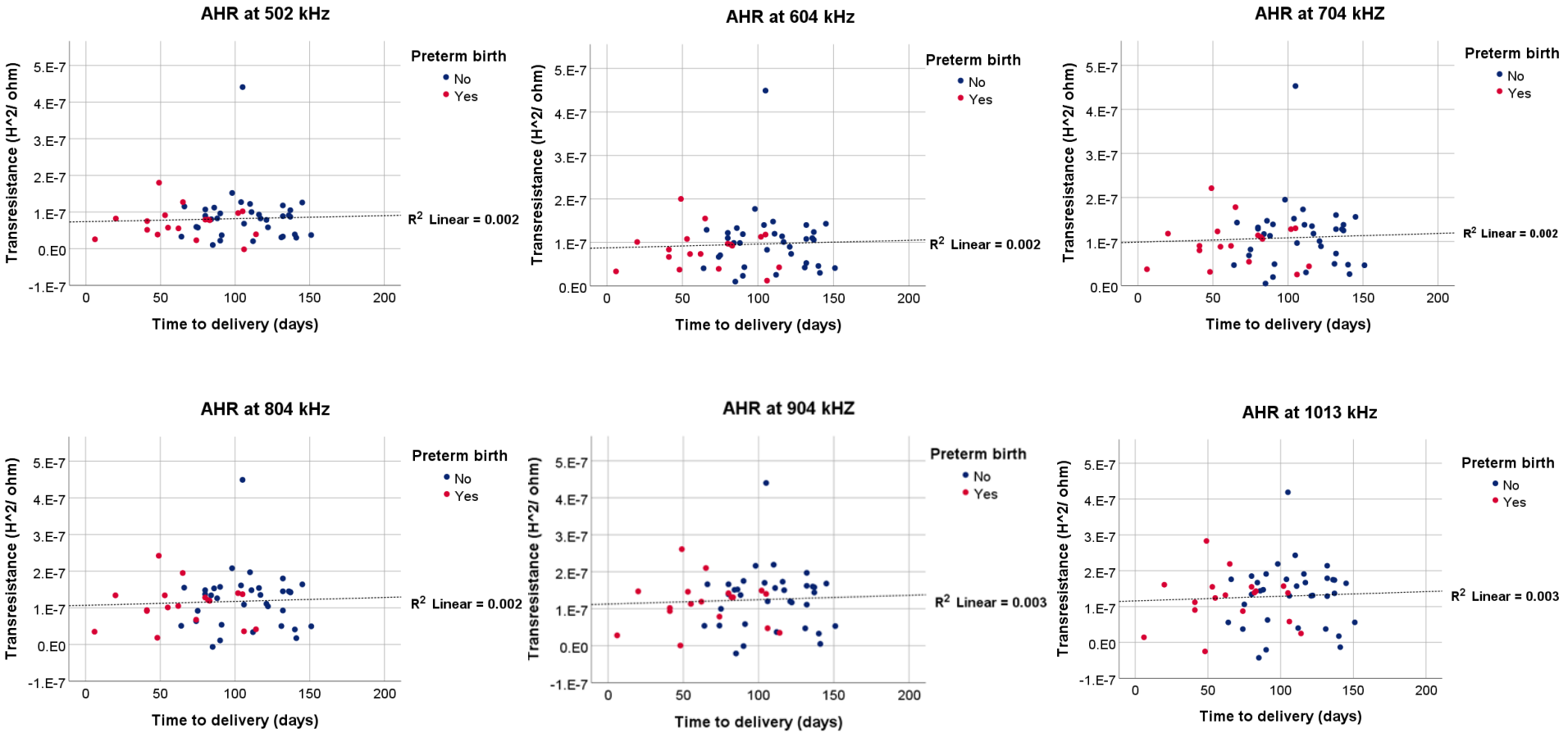

Figure E.2. AHR probe A cervical transresistance is plotted against time to delivery (days) and colour-coded based on delivery outcome (red=PTB, blue=term) for the range 502-1013 kHz. *AHR: asymptomatic high risk*

SYMP: probe A cervical transresistance based on time to delivery

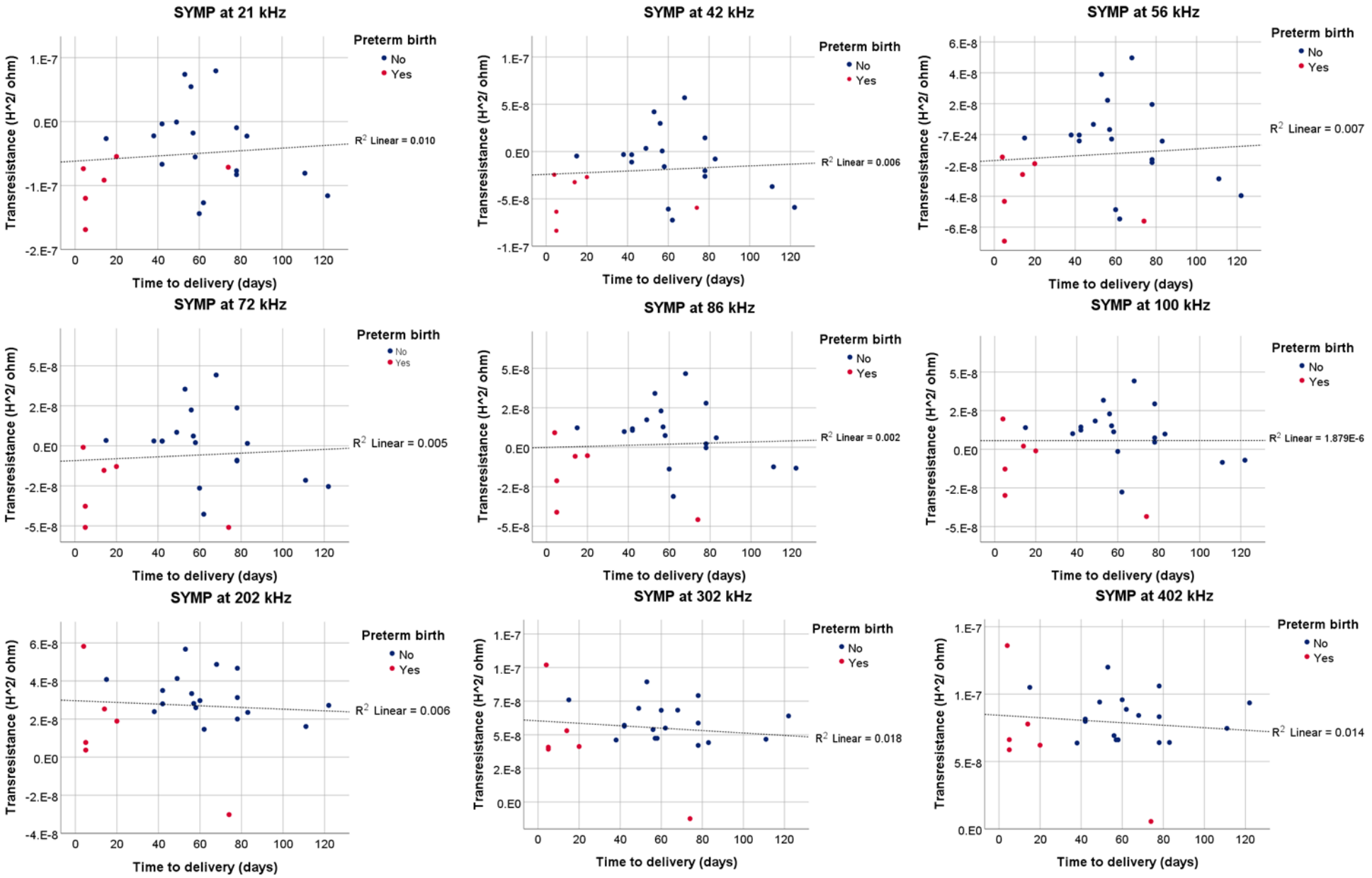

Figure E.3. SYMP probe A cervical transresistance is plotted against time to delivery (days) and colour-coded based on delivery outcome (red=PTB, blue=term) for the range 21-402 kHz. *SYMP: symptomatic*

SYMP: probe A cervical transresistance based on time to delivery

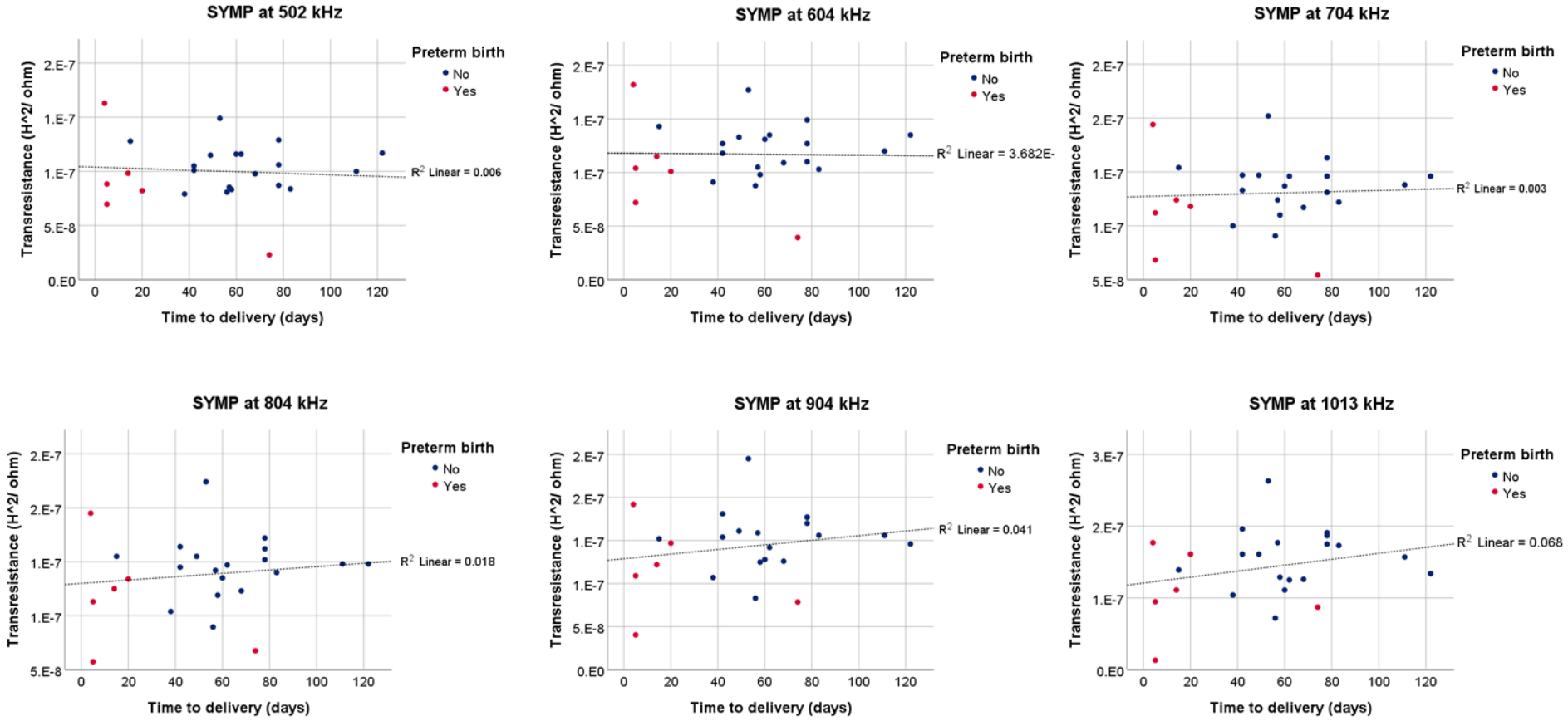

Figure E.4. SYMP probe A cervical transresistance is plotted against time to delivery (days) and colour-coded based on delivery outcome (red=PTB, blue=term) for the range 502-1013 kHz. *SYMP: symptomatic*

Appendix F

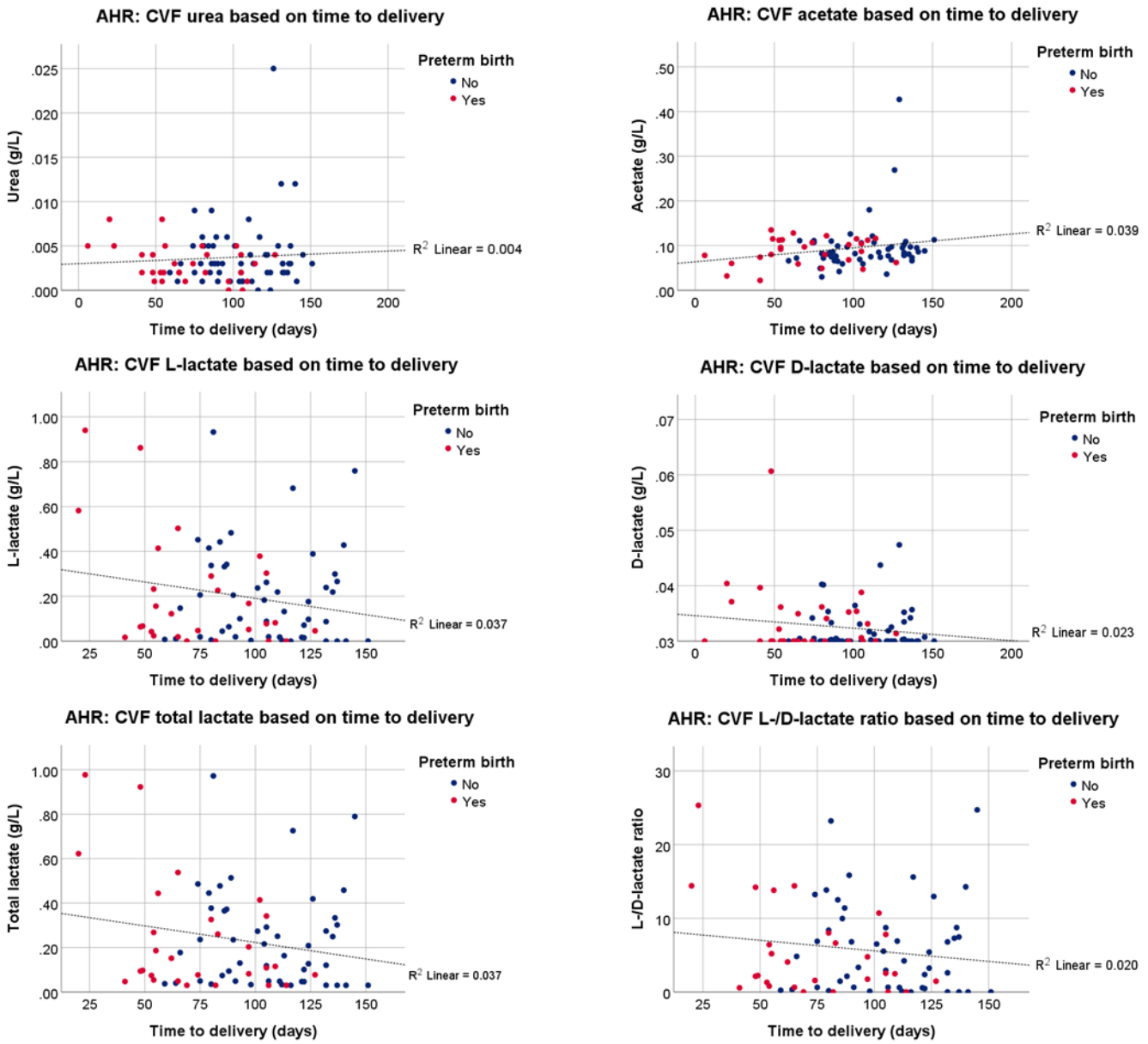

Figure F.1. AHR CVF metabolites plotted against time to delivery (days) and colour-coded based on delivery outcome (red=PTB, blue=term) *AHR: asymptomatic high risk*

SYMP: CVF metabolites based on time to delivery

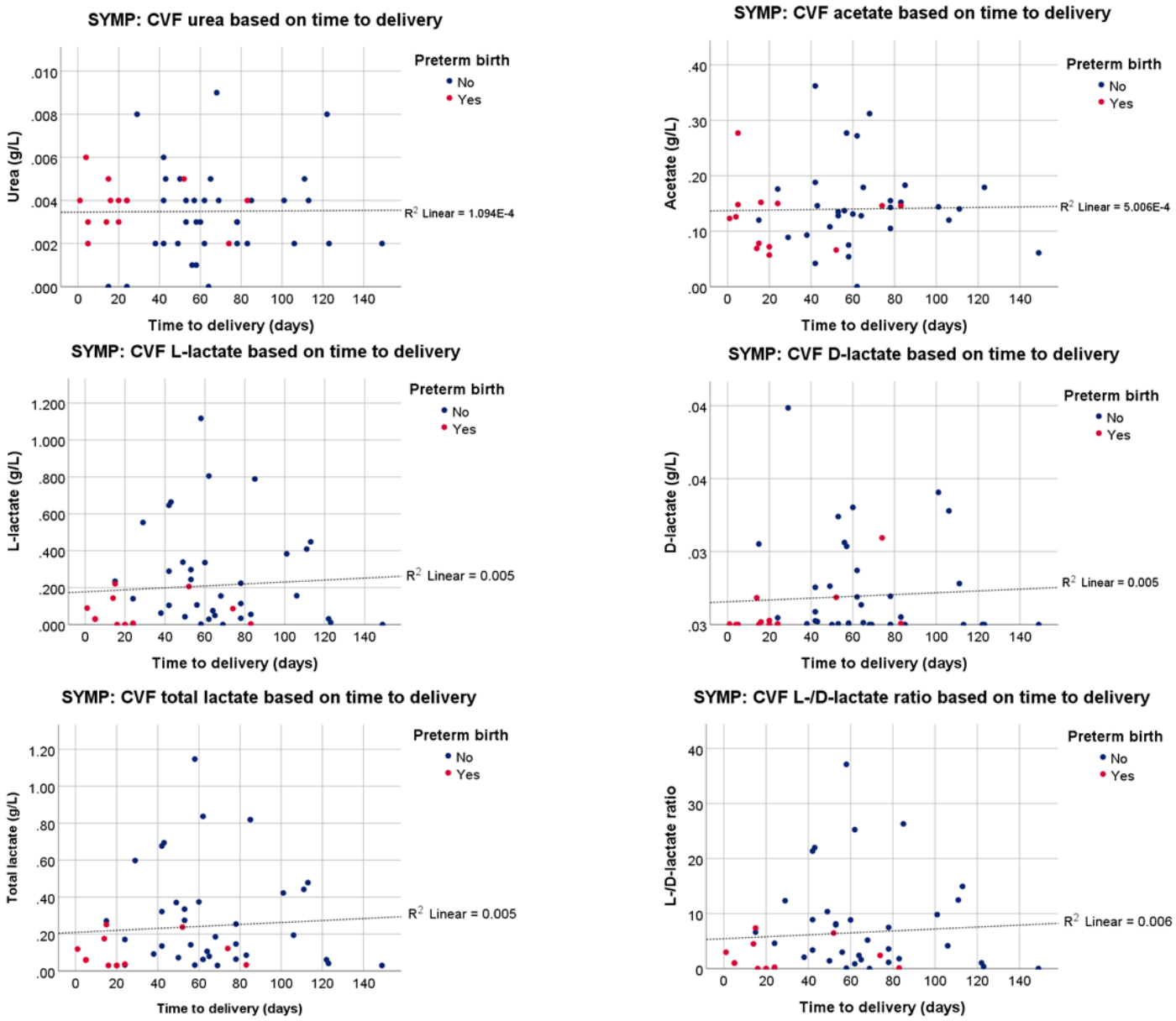

Figure F.2. SYMP CVF metabolites plotted against time to delivery (days) and colour-coded based on delivery outcome (red=PTB, blue=term) *SYMP: symptomatic*